THE ROLE OF IRON IN CANCER PROGRESSION

EDITED BY: Maryam Mehrpour, Ahmed Hamaï and Chang Gong
PUBLISHED IN: Frontiers in Cell and Developmental Biology and Frontiers in Oncology

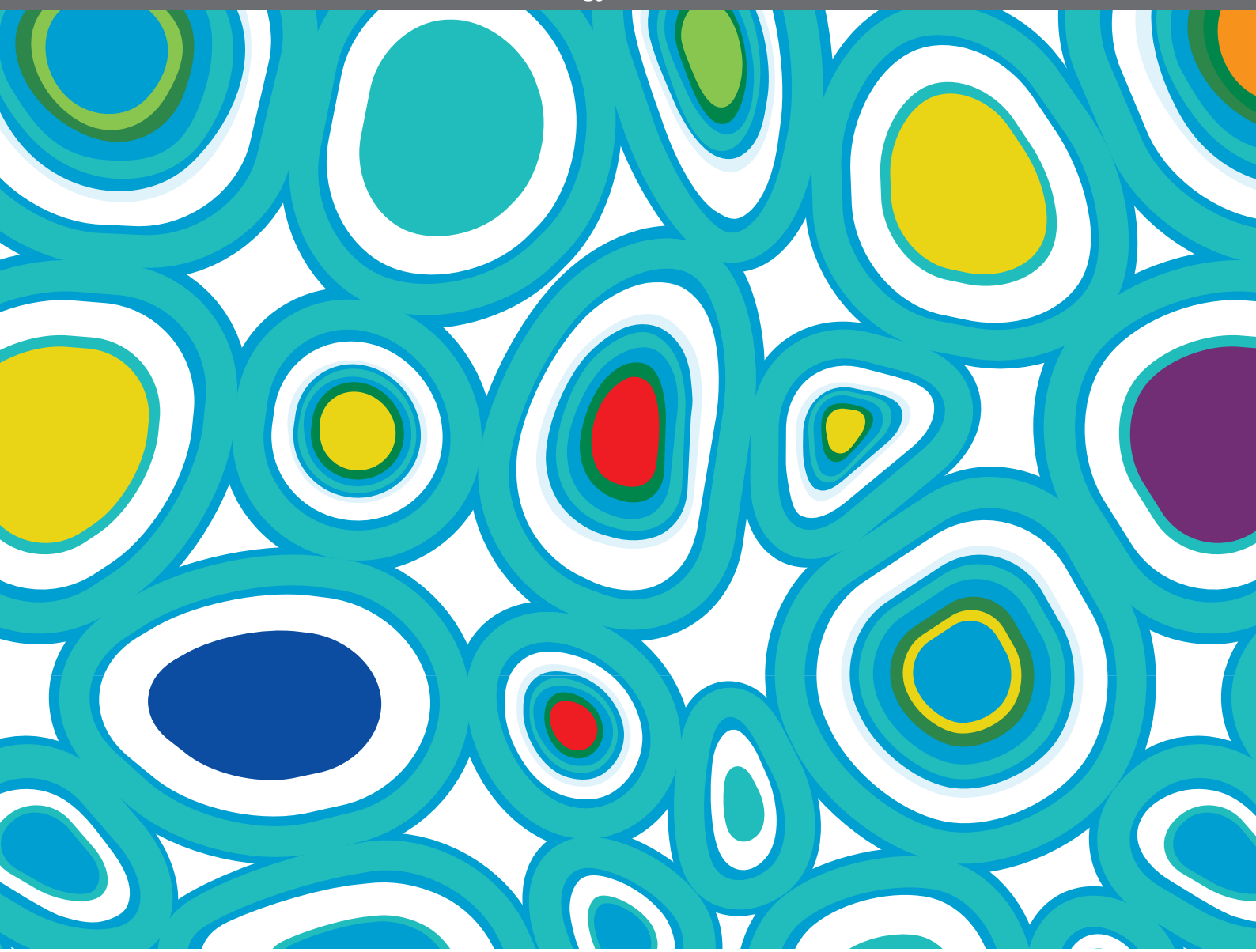

frontiers Research Topics

frontiers

ISSN 1664-8714
ISBN 978-2-83250-411-6
DOI 10.3389/978-2-83250-411-6

About Frontiers

Frontiers is more than just an open-access publisher of scholarly articles: it is a pioneering approach to the world of academia, radically improving the way scholarly research is managed. The grand vision of Frontiers is a world where all people have an equal opportunity to seek, share and generate knowledge. Frontiers provides immediate and permanent online open access to all its publications, but this alone is not enough to realize our grand goals.

Frontiers Journal Series

The Frontiers Journal Series is a multi-tier and interdisciplinary set of open-access, online journals, promising a paradigm shift from the current review, selection and dissemination processes in academic publishing. All Frontiers journals are driven by researchers for researchers; therefore, they constitute a service to the scholarly community. At the same time, the Frontiers Journal Series operates on a revolutionary invention, the tiered publishing system, initially addressing specific communities of scholars, and gradually climbing up to broader public understanding, thus serving the interests of the lay society, too.

Dedication to Quality

Each Frontiers article is a landmark of the highest quality, thanks to genuinely collaborative interactions between authors and review editors, who include some of the world's best academicians. Research must be certified by peers before entering a stream of knowledge that may eventually reach the public - and shape society; therefore, Frontiers only applies the most rigorous and unbiased reviews.
Frontiers revolutionizes research publishing by freely delivering the most outstanding research, evaluated with no bias from both the academic and social point of view. By applying the most advanced information technologies, Frontiers is catapulting scholarly publishing into a new generation.

What are Frontiers Research Topics?

Frontiers Research Topics are very popular trademarks of the Frontiers Journals Series: they are collections of at least ten articles, all centered on a particular subject. With their unique mix of varied contributions from Original Research to Review Articles, Frontiers Research Topics unify the most influential researchers, the latest key findings and historical advances in a hot research area! Find out more on how to host your own Frontiers Research Topic or contribute to one as an author by contacting the Frontiers Editorial Office: frontiersin.org/about/contact

THE ROLE OF IRON IN CANCER PROGRESSION

Topic Editors:
Maryam Mehrpour, INSERM U1151 Institut Necker Enfants Malades, France
Ahmed Hamaï, Institut National de la Santé et de la Recherche Médicale (INSERM), France
Chang Gong, Sun Yat-sen University, China

Citation: Mehrpour, M., Hamaï, A., Gong, C., eds. (2022). The Role of Iron in Cancer Progression. Lausanne: Frontiers Media SA.
doi: 10.3389/978-2-83250-411-6

Table of Contents

frontiers | Frontiers in Oncology

TYPE Editorial
PUBLISHED 21 September 2022
DOI 10.3389/fonc.2022.1026420

OPEN ACCESS

EDITED AND REVIEWED BY
Tao Liu,
University of New South Wales, Australia

*CORRESPONDENCE
Ahmed Hamaï
ahmed.hamai@inserm.fr

SPECIALTY SECTION
This article was submitted to Molecular and Cellular Oncology, a section of the journal Frontiers in Oncology

RECEIVED 23 August 2022
ACCEPTED 26 August 2022
PUBLISHED 21 September 2022

CITATION
Hamaï A, Gong C and Mehrpour M (2022) Editorial: The role of iron in cancer progression.
Front. Oncol. 12:1026420.
doi: 10.3389/fonc.2022.1026420

Editorial: The role of iron in cancer progression

Ahmed Hamaï[1,2]*, Chang Gong[3,4] and Maryam Mehrpour[1,2]

[1]Inserm U1151, Institut Necker Enfants Malades, Faculté de Médecine, Team 5, Université Paris Cité, Paris, France, [2]FEROSTEM Group, Institut Necker Enfants Malades, Inserm U1151, Université Paris Cité, Paris, France, [3]Guangdong Provincial Key Laboratory of Malignant Tumor Epigenetics and Gene Regulation, Sun Yat-Sen Memorial Hospital, Sun Yat-Sen University, Guangzhou, China, [4]Breast Tumor Center, Sun Yat-Sen Memorial Hospital, Sun Yat-Sen University, Guangzhou, China

KEYWORDS

iron, cancer, ferritinophagy, ferroptosis, antitumor immunity, cancer stem cell (CSC), ferroptosis-related gene prognostic index

Editorial on the Research Topic
The role of iron in cancer progression

Iron is an essential nutrient in all mammals, involved in key biological processes, including oxygen transport, mitochondrial respiration, metabolism, detoxification, and immune defense. The ability of iron to alternate between the oxidized form and the reduced form contributes to the formation of free radicals, with an excess leading to lipid peroxidation, increased production of reactive oxygen species (ROS), oxidative stress, and DNA damage. The accumulation of iron and ROS are linked to various pathologies, including iron overload diseases and cancer. Indeed, cancer cells exhibit an increased iron demand compared to non-cancer cells. Furthermore, pathways of iron uptake, storage, mobilization, trafficking, and regulation are all perturbed in cancer, suggesting that the reprogramming of iron metabolism is a central aspect of tumor cell survival (1). Anemia is frequently observed in many patients with cancer, and iron dyshomeostasis is implicated in numerous types of cancer (2). Recent studies have shed light on the role of iron metabolism in cancer stem cells (CSC) and suggest that specific targeting of iron metabolism in CSCs may improve the efficacy of cancer therapy (3–6). This iron dependency can make CSC and non-CSC cells more vulnerable to a non-apoptotic form of regulated cell death, referred to as ferroptosis. This cell death process characterized by the iron-dependent accumulation of lipid peroxides is morphologically, biochemically, and genetically different from other well-known modalities of regulated cell death, including apoptosis, necroptosis, various forms of necrosis, and autophagy. In distinct cancer types, metabolic reprogramming has been linked to an acquired sensitivity to ferroptosis, thus opening new opportunities to treat tumors unresponsive to other therapies. The activation of ferritinophagy, a specific form of macroautophagy required for the degradation of ferritin, the main cellular iron-storage protein, seems to occur during the early initiation stage of ferroptosis (7). Recent discoveries have highlighted the importance of transferrin trafficking and ferritinophagy, as critical determinants of ferroptosis sensitivity *via* an increase in the so-called labile iron pool. Guo et al., bring us a review of the latest research about iron metabolism disorders in various types of tumors, the functions and properties of iron in ferroptosis and ferritinophagy, and new

opportunities for iron-based on treatment methods for tumors, providing more information regarding the prevention and treatment of tumors. In their review, Chen et al. focus on the regulatory roles of the human six-transmembrane epithelial antigen of the prostate (STEAP) metaloxidoreductase proteins in the occurrence and development of malignant tumors. In addition, Zhang et al. summarize for us the recent findings on the role of Nuclear Factor (erythroid-derived 2)-like 2 (NRF2) as a potential modulator for orchestrating iron homeostasis and redox balance in cancer cells. Accordingly, Bajbouj et al. identified how vitamin D alters the redox balance in breast cancer cells by disrupting the cellular iron metabolism to induce oxidative stress and cell death. Zhang et al. performed us a bibliometric and knowledge-map analysis to evaluate the knowledge base, find the hotspot trends, and detect the emerging topics regarding ferroptosis research. From the FerrDb website database (the first database of ferroptosis genes and ferroptosis-diseases associations) or MSigDB and public databases, several studies presented here systematically investigated the correlation between ferroptosis-related genes and tumor patient prognosis and establish/validate a novel prognostic model of tumor patient based on ferroptosis-related gene (FRG) signature in order to develop individualized treatments and to improve their overall survival. Tian et al. validated their 7-FRG prognostic signature (including *ALOX12B*, *ALOX15*, *GPX2*, *DDIT4*, *GDF15*, *SLC2A1*, *RRM2*) in lung adenocarcinoma. For overall survival prediction in patients with breast cancer, Zhu et al. and Li et al., developed and validated a novel robust FRG panel, consisting with the 11-gene core (*CISD1*, *TP63*, *BRD4*, *PROM2*, *EMC2*, *G6PD*, *PI3KCA*, *FLT3*, *IFNG*, *ANO6*, *SLC1A4*) and the 9-gene core (*ALDH3A2*, *SIAH2*, *G6PD*, *SLC1A4*, *FLT3*, *SQLE*, *EGLN2*, *SFXN5*, *CHAC1*), respectively. In addition, He et al., identified and validated the prognostic value of a 10 FRG core signature (including *MAP1LC3A*, *SLC7A5*, *OTUB1*, *PRDX6*, *MAP3K5*, *SOCS1*, *ATG5*, *DDIT4*, *ACSL3*, *PRKAA2*) in patients with head and neck squamous cell carcinoma. Lv et al. identified 17 FRG associated with long-term of prostate cancer and finally constructed a signature based on nine FRGs (*AIFM2*, *AKR1C1*, *AKR1C*, *CBS*, *FANCD2*, *FTH1*, *G6PD*, *NFS1*, *SLC1A5*), with a prognostic value in patients with prostate cancer. If iron metabolism plays a crucial role in the occurrence and development of colon adenocarcinoma, Yuan et al., revealed the prognostic value of iron metabolism-related genes *SLC48A1* and *SLC39A8* in colon cancer. These findings provide evidence on the key role of ferroptosis in cancer development. Interestingly, most of these studies found a strong correlation between ferroptosis and immune status and immune checkpoint genes. Indeed, iron metabolism, inflammation, and immunity are tightly interlinked (8). Recent data demonstrate that immune checkpoint inhibition stimulates interferon-γ production by CD8+ T cells to kill cancer cells through the induction of ferroptosis cell death (9). In contrast, a newly developed hypothesis suggests that a ferroptosis-sensitive state may allow cancer cells to generate lipid-derived mediators modulating intra- and intercellular signaling pathways that would lead to the growth of the tumor (8). This theory suggests an inverse correlation between cellular peroxide tone and immune evasion. Thus, it is essential to explore the molecular mechanism offerroptosis that inhibits tumor growth as well as the consequence of cancer cell death by ferroptosis, which potentially dampens antitumor immunity and promotes tumor growth. Yu et al. bring us a prognostic model in pancreatic cancer based on 6-FRGs (*CD44*, *MT1G*, *PTGS2*, *SAT1*, *TFRC*, *STEAP3*) to determine its immune landscape and underlying mechanisms. In line with this, Liu et al. also identified a prognostic signature associated with tumor immune microenvironment based on 6-FRGs (*HMOX1*, *KEAP1*, *HSBP1*, *SAT1*, *CISD1*, *GPX4*) in uterine corpus endometrial carcinoma. If long non-coding RNAs (lncRNAs) have been reported to be involved in tumorigenesis in several cancers, He et al. identified a ferroptosis-related lncRNA signature that could effectively stratify the prognosis of glioma patients with adequate predictive performance to all clinical index. Interestingly, the authors indicated that there was increased immune infiltration in the high-risk group defined by the ferroptosis-related lncRNA signature. Accordingly, Duan et al., explored the prognostic value of a novel comprehensive biomarker, the iron-monocyte-to-lymphocyte ratio or IronMLR score, in patients with early-stage triple-negative breast cancer, illustrating that the iron-inflammation axis might be a potential prognostic biomarker of survival outcomes. Hua et al. and Duan et al. also explored a novel prognostic model based on the serum metal levels, iron and copper, respectively, for patients with early-stage triple-negative breast cancer as a practical tool for individualized survival predictions and treatment guidance.

Overall, we believe that this Research Topic opens up new and exciting fields of investigation into iron metabolism in cancer progression and in cancer treatments, and hope readers will enjoy it.

Author contributions

All authors listed have made a substantial, direct, and intellectual contribution to the work and approved it for publication.

Funding

The authors gratefully acknowledge funding from INSERM, Université Paris Cité, la ligue nationale contre le cancer, and Comité de Paris de la ligue contre le cancer.

Conflict of interest

The authors declare that the research was conducted in the absence of any commercial or financial relationships that could be construed as a potential conflict of interest.

Publisher's note

References

1. Torti SV, Torti FM. Iron: The cancer connection. *Mol Aspects Med* (2020) 75:100860. doi: 10.1016/j.mam.2020.100860

2. Muñoz M, Gómez-Ramírez S, Martín-Montañez E, Auerbach M. Perioperative anemia management in colorectal cancer patients: A pragmatic approach. *World J Gastroenterol* (2014) 20:1972–85. doi: 10.3748/wjg.v20.i8.1972

3. Cosialls E, El Hage R, Dos Santos L, Gong C, Mehrpour M, Hamaï A. Ferroptosis: Cancer stem cells rely on iron until "to die for" it. *Cells* (2021) 10:2981. doi: 10.3390/cells10112981

4. El Hout M, Dos Santos L, Hamaï A, Mehrpour M. A promising new approach to cancer therapy: Targeting iron metabolism in cancer stem cells. *Semin Cancer Biol* (2018) 53:125–38. doi: 10.1016/j.semcancer.2018.07.009

5. Hamaï A, Cañeque T, Müller S, Mai TT, Hienzsch A, Ginestier C, et al. An iron hand over cancer stem cells. *Autophagy* (2017) 13:1465–6. doi: 10.1080/15548627.2017.1327104

6. Mai TT, Hamaï A, Hienzsch A, Cañeque T, Müller S, Wicinski J, et al. Salinomycin kills cancer stem cells by sequestering iron in lysosomes. *Nat Chem* (2017) 9:1025–33. doi: 10.1038/nchem.2778

7. Hou W, Xie Y, Song X, Sun X, Lotze MT, Zeh HJ, et al. Autophagy promotes ferroptosis by degradation of ferritin. *Autophagy* (2016) 12:1425–8. doi: 10.1080/15548627.2016.1187366

8. Friedmann Angeli JP, Krysko DV, Conrad M. Ferroptosis at the crossroads of cancer-acquired drug resistance and immune evasion. *Nat Rev Cancer* (2019) 19:405–14. doi: 10.1038/s41568-019-0149-1

9. Wang W, Green M, Choi JE, Gijón M, Kennedy PD, Johnson JK, et al. CD8+ T cells regulate tumour ferroptosis during cancer immunotherapy. *Nature* (2019) 569:270–4. doi: 10.1038/s41586-019-1170-y

frontiers in Oncology

ORIGINAL RESEARCH
published: 03 June 2021
doi: 10.3389/fonc.2021.686726

Knowledge Domain and Emerging Trends in Ferroptosis Research: A Bibliometric and Knowledge-Map Analysis

Jie Zhang[1,2], *Luxia Song*[1,2], *Liyan Xu*[3], *Yixuan Fan*[1,2], *Tong Wang*[1,2], *Wende Tian*[2,4], *Jianqing Ju*[2*] and *Hao Xu*[2*]

[1] Graduate School, Beijing University of Chinese Medicine, Beijing, China, [2] National Clinical Research Center for Chinese Medicine Cardiology, Xiyuan Hospital, China Academy of Chinese Medical Sciences, Beijing, China, [3] Department of Computer Science, Emory University, Atlanta, GA, United States, [4] Graduate School, China Academy of Chinese Medical Sciences, Beijing, China

OPEN ACCESS

Edited by:
Maryam Mehrpour, INSERM U1151 Institut Necker enfants Malades, France

Reviewed by:
Andy Wai Kan Yeung, The University of Hong Kong, China
Carlos Mulet Forteza, University of the Balearic Islands, Spain

***Correspondence:**
Jianqing Ju
jujianqing@163.com
Hao Xu
xuhaotcm@hotmail.com

Specialty section:
This article was submitted to Molecular and Cellular Oncology, a section of the journal Frontiers in Oncology

Received: *27 March 2021*
Accepted: *05 May 2021*
Published: *03 June 2021*

Citation:
Zhang J, Song L, Xu L, Fan Y, Wang T, Tian W, Ju J and Xu H (2021) Knowledge Domain and Emerging Trends in Ferroptosis Research: A Bibliometric and Knowledge-Map Analysis. Front. Oncol. 11:686726. doi: 10.3389/fonc.2021.686726

Objectives: To identify the cooperation and impact of authors, countries, institutions, and journals, evaluate the knowledge base, find the hotspot trends, and detect the emerging topics regarding ferroptosis research.

Methods: The articles and reviews related to ferroptosis were obtained from the Web of Science Core Collection on November 1, 2020. Two scientometric software (CiteSpace 5.7 and VOSviewer 1.6.15) were used to perform bibliometric and knowledge-map analysis.

Results: A total of 1,267 papers were included, in 466 academic journals by 6,867 authors in 438 institutions from 61 countries/regions. The ferroptosis-related publications were increasing rapidly. *Cell Death & Disease* published the most papers on ferroptosis, while *Cell* was the top co-cited journal, publication journals and co-cited journals were major in the molecular and biology fields. The United States and China were the most productive countries; meanwhile, the University of Pittsburgh, Columbia University and Guangzhou Medical University were the most active institutions. Brent R Stockwell published the most papers, while Scott J Dixon had the most co-citations; simultaneously, active cooperation existed in ferroptosis researchers. Ten references on reviews, mechanisms, and diseases were regarded as the knowledge base. Five main aspects of ferroptosis research included regulation mechanisms, nervous system injury, cancer, relationships with other types of cell death, and lipid peroxidation. The latest hotspots were nanoparticle, cancer therapy, iron metabolism, and in-depth mechanism. Notably Nrf2 might have turning significance. The emerging topics on ferroptosis research were the further molecular mechanism of ferroptosis and the wider application of ferroptosis-related disease with advanced technology.

Conclusion: This study performed a full overview of the ferroptosis research using bibliometric and visual methods. The information would provide helpful references for scholars focusing on ferroptosis.

Keywords: ferroptosis, bibliometric, knowledge-map, CiteSpace, VOSviewer

INTRODUCTION

Ferroptosis is an iron-dependent regulated necrosis caused by unrestricted lipid peroxidation and subsequent membrane damage (1). Scott J Dixon (2) proposed the term ferroptosis in 2012 to describe a type of cell death induced by the small molecule erastin, which could lead to glutathione (GSH) depletion and glutathione peroxidase 4 (GPX4) inactivation (1, 3). In addition to the necrotic morphological changes, ferroptotic cell death usually shows mitochondrial abnormalities, such as increased membrane density, reduced or absent crista, condensation or swelling, and rupture of the outer membrane (2, 4–7). Existing evidence proves that ferroptosis plays an important role in the development of many diseases (7, 8), such as cancer, neurodegenerative diseases, ischemia/reperfusion injury, acute kidney injury, atherosclerosis, chronic obstructive pulmonary disease, and immune system diseases. Therefore, as an evolutionary program offers various druggable nodes, ferroptosis is supposed to be an emerging way to cure many kinds of diseases (9–14). Especially as a therapeutic model in cancer treatment and prevention of ischemic organ damage, ferroptosis has been convincingly established (15).

According to its great potential, ferroptosis has gained scholars' keen interest in better understanding the process of ferroptosis with a rapidly increasing number of publications (16). Many scholars have reviewed ferroptosis research from various aspects. For instance, Daolin Tang etc. (7) summarized the progress of ferroptosis research mainly from molecular mechanisms, including hallmarks, regulation, oxidant system, antioxidant system, membrane repair, degradation systems, transcription factors and cofactors, epigenetic regulation, assays, and the implications in disease. Xuejun Jiang etc. (17) overviewed ferroptosis from the mechanisms, pathways, biological functions in tumor suppression and immune surveillance, and the implications in cancer and ischemic damage. Marcus Conrad etc. (12) outlined ferroptosis mainly from its effects on as-yet- incurable disease, including ischemia-reperfusion injury, organ failure, neurodegenerative disease and therapy-resistant cancer. However, there is no comprehensive and objective report on the publication trends, influential authors or institutions and their cooperation, knowledge base, hotspots evolution, or the emerging topics in ferroptosis research to our knowledge.

Nowadays, there are kinds of approaches to systemically review a research field, of which bibliometrics is one of the most popular methods (18). Bibliometrics can not only qualitatively and quantitatively analyze the contribution and cooperation of authors, institutions, countries, and journals, but also evaluate the development and emerging trends in scientific research (18–23). That which other methods, such as traditional review, meta-analysis, or experiment research, cannot perform. According to the strengths, it is becoming increasingly important in evaluating research trends and formulating guidelines (24). Therefore, bibliometrics is suitable for evaluating and overviewing ferroptosis research.

This study aimed to use two commonly used bibliometric tools, CiteSpace and VOSviewer, to objectively describe the knowledge domain and emerging trends of ferroptosis research from three aspects as follows. (1) We designed to quantify and identify the general information in ferroptosis research, such as the individual impact and the cooperation information, by analyzing annual publications, journals, co-cited journals, countries/regions, institutions, authors and co-cited authors. (2) We planned to find and analyze the most co-cited papers by co-cited reference analysis to evaluate the knowledge base of ferroptosis. (3) Most importantly, finding the knowledge structure and hotspots evolution, and detecting the emerging topics of ferroptosis by keywords analysis and co-cited reference burst analysis. Overall, these three aspects cover the status quo and trends of ferroptosis research.

MATERIALS AND METHODS

Data Collection

The Web of Science Core Collection (WoSCC) database is commonly used in bibliometric analysis (19, 22, 25–27). We also chose it because it can provide comprehensive information bibliometric software needs and is regarded as the most influential database (28).

Data were retrieved from the WoSCC database on November 1, 2020. We searched "ferroptosis" and "ferroptotic" as the term and set the timespan from the inception of Web of Science (WoS) to November 1, 2020. The language was restricted to English, and the article type was limited to Article or Review. Search results were downloaded with the record content of "Full Record and Cited References" and the file format of "Plain Text". Then, we renamed the files for further analysis because CiteSpace can only recognize files named "download *.txt".

Data Analysis and Visualization

At present, the commonly used bibliometric software includes VOSViewer, CiteSpace, SCI2, NetDraw, and HistCite (29). There is no consensus on which bibliographic method is the best (30). Considering their characteristics and advantages,

this research used both VOSviewer and CiteSpace (22, 25, 29, 31).

VOSviewer, developed by Leiden University, is a software that does well in creating, visualizing, and exploring maps based on network data (32, 33). We used VOSviewer 1.6.15 to identify productive journals, co-cited journals, authors, co-cited authors, as well as the related knowledge-maps based on bibliographic data. In addition, we created the keywords co-occurrence and cluster map based on text data. Terms were obtained from titles and abstracts fields using natural language processing algorithms and complemented with a VOSviewer corpus file (33). Firstly, we cleaned the data, such as merged "van raan, a" and "vanraan, a" in author analysis, unified "glutathione" and "gsh" as "gsh," and deleted meaningless terms such as "focus" and "year" in term analysis (34). Secondly, we used fractional counting as the counting method and set the maximum number of authors per document as 25 (35). The difference between full counting and fractional counting is the strength of the links (33). The fractional counting method calculated the link strength by splitting papers according to the weight (18, 30, 33). For example, if three authors co-author a paper, each of their link strength will be counted as 1/3 in fractional counting, while it will be counted as one in full counting. It can be identified that fractional counting performs more reasonable in author analysis (36), and after comparing two methods in other sections, the data in our study showed more reasonably and clearly by the fractional counting method. Besides, in term analysis, each term was calculated a relevance score, which represented that terms with a high relevance score tend to represent specific topics, while terms with a low relevance score tend not to be representative of any specific topic (33). Therefore, we selected the terms that not only appeared more than ten times but also at the top 60% relevance score to analyze. Other thresholds (T) of items were set based on different situations (19), which were marked in corresponding tables and figures.

CiteSpace, developed by Prof. Chaomei Chen, is a bibliometric and visual analysis tool good at exploring cooperation, key points, internal structure, potential trends and dynamics in a certain field (37). Therefore, we used CiteSpace 5.7 to analyze and visualize the co-occurrence of countries/regions and institutions, dual-map of journals, trends of high-frequency keywords, co-cited references, and citation bursts for references. We cleaned the data before analyzing; for instance, in countries/regions analysis, publications from Taiwan were reclassified to China (35), and those from England, Scotland, Northern Ireland, and Wales were assigned to the United Kingdom (36). Similarly, we merged the synonyms such as "GPX4" and "glutathione peroxidase 4" in keyword evolution analysis. The CiteSpace settings were as follows: time span (2012–2020), years per slice (1), pruning (Minimum Spanning Tree and Pruning Sliced Networks), selection criteria (Top N=50), and others followed the default.

We used Microsoft Office Excel 2019 to manage the database and analyze the annual publications.

Besides, we obtained the 2019 impact factor (IF) and JCR division of journals from the Web of Science InCites Journal Citation Reports on November 15, 2020.

RESULTS

Annual Growth Trend

According to the data collection strategy, we collected 1,268 papers but these contained one duplicate. Finally, a total of 1,267 eligible papers were included (Annexes 1), published between 2012 and 2020. As we can see from **Figure 1**, ferroptosis-related references showed an annual upward tendency. Significantly, the yearly output is almost twice as much as the previous year in the last three years (2018 to present).

Journals and Co-Cited Journals

We used VOSviewer to conduct co-citation and co-cited journal analysis, finding the most active and most influential journals in the ferroptosis field. The results showed that the 1,267 references were published in 466 academic journals. *Cell Death & Disease* published the most papers (41, 3.21%), followed by *Biochemical and Biophysical Research Communications*, *Free Radical Biology and Medicine*, *Redox Biology*, and *Cell Death and Differentiation* (**Table 1**). Among the top10 journals, seven were at the Q1 JCR division, and six had an Impact Factor (IF) of more than five (**Table 1**).

Among 4,781 co-cited journals, eleven journals had citations over 1,000. As we can see from **Table 2**, *Cell* had the most co-citations (3,926, 4.21%), followed by *Nature*, *Journal of Biological Chemistry*, and *Proceedings of the National Academy of Sciences of the United States of America (PNAS)*. Among the top 10 co-cited journals, eight were at the Q1 JCR division with an Impact Factor (IF) of more than six, seven were from the United States.

The dual-map overlay of journals stands for the topic distribution of academic journals (38) (**Figure 2**). The citing journals were located on the left while the cited journals were on the right, and the colored paths indicated the citation relationships. Only one primary citation path colored orange was identified, which means the studies published in Molecular/Biology/Genetics journals were mainly cited by the studies published in Molecular/Biology/Immunology journals.

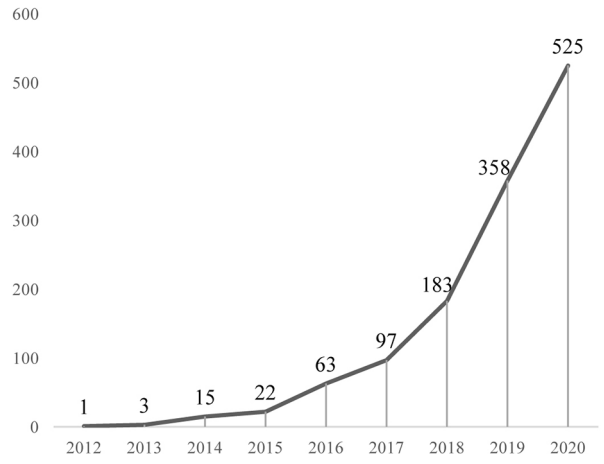

FIGURE 1 | Annual output of ferroptosis research.

TABLE 1 | The top 10 journals of ferroptosis research.

Rank	Journal	N (%)	IF(2019)[#]	JCR division	Country
1	Cell Death & Disease	41 (3.21%)	6.304	Q1	UK
2	Biochemical and Biophysical Research Communications	36 (2.82%)	2.985	Q2/Q3	USA
3	Free Radical Biology and Medicine	31 (2.43%)	6.170	Q1	USA
4	Redox Biology	27 (2.12%)	9.986	Q1	Netherlands
5	Cell Death and Differentiation	21 (1.65%)	10.717	Q1	UK
6	Oxidative Medicine and Cellular Longevity	20 (1.57%)	5.076	Q2	USA
7	International Journal of Molecular Sciences	20 (1.57%)	4.556	Q1/Q2	Switzerland
8	Scientific Reports	16 (1.25%)	3.998	Q1	UK
9	Frontiers in Neuroscience	15 (1.18%)	3.707	Q2	Switzerland
10	Cell Chemical Biology	15 (1.18%)	7.739	Q1	USA

[#]*IF: Impact Factor.*

TABLE 2 | The top 10 co-cited journals of ferroptosis research.

Rank	Co-cited Journal	N (%)	IF(2019)[#]	JCR division	Country
1	Cell	3,926 (4.21%)	38.637	Q1	USA
2	Nature	2,912 (3.12%)	42.779	Q1	Germany
3	Journal of Biological Chemistry	2,661 (2.85%)	4.238	Q2	USA
4	Proceedings of The National Academy of Sciences of the United States of America	2,475 (2.65%)	9.412	Q1	USA
5	Cell Death and Differentiation	1,766 (1.89%)	10.717	Q1	UK
6	Free Radical Biology and Medicine	1,758 (1.88%)	6.170	Q1	USA
7	Nature Chemical Biology	1,270 (1.36%)	12.587	Q1	Germany
8	Plos One	1,152 (1.23%)	2.74	Q2	USA
9	Cancer Research	1,066 (1.14%)	9.727	Q1	USA
10	Science	1,061 (1.14%)	41.846	Q1	USA

[#]*IF, impact factor.*

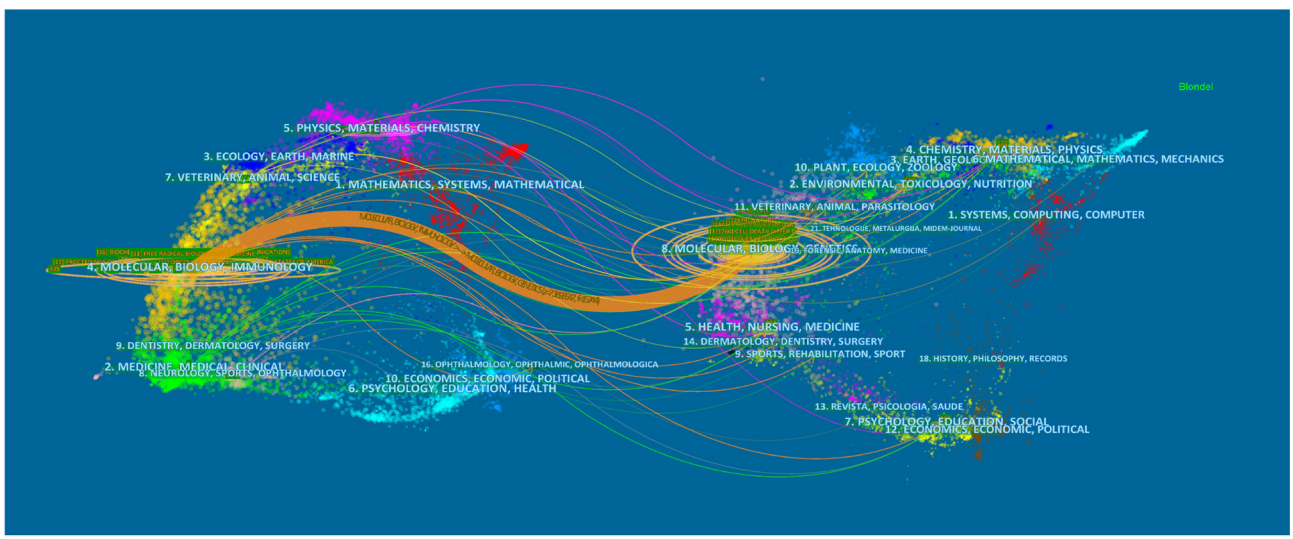

FIGURE 2 | The dual-map overlay of journals related to ferroptosis research. Notes: The citing journals were at left, the cited journals were on the right, and the colored path represents citation relationship.

Countries/Regions and Institutions

A total of 1,267 publications were co-authored by 438 institutions from 61 countries/regions. The largest number of publications were originated from China (562, 31.03%), followed by the United States (410, 22.64%), Germany (157, 8.67%), and Japan (103, 5.69%) (**Table 3**). Some nodes, such as the United States, France, Germany, Australia, the United Kingdom and Canada, were colored purple round in **Figure 3A** in terms of their high betweenness centrality (≥0.10), which is usually regarded as the important turning points that may lead to transformative discoveries and acts as a bridge (37, 39–41). Furthermore, according to the color of links, the USA (2012), Germany

TABLE 3 | The top 10 countries/regions and institutions involved in ferroptosis research.

Rank	Country/region	N (%)	Centrality	Institution	Country/region	N (%)	Centrality
1	China	562 (31.03%)	0.09	University of Pittsburgh	USA	59 (3.34%)	0.20
2	USA	410 (22.64%)	0.18	Columbia University	USA	57 (3.23%)	0.14
3	Germany	157 (8.67%)	0.31	Guangzhou Medical University	China	41 (2.32%)	0.08
4	Japan	103 (5.69%)	0.10	Chinese Academy of Sciences	China	33 (1.87%)	0.08
5	France	55 (3.04%)	0.39	Zhejiang University	China	32 (1.81%)	0.07
6	Australia	49 (2.71%)	0.21	Harvard University	USA	29 (1.64%)	0.11
7	UK	48 (2.65%)	0.19	Stanford University	USA	28 (1.59%)	0.10
8	Canada	42 (2.32%)	0.15	Central South University	China	27 (1.53%)	0.03
9	Italy	39 (2.15%)	0.01	Jilin University	China	25 (1.42%)	0.07
10	Russia	33 (1.82%)	0.02	Helmholtz Zentrum München	Germany	25 (1.42%)	0.06
10				Shanghai Jiao Tong University	China	25 (1.42%)	0.03
10				The University of Melbourne	Australia	25 (1.42%)	0.10

(2013), France (2013), and Russia (2013) were the earliest countries to take up the ferroptosis research. We used minimum spanning tree pruning to make the network clear (**Figure 3A**). Actually, no-pruning countries/regions co-occurrence map contained 61 nodes and 302 links with a density equal to 0.165, indicating active collaborations among different countries/regions. For instance, the USA had cooperation with 34 countries/regions, followed by Germany (n = 30), China (n = 26), France (n = 24), and UK (n = 24).

The top 12 institutions were from China (6/12), USA (4/12), Germany (1/12) and Australia (1/12) (**Table 3**). University of Pittsburgh (59, 3.34%) published the most papers, followed by Columbia University (57, 3.23%), Guangzhou Medical University (41, 2.32%), Chinese Academy of Sciences (33, 1.87%), and Zhejiang University (32, 1.81%) (**Table 3**).

Authors and Co-Cited Authors

A total of 6,867 authors were involved in ferroptosis research. Eighteen authors published more than ten articles. Brent R Stockwell published the most papers (n = 39), followed by Daolin Tang (n = 36), Rui Kang (n = 35), Marcus Conrad (n = 31) and Andreas Linkermann (n = 26) (**Table 4**). The authors (n = 135) who published at least five papers (T≥5) were included to build the network map of authors (**Figure 4**). The same color represented the same cluster. There were active collaborations in ferroptosis research, especially among authors in the same cluster, such as Brent R Stockwell and Scott J Dixon, Daolin Tang and Rui Kang, etc. Close cooperation was also observed among clusters, such as Brent R Stockwell and Andreas Linkermann, Brent R Stockwell and Marcus Conrad, Brent R Stockwell, and Xuejun Jiang, etc.

Co-cited authors are authors who have been co-cited together in a range of publications (42). Among 36,666 co-cited authors, 16 were co-cited over 200. Scott J Dixon (n = 1566) ranked first, followed by Wan Seok Yang (n = 1304), Jose Pedro Friedmann Angeli (n = 557), Minghui Gao (n = 519), Andreas Linkermann (n = 462), and Brent R Stockwell (n = 462). The remaining four top authors were co-cited from 327 to 413 (**Table 4**). The authors (n = 43) with co-citations of at least 100 (T ≥ 100) were used to make the density map (**Figure 5**); this type of knowledge-map could present the high-frequency co-

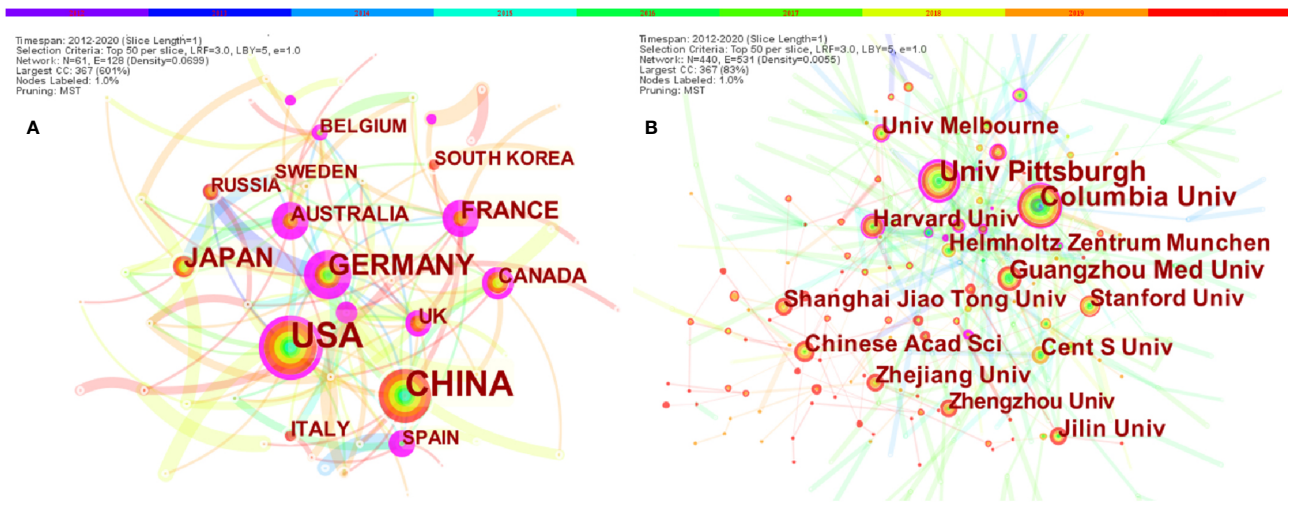

FIGURE 3 | The co-occurrence map of **(A)** countries/regions and **(B)** institutions in ferroptosis research (T≥20). Notes: The size of node reflects the co-occurrence frequencies, and the links indicate the co-occurrence relationships. The color of node and line represents different years, colors vary from purple to red as time goes from 2012 to 2020; and node with purple round means high betweenness centrality (>0.1).

TABLE 4 | The top 10 authors and co-cited authors of ferroptosis research.

Rank	Author	Count	Co-cited author	Co-citation
1	Brent R Stockwell	39	Scott J Dixon	1,566
2	Daolin Tang	36	Wan Seok Yang	1,304
3	Rui Kang	35	Jose Pedro Friedmann Angeli	557
4	Marcus Conrad	31	Minghui Gao	519
5	Andreas Linkermann	26	Andreas Linkermann	462
6	Scott J Dixon	22	Brent R Stockwell	462
7	Jose Pedro Friedmann Angeli	14	Sebastian Doll	413
8	Valerian E Kagan	13	Lorenzo Galluzzi	383
9	Guido Kroemer	13	Yangchun Xie	344
10	Jiao Liu	13	Li Jiang	327
10	Shinya Toyokuni	13		

cited authors clearly. According to **Figure 5**, Scott J Dixon and Wan Seok Yang had the hottest color for the most co-cited.

Keyword Co-Occurrence, Clusters, and Evolution

VOSviewer was used to present the term co-occurrence (**Table 5**, **Figure 6**, **7**) and cluster analysis (**Figure 7**). A total of 25,413 terms were extracted, of which 595 appeared more than ten times and 51 appeared more than 100 times. The density map (**Figure 6**) of terms can find the high-frequency co-occurrence terms, which reveal the hotspots in a specific research field. As we can see from **Figure 6** and **Table 5**, peroxidation was the most important term with 350 (2.97%) co-occurrences, followed by disease, tumor cell, tumor, review and necroptosis.

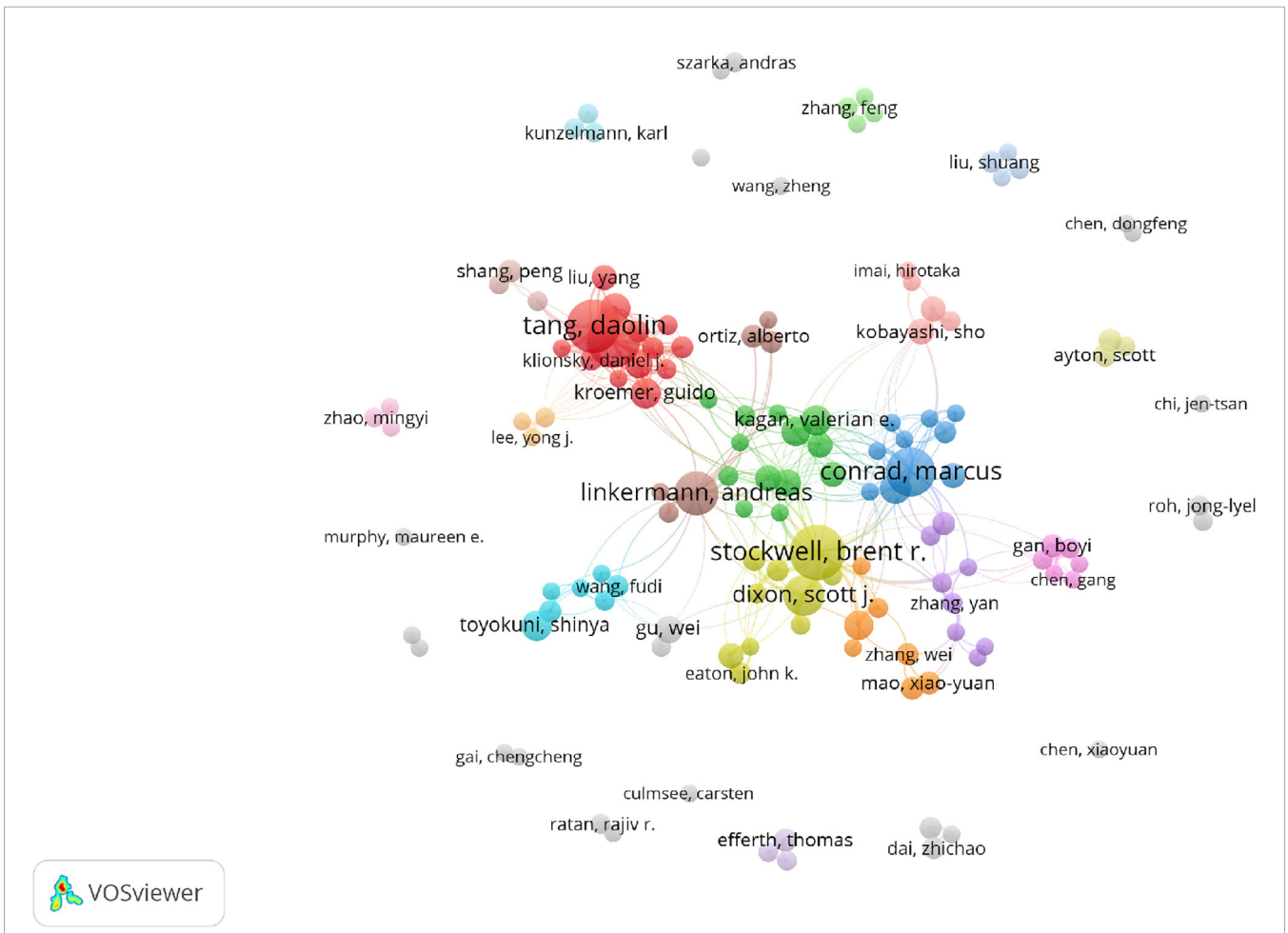

FIGURE 4 | The co-occurrence map of authors in ferroptosis research (T≥5). Notes: The size of node reflects the author's co-occurrence frequencies, the link indicate the co-occurrence relationship between authors, and the same color of node represent the same cluster.

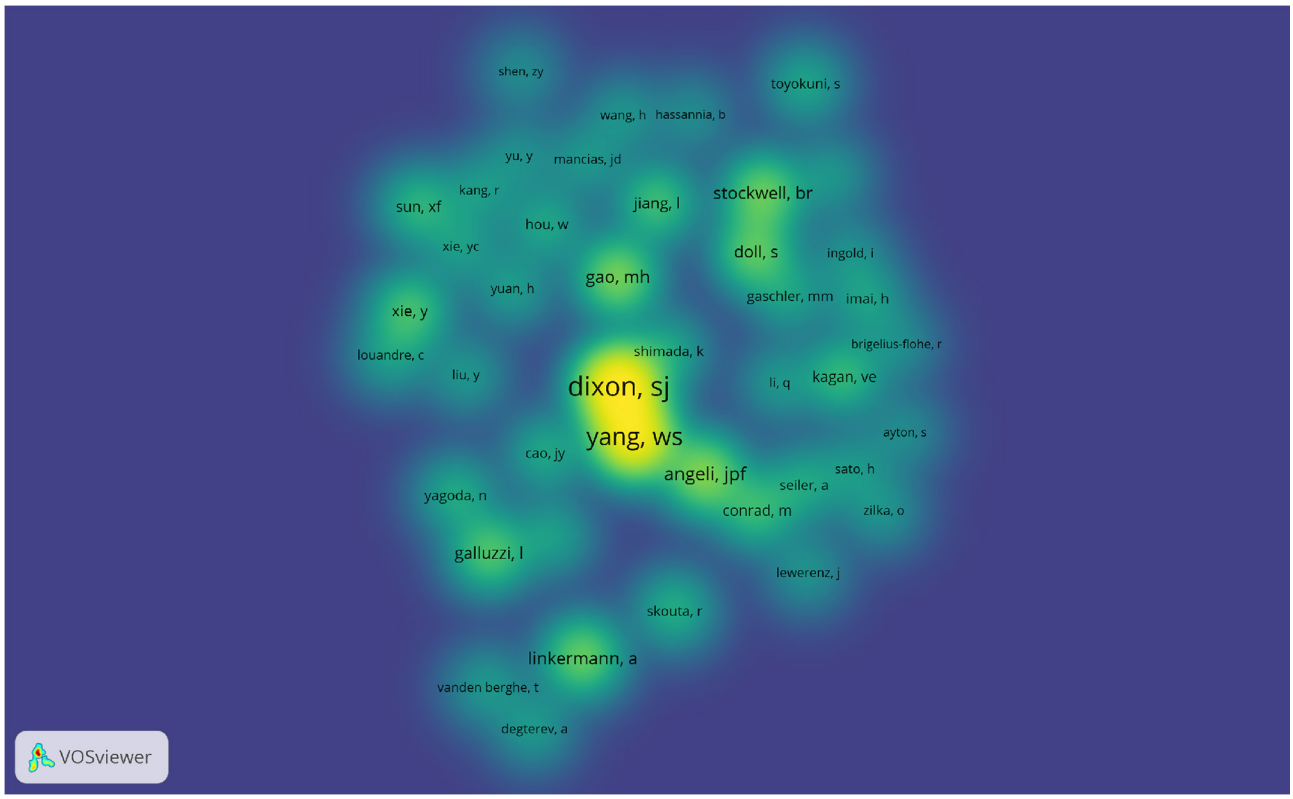

FIGURE 5 | The density map of co-cited authors in ferroptosis research (≥100). Notes: The size of word, the size of round, and the opacity of yellow is positively related to the co-cited frequency.

Cluster analysis can show the knowledge structure of the research field (29). According to the link strength of term co-occurrence, the network was divided into five clusters (**Figure 7**). It is highly homogeneous between the terms in one cluster. Cluster 1 (red) is the largest cluster with 110 co-occurrence terms: erastin, cell line, ferrostatin-1, cell viability, knockdown, cytotoxicity, cell viability, SLC7A11, malonaldehyde (MDA), sorafenib, caspase, ferrous iron, system xc-, RSL3, miRNA, siRNA, etc. The topic of Cluster1 is the mechanism of ferroptosis. Cluster 2 (green) is mainly related to nervous system injury, which includes 73 terms: disease, neurodegeneration, dysfunction, pathogenesis, neuron, iron homeostasis, Parkinson's disease, Alzheimer, stroke, neuronal death, etc. Cluster 3 (blue) focuses on cancer, which contains 69 terms: tumor cell, tumor, anti-cancer therapy, peroxide, potential, application, chemotherapy, nanomaterial, new strategy, tumor microenvironment, photothermal therapy, photodynamic therapy, etc. Cluster 4 (yellow) is mainly related to cell death with 63 terms: review, necroptosis, necrosis, injury, inflammation, cell death pathway, pyroptosis, regulated necrosis,

TABLE 5 | The top 20 terms of ferroptosis research (relevance score>0.081).

Rank	Term	Count	Rank	Term	Count
1	peroxidation	350 (2.97%)	12	neurodegeneration	106 (0.90%)
2	disease	321 (2.73%)	13	cancer therapy	99 (0.84%)
3	tumor cell	258 (2.19%)	13	inflammation	99 (0.84%)
4	tumor	186 (1.58%)	15	dysfunction	96 (0.82%)
5	review	185 (1.57%)	16	peroxide	92 (0.78%)
6	necroptosis	168 (1.43%)	17	potential	88 (0.75%)
7	erastin	148 (1.26%)	18	cell death pathway	86 (0.73%)
8	injury	141 (1.20%)	19	release	85 (0.72%)
9	necrosis	121 (1.03%)	20	ferroptosis inhibitor	84 (0.71%)
10	cell line	113 (0.96%)	20	pyroptosis	84 (0.71%)
11	ferrostatin-1	111 (0.94%)	20	sensitivity	84 (0.71%)

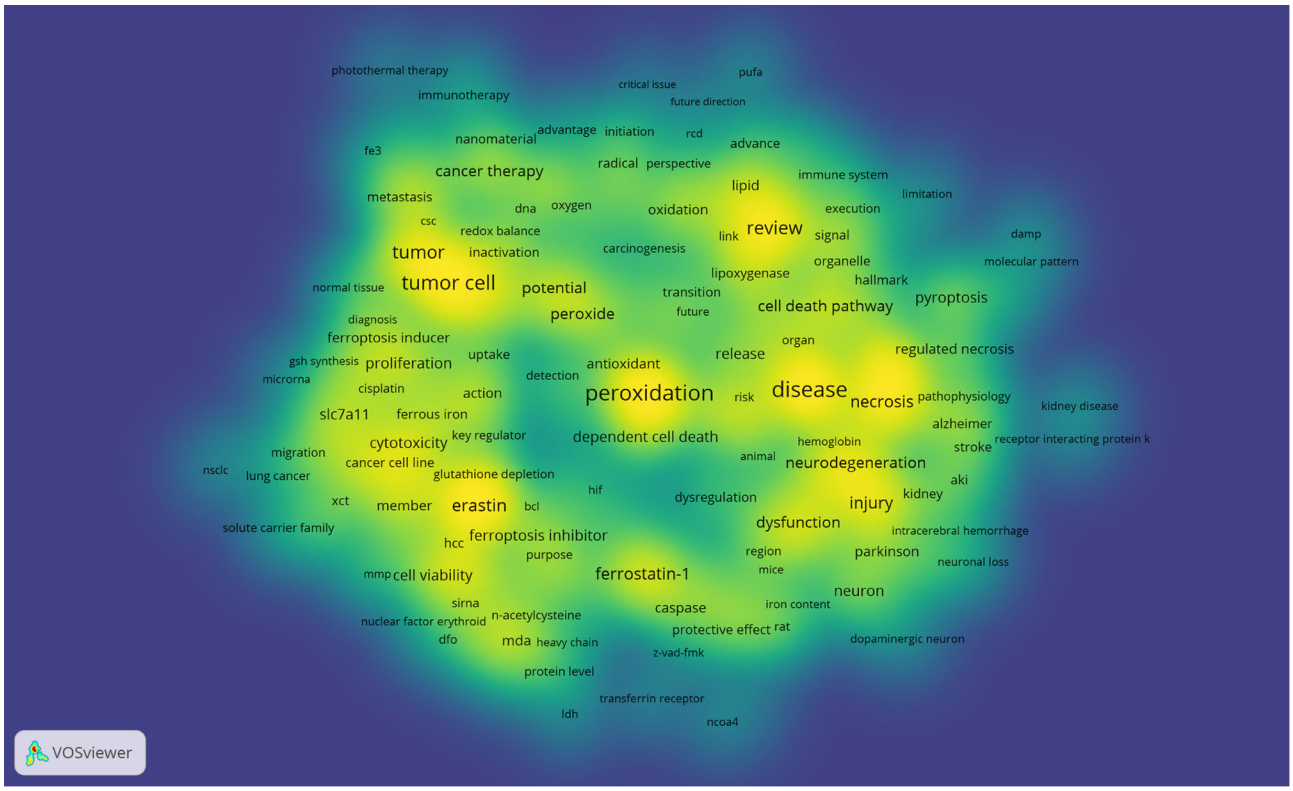

FIGURE 6 | The density map of terms in ferroptosis research (T≥10, relevance score ≥0.081) Notes: The size of word, the size of round, and the opacity of yellow is positively related to the co-occurrence frequency.

cell death mechanism, ischemia-reperfusion, acute kidney injury (AKI), etc. Cluster 5 (purple) is related to lipid peroxidation, which includes 42 terms: peroxidation, oxidation, lipid, antioxidant, phospholipid, lipoxygenase, lipid hydroperoxide, acyl-CoA synthetase long chain family member 4 (ACSL4), polyunsaturated fatty acid (PUFAs), etc.

Keywords time zone view was designed by CiteSpace, which could show the evolution of high-frequency keywords clearly. Keywords were located in the year they first co-occurred, and the color of links represents the first year two keywords appear simultaneously. High-frequency keywords (T≥50) were shown in **Figure 8**, while the threshold was a cumulative figure, leading some latest keywords had not accumulated 50 enough. Consequently, we added the annual top three high-frequency keywords from 2016 to 2019 to supplement the timezone map (**Figure 8**). Among them, nuclear factor erythroid-2 related factor 2 (Nrf2) may have turning point significance with a high centrality (0.12) more than 0.10 (41).

Co-Cited Reference and Reference Burst

We used CiteSpace to detect the co-cited references. **Table 6** showed that the top 10 co-cited references were co-cited at least 196 times, especially three of them were co-cited over 300 times. The most co-cited reference was a review published in *Cell* by Brent R Stockwell, etc. in 2017 (1), entitled "Ferroptosis: A Regulated Cell Death Nexus Linking Metabolism, Redox Biology, and Disease", followed by an article entitled "Regulation of ferroptotic cancer cell death by GPX4" (3).

References with citation bursts are defined as those that are cited frequently over a while (41). In CiteSpace, we set the burst duration to at least two years, from which we detected 55 references with the strongest citation bursts (**Figure 9**). **Figure 9** showed that 34.55% (19/55) of the references appeared citation burstness in 2014, followed by 2016 (15/55,27.27%) and 2015 (7/55,12.73%). Notably, nine references (16.36%) were in burstness until 2020. The paper with the strongest burstness (strength=79.99) was entitled "Ferroptosis: an iron-dependent form of non-apoptotic cell death" (2), published in *Cell* by Scott J Dixon, etc. in 2012, with citation burstness from 2013 to 2017.

DISCUSSION

General Information

Based on the data from WoSCC database up to November 1, 2020, a total of 1,267 ferroptosis researches were published in 466 academic journals by 6,867 authors in 438 institutions from 61 countries/regions.

Change of the annual output is an essential indicator for the development trend in the field (29, 35). The ferroptosis research

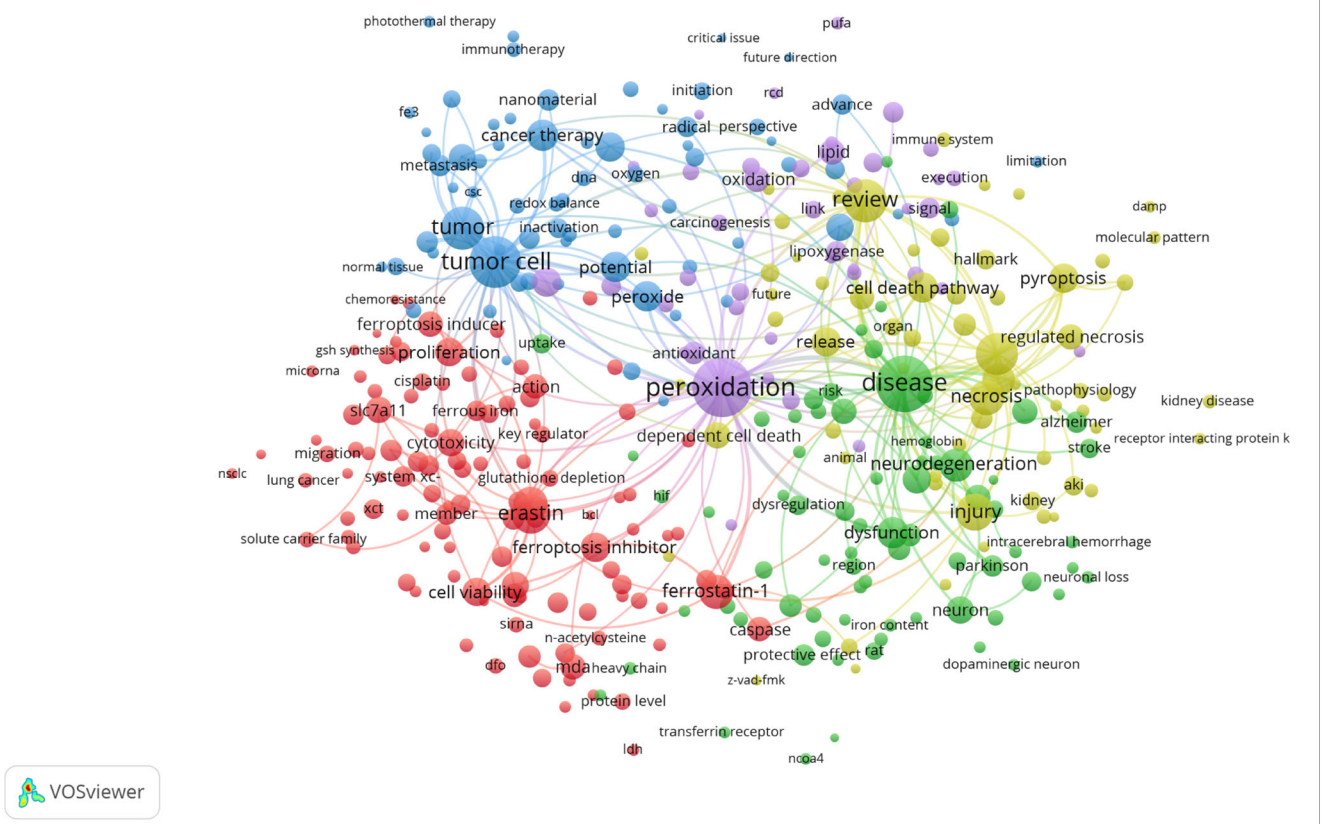

FIGURE 7 | Terms co-occurrence network and clusters in ferroptosis research (T≥10, relevance score ≥0.081, contains 357 items, 5 clusters and 25,151links; max lines = 200.). Notes: The size of node and word reflects the co-occurrence frequencies, the link indicate the co-occurrence relationship, and the same color of node represent the same cluster.

officially started in 2012, the year Scott J Dixon presented "ferroptosis" (2), and showed an upward tendency overall (**Figure 1**). It could be divided into three stages, namely, "Germination," "Stable growth," and "Rapid development." "Germination"(2012–2013): The concept of ferroptosis was officially proposed (2), and there were four articles in these 2 years. "Stable growth" (2014–2017): In this stage, ferroptosis gained more scientists' interest and the annual output grew steadily. "Rapid development" (2018 to present): During this period, the number of annual publications was approximately twice that of the previous year, indicating that ferroptosis research has attracted mounting researchers' attention and developed rapidly. Furthermore, the increasing trend looks promising.

Journals and co-cited journals analysis (**Table 1**) showed that *Cell Death & Disease* published the most ferroptosis research, while *Cell* received the largest number of co-cited references. Both of these are journals on cell biology, which is consistent with the dual-map analysis (**Figure 2**). The dual-map overlay of journals stands for the topic distribution of academic journals (38); **Figure 2** showed only one main citation path from Molecular/Biology/Genetics co-cited journals to Molecular/Biology/Immunology journals, implying that ferroptosis-related studies are focused on basic research nowadays, while researches on translational medicine is still limited (7). Meanwhile, journals at the Q1 JCR division with high IF accounted for the majority of top 10 journals (70%) and co-cited journals (80%), suggesting that these journals have interests and play essential roles in ferroptosis-related researches.

Are there differences among countries/institutions in ferroptosis studies? **Table 3** and **Figure 3** showed that China, the USA, and Germany were the top 3 productive countries. However, the USA, France, Germany, Australia, the United Kingdom, and Canada were regarded as important turning points that may lead to transformative discoveries (37, 39–41). Furthermore, the United States was the earliest country to take up the ferroptosis study, followed by Germany, France, and Russia; these four countries were also the top 10 productive countries. Indicating that the United States is always a productive and influential country in ferroptosis research; noticeably, China started later but has emerged as one of the most productive contributors in recent years. That is consistent with the finding in neuroscience research, and may be related to the economic development and financial input into academic research of these countries (50). Besides, there were active collaborations among different countries/regions, especially the United States, indicating ferroptosis-related research had gained interest

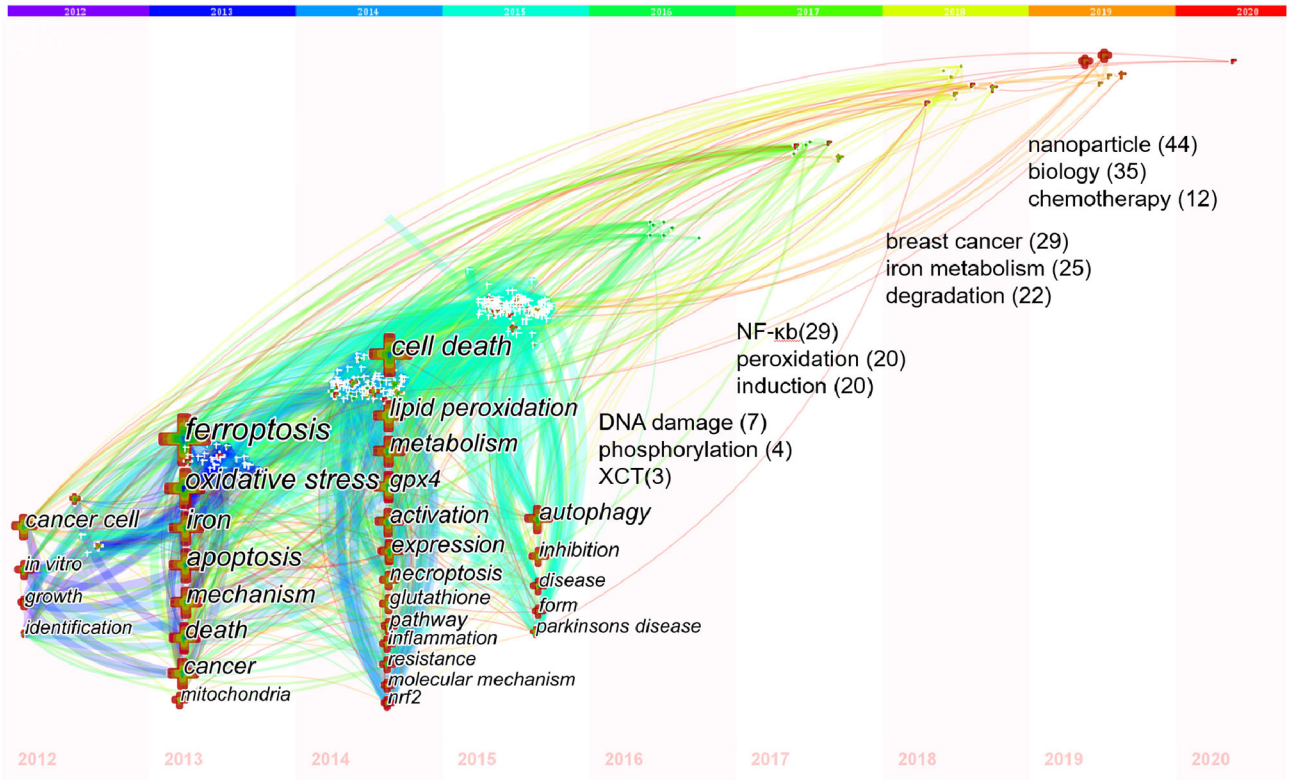

FIGURE 8 | Keywords timezone view of ferroptosis research. Notes: In 2012-2015, keywords with co-occurrence ≥50 were showed; In 2016-2019, the annual top3 keywords were showed with its co-occurrence frequency. The size of cross and word reflects the co-occurrence frequencies, the link indicate the co-occurrence relationship. The color of node and line represents different years, colors vary from purple to red as time goes from 2012 to 2020.

worldwide, and the United States was the main collaborating center. The top 12 institutions were from four countries; three-fifths were from China, while the top 2 were from the USA. The University of Pittsburgh, Columbia University, and Guangzhou Medical University published the most. Moreover, we found active cooperation among the University of Pittsburgh, Columbia University, Harvard University, and other institutions, implying their notable contributions to the ferroptosis field.

Highlighting the contributions of influential researchers, such as the authors with many co-occurrences or co-cited papers in a specific field, can help scholars move along the road and provide further directions and guidelines (51). In our analysis (**Table 4**, **Figures 4** and **5**), Brent R Stockwell published the most papers, while Scott J Dixon had the most co-citations. Meanwhile, we found four scholars who were not only the top 10 productive authors but also the top 10 co-cited authors, namely Brent R Stockwell, Andreas Linkermann, Scott J Dixon, and Jose Pedro Friedmann Angeli. Implying that these four authors had an outstanding contribution to ferroptosis field. Furthermore, the map of authors and co-cited authors provides information about potential collaborators and influential research groups (52).

TABLE 6 | Top 10 co-cited references for ferroptosis research.

Rank	ID	Title	Journal	Co-citation
1	Stockwell BR (1)	Ferroptosis: A Regulated Cell Death Nexus Linking Metabolism, Redox Biology, and Disease	Cell	433
2	Yang WS (3)	Regulation of ferroptotic cancer cell death by GPX4	Cell	374
3	Xie Y (43)	Ferroptosis: process and function	Cell Death Differ	335
4	Jiang L (44)	Ferroptosis as a p53-mediated activity during tumor suppression	Nature	279
5	Doll S (45)	ACSL4 dictates ferroptosis sensitivity by shaping cellular lipid composition	Nat Chem Biol	276
6	Yang WS (46)	Ferroptosis: Death by Lipid Peroxidation	Trends Cell Biol	273
7	Angeli JPF (4)	Inactivation of the ferroptosis regulator Gpx4 triggers acute renal failure in mice	Nat Cell Biol	271
8	Gao MH (47)	Glutaminolysis and Transferrin Regulate Ferroptosis	Mol Cell	240
9	Kagan VE (48)	Oxidized arachidonic and adrenic PEs navigate cells to ferroptosis	Nat Chem Biol	234
10	Yang WS (49)	Peroxidation of polyunsaturated fatty acids by lipoxygenases drives ferroptosis	Proc Natl Acad Sci U S A	196

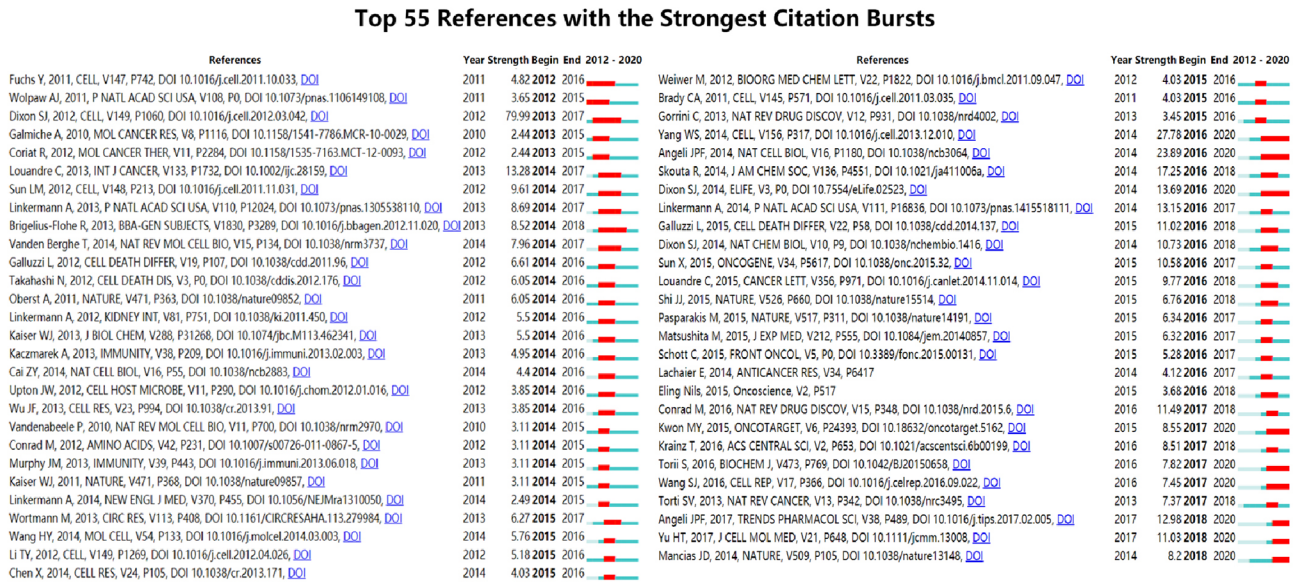

FIGURE 9 | Top 55 references with the strongest citation bursts (sorted by the beginning year of burst). Notes: The Blue bars mean the reference had been published; the red bars mean citation burstness.

In the ferroptosis field, researchers have active cooperation within and between institutions, especially among the influential authors. For example, 27 researchers from 24 institutions presented the most co-cited review entitled "Ferroptosis: A Regulated Cell Death Nexus Linking Metabolism, Redox Biology, and Disease" (1). It is suggesting that these influential teams could be potential collaborators for researchers.

Knowledge Base

Co-cited references are references that have been cited together by other publications. However, the knowledge base is the collection of co-cited references cited by the corresponding research community (41, 53–55), which is not entirely equivalent to highly cited references. In this bibliometric analysis, the top 10 references co-cited by the included ferroptosis literature (**Table 6**) were as follows.

In 2017, *Cell* published the most co-cited study (n=430) co-authored by Brent R Stockwell and 26 other scholars (1) outstanding in ferroptosis research. This review summarized the mechanisms of ferroptosis, highlighted connections with other biological and medical areas, and recommended guidelines for studying ferroptosis. Wan Seok Yang et al. (3) published the second co-cited study in *Cell* in 2014. This study found GPX4 is an essential regulator of ferroptotic cancer cell death; before that, GPX4 had been proved to protect against lipid peroxidation (56) and oxidative stress damage (57). The third co-cited publication was published in 2016 by Y Xie et al. (43) This review summarized the mechanisms, signaling pathways, and measuring methods of ferroptosis and discussed the role of ferroptosis in disease. The fourth co-cited paper was published by Le Jiang et al. (44) in *Nature* in 2015. This study showed that p53 inhibits cystine uptake and sensitizes cells to ferroptosis by repressing the expression of SLC7A11, a vital component of the cystine/glutamate antiporter. In 2017, Sebastian Doll et al. (45) established the essential role of ACSL4 in ferroptosis and published the fifth co-cited study. They used two approaches, genome-wide CRISPR-based genetic screen and microarray analysis of ferroptosis-resistant cell lines, to reveal that ACSL4 dictates ferroptosis sensitivity by shaping cellular lipid composition. The sixth co-cited paper was published by Wan Seok Yang et al. (46) in 2016. This review summarized the discovery of ferroptosis, the molecular mechanisms controlling ferroptosis, and its increasingly appreciated relevance to health and disease. *Nature Cell Biology* published the seventh co-cited experiment research by Jose Pedro Friedmann Angeli et al. in 2014 (4). This study used inducible Gpx4(−/−) mice to elucidate an essential role for the GSH/Gpx4 axis in preventing lipid-oxidation-induced acute renal failure. Furthermore, they found Liproxstatin-1, a spiroquinoxalinamine derivative, is a potent ferroptosis inhibitor in cells, Gpx4(−/−) mice, and a pre-clinical model of ischemia/reperfusion-induced hepatic damage. The eighth co-cited paper was published by Minghui Gao et al. (47) in *Molecular Cell* in 2015. This study detected that the iron-carrier protein transferrin and amino acid glutamine are the inducers of ferroptosis; and glutaminolysis, the cell surface transferrin receptor and the glutamine-fueled intracellular metabolic pathway, plays crucial roles in the ferroptosis process. Furthermore, this study proved that inhibiting glutaminolysis can reduce ischemia/reperfusion-induced heart damage. In 2017, *Nature Chemical Biology* published the ninth co-cited study authored by Valerian E Kagan et al. (48). This study used quantitative redox lipidomics, reverse genetics, bioinformatics, and systems biology to detect the peroxidation

mechanism of ferroptosis, and discovered that oxidized arachidonic and adrenic PEs navigate cells to ferroptosis, which may be useful to anti-cancer therapy. In 2016, the tenth co-cited paper was published by Wan Seok Yang et al. (49) in *PNAS*. They demonstrated that PUFAs are susceptible to lipid peroxidation by lipoxygenases and hence execute ferroptosis.

Generally, the top 10 co-cited references focused on reviews (three reviews were published in 2017 and 2016), mechanisms (include targets and genes, such as GPX4, glutamine, GSH, iron-carrier protein transferrin, p53, SLC7A11, ACSL4, system xc–, PUFAs, lipoxygenase, etc.), and related diseases of ferroptosis (such as cancers, acute renal failure, ischemia/reperfusion-induced hepatic and heart damage etc.), all these were the foundations of ferroptosis research.

Hotspot Evolution, Knowledge Structure, and Emerging Topics

In bibliometrics, keywords/terms co-occurrence (**Table 5** and **Figure 6**) can reflect the hotspots of an academic field (58), and the timezone view (**Figure 8**) can show the evolution of new hotspots (59). The high-frequency terms of ferroptosis (**Table 5** and **Figure 6**) included peroxidation, inflammation, disease, tumor, cancer therapy, neurodegeneration, review, necroptosis, pyroptosis, etc., which were regarded as the hotspots in ferroptosis research. As time goes on, emerging topics occurred continuously (**Figure 8**). In the germination stage (2012–2013), rising terms included cancer cell, oxidative, mechanism, mitochondria, etc. While in the stable-growth stage (2014–2017), new terms contained more mechanism detection and pay more attention to different diseases, including lipid peroxidation, GPX4, glutathione, pathway, inflammation, resistance, molecule mechanism, Nrf2, disease, Parkinson's disease, DNA damage, nuclear factor kappa-B (NF-κb), peroxidation, induction, etc. Notably, Nrf2 may have turning significance with a high centrality (41, 60). In the rapid development stage (2018-now), emerging topics, such as breast cancer, iron metabolism, degradation, nanoparticle, biology, did not only continue the characteristics of the stable-growth stage but also used more technology, such as the emerging application of nanoparticles in cancer treatment (61–67). Unfortunately, although many essential regulatory molecules were demonstrated and transferrin receptor 1 protein (TfR1) was considered as a specific marker of ferroptosis by some scholars (68), there are still no acknowledged specific biomarkers of ferroptosis, such as caspase activation for apoptosis or autophagy lysosome formation for autophagy (9, 69).

Moreover, the cluster of keywords/terms could describe the internal knowledge structure and reveal the research frontier of the discipline (29). Cluster analysis showed five main clusters in the ferroptosis field (**Figure 7**), including regulation mechanisms, nervous system injury (including neurodegenerative disease), cancer, the relationship with other types of cell death, and lipid peroxidation, representing five main aspects of ferroptosis research to some extent. As we know, there is cross-talk between ferroptosis and other types of cell death in some similar signals and molecular regulators [e.g., apoptosis (70) and autophagy (71)], while the mechanisms that direct cells to choose among different cell death ways are still an enigma (7). Besides, lipid peroxidation is proved to be a vital mechanism in ferroptosis, but it is still unknown why and how lipid peroxidation leads to the death of cells in ferroptosis, and this is regarded as one of three key areas of future ferroptosis research (72). As for disease, ferroptosis in cancers has been a hotspot from initial stage to now, and there is also a large amount of research on nervous system injury.

References with strong citation bursts (**Figure 9**) could also characterize the emerging topics of a field (35, 41, 73). The strongest citation burstness came from a landmark study published by Dixon SJ et al. (2) in 2012 (79.30, 2013–2017), which coined the term ferroptosis. Early research only recognized that cysteine is necessary to maintain the biosynthesis of glutathione and inhibit a type of cell death in mammalian cells (74, 75) that is also preventable by iron chelators or lipophilic antioxidants (76). While in this study, Dixon SJ's team found that erastin could trigger a unique iron-dependent form of non-apoptotic cell death and named it ferroptosis. Since then, additional compounds and regulatory mechanisms have been identified, and ferroptosis becomes an emerging focus of regulated cell death. More importantly, among the top 55 references with the strongest citation burst (**Figure 9**), nine references are still in burstness. These nine references represent the latest emerging topics of ferroptosis hence they deserve further discussion (19, 35). Ranking by burstness strength, the first paper (strength=27.78) was published by Wan Seok Yang et al. (3) in *Cell* in 2014, with the citation burstness lasted for five years (2016–2020), proving that GPX4 is an essential regulator of ferroptotic cancer cell death. Jose Pedro Friedmann Angeli et al. (4) detected that inactivation of Gpx4 triggers acute renal failure in mice. The study was published in *Nature Cell Biology* in 2014 with the second strongest citation burstness (strength=23.89) lasting for five years (2016–2020). Scott J Dixon et al. (77) published the third reference in 2014 (13.69, 2016–2020). They found that erastin is a potent inhibitor of system xc– function, which is much more potent than sulfasalazine, the known best inhibitor of system xc–. They also discovered that the anti-cancer drug sorafenib inhibits system xc– function and could trigger endoplasmic reticulum stress and ferroptosis. The reference with the fourth-strongest citation burstness was published in *Trends in Pharmacological Science* by Jose Pedro Friedmann Angeli et al. (78) in 2017 (12.98, 2018–2020). This review mainly summarized the fundamental aspects of lipid peroxidation in ferroptosis and their potential contribution to disease; furthermore, they discussed the potential pharmacological approaches aiming to subvert lipid peroxidation and suppress ferroptosis. The fifth paper is a review authored by Haitao Yu et al. (79) in 2017 (11.03, 2018–2020), focusing on the relationship between ferroptosis and human tumorous diseases. Min-Young Kwon et al. (80) published the sixth study in 2015 (8.55, 2017–2020). They elucidated that heme oxygenase-1 (HO-1) accelerates erastin-induced lipid peroxidation and ferroptosis. The seventh reference (81) was published in *Nature* in 2014 (8.2, 2018–2020). This work identified nuclear receptor coactivator 4 (NCOA4) as a selective cargo receptor for autophagic turnover of ferritin. In previous studies, genetic overexpression or knockdown of NCOA4 has been shown to trigger or prevent erastin-induced

ferroptosis in several (82). Indeed, ferroptosis has been suggested as a type of autophagy-dependent cell death (71). The eighth study (83) (7.82, 2017–2020) detected that functional lysosomes play an essential role in functional lysosomes in the ferroptosis of cancer cells. Moreover, the ninth study (84) (7.45, 2017-2020) demonstrated the vital role of p53 acetylation in ferroptosis and its remaining tumor suppression activity. The citation burstness analysis showed that exploring the mechanism of ferroptosis (such as GPX4, lipid peroxidation, HO-1, NCOA4, functional lysosomes, p53 acetylation, etc.) and applying to related disease (such as tumor, acute renal failure, etc.) were the recent major topics in the field of ferroptosis research.

From the above analysis, we can see that ferroptosis research initially focused on experimental research and cancer. Afterward, in-depth experimental research detected more star mechanisms (such as GPX4, Nrf2, GSH, p53, SLC7A11, ACSL4, system xc−, phospholipids, NAD(P)H, CoQ10, lipid peroxidation, etc.), used new technologies, and related ferroptosis to more diseases (such as kinds of cancer, Alzheimer, Parkinson's disease, stroke, ischemia-reperfusion damage, kidney disease, liver disease, atherosclerosis, drug resistance, etc.). Furthermore, ferroptosis research began to do clinical trials (85), while there are still no human intervention trials, indicating that the clinical translational application of ferroptosis theories is still ongoing (12). The reason might be that the ferroptosis inhibitors such as ferrostatin-1 and liproxstatin-1 may inhibit other ROS-dependent forms of cell death, although they are safe in pre-clinical animal studies (7). In the latest traditional review, Daolin Tang (7) pointed out that we are at the dawn of ferroptosis research; challenges require more specific drugs, sophisticated pre-clinical models, and innovative technology. That is consistent with our bibliometric detecting.

Limitations

This study also comes with certain limitations inherent in bibliometrics. Firstly, data were retrieved only from the WoSCC database, while a few studies not included in WoSCC were missed. However, WoSCC is the most commonly applied database for scientometric analysis (19, 28); data from WoSCC could represent most information in a degree. Secondly, all information was extracted by bibliometric tools basing on machine learning and natural language processing, which may lead to bias as reported in other bibliometric studies (86). Nevertheless, compared to the latest traditional reviews (7, 9, 72, 87, 88), our results are basically consistent with them while providing researchers with richer objective information, knowledge and insight.

CONCLUSION

In conclusion, ferroptosis research is in a rapid development stage with active cooperation worldwide, of which the United States is the main collaborating center. Current publications are mainly in the molecular and biology field. Five main aspects of ferroptosis research included regulation mechanisms, nervous system injury, cancer, relationships with other types of cell death, and lipid peroxidation. The latest hotspots are nanoparticle, cancer therapy, iron metabolism, and in-depth mechanism. Notably, Nrf2 may have turning significance. Based on the results, the emerging topics would be the further regulatory mechanism of ferroptosis and the broader application of ferroptosis-related disease with advanced technology.

Overall, this is the first study to systematically analyze the ferroptosis-related publications by bibliometric and knowledge-map. Moreover, we analyzed data by both CiteSpace and VosViewer, which could obtain richer results from different perspectives. Compared to traditional reviews, this study provides an original and objective insight into ferroptosis research. We believe the results of this study would provide helpful references for further research.

AUTHOR'S NOTE

The data used for analysis is in Annexes 1, and the result data is in Annexes 2.

DATA AVAILABILITY STATEMENT

The original contributions presented in the study are included in the article/**Supplementary Material**. Further inquiries can be directed to the corresponding authors.

AUTHOR CONTRIBUTIONS

HX and JJ designed this study. YF collected the data. JZ and LX performed the analysis. TW and WT normalized the pictures. JZ and LS wrote the original draft. All authors contributed to the article and approved the submitted version.

FUNDING

The work was supported by the National Natural Science Foundation of China (No. 81874412), National Natural Science Foundation of China (No.82004145), Beijing Natural Science Foundation (No.7204298), and Central Public Welfare Research Institutes of China Academy of Chinese Medical Sciences (No. ZZ13-YQ-017).

ACKNOWLEDGMENTS

The authors would like to thank National Clinical Research Center for Chinese Medicine Cardiology for supporting that work.

SUPPLEMENTARY MATERIAL

The Supplementary Material for this article can be found online at: https://www.frontiersin.org/articles/10.3389/fonc.2021.686726/full#supplementary-material.

REFERENCES

1. Stockwell BR, Friedmann Angeli JP, Bayir H, Bush AI, Conrad M, Dixon SJ, et al. Ferroptosis: A Regulated Cell Death Nexus Linking Metabolism, Redox Biology, and Disease. *Cell* (2017) 171(2):273–85. doi: 10.1016/j.cell.2017.09.021
2. Dixon SJ, Lemberg KM, Lamprecht MR, Skouta R, Zaitsev EM, Gleason CE, et al. Ferroptosis: An Iron-Dependent Form of Nonapoptotic Cell Death. *Cell* (2012) 149(5):1060–72. doi: 10.1016/j.cell.2012.03.042
3. Yang WS, SriRamaratnam R, Welsch ME, Shimada K, Skouta R, Viswanathan VS, et al. Regulation of Ferroptotic Cancer Cell Death by GPX4. *Cell* (2014) 156(1-2):317–31. doi: 10.1016/j.cell.2013.12.010
4. Friedmann Angeli JP, Schneider M, Proneth B, Tyurina YY, Tyurin VA, Hammond VJ, et al. Inactivation of the Ferroptosis Regulator Gpx4 Triggers Acute Renal Failure in Mice. *Nat Cell Biol* (2014) 16(12):1180–91. doi: 10.1038/ncb3064
5. Yagoda N, von Rechenberg M, Zaganjor E, Bauer AJ, Yang WS, Fridman DJ, et al. Ras-RAF-MEK-Dependent Oxidative Cell Death Involving Voltage-Dependent Anion Channels. *Nature* (2007) 447(7146):864–8. doi: 10.1038/nature05859
6. Vanden Berghe T, Linkermann A, Jouan-Lanhouet S, Walczak H, Vandenabeele P. Regulated Necrosis: The Expanding Network of Non-Apoptotic Cell Death Pathways. *Nat Rev Mol Cell Biol* (2014) 15(2):135–47. doi: 10.1038/nrm3737
7. Tang D, Chen X, Kang R, Kroemer G. Ferroptosis: Molecular Mechanisms and Health Implications. *Cell Res* (2021) 31(2):107–25. doi: 10.1038/s41422-020-00441-1
8. Ingold I, Berndt C, Schmitt S, Doll S, Poschmann G, Buday K, et al. Selenium Utilization by GPX4 Is Required to Prevent Hydroperoxide-Induced Ferroptosis. *Cell* (2018) 172(3):409–22.e21. doi: 10.1016/j.cell.2017.11.048
9. Li J, Cao F, Yin HL, Huang ZJ, Lin ZT, Mao N, et al. Ferroptosis: Past, Present and Future. *Cell Death Dis* (2020) 11(2):88. doi: 10.1038/s41419-020-2298-2
10. Wang H, Cheng Y, Mao C, Liu S, Xiao D, Huang J, et al. Emerging Mechanisms and Targeted Therapy of Ferroptosis in Cancer. *Mol Ther* (2021). doi: 10.1016/j.ymthe.2021.03.022
11. El Hout M, Dos Santos L, Hamaï A, Mehrpour M. A Promising New Approach to Cancer Therapy: Targeting Iron Metabolism in Cancer Stem Cells. *Semin Cancer Biol* (2018) 53:125–38. doi: 10.1016/j.semcancer.2018.07.009
12. Conrad M, Lorenz SM, Proneth B. Targeting Ferroptosis: New Hope for As-Yet-Incurable Diseases. *Trends Mol Med* (2021) 27(2):113–22. doi: 10.1016/j.molmed.2020.08.010
13. Jin Y, Zhuang Y, Liu M, Che J, Dong X. Inhibiting Ferroptosis: A Novel Approach for Stroke Therapeutics. *Drug Discovery Today* (2021) 26(4):916–30. doi: 10.1016/j.drudis.2020.12.020
14. Wu X, Li Y, Zhang S, Zhou X. Ferroptosis as a Novel Therapeutic Target for Cardiovascular Disease. *Theranostics* (2021) 11(7):3052–9. doi: 10.7150/thno.54113
15. Chen X, Kang R, Kroemer G, Tang D. Broadening Horizons: The Role of Ferroptosis in Cancer. *Nat Rev Clin Oncol* (2021) 18(5):280–96. doi: 10.1038/s41571-020-00462-0
16. Zheng J, Conrad M. The Metabolic Underpinnings of Ferroptosis. *Cell Metab* (2020) 32(6):920–37. doi: 10.1016/j.cmet.2020.10.011
17. Jiang X, Stockwell BR, Conrad M. Ferroptosis: Mechanisms, Biology and Role in Disease. *Nat Rev Mol Cell Biol* (2021) 22(4):266–82. doi: 10.1038/s41580-020-00324-8
18. Forteza CM, Lunn E, Merigó JM, Horrach P. Research Progress in Tourism, Leisure and Hospitality in Europe (1969–2018). *Int J Contemp Hospital Manage* (2020) 33(1):48–74. doi: 10.1108/IJCHM-06-2020-0521
19. Ke L, Lu C, Shen R, Lu T, Ma B, Hua Y. Knowledge Mapping of Drug-Induced Liver Injury: A Scientometric Investigation (2010-2019). *Front Pharmacol* (2020) 11:842. doi: 10.3389/fphar.2020.00842
20. de Castilhos Ghisi N, Zuanazzi NR, Fabrin TMC, Oliveira EC. Glyphosate and its Toxicology: A Scientometric Review. *Sci Total Environ* (2020) 733:139359. doi: 10.1016/j.scitotenv.2020.139359
21. Chen C, Song M. Visualizing a Field of Research: A Methodology of Systematic Scientometric Reviews. *PloS One* (2019) 14(10):e0223994. doi: 10.1371/journal.pone.0223994
22. Ma C, Su H, Li H. Global Research Trends on Prostate Diseases and Erectile Dysfunction: A Bibliometric and Visualized Study. *Front Oncol* (2020) 10:627891. doi: 10.3389/fonc.2020.627891
23. Devos P, Ménard J. Trends in Worldwide Research in Hypertension Over the Period 1999-2018: A Bibliometric Study. *Hypertension* (2020) 76(5):1649–55. doi: 10.1161/hypertensionaha.120.15711
24. Chen C, Lou Y, Li XY, Lv ZT, Zhang LQ, Mao W. Mapping Current Research and Identifying Hotspots on Mesenchymal Stem Cells in Cardiovascular Disease. *Stem Cell Res Ther* (2020) 11(1):498. doi: 10.1186/s13287-020-02009-7
25. Huang X, Fan X, Ying J, Chen S. Emerging Trends and Research Foci in Gastrointestinal Microbiome. *J Transl Med* (2019) 17(1):67. doi: 10.1186/s12967-019-1810-x
26. Zhu X, Kong Q, Niu X, Chen L, Ge C. Mapping Intellectual Structure and Research Performance for the Nanoparticles in Pancreatic Cancer Field. *Int J Nanomed* (2020) 15:5503–16. doi: 10.2147/ijn.S253599
27. Zhang XL, Zheng Y, Xia ML, Wu YN, Liu XJ, Xie SK, et al. Knowledge Domain and Emerging Trends in Vinegar Research: A Bibliometric Review of the Literature From Woscc. *Foods* (2020) 9(2):166. doi: 10.3390/foods9020166
28. Mulet-Forteza C, Genovart-Balaguer J, Mauleon-Mendez E, Merigó JM. A Bibliometric Research in the Tourism, Leisure and Hospitality Fields. *J Business Res* (2019) 101:819–27. doi: 10.1016/j.jbusres.2018.12.002
29. Qin Y, Zhang Q, Liu Y. Analysis of Knowledge Bases and Research Focuses of Cerebral Ischemia-Reperfusion From the Perspective of Mapping Knowledge Domain. *Brain Res Bull* (2020) 156:15–24. doi: 10.1016/j.brainresbull.2019.12.004
30. Merigó JM, Mulet-Forteza C, Valencia C, Lew AA. Twenty Years of Tourism Geographies : A Bibliometric Overview. *Tourism Geograph* (2019) 21(5):881–910. doi: 10.1080/14616688.2019.1666913
31. Chen L, Ma S, Hu D, Lin H, Zhu Y, Chen K, et al. Bibliometric Study of Sodium Glucose Cotransporter 2 Inhibitors in Cardiovascular Research. *Front Pharmacol* (2020) 11:561494. doi: 10.3389/fphar.2020.561494
32. van Eck NJ, Waltman L. Software Survey: VOSviewer, A Computer Program for Bibliometric Mapping. *Scientometrics* (2010) 84(2):523–38. doi: 10.1007/s11192-009-0146-3
33. Eck N, Waltman L. *Vosviewer Manual*. Leiden: Leiden University (2020).
34. Paunkov A, Chartoumpekis DV, Ziros PG, Sykiotis GP. A Bibliometric Review of the Keap1/Nrf2 Pathway and Its Related Antioxidant Compounds. *Antioxid (Basel)* (2019) 8(9):353. doi: 10.3390/antiox8090353
35. Gao Y, Shi S, Ma W, Chen J, Cai Y, Ge L, et al. Bibliometric Analysis of Global Research on PD-1 and PD-L1 in the Field of Cancer. *Int Immunopharmacol* (2019) 72:374–84. doi: 10.1016/j.intimp.2019.03.045
36. Forteza CM, Balaguer JG, Merigó JM, Mendez EM. Bibliometric Structure of IJCHM in its 30 Years. *Int J Contemp Hospital Manage* (2019) 31(12):4574–604. doi: 10.1108/IJCHM-10-2018-0828
37. Chaomei C. Searching for Intellectual Turning Points: Progressive Knowledge Domain Visualization. *Proc Natl Acad Sci USA* (2004) 101(Suppl 1):5303–10. doi: 10.1073/pnas.0307513100
38. Chen C, Leydesdorff L. Patterns of Connections and Movements in Dual-Map Overlays: A New Method of Publication Portfolio Analysis. *J Assoc Inf Sci Technol* (2014) 65(2):334–51. doi: 10.1002/asi.22968
39. Chen C, Hu Z, Liu S, Tseng H. Emerging Trends in Regenerative Medicine: A Scientometric Analysis in Citespace. *Expert Opin Biol Ther* (2012) 12(5):593–608. doi: 10.1517/14712598.2012.674507
40. Chen C. Searching for Intellectual Turning Points: Progressive Knowledge Domain Visualization. *Proc Natl Acad Sci USA* (2004) 101 Suppl 1(Suppl 1):5303–10. doi: 10.1073/pnas.0307513100
41. Chen C. Science Mapping:A Systematic Review of the Literature. *J Data Inf Sci* (2017) 2(02):1–40. doi: 10.1515/jdis-2017-0006
42. Li C, Wu K, Wu J. A Bibliometric Analysis of Research on Haze During 2000-2016. *Environ Sci Pollut Res Int* (2017) 24(32):24733–42. doi: 10.1007/s11356-017-0440-1
43. Xie Y, Hou W, Song X, Yu Y, Huang J, Sun X, et al. Ferroptosis: Process and Function. *Cell Death Differ* (2016) 23(3):369–79. doi: 10.1038/cdd.2015.158
44. Jiang L, Kon N, Li T, Wang SJ, Su T, Hibshoosh H, et al. Ferroptosis as a p53-Mediated Activity During Tumour Suppression. *Nature* (2015) 520(7545):57–62. doi: 10.1038/nature14344

45. Doll S, Proneth B, Tyurina YY, Panzilius E, Kobayashi S, Ingold I, et al. ACSL4 Dictates Ferroptosis Sensitivity by Shaping Cellular Lipid Composition. *Nat Chem Biol* (2017) 13(1):91–8. doi: 10.1038/nchembio.2239
46. Yang WS, Stockwell BR. Ferroptosis: Death by Lipid Peroxidation. *Trends Cell Biol* (2016) 26(3):165–76. doi: 10.1016/j.tcb.2015.10.014
47. Gao M, Monian P, Quadri N, Ramasamy R, Jiang X. Glutaminolysis and Transferrin Regulate Ferroptosis. *Mol Cell* (2015) 59(2):298–308. doi: 10.1016/j.molcel.2015.06.011
48. Kagan VE, Mao G, Qu F, Angeli JP, Doll S, Croix CS. Oxidized Arachidonic and Adrenic PEs Navigate Cells to Ferroptosis. *Nat Chem Biol* (2017) 13 (1):81–90. doi: 10.1038/nchembio.2238
49. Yang WS, Kim KJ, Gaschler MM, Patel M, Shchepinov MS, Stockwell BR. Peroxidation of Polyunsaturated Fatty Acids by Lipoxygenases Drives Ferroptosis. *Proc Natl Acad Sci USA* (2016) 113(34):E4966–75. doi: 10.1073/pnas.1603244113
50. Yeung AW, Goto TK, Leung WK. The Changing Landscape of Neuroscience Research, 2006-2015: A Bibliometric Study. *Front Neurosci* (2017) 11:120. doi: 10.3389/fnins.2017.00120
51. Kodonas K, Fardi A, Gogos C, Economides N. Scientometric Analysis of Vital Pulp Therapy Studies. *Int Endod J* (2021) 54(2):220–30. doi: 10.1111/iej.13422
52. Liang YD, Li Y, Zhao J, Wang XY, Zhu HZ, Chen XH. Study of Acupuncture for Low Back Pain in Recent 20 Years: A Bibliometric Analysis Via Citespace. *J Pain Res* (2017) 10:951–64. doi: 10.2147/jpr.S132808
53. Chaomei C. Citespace II: Detecting and Visualizing Emerging Trends and Transient Patterns in Scientific Literature. *J Am Soc Inf Sci Technol* (2005) 57 (3):359–77. doi: 10.1002/asi.20317
54. Lu C, Liu M, Shang W, Yuan Y, Li M, Deng X, et al. Knowledge Mapping of Angelica Sinensis (Oliv.) Diels (Danggui) Research: A Scientometric Study. *Front Pharmacol* (2020) 11:294. doi: 10.3389/fphar.2020.00294
55. Chen C, Song M. Science Mapping Tools and Applications, In *Representing Scientific Knowledge: The Role of Uncertainty*. Springer (2017). p. 57–137.
56. Aitken RJ, Clarkson JS. Cellular Basis of Defective Sperm Function and its Association With the Genesis of Reactive Oxygen Species by Human Spermatozoa. *J Reprod Fertil* (1987) 81(2):459–69. doi: 10.1530/jrf.0.0810459
57. Yant LJ, Ran Q, Rao L, Van Remmen H, Shibatani T, Belter JG, et al. The Selenoprotein GPX4 is Essential for Mouse Development and Protects From Radiation and Oxidative Damage Insults. *Free Radic Biol Med* (2003) 34 (4):496–502. doi: 10.1016/s0891-5849(02)01360-6
58. Xiao F, Li C, Sun J, Zhang L. Knowledge Domain and Emerging Trends in Organic Photovoltaic Technology: A Scientometric Review Based on CiteSpace Analysis. *Front Chem* (2017) 5:67. doi: 10.3389/fchem.2017.00067
59. Liu G, Jiang R, Jin Y. Sciatic Nerve Injury Repair: A Visualized Analysis of Research Fronts and Development Trends. *Neural Regen Res* (2014) 9 (18):1716–22. doi: 10.4103/1673-5374.141810
60. Anandhan A, Dodson M, Schmidlin CJ, Liu P, Zhang DD. Breakdown of an Ironclad Defense System: The Critical Role of NRF2 in Mediating Ferroptosis. *Cell Chem Biol* (2020) 27(4):436–47. doi: 10.1016/j.chembiol.2020.03.011
61. Davis ME, Chen ZG, Shin DM. Nanoparticle Therapeutics: An Emerging Treatment Modality for Cancer. *Nat Rev Drug Discovery* (2008) 7(9):771–82. doi: 10.1038/nrd2614
62. Shen Z, Liu T, Li Y, Lau J, Yang Z, Fan W, et al. Fenton-Reaction-Acceleratable Magnetic Nanoparticles for Ferroptosis Therapy of Orthotopic Brain Tumors. *ACS Nano* (2018) 12(11):11355–65. doi: 10.1021/acsnano.8b06201
63. Jiang Q, Wang K, Zhang X, Ouyang B, Liu H, Pang Z, et al. Platelet Membrane-Camouflaged Magnetic Nanoparticles for Ferroptosis-Enhanced Cancer Immunotherapy. *Small* (2020) 16(22):e2001704. doi: 10.1002/smll.202001704
64. Kim SE, Zhang L, Ma K, Riegman M, Chen F, Ingold I, et al. Ultrasmall Nanoparticles Induce Ferroptosis in Nutrient-Deprived Cancer Cells and Suppress Tumour Growth. *Nat Nanotechnol* (2016) 11(11):977–85. doi: 10.1038/nnano.2016.164
65. Li L, Sun S, Tan L, Wang Y, Wang L, Zhang Z, et al. Polystyrene Nanoparticles Reduced ROS and Inhibited Ferroptosis by Triggering Lysosome Stress and TFEB Nucleus Translocation in a Size-Dependent Manner. *Nano Lett* (2019) 19(11):7781–92. doi: 10.1021/acs.nanolett.9b02795
66. Li L, Sun S, Tan L, Wang Y, Wang L, Zhang Z, et al. Correction to "Polystyrene Nanoparticles Reduced ROS and Inhibited Ferroptosis by Triggering Lysosome Stress and TFEB Nucleus Translocation in a Size-Dependent Manner". *Nano Lett* (2019) 19(12):9170. doi: 10.1021/acs.nanolett.9b04770
67. Zhang J, Yang J, Zuo T, Ma S, Xokrat N, Hu Z, et al. Heparanase-Driven Sequential Released Nanoparticles for Ferroptosis and Tumor Microenvironment Modulations Synergism in Breast Cancer Therapy. *Biomaterials* (2021) 266:120429. doi: 10.1016/j.biomaterials.2020.120429
68. Feng H, Schorpp K, Jin J, Yozwiak CE, Hoffstrom BG, Decker AM, et al. Transferrin Receptor Is a Specific Ferroptosis Marker. *Cell Rep* (2020) 30 (10):3411–23.e7. doi: 10.1016/j.celrep.2020.02.049
69. Chen X, Comish PB, Tang D, Kang R. Characteristics and Biomarkers of Ferroptosis. *Front Cell Dev Biol* (2021) 9:637162. doi: 10.3389/fcell.2021.637162
70. Lee YS, Lee DH, Choudry HA, Bartlett DL, Lee YJ. Ferroptosis-Induced Endoplasmic Reticulum Stress: Cross-Talk Between Ferroptosis and Apoptosis. *Mol Cancer Res* (2018) 16(7):1073–6. doi: 10.1158/1541-7786.Mcr-18-0055
71. Zhou B, Liu J, Kang R, Klionsky DJ, Kroemer G, Tang D. Ferroptosis Is a Type of Autophagy-Dependent Cell Death. *Semin Cancer Biol* (2020) 66:89–100. doi: 10.1016/j.semcancer.2019.03.002
72. Stockwell BR, Jiang X, Gu W. Emerging Mechanisms and Disease Relevance of Ferroptosis. *Trends Cell Biol* (2020) 30(6):478–90. doi: 10.1016/j.tcb.2020.02.009
73. Chen C, Dubin R, Kim MC. Orphan Drugs and Rare Diseases: A Scientometric Review (2000–2014). *Expert Opin Orphan Drugs* (2014) 2 (7):709–24. doi: 10.1517/21678707.2014.920251
74. Eagle H. Nutrition Needs of Mammalian Cells in Tissue Culture. *Science* (1955) 122(3168):501–14. doi: 10.1126/science.122.3168.501
75. Bannai S, Tsukeda H, Okumura H. Effect of Antioxidants on Cultured Human Diploid Fibroblasts Exposed to Cystine-Free Medium. *Biochem Biophys Res Commun* (1977) 74(4):1582–8. doi: 10.1016/0006-291x(77)90623-4
76. Murphy TH, Miyamoto M, Sastre A, Schnaar RL, Coyle JT. Glutamate Toxicity in a Neuronal Cell Line Involves Inhibition of Cystine Transport Leading to Oxidative Stress. *Neuron* (1989) 2(6):1547–58. doi: 10.1016/0896-6273(89)90043-3
77. Dixon SJ, Patel DN, Welsch M, Skouta R, Lee ED, Hayano M, et al. Pharmacological Inhibition of Cystine-Glutamate Exchange Induces Endoplasmic Reticulum Stress and Ferroptosis. *Elife* (2014) 3:e02523. doi: 10.7554/eLife.02523
78. Angeli JPF, Shah R, Pratt DA, Conrad M. Ferroptosis Inhibition: Mechanisms and Opportunities. *Trends Pharmacol Sci* (2017) 38(5):489–98. doi: 10.1016/j.tips.2017.02.005
79. Yu H, Guo P, Xie X, Wang Y, Chen G. Ferroptosis, a New Form of Cell Death, and its Relationships With Tumourous Diseases. *J Cell Mol Med* (2017) 21 (4):648–57. doi: 10.1111/jcmm.13008
80. Kwon MY, Park E, Lee SJ, Chung SW. Heme Oxygenase-1 Accelerates Erastin-Induced Ferroptotic Cell Death. *Oncotarget* (2015) 6(27):24393–403. doi: 10.18632/oncotarget.5162
81. Mancias JD, Wang X, Gygi SP, Harper JW, Kimmelman AC. Quantitative Proteomics Identifies NCOA4 as the Cargo Receptor Mediating Ferritinophagy. *Nature* (2014) 509(7498):105–9. doi: 10.1038/nature13148
82. Zhang Z, Yao Z, Wang L, Ding H, Shao J, Chen A, et al. Activation of Ferritinophagy Is Required for the RNA-Binding Protein ELAVL1/HuR to Regulate Ferroptosis in Hepatic Stellate Cells. *Autophagy* (2018) 14(12):2083–103. doi: 10.1080/15548627.2018.1503146
83. Torii S, Shintoku R, Kubota C, Yaegashi M, Torii R, Sasaki M, et al. An Essential Role for Functional Lysosomes in Ferroptosis of Cancer Cells. *Biochem J* (2016) 473(6):769–77. doi: 10.1042/bj20150658
84. Wang SJ, Li D, Ou Y, Jiang L, Chen Y, Zhao Y, et al. Acetylation Is Crucial for P53-Mediated Ferroptosis and Tumor Suppression. *Cell Rep* (2016) 17 (2):366–73. doi: 10.1016/j.celrep.2016.09.022
85. Devos D, Moreau C, Kyheng M, Garcon G, Rolland AS, Blasco H, et al. A Ferroptosis-Based Panel of Prognostic Biomarkers for Amyotrophic Lateral Sclerosis. *Sci Rep* (2019) 9(1):2918. doi: 10.1038/s41598-019-39739-5
86. Yan WT, Lu S, Yang YD, Ning WY, Cai Y, Hu XM, et al. Research Trends, Hot Spots and Prospects for Necroptosis in the Field of Neuroscience. *Neural Regener Res* (2021) 16(8):1628–37. doi: 10.4103/1673-5374.303032
87. Qiu Y, Cao Y, Cao W, Jia Y, Lu N. The Application of Ferroptosis in Diseases. *Pharmacol Res* (2020) 159:104919. doi: 10.1016/j.phrs.2020.104919

88. Stockwell BR, Jiang X. The Chemistry and Biology of Ferroptosis. *Cell Chem Biol* (2020) 27(4):365–75. doi: 10.1016/j.chembiol.2020.03.013

Conflict of Interest: The authors declare that the research was conducted in the absence of any commercial or financial relationships that could be construed as a potential conflict of interest.

frontiers in Cell and Developmental Biology

ORIGINAL RESEARCH
published: 17 June 2021
doi: 10.3389/fcell.2021.670184

A Novel Ferroptosis-Related Gene Signature for Overall Survival Prediction in Patients With Breast Cancer

Lizhe Zhu[1†], Qi Tian[2†], Siyuan Jiang[1], Huan Gao[2], Shibo Yu[1], Yudong Zhou[1], Yu Yan[1], Yu Ren[1], Jianjun He[1] and Bin Wang[1*]*

[1] Department of Breast Surgery, The First Affiliated Hospital of Xi'an Jiaotong University, Xi'an, China, [2] Department of Medical Oncology, The First Affiliated Hospital of Xi'an Jiaotong University, Xi'an, China

OPEN ACCESS

Edited by:
Maryam Mehrpour,
Université Paris Descartes, France

Reviewed by:
Peng-Chan Lin,
National Cheng Kung University, Taiwan
Xiongjian Rao,
University of Kentucky, United States

***Correspondence:**
Jianjun He
chinahjj@163.com
Bin Wang
february111@163.com

[†] These authors have contributed equally to this work

Specialty section:
This article was submitted to Molecular and Cellular Oncology, a section of the journal Frontiers in Cell and Developmental Biology

Received: 20 February 2021
Accepted: 14 May 2021
Published: 17 June 2021

Citation:
Zhu L, Tian Q, Jiang S, Gao H, Yu S, Zhou Y, Yan Y, Ren Y, He J and Wang B (2021) A Novel Ferroptosis-Related Gene Signature for Overall Survival Prediction in Patients With Breast Cancer. Front. Cell Dev. Biol. 9:670184. doi: 10.3389/fcell.2021.670184

Introduction: Breast cancer is the most common malignant tumor in women worldwide. However, advanced multidisciplinary therapy cannot rescue the mortality of high-risk breast cancer metastasis. Ferroptosis is a newly discovered form of regulating cell death that related to cancer treatment, especially in eradicating aggressive malignancies that are resistant to traditional therapies. However, the prognostic value of ferroptosis-related gene in breast cancer remains unknown.

Materials and Methods: In this study, a total of 1,057 breast cancer RNA expression data with clinical and follow-up information were downloaded from the TCGA cohort, multivariate Cox regression was used to construct the 11-gene prognostic ferroptosis-related gene signature. The breast cancer patients from the GEO cohort were used for validation. The expression levels of core prognostic genes were also verified in erastin-treated breast cancer cell lines by real-time polymerase chain action (PCR).

Results and Discussion: Our results showed that 78% ferroptosis-related genes were differentially expressed between breast cancer tumor tissue and adjacent non-tumorous tissues, including 29 of them which were significantly correlated with OS in the univariate Cox regression analysis. Patients were divided into high-risk group and low-risk group by the 11-gene signature. Patients with high-risk scores had a higher probability of death earlier than the low-risk group both in the TCGA construction cohort and in the GEO validation cohort (all $P < 0.001$). Meanwhile, the risk score was proved to be an independent predictor for OS in both univariate and multivariate Cox regression analyses (HR > 1, $P < 0.01$). The predictive efficacy of the prognostic signature for OS was further verified by the time-dependent ROC curves. Moreover, we also enriched many immune-related biological processes in later functional analysis; the immune status showed a statistical difference between the two risk groups. In addition,

the differences in expression levels of 11 core prognostic genes were examined in ferroptosis inducer-treated breast cancer cell lines.

Conclusion: In conclusion, a novel ferroptosis-related gene model can be used for prognostic prediction in breast cancer. New ferroptosis-related genes may be used for breast cancer targeting therapy in the future.

Keywords: breast cancer, ferroptosis, gene signature, overall survival, immune status

INTRODUCTION

Breast cancer is the most common malignant tumor in women worldwide; among 70–80% patients with early, non-metastatic disease can be cured. However, advanced breast cancer with distant organ metastasis is considered to be incurable by the currently available treatment methods (Harbeck et al., 2019). Meanwhile, the chemotherapy or endocrine therapy resistance of breast cancer patients also brings certain challenges to their treatment. In addition, the global incidence of breast cancer is increasing at a rate of 3.1% per year, from 641,000 cases in 1980 to 1.6 million cases in 2010 (Bray et al., 2015). Under the joint multidisciplinary diagnosis and treatment model of surgery, radiotherapy, chemotherapy, endocrinology, and targeted precision therapy, the mortality of advanced breast cancer or high-risk breast cancer with metastasis has not been significantly improved (Emens, 2018). All these data highlight the additional need for innovative methods to identify patients with high-risk disease.

Ferroptosis is a newly discovered form of regulating cell death, which is related to metabolism, redox biology, and human health. Emerging evidence suggests that it may trigger ferroptosis for cancer treatment, especially in eradicating aggressive malignancies that are resistant to traditional therapies (Liang et al., 2019). Previous studies have shown that ferroptotic cell death is a type of cell death that is different from apoptosis, various forms of necrosis, and autophagy. It is different in morphology, biochemistry, and genetics. Different from other forms of apoptosis and non-apoptotic death, the feature of this process is the iron-dependent accumulation of reactive oxygen species (ROS) (Yagoda et al., 2007; Christofferson and Yuan, 2010; Dixon et al., 2012). There have been some studies related to breast cancer and ferroptosis. Ma et al. discovered that ferroptosis was induced following siramesine and lapatinib treatment of breast cancer cells (Ma et al., 2016). Yu et al. found that target exosome-encapsulated erastin induced ferroptosis in triple-negative breast cancer cells (Yu et al., 2019b). There was also a study that explored that sulfasalazine-induced ferroptosis in breast cancer cells was reduced by the inhibitory effect of the estrogen receptor on the transferrin receptor (Yu et al., 2019a). In addition, Qiao et al. discovered that NR5A2 synergized with NCOA3 could induce breast cancer resistance to the BET inhibitor by regulating NRF2 to attenuate ferroptosis (Qiao et al., 2020). However, studies on the ferroptosis-related genes in the prognosis of breast cancer remain largely unknown.

In this study, we downloaded the mRNA expression data and corresponding clinical data of breast cancer patients from the TCGA database. Then, we constructed a prognostic ferroptosis-related gene signature based on the TCGA cohort and validated this model in the GEO cohort. We further did the functional enrichment analysis to identify the potential mechanisms.

MATERIALS AND METHODS

Data Collection and Ferroptosis-Related Gene Definition

A total of 1057 breast cancer RNA expression data with clinical and follow-up information were downloaded from the TCGA cohort[1]. In addition, the breast cancer RNA expression data with clinical and follow-up information of three external validation cohorts were downloaded from the Gene Expression Omnibus (GEO) database[2], including 327 samples of GSE20685, 88 samples of GSE20711, and 104 samples of GSE42568. The baseline clinical characteristics of the breast cancer patients in this study are shown in **Table 1**. All the data from TCGA and GEO were public. This study was exempted from the approval of the local ethics committees. The present study followed the TCGA and GEO data access policies and publication guidelines.

Later, 259 ferroptosis-related genes were obtained from the FerrDb website[3], which was the first database of ferroptosis regulators and markers and ferroptosis–disease associations. It classified ferroptosis-related genes into three subgroups, including drivers which were genes that promote ferroptosis, suppressors which were genes that prevent ferroptosis, and markers which were genes that indicated the occurrence of ferroptosis (Zhou and Bao, 2020). We further removed the duplicate genes of the three subgroups of ferroptosis gene sets and obtained a total of 259 genes for subsequent analysis. The detailed information and classification of ferroptosis-related genes are found in **Supplementary Table 1**.

Construction and Validation of a Prognostic Ferroptosis-Related Gene Signature

The "limma" R package was used to identify the differentially expressed genes (DEGs) between breast cancer tissues and adjacent normal breast tissues; it was filtered by the cutoff values of false discovery rate (FDR) < 0.05 and $\log2|\text{fold change}| > 1$ in the TCGA cohort. Later, we used univariate

[1]https://portal.gdc.cancer.gov

[2]http://www.ncbi.nlm.nih.gov/geo

[3]http://www.zhounan.org/ferrdb

TABLE 1 | The baseline clinical characteristics of the breast cancer patients in this study.

	TCGA cohort	GEO cohort			*P*-value
		GSE20685	GSE20711	GSE42568	
No. of patients	1057	327	88	104	/
Age (median, range)	58 (26–90)	46 (24–84)	/	56 (31–90)	/
Stage (%)					
I	181	/	/	/	/
II	598	/	/	/	
III	237	/	/	/	
IV	30	/	/	/	
Unknown	11	/	/	/	
T					
1	278	101	/	/	0.092
2	607	188	/	/	
3	132	26	/	/	
4	37	12	/	/	
Unknown	3	0	/	/	
N					
0	497	137	/	/	<0.01
1	352	87	/	/	
2	119	63	/	/	
3	72	40	/	/	
Unknown	17	0	/	/	
M					
0	879	319	/	/	0.908
1	21	8	/	/	
Unknown	157	0	/	/	
Survival status					
OS days (median)	858	1862	2216	2197	/

The P-value represents the comparison of clinicopathological parameters of patients between the TCGA cohort and GSE20685.

Cox analysis of overall survival (OS) to select the potential ferroptosis-related prognostic genes by R "survival" filtered by $p < 0.05$. In addition, the R "venn" package was used to get the intersect genes between ferroptosis-related DEGs and prognostic genes. We further used the intersect candidate genes for the construction of the prognostic signature. A ferroptosis-related prognostic signature-based prediction model was constructed by using coefficients (β) calculated from multivariate Cox regression as the weights. The risk score for each patient in the TCGA cohort was calculated based on the risk formula: risk score = expression of gene1 × β1 + expression of gene2 × β2 + ... expression of genen × βn. The breast cancer samples were then divided into high-risk group and low-risk group according to the median value of risk scores. For the survival analysis, the optimal cutoff expression value was determined by the "survminer" R packages. We also used the "survivalROC" R package to conduct the time-dependent ROC curve analyses for evaluating the predictive power of our 11-gene signature prediction model. Besides, univariate and multivariate Cox regression analyses were used to explore whether the risk score calculated from our model could play as an independent prognostic factor for breast cancer patients after considering other clinical factors, including age, stage, T stage, N stage, and M stage.

Functional Enrichment Analysis

The Gene Ontology (GO) and Kyoto Encyclopedia of Genes and Genomes (KEGG) were analyzed by the "clusterProfiler" R package through identifying the DEGs ($|\log2FC| \geq 1$, FDR < 0.05) between the high-risk and low-risk groups. Later, the ssGSEA algorithm was used to calculate the enrichment degree of 29 immune-related gene sets, including immune cell types, functions, or pathways. The annotated gene sets are concluded in **Supplementary Table 2**.

Cell Culture

Human breast cancer cells MDA-MB-231 and MCF-7 were maintained in L15 and DMEM High Glucose (Gibco; Thermo Fisher Scientific, Inc., Waltham, MA, United States), respectively, and were supplied with 10% fetal bovine serum (FBS; Gibco; Thermo Fisher Scientific, Inc.) at 37°C with 5% CO_2. The MCF-10A cells were cultured in DMEM/F12 (1:1) (Gibco; Thermo Fisher Scientific, Inc., Waltham, MA, United States) that was supplemented with 100 ng/ml cholera toxin (Sigma, St. Louis, MO, United States), 20 ng/ml epidermal growth factor (EGF) (Thermo Fisher Scientific, Inc., Waltham, MA, United States), 10 μg/ml insulin, 500 ng/ml hydrocortisone, and 5% heat-inactivated horse serum (all from Sigma) at 37°C with 5% CO_2. BT-549 cells were cultured in 1640 medium (Gibco; Thermo Fisher Scientific, Inc., Waltham, MA, United States) with 10% FBS, 1μg/ml insulin (Sigma) at 37°C with 5% CO_2. SUM-159 cells were maintained in DMEM/F12 with 10% FBS at 37°C with 5% CO_2. The old cell culture medium was replaced with fresh medium every other day.

Cell Viability Assay

MDA-MB-231 and MCF-7 cells were seeded in 96-well plates at a density of 3,000 cells per well and incubated in a humidified cell incubator at 37°C, 5% CO_2 for 24 h. The cells were then treated with erastin (T-1765, TargetMol, Boston, MA, United States) of 0, 10, 20, and 40 μM for 24, 48, and 72 h. MCF-10A, BT-549, and SUM-159 cells were seeded in 96-well plates at a density of 3,000, 4,000, and 2,500 cells per well, respectively, and then incubated in a humidified cell incubator at 37°C, 5% CO_2, for 24 h. The cells were then treated with erastin (T-1765, TargetMol) of 0, 10, 20, and 40 μM for 24 and 48 h. The Cell Counting Kit-8 (CCK-8) (TargetMol) reagent was then added, and the 96-well plate was continued to incubate for another 2 h. The OD (optical density) values were measured at 450 nm with a microplate reader. The experiments in all groups were performed in triplicates and repeated for three times.

Detection of ROS

MDA-MB-231 and MCF-7 cells were incubated in a 60-mm dish for 24 h, then different treatment groups were treated with DMSO, a ferroptosis activator (erastin, 10, 20, 40 μM), for another 48 h. Later, cells were incubated in a 60-mm dish containing 5 μM BODIPY 581/591 C11 dye (D3861, Invitrogen, Carlsbad, CA, United States) for 30 min at 37°C; cells were washed with PBS and trypsinized, then stained with PI (propidium iodide) in PBS for 5 min. Cells were then subjected to flow cytometry analysis using flow cytometry. The FL1 channel signal in live cells was plotted as shown in the figures.

RNA Isolation and Real-Time PCR

Total RNA from MDA-MB-231, MCF-7, MCF-10A, BT-549, and SUM-159 cells treated with erastin was extracted with the

RNeasy Mini Kit (Qiagen, Valencia, CA, United States) according to the manufacturer's protocol. The concentration and purity of all RNA samples were determined at an absorbance ratio of 260/280 nm. A total of 1 μg RNA was reverse-transcribed using iScript cDNA Synthesis kit from Bio-Rad™ (Hercules, CA, United States). Real-time PCR analysis was set up with the SYBR Green qPCR Supermix kit (Invitrogen, Carlsbad, CA, United States) and carried out in the iCycler thermal cycler. It was used to detect the mRNA expression levels of core prognostic genes. The relative level of mRNA expression of a gene was determined by normalizing with GAPDH. The primers used for real-time PCR are listed in **Supplementary Table 3** and were purchased from Sangon Biotech (Shanghai, China).

Western Blot

The proteins from MDA-MB-231, MCF-7, MCF-10A, BT-549, and SUM-159 cells treated with erastin were lysed in RIPA buffer, containing the phosphatase and protease inhibitor, by using an ultrasonic crusher (Sonics & Materials, Inc., Newtown, CT, United States). Later, the cell mixture was kept on ice for 30 min and transferred to a centrifuge tube for centrifugation at 4°C, 12,000 rpm, for 20 min. The breast cancer proteins from the upper part of the supernatant were collected and detected by BCA Protein Assay Kit (Pierce; Thermo Fisher Scientific, Inc.). Thirty-five micrograms of protein was separated on 10% SDS-PAGE gels and transferred to polyvinylidene fluoride (PVDF) membranes. Then, the PVDF membranes were blocked with 5% non-fat milk in TBST to prevent non-specific binding and subsequently incubated with a primary antibody (G6PD: cat no. sc-373886; Santa Cruz Biotechnology, Inc., Dallas, TX, United States; dilution, 1:500; BRD4: cat no. sc-518021; Santa Cruz Biotechnology, Inc.; dilution, 1:500; PI 3-kinase p110: cat no. sc-8010; Santa Cruz Biotechnology, Inc.; dilution, 1:500; GAPDH: cat no. 5174; Cell Signaling Technology, Inc., Danvers, MA, United States; dilution, 1:1,000) overnight at 4°C. All samples were incubated with anti-horseradish peroxidase-linked IgG secondary antibody (cat no. 7074; Cell Signaling Technology, Inc.; dilution, 1:2,000) at room temperature for 2 h and detected *via* chemiluminescence detection system (version 3.0; Bio-Rad Laboratories, Inc., Hercules, CA, United States).

Plasmids and Cell Transfection

pcDNA3.1 G6PD plasmid was kindly provided by Professor Ke Wang (XJTU). To overexpress G6PD, MDA-MB-231 cells were transfected with the empty vector pcDNA3.1 and pcDNA3.1 encoding G6PD, and cells were yielded to Western blot for transfect efficiency verification and then subjected to the following experiment. Transfections were performed using Lipofectamine 3000 (Invitrogen) according to the manufacturer's instructions.

Statistical Analysis

All data were analyzed using R version 4.0.2 or GraphPad Prism 8, and all experiments were repeated at least three times. These results were presented as mean ± standard deviation (SD). We used Student's *t*-test to compare the gene expression between tumor tissues and adjacent normal tissues. The Mann–Whitney test with *P*-values was used to compare the ssGSEA scores of immune cells and pathways between the high-risk and low-risk groups. Kaplan–Meier analysis with the log-rank test was used to compare the OS between the high-risk and low-risk groups. Besides, univariate and multivariate Cox regression analyses were used to identify the independent predictors of OS. The comparison of patients' clinicopathological parameters between the TCGA cohort and GSE20685 was analyzed by the χ^2-test. All statistical analyses were performed with R software (Version 4.0.2). All $P < 0.05$ was considered statistically significant.

RESULTS

Figure 1 shows the flowchart of construction and validation of data collection and analysis. We totally enrolled 1,057 breast cancer patients from the TCGA as the derivation cohort and 519 breast cancer patients from GEO as the validation cohort. The baseline clinical characteristics of the breast cancer patients in this study are summarized in **Table 1**.

Identification of Prognostic Ferroptosis-Related DEGs in the TCGA Cohort

We totally included 259 well-defined ferroptosis-related genes in this study, including 108 drivers that promote ferroptosis, 69 suppressors that prevent ferroptosis, and 111 markers that indicate the occurrence of ferroptosis. **Supplementary Table 1** shows the detailed information of ferroptosis-related gene sets that were used in our analyses. After the identification of prognostic ferroptosis-related DEGs in the TCGA cohort, results showed that most of the ferroptosis-related genes (202/259, 78%) were differentially expressed between breast cancer tumor tissues and adjacent non-tumorous tissues, including 29 of them which were significantly correlated with OS in the univariate Cox regression analysis (**Figure 2A**). A total of 29 prognostic ferroptosis-related DEGs were identified by the criteria of FDR < 0.05 (**Figures 2B,C**). The heatmap in **Figure 2B** depicts the expression level and distribution of those 29 prognostic ferroptosis-related DEGs. The forest plot of **Figure 2C** shows the results of univariate Cox regression analysis of these 29 genes. The results demonstrated that 13 of these genes played protective roles in breast cancer patients with HR less than 1 (GPX4, TP63, BRD4, JUN, CHMP6, ACSF2, FLT3, SOCS1, BAP1, IFNG, EGLN2, SLC1A4, IL33), while the other 16 genes (GCLC, CISD1, PROM2, CS, EMC2, G6PD, PIK3CA, SLC38A1, ALOX15, ANO6, MTDH, PANX1, TXNRD1, BNIP3, SLC7A5, NGB) were risk factors with HR more than 1. We further used the STRING database to detect the protein–protein interaction network among those 29 genes (**Figure 2D**). The interaction network indicated that JUN, FLT3, PIK3CA, G6PD, and GPX4 were the hub genes. The correlation network of the selected candidate genes is shown in **Figure 2E**, among which different colors represented different degrees of the correlation coefficient.

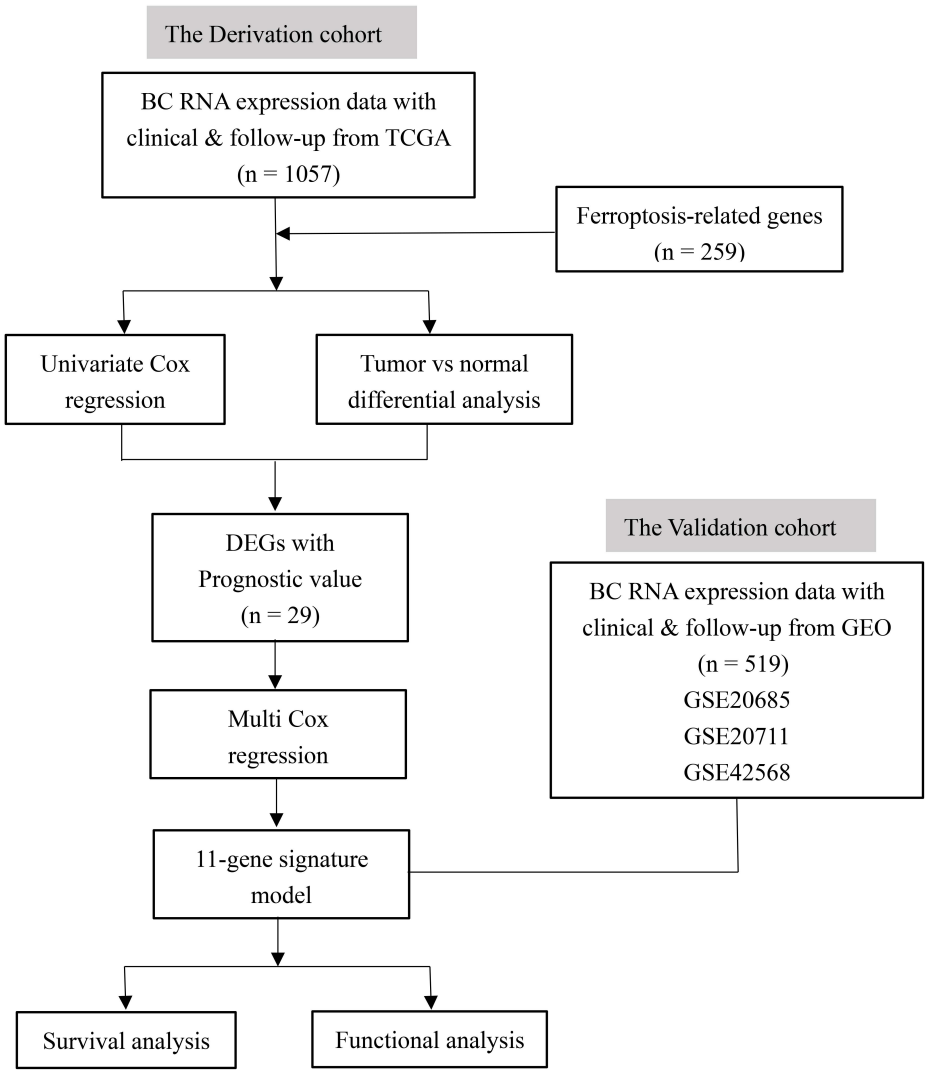

FIGURE 1 | The flowchart of construction and validation of data collection and analysis.

Construction of the Ferroptosis-Related Prognostic Signature in TCGA Cohort

Multi-Cox regression analysis was applied to construct an 11-gene prognostic model using the expression of 29 genes mentioned above. The risk score could be calculated by the following formula: risk score = 0.366 * expression level of CISD1 + (–0.272) * expression level of TP63 + (–0.499) * expression level of BRD4 + 0.290 * expression level of PROM2 + 0.277 * expression level of EMC2 + 0.217 * expression level of G6PD + 0.294 * expression level of PIK3CA + (–0.179) * expression level of FLT3 + (–0.666) * expression level of IFNG + 0.500 * expression level of ANO6 + (–0.275) * expression level of SLC1A4. We stratified all breast cancer patients in the TCGA cohort into the high-risk group (n = 528) and low-risk (n = 529) group according to the median value of risk scores (**Figure 3A**). In addition, **Figure 3B** reflects that patients with high-risk scores were more likely to die earlier than those with-low risk scores. Consistently, the Kaplan–Meier survival curve in **Figure 3C** shows that OS of breast cancer patients in the high-risk group was significantly worse than those in the low-risk group (p = 4.919e–10). We further evaluated the predictive efficacy of the prognostic signature for OS in breast cancer patients by the time-dependent ROC curves, and the area under the curve (AUC) reached 0.700 at 1 year, 0.749 at 2 years and 0.720 at 3 years (**Figure 3D**).

Validation of the Ferroptosis-Related Prognostic Signature in GEO Cohort

In order to test the robustness of the 11-gene model constructed from the TCGA cohort, GEO cohorts (GSE20685, GSE20711, and GSE42568) from the GEO database were used for external validation. The patients from the GEO cohort were divided into the high-risk group and low-risk group by the median value of risk scores calculated with the same formula from the TCGA

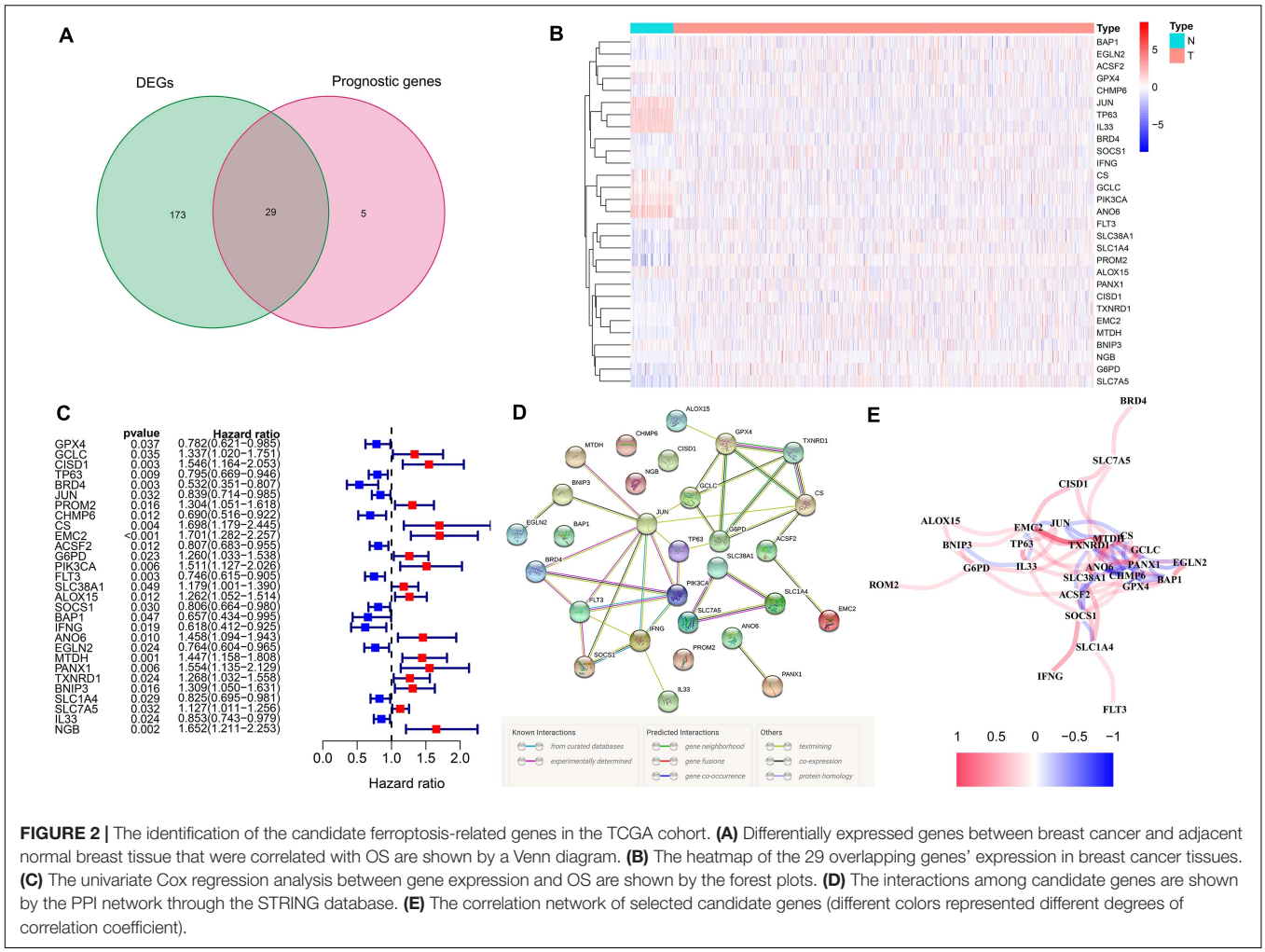

FIGURE 2 | The identification of the candidate ferroptosis-related genes in the TCGA cohort. **(A)** Differentially expressed genes between breast cancer and adjacent normal breast tissue that were correlated with OS are shown by a Venn diagram. **(B)** The heatmap of the 29 overlapping genes' expression in breast cancer tissues. **(C)** The univariate Cox regression analysis between gene expression and OS are shown by the forest plots. **(D)** The interactions among candidate genes are shown by the PPI network through the STRING database. **(E)** The correlation network of selected candidate genes (different colors represented different degrees of correlation coefficient).

cohort (**Figure 4A**). Similar to the results that were obtained from the TCGA cohort, in the GEO validation cohort, patients with high-risk scores had a higher probability of death earlier than the low-risk group (**Figure 4B**). Likewise, the Kaplan–Meier survival curve showed that OS of breast cancer patients in the high-risk group was worse than that in the low-risk group with statistical significance (p = 5.431e-04). In addition, the AUC of the 11-gene signature was 0.709 at 1 year, 0.671 at 2 years, and 0.661 at 3 years (**Figures 4C, D**).

Independent Prognostic Value of the 11-Gene Ferroptosis-Related Prognostic Signature

Subsequently, we extracted the available clinical variables in the TCGA database and GEO database. Univariate and multivariate Cox regression analyses were used to detect whether the risk score could play an independent prognostic role in predicting OS of breast cancer. **Figures 5A,C** show that the risk score was an independent prognostic predictor for OS in both TCGA cohort (HR = 1.403, 95% CI = 1.261–1.560, $P < 0.001$) and GEO cohort (GSE20685: HR = 1.061, 95% CI = 1.027–1.097, $P < 0.001$). Multivariate Cox regression further proved that our risk score could work as an independent predictor for OS in both cohorts (TCGA: HR = 1.412, 95% CI = 1.267–1.574, $P < 0.001$; GEO: HR = 1.055, 95% CI = 1.021–1.091, $P = 0.002$) (**Figures 5B,D**).

Functional Analyses of the Prognostic Signature-Related Biological Pathways

In order to elucidate the underlying biological functions and pathways that were correlated with our 11-gene prognostic signature-related model, we performed GO enrichment and KEGG pathway analyses by analyzing the DEGs between the high-risk and low-risk groups. Interestingly, results showed that the DEGs from the TCGA cohort were obviously enriched in many immune-related biological processes in GO enrichment (**Figures 6A,B**). The representing immune-related biological processes and molecular functions include immunoglobulin-mediated immune response, lymphocyte-mediated immunity, humoral immune response, adaptive immune response, immune response-activating cell surface receptor signaling pathway, and immune response-activating signal transduction. Similarly, the KEGG pathway analyses also indicated immune-related pathways

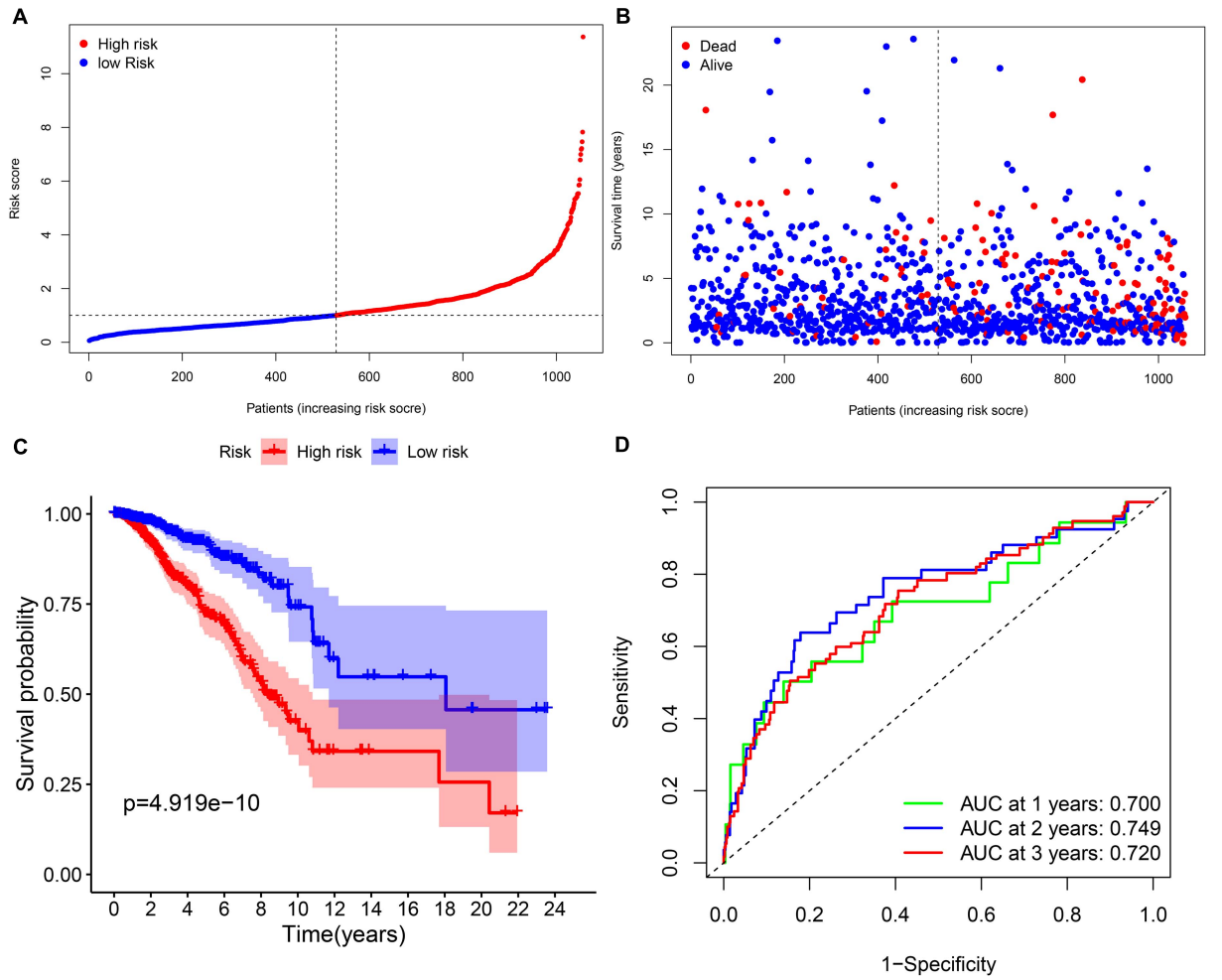

FIGURE 3 | The prognostic analysis of the 11-gene signature model in the TCGA cohort. **(A)** The distribution and median value of the risk scores in the TCGA cohort. **(B)** The distribution of OS, OS status, and risk score in the TCGA cohort. **(C)** The Kaplan–Meier curves for the OS of patients in the TCGA cohort which was divided into high-risk group and low-risk group. **(D)** The AUC of time-dependent ROC curves was used to verify the prognostic performance of the risk score in the TCGA cohort.

such as primary immunodeficiency, T cell receptor signaling pathway, PD-L1 expression and PD-1 checkpoint pathway in cancer, Th1 and Th2 cell differentiation, and Th17 cell differentiation (**Figures 6C,D**).

In order to further explore the correlation between the 11-gene signature risk score and immune status, we used ssGSEA to quantify the enrichment scores of different immune cell subgroups, related functions, or pathways. As we expected, the contents of the antigen presentation process showed statistical difference between the high-risk group and low-risk group in the TCGA cohort, including aDCs, B cells, CD8 + T cells, DCs, iDCs, macrophages, mast cells, NK cells, pDCs, T helper cells, Tfh, Th1 cells, Th2 cells, TIL, APC co-inhibition, cytokine–cytokine receptor (CCR), checkpoint, cytolytic activity, HLA, T cell co-inhibition, and T cell co-stimulation (**Figure 7**). In particular, the scores of Th1 cells, Th2 cells, and T cell co-inhibition and co-stimulation were reflected significantly different between the high-risk group and low-risk group; this finding could correspond with the above enrichment in KEGG analysis.

Effects of Erastin on the Expression Levels of 11 Core Prognostic Genes in Breast Cancer Cell Lines *in vitro*

Breast cancer cell lines MDA-MB-231 and MCF-7 were then treated with ferroptosis inducer erastin in order to explore the role of the 11-core prognostic genes. In **Figure 8A,B**, the cell viability assay showed that the ferroptosis inducer erastin could inhibit the proliferation of MDA-MB-231 and MCF-7 in a dose-dependent manner. The experiment results showed that the growth inhibitory effects of erastin in both breast cancer cell lines were statistically significant when the concentration was over 20 μM. The growth of MDA-MB-231 and MCF-7 was almost completely inhibited when the erastin treatment concentration reached 40 μM. The correspondence images of

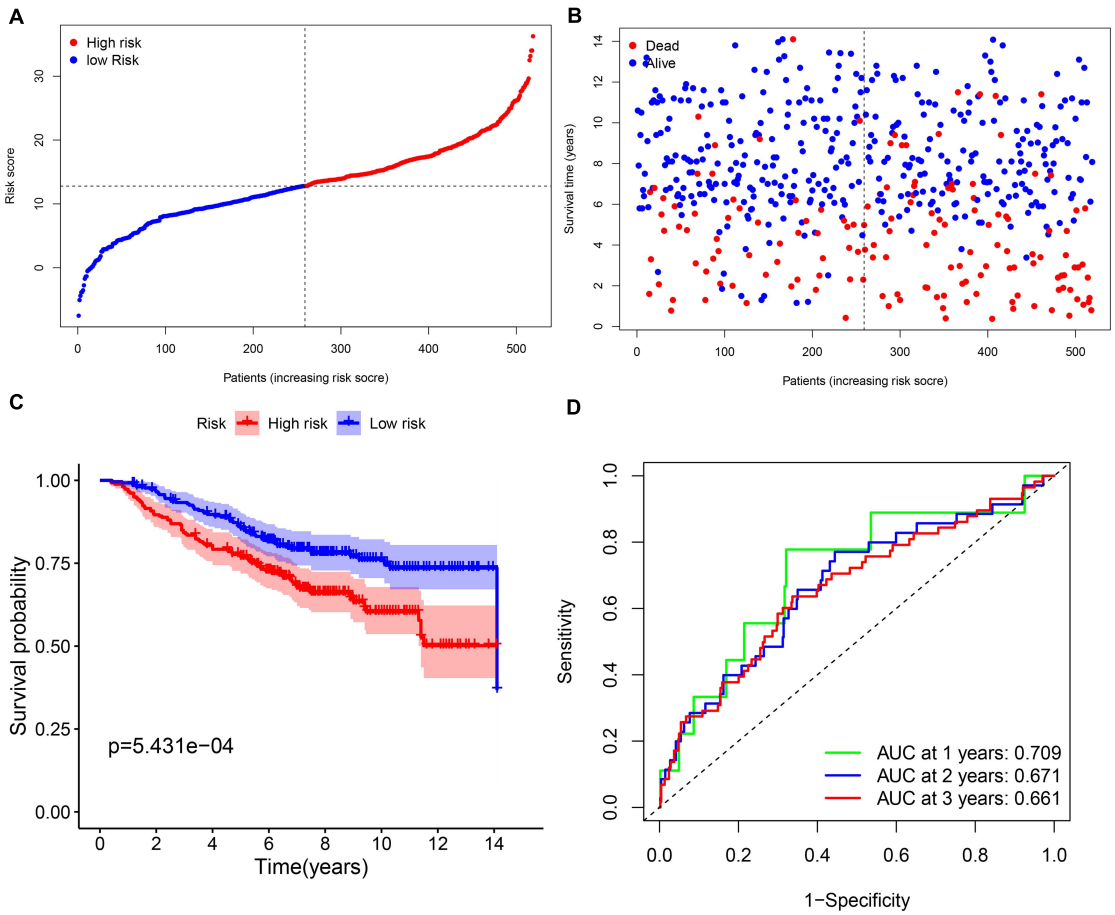

FIGURE 4 | The validation of the 11-gene signature model in the GEO cohort. **(A)** The distribution and median value of the risk scores in the GEO cohort. **(B)** The distribution of OS, OS status, and risk score in the GEO cohort. **(C)** The Kaplan–Meier curves for the OS of patients in the GEO cohort which was divided into high-risk group and low-risk group. **(D)** The AUC of time-dependent ROC curves in the GEO cohort.

MCF-7's cell viability and MDA-MB-231 treated by erastin are found in **Supplementary Figure 1**. In addition, more cell lines such as MCF-10A, BT-549, and SUM-159 were used to test erastin's inhibition on cell viability. Similar results are found in **Supplementary Figure 2**. Later, we detected that erastin treatment at 10, 20, and 40 μM could significantly increase ROS accumulation by FACS (**Figures 8C,D**). Finally, RT-PCR was used to investigate the expression of 11-core prognostic genes in MDA-MB-231 and MCF-7 after being treated with erastin of 20 μM for 48 h. Results showed that mRNA expression levels of six genes (EMC2, G6PD, FLT3, IFNG, ANO6, and SLC1A4) were increased and three genes (CISD1, TP63, and BRD4) were decreased after erastin treatment. However, the increase of PIK3CA was not statistically significant in MCF-7-erastin cells and PROM2 was barely decreased in MDA-MB-231 cells (**Figures 8E,F**). The results indicated that EMC2, G6PD, FLT3, IFNG, ANO6, and SLC1A4 were positively correlated with ferroptosis while CISD1, TP63, and BRD4 were negatively correlated with ferroptosis in breast cancer. Western blotting of G6PD, PIK3CA, and BRD4 was performed to test future PCR results (**Figure 8G**). Our results showed that the protein alteration was consistent with the PCR result except G6PD in MCF-7, which indicated that our 11-gene model could be verified by cell line experiment. Since G6PD produces NADPH which is a scavenger of ROS, we also overexpressed G6PD in MDA-MB-231 to detect erastin sensitivity. The results suggested that overexpression of G6PD would result in decrease in the sensitivity of cells to erastin (**Supplementary Figure 3**). In addition, more cell lines such as MCF10A, BT549, and SUM159 were used to detect our 11-gene alteration after adding erastin; similar results are found in **Supplementary Figure 4**. This result indicated the different stages of breast cancer cell lines with ferroptotic inducers had the same trend.

DISCUSSION

In our study, we explored a total of 259 well-defined ferroptosis-related genes in breast cancer tissues and their correlations with OS. A novel 11-gene ferroptosis-related prognostic model was constructed and validated by the external cohort. We further did

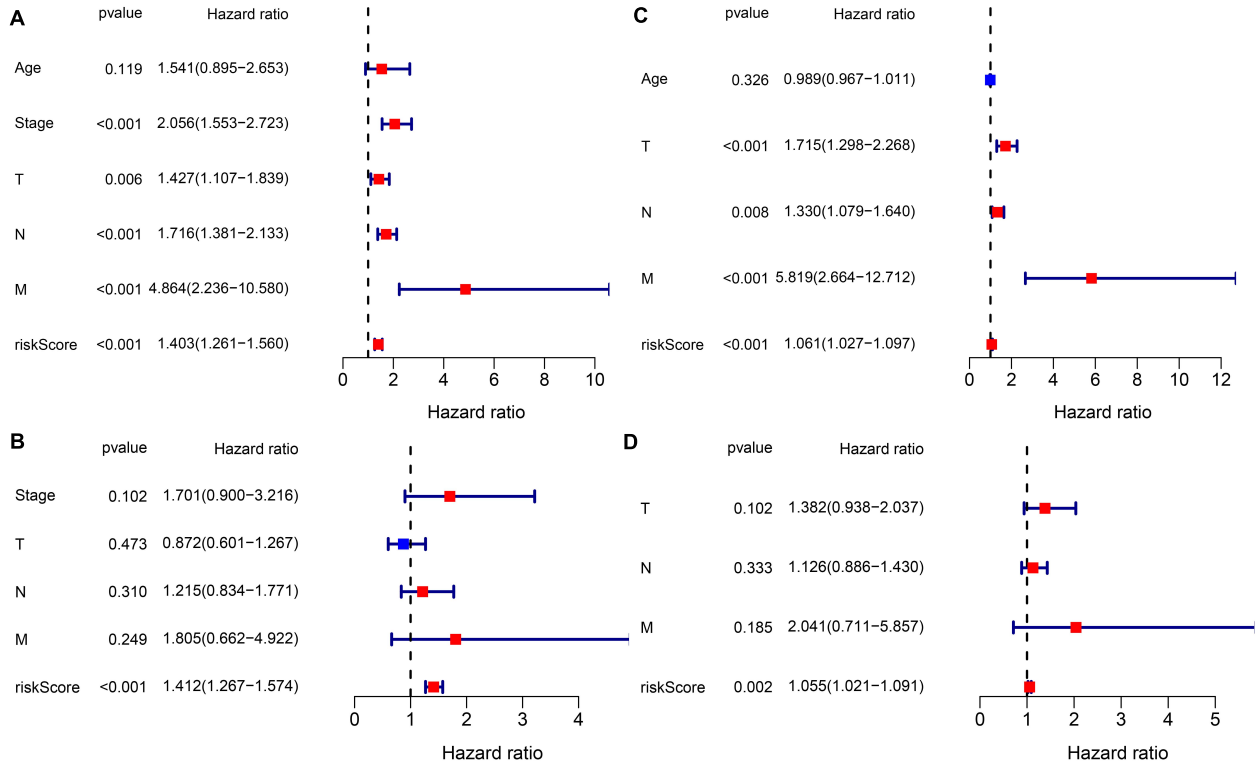

FIGURE 5 | Results of the Cox regression analyses regarding OS in the TCGA derivation cohort and GEO validation cohort. **(A)** The univariate Cox regression analyses regarding OS in the TCGA derivation cohort. **(B)** The multivariate Cox analyses regarding OS in the TCGA derivation cohort. **(C)** The univariate Cox regression analyses regarding OS in the GEO validation cohort. **(D)** The multivariate Cox analyses regarding OS in the GEO validation cohort.

functional analyses and surprisingly found some immune-related biological processes.

A few studies have discovered that certain drugs might cause ferroptosis in breast cancer (Ma et al., 2016; Yu et al., 2019a,b); however, there are still few studies on whether there exist specific ferroptosis-related genes in regulating the progression of breast cancer. The relationship between ferroptosis and the prognosis of breast cancer remains to be clarified. Interestingly, 78% ferroptosis-related genes were differentially expressed between breast cancer tumor tissue and adjacent non-tumorous tissues, including 29 of them which were significantly correlated with OS in the univariate Cox regression analysis. These results fully demonstrated that ferroptosis might play an important role in breast cancer and the possibility of using these ferroptosis-related genes to establish a prognostic model.

Our 11-gene prognostic signature-related model includes CISD1, TP63, BRD4, PROM2, EMC2, G6PD, PIK3CA, FLT3, IFNG, ANO6, and SLC1A4. These genes could be classified into three subgroups, including drivers (EMC2, G6PD, PIK3CA, FLT3, IFNG, ANO6) which were genes that promote ferroptosis, suppressors (CISD1, TP63, BRD4, PROM2) which were genes that prevent ferroptosis, and markers (SLC1A4) which were genes that indicated the occurrence of ferroptosis. By using an shRNA library that targets plenty of genes which encode mitochondrial proteins, EMC2 (ER membrane protein complex subunit 2, also referred as TTC35) has been identified to play an important role in erastin-induced ferroptosis in HT-1080 fibrosarcoma cells (Dixon et al., 2012). G6PD (glucose-6-phosphate dehydrogenase) is involved in the pentose phosphate pathway of energy metabolism and has been verified to prevent erastin-induced ferroptosis in human lung adenocarcinoma cells while it was knocked down by the corresponding shRNA (Dixon et al., 2012). Our result also showed that overexpression of G6PD can reduce sensitivity to erastin in MDA-MB-231. We considered the increase in G6PD as a compensatory adjustment to erastin-induced ferroptosis which is consistent with their study. Kang et al. demonstrated that both FLT3 and PIK3CA inhibitors play protective roles against glutamate-induced oxidative stress and prove the involvement of lipid peroxidation-mediated ferroptosis (Kang et al., 2014). In addition, IFNG releases from CD8 + T cells could downregulate two subunits of glutamate-cystine antiporter system xc-, restrain tumor cell cystine uptake, and finally promote tumor cell lipid peroxidation and ferroptosis (Wang et al., 2019). German scientists discovered that ANO6 is activated during erastin and RSL3-induced ferroptosis; however, inhibition of ANO6 could also lead to cell death. They concluded that the activation of ANO6 might be an important component during ferroptosis cell death and induce cell death in cancer cells (Ousingsawat et al., 2019). In contrast, CISD1, TP63, BRD4, and PROM2 were all genes that prevent ferroptosis. It has been explored that genetic inhibition of CISD1 (CDGSH iron sulfur domain 1, also termed mitoNEET) could increase

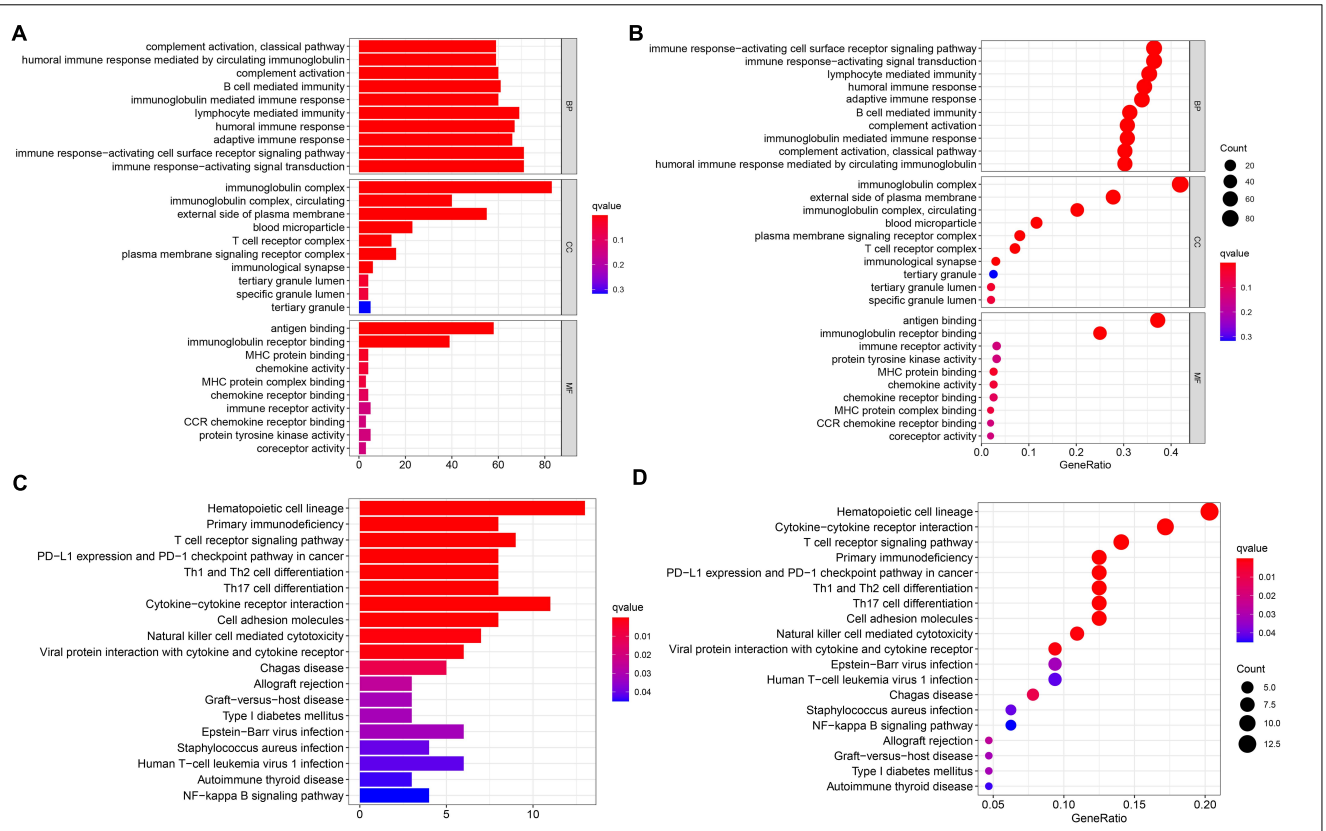

FIGURE 6 | Results of GO and KEGG analyses in the TCGA cohort. **(A,B)** The significant GO enrichment in the TCGA cohort. **(C,D)** The significant KEGG pathways in the TCGA cohort.

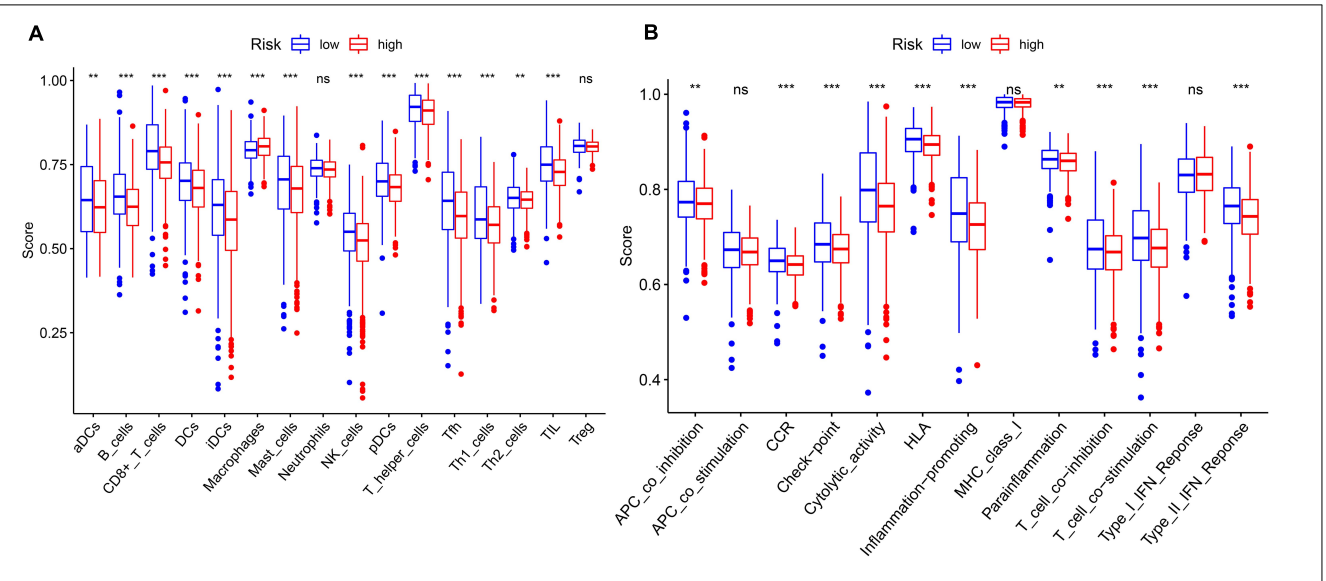

FIGURE 7 | The ssGSEA scores between different risk groups in the TCGA cohort. **(A)** The scores of 16 immune cells in the boxplot. **(B)** The 13 immune-related functions in boxplots. The adjusted *P*-values are shown in the analyses. ns, not significant; $^{**}P < 0.01$; $^{***}P < 0.001$.

iron-mediated intramitochondrial lipid peroxidation, resulting in erastin-induced ferroptosis. On the contrary, pioglitazone stabilizes the iron sulfur cluster of CISD1 and inhibits the mitochondrial iron uptake as well as lipid peroxidation which finally leads to ferroptosis (Yuan et al., 2016). TP63 has been validated to inhibit oxidative stress-induced cell death

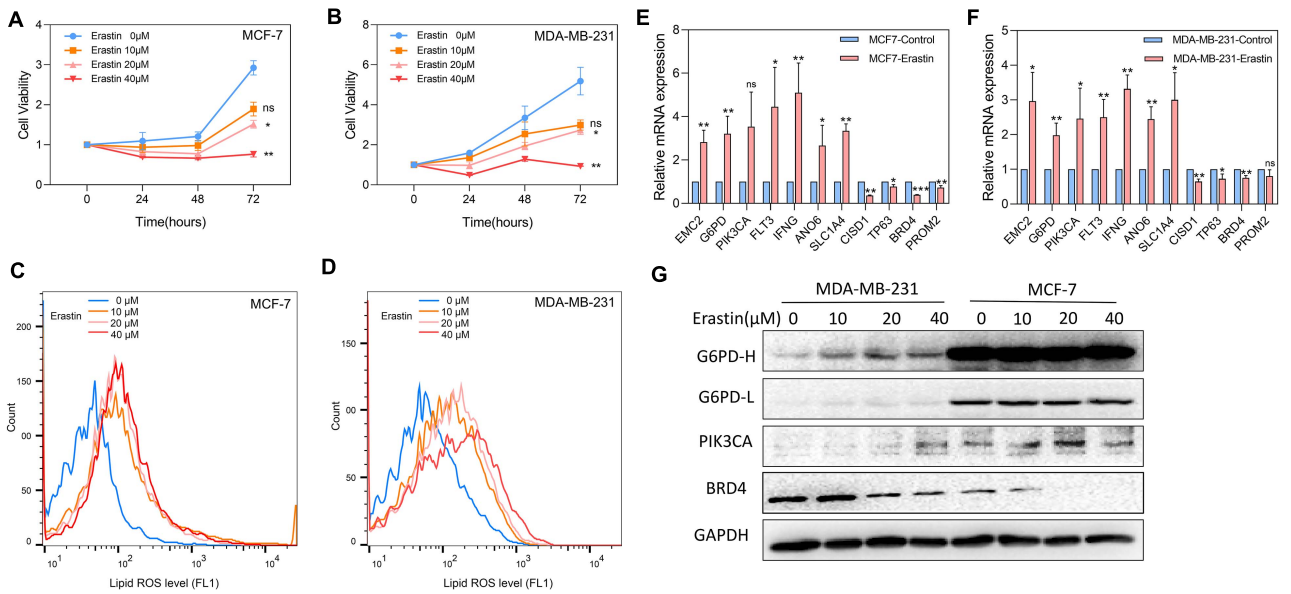

FIGURE 8 | Effects of ferroptosis inducer on expression levels of 11-core prognostic genes in breast cancer cell lines *in vitro*. **(A,B)** The cell viability of MCF-7 **(A)** and MDA-MB-231 **(B)** treated by erastin was tested by CCK8 assay. **(C,D)** Lipid peroxidation of MCF-7 **(C)** and MDA-MB-231 **(D)** treated by erastin was assessed by flow cytometry after C11-BODIPY staining. **(E,F)** The expression changes of 11-core prognostic genes in MCF-7 **(E)** and MDA-MB-231 **(F)** after being treated with 20 μM erastin were detected by real time-PCR. **(G)** The expression changes of G6PD, PIK3CA, and BRD4 genes in MDA-MB-231 and MCF-7 after being treated with erastin for 48 h were detected by western blot (G6PD-H means high exposure, G6PD-L means short exposure). * $P < 0.05$; ** $P < 0.01$; *** $P < 0.001$.

ferroptosis through cooperating with the BCL-2 family to promote clonogenic survival (Wang et al., 2017). In addition, after knockdown of BRD4 or under (+)-JQ1 (an inhibitor of the tumor-driver bromodomain protein BRD4), the expressions of ferroptosis-associated genes GPX4, SLC7A11, and SLC3A2 are downregulated. It indicated that knockdown or inhibition of BRD4 would induce ferroptosis *via* ferritinophagy or regulating ferroptosis-associated genes through epigenetic repression of BRD4 (Sui et al., 2019). Furthermore, Brown explored that PROM2 could facilitate ferroptosis resistance in mammary epithelial and breast cancer cell lines; in detail, PROM2 promotes the formation of ferritin-containing multivesicular bodies and exosomes which transport iron out of the cell, therefore, inhibiting ferroptosis (Brown et al., 2019). Besides, SLC1A4 was also indicated to correlate with the occurrence of ferroptosis (Dixon et al., 2014). These genes are all associated with the promotion or prevention of ferroptosis in different cancers through multiple mechanisms; however, whether these genes play a vital role in the prognosis of breast cancer patients through influencing ferroptosis remains unclear.

There are already some researches surrounding the ferroptosis and cancer progression mechanisms in the recent years; however, the potential relationship between ferroptosis and cancer immunity remains to be elucidated. In our study, we performed GO enrichment and KEGG pathway analyses by analyzing the DEGs between the high-risk and low-risk groups based on our 11-gene model. Interestingly, we discovered some immune-related biological processes in GO enrichment. These gene enrichment analyses suggested that our ferroptosis might be closely related to the immune response of breast cancer. Besides, our results also revealed that breast cancer patients in the high-risk group had decreased infiltration degrees of B cells, $CD8^+$ T cells, dendritic cells, T helper cells, Tfh cells, Th1 cells, Th2 cells, and TIL. The risk score formed by our 11-gene signature is negatively correlated with immune cell infiltration, suggesting that this model might be a predictor of local immune response in the tumor bed. At present, studies have shown that tumor-infiltrating B cells express and secrete antibodies which could promote tumor cell lysis and apoptosis (Ruffell et al., 2012). The direct and indirect cytotoxic effects of $CD8^+$ T cells support the findings that CD8 + T cell infiltration is associated with good survival outcomes (Mahmoud et al., 2011; Matsumoto et al., 2016). There has been a discovery that neutrophil infiltration is also an independent prognostic factor which correlated with better overall survival in breast cancer (Zeindler et al., 2019). However, the infiltration level of neutrophil in the low-risk group and high-risk group of our model states no statistical significance. It is well known that dendritic cell-mediated T cell activation is a key step in antitumor immunity. Studies have found that the functional defects of dendritic cells in patients with early breast cancer might be an important factor in tumor progression (Satthaporn et al., 2004). Consistent with our research, in the ferroptosis-related model we constructed, the proportion of dendritic cells in breast cancer patients in the high-risk group was significantly reduced in the low-risk group. In summary, the imbalance of immune infiltration and immune response dysfunction in the surrounding environment of the tumor may be at least partially attributed to the high-risk score.

Besides, there also exist some limitations in our study. Firstly, our ferroptosis-related prognostic model was constructed and

validated in public databases with retrospective data. We will further use our prospective multicenter clinical data for further verification in the future. Secondly, we only used ferroptosis-related genes to construct this prognostic model; therefore, many other hot biomarkers might be excluded. Also, the correlation between our model and immune-related pathways needed further experimental validation.

CONCLUSION

In conclusion, a novel ferroptosis-related gene model can be used for prognostic prediction in breast cancer. New ferroptosis-related genes might be used for breast cancer targeting therapy in the future.

DATA AVAILABILITY STATEMENT

The datasets supporting the results and conclusions of this study were downloaded from the TCGA (http://tcga-data.nci.nih.gov/tcga/) and GEO (http://www.ncbi.nlm.nih.gov/geo/), and we thank The Cancer Genome Atlas (TCGA) and Gene Expression Omnibus (GEO) for providing transcriptomics and clinicopathological data.

AUTHOR CONTRIBUTIONS

LZ: collection and assembly of data, data analysis and interpretation, manuscript writing, and methodology and software. QT: collection and assembly of data, data analysis and interpretation, and manuscript writing and editing. SJ and HG: data analysis, manuscript writing and interpretation. SY and YZ: manuscript writing and project administration. YY: manuscript writing. YR: conception and design. JH and BW: conception and design, supervision and editing. All authors: article writing and final approval of article.

FUNDING

This study was supported by grants from the National Natural Science Fund of China (Nos. 81702633 and 81970365).

SUPPLEMENTARY MATERIAL

The Supplementary Material for this article can be found online at: https://www.frontiersin.org/articles/10.3389/fcell.2021.670184/full#supplementary-material

Supplementary Figure 1 | The images about MCF7 cell viability and MDA-MB-231 treated by erastin.

Supplementary Figure 2 | The cell viability of MCF-10A **(A)**, BT-549 **(B)**, and SUM-159 **(C)** treated by erastin was tested by CCK8 assay.

Supplementary Figure 3 | The transfection of overexpression plasmid G6PD in MDA-MB-231 and the cell viability test. **(A)** The transfection efficiency was tested by western blot. **(B)** The viability of MDA-MB-231 con and MDA-MB-231 overexpression G6PD were tested by CCK8 assay.

Supplementary Figure 4 | Effects of ferroptosis inducer on expression levels of 11 core prognostic genes in breast cancer cell lines *in vitro*. **(A–C)** The expression changes of 11 core prognostic genes in MCF-10A **(A)**, BT-549 **(B)**, and SUM-159 **(C)** after treated with 20μM erastin were detected by real time-PCR. **(D)** The expression changes of G6PD, PIK3CA, and BRD4 genes in MCF-10A, BT-549, and SUM-159 after treated with erastin for 48 h was detected by western blot.

REFERENCES

Bray, F., Ferlay, J., Laversanne, M., Brewster, D. H., Gombe Mbalawa, C., Kohler, B., et al. (2015). Cancer incidence in five continents: inclusion criteria, highlights from volume X and the global status of cancer registration. *Int. J. Cancer* 137, 2060–2071. doi: 10.1002/ijc.29670

Brown, C. W., Amante, J. J., Chhoy, P., Elaimy, A. L., Liu, H., Zhu, L. J., et al. (2019). Prominin2 drives ferroptosis resistance by stimulating iron export. *Dev. Cell* 51, 575–586. doi: 10.1016/j.devcel.2019.10.007

Christofferson, D. E., and Yuan, J. (2010). Necroptosis as an alternative form of programmed cell death. *Curr. Opin. Cell Biol.* 22, 263–268. doi: 10.1016/j.ceb.2009.12.003

Dixon, S. J., Lemberg, K. M., Lamprecht, M. R., Skouta, R., Zaitsev, E. M., Gleason, C. E., et al. (2012). Ferroptosis: an iron-dependent form of nonapoptotic cell death. *Cell* 149, 1060–1072. doi: 10.1016/j.cell.2012.03.042

Dixon, S. J., Patel, D. N., Welsch, M., Skouta, R., Lee, E. D., Hayano, M., et al. (2014). Pharmacological inhibition of cystine-glutamate exchange induces endoplasmic reticulum stress and ferroptosis. *Elife* 3:e02523. doi: 10.7554/eLife.02523

Emens, L. A. (2018). Breast cancer immunotherapy: facts and hopes. *Clin. Cancer. Res.* 24, 511–520. doi: 10.1158/1078-0432.CCR-16-3001

Harbeck, N., Penault-Llorca, F., Cortes, J., Gnant, M., Houssami, N., Poortmans, P., et al. (2019). Breast cancer. *Nat. Rev. Dis. Primers* 5:66. doi: 10.1038/s41572-019-0111-2

Kang, Y., Tiziani, S., Park, G., Kaul, M., and Paternostro, G. (2014). Cellular protection using Flt3 and PI3Kα inhibitors demonstrates multiple mechanisms of oxidative glutamate toxicity. *Nat. Commun.* 5:3672. doi: 10.1038/ncomms4672

Liang, C., Zhang, X., Yang, M., and Dong, X. (2019). Recent progress in ferroptosis inducers for cancer therapy. *Adv. Mater.* 31:e1904197. doi: 10.1002/adma.201904197

Ma, S., Henson, E. S., Chen, Y., and Gibson, S. B. (2016). Ferroptosis is induced following siramesine and lapatinib treatment of breast cancer cells. *Cell Death Dis.* 7:e2307. doi: 10.1038/cddis.2016.208

Mahmoud, S. M., Paish, E. C., Powe, D. G., Macmillan, R. D., Grainge, M. J., Lee, A. H., et al. (2011). Tumor-infiltrating CD8+ lymphocytes predict clinical outcome in breast cancer. *J. Clin. Oncol.* 29, 1949–1955. doi: 10.1200/JCO.2010.30.5037

Matsumoto, H., Thike, A. A., Li, H., Yeong, J., Koo, S. L., Dent, R. A., et al. (2016). Increased CD4 and CD8-positive T cell infiltrate signifies good prognosis in a subset of triple-negative breast cancer. *Breast Cancer Res. Treat.* 156, 237–247. doi: 10.1007/s10549-016-3743-x

Ousingsawat, J., Schreiber, R., and Kunzelmann, K. (2019). TMEM16F/Anoctamin 6 in ferroptotic cell death. *Cancer* 11:625. doi: 10.3390/cancers11050625

Qiao, J., Chen, Y., Mi, Y., Jin, H., Huang, T., Liu, L., et al. (2020). NR5A2 synergizes with NCOA3 to induce breast cancer resistance to BET inhibitor by upregulating NRF2 to attenuate ferroptosis. *Biochem. Biophys. Res. Commun.* 530, 402–409. doi: 10.1016/j.bbrc.2020.05.069

Ruffell, B., Au, A., Rugo, H. S., Esserman, L. J., Hwang, E. S., and Coussens, L. M. (2012). Leukocyte composition of human breast cancer. *Proc. Natl. Acad. Sci. U.S.A.* 109, 2796–2801. doi: 10.1073/pnas.1104303108

Satthaporn, S., Robins, A., Vassanasiri, W., El-Sheemy, M., Jibril, J. A., Clark, D., et al. (2004). Dendritic cells are dysfunctional in patients with operable breast cancer. *Cancer Immunol. Immunother.* 53, 510–518. doi: 10.1007/s00262-003-0485-5

Sui, S., Zhang, J., Xu, S., Wang, Q., Wang, P., and Pang, D. (2019). Ferritinophagy is required for the induction of ferroptosis by the bromodomain protein BRD4 inhibitor (+)-JQ1 in cancer cells. *Cell Death Dis.* 10:331. doi: 10.1038/s41419-019-1564-7

Wang, G. X., Tu, H. C., Dong, Y., Skanderup, A. J., Wang, Y., Takeda, S., et al. (2017). ΔNp63 Inhibits oxidative stress-induced cell death, including ferroptosis, and cooperates with the BCL-2 family to promote clonogenic survival. *Cell Rep.* 21, 2926–2939. doi: 10.1016/j.celrep.2017.11.030

Wang, W., Green, M., Choi, J. E., Gijón, M., Kennedy, P. D., Johnson, J. K., et al. (2019). CD8+ T cells regulate tumour ferroptosis during cancer immunotherapy. *Nature* 569, 270–274. doi: 10.1038/s41586-019-1170-y

Yagoda, N., von Rechenberg, M., Zaganjor, E., Bauer, A. J., Yang, W. S., Fridman, D. J., et al. (2007). RAS-RAF-MEK-dependent oxidative cell death involving voltage-dependent anion channels. *Nature* 447, 864–868. doi: 10.1038/nature05859

Yu, H., Yang, C., Jian, L., Guo, S., Chen, R., Li, K., et al. (2019a). Sulfasalazine-induced ferroptosis in breast cancer cells is reduced by the inhibitory effect of estrogen receptor on the transferrin receptor. *Oncol. Rep.* 42, 826–838. doi: 10.3892/or.2019.7189

Yu, M., Gai, C., Li, Z., Ding, D., Zheng, J., Zhang, W., et al. (2019b). Targeted exosome-encapsulated erastin induced ferroptosis in triple negative breast cancer cells. *Cancer Sci.* 110, 3173–3182. doi: 10.1111/cas.14181

Yuan, H., Li, X., Zhang, X., Kang, R., and Tang, D. (2016). CISD1 inhibits ferroptosis by protection against mitochondrial lipid peroxidation. *Biochem. Biophys. Res. Commun.* 478, 838–844. doi: 10.1016/j.bbrc.2016.08.034

Zeindler, J., Angehrn, F., Droeser, R., Däster, S., Piscuoglio, S., Ng, C. K. Y., et al. (2019). Infiltration by myeloperoxidase-positive neutrophils is an independent prognostic factor in breast cancer. *Breast Cancer Res. Treat.* 177, 581–589. doi: 10.1007/s10549-019-05336-3

Zhou, N., and Bao, J. (2020). FerrDb: a manually curated resource for regulators and markers of ferroptosis and ferroptosis-disease associations. *Database* 2020:baaa021. doi: 10.1093/database/baaa021

Conflict of Interest: The authors declare that the research was conducted in the absence of any commercial or financial relationships that could be construed as a potential conflict of interest.

frontiers in Cell and Developmental Biology

ORIGINAL RESEARCH
published: 07 July 2021
doi: 10.3389/fcell.2021.684259

Development and Validation of a Ferroptosis-Related Gene Signature for Overall Survival Prediction in Lung Adenocarcinoma

*Qi Tian[1], Yan Zhou[1], Lizhe Zhu[2], Huan Gao[1] and Jin Yang[1]**

[1] Department of Medical Oncology, The First Affiliated Hospital of Xi'an Jiaotong University, Xi'an, China, [2] Department of Breast Surgery, The First Affiliated Hospital of Xi'an Jiaotong University, Xi'an, China

Background: Ferroptosis is an iron-dependent programmed cell death process. Recent studies have found that ferroptosis inducers hold promising potential in the treatment of lung adenocarcinoma (LUAD). However, the comprehensive analysis about the prognostic value of ferroptosis-related genes in LUAD remains to be elucidated.

Methods: The RNA sequencing data and corresponding clinical information were obtained from The Cancer Genome Atlas (TCGA) and Gene Expression Omnibus (GEO) databases. A total of 259 ferroptosis-related genes were extracted from FerrDb website. The ferroptosis-related prognostic signature was developed by least absolute shrinkage and selection operator (LASSO) Cox regression analysis in TCGA LUAD cohort, and then validated by 5 independent GEO cohorts. Gene Ontology (GO), Kyoto Encyclopedia of Genes and Genomes (KEGG), and gene set enrichment analysis (GSEA) were performed to identify the difference in biological processes and functions between different risk groups. The expression levels of core prognostic genes were then verified in LUAD samples by immunohistochemistry (IHC) and erastin-treated LUAD cell lines by real-time polymerase chain reaction (PCR). The potential roles of GPX2 and DDIT4 as ferroptosis drivers in LUAD cell line were further confirmed by *in vitro* experiments.

Results: A total of 20 intersecting genes between 70 ferroptosis-related DEGs and 45 potential prognostic genes were obtained for LASSO Cox regression analysis. The ferroptosis-related prognostic signature was developed by 7 core prognostic DEGs, and stratified LUAD patients into two risk groups. Kaplan-Meier analysis showed that the overall survival (OS) of LUAD patients in the high-risk group was significantly worse than that of the low-risk group. External validation of 5 independent GEO cohorts further confirmed that the ferroptosis-related prognostic signature was an ideal biomarker for predicting the survival of LUAD patients. Significant enrichment of fatty acid metabolism and cell cycle-related pathways were found in different risk groups. The expression patterns of 7 core prognostic genes in LUAD and adjacent normal lung tissues were validated by IHC, which was almost consistent with the results from public database. Furthermore, the changes related to cell cycle and ferroptosis after erastin treatment

OPEN ACCESS

Edited by:
Maryam Mehrpour, Université Paris Descartes, France

Reviewed by:
Min Yu, Hangzhou Medical College, China
Junjie Kong, Shandong Provincial Hospital, China

****Correspondence:***
Jin Yang
yangjin@xjtu.edu.cn

Specialty section:
This article was submitted to Molecular and Cellular Oncology, a section of the journal Frontiers in Cell and Developmental Biology

Received: *23 March 2021*
Accepted: *18 June 2021*
Published: *07 July 2021*

Citation:
Tian Q, Zhou Y, Zhu L, Gao H and Yang J (2021) Development and Validation of a Ferroptosis-Related Gene Signature for Overall Survival Prediction in Lung Adenocarcinoma. Front. Cell Dev. Biol. 9:684259. doi: 10.3389/fcell.2021.684259

were also validated in LUAD cell lines. In addition, silencing GPX2 or DDIT4 could partially reverse the erastin-induced ferroptosis.

Conclusion: In summary, the ferroptosis-related prognostic signature based on 7 core prognostic DEGs indicated superior predictive performance of LUAD patients. Targeting ferroptosis holds potential to be a therapeutic alternative for LUAD.

Keywords: lung adenocarcinoma, ferroptosis, prognostic signature, overall survival, cell cycle

INTRODUCTION

Lung cancer remains the most prevalent cancer and the leading cause of cancer death worldwide (Siegel et al., 2020). Non-small cell lung cancer (NSCLC) accounts for almost 80% of lung cancer, and lung adenocarcinoma (LUAD) is the predominant histological subtype of NSCLC (Shukla et al., 2017). Despite the clinical application of epithelial growth factor receptor (EGFR)-targeted tyrosine kinase inhibitors (TKIs) and immunotherapy targeting PD-1 or PD-L1 in recent years, the 5-year overall survival (OS) rate for LUAD patients still remains 16% (Miller et al., 2016). Therefore, it is urgent to further discover specific prognostic prediction methods for LUAD patients in order to find new therapeutic targets and improve patients' survival.

Ferroptosis is an iron-dependent programmed cell death process, which is different from other forms of cell death, such as apoptosis, necrosis and autophagy. The main characteristic of ferroptosis is that it is induced by the imbalance of cellular redox homeostasis, leading to excessive lipid peroxidation and finally resulting in cell death. The ferroptosis-related diseases mainly include neurodegenerative diseases (Ren et al., 2020), organ injury induced by ischemia (Friedmann Angeli et al., 2014), and several types of cancers (Jiang et al., 2020). The rapid growth of studies on the role of ferroptosis in cancer has boosted a perspective for its application in cancer treatment. Recently, Alvarez et al. (2017) reported that inhibition of iron-sulfur cluster biosynthetic enzyme NFS1 in LUAD cooperated with suppression of cysteine transport to trigger ferroptosis *in vitro* and slow tumor growth. Besides, Liu et al. (2020) found that the transcription factor nuclear factor-erythroid 2-like 2 (NRF2) inhibitor (Brusatol) could enhance the sensitivity of NSCLC cells to cystine deprivation-induced ferroptosis by FOCAD-FAK signaling, and the combination use of Brusatol and erastin showed better therapeutic action against NSCLC. Other novel compounds, such as erianin, could exert anti-tumor effects in lung cancer by inducing Ca^{2+}/CaM-dependent ferroptosis and inhibiting cell migration (Chen P. et al., 2020). In summary, ferroptosis inducers hold promising potential in the treatment of patients with NSCLC, especially for tumors resistant to traditional treatment. Recent studies have suggested that ferroptosis may play a role in tumor suppression by inducing cell cycle arrest and metabolic regulation imbalance (Li et al., 2020). In addition, almost all of the well-recognized ferroptosis regulators are main components modulating cellular redox (Bersuker et al., 2019; Doll et al., 2019) and cell cycle (Jiang et al., 2015; Ou et al., 2016). However, there is still a lack of comprehensive understanding of ferroptosis-related genes in the prognosis of LUAD, and the function of ferroptosis in LUAD remains largely unknown.

In the present study, we developed a 7-gene ferroptosis-related prognostic signature by analyzing the RNA-seq data and corresponding clinical information of LUAD patients from TCGA database. We further validated our 7-gene model in 5 independent GEO cohorts. Moreover, we detected the expression profiles of core genes in clinical tissue samples. The possible role and functions of core genes in regulating ferroptosis in LUAD cell lines were also explored.

MATERIALS AND METHODS

Patients and Datasets

All public datasets included in this study meet the following inclusion criteria: (1) More than 50 patients were included in each cohort; (2) Included patients had been pathologically confirmed with LUAD; (3) The clinical characteristics of included patients were relatively complete; (4) Included patients had follow-up information of OS. A total of 1163 LUAD samples from six public datasets were included in our study. RNA-Seq expression profile of 594 samples (including 535 LUAD samples and 59 normal lung samples), and the corresponding clinical information of 522 samples were downloaded from the Cancer Genome Atlas (TCGA) database. In addition, the transcriptome and clinical information of 5 external validation cohorts were downloaded from Gene Expression Omnibus (GEO) database, including 90 samples of GSE11969 (Takeuchi et al., 2006), 117 samples of GSE13213 (Tomida et al., 2009), 83 samples of GSE30219 (Rousseaux et al., 2013), 158 samples of GSE31210 (Okayama et al., 2012), and 180 samples of GSE41271 (Sato et al., 2013). The main demographic and clinical characteristics of LUAD samples in the datasets mentioned above were summarized in **Table 1**. Patients with survival time less than 90 days were excluded for Cox and Kaplan-Meier analysis.

Ferroptosis-Related Genes Definition

259 ferroptosis-related genes were obtained from the FerrDb website[1], the first database of ferroptosis regulators and markers and ferroptosis-disease associations, which classified ferroptosis-related genes into 3 subgroups, including drivers, suppressors and markers (Zhou and Bao, 2020). After removing the duplicated genes of the above three subgroups of ferroptosis gene sets, we obtained a total of 259 genes for the subsequent analysis.

[1]http://www.zhounan.org/ferrdb

TABLE 1 | Main demographic and clinical characteristics of LUAD patients in different datasets.

Characteristics	TCGA	GSE11969	GSE13213	GSE30219	GSE31210	GSE41271	IHC cohort
Number	522	90	117	85	158	184	30
Age, median (range)	66 (33–88)	62 (32–84)	61 (32–84)	60 (44–84)	60.5 (30–75)	–	63 (38–83)
Gender (%)							
Female	280, 53.6%	43, 47.8%	57, 48.7%	19, 22.4%	94, 59.5%	91, 49.5%	13, 43.3%
Male	242, 46.4%	47, 52.2%	60, 51.3%	66, 77.6%	64, 40.5%	93, 50.5%	17, 56.7%
TNM stage							
I	279, 53.4%	52, 57.8%	79, 67.5%	84, 98.8%	120, 75.9%	101, 54.9%	13, 43.3%
II	124, 23.8%	13, 14.4%	13, 11.1%		38, 24.1%	29, 15.8%	11, 36.7%
III	85, 16.3%	25, 27.8%	25, 21.4%	1, 1.2%	0	50, 27.2%	6, 20.0%
IV	26, 5.0%	0	0	0	0	4, 2.2%	0
Smoking history							
Yes	446, 85.4%	45, 50.0%	61, 52.1%	–	74, 46.8%	158, 85.9%	12, 40.0%
No	76, 14.6%	45, 50.0%	56, 47.9%	–	84, 53.2%	25, 13.6%	18, 60.0%
Survival status							
OS days (median)	661	2344.5	2,041	2,040	1825.5	1176.5	NA
Censored (%)	188, 36.0%	40, 44.4%	49, 41.9%	45, 52.9%	19, 12.0%	72, 39.1%	NA

The detailed information and classification of ferroptosis-related genes were attached in **Supplementary Table 1**.

Identification of Intersecting Genes to Build the Prognostic Signature

Ferroptosis-related differentially expressed genes (DEGs) between LUAD and adjacent normal lung samples were obtained by R "limma" package, filtered by the cutoff values of false discovery rate (FDR) < 0.05 and log2| fold change (FC)| > 1. The potential ferroptosis-related prognostic genes were selected by univariate Cox analysis by R "survival" filtered by $p < 0.05$. The intersect genes between ferroptosis-related DEGs and prognostic genes were obtained and showed via R "venn" package.

Development of the Prognostic Signature of Ferroptosis-Related Genes

The intersecting genes between ferroptosis-related DEGs and potential prognostic genes were used as candidates for the construction of the prognostic signature. LASSO (least absolute shrinkage and selection operator)-Cox regression analysis was applied to identify the core prognostic DEGs by the R "glmnet" package, and the value of the penalty parameter (λ) was determined according to the lowest partial likelihood deviance by 10-fold cross-validation. The ferroptosis-related risk scores for each patient was calculated by the following formula:

$$\text{Risk score} = \beta1^{*}\text{expG1} + \beta2^{*}\text{expG2} + \ldots + \beta n^{*}\text{expGn},$$

Where β is the regression coefficient obtained through LASSO-Cox regression, and expG is the expression level of core prognostic genes. The LUAD samples were divided into low-risk and high-risk groups according to the median value of risk scores. Subsequently, principal component analysis (PCA) by "prcomp" function and t-distributed stochastic neighbor embedding (t-SNE) algorithm by "Rtsne" package were applied to dimensionality reduction analysis between the two risk groups.

Prognostic Meta-Analysis

To evaluate the efficacy of the prognostic signature based on ferroptosis-related genes in predicting survival of LUAD patients in different public cohorts, a meta-analysis of HR values was performed by random-effects model by STATA 15.0 software.

Functional Enrichment Analysis

DEGs between high-risk and low-risk groups were identified by the cutoff value of log2| FC| > 1 and FDR < 0.05, and then the Gene Ontology (GO) and Kyoto Encyclopedia of Genes and Genomes (KEGG) analyses based on DEGs were conducted by "clusterProfiler" R package. Gene set enrichment analysis (GSEA) was performed using GSEA4.1.0 software[2]. The c2.cp.kegg.v7.0.symbols.gmt in MSigDB was used as the reference gene sets in GSEA.

Cell Culture

A549 and H1299 cells were obtained from Beijing union medical college hospital cell resource sharing platform. A549 and H1299 cells were cultured in RPMI 1640 medium with 10% fetal bovine serum (FBS) and 1% Penicillin-Streptomycin, and maintained in a humidified incubator at 37°C, 5% CO_2. Medium, FBS and Penicillin-Streptomycin were purchased from Corning.

Cell Viability Assay

Cell Counting Kit-8 (CCK-8) (TargetMol) assay was performed to measure cell viability according to the manufacturer's instructions. Erastin (T-1765) was purchased from TargetMol. A549 and H1299 cells were seeded in 96-well plates at a density of 3,000 cells per well and incubated in a humidified cell incubator at 37°C, 5% CO_2 for 24 h. The cells were then treated with erastin of 0, 10, and 20 for 24, 48, and 72 h. The WST-8 reagent was then added and the 96-well plate was continued to incubate for another 2 h. The OD (optical density) values were measured at

[2]http://www.broadinstitute.org/gsea/index.jsp

450 nm with a microplate reader. The experiments in all groups were performed in triplicates and repeated 3 times.

Detection of Lipid Peroxidation

A549 and H1299 cells were seeded in a 6-well plate at a density of 1×10^6 cells per well and incubated for 24 h, and then treated with erastin (0, 10, and 20 μM) for another 48 h. Then the cells were harvested by trypsinization and resuspended in 500 μL of PBS containing the BODIPY 581/591 C11 dye (Invitrogen, D3861). Cells were then incubated for 30 min at 37°C and analyzed using a flow cytometer.

Determination of Iron Concentration

A549 and H1299 cells were seeded in a 6-well plate at a density of 1×10^6 cells per well and treated with erastin (0, 10, and 20μM) for 48 h. Cells were then washed and lysed. The iron concentration was determined with an iron assay kit (Abcam, ab83366) according to the manufacturer's instructions.

RNA Isolation and Real-Time PCR

Total RNA from A549 and H1299 cells treated with erastin was extracted using TRIzol reagent (Invitrogen), and then converted to cDNA using the PrimeScript^{TM} RT Master Mix (Takara) in accordance with the manufacturer's instructions. Real-time PCR was conducted with the SYBR-Green kit (Takara) to detect the mRNA expression levels of core prognostic genes. The primers used for real-time PCR were listed in **Supplementary Table 2** and purchased from Sangon Biotech.

IHC

The samples used for IHC staining had to meet the following inclusion criteria: (1) Age > 18; (2) All included patients had been pathologically confirmed with LUAD; (3) The patients included had no other serious systemic comorbidities; (4) No other primary tumors were found in patients; (5) Good patients' compliance to continue follow-up. A total of 30 cases of LUAD and 12 cases of adjacent non-cancerous lung tissues were obtained from the First Affiliated Hospital of Xi'an Jiaotong University. Our study was approved by the Ethics Committee on Human Research of the First Affiliated Hospital of Xi'an Jiaotong University. Primary antibodies used in IHC including ALOX12B (ab121785, 1:50 for IHC), ALOX15 (ab244205, 1:200 for IHC), GPX2 (ab140130, 1:200 for IHC), DDIT4 (ab191871, 1:200 for IHC), GDF15 (ab180929, 1:200 for IHC), SLC2A1 (ab115730, 1:500 for IHC), and RRM2 (ab172476, 1:100 for IHC) were purchased from Abcam. The paraffin-embedded tissue sections were roasted at 60°C for 6 h and deparaffinized in xylene and dehydrated in gradient concentration of ethanol. Antigen repair of tissue slides was subsequently performed in sodium citrate buffer (PH = 9.0) in a microwave oven. The endogenous peroxidase was then deactivated by 3% hydrogen peroxide for 15 min. Subsequently, 5% BSA (bovine serum albumin) was applied to block non-specific antigens at room temperature for 30 min and the incubation with primary antibodies in a certain concentration was performed overnight at 4°C. On the second day, the slides were incubated with the homologous secondary antibody at room temperature for 1 h. Then, DAB (diaminobenzidine) staining, hematoxylin staining, dehydration in gradient ethanol and transparency in xylene were followed to handle the slides. 10 random fields of each tissue section were selected for semi-quantitative scoring, and the scoring method was as follows: (1) Positive cell rate score—0 for < 10% positive cells, 1 for 10∼25% positive cells, 2 for 25∼50% positive cells, 3 for 50∼75% positive cells and 4 for > 75% positive cells; (2) Dyeing strength score—1 for light yellow, 2 for brown yellow and 3 for tan; (3) The total score was the product of the positive cell rate score and staining intensity score. The Ki67 and TNM stage information of all samples were obtained from the postoperative pathological reports of the Department of Pathology in our hospital. All LUAD samples were divided into Ki67-low and Ki67-high two groups according to the median value of Ki67 (35%, range from 5 to 60%).

Small Interfering RNA (siRNA) Transfection

The siRNAs targeting GPX2 and DDIT4 were synthesized from GenePharma and transfected with Lipofectamine 2000 reagent (Invitrogen) according to the manufacturer's protocol. The knockdown efficiency was evaluated by Western blotting after 48h transfection. The sequences of siRNAs are the following: si-Ctrl: 5′-UUCUCCGAACGUGUCACGUTT-3′; si-GPX2-1: 5′-GCUAGAAGAGACC-AAUAAAGG-3′; si-GPX2-2: 5′-GGGAGAAGGUAGAUUUCAAUA-3′; si-DDIT4-1: 5′-GUACU-GUAGCAUGAAACAAAG-3′; and si-DDIT4-2: 5′-GAGGAGUGUUGAACUUCAACC-3′. The siRNA sequences used in cell viability assay and iron concentration detection were siGPX2#1 and siDDI4#1.

Western Blotting

Whole cell lysates were prepared by RIPA buffer, then proteins were separated with SDS/PAGE gel and transferred to PVDF membranes, which were incubated overnight with corresponding primary antibodies. Primary antibodies used in Western blotting included CDK4 (#12790 from CST, 1:1,000), CDK6 (#3136 from CST, 1:2,000), p21 (#2947 from CST, 1:1,000), p27 (#3686 from CST, 1:1,000), GPX2 (ab140130 from abcam, 1:5,000), DDIT4 (ab191871 from abcam, 1:1,000), and HRP-labeled GAPDH (HRP-60004 from proteintech, 1:15,000). Subsequently, HRP-conjugated secondary antibodies (Cell Signaling Technology) were incubated and chemiluminescent signals were detected by ECL (Millipore).

Statistical Analysis

All data were analyzed using R version 3.5.2 or Graphpad Prism 8, and all experiments were repeated at least 3 times. These results were presented as mean ± standard deviation (SD). Student's two-sided *t*-test was used to compare the differences between two groups. Differences in survival between different risk groups were compared by Kaplan-Meier curves followed by log-rank test. $P < 0.05$ was considered as statistically significant.

RESULTS

The overall design and flow chart of this study were shown in **Figure 1**. 522 LUAD patients in TCGA database and 628 LUAD patients in GEO database were included in this study. The main demographic and clinical characteristics of patients in different datasets were summarized in **Table 1**.

The Prognostic Significance of Ferroptosis-Related Genes in LUAD

A total of 259 well-defined ferroptosis-related genes were included in this study, including 108 drivers that promote ferroptosis, 69 suppressors that prevent ferroptosis, and 111 markers that indicate the occurrence of ferroptosis. There is an overlap between these three gene sets. The detailed ferroptosis-related gene sets could be found in **Supplementary Table 1**. The univariate Cox proportional hazards regression analysis was applied to assess the relationship between the expression levels of ferroptosis-related genes and prognosis of LUAD patients of TCGA database. A total of 45 potential prognostic ferroptosis-related genes were identified (p-value < 0.05), and the prognostic information of these 45 genes was shown in **Table 2**. Among these 45 genes, 15 genes were identified as "protective" factors with hazard ratios (HRs) < 1, while the remaining 30 genes were considered as "risk" factors with HRs > 1.

Identification of Prognostic Ferroptosis-Related DEGs in LUAD

A total of 70 ferroptosis-related DEGs between LUAD and adjacent non-tumorous samples of TCGA database were identified by the criteria of $\log2|FC| > 1$, FDR < 0.05. The heatmap and volcano map in **Supplementary Figure 1** depicted the expression level and distribution of these ferroptosis-related DEGs, including 47 DEGs up-regulated and 23 DEGs down-regulated in LUAD. Subsequently, 20 intersection genes of 70 ferroptosis-related DEGs and 45 potential prognostic genes were obtained as the potential prognostic ferroptosis-related DEGs, which was shown in the venn diagram of **Figure 2A**. The forest plot of **Figure 2B** showed the results of univariate COX regression analysis of these 20 genes, which demonstrated that 6 of these genes (DUOX1, ALOX15, DPP4, CDO1, GDF15, IL33) were "protective" factors for LUAD patients, while the other 14 genes were "risk" factors. The protein interaction network among these genes from the STRING database was shown in **Figure 2C**. The heatmap in **Figure 2D** showed the expression levels of these 20-potential prognostic ferroptosis-related DEGs in LUAD and normal lung tissues, from which we could found that only 4 genes (ALOX15, DUOX1, CDO1, and IL33) were highly expressed in normal tissues, while the remaining 16 genes were highly expressed in tumor tissues. The boxplot in **Supplementary Figure 1C** also detected the difference in expression levels of these 20 genes in tumor and normal tissues.

Development of the Ferroptosis-Related Prognostic Signature in TCGA Cohort

The expression levels of the above mentioned 20 potential prognostic ferroptosis-related DEGs and the OS data of LUAD patients with survival time greater than 90 days were then extracted from TCGA database for LASSO Cox regression analysis. The prognostic signature based on 7 core prognostic ferroptosis-related DEGs was then constructed by the optimal penalty parameter (λ) for the LASSO model was determined via 10-fold cross-validation. The risk scores for this model can be obtained by the following formula: Risk score = 0.139 * expression level of ALOX12B + (−0.033)* expression level of ALOX15 + 0.029 * expression level of GPX2 + 0.089 * expression level of DDIT4 + (−0.021) * expression level of GDF15 + 0.088 * expression level of SLC2A1 + 0.150 * expression level of RRM2. Subsequently, the LUAD patients were stratified into two different risk groups: high-risk (n = 236) and low-risk (n = 237) according to the median value of risk scores. Patients in the high-risk group had a higher death probability than those in the low-risk group (**Figure 3A**). Dimensionality reduction algorithms of PCA and t-SNE were then used to confirm the samples of the above two risk groups were separately distributed (**Figures 3B,C**). Kaplan-Meier survival curve in **Figure 3D** showed that OS of LUAD patients in the high-risk group was significantly worse than that of the low-risk group, with the HR value of 2.396 (95% confidence interval: 1.771–3.242, $p < 0.001$). The predictive efficacy of the prognostic signature for OS in LUAD patients was evaluated by the time-dependent ROC curves, and the area under the curve (AUC) reached 0.702 for 1-year, 0.700 for 2-year, and 0.705 for 3-year, respectively (**Figure 3E**).

Validation of the Ferroptosis-Related Prognostic Signature in Independent GEO Cohorts

In order to verify the stability and reproducibility of the ferroptosis-related prognostic signature of LUAD, 5 independent NSCLC cohorts from the GEO database were used for external validation. The expression levels of ferroptosis-related genes and prognostic information of LUAD patients were obtained from these 5 cohorts. The main demographic and clinical information were provided in **Table 1**. The formula obtained from the TCGA training cohort was then used to calculate the risk scores of LUAD patients in the GEO validation cohorts. K-M survival analysis showed that the OS of LUAD patients in the high-risk group was significantly worse than that of the low-risk group in 4 GEO validation cohorts, except for the no statistically significant difference found in GSE13213 (**Figures 4A–E**). Moreover, a meta-analysis was conducted to comprehensively evaluate the HR values obtained from TCGA and GEO cohorts, and the pooled analysis further confirmed that the high-risk group was a risk factor for LUAD patients with combined HR of 2.33 (95% CI: 1.84–2.83, $p < 0.001$) (**Figure 4F**).

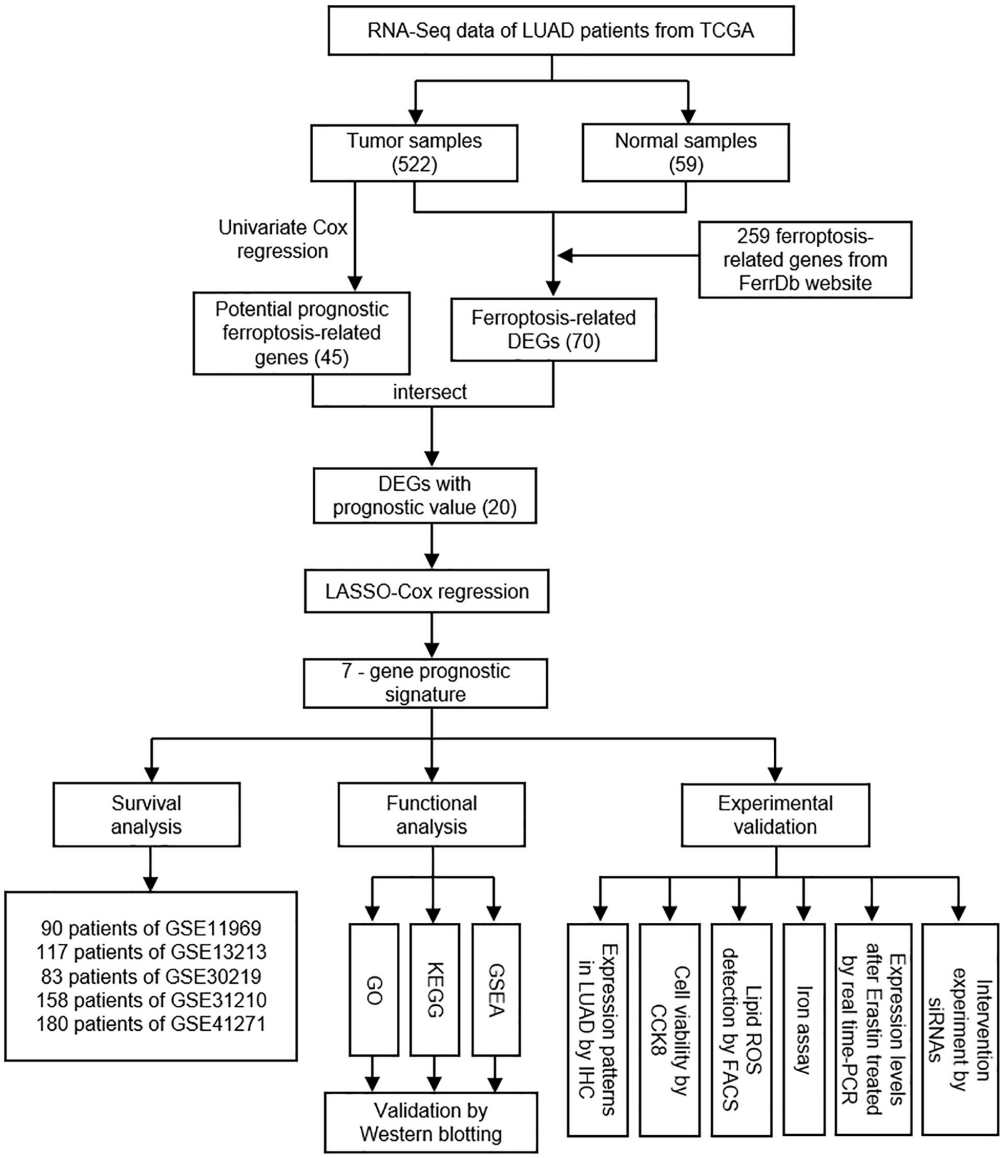

FIGURE 1 | The overall study design and workflow.

Independent Prognostic Value of the Ferroptosis-Related Prognostic Signature

Subsequently, we extracted the main clinical characteristics of LUAD patients in TCGA database, including age, sex, smoking history, radiation history, pharmaceutical history, T, N, M, and stage. Both univariate and multivariate Cox analyses were carried out among these available variables in combination with risk scores obtained by the ferroptosis-related prognostic signature. The results of univariate Cox analysis confirmed that receiving radiation treatment, higher T/N/M and stage, as well as higher risk scores were risk factors for LUAD patients with HRs > 1, $p < 0.05$ (**Figure 5**). Multivariate Cox analysis further conducted by including radiation history, stage and risk scores, after other confounding factors were removed, and results showed that higher stage and higher risk scores proved to be independent prognostic factors for OS of LUAD patients (HR for stage = 1.485, 95% CI: 1.264–1.744, $p < 0.001$; HR for risk score = 3.210, 95% CI: 2.020–5.099, $p < 0.001$; **Figure 5**).

Identification of the Prognostic Signature-Related Biological Pathways

To investigate the underlying difference in biological processes and functions between the different risk groups, DEGs between high-risk and low-risk groups were identified by the cutoff value of $\log2|\ FC|\ > 1$ and FDR < 0.05, and enrichment analyses of GO and KEGG pathways of DEGs were then performed. Interestingly, DEGs up-regulated in high-risk group

TABLE 2 | Univariate Cox analysis of ferroptosis-related genes in TCGA cohort.

Official symbol	Classification	HR	HR.95L	HR.95H	*p*-value
SLC7A11	Suppressor, marker	1.1436	1.0264	1.2741	0.0150
GCLC	Suppressor	1.1311	1.0274	1.2453	0.0120
SLC3A2	Suppressor, marker	1.2903	1.0164	1.6379	0.0363
CISD1	Suppressor	1.4746	1.0815	2.0106	0.0141
FANCD2	Suppressor	1.4818	1.1262	1.9496	0.0050
HELLS	Suppressor	1.2736	1.0203	1.5899	0.0326
VDAC2	Driver, suppressor	1.5990	1.2089	2.1150	0.0010
CISD2	Suppressor	1.4245	1.0326	1.9651	0.0311
ISCU	Suppressor	0.5316	0.3645	0.7753	0.0010
ACSL3	Suppressor	1.4123	1.1310	1.7635	0.0023
ARNTL	Suppressor	0.6487	0.4691	0.8971	0.0089
ATP5MC3	Driver, marker	1.3624	1.0458	1.7748	0.0219
DUOX1	Driver	0.8690	0.7636	0.9891	0.0335
PGD	Driver	1.1832	1.0226	1.3691	0.0238
FLT3	Driver	0.4923	0.2676	0.9058	0.0227
NRAS	Driver	1.3643	1.0743	1.7327	0.0108
KRAS	Driver	1.3267	1.0652	1.6524	0.0116
GLS2	Driver	0.3929	0.1930	0.8000	0.0100
ALOX12B	Driver	1.5515	1.0374	2.3206	0.0325
ALOX15	Driver, marker	0.8494	0.7296	0.9890	0.0355
ALOX15B	Driver	0.9102	0.8330	0.9946	0.0375
ALOXE3	Driver	1.6274	1.0031	2.6403	0.0486
PHKG2	Driver	0.7183	0.5258	0.9814	0.0377
DPP4	Driver	0.9036	0.8279	0.9863	0.0233
PEBP1	Driver	0.6239	0.4811	0.8091	0.0004
CDO1	Driver	0.7163	0.5199	0.9870	0.0413
PANX1	Driver	1.3978	1.0663	1.8323	0.0153
UBC	Marker	1.4774	1.0163	2.1477	0.0409
TXNRD1	Marker	1.1429	1.0354	1.2615	0.0081
SRXN1	Marker	1.1887	1.0130	1.3949	0.0341
GPX2	Marker	1.0511	1.0004	1.1043	0.0481
DDIT4	Marker	1.2211	1.0740	1.3883	0.0023
TSC22D3	Marker	0.8428	0.7269	0.9771	0.0234
SLC7A5	Marker	1.1724	1.0379	1.3244	0.0105
HERPUD1	Marker	0.6625	0.5232	0.8389	0.0006
GDF15	Marker	0.8923	0.8103	0.9825	0.0204
CEBPG	Marker	1.3520	1.0752	1.6999	0.0099
EIF2S1	Marker	1.7254	1.2530	2.3757	0.0008
RELA	Marker	1.6419	1.0522	2.5623	0.0290
IL33	Marker	0.8559	0.7507	0.9758	0.0200
SLC2A1	Marker	1.2901	1.1569	1.4386	0.0000
RRM2	Marker	1.3596	1.1913	1.5517	0.0000
HNF4A	Marker	1.2844	1.1014	1.4978	0.0014
YWHAE	Marker	1.4306	1.0352	1.9769	0.0300
AURKA	Marker	1.3003	1.1259	1.5018	0.0004

were obviously enriched in a variety of cell cycle-related pathways and functions. In **Figure 6A**, GO analysis showed that the DEGs were significantly enriched in biological process (BP) associated with cell division, including organelle fission, nuclear division, chromosome segregation and etc. For cellular component (CC) item, the up-regulated DEGs were also enriched in chromosome-associated structure (such as chromosomal region, spindle, centromeric region, and kinetochore). The bar plot of **Figure 6B** showed that the significantly enriched KEGG pathways, including cell cycle,

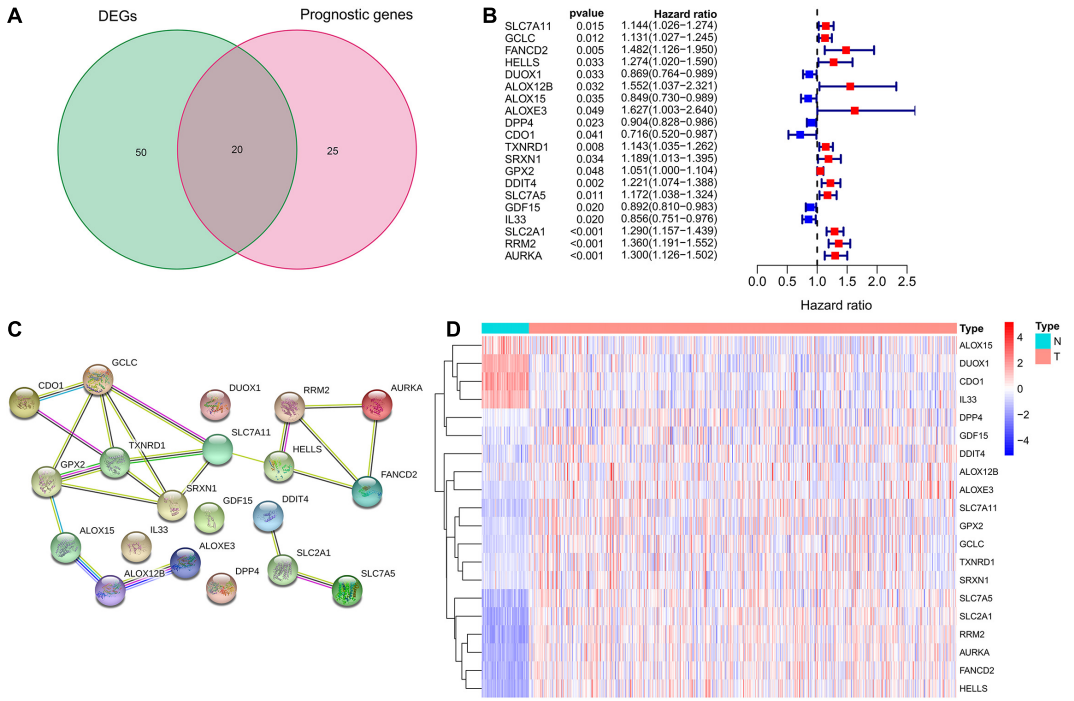

FIGURE 2 | Identification of potential prognostic ferroptosis-related DEGs in LUAD. **(A)** Venn diagram to show the 20 intersection genes of 70 ferroptosis-related DEGs between LUAD and adjacent non-tumorous samples and 45 potential prognostic genes identified by univariate Cox analysis. **(B)** The forest plot showing the results of univariate Cox regression analysis of these 20 ferroptosis-related genes. **(C)** The protein interaction network among these 20 genes from the STRING database. **(D)** The heatmap showing the expression levels of these 20 genes in LUAD and normal lung tissues. DEGs, differentially expressed genes; LUAD, lung adenocarcinoma.

complement and coagulation cascades, p53 signaling, cellular senescence and fatty acid metabolism. Multiple-GSEA analysis also confirmed the enrichment of cell cycle-associated pathways, p53 signaling and metabolic-related pathways (**Figure 6C**).

Validation of the Expression Levels of 7 Core Prognostic Genes in LUAD and Paracancerous Normal Lung Tissues

To verify the reliability of the above results obtained from the public database, we collected 30 cases of LUAD samples and 12 cases of adjacent normal lung tissues to test the expression levels of the 7 ferroptosis-related genes consisting of our prognostic signature by IHC. As shown in **Figure 7**, the expression levels of ALOX12B, GPX2, DDIT4, GDF15, and RRM2 in tumor tissues were significantly higher than those in the normal lung tissues. Only ALOX15 showed high expression in normal lung samples. However, there was no significant difference in the expression level of SLC2A1 between LUAD and adjacent tissues. The above protein expression results of the prognostic genes in clinical tissue samples by IHC were almost consistent with the RNA sequencing data analyzed by the TCGA database. The above 7 prognostic biomarkers were mainly located in the cytoplasm and membrane of LUAD samples with moderate to strong positive staining. Furthermore, we analyzed the relationship between the expression profiles of the 7 core prognostic genes with Ki67 and TNM stage, and found only ALOX15 was significantly low expressed in Ki67-high samples, while GPX2, DDIT4, and SLC2A1 were high expressed in Ki67-high samples. There was no significant difference in the distribution of the other 3 genes in LUAD samples with different Ki67 levels and all 7 genes in samples with different TNM stage.

Effects of Ferroptosis Inducer Erastin on the Expression Levels of 7 Core Prognostic Genes in LUAD Cell Lines *in vitro*

LUAD cell lines A549 and H1299 were then treated with ferroptosis inducer erastin to investigate the role of ferroptosis-related prognostic genes. As shown in **Figure 8A**, CCK8 assay identified that erastin could inhibit the proliferation of A549 and H1299 in a dose-dependent manner. When the concentration was greater than 20 μM, the growth inhibitory effects of erastin on both A549 and H1299 were statistically significant. Subsequently, we confirmed that erastin treatment of 10 and 20 μM significantly increased the lipid ROS accumulation (**Figure 8B**) and iron concentration (**Figure 8C**). Furthermore, to validate the relevance of erastin-induced ferroptosis and cell cycle regulation, we explored the changes in several regulators involved in G1/S transition after erastin treatment of A549 and H1299 cells by Western blotting. As shown in **Figure 8D**, decreased expression levels of CDK4 and CDK6 were observed, whereas

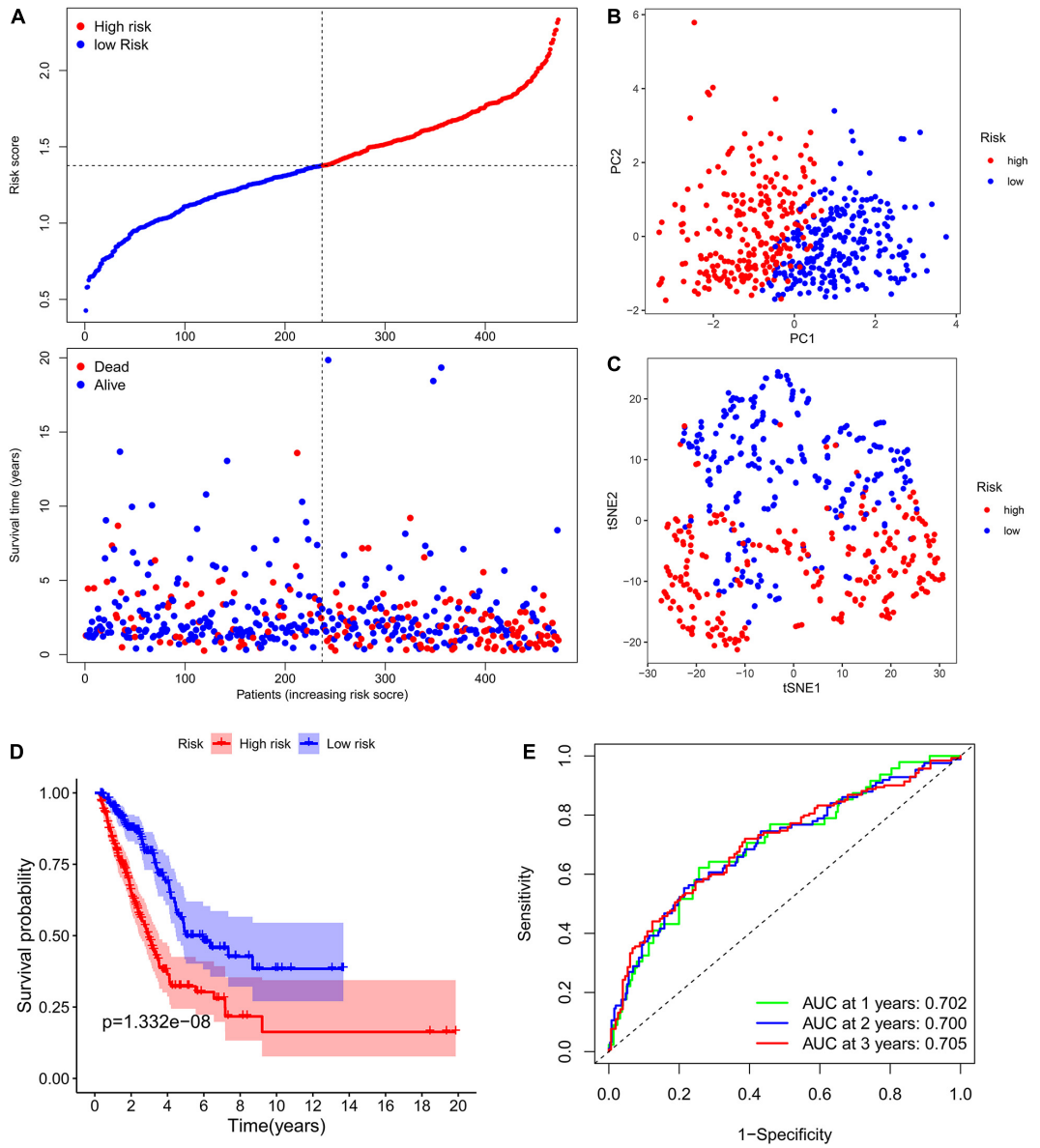

FIGURE 3 | Construction of the ferroptosis-related prognostic signature in the TCGA cohort. **(A)** Distribution of risk scores and survival status in TCGA cohort. **(B,C)** Dimensionality reduction algorithms of PCA **(B)** and t-SNE **(C)** to show the samples of different ferroptosis-related risk groups were separately distributed. **(D)** Kaplan-Meier survival curve showing the OS of LUAD patients in the high-risk group was significantly worse than that of the low-risk group. **(E)** AUC of time-dependent ROC curves to evaluate the predictive efficacy of the prognostic signature for OS in LUAD patients. TCGA, the Cancer Genome Atlas; PCA, principal component analysis; t-SNE, t-distributed stochastic neighbor embedding algorithm; OS, overall survival; AUC, area under the curve; ROC, receiver operating characteristic curve.

increased expression levels of p21 and p27 were found. Next, real time-PCR was applied to test the expression changes of 7 core prognostic genes in A549 and H1299 after treated with erastin of 20 μM for 48 h. We found that mRNA expression levels of 5 genes (ALOX12B, ALOX15, GPX2, DDIT4, and GDF15) were increased and the other 2 (SLC2A1 and RRM2) were decreased after erastin treatment, although the increase of GPX2 was not statistically significant in A549 and GDF15 was barely changed in H1299 (**Figure 8E**). To validate the specific role in ferroptosis of individual gene in our prognostic model, silencing GPX2 and DDIT4 were also performed in A549 by siRNAs. Western blotting was used to verify that the expression of GPX2 and DDIT4 would not be affected by the sequence of siCtrl, while two different sequences of siRNAs targeting GPX2 or DDIT4 could effectively reduce the expression of their target genes (**Figure 8F**). Subsequently, we found that down-regulation of either GPX2 or DDIT4 could partially reverse the cell proliferation arrest (**Figure 8G**) and the elevation of lipid ROS (**Figure 8H**) and

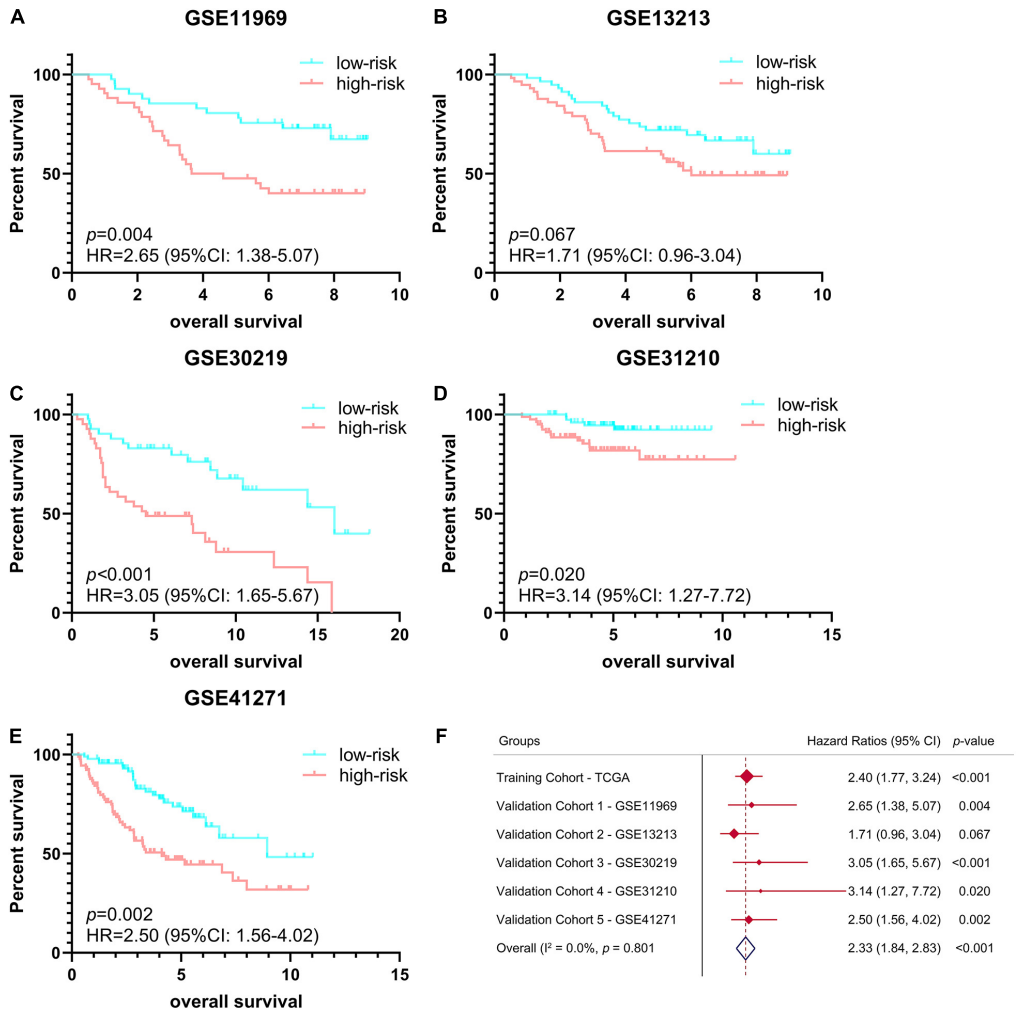

FIGURE 4 | Validation of ferroptosis-related prognostic signature in LUAD from different GEO cohorts. **(A–E)** Kaplan-Meier survival curves of OS in 5 independent GEO cohorts, **(A)** GSE11969 (*n* = 90), **(B)** GSE13213 (*n* = 117), **(C)** GSE30219 (*n* = 85), **(D)** GSE31210 (*n* = 158), **(E)** GSE41271 (*n* = 184). **(F)** Meta-analysis was performed to combine HR values obtained from TCGA and 5 GEO cohorts. GEO, Gene Expression Omnibus; HR, hazard ratio.

iron concentration (**Figure 8I**) induced by erastin in A549 cells, whereas these reversing effects could not be observed in the siCtrl group. The validation of other prognostic genes in our model will be further investigated in our future studies.

DISCUSSION

Ferroptosis is a novel programmed cell death pattern, mainly caused by iron-dependent lipid peroxidation (Liu et al., 2020). In recent years, the role and mechanism of ferroptosis in different diseases have been extensively investigated, especially in the field of tumor research and treatment. Several studies have already found that some traditional chemotherapy-resistant tumors are highly sensitive to ferroptosis inducers, so ferroptosis is expected to bring novel promising strategies to some refractory tumors (Jiang et al., 2020). In lung cancer, limited ferroptosis-related studies mainly focused on the role of potential ferroptosis biomarkers in the ferroptosis-inducing process of well-recognized inducers (Alvarez et al., 2017; Chen P. et al., 2020; Kwon et al., 2020; Liu et al., 2020; Lou et al., 2020). There is a lack of comprehensive and systematic analysis of ferroptosis in the malignant progression and treatment strategy for lung cancer. In this study, we systematically analyzed the expression profiles and prognostic values of 259 ferroptosis-related genes provided by the latest online FerrDb database (Zhou and Bao, 2020). Additionally, the ferroptosis-related prognostic signature for LUAD patients was developed and validated by available public databases. The cell cycle signaling was identified as the main enrichment pathway between different risk subgroups.

According to the detailed information of ferroptosis-related genes provided by FerrDb website, which was developed by manually extracted 784 ferroptosis-related articles from PubMed, 108 drivers, 69 suppressors, and 111 markers were included in our study as potential prognostic ferroptosis-related genes. Because there are 28 genes reported to function in multiple

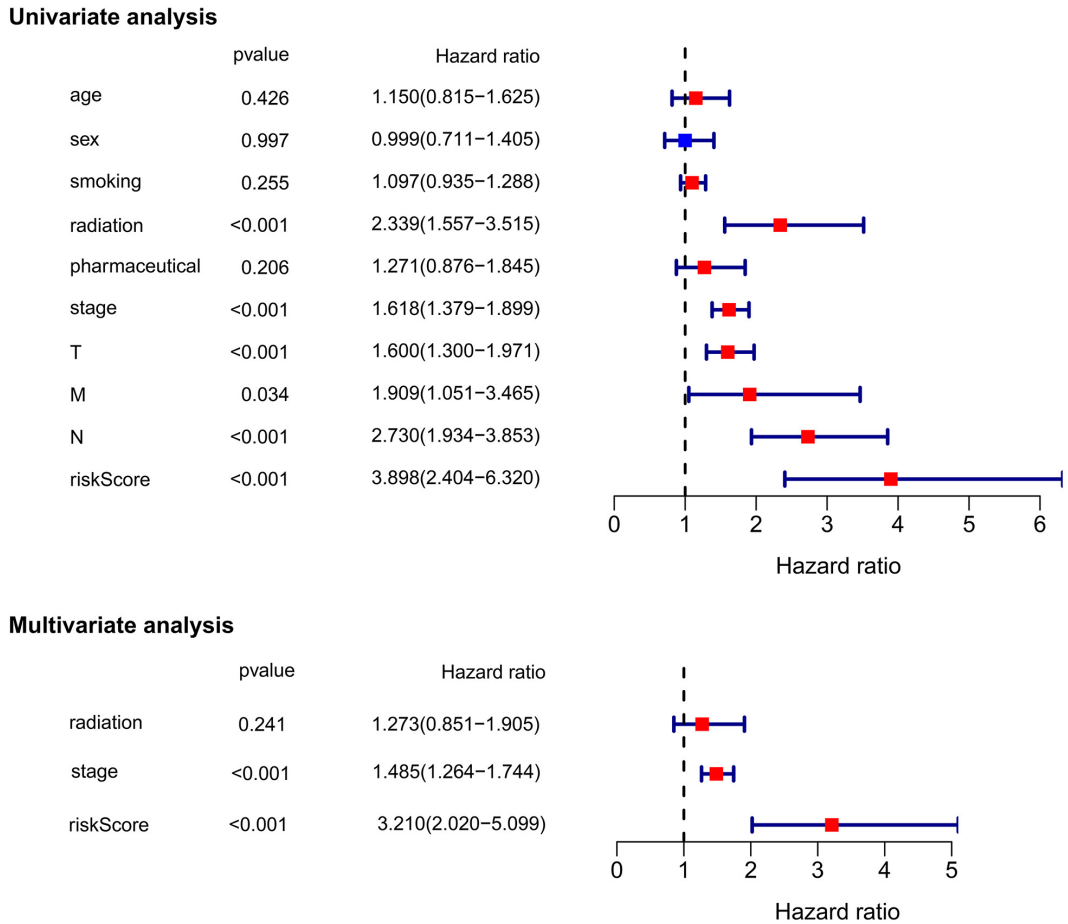

FIGURE 5 | Univariate and multivariate Cox regression analysis of the ferroptosis-related prognostic signature and other clinical characteristics in TCGA cohort.

processes of ferroptosis, these genes were multi-annotated in different subclasses of ferroptosis genes (Zhou and Bao, 2020). Among the 259 ferroptosis-related genes, 27.0% (70/259) were differentially expressed in tumor and adjacent normal tissues of LUAD samples, and 17.3% (45/259) were correlated with prognosis in the univariate Cox analysis. The intersecting genes between ferroptosis-related DEGs and prognostic genes were obtained for the following study. Among the 20 intersecting genes, only 4 were highly expressed in normal lung tissues, and all 4 genes were protective markers according to univariate Cox analysis, which was consistent with the expression status. The remaining 16 genes were highly expressed in tumor tissues of LUAD patients, and most of them (14/16) were identified as risk factors for LUAD patients, except for DPP4 and GDF15. DPP4 (dipeptidyl peptidase 4) is considered as a ferroptosis driver in colorectal cancer. Xie et al. (2017) reported that loss of TP53 could prevent the nuclear translocation of DPP4, thus promoting the plasma membrane-related DPP4-dependent lipid peroxidation process and ultimately leading to ferroptosis, which was consistent with its protective role identified in our analysis. However, study of DPP4 in LUAD showed that it was highly expressed in LUAD compared to adjacent normal lung tissues, and the DPP4 inhibitor could inhibit lung cancer growth by promoting the pro-inflammatory activity of macrophages (Jang et al., 2019). Thus, the specific role of DPP4 in ferroptosis process in LUAD still need to be further studied. According to the study of GDF15 (growth differentiation factor 15) in gastric cancer cell line MGC803, GDF15 functions as a ferroptosis inhibitor in gastric cancer, for knockdown of GDF15 could promote erastin-induced ferroptosis by reducing the expression of SLC7A11 (Chen L. et al., 2020). However, GDF15 was identified as a protective factor for LUAD patients according to the univariate Cox analysis, and how GDF15 functions by ferroptosis process in lung cancer has not been reported.

The prognostic signature developed by LASSO Cox regression was consisted of 7 ferroptosis-related genes, among which the expression of ALOX12B, GPX2, DDIT4, SLC2A1, and RRM2 were positively correlated with the survival risk of LUAD patients, while the levels of ALOX15 and GDF15 were negatively associated with the survival risk. According to FerrDb database, only ALOX12B and ALOX15 were definitely labeled as ferroptosis drivers, while the remaining 5 genes in addition to ALOX15 were labeled as ferroptosis markers, indicating that their definite roles in ferroptosis process remained unclear. After

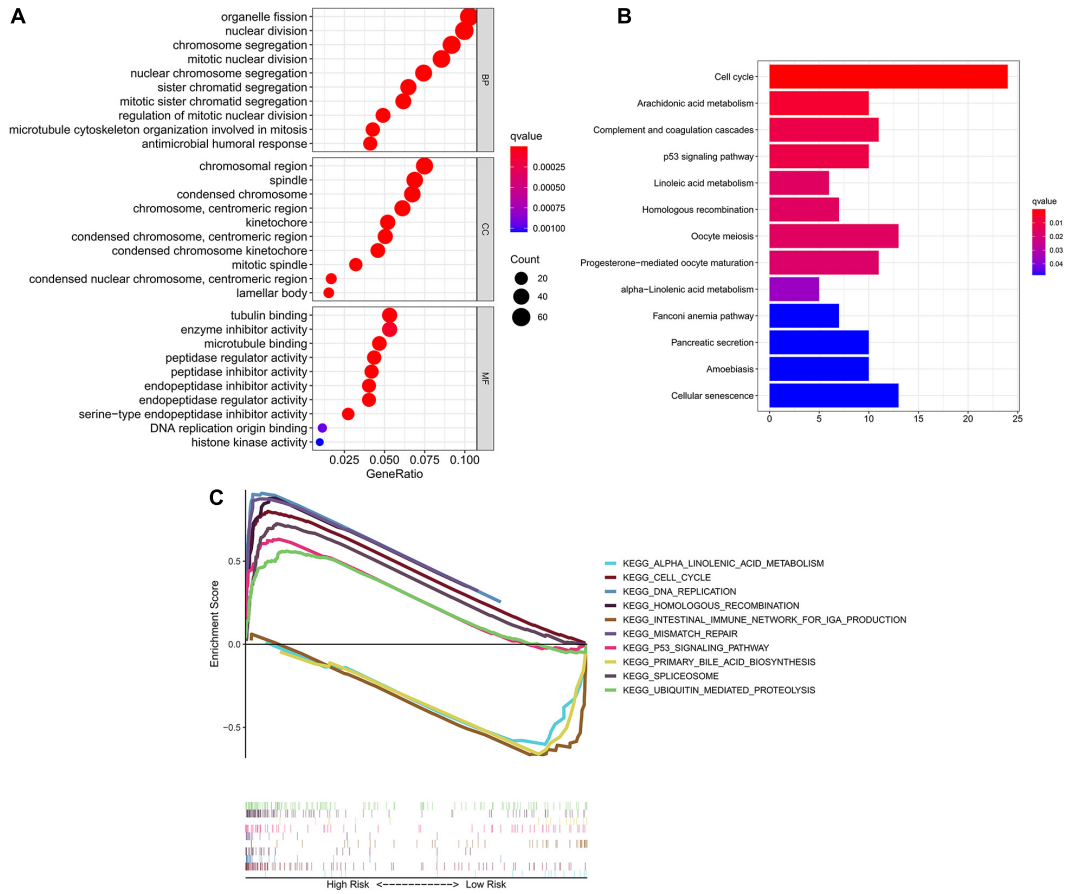

FIGURE 6 | Identification of biological pathways associated with the risk of ferroptosis. **(A)** GO analysis of DEGs between different risk groups into three functional groups, including BP, CC and MF. **(B)** KEGG analysis of DEGs between different risk groups. **(C)** Multiple-GSEA between the high-risk and low-risk groups of TCGA cohort. GO, Gene Ontology; BP, biological process; CC, cellular component; MF, molecular function; KEGG, Kyoto Encyclopedia of Genes and Genomes; GSEA, Gene set enrichment analysis.

reviewing related references systematically, we summarized the research status in ferroptosis of the above 7 genes included in our prognostic signature as follows: ALOX12B and ALOX15 are two of the six ALOX (arachidonate lipoxygenase) genes in humans. Yang et al. (2016) confirmed that targeted silence of the ALOX family genes by a pool of siRNAs or pharmacological inhibitors in G-401, BJeLR, and HT-1080 cell lines could effectively prevent erastin- or IKE (Imidazole Ketoerastin)-induced ferroptosis, confirming the role of lipoxygenases as ferroptosis drivers. The study by Ou et al. (2016) had found that in various cell lines, including NSCLC H1299, the activation of SAT1 (spermidine N1-acetyltransferase 1) expression induced by TP53 could promote lipid peroxidation and increase the sensitivity to ferroptosis, while PD146176, the specific inhibitor of ALOX15, significantly abrogate the SAT1-induced ferroptosis. Shintoku et al. (2017) also confirmed that, in fibrosarcoma HT1080, pancreatic cancer PANC-1, and NSCLC Calu-1, the cell membrane localized ALOX15 promoted erastin- and RSL3-induced ferroptosis. Glutathione-dependent peroxidases (GPXs) play an important role in catalyzing the reduction reaction of hydrogen peroxide and organic peroxides (Yang et al., 2014), and among them, GPX4 has been identified as a common crucial mediator for ferroptosis, for it reduces hydroperoxyl groups of lipid complexes and inhibits lipoxygenases (Brigelius-Flohe and Flohe, 2020). Also, as a member of GPXs family, GPX2 was proved to control the balance between the regenerative and apoptotic cells in the intestinal epithelium, and restrained the inflammation-induced tumorigenesis in the gut (Brigelius-Flohe and Flohe, 2020). However, its specific role in ferroptosis has not been clarified. DDIT4 (DNA damage inducible transcript 4) was found upregulated by erastin, which was associated with the activation of ER (endoplasmic reticulum) stress response pathway, and the upregulation of CHAC1 (cation transport regulator homolog 1), an ER stress response gene, could be regarded as a marker for pharmacodynamic inhibition of cystine-glutamate exchange (Dixon et al., 2014). Our results also confirmed that knockdown of GPX2 or DDIT4 in A549 could partially reverse the increase of lipid ROS and iron concentration induced by erastin, which further verified the potential role of GPX2 and DDIT4 as ferroptosis drivers. GDF15 (growth

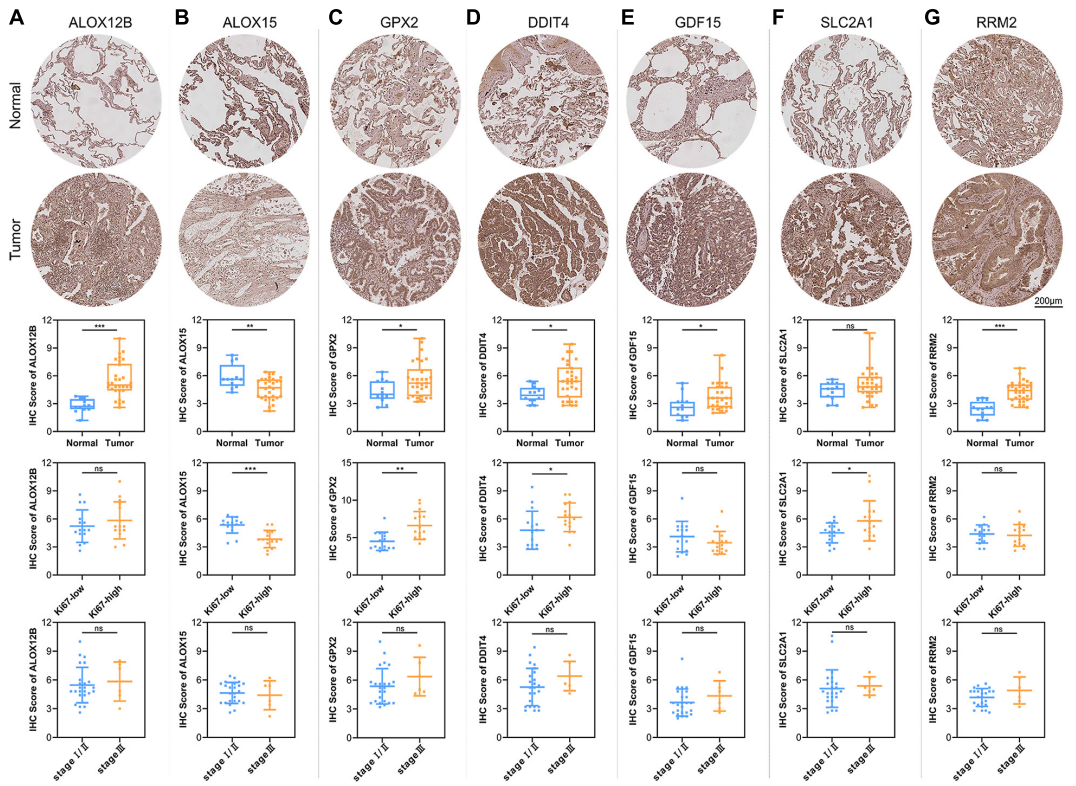

FIGURE 7 | Validation of the expression patterns of 7 core prognostic genes in LUAD tissue samples. The figures of IHC staining showed the representative images of the expression levels of ALOX12B **(A)**, ALOX15 **(B)**, GPX2 **(C)**, DDIT4 **(D)**, GDF15 **(E)**, SLC2A1 **(F)**, and RRM2 **(G)** in adjacent normal lung tissues and LUAD. The box plots showed the statistical results of the expression of the above 7 core prognostic genes in 30 LUAD and 12 adjacent normal lung tissues. The scatter plots showed the distribution of 7 core prognostic genes in LUAD samples with different Ki67 levels and TNM stage. ns, not significant; $^{*}P < 0.05$; $^{**}P < 0.01$; $^{***}P < 0.001$.

differentiation factor 15), as described above, was considered as a ferroptosis inhibitor in gastric cancer (Chen L. et al., 2020), whereas it was upregulated in erastin-treated samples in HT-1080 (Dixon et al., 2014). The above differences may be associated with the heterogeneity and mutant spectrum of different tumors. SLC2A1 (solute carrier family 2 member 1), also known as GLUT1 (glucose transporter 1), plays an important role in glucose transport. Jiang et al. (2017) identified a DNA methylation modifier, LSH (lymphoid-specific helicase), could inhibit ferroptosis in lung cancer by directly transcriptional activation of SLC2A1 expression. RRM2 was reported to be down-regulated in erastin-treated HCC cell lines Bel-7402 and HepG2, and possibly suppress ferroptosis in a GSH-dependent manner (Zhang et al., 2019). In summary, four of the genes (ALOX12B, ALOX15, GPX2, DDIT4) in our prognostic signature have been reported to promote ferroptosis, while SLC2A1 and RRM2 have been regarded as ferroptosis inhibitors, and the role of GDF15 in ferroptosis is not consistent in different tumors.

Although some researchers have investigated the mechanism and clinical application value of ferroptosis, especially in the field of tumor therapy, the underlying mechanism of tumor susceptibility to ferroptosis still needs to be clarified. It is reasonable to find a significant difference in fatty acid metabolism and cell cycle-related pathways in patients with different ferroptosis-related risks. Lipid peroxidation of cell membrane induced by the redox imbalance was the main cause of ferroptosis; thus a significant differential expression of arachidonic acid and linoleic acid metabolism-related genes could be found in different risk groups. Dysregulation of cell cycle-related pathways may be the consequence of ferroptosis imbalance, meanwhile, the abnormal expression of cell cycle-regulating molecules may also lead to different ferroptosis-related risks in LUAD patients. We detected the expression levels of several main cell cycle regulators in A549 and H1299 after treated with erastin, and we found that the positive regulators for cell cycle were down-regulated and the negative regulators were obviously up-regulated. However, the specific modulation relationship between cell cycle regulation and ferroptosis remains to be further elucidated.

Several limitations should be acknowledged in our study: (1) Due to few studies about the role of ferroptosis in tumors, the information of ferroptosis-related genes provided by FerrDb website may not be accurate enough, for the references were manually extracted from the previous literature reports, so some unidentified crucial ferroptosis-mediating genes may be missing in the ferroptosis gene sets. (2) Although all of the 7 genes

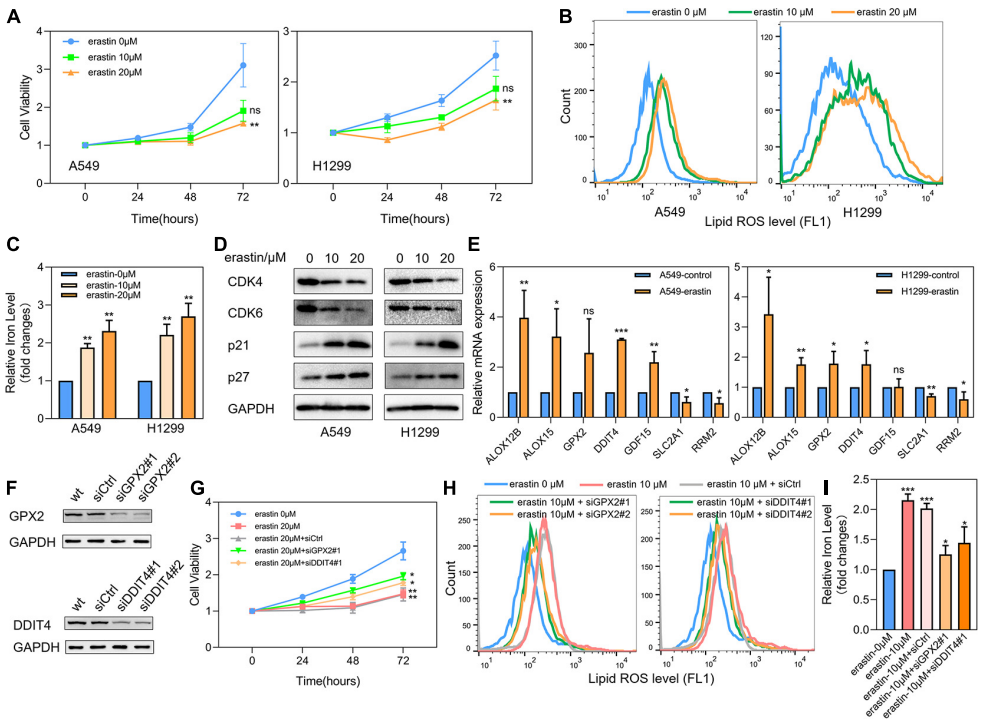

FIGURE 8 | Effects of ferroptosis inducer on expression levels of 7 core prognostic genes in LUAD cell lines *in vitro*. **(A)** The cell viability of A549 and H1299 treated by erastin was tested by CCK8 assay. **(B)** Lipid ROS levels of A549 and H1299 treated by erastin were detected by FACS. **(C)** Iron concentrations of A549 and H1299 treated by erastin were detected by iron colorimetric assay. **(D)** The expression levels of several cell cycle regulators in A549 and H1299 after erastin treatment were assayed by Western blotting. **(E)** The expression changes of 7 core prognostic genes in A549 and H1299 after treated with erastin were detected by real time PCR. **(F)** Silencing of GPX2 and DDIT4 in A549 by siRNAs. **(G)** The cell viability of A549 after erastin treatment in combination with or without GPX2 or DDIT4 silencing were detected by CCK8 assay. **(H)** Lipid ROS levels of A549 after erastin treatment in combination with or without GPX2 or DDIT4 silencing were detected by FACS. **(I)** Iron concentrations of A549 after erastin treatment in combination with or without GPX2 or DDIT4 silencing were detected by iron colorimetric assay. ns, not significant; $^{*}P < 0.05$; $^{**}P < 0.01$; $^{***}P < 0.001$.

constituting the ferroptosis-related prognosis signature have been reported to mediating ferroptosis, there is almost no evidence that they could regulate ferroptosis in lung cancer except for ALOX15 and SLC2A1. Therefore, further experimental evidence is needed to validate the ferroptosis-regulating functions of these core prognostic genes in LUAD. 3) A total of 6 cohorts (LUAD cohort of TCGA and 5 GEO cohorts) were used for the construction and external validation of the prognostic signature, however, all the sample information was extracted from the public database. We think this ferroptosis-related prognostic signature would be more reliable if it is tested by a prospective clinical trial cohort in our research center.

CONCLUSION

In summary, we systematically analyzed the expression profiles and prognostic significance of 259 ferroptosis-related genes in LUAD patients, and developed a ferroptosis-related prognostic signature consisting of 7 core prognostic DEGs. The efficacy of our prognostic signature was further tested by external validation cohorts. The ferroptosis-related risk was proven to be an independent prognostic factor for LUAD patients. Besides, the expression patterns of 7 core prognostic genes in LUAD and normal lung tissues were confirmed by IHC. The changes related to cell cycle and ferroptosis in LUAD cell line after erastin treatment were also verified by *in vitro* experiments. The potential roles of GPX2 and DDIT4 as ferroptosis drivers in LUAD cell line were further confirmed by siRNA experiments. However, the specific role and regulatory mechanism of these 7 ferroptosis-related genes in LUAD is still needed further experimental verifications. The prospective clinical studies are also needed to validate the clinical application value of our prognostic signature.

DATA AVAILABILITY STATEMENT

The datasets presented in this study can be found in online repositories. The names of the repository/repositories and accession number(s) can be found in the article/**Supplementary Material**.

ETHICS STATEMENT

The studies involving human participants were reviewed and approved by the Ethics Committee of the First Affiliated Hospital

of Xi'an Jiaotong University. The patients/participants provided their written informed consent to participate in this study.

AUTHOR CONTRIBUTIONS

QT and LZ contributed to the study design and performed the experiments. YZ and HG contributed to data collection. QT, YZ, and JY performed statistical analysis and interpretation. QT and JY drafted the manuscript. All authors contributed to critical revision of the final manuscript.

FUNDING

This study was supported by the National Natural Science Foundation of China (No. 82002794) and Key Research and Development Program of Shaanxi Province (No. 2020GXLH-Y-018).

ACKNOWLEDGMENTS

We thank The Cancer Genome Atlas (TCGA) and Gene Expression Omnibus (GEO) for providing transcriptomics and clinicopathological data.

SUPPLEMENTARY MATERIAL

The Supplementary Material for this article can be found online at: https://www.frontiersin.org/articles/10.3389/fcell.2021.684259/full#supplementary-material

Supplementary Figure 1 | Differential expression of ferroptosis-related genes in LUAD and normal lung tissues. The heatmap **(A)** and volcano map **(B)** depicted the expression levels and distribution of 70 ferroptosis-related DEGs. The boxplot **(C)** showed the difference in expression levels of 20 potential prognostic ferroptosis-related DEGs in tumor and normal tissues.

Supplementary Figure 2 | Establishment of the prognostic model by LASSO Cox regression. **(A,B)** LASSO regression coefficient profiles. **(C)** Table of regression coefficients of 7 core prognostic genes.

REFERENCES

Alvarez, S. W., Sviderskiy, V. O., Terzi, E. M., Papagiannakopoulos, T., Moreira, A. L., Adams, S., et al. (2017). NFS1 undergoes positive selection in lung tumours and protects cells from ferroptosis. *Nature* 551, 639–643. doi: 10.1038/nature24637

Bersuker, K., Hendricks, J. M., Li, Z., Magtanong, L., Ford, B., and Tang, P. H. (2019). The CoQ oxidoreductase FSP1 acts parallel to GPX4 to inhibit ferroptosis. *Nature* 575, 688–692. doi: 10.1038/s41586-019-1705-2

Brigelius-Flohe, R., and Flohe, L. (2020). Regulatory phenomena in the glutathione peroxidase superfamily. *Antioxid. Redox Signal.* 33, 498–516. doi: 10.1089/ars.2019.7905

Chen, L., Qiao, L., Bian, Y., and Sun, X. (2020). GDF15 knockdown promotes erastin-induced ferroptosis by decreasing SLC7A11 expression. *Biochem. Biophys. Res. Commun.* 526, 293–299. doi: 10.1016/j.bbrc.2020.03.079

Chen, P., Wu, Q., Feng, J., Yan, L., Sun, Y., Liu, S., et al. (2020). Erianin, a novel dibenzyl compound in *Dendrobium* extract, inhibits lung cancer cell growth and migration via calcium/calmodulin-dependent ferroptosis. *Signal Transduct. Target. Ther.* 5:51.

Dixon, S. J., Patel, D. N., Welsch, M., Skouta, R., Lee, E. D., Hayano, M., et al. (2014). Pharmacological inhibition of cystine–glutamate exchange induces endoplasmic reticulum stress and ferroptosis. *Elife* 3:e02523.

Doll, S., Freitas, F. P., Shah, R., Aldrovandi, M., da Silva, M. C., Ingold, I., et al. (2019). FSP1 is a glutathione-independent ferroptosis suppressor. *Nature* 575, 693–698. doi: 10.1038/s41586-019-1707-0

Friedmann Angeli, J. P., Schneider, M., Proneth, B., Tyurina, Y. Y., Tyurin, V. A., Hammond, V. J., et al. (2014). Inactivation of the ferroptosis regulator Gpx4 triggers acute renal failure in mice. *Nat. Cell Biol.* 16, 1180–1191. doi: 10.1038/ncb3064

Jang, J.-H., Janker, F., De Meester, I., Arni, S., Borgeaud, N., Yamada, Y., et al. (2019). The CD26/DPP4-inhibitor vildagliptin suppresses lung cancer growth via macrophage-mediated NK cell activity. *Carcinogenesis* 40, 324–334. doi: 10.1093/carcin/bgz009

Jiang, L., Kon, N., Li, T., Wang, S. J., Su, T., Hibshoosh, H., et al. (2015). Ferroptosis as a p53-mediated activity during tumour suppression. *Nature* 520, 57–62. doi: 10.1038/nature14344

Jiang, M., Qiao, M., Zhao, C., Deng, J., Li, X., and Zhou, C. (2020). Targeting ferroptosis for cancer therapy: exploring novel strategies from its mechanisms and role in cancers. *Transl. Lung Cancer Res.* 9, 1569–1584. doi: 10.21037/tlcr-20-341

Jiang, Y., Mao, C., Yang, R., Yan, B., Shi, Y., Liu, X., et al. (2017). EGLN1/c-Myc induced lymphoid-specific helicase inhibits ferroptosis through lipid metabolic gene expression changes. *Theranostics* 7, 3293–3305. doi: 10.7150/thno.19988

Kwon, O. S., Kwon, E. J., Kong, H. J., Choi, J. Y., Kim, Y. J., Lee, E. W., et al. (2020). Systematic identification of a nuclear receptor-enriched predictive signature for erastin-induced ferroptosis. *Redox Biol.* 37:101719. doi: 10.1016/j.redox.2020.101719

Li, J., Cao, F., Yin, H. L., Huang, Z. J., Lin, Z. T., Mao, N., et al. (2020). Ferroptosis: past, present and future. *Cell Death Dis.* 11:88.

Liu, P., Wu, D., Duan, J., Xiao, H., Zhou, Y., Zhao, L., et al. (2020). NRF2 regulates the sensitivity of human NSCLC cells to cystine deprivation-induced ferroptosis via FOCAD-FAK signaling pathway. *Redox Biol.* 37:101702. doi: 10.1016/j.redox.2020.101702

Lou, J. S., Zhao, L. P., Huang, Z. H., Chen, X. Y., Xu, J. T., Tai, W. C., et al. (2020). Ginkgetin derived from *Ginkgo biloba* leaves enhances the therapeutic effect of cisplatin via ferroptosis-mediated disruption of the Nrf2/HO-1 axis in EGFR wild-type non-small-cell lung cancer. *Phytomedicine* 80:153370. doi: 10.1016/j.phymed.2020.153370

Miller, K. D., Siegel, R. L., Lin, C. C., Mariotto, A. B., Kramer, J. L., Rowland, J. H., et al. (2016). Cancer treatment and survivorship statistics, 2016. *CA Cancer J. Clin.* 66, 271–289.

Okayama, H., Kohno, T., Ishii, Y., Shimada, Y., Shiraishi, K., Lwakawa, R., et al. (2012). Identification of genes upregulated in ALK-positive and EGFR/KRAS/ALK-negative lung adenocarcinomas. *Cancer Res.* 72, 100–111. doi: 10.1158/0008-5472.can-11-1403

Ou, Y., Wang, S.-J., Li, D., Chu, B., and Gu, W. (2016). Activation of SAT1 engages polyamine metabolism with p53-mediated ferroptotic responses. *Proc. Natl. Acad. Sci. U.S.A.* 113, E6806–E6812.

Ren, J. X., Sun, X., Yan, X. L., Guo, Z. N., and Yang, Y. (2020). Ferroptosis in neurological diseases. *Front. Cell. Neurosci.* 14:218. doi: 10.3389/fncel.2020.00218

Rousseaux, S., Debernardi, A., Jacquiau, B., Vitte, A. L., Vesin, A., Mignotte, H. N., et al. (2013). Ectopic activation of germline and placental genes identifies aggressive metastasis-prone lung cancers. *Sci. Transl. Med.* 5:186ra66. doi: 10.1126/scitranslmed.3005723

Sato, M., Larsen, J. E., Lee, W., Sun, H., Shames, D. S., Dalvi, M. P., et al. (2013). Human lung epithelial cells progressed to malignancy through specific oncogenic manipulations. *Mol. Cancer Res.* 11, 638–650. doi: 10.1158/1541-7786.mcr-12-0634-t

Shintoku, R., Takigawa, Y., Yamada, K., Kubota, C., Yoshimoto, Y., Takeuchi, T., et al. (2017). Lipoxygenase-mediated generation of lipid peroxides enhances

ferroptosis induced by erastin and RSL3. *Cancer Sci.* 108, 2187–2194. doi: 10.1111/cas.13380

Shukla, S., Evans, J. R., Malik, R., Feng, F. Y., Dhanasekaran, S. M., Cao, X., et al. (2017). Development of a RNA-Seq based prognostic signature in lung adenocarcinoma. *J. Natl. Cancer Inst.* 109:djw200. doi: 10.1093/jnci/djw200

Siegel, R. L., Miller, K. D., and Jemal, A. (2020). Cancer statistics, 2020. *CA Cancer J. Clin.* 70, 7–30.

Takeuchi, T., Tomida, S., Yatabe, Y., Kosaka, T., Osada, H., Yanagisawa, K., et al. (2006). Expression profile-defined classification of lung adenocarcinoma shows close relationship with underlying major genetic changes and clinicopathologic behaviors. *J. Clin. Oncol.* 24, 1679–1688. doi: 10.1200/jco.2005.03.8224

Tomida, S., Takeuchi, T., Shimada, Y., Arima, C., Matsuo, K., Mitsudomi, T., et al. (2009). Relapse-related molecular signature in lung adenocarcinomas identifies patients with dismal prognosis. *J. Clin. Oncol.* 27, 2793–2799. doi: 10.1200/jco.2008.19.7053

Xie, Y., Zhu, S., Song, X., Sun, X., Fan, Y., Liu, J., et al. (2017). The tumor suppressor p53 limits ferroptosis by blocking DPP4 activity. *Cell Rep.* 20, 1692–1704. doi: 10.1016/j.celrep.2017.07.055

Yang, W. S., Kim, K. J., Gaschler, M. M., Patel, M., Shchepinov, M. S., and Stockwell, B. R. (2016). Peroxidation of polyunsaturated fatty acids by lipoxygenases drives ferroptosis. *Proc. Natl Acad. Sci. U.S.A.* 113, E4966–E4975.

Yang, W. S., SriRamaratnam, R., Welsch, M. E., Shimada, K., Skouta, R., Viswanathan, V. S., et al. (2014). Regulation of ferroptotic cancer cell death by GPX4. *Cell* 156, 317–331. doi: 10.1016/j.cell.2013.12.010

Zhang, X., Du, L., Qiao, Y., Zhang, X., Zheng, W., Wu, Q., et al. (2019). Ferroptosis is governed by differential regulation of transcription in liver cancer. *Redox Biol.* 24:101211. doi: 10.1016/j.redox.2019.101211

Zhou, N., and Bao, J. (2020). FerrDb: a manually curated resource for regulators and markers of ferroptosis and ferroptosis-disease associations. *Database* 2020:baaa021.

Conflict of Interest: The authors declare that the research was conducted in the absence of any commercial or financial relationships that could be construed as a potential conflict of interest.

frontiers in Cell and Developmental Biology

HYPOTHESIS AND THEORY
published: 13 September 2021
doi: 10.3389/fcell.2021.728172

Nrf2 Is a Potential Modulator for Orchestrating Iron Homeostasis and Redox Balance in Cancer Cells

Lingyan Zhang, Jian Zhang, Yuanqing Jin, Gang Yao, Hai Zhao, Penghai Qiao and Shuguang Wu*

Institute of Laboratory Animal Science, Guizhou University of Traditional Chinese Medicine, Guiyang, China

Iron is an essential trace mineral element in almost all living cells and organisms. However, cellular iron metabolism pathways are disturbed in most cancer cell types. Cancer cells have a high demand of iron. To maintain rapid growth and proliferation, cancer cells absorb large amounts of iron by altering expression of iron metabolism related proteins. However, iron can catalyze the production of reactive oxygen species (ROS) through Fenton reaction. Nuclear factor (erythroid-derived 2)-like 2 (Nrf2) is an important player in the resistance to oxidative damage by inducing the transcription of antioxidant genes. Aberrant activation of Nrf2 is observed in most cancer cell types. It has been revealed that the over-activation of Nrf2 promotes cell proliferation, suppresses cell apoptosis, enhances the self-renewal capability of cancer stem cells, and even increases the chemoresistance and radioresistance of cancer cells. Recently, several genes involving cellular iron homeostasis are identified under the control of Nrf2. Since cancer cells require amounts of iron and Nrf2 plays pivotal roles in oxidative defense and iron metabolism, it is highly probable that Nrf2 is a potential modulator orchestrating iron homeostasis and redox balance in cancer cells. In this hypothesis, we summarize the recent findings of the role of iron and Nrf2 in cancer cells and demonstrate how Nrf2 balances the oxidative stress induced by iron through regulating antioxidant enzymes and iron metabolism. This hypothesis provides new insights into the role of Nrf2 in cancer progression. Since ferroptosis is dependent on lipid peroxide and iron accumulation, Nrf2 inhibition may dramatically increase sensitivity to ferroptosis. The combination of Nrf2 inhibitors with ferroptosis inducers may exert greater efficacy on cancer therapy.

Keywords: Nrf2, iron homeostasis, redox balance, cancer, ferroptosis

OPEN ACCESS

Edited by:
Ahmed Hamaï, Institut National de la Santé et de la Recherche Médicale (INSERM), France

Reviewed by:
Milena Botelho Pereira Soares, Gonçalo Moniz Institute (IGM), Brazil
Esmaa Bouhamida, University of Ferrara, Italy

****Correspondence:***
Jian Zhang
zhangjian075@gzy.edu.cn

Specialty section:
This article was submitted to Molecular and Cellular Oncology, a section of the journal Frontiers in Cell and Developmental Biology

Received: *21 June 2021*
Accepted: *16 August 2021*
Published: *13 September 2021*

Citation:
Zhang L, Zhang J, Jin Y, Yao G, Zhao H, Qiao P and Wu S (2021) Nrf2 Is a Potential Modulator for Orchestrating Iron Homeostasis and Redox Balance in Cancer Cells. Front. Cell Dev. Biol. 9:728172. doi: 10.3389/fcell.2021.728172

INTRODUCTION

Iron is an essential trace mineral element in the body and is engaged in a wide range of biological processes, such as oxygen transport, electron transport, energy metabolism, DNA synthesis and repair, etc. (Torti et al., 2018). Cancer cells have a high demand for iron compared with normal cells to initiate carcinogenesis, sustain uncontrolled proliferation, and other events necessary for cancer progression. However, excess iron is toxic. Iron can catalyze the production of a highly

toxic hydroxyl radical *via* Fenton/Haber–Weiss reaction cycle (Torti and Torti, 2020). Iron-mediated oxidative stress not only induces oxidative damage but also induces ferroptosis *via* lipid peroxidation (Anandhan et al., 2020; Chen et al., 2020). Considering the high levels of intracellular iron within cancer cells, ferroptosis induction provides an alternative strategy for cancer therapy.

Nuclear factor (erythroid-derived 2)-like 2 (Nrf2) is an important transcription regulator of cellular resistance to oxidative stress (Bellezza et al., 2018). Nrf2 is found to mediate transcription of a set of antioxidant and cellular protective genes, attenuating cellular injury from oxidative stress. Nrf2-mediated antioxidant capabilities have been demonstrated to prevent multiple diseases, including neurodegenerative diseases (Song and Long, 2020), cardiovascular disorders (Vashi and Patel, 2021), osteoporosis (Sun et al., 2015), and inflammation (Ahmed et al., 2017). Oxidative stress is suggested to be involved in cancer initiation and progression. To maintain redox balance and avoid oxidative damage, cancer cells upregulate their antioxidant capacity (Reczek and Chandel, 2017). Indeed, a variety of cancers exhibit hyperactivation of Nrf2, conferring aggressive proliferation (Okazaki et al., 2020), metastasis (Lignitto et al., 2019), chemoresistance (Jeong et al., 2020), and radioresistance (Wang Z. et al., 2020). Nrf2 hyperactivation counteracts the large amount of reactive oxygen species (ROS) production induced by excess iron (Wu et al., 2019; Zimta et al., 2019). On the other hand, ferritin (an iron storage protein) and ferroportin 1 (FPN1, an iron exporter protein) are under the control of Nrf2 (Kasai et al., 2018). Ferritin and FPN1 reduce the cellular free iron by enhancing iron sequestration and export (Chen et al., 2021). Since cancer cells have an enhanced iron uptake and Nrf2 plays pivotal roles in oxidative defense and iron metabolism, it is highly probable that Nrf2 is a potential modulator orchestrating iron homeostasis and redox balance in cancer cells. Oxidative stress can be induced by the high levels of iron accumulation in cancer cells and activates the Nrf2 pathway (Bellezza et al., 2018; Nakamura et al., 2019). Nrf2 not only eliminates ROS by inducing expression of antioxidant genes but also removes iron by FPN1 and neutralizes free iron by ferritin. From this point, Nrf2 exhibits pro-oncogenic activity (Jung et al., 2018). Nrf2 inhibition has attracted more attention on cancer therapy (Qin et al., 2019). However, most of the Nrf2 inhibitors exhibit low potency, limiting its clinical application (Jung et al., 2018; Qin et al., 2019). A combination of Nrf2 inhibitors with ferroptosis inducers may exert greater efficacy on cancer therapy.

IRON, OXIDATIVE STRESS, AND FERROPTOSIS

As a transition metal, iron in its free state is toxic to our body. Circulating ferric iron is bound by transferrin (Tf) and is taken up through transferrin receptor 1 (TfR1) mediated endocytosis. The ferric iron is then released from transferrin and is reduced to ferrous iron by ferrireductase six-transmembrane epithelial antigen of the prostate 3 (STEAP3) proteins in the endosomes. Subsequently, the ferrous iron enters the cytoplasm *via* divalent metal transporter 1 (DMT1) and is utilized for the synthesis of heme and iron-sulfur (Fe/S) clusters. The excess iron can be stored in ferritin, the major iron-storage protein at the cellular level, or is exported from cells through FPN1, the only known iron exporter (Sacco et al., 2021; Zhang et al., 2021). Hepcidin, an iron regulator synthesized in the liver, controls iron export from cells by inducing the internalization and degradation of FPN1 (Camaschella et al., 2020). Under normal condition, the cellular iron homeostasis is tightly regulated to avoid the enhanced labile iron pool (LIP), a pool of chelatable and redox-active iron (Nakamura et al., 2019). As a transition metal, iron can undergo redox cycling reactions between ferrous (Fe^{2+}) and ferric (Fe^{3+}) oxidation states. This redox activity enables ferrous iron to transfer an electron to hydrogen peroxide to generate highly toxic hydroxyl radical (HO•) and ferric iron (Nakamura et al., 2019). The reaction between ferrous iron and hydrogen peroxide to yield hydroxyl radicals is called Fenton reaction. In the presence of superoxide, the ferric iron can be reduced back to ferrous iron, which then undergoes Fenton reactions. Hydroxyl radicals are responsible for the cytotoxic effects by reacting with lipids, proteins, and nucleic acids (Nakamura et al., 2019).

Ferroptosis is a type of iron dependent oxidative cell death caused by the accumulation of ROS from the Fenton reaction and iron-mediated lipid peroxidation (Chen et al., 2020). Morphologically, cells undergoing ferroptosis exhibit unique characteristics, including reduced mitochondrial volume, increased bilayer membrane density, and reduction or disappearance of mitochondrial crista. Glutathione peroxidase 4 (GPX4), a kind of GSH-dependent reductase, plays a central role in regulating ferroptosis. GPX4 converts lipid hydroperoxides to lipid alcohols, preventing the formation of toxic lipid ROS. Inactivation of antioxidant GPX4 dependent systems provokes ferroptosis (Lei et al., 2021). Cellular iron is considered as an essential factor in ferroptosis. Increased intracellular ferrous iron levels are often observed during the induction of ferroptosis (Hou et al., 2016). Enhanced iron uptake markedly increases the sensitivity of cells to ferroptosis inducers and even directly induces ferroptosis (Gao et al., 2019). Iron chelators significantly inhibit the occurrence of ferroptosis (Chen et al., 2020). Ferroptosis opens new avenues for those chemoresistant and radioresistant cancers. The relationships among iron, oxidative stress, and ferroptosis are summarized in **Figure 1**.

IRON AND CANCER

Epidemiological Studies

People with iron overload have a higher cancer risk (Torti et al., 2018). Many epidemiological studies have investigated the association between iron status and cancer risk. The risk of cancer occurrence and mortality in the group with above 60% transferrin saturation relative to the 0–30% group is 1.81 and 1.73 (Stevens et al., 1994). For participants with serum iron higher than 141 μg/dl, their relative risks of cancer mortality are 1.86 compared with those with serum iron of 61–94 μg/dl (Wu et al., 2004). For people with transferrin saturation more than 43%, dietary iron more than 18 mg/day increases cancer

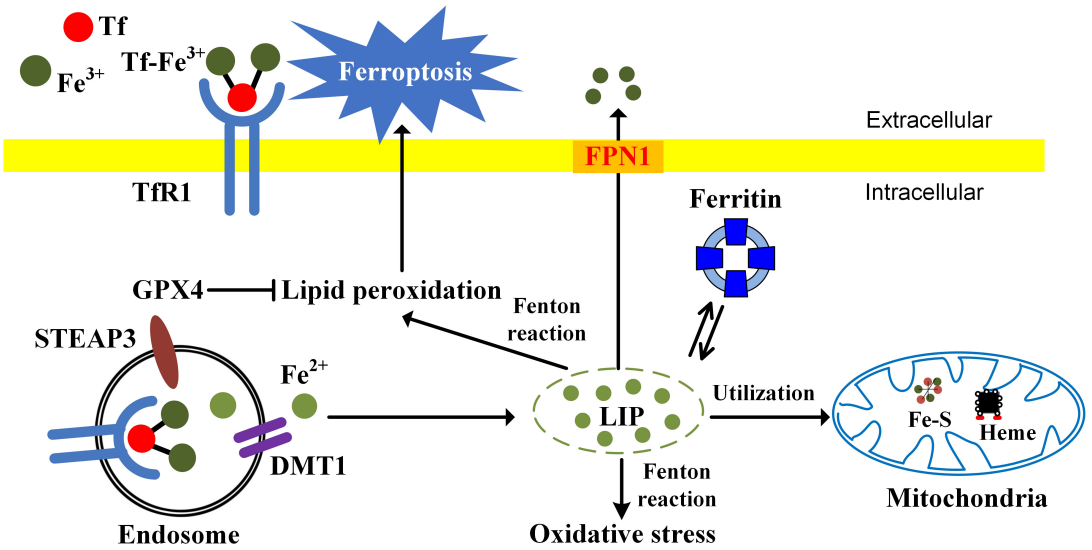

FIGURE 1 | The relationships among iron, oxidative stress, and ferroptosis. TfR1-mediated iron uptake is the major way for iron acquisition by most mammalian cells. When Tf binds to the cell-surface TfR1, the complex is internalized by receptor-mediated endocytosis. Ferric iron is then released and reduced to the ferrous state by ferrireductase STEAP3. After that, Fe^{2+} is transported into the cytosol from the endosome by DMT1. In mitochondria, iron is utilized for the synthesis of Fe-S clusters and heme. Ferritin is the major iron-storage protein. Cellular free iron catalyzes the formation of ROS and causes oxidative stress *via* Fenton reaction. The excessive iron-dependent generation of lipid peroxidation can lead to ferroptosis.

risk (Mainous et al., 2005). Women with serum ferritin higher than 160 μg/L may have an increased risk of cancers (Hercberg et al., 2005). Cancers of the esophagus, colon, rectum, lung, and bladder are strongly associated with body iron level (Stevens et al., 1994). High iron stores, as indicated by the level of transferrin saturation exceeding 60%, increase the risks of colorectal cancer. The relative risks, adjusted for age, sex, and smoking, are 3.04 for colorectal cancer in comparison with subjects with lower iron levels (Knekt et al., 1994). Moreover, heme iron intake, serum iron, and transferrin saturation are associated with increased risks of breast cancer and death in women (Kallianpur et al., 2008; Gaur et al., 2013; Chua et al., 2016; Chang et al., 2019). High serum iron (≥120 μg/dl) is associated with elevated risks of incidence and mortality from all cancers, particularly liver and breast cancers (Wen et al., 2014). Hepcidin, encoded by the hepatic antimicrobial protein gene (*HAMP*), is a key regulator of systemic iron metabolism. It inhibits iron export by binding to FPN1, inducing its internalization and degradation. Hepcidin deficiency causes accumulation of cellular iron. The polymorphism rs10421768 in *HAMP* is reported to be associated with a three-times higher lung cancer risk (Sukiennicki et al., 2019). This polymorphism is considered to be a modulator of iron overload (Radio et al., 2015).

Some reports suggest positive correlations between iron intake and certain cancers (Beguin et al., 2014). A significant association is found between colorectal cancer risk and higher intake of heme iron and iron from red meat (Luo et al., 2019). Some endemiological studies show that people with high dietary iron intake are at a high risk for lung cancer (Kuang and Wang, 2019; Ward et al., 2019). High intake of heme iron, which is present predominantly in meat, is positively associated with breast cancer risk (Chang et al., 2019). There is a modest positive association between heme iron, total iron, and liver intakes and endometrial cancer risk (Genkinger et al., 2012).

Hereditary hemochromatosis, characterized by iron overload, is a genetic disease resulting in increased intestinal iron absorption. Patients (particularly men) with hereditary hemochromatosis are at an increased risk for hepatocellular cancer (Fracanzani et al., 2001; Elmberg et al., 2003). Blood transfusions or donation may influence the cancer risks through regulating iron stores. Donating blood removes iron from the body. Repeated blood transfusions cause iron overload. Blood donors had significantly lower mortality compared with non-donor cancer patients (Vahidnia et al., 2013). Iron reduction by phlebotomy in patients with peripheral arterial disease reduces the risk of new cancers, including lung, colorectal, upper aerodigestive, and prostate cancers (Zacharski et al., 2008). Long-term phlebotomy with low-iron diet therapy lowers the risk of development of hepatocellular carcinoma from chronic hepatitis C (Kato et al., 2007). In contrast, blood transfusion increases cancer risk (Hjalgrim et al., 2007).

Iron Is Involved in Carcinogenesis and Tumor Growth

Carcinogenesis

Oxidative damage to DNA is intimately associated with carcinogenesis. Mitochondria and nicotinamide adenine dinucleotide phosphate (NADPH) oxidases (NOX) are the major sources of ROS. During the flow of electrons through the electron transport chain, some electrons leak from the electron transport chain and combine with oxygen to form superoxide. NOX transfers an electron from NADPH to

molecular oxygen to generate superoxide (Panday et al., 2015). After that, the intracellular superoxide can be rapidly dismutated to hydrogen peroxide (H_2O_2) through superoxide dismutase (SOD). Hydrogen peroxide can be removed by the antioxidant enzyme catalase, catalyzing the conversion of hydrogen peroxide to harmless water and oxygen. If the cells have a high level of LIP, more hydroxyl radicals can be induced through Fenton reactions. Unlike superoxide and hydrogen peroxide, hydroxyl radical cannot be eliminated by antioxidant enzymes. Furthermore, hydroxyl radical has an extremely high reactivity. Hydrogen peroxide can aggressively react with any biochemical or macromolecules and causes more severe damage to the cell than any other free radicals. Hydroxyl radicals tend to cause DNA damage, resulting in the accumulation of oncogenes and mutations of tumor suppressor genes (Torti and Torti, 2020). However, direct evidence linking iron overload to carcinogenesis is still lacking.

Diseases with iron overload, such as hereditary hemochromatosis and β-thalassemia, have a high risk of liver cancer, for liver is the main site of iron storage (Fracanzani et al., 2001; Maakaron et al., 2013). Recently, Muto et al. (2019) evaluated the effects of iron overload on liver carcinogenesis. They generate a mouse model of hepatocarcinogenesis induced by hepatic iron overload, in which F-box and leucine rich repeat protein 5 (*FBLX5*) is specifically deleted in hepatocytes (Muto et al., 2019). FBLX5 is an iron–sulfur cluster protein. The oxidation state of the cluster regulates iron regulatory protein 2 (IRP2) polyubiquitination and degradation in response to both iron and oxidative stress (Wang H. et al., 2020). *FBLX5* deletion induces iron accumulation by upregulating IRP2, leading to oxidative stress, inflammation, DNA damage, liver damage, and compensatory proliferation of hepatocytes (Muto et al., 2019). These alterations consequently promote liver carcinogenesis induced by exposure to the chemical carcinogen diethylnitrosamine. *IRP2* deletion rescues the increased carcinogenesis induced by *FBLX5* deficiency (Muto et al., 2019). FBLX5–IRP2 axis is a potential therapeutic target for hepatocellular carcinoma associated with cellular iron dysregulation. It should be noted that the association between iron and carcinogenesis arises from epidemiological studies and theoretical analysis. There is limited experimental evidence regarding the role of iron in carcinogenesis. Further studies are still needed to evaluate the underlying mechanisms of how iron overload initiates and promotes carcinogenesis.

Tumor Growth

Iron is closely associated with cancer growth. Excess iron facilitates cancer growth, while iron deficiency caused by reduced dietary intake or iron chelators has an inhibitory effect (Torti et al., 2018). Disruption of iron homeostasis also influences tumor growth. Reduction of iron uptake through blocking TfR1 or enhancing iron efflux through overexpression of FPN1 decreases tumor growth (White et al., 1990; Pinnix et al., 2010; Deng et al., 2019). DMT1 inhibition also negatively affects the proliferation of colorectal cancer cells (Xue et al., 2016). Cancer cells require a high level of energy to support proliferation, migration, and invasion. To meet their higher demand for energy, cancer cells have an increased mitochondrial biogenesis. Complexes I, III, and IV of the mitochondrial electron transport chain contains Fe-S clusters. For this reason, mitochondria biogenesis demands cellular iron uptake. Iron may contribute to cancer progression by supporting mitochondrial electron transport chain and ATP generation. Furthermore, iron and NOX can synergistically stimulate ROS production. Iron accentuates ROS production by NOX in activated microglia. NOX2 and NOX4 inhibition significantly reduces ROS production in microglia treated with iron (Yauger et al., 2019).

Intracellular Iron Regulation Is Altered in Cancer Cells

Generally, cancer cells require a high level of metabolically available iron by increasing iron uptake and decreasing iron storage and efflux. Manipulation of the proteins of iron metabolism may contribute to cancer growth and progression. TfR1 is highly expressed in a variety of cancers, such as leukemia, lymphoma, breast cancer, lung cancer, glioma, and others (Daniels et al., 2012). Furthermore, increased iron storage is also observed in cancer stem cells (Schonberg et al., 2015). TfR1 is a candidate marker of poor prognosis in breast cancer (Habashy et al., 2010). Therefore, TfR1 is a promising target in treating the cancers with overexpressed TfR1 and increased iron demands (Candelaria et al., 2021). Anti-TfR1 antibodies have been demonstrated to be an efficient therapy for leukemias and lymphomas (Neiveyans et al., 2019).

Serum ferritin is associated with poor prognosis in various cancers, including hepatobiliary cancer (Facciorusso et al., 2014; Song et al., 2018), lung cancer (Ji et al., 2014), pancreas cancer (Kalousová et al., 2012), T-cell lymphoma (Koyama et al., 2017), renal cancer (Singh et al., 2005) and colorectal cancer (Lee et al., 2016). Ferritin is also associated with many signaling pathways in cancer, such as p53, NF-κB (nuclear factor kappa-light-chain-enhancer of activated B cells), anti-apoptosis process, invasion, and metastasis (Alkhateeb and Connor, 2013; Min and James, 2015). Ferritin may serve as a promising and effective anticancer target. Some studies have demonstrated the therapeutic roles of ferritin in cancer treatments. Downregulation of ferritin enhances the chemosensitivity of breast cancer cells and glioma cells to chemotherapy (Liu et al., 2011; Shpyleva et al., 2011), and significantly reduces the growth rate of the tumor xenograft of melanoma cells (Di Sanzo et al., 2011).

Ferroportin 1 is the only known cellular iron efflux pump. FPN1 is downregulated in breast (Pinnix et al., 2010), prostate (Tesfay et al., 2015), and ovarian (Basuli et al., 2017) cancers. Transfection of breast cancer cells with FPN1 significantly reduces the level of intracellular iron and its growth. Increased FPN1 is associated with a cohort of breast cancer patients who have a 10-year survival rate of >90% (Pinnix et al., 2010). Overexpression of FPN1 decreases tumorigenicity and invasion of ovarian cancer cells (Basuli et al., 2017). FPN1 is tightly regulated by hepcidin, a circulating hormone mainly synthesized in the liver. However, recent studies show that hepcidin is also expressed in prostate and breast epithelial cells (Pinnix et al., 2010; Tesfay et al., 2015). Hepcidin downregulates FPN1 as an

autocrine hormone, increases intracellular iron, and contributes to cancer cell progression (Pinnix et al., 2010; Tesfay et al., 2015).

These results suggest that the measurement of proteins involved in cellular iron homeostasis could be helpful in cancer prognosis. Decreasing cellular iron uptake by blocking TfR1 and increasing cellular iron export by overexpression of FPN1 are promising strategies for cancer therapy.

Ferroptosis

Ferroptosis is a morphologically, biochemically, and genetically distinct form of regulated cell death characterized by its dependence on iron. Intracellular iron accumulation causes oxidative stress, promotes lipid peroxidation, and consequently leads to cell death (Wu et al., 2020). Compared with normal cells, several cancers strongly rely on iron to support their growth. Enhanced iron uptake and retention are considered to be the hallmarks of cancer. Since ferroptosis is a result of metabolic dysfunction involving iron and ROS, the elevated levels of iron make cancer cells more vulnerable to ferroptosis (Torti and Torti, 2020). These features suggest that ferroptosis inducers could be used to improve the efficacy of cancer therapy. Ferroptosis offers a new way of targeted cancer therapy.

Iron accumulation and lipid peroxidation are two key factors initiating ferroptosis. Alterations of proteins involved in iron import, storage, and export have been demonstrated to influence sensitivity to ferroptosis (**Figure 2**; Hassannia et al., 2019). Knockdown of TfR1 suppresses ferroptosis induced by erastin or cystine deprivation (Yang and Stockwell, 2008; Gao et al., 2015). FTH1 expression levels are negatively associated with ferroptosis sensitivity (Yang and Stockwell, 2008). Knockdown of FTH1 by RNA interference enhances ferroptosis induced by erastin or sorafenib in hepatocellular carcinoma cells (Sun et al., 2016). Overexpression of PFN1 enhanced iron efflux lowers intracellular iron level and sensitizes ovarian cancer cells to ferroptosis (Basuli et al., 2017), while knockdown of ferroportin accelerates erastin (a ferroptosis inducer)-induced ferroptosis in neuroblastoma cells (Geng et al., 2018). Dysregulation of IRP cellular iron homeostasis is regulated by IRP. In iron-starved cells, IRP2 increases cellular iron levels by stabilizing TfR1 mRNA and inhibiting translation of ferritin and FPN1 (Sacco et al., 2021). Knockdown of IRP2 suppresses the sensitivity of cancer cells to ferroptosis inducers (Dixon et al., 2012). Ferritinophagy plays a pivotal role in maintaining cellular iron homeostasis by regulating the autophagic degradation of iron-storage protein ferritin (Tang et al., 2018). This process is mediated by nuclear receptor coactivator 4 (NCOA4), acting as a specific cargo receptor, binding ferritin and targeting it to emerging autophagosome (Mancias et al., 2014). Knockdown of NCOA4 inhibits iron release from ferritin. Ferritinophagy has been demonstrated to contribute to ferroptosis in cancer cells. Genetic inhibition of NCOA4 not only inhibits ferritin degradation but also suppresses ferroptosis induced by erastin or cystine deprivation (Gao M. et al., 2016; Hou et al., 2016).

Mitochondria are the center of iron utilization. In mitochondria, iron is used for the synthesis of iron–sulfur clusters and heme. Alterations of mitochondrial iron metabolism influence ferroptosis. CDGSH iron sulfur domain 1 (CISD1, also termed mitoNEET) regulates mitochondrial iron transport. Knockdown of *CISD1* is found to cause mitochondrial iron overload and to enhance erastin-induced ferroptosis (Yuan et al., 2016). Aconitase 1 (ACO1) is bifunctional. When cellular iron levels are high, it binds to iron–sulfur and catalyzes citrate to isocitrate. When cellular iron levels are low, ACO1 interacts with iron-response elements (IREs) to controls the levels of iron inside cells. Knockdown of ACO1 suppresses ferroptosis induced by cystine deprivation (Gao M. et al., 2016). NFS1 (cysteine desulfurase) is an enzyme involving synthesizing iron-sulfur clusters using sulfur from cysteine. Suppression of NFS1 cooperates with inhibition of cysteine transport to trigger ferroptosis (Alvarez et al., 2017).

It is recognized that mitochondria are one of the major sources of intracellular ROS. Mitochondrial ROS is not only important for apoptosis but also contributes to ferroptosis (Wu et al., 2021). Ferroptosis inducers, erastin or RSL3, trigger a substantial generation of mitochondrial ROS in HT-22 and MEF cells (Neitemeier et al., 2017; Jelinek et al., 2018). MitoQ, a mitochondria-targeted antioxidant, inhibits ferroptosis induced by RSL3 (Neitemeier et al., 2017). Lipid peroxidation also occurs in mitochondria during ferroptosis (Feng and Stockwell, 2018). Upon erastin treatment, lipid peroxidation first appears in mitochondria and then in plasma membrane (Gao et al., 2019). CISD1 deletion induces iron accumulation within mitochondria, and facilitates the generation of iron-mediated mitochondrial lipid peroxidation (Yuan et al., 2016). It should be noted that mitochondria play a crucial role in cysteine deprivation-induced ferroptosis but not in that induced by inhibiting GPX4 (Gao et al., 2019). Inhibition of mitochondrial tricarboxylic acid cycle (TCA cycle) or electron transfer chain (ETC) mitigates lipid peroxide accumulation and ferroptosis (Gao et al., 2019).

REDOX BALANCE REGULATED BY Nrf2 DURING CANCER PROGRESSION

Nrf2-Mediated Antioxidant Response

Nrf2 is a Cap "n" Collar (CNC) basic leucine zipper (bZIP) transcription factor and is considered to be a critical regulator of cytoprotective response against oxidative and xenobiotic (or electrophilic) stresses (Bellezza et al., 2018). The Kelch-like ECH-associated protein 1 (Keap1)/Nrf2 signaling pathway plays a pivotal role in protecting against oxidative stress to maintain redox balance. Under physiological conditions, Nrf2 is constitutively maintained at a low protein level through rapid degradation *via* the Keap1-dependent proteasomal degradation. Keap1 recruits Nrf2 through binding to DLG and ETGE motifs, promotes the polyubiquitination of Nrf2 by Cullin-3 E3 ubiquitin ligase, and then induces proteasome-dependent degradation of Nrf2 by 26S proteasomal pathway. In case of oxidative stress, Nrf2 detaches from Keap1 and translocates to the nucleus, where it binds to antioxidant responsive elements (ARE) in the DNA promoter region and regulates an array of antioxidant genes, including catalase (CAT), heme oxygenase-1 (HO-1), NAD(P)H quinone dehydrogenase 1 (NQO-1), and enzymes involved in glutathione metabolism (Bellezza et al., 2018).

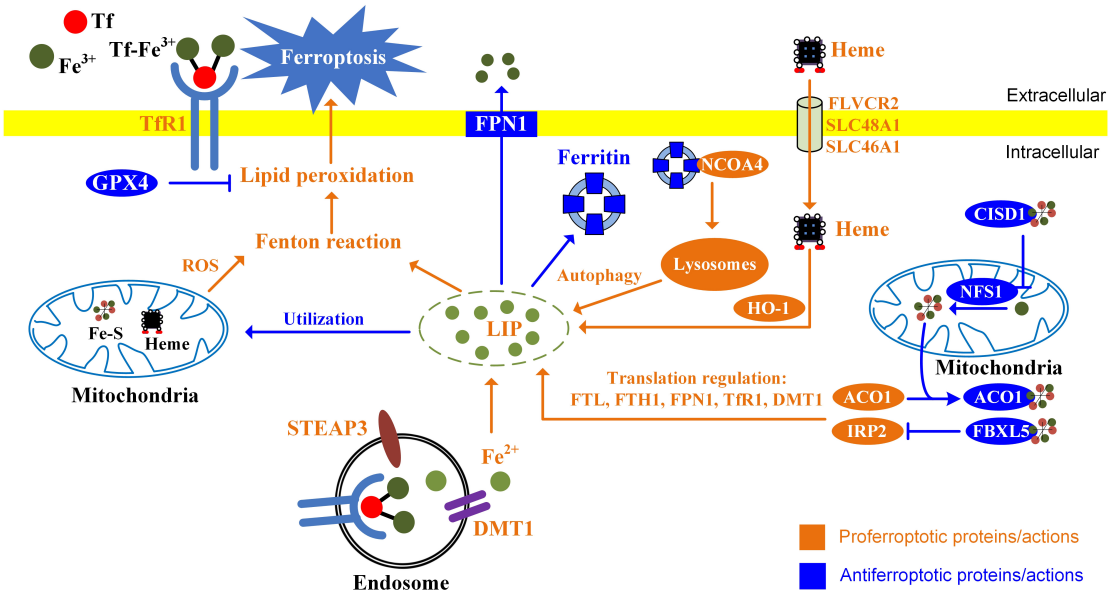

FIGURE 2 | Alterations of iron metabolism influence ferroptosis in cancer cells. The ways of increasing absorption, reducing iron storage, and limiting iron efflux contribute to ferroptosis. Endocytosis of diferric Tf is the major way for cellular iron uptake. In the endosomes, ferric iron is released from Tf, reduced by STEAP3, and transported to the cytosol through DMT1. Heme provides additional sources of iron through FLVCR2, SLC48A1, and SLC46A1 in the cell membrane. HO-1 catalyzes oxidative degradation of heme to liberate ferrous iron. Ferritin is a protein that stores iron, while NCOA4-mediated ferritinophagy promotes ferritin degradation and releases ferrous iron. Iron can be utilized for the synthesis of Heme and Fe-S clusters. Mitochondrial proteins regulating iron utilization (CISD1 and NFS1) negatively regulate ferroptosis. Iron-regulatory proteins ACO1 and IRP2 regulate ferroptosis by modulating FTL, FTH1, FPN1, TfR1, and DMT1 at the translational level.

Nrf2-mediated antioxidant response maintains redox homeostasis and exerts anti-inflammation and anticancer activities in normal cells. However, accumulating studies suggest that Nrf2 is aberrantly activated in many cancer types, including skin, breast, prostate, and lung. Nrf2 activation is associated with poor prognosis. Nrf2 promotes cancer cell proliferation, self−renewal of cancer stem cells, anti-inflammation activities, angiogenesis, chemoresistance, and radioresistance (Wu et al., 2019). Nrf2 activation promotes aggressive lung cancer. Patients with Nrf2-activated non-squamous or squamous tumors have poor prognosis and show limited response to anti-programmed death-ligand 1 (PD-L1) treatment (Singh et al., 2021). Nrf2 activation promotes the recurrence of dormant tumor cells. Nrf2 is found to be activated in recurrent tumors in animal models and patients with breast cancer with poor prognosis. Suppression of Nrf2 impairs recurrence (Fox et al., 2020).

Nrf2 Is Aberrantly Activated in Cancer Cells

The enhanced production of ROS is one of the fundamental features of cancer cells. Increased levels of ROS are pro-tumorigenic; supporting death evasion; uncontrolled proliferation; deregulating the cellular energetics; evading the immune response; provoking inflammation; inducing genome instability and mutations; and developing drug resistance, angiogenesis, invasiveness, and metastasis (Fouad and Aanei, 2017). Several mechanisms by which ROS production is enhanced in cancer cells have been described, such as oncogene activation, loss of cancer suppressors, and enhanced metabolism (Reczek and Chandel, 2017). Although enhanced ROS is essential for cancer survival and growth, the excess ROS must be eliminated to prevent cell death. To maintain redox balance and avoid oxidative damage, cancer cells upregulate their antioxidant capacity.

Constitutive Nrf2 activation maintains redox homeostasis by inducing the expression of antioxidants, enzymes involving GSH metabolism, and detoxification enzymes. Indeed, Nrf2 activation has been observed in various cancer types, including bladder cancer, breast cancer, cervical cancer, colon cancer, gastric cancer, globlastoma, glioma, hepatocellular carcinoma, lung cancer, multiple myeloma, pancreatic cancer, and ovarian cancer (Zimta et al., 2019). Nrf2 activation contributes to tumor growth, metastasis, and resistance to chemotherapy (Zimta et al., 2019). Constitutive activation of Nrf2 accelerates the recurrence of dormant tumor cells following therapy through regulation of redox and nucleotide metabolism (Fox et al., 2020). Furthermore, Nrf2 activation promotes NADPH production by regulating the pentose phosphate pathway and serine biosynthesis pathways (Wu et al., 2011; DeNicola et al., 2015). Hypoxia arises in tumor regions due to inadequate oxygen delivery, when the tumor rapidly outgrows its blood supply (Toth and Warfel, 2017). Hypoxia is well known to increase ROS production, eliciting oxidative stress. In response to hypoxia, Nrf2-mediated antioxidant pathway is also activated to improve hypoxia adaptation and cancer pathogenesis (Shi et al., 2019).

Several studies have demonstrated the underlying mechanisms of the constitutive activation of Nrf2 in cancers. Oncogenes,

K-Ras, B-Raf, and Myc each increased the transcription of Nrf2 and lower intracellular ROS (DeNicola et al., 2011). Loss of KEAP1 interaction domain by missing exon 2, or exons 2, and 3 in *NFE2L2* gene (encoding Nrf2), results in the failure of interaction with Keap1 (Goldstein et al., 2016). Succination of Keap1 cysteine residues abrogates its binding affinity with Nrf2 (Adam et al., 2011). Somatic mutations in Nrf2, CUL3, and SIRT1 confer an Nrf2 activation phenotype in cancer cells (Ooi et al., 2013). P1 region, including 12 CpG sites, is highly methylated in the Keap1 promoter, resulting in Keap1 downregulation (Wang et al., 2008). p62 interacts with the Nrf2-binding site on Keap1, leading to stabilization of Nrf2 (Komatsu et al., 2010). The KRR motif in p21 directly interacts with the DLG and ETGE motifs in Nrf2 and thus competes with Keap1 for Nrf2 binding, compromising the ubiquitination of Nrf2 (Chen et al., 2009).

Nrf2 Is a Potential Target for Cancer Therapy

Induction of ROS and oxidative stress is suggested to be involved in cancer initiation and progression. Cancer cells exhibit higher levels of ROS than normal cells (Hayes et al., 2020). The large amount of ROS activates Nrf2, preventing the possible oxidative damage induced by excess ROS. Nrf2 plays an important role in cancer progression, therapy resistance, and poor prognosis (Panieri and Saso, 2019). Therefore, Nrf2 is a potential therapeutic target in cancer therapy. Some Nrf2 inhibitors have been found with anti-cancer efficacy by suppressing Nrf2 expression, causing Nrf2 degradation or inhibiting Nrf2 nuclear translocation (Qin et al., 2019). These Nrf2 inhibitors include natural compounds derived from medicinal plants and some commercial drugs, such as procyanidin (Ohnuma et al., 2015, 2017), flavonoid luteolin (Chian et al., 2014), alkaloid trigonelline (Arlt et al., 2013), quassinoid brusatol (Tao et al., 2014; Olayanju et al., 2015; Karathedath et al., 2017; Wang M. et al., 2018), chrysin (Wang J. et al., 2018), oridonin (Lu et al., 2018), convallatoxin (Lee et al., 2018), honokiol (Gao D. Q. et al., 2016), wogonin (Qian et al., 2014; Xu et al., 2014, 2017; Kim et al., 2016), etc. Moreover, some commercial drugs, such as ascorbic acid (Tarumoto et al., 2004), retinoic acid (Valenzuela et al., 2014), antitubercular agent isoniazid (Verma et al., 2018), CDK inhibitor PHA-767491 (Liu et al., 2018), sorafenib (Zhou et al., 2013), valproic acid (Cha et al., 2016), metformin (Do et al., 2013, 2014; Yu et al., 2017; Sena et al., 2018), and glucocorticoid clobetasol propionate (Choi et al., 2017) also have anti-Nrf2 activity (Jung et al., 2018;

TABLE 1 | Nrf2 inhibitors in cancer research.

Compounds	Types of cancer/cell lines	Main findings	References
Procyanidin	Non-small-cell lung cancer/A549.	Reduce Nrf2 expression, and promote proteasome-independent degradation of nuclear Nrf2.	Ohnuma et al., 2015, 2017;
Luteolin	Non-small-cell lung cancer/A549.	Reduce Nrf2 expression and its downstream antioxidant enzymes.	Chian et al., 2014
Trigonelline	Pancreatic carcinoma/Panc1, Colo357, and MiaPaca2.	Block Nrf2-dependent proteasome activity.	Arlt et al., 2013
Brusatol	Acute myeloid leukemia/TPH1; Non-small-cell lung cancer/A549; Hepatoma/Hepa-1c1c7; Pancreatic cancer/PATU-8988 and PANC-1; Melanoma/A375.	Suppress Nrf2 pathway.	Tao et al., 2014; Olayanju et al., 2015; Karathedath et al., 2017; Wang M. et al., 2018
Chrysin	Glioblastoma/T98, U251, and U87.	Inhibit ERK/Nrf2 pathway.	Wang J. et al., 2018
Oridonin	Osteosarcoma/MG63 and HOS.	Suppress Nrf2 mediated antioxidant pathways.	Lu et al., 2018
Convallatoxin	Non-small-cell lung cancer/A549.	Suppression of Nrf2 is regulated at the level of proteolysis.	Lee et al., 2018
Honokiol	Lymphoid cancer/Raji and Molt4	Attenuate Nrf2 and NF-κB.	Gao D. Q. et al., 2016
Wogonin	Hepatoma/HepG2; Head and neck cancer/HNC; Leukemia/K562.	Inhibit Nrf2 *via* Stat3/NF-κB signaling.	Qian et al., 2014; Xu et al., 2014; Kim et al., 2016; Xu et al., 2017
Ascorbic acid	Leukemia/Imatinib-resistant KCL22.	Inhibit Nrf2 nuclear translocation.	Tarumoto et al., 2004
Retinoic acid	Acute myeloid leukemia/HL60.	Inhibit Nrf2 nuclear translocation.	Valenzuela et al., 2014
Isoniazid	Hepatoma/HepG2.	Inhibit Nrf2 nuclear translocation.	Verma et al., 2018
PHA-767491	Hepatoma/HepG2; Myeloma/MM.1S, L363, and U266.	Inhibit Nrf2 nuclear translocation.	Liu et al., 2018
Sorafenib	Hepatoma/5-FU resistant Bel-7402.	Suppress Nrf2 expression.	Zhou et al., 2013
Valproic acid	Papillary thyroid cancer/TPC1 and BCPAP.	Inhibit Nrf2 nuclear expression.	Cha et al., 2016
Metformin	Hepatoma/HepG2; Breast cancer/MCF-7; Colon cancer/HT29; Non-small-cell lung cancer/A549, H1299, and H460.	Suppress Nrf2 expression *via* downregulating PPARγ transcriptional activity.	Do et al., 2013; Do et al., 2014; Yu et al., 2017; Sena et al., 2018
Clobetasol propionate	Non-small-cell lung cancer/A549.	Suppress Nrf2 nuclear translocation and promote its degradation.	Choi et al., 2017

Panieri and Saso, 2019). These Nrf2 inhibitors are summarized in **Table 1**.

THE REGULATORY ROLE OF Nrf2 IN IRON HOMEOSTASIS

Free iron is toxic to the body by catalyzing the production of highly reactive hydroxyl radicals (OH·) through Fenton reaction. Therefore, the intracellular LIP must be tightly regulated. To date, most of the current researches on Nrf2 focus on its antioxidant properties. However, Nrf2 has been demonstrated to play a pivotal role in iron homeostasis. Nrf2 can regulate iron storage and iron efflux through ferritin, FPN1, and HO-1 gene transcription (Kasai et al., 2018).

Cellular Iron Homeostasis

Ferritin is a highly conserved and universal iron storage protein composed of 24 subunits of two types, ferritin heavy chain (FTH) and ferritin light chain (FTL). Ferritin can carry up to 4,500 iron atoms in its core and prevents iron-mediated formation of harmful ROS (Arosio et al., 2017). Therefore, ferritin has an antioxidant effect to some extent. The effects of Nrf2 on iron storage are first found in Nrf2-deficient mice. The *Nrf2*$^{-/-}$ mice exhibit abnormally white teeth due to defective iron utilization during the development of tooth enamel (Yanagawa et al., 2004). Subsequent research shows Nrf2 activation is responsible for the induction of ferritin. Some chemo-preventive agents, such as sulforaphane and 1,2-dithiole-3-thione, can activate Nrf2 and induce ferritin transcription (Kwak et al., 2001; Thimmulappa et al., 2002). Electrophoretic mobility shift assays demonstrate that Nrf2 binds ARE elements and mediates the transcriptional activation of ferritin (Pietsch et al., 2003). The induction of ferritin is not observed in Nrf2 knockout cells. These results suggest that Nrf2 mediates the induction of ferritin H and L in response to xenobiotics (Pietsch et al., 2003).

Nrf2 not only regulates iron homeostasis by inducing ferritin transcription but also decreases LIP by enhancing iron efflux of the cell. FPN1 is the only known mammalian iron exporter of non-heme iron. Nrf2 activation promotes FPN1 mRNA expression and enhances iron release (Harada et al., 2011). The ARE element located at position -7007/-7016 of *FPN1* promoter is involved in Nrf2-mediated transcription (Marro et al., 2010). The induction of *FPN1* by Nrf2 can be also regulated by BTB and CNC homology 1 (Bach1). Bach1 and Nrf2 compete to bind ARE-like enhancers in cells and regulate ARE-mediated FPN1 expression. The role of Bach1 in Nrf2-mediated *FPN1* regulation arises from studies on the heme induced *FPN1* expression in macrophages. Before erythrophagocytosis or Heme treatment, Bach1 binds to the ARE of *FPN1*. Upon Heme treatment, the heme-sensitive Bach1 releases from DNA and allows Nrf2 to bind, consequently promoting *FPN1* transcription (Marro et al., 2010). Whether Bach1 inactivation is involved in the regulation of ferritin transcription needs further investigation.

Heme, an iron-containing molecule, plays an essential role in mitochondrial electron transport as a cofactor of cytochromes. Heme can enter cell through FLVCR2 (feline leukemia virus subgroup C receptor-related protein 2), SLC48A1, and SCL46A1 in the cell membrane (Cao and Fleming, 2015). Its degradation is regulated by HO-1, which is also an Nrf2-regulated gene. HO-1 (encoded by *HMOX1*) is an initial and rate-limiting enzyme catalyzing the oxidative degradation of heme to produce biliverdin, ferrous iron, and carbon monoxide. Biliverdin is subsequently converted to bilirubin by biliverdin reductase (Chau, 2015). HO-1 overexpression may lead to the accumulation of iron derived from HO-1 catabolism and mediates the development of ferroptosis induced by erastin, withaferin A, and BAY 11-7058 (Kwon et al., 2015; Chang et al., 2018; Hassannia et al., 2018). Pharmacological inhibition or knockdown of HO-1 has an inhibitory effect (Kwon et al., 2015; Chang et al., 2018; Hassannia et al., 2018). It has been proven that Nrf2/HO-1 mediates tagitinin C-induced ferroptosis (Wei R. et al., 2021). In addition to its primary role in heme catabolism, HO-1 exhibits anti-oxidative functions *via* the actions of bilirubin (Chau, 2015). Activation of Nrf2/HO-1 axis is also involved in the cytoprotective effects against ferroptosis (Jiang et al., 2020; Ma et al., 2020; Wang et al., 2021; Wei N. et al., 2021). Whether HO-1 is cytoprotective or cytotoxic, it may depend on the degree of its expression. Excessive upregulation of HO-1 releases a significant amount of ferrous iron from heme and enhances the generation of ROS through Fenton reaction, while a moderate upregulation may be cytoprotective (Hassannia et al., 2019).

Systemic Iron Homeostasis

Nrf2 deficiency dysregulates iron homeostasis in the body. Nrf2 deficiency aging mice exhibit an increased accumulation of iron in liver, spleen, and serum. Iron regulatory genes responsible for uptake (TfR1 and DMT1) and excretion (FPN1) are decreased, while ferritin responsible for iron deposition (FTL and FTH1) is upregulated (Liu et al., 2020). If Nrf2 is responsible for the dysregulation of iron homeostasis, the ferritin should be decreased. However, Nrf2 knockout enhances ferritin expression in aging mice. These results suggest that ferritin, FPN1, DMT1, and TfR1 may be regulated by IRP-iron responsive element (IRE) system in Nrf2 deficiency mice. Nrf2 controls systemic iron homeostasis *via* BMP6/hepcidin in hepatocytes (Lim et al., 2019). Nrf2 regulates Bmp6 expression and is required for the induction of hepatic hepcidin in response to mitochondrial ROS and oxidative damage mediated by iron. Nrf2-deficient mice with iron overload exhibit defective hepcidin induction (Lim et al., 2019). Pharmacological Nrf2 activation not only improves iron homeostasis in hemochromatosis and thalassemia but also induces antioxidant/detoxifying enzyme gene expression to alleviate iron-mediated oxidative damage (Lim et al., 2019).

Nrf2 IS A POTENTIAL MODULATOR ORCHESTRATING IRON HOMEOSTASIS AND REDOX BALANCE IN CANCER CELLS

Cancer cells have extremely higher energy demands, which provides a fundamental advantage for proliferation, migration,

and metastasis. Therefore, the reliance on mitochondrial energy generation is much greater than normal cells. To meet their high energy demand, cancer cells have an enhanced mitochondrial biogenesis and possess abundant mitochondria (Zong et al., 2016). Iron is an essential trace element for mitochondrial biogenesis. Mitochondria contain up to 20–50% of total cellular iron (Ward and Cloonan, 2019). Mitochondrial iron is utilized for the biosynthesis of Fe-S clusters involving in electron transport. Alterations in mitochondrial iron concentrations can impair the biosynthesis of Fe-S clusters, leading to mitochondrial dysfunction, and increase oxidative stress. Iron depletion initiates a rapid and reversible decrease in mitochondrial biogenesis through dampening the transcription of genes encoding mitochondrial proteins (Rensvold et al., 2016). Therefore, cancer cells require abundant iron uptake to support tumor growth and migration. However, excess iron may generate a large abundant of ROS through Fenton reaction and induce oxidative stress and even damage to the cells. As the major source of ROS, 90% intracellular ROS is demonstrated to be generated in mitochondria. Since the cancer cells have a large number of mitochondria, cancer cells overproduce about a 10-fold level of ROS compared with normal cells (Zhang et al., 2019). How the cancer cells perceive the intracellular iron concentration, regulate iron uptake, and stimulate antioxidant system is of great importance.

Nrf2 is a potential modulator capable of orchestrating iron homeostasis and redox balance. Nrf2 is first identified to have redox-regulating capacities by recognizing ARE for transcription activation of antioxidant genes, including HO-1, CAT, NQO-1, glutamate-cysteine ligase catalytic subunit (Gclc), etc. Recent studies have revealed that Nrf2 is involved in iron homeostasis. *FPN1* (iron efflux proteins) and *ferritin* (including *FTH1* and *FTL*) are the new target genes of Nrf2. Iron-mediated ROS production activates Nrf2 and causes Nrf2 nuclear translocation. Nrf2 not only induces the gene expression of anti-oxidant enzymes but also gene expression involved in iron metabolism. FPN1 controls iron export from cells. The iron storage protein ferritin contributes to iron storage. Both FPN1 and ferritin reduce the intracellular free iron and limit the production of iron-mediated ROS (**Figure 3**). Nrf2 is a potential modulator for orchestrating iron homeostasis and redox balance in cancer cells.

THE POTENTIAL APPLICATION

In view of the constitutive activation of Nrf2 in various cancers, Nrf2 is believed to be a potential therapeutic target. Therefore, inhibition of the Nrf2 pathway is a useful strategy for cancer therapy and reversing drug resistance. Some Nrf2 inhibitors have been identified and reported to have anti-cancer activities.

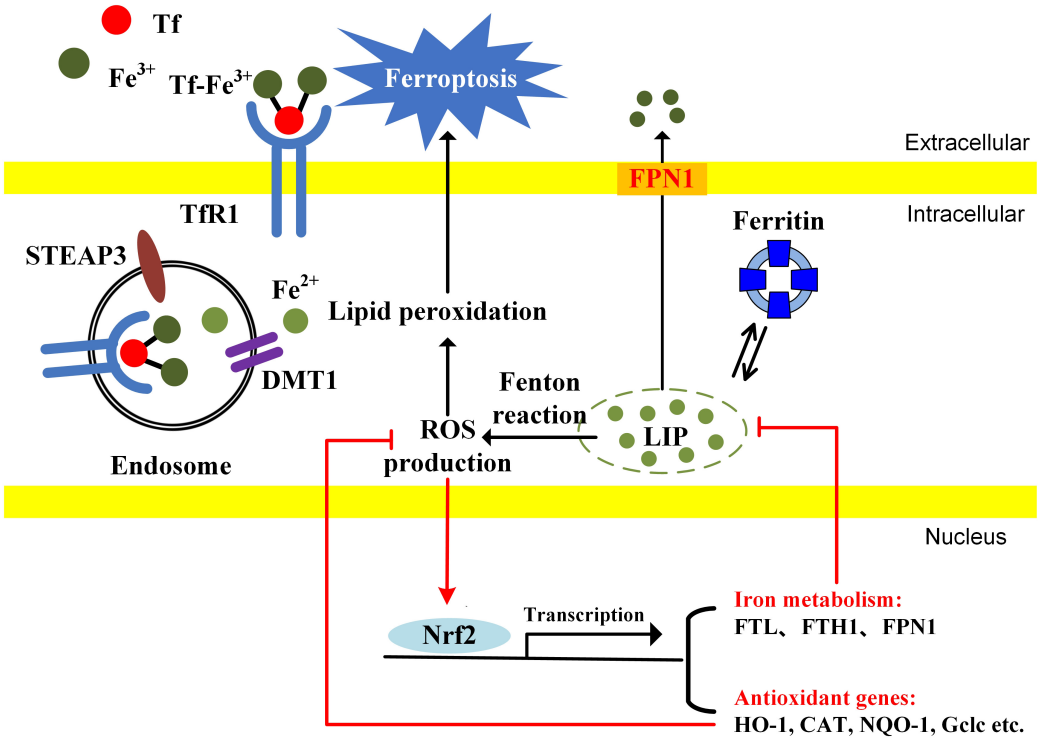

FIGURE 3 | The possible mechanisms of Nrf2 modulating iron metabolism and redox balance in cancer cells. The cancer cells have an enhanced iron uptake compared with normal cells. The LIP, a free cellular iron pool, generates ROS through Fenton reaction, causing the activation of Nrf2. Nrf2 translocates into the nucleus and promotes the transcription of genes associated with antioxidant enzymes and iron metabolism. Ferritin and FPN1 reduce the cellular free iron. Antioxidant enzymes reduce the ROS accumulation. Since cellular free iron and iron-dependent lipid peroxidation are essential for ferroptosis induction, Nrf2 inhibition probably contributes to ferroptosis by simultaneously enhancing LIP and oxidative stress.

However, most of these Nrf2 inhibitors exhibit low potency, non-specificity, and inconsistency. There have been no inhibitors currently and clinically available or under clinical trial (Jung et al., 2018; Panieri and Saso, 2019).

Increased iron stores are associated with cancer induction, malignant progression, therapy resistance, and immune evasion. The enhanced iron demand makes cancer cells more vulnerable to iron-dependent ferroptosis. However, excess iron induces ROS production *via* Fenton reaction, activating Nrf2 mediated antioxidant pathways to avoid iron-induced oxidative damage. Since ferroptosis is strongly dependent on antioxidant metabolism and iron homeostasis, genes or pathways associated with metabolism in iron or antioxidative stress may potentially regulate sensitivity to ferroptosis. Nrf2 regulates genes involving not only antioxidant defenses but also the synthesis of heme and Fe-S clusters, iron storage, and iron export. Nrf2 is a core regulator orchestrating the activation of antioxidant defenses to protect against iron toxicity. If cancer cells are treated with ferroptosis inducers along with Nrf2 inhibitors, it may effectively increase the sensitivity to ferroptosis. Indeed, Nrf2 plays a central role in protecting against ferroptosis by activating transcription of NQO-1, HO-1, and FTH1. Inhibition of Nrf2 or its downstream antioxidant genes and FTH1 promotes ferroptosis in response to ferroptosis-inducing compounds (erastin and sorafenib) (Sun et al., 2016). Nrf2 inhibition reverses the resistance of cisplatin-resistant head and neck cancer cells to artesunate-induced ferroptosis (Roh et al., 2017). Nrf2 inhibition also reverses resistance to GPX4 inhibitor-induced ferroptosis in head and neck cancer (Shin et al., 2018). Nrf2 inhibitors are the promising modulators of ferroptosis.

CONCLUSION

In this hypothesis, we highlight the role of Nrf2 in ferroptosis through regulating iron and ROS homeostasis. Nrf2 plays dual roles in both iron homeostasis and redox balance. Iron promotes carcinogenesis, tumor growth, and migration. On the other hand, excess iron also causes overproduction of ROS through Fenton reaction and mitochondrial oxidative respiration. To avoid the excess of redox-active iron and oxidative damage, it is highly probable that Nrf2 modulates the balance between iron status and oxidative stress. Nrf2 can be activated by iron-induced ROS and induces transcriptions of antioxidant genes, FPN1, and ferritin. Hence, Nrf2 not only reduces cellular oxidative stress but also decreases the free iron level. Since ferroptosis is dependent on lipid peroxide and iron accumulation, Nrf2 inhibition may dramatically increase the sensitivity to ferroptosis. The combination of Nrf2 inhibitors with ferroptosis inducers may exert greater efficacy on cancer therapy.

DATA AVAILABILITY STATEMENT

The original contributions presented in the study are included in the article/supplementary material, further inquiries can be directed to the corresponding author/s.

AUTHOR CONTRIBUTIONS

JZ contributed to the study conception and design and wrote the manuscript. LZ conducted the literature search. YJ drew the figures. GY, HZ, PQ, and SW revised the manuscript. All authors contributed to the article and approved the submitted version.

FUNDING

This work was supported by the Basic Research Project of Guizhou Science and Technology Department [Qian Ke He Ji Chu-ZK (2021)-Yi Ban 398], National Natural Science Foundation of China (82060168), Youth Science and Technology Talents Growth Project of Guizhou Education Department [Qian Jiao He KY Zi (2021)199], and the Science and Technology Fund of the Guizhou Health Commission (gzwjkj2019-1-226).

REFERENCES

Adam, J., Hatipoglu, E., O'Flaherty, L., Ternette, N., Sahgal, N., Lockstone, H., et al. (2011). Renal cyst formation in Fh1-deficient mice is independent of the Hif/Phd pathway: roles for fumarate in KEAP1 succination and Nrf2 signaling. *Cancer Cell* 20, 524–537. doi: 10.1016/j.ccr.2011.09.006

Ahmed, S. M., Luo, L., Namani, A., Wang, X. J., and Tang, X. (2017). Nrf2 signaling pathway: pivotal roles in inflammation. *Biochim. Biophys. Acta Mol. Basis Dis.* 1863, 585–597. doi: 10.1016/j.bbadis.2016.11.005

Alkhateeb, A. A., and Connor, J. R. (2013). The significance of ferritin in cancer: anti-oxidation, inflammation and tumorigenesis. *Biochim. Biophys. Acta* 1836, 245–254. doi: 10.1016/j.bbcan.2013.07.002

Alvarez, S. W., Sviderskiy, V. O., Terzi, E. M., Papagiannakopoulos, T., Moreira, A. L., Adams, S., et al. (2017). NFS1 undergoes positive selection in lung tumours and protects cells from ferroptosis. *Nature* 551, 639–643. doi: 10.1038/nature24637

Anandhan, A., Dodson, M., Schmidlin, C. J., Liu, P., and Zhang, D. D. (2020). Breakdown of an Ironclad defense system: the critical role of NRF2 in mediating ferroptosis. *Cell Chem. Biol.* 27, 436–447. doi: 10.1016/j.chembiol.2020.03.011

Arlt, A., Sebens, S., Krebs, S., Geismann, C., Grossmann, M., Kruse, M. L., et al. (2013). Inhibition of the Nrf2 transcription factor by the alkaloid trigonelline renders pancreatic cancer cells more susceptible to apoptosis through decreased proteasomal gene expression and proteasome activity. *Oncogene* 32, 4825–4835. doi: 10.1038/onc.2012.493

Arosio, P., Elia, L., and Poli, M. (2017). Ferritin, cellular iron storage and regulation. *IUBMB Life* 69, 414–422. doi: 10.1002/iub.1621

Basuli, D., Tesfay, L., Deng, Z., Paul, B., Yamamoto, Y., Ning, G., et al. (2017). Iron addiction: a novel therapeutic target in ovarian cancer. *Oncogene* 36, 4089–4099. doi: 10.1038/onc.2017.11

Beguin, Y., Aapro, M., Ludwig, H., Mizzen, L., and Osterborg, A. (2014). Epidemiological and nonclinical studies investigating effects of iron in carcinogenesis–a critical review. *Crit. Rev. Oncol. Hematol.* 89, 1–15. doi: 10.1016/j.critrevonc.2013.10.008

Bellezza, I., Giambanco, I., Minelli, A., and Donato, R. (2018). Nrf2-Keap1 signaling in oxidative and reductive stress. *Biochim. Biophys. Acta Mol. Cell Res.* 1865, 721–733. doi: 10.1016/j.bbamcr.2018.02.010

Camaschella, C., Nai, A., and Silvestri, L. (2020). Iron metabolism and iron disorders revisited in the hepcidin era. *Haematologica* 105, 260–272. doi: 10.3324/haematol.2019.232124

Candelaria, P. V., Leoh, L. S., Penichet, M. L., and Daniels-Wells, T. R. (2021). Antibodies targeting the transferrin receptor 1 (TfR1) as direct anti-cancer agents. *Front. Immunol.* 12:607692. doi: 10.3389/fimmu.2021.607692

Cao, C., and Fleming, M. D. (2015). The ins and outs of erythroid heme transport. *Haematologica* 100:703. doi: 10.3324/haematol.2015.127886

Cha, H. Y., Lee, B. S., Chang, J. W., Park, J. K., Han, J. H., Kim, Y. S., et al. (2016). Downregulation of Nrf2 by the combination of TRAIL and Valproic acid induces apoptotic cell death of TRAIL-resistant papillary thyroid cancer cells via suppression of Bcl-xL. *Cancer Lett.* 372, 65–74. doi: 10.1016/j.canlet.2015.12.016

Chang, L. C., Chiang, S. K., Chen, S. E., Yu, Y. L., Chou, R. H., and Chang, W. C. (2018). Heme oxygenase-1 mediates BAY 11-7085 induced ferroptosis. *Cancer Lett.* 416, 124–137. doi: 10.1016/j.canlet.2017.12.025

Chang, V. C., Cotterchio, M., and Khoo, E. (2019). Iron intake, body iron status, and risk of breast cancer: a systematic review and meta-analysis. *BMC Cancer* 19:543. doi: 10.1186/s12885-019-5642-0

Chau, L. Y. (2015). Heme oxygenase-1: emerging target of cancer therapy. *J. Biomed. Sci.* 22:22. doi: 10.1186/s12929-015-0128-0

Chen, W., Sun, Z., Wang, X. J., Jiang, T., Huang, Z., Fang, D., et al. (2009). Direct interaction between Nrf2 and p21(Cip1/WAF1) upregulates the Nrf2-mediated antioxidant response. *Mol. Cell* 34, 663–673. doi: 10.1016/j.molcel.2009.04.029

Chen, X., Kang, R., Kroemer, G., and Tang, D. (2021). Broadening horizons: the role of ferroptosis in cancer. Nature reviews. *Clinical Oncolo.* 18, 280–296. doi: 10.1038/s41571-020-00462-0

Chen, X., Yu, C., Kang, R., and Tang, D. (2020). Iron metabolism in ferroptosis. *Front. Cell Dev. Biol.* 8:590226. doi: 10.3389/fcell.2020.590226

Chian, S., Thapa, R., Chi, Z., Wang, X. J., and Tang, X. (2014). Luteolin inhibits the Nrf2 signaling pathway and tumor growth in vivo. *Biochem. Biophys. Res. Commun.* 447, 602–608. doi: 10.1016/j.bbrc.2014.04.039

Choi, E. J., Jung, B. J., Lee, S. H., Yoo, H. S., Shin, E. A., Ko, H. J., et al. (2017). A clinical drug library screen identifies clobetasol propionate as an NRF2 inhibitor with potential therapeutic efficacy in KEAP1 mutant lung cancer. *Oncogene* 36, 5285–5295. doi: 10.1038/onc.2017.153

Chua, A. C., Knuiman, M. W., Trinder, D., Divitini, M. L., and Olynyk, J. K. (2016). Higher concentrations of serum iron and transferrin saturation but not serum ferritin are associated with cancer outcomes. *Am. J. Clin. Nutr.* 104, 736–742. doi: 10.3945/ajcn.115.129411

Daniels, T. R., Bernabeu, E., Rodríguez, J. A., Patel, S., Kozman, M., Chiappetta, D. A., et al. (2012). The transferrin receptor and the targeted delivery of therapeutic agents against cancer. *Biochim. Biophys. Acta* 1820, 291–317. doi: 10.1016/j.bbagen.2011.07.016

Deng, Z., Manz, D. H., Torti, S. V., and Torti, F. M. (2019). Effects of ferroportin-mediated iron depletion in cells representative of different histological subtypes of prostate Cancer. *Antioxidants Redox Signal.* 30, 1043–1061. doi: 10.1089/ars.2017.7023

DeNicola, G. M., Chen, P. H., Mullarky, E., Sudderth, J. A., Hu, Z., Wu, D., et al. (2015). NRF2 regulates serine biosynthesis in non-small cell lung cancer. *Nat. Genet.* 47, 1475–1481. doi: 10.1038/ng.3421

DeNicola, G. M., Karreth, F. A., Humpton, T. J., Gopinathan, A., Wei, C., Frese, K., et al. (2011). Oncogene-induced Nrf2 transcription promotes ROS detoxification and tumorigenesis. *Nature* 475, 106–109. doi: 10.1038/nature10189

Di Sanzo, M., Gaspari, M., Misaggi, R., Romeo, F., Falbo, L., De Marco, C., et al. (2011). H ferritin gene silencing in a human metastatic melanoma cell line: a proteomic analysis. *J. Proteome Res.* 10, 5444–5453. doi: 10.1021/pr200705z

Dixon, S. J., Lemberg, K. M., Lamprecht, M. R., Skouta, R., Zaitsev, E. M., Gleason, C. E., et al. (2012). Ferroptosis: an iron-dependent form of nonapoptotic cell death. *Cell* 149, 1060–1072. doi: 10.1016/j.cell.2012.03.042

Do, M. T., Kim, H. G., Choi, J. H., and Jeong, H. G. (2014). Metformin induces microRNA-34a to downregulate the Sirt1/Pgc-1α/Nrf2 pathway, leading to increased susceptibility of wild-type p53 cancer cells to oxidative stress and therapeutic agents. *Free Radic. Biol. Med.* 74, 21–34. doi: 10.1016/j.freeradbiomed.2014.06.010

Do, M. T., Kim, H. G., Khanal, T., Choi, J. H., Kim, D. H., Jeong, T. C., et al. (2013). Metformin inhibits heme oxygenase-1 expression in cancer cells through inactivation of Raf-ERK-Nrf2 signaling and AMPK-independent pathways. *Toxicol. Appl. Pharmacol.* 271, 229–238. doi: 10.1016/j.taap.2013.05.010

Elmberg, M., Hultcrantz, R., Ekbom, A., Brandt, L., Olsson, S., Olsson, R., et al. (2003). Cancer risk in patients with hereditary hemochromatosis and in their first-degree relatives. *Gastroenterology* 125, 1733–1741. doi: 10.1053/j.gastro.2003.09.035

Facciorusso, A., Del Prete, V., Antonino, M., Neve, V., Crucinio, N., Di Leo, A., et al. (2014). Serum ferritin as a new prognostic factor in hepatocellular carcinoma patients treated with radiofrequency ablation. *J. Gastroenterol. Hepatol.* 29, 1905–1910. doi: 10.1111/jgh.12618

Feng, H., and Stockwell, B. R. (2018). Unsolved mysteries: how does lipid peroxidation cause ferroptosis? *PLoS Biol.* 16:e2006203. doi: 10.1371/journal.pbio.2006203

Fouad, Y. A., and Aanei, C. (2017). Revisiting the hallmarks of cancer. *Am. J. Cancer Res.* 7, 1016–1036.

Fox, D. B., Garcia, N. M. G., McKinney, B. J., Lupo, R., Noteware, L. C., Newcomb, R., et al. (2020). NRF2 activation promotes the recurrence of dormant tumour cells through regulation of redox and nucleotide metabolism. *Nat. Metab.* 2, 318–334. doi: 10.1038/s42255-020-0191-z

Fracanzani, A. L., Conte, D., Fraquelli, M., Taioli, E., Mattioli, M., Losco, A., et al. (2001). Increased cancer risk in a cohort of 230 patients with hereditary hemochromatosis in comparison to matched control patients with non-iron-related chronic liver disease. *Hepatology* 33, 647–651. doi: 10.1053/jhep.2001.22506

Gao, D. Q., Qian, S., and Ju, T. (2016). Anticancer activity of Honokiol against lymphoid malignant cells via activation of ROS-JNK and attenuation of Nrf2 and NF-κB. *J. BUON* 21, 673–679.

Gao, M., Monian, P., Pan, Q., Zhang, W., Xiang, J., and Jiang, X. (2016). Ferroptosis is an autophagic cell death process. *Cell Res.* 26, 1021–1032. doi: 10.1038/cr.2016.95

Gao, M., Monian, P., Quadri, N., Ramasamy, R., and Jiang, X. (2015). Glutaminolysis and transferrin regulate ferroptosis. *Mol. Cell* 59, 298–308. doi: 10.1016/j.molcel.2015.06.011

Gao, M., Yi, J., Zhu, J., Minikes, A. M., Monian, P., Thompson, C. B., et al. (2019). Role of mitochondria in ferroptosis. *Mol. Cell* 73, 354.e3–363.e3. doi: 10.1016/j.molcel.2018.10.042

Gaur, A., Collins, H., Wulaningsih, W., Holmberg, L., Garmo, H., Hammar, N., et al. (2013). Iron metabolism and risk of cancer in the Swedish AMORIS study. *Cancer Causes Control* 24, 1393–1402. doi: 10.1007/s10552-013-0219-8

Geng, N., Shi, B. J., Li, S. L., Zhong, Z. Y., Li, Y. C., Xua, W. L., et al. (2018). Knockdown of ferroportin accelerates erastin-induced ferroptosis in neuroblastoma cells. *Eur. Rev. Med. Pharmacol. Sci.* 22, 3826–3836. doi: 10.26355/eurrev_201806_15267

Genkinger, J. M., Friberg, E., Goldbohm, R. A., and Wolk, A. (2012). Long-term dietary heme iron and red meat intake in relation to endometrial cancer risk. *Am. J. Clin. Nutr.* 96, 848–854. doi: 10.3945/ajcn.112.039537

Goldstein, L. D., Lee, J., Gnad, F., Klijn, C., Schaub, A., Reeder, J., et al. (2016). Recurrent loss of NFE2L2 Exon 2 is a mechanism for Nrf2 pathway activation in human Cancers. *Cell Rep.* 16, 2605–2617. doi: 10.1016/j.celrep.2016.08.010

Habashy, H. O., Powe, D. G., Staka, C. M., Rakha, E. A., Ball, G., Green, A. R., et al. (2010). Transferrin receptor (CD71) is a marker of poor prognosis in breast cancer and can predict response to tamoxifen. *Breast Cancer Res. Treat.* 119, 283–293. doi: 10.1007/s10549-009-0345-x

Harada, N., Kanayama, M., Maruyama, A., Yoshida, A., Tazumi, K., Hosoya, T., et al. (2011). Nrf2 regulates ferroportin 1-mediated iron efflux and counteracts lipopolysaccharide-induced ferroportin 1 mRNA suppression in macrophages. *Arch. Biochem. Biophys.* 508, 101–109. doi: 10.1016/j.abb.2011.02.001

Hassannia, B., Vandenabeele, P., and Vanden Berghe, T. (2019). Targeting ferroptosis to iron out cancer. *Cancer Cell* 35, 830–849. doi: 10.1016/j.ccell.2019.04.002

Hassannia, B., Wiernicki, B., Ingold, I., Qu, F., Van Herck, S., Tyurina, Y. Y., et al. (2018). Nano-targeted induction of dual ferroptotic mechanisms eradicates high-risk neuroblastoma. *J. Clin. Invest,* 128, 3341–3355. doi: 10.1172/jci99032

Hayes, J. D., Dinkova-Kostova, A. T., and Tew, K. D. (2020). Oxidative stress in Cancer. *Cancer Cell* 38, 167–197. doi: 10.1016/j.ccell.2020.06.001

Hercberg, S., Estaquio, C., Czernichow, S., Mennen, L., Noisette, N., Bertrais, S., et al. (2005). Iron status and risk of cancers in the SU.VI.MAX cohort. *J. Nutr.* 135, 2664–2668. doi: 10.1093/jn/135.11.2664

Hjalgrim, H., Edgren, G., Rostgaard, K., Reilly, M., Tran, T. N., Titlestad, K. E., et al. (2007). Cancer incidence in blood transfusion recipients. *J. Natl. Cancer Inst.* 99, 1864–1874. doi: 10.1093/jnci/djm248

Hou, W., Xie, Y., Song, X., Sun, X., Lotze, M. T., Zeh, H. J. III, et al. (2016). Autophagy promotes ferroptosis by degradation of ferritin. *Autophagy* 12, 1425–1428. doi: 10.1080/15548627.2016.1187366

Jelinek, A., Heyder, L., Daude, M., Plessner, M., Krippner, S., Grosse, R., et al. (2018). Mitochondrial rescue prevents glutathione peroxidase-dependent ferroptosis. *Free Radic. Biol. Med.* 117, 45–57. doi: 10.1016/j.freeradbiomed.2018.01.019

Jeong, Y., Hellyer, J. A., Stehr, H., Hoang, N. T., Niu, X., Das, M., et al. (2020). Role of KEAP1/NFE2L2 mutations in the chemotherapeutic response of patients with non-small cell lung cancer. *Clin. Cancer Res.* 26, 274–281. doi: 10.1158/1078-0432.Ccr-19-1237

Ji, M., Li, X. D., Shi, H. B., Ning, Z. H., Zhao, W. Q., Wang, Q., et al. (2014). Clinical significance of serum ferritin in elderly patients with primary lung carcinoma. *Tumour Biol.* 35, 10195–10199. doi: 10.1007/s13277-014-2317-y

Jiang, T., Cheng, H., Su, J., Wang, X., Wang, Q., Chu, J., et al. (2020). Gastrodin protects against glutamate-induced ferroptosis in HT-22 cells through Nrf2/HO-1 signaling pathway. *Toxicol. Vitro* 62:104715. doi: 10.1016/j.tiv.2019.104715

Jung, B. J., Yoo, H. S., Shin, S., Park, Y. J., and Jeon, S. M. (2018). Dysregulation of NRF2 in Cancer: from molecular mechanisms to therapeutic opportunities. *Biomol. Ther.* 26, 57–68. doi: 10.4062/biomolther.2017.195

Kallianpur, A. R., Lee, S. A., Gao, Y. T., Lu, W., Zheng, Y., Ruan, Z. X., et al. (2008). Dietary animal-derived iron and fat intake and breast cancer risk in the shanghai breast cancer study. *Breast Cancer Res. Treat.* 107, 123–132. doi: 10.1007/s10549-007-9538-3

Kalousová, M., Krechler, T., Jáchymová, M., Kubìna, A. A., Zák, A., and Zima, T. (2012). Ferritin as an independent mortality predictor in patients with pancreas cancer. Results of a pilot study. *Tumour Biol.* 33, 1695–1700. doi: 10.1007/s13277-012-0426-z

Karathedath, S., Rajamani, B. M., Musheer Aalam, S. M., Abraham, A., Varatharajan, S., Krishnamurthy, P., et al. (2017). Role of NF-E2 related factor 2 (Nrf2) on chemotherapy resistance in acute myeloid leukemia (AML) and the effect of pharmacological inhibition of Nrf2. *PLoS One* 12:e0177227. doi: 10.1371/journal.pone.0177227

Kasai, S., Mimura, J., Ozaki, T., and Itoh, K. (2018). Emerging regulatory role of Nrf2 in Iron, Heme, and hemoglobin metabolism in physiology and disease. *Front. Vet. Sci.* 5:242. doi: 10.3389/fvets.2018.00242

Kato, J., Miyanishi, K., Kobune, M., Nakamura, T., Takada, K., Takimoto, R., et al. (2007). Long-term phlebotomy with low-iron diet therapy lowers risk of development of hepatocellular carcinoma from chronic hepatitis C. *J. Gastroenterol.* 42, 830–836. doi: 10.1007/s00535-007-2095-z

Kim, E. H., Jang, H., Shin, D., Baek, S. H., and Roh, J. L. (2016). Targeting Nrf2 with wogonin overcomes cisplatin resistance in head and neck cancer. *Apoptosis* 21, 1265–1278. doi: 10.1007/s10495-016-1284-8

Knekt, P., Reunanen, A., Takkunen, H., Aromaa, A., Heliövaara, M., and Hakulinen, T. (1994). Body iron stores and risk of cancer. *Int. J. Cancer* 56, 379–382. doi: 10.1002/ijc.2910560315

Komatsu, M., Kurokawa, H., Waguri, S., Taguchi, K., Kobayashi, A., Ichimura, Y., et al. (2010). The selective autophagy substrate p62 activates the stress responsive transcription factor Nrf2 through inactivation of Keap1. *Nat. Cell Biol.* 12, 213–223. doi: 10.1038/ncb2021

Koyama, S., Fujisawa, S., Watanabe, R., Itabashi, M., Ishibashi, D., Ishii, Y., et al. (2017). Serum ferritin level is a prognostic marker in patients with peripheral T-cell lymphoma. *Int. J. Lab. Hematol.* 39, 112–117. doi: 10.1111/ijlh.12592

Kuang, Y., and Wang, Q. (2019). Iron and lung cancer. *Cancer Lett.* 464, 56–61. doi: 10.1016/j.canlet.2019.08.007

Kwak, M. K., Itoh, K., Yamamoto, M., Sutter, T. R., and Kensler, T. W. (2001). Role of transcription factor Nrf2 in the induction of hepatic phase 2 and antioxidative enzymes in vivo by the cancer chemoprotective agent, 3H-1, 2-dimethiole-3-thione. *Mol. Med.* 7, 135–145.

Kwon, M. Y., Park, E., Lee, S. J., and Chung, S. W. (2015). Heme oxygenase-1 accelerates erastin-induced ferroptotic cell death. *Oncotarget* 6, 24393–24403. doi: 10.18632/oncotarget.5162

Lee, J., Kang, J. S., Nam, L. B., Yoo, O. K., and Keum, Y. S. (2018). Suppression of NRF2/ARE by convallatoxin sensitises A549 cells to 5-FU-mediated apoptosis. *Free Radic. Res.* 52, 1416–1423. doi: 10.1080/10715762.2018.1489132

Lee, S., Song, A., and Eo, W. (2016). Serum ferritin as a prognostic biomarker for survival in relapsed or refractory metastatic colorectal cancer. *J. Cancer* 7, 957–964. doi: 10.7150/jca.14797

Lei, G., Mao, C., Yan, Y., Zhuang, L., and Gan, B. (2021). Ferroptosis, radiotherapy, and combination therapeutic strategies. *Protein Cell* [Epub ahead of print]. doi: 10.1007/s13238-021-00841-y

Lignitto, L., LeBoeuf, S. E., Homer, H., Jiang, S., Askenazi, M., Karakousi, T. R., et al. (2019). Nrf2 activation promotes lung cancer metastasis by inhibiting the degradation of Bach1. *Cell* 178, 316.e18–329.e18. doi: 10.1016/j.cell.2019.06.003

Lim, P. J., Duarte, T. L., Arezes, J., Garcia-Santos, D., Hamdi, A., Pasricha, S. R., et al. (2019). Nrf2 controls iron homeostasis in haemochromatosis and thalassaemia via Bmp6 and hepcidin. *Nat. Metab.* 1, 519–531. doi: 10.1038/s42255-019-0063-6

Liu, H. Y., Tuckett, A. Z., Fennell, M., Garippa, R., and Zakrzewski, J. L. (2018). Repurposing of the CDK inhibitor PHA-767491 as a NRF2 inhibitor drug candidate for cancer therapy via redox modulation. *Invest. New Drugs* 36, 590–600. doi: 10.1007/s10637-017-0557-6

Liu, X., Madhankumar, A. B., Slagle-Webb, B., Sheehan, J. M., Surguladze, N., and Connor, J. R. (2011). Heavy chain ferritin siRNA delivered by cationic liposomes increases sensitivity of cancer cells to chemotherapeutic agents. *Cancer Res.* 71, 2240–2249. doi: 10.1158/0008-5472.Can-10-1375

Liu, Z., Han, K., Huo, X., Yan, B., Gao, M., Lv, X., et al. (2020). Nrf2 knockout dysregulates iron metabolism and increases the hemolysis through ROS in aging mice. *Life Sci.* 255:117838. doi: 10.1016/j.lfs.2020.117838

Lu, Y., Sun, Y., Zhu, J., Yu, L., Jiang, X., Zhang, J., et al. (2018). Oridonin exerts anticancer effect on osteosarcoma by activating PPAR-γ and inhibiting Nrf2 pathway. *Cell Death Dis.* 9:15. doi: 10.1038/s41419-017-0031-6

Luo, H., Zhang, N. Q., Huang, J., Zhang, X., Feng, X. L., Pan, Z. Z., et al. (2019). Different forms and sources of iron in relation to colorectal cancer risk: a case-control study in China. *Br. J. Nutr.* 121, 735–747. doi: 10.1017/s0007114519000023

Ma, H., Wang, X., Zhang, W., Li, H., Zhao, W., Sun, J., et al. (2020). Melatonin suppresses ferroptosis induced by high glucose via activation of the Nrf2/HO-1 signaling pathway in Type 2 diabetic osteoporosis. *Oxid. Med. Cell. Longev.* 2020:9067610. doi: 10.1155/2020/9067610

Maakaron, J. E., Cappellini, M. D., Graziadei, G., Ayache, J. B., and Taher, A. T. (2013). Hepatocellular carcinoma in hepatitis-negative patients with thalassemia intermedia: a closer look at the role of siderosis. *Ann. Hepatol.* 12, 142–146. doi: 10.1016/S1665-2681(19)31397-3

Mainous, A. G. III, Gill, J. M., and Everett, C. J. (2005). Transferrin saturation, dietary iron intake, and risk of cancer. *Ann. Fam. Med.* 3, 131–137. doi: 10.1370/afm.283

Mancias, J. D., Wang, X., Gygi, S. P., Harper, J. W., and Kimmelman, A. C. (2014). Quantitative proteomics identifies NCOA4 as the cargo receptor mediating ferritinophagy. *Nature* 509, 105–109. doi: 10.1038/nature13148

Marro, S., Chiabrando, D., Messana, E., Stolte, J., Turco, E., Tolosano, E., et al. (2010). Heme controls ferroportin1 (FPN1) transcription involving Bach1, Nrf2 and a MARE/ARE sequence motif at position -7007 of the FPN1 promoter. *Haematologica* 95, 1261–1268. doi: 10.3324/haematol.2009.020123

Min, P. B. S., and James, R. C. (2015). Role of ferritin in Cancer biology. *J. Cancer Sci. Ther.* 7, 155–160. doi: 10.4172/1948-5956.1000341

Muto, Y., Moroishi, T., Ichihara, K., Nishiyama, M., Shimizu, H., Eguchi, H., et al. (2019). Disruption of FBXL5-mediated cellular iron homeostasis promotes liver carcinogenesis. *J. Exp. Med.* 216, 950–965. doi: 10.1084/jem.20180900

Nakamura, T., Naguro, I., and Ichijo, H. (2019). Iron homeostasis and iron-regulated ROS in cell death, senescence and human diseases. *Biochim. Biophys. Acta Gen. Sub.* 1863, 1398–1409. doi: 10.1016/j.bbagen.2019.06.010

Neitemeier, S., Jelinek, A., Laino, V., Hoffmann, L., Eisenbach, I., Eying, R., et al. (2017). BID links ferroptosis to mitochondrial cell death pathways. *Redox Biol.* 12, 558–570. doi: 10.1016/j.redox.2017.03.007

Neiveyans, M., Melhem, R., Arnoult, C., Bourquard, T., Jarlier, M., Busson, M., et al. (2019). A recycling anti-transferrin receptor-1 monoclonal antibody as an efficient therapy for erythroleukemia through target up-regulation and antibody-dependent cytotoxic effector functions. *mAbs* 11, 593–605. doi: 10.1080/19420862.2018.1564510

Ohnuma, T., Anzai, E., Suzuki, Y., Shimoda, M., Saito, S., Nishiyama, T., et al. (2015). Selective antagonization of activated Nrf2 and inhibition of cancer cell proliferation by procyanidins from Cinnamomi Cortex extract. *Arch. Biochem. Biophys.* 585, 17–24. doi: 10.1016/j.abb.2015.09.007

Ohnuma, T., Sakamoto, K., Shinoda, A., Takagi, C., Ohno, S., Nishiyama, T., et al. (2017). Procyanidins from cinnamomi cortex promote proteasome-independent degradation of nuclear Nrf2 through phosphorylation of insulin-like growth factor-1 receptor in A549 cells. *Arch. Biochem. Biophys.* 635, 66–73. doi: 10.1016/j.abb.2017.10.007

Okazaki, K., Papagiannakopoulos, T., and Motohashi, H. (2020). Metabolic features of cancer cells in NRF2 addiction status. *Biophys. Rev.* 12, 435–441. doi: 10.1007/s12551-020-00659-8

Olayanju, A., Copple, I. M., Bryan, H. K., Edge, G. T., Sison, R. L., Wong, M. W., et al. (2015). Brusatol provokes a rapid and transient inhibition of Nrf2 signaling and sensitizes mammalian cells to chemical toxicity-implications for therapeutic targeting of Nrf2. *Free Radic. Biol. Med.* 78, 202–212. doi: 10.1016/j.freeradbiomed.2014.11.003

Ooi, A., Dykema, K., Ansari, A., Petillo, D., Snider, J., Kahnoski, R., et al. (2013). CUL3 and NRF2 mutations confer an NRF2 activation phenotype in a sporadic form of papillary renal cell carcinoma. *Cancer Res.* 73, 2044–2051. doi: 10.1158/0008-5472.Can-12-3227

Panday, A., Sahoo, M. K., Osorio, D., and Batra, S. (2015). NADPH oxidases: an overview from structure to innate immunity-associated pathologies. *Cell. Mol. Immunol.* 12, 5–23. doi: 10.1038/cmi.2014.89

Panieri, E., and Saso, L. (2019). Potential applications of NRF2 inhibitors in cancer therapy. *Oxid. Med. Cell. Longev.* 2019:8592348. doi: 10.1155/2019/8592348

Pietsch, E. C., Chan, J. Y., Torti, F. M., and Torti, S. V. (2003). Nrf2 mediates the induction of ferritin H in response to xenobiotics and cancer chemopreventive dithiolethiones. *J. Biol. Chem.* 278, 2361–2369. doi: 10.1074/jbc.M210664200

Pinnix, Z. K., Miller, L. D., Wang, W., D'Agostino, R. Jr., Kute, T., Willingham, M. C., et al. (2010). Ferroportin and iron regulation in breast cancer progression and prognosis. *Sci. Transl. Med.* 2:43ra56. doi: 10.1126/scisignal.3001127

Qian, C., Wang, Y., Zhong, Y., Tang, J., Zhang, J., Li, Z., et al. (2014). Wogonin-enhanced reactive oxygen species-induced apoptosis and potentiated cytotoxic effects of chemotherapeutic agents by suppression Nrf2-mediated signaling in HepG2 cells. *Free Radic. Res.* 48, 607–621. doi: 10.3109/10715762.2014.897342

Qin, J. J., Cheng, X. D., Zhang, J., and Zhang, W. D. (2019). Dual roles and therapeutic potential of Keap1-Nrf2 pathway in pancreatic cancer: a systematic review. *Cell Commun. Signal.* 17:121. doi: 10.1186/s12964-019-0435-2

Radio, F. C., Majore, S., Aurizi, C., Sorge, F., Biolcati, G., Bernabini, S., et al. (2015). Hereditary hemochromatosis type 1 phenotype modifiers in Italian patients. The controversial role of variants in HAMP, BMP2, FTL and SLC40A1 genes. *Blood Cells Mol. Dis.* 55, 71–75. doi: 10.1016/j.bcmd.2015.04.001

Reczek, C. R., and Chandel, N. S. (2017). The two faces of reactive oxygen species in cancer. *Annu. Rev. Cancer Biol.* 1, 79–98. doi: 10.1146/annurev-cancerbio-041916-065808

Rensvold, J. W., Krautkramer, K. A., Dowell, J. A., Denu, J. M., and Pagliarini, D. J. (2016). Iron deprivation induces transcriptional regulation of mitochondrial biogenesis. *J. Biol. Chem.* 291, 20827–20837. doi: 10.1074/jbc.M116.727701

Roh, J. L., Kim, E. H., Jang, H., and Shin, D. (2017). Nrf2 inhibition reverses the resistance of cisplatin-resistant head and neck cancer cells to artesunate-induced ferroptosis. *Redox Biol.* 11, 254–262. doi: 10.1016/j.redox.2016.12.010

Sacco, A., Battaglia, A. M., Botta, C., Aversa, I., Mancuso, S., Costanzo, F., et al. (2021). Iron metabolism in the tumor microenvironment-implications for anti-cancer immune response. *Cells* 10:303. doi: 10.3390/cells10020303

Schonberg, D. L., Miller, T. E., Wu, Q., Flavahan, W. A., Das, N. K., Hale, J. S., et al. (2015). Preferential Iron trafficking characterizes glioblastoma stem-like cells. *Cancer Cell* 28, 441–455. doi: 10.1016/j.ccell.2015.09.002

Sena, P., Mancini, S., Benincasa, M., Mariani, F., Palumbo, C., and Roncucci, L. (2018). Metformin induces apoptosis and alters cellular responses to oxidative stress in Ht29 Colon cancer cells: preliminary findings. *Int. J. Mol. Sci.* 19:1478. doi: 10.3390/ijms19051478

Shi, Y., Fan, S., Wu, M., Zuo, Z., Li, X., Jiang, L., et al. (2019). YTHDF1 links hypoxia adaptation and non-small cell lung cancer progression. *Nat. Commun.* 10:4892. doi: 10.1038/s41467-019-12801-6

Shin, D., Kim, E. H., Lee, J., and Roh, J. L. (2018). Nrf2 inhibition reverses resistance to GPX4 inhibitor-induced ferroptosis in head and neck cancer. *Free Radic. Biol. Med.* 129, 454–462. doi: 10.1016/j.freeradbiomed.2018.10.426

Shpyleva, S. I., Tryndyak, V. P., Kovalchuk, O., Starlard-Davenport, A., Chekhun, V. F., Beland, F. A., et al. (2011). Role of ferritin alterations in human breast cancer cells. *Breast Cancer Res. Treat.* 126, 63–71. doi: 10.1007/s10549-010-0849-4

Singh, A., Daemen, A., Nickles, D., Jeon, S. M., Foreman, O., Sudini, K., et al. (2021). NRF2 activation promotes aggressive lung cancer and associates with poor clinical outcomes. *Clin. Cancer Res.* 27, 877–888. doi: 10.1158/1078-0432.Ccr-20-1985

Singh, K. J., Singh, S. K., Suri, A., Vijjan, V., Goswami, A. K., and Khullar, M. (2005). Serum ferritin in renal cell carcinoma: effect of tumor size, volume grade, and stage. *Indian J. Cancer* 42, 197–200.

Song, A., Eo, W., Kim, S., Shim, B., and Lee, S. (2018). Significance of serum ferritin as a prognostic factor in advanced hepatobiliary cancer patients treated with Korean medicine: a retrospective cohort study. *BMC Compl. Altern. Med.* 18:176. doi: 10.1186/s12906-018-2240-7

Song, X., and Long, D. (2020). Nrf2 and ferroptosis: a new research direction for neurodegenerative diseases. *Front. Neurosci.* 14:267. doi: 10.3389/fnins.2020.00267

Stevens, R. G., Graubard, B. I., Micozzi, M. S., Neriishi, K., and Blumberg, B. S. (1994). Moderate elevation of body iron level and increased risk of cancer occurrence and death. *Int. J. Cancer* 56, 364–369. doi: 10.1002/ijc.2910560312

Sukiennicki, G. M., Marciniak, W., Muszyńska, M., Baszuk, P., Gupta, S., Białkowska, K., et al. (2019). Iron levels, genes involved in iron metabolism and antioxidative processes and lung cancer incidence. *PLoS One* 14:e0208610. doi: 10.1371/journal.pone.0208610

Sun, X., Ou, Z., Chen, R., Niu, X., Chen, D., Kang, R., et al. (2016). Activation of the p62-Keap1-NRF2 pathway protects against ferroptosis in hepatocellular carcinoma cells. *Hepatology* 63, 173–184. doi: 10.1002/hep.28251

Sun, Y. X., Xu, A. H., Yang, Y., and Li, J. (2015). Role of Nrf2 in bone metabolism. *J. Biomed. Sci.* 22:101. doi: 10.1186/s12929-015-0212-5

Tang, M., Chen, Z., Wu, D., and Chen, L. (2018). Ferritinophagy/ferroptosis: iron-related newcomers in human diseases. *J. Cell. Physiol.* 233, 9179–9190. doi: 10.1002/jcp.26954

Tao, S., Wang, S., Moghaddam, S. J., Ooi, A., Chapman, E., Wong, P. K., et al. (2014). Oncogenic KRAS confers chemoresistance by upregulating NRF2. *Cancer Res.* 74, 7430–7441. doi: 10.1158/0008-5472.Can-14-1439

Tarumoto, T., Nagai, T., Ohmine, K., Miyoshi, T., Nakamura, M., Kondo, T., et al. (2004). Ascorbic acid restores sensitivity to imatinib via suppression of Nrf2-dependent gene expression in the imatinib-resistant cell line. *Exp. Hematol.* 32, 375–381. doi: 10.1016/j.exphem.2004.01.007

Tesfay, L., Clausen, K. A., Kim, J. W., Hegde, P., Wang, X., Miller, L. D., et al. (2015). Hepcidin regulation in prostate and its disruption in prostate cancer. *Cancer Res.* 75, 2254–2263. doi: 10.1158/0008-5472.Can-14-2465

Thimmulappa, R. K., Mai, K. H., Srisuma, S., Kensler, T. W., Yamamoto, M., and Biswal, S. (2002). Identification of Nrf2-regulated genes induced by the chemopreventive agent sulforaphane by oligonucleotide microarray. *Cancer Res.* 62, 5196–5203.

Torti, S. V., Manz, D. H., Paul, B. T., Blanchette-Farra, N., and Torti, F. M. (2018). Iron and Cancer. *Annu. Rev. Nutr.* 38, 97–125. doi: 10.1146/annurev-nutr-082117-051732

Torti, S. V., and Torti, F. M. (2020). Iron and Cancer: 2020 Vision. *Cancer Res.* 80, 5435–5448. doi: 10.1158/0008-5472.Can-20-2017

Toth, R. K., and Warfel, N. A. (2017). Strange bedfellows: nuclear factor, Erythroid 2-Like 2 (Nrf2) and hypoxia-inducible Factor 1 (HIF-1) in tumor hypoxia. *Antioxidants* 6:27. doi: 10.3390/antiox6020027

Vahidnia, F., Hirschler, N. V., Agapova, M., Chinn, A., Busch, M. P., and Custer, B. (2013). Cancer incidence and mortality in a cohort of US blood donors: a 20-Year study. *J. Cancer Epidemiol.* 2013:814842. doi: 10.1155/2013/814842

Valenzuela, M., Glorieux, C., Stockis, J., Sid, B., Sandoval, J. M., Felipe, K. B., et al. (2014). Retinoic acid synergizes ATO-mediated cytotoxicity by precluding Nrf2 activity in AML cells. *Br. J. Cancer* 111, 874–882. doi: 10.1038/bjc.2014.380

Vashi, R., and Patel, B. M. (2021). NRF2 in cardiovascular diseases: a ray of hope! *J. Cardiovas. Transl. Res.* 14, 573–586. doi: 10.1007/s12265-020-10083-8

Verma, A. K., Yadav, A., Singh, S. V., Mishra, P., and Rath, S. K. (2018). Isoniazid induces apoptosis: role of oxidative stress and inhibition of nuclear translocation of nuclear factor (erythroid-derived 2)-like 2 (Nrf2). *Life Sci.* 199, 23–33. doi: 10.1016/j.lfs.2018.02.037

Wang, C., Liu, T., Tong, Y., Cui, R., Qu, K., Liu, C., et al. (2021). Ulinastatin protects against acetaminophen-induced liver injury by alleviating ferroptosis via the SIRT1/NRF2/HO-1 pathway. *Am. J. Transl. Res.* 13, 6031–6042.

Wang, H., Shi, H., Rajan, M., Canarie, E. R., Hong, S., Simoneschi, D., et al. (2020). FBXL5 regulates IRP2 stability in iron homeostasis via an oxygen-responsive [2Fe2S] cluster. *Mol. Cell* 78, 31.e5–41.e5. doi: 10.1016/j.molcel.2020.02.011

Wang, J., Wang, H., Sun, K., Wang, X., Pan, H., Zhu, J., et al. (2018). Chrysin suppresses proliferation, migration, and invasion in glioblastoma cell lines via mediating the ERK/Nrf2 signaling pathway. *Drug Design Dev. Ther.* 12, 721–733. doi: 10.2147/dddt.S160020

Wang, M., Shi, G., Bian, C., Nisar, M. F., Guo, Y., Wu, Y., et al. (2018). UVA irradiation enhances brusatol-mediated inhibition of melanoma growth by downregulation of the Nrf2-mediated antioxidant response. *Oxid. Med. Cell. Longev.* 2018:9742154. doi: 10.1155/2018/9742154

Wang, R., An, J., Ji, F., Jiao, H., Sun, H., and Zhou, D. (2008). Hypermethylation of the Keap1 gene in human lung cancer cell lines and lung cancer tissues. *Biochem. Biophys. Res. Commun.* 373, 151–154. doi: 10.1016/j.bbrc.2008.06.004

Wang, Z., Zhang, J., Li, M., Kong, L., and Yu, J. (2020). The expression of p-p62 and nuclear Nrf2 in esophageal squamous cell carcinoma and association with radioresistance. *Thorac. Cancer* 11, 130–139. doi: 10.1111/1759-7714.13252

Ward, D. M., and Cloonan, S. M. (2019). Mitochondrial Iron in human health and disease. *Annu. Rev. Physiol.* 81, 453–482. doi: 10.1146/annurev-physiol-020518-114742

Ward, H. A., Whitman, J., Muller, D. C., Johansson, M., Jakszyn, P., Weiderpass, E., et al. (2019). Haem iron intake and risk of lung cancer in the European prospective investigation into cancer and nutrition (EPIC) cohort. *Eur. J. Clin. Nutr.* 73, 1122–1132. doi: 10.1038/s41430-018-0271-2

Wei, N., Lu, T., Yang, L., Dong, Y., and Liu, X. (2021). Lipoxin A4 protects primary spinal cord neurons from Erastin-induced ferroptosis by activating the Akt/Nrf2/HO-1 signaling pathway. *FEBS Open Bio* 97, 905–910. doi: 10.1002/2211-5463.13203

Wei, R., Zhao, Y., Wang, J., Yang, X., Li, S., Wang, Y., et al. (2021). Tagitinin C induces ferroptosis through PERK-Nrf2-HO-1 signaling pathway in colorectal cancer cells. *Int. J. Biol. Sci.* 17, 2703–2717. doi: 10.7150/ijbs.59404

Wen, C. P., Lee, J. H., Tai, Y. P., Wen, C., Wu, S. B., Tsai, M. K., et al. (2014). High serum iron is associated with increased cancer risk. *Cancer Res.* 74, 6589–6597. doi: 10.1158/0008-5472.Can-14-0360

White, S., Taetle, R., Seligman, P. A., Rutherford, M., and Trowbridge, I. S. (1990). Combinations of anti-transferrin receptor monoclonal antibodies inhibit human tumor cell growth in vitro and in vivo: evidence for synergistic antiproliferative effects. *Cancer Res.* 50, 6295–6301.

Wu, H., Wang, F., Ta, N., Zhang, T., and Gao, W. (2021). The multifaceted regulation of mitochondria in ferroptosis. *Life* 11:222. doi: 10.3390/life11030222

Wu, K. C., Cui, J. Y., and Klaassen, C. D. (2011). Beneficial role of Nrf2 in regulating NADPH generation and consumption. *Toxicol. Sci.* 123, 590–600. doi: 10.1093/toxsci/kfr183

Wu, S., Lu, H., and Bai, Y. (2019). Nrf2 in cancers: a double-edged sword. *Cancer Med.* 8, 2252–2267. doi: 10.1002/cam4.2101

Wu, T., Sempos, C. T., Freudenheim, J. L., Muti, P., and Smit, E. (2004). Serum iron, copper and zinc concentrations and risk of cancer mortality in US adults. *Ann. Epidemiol.* 14, 195–201. doi: 10.1016/s1047-2797(03)00119-4

Wu, Y., Yu, C., Luo, M., Cen, C., Qiu, J., Zhang, S., et al. (2020). Ferroptosis in cancer treatment: another way to rome. *Front. Oncol.* 10:571127. doi: 10.3389/fonc.2020.571127

Xu, X., Zhang, X., Zhang, Y., Yang, L., Liu, Y., Huang, S., et al. (2017). Wogonin reversed resistant human myelogenous leukemia cells via inhibiting Nrf2 signaling by Stat3/NF-κB inactivation. *Sci. Rep.* 7:39950. doi: 10.1038/srep39950

Xu, X., Zhang, Y., Li, W., Miao, H., Zhang, H., Zhou, Y., et al. (2014). Wogonin reverses multi-drug resistance of human myelogenous leukemia K562/A02 cells via downregulation of MRP1 expression by inhibiting Nrf2/ARE signaling pathway. *Biochem. Pharmacol.* 92, 220–234. doi: 10.1016/j.bcp.2014.09.008

Xue, X., Ramakrishnan, S. K., Weisz, K., Triner, D., Xie, L., Attili, D., et al. (2016). Iron uptake via DMT1 integrates cell cycle with JAK-STAT3 signaling to promote colorectal tumorigenesis. *Cell Metab.* 24, 447–461. doi: 10.1016/j.cmet.2016.07.015

Yanagawa, T., Itoh, K., Uwayama, J., Shibata, Y., Yamaguchi, A., Sano, T., et al. (2004). Nrf2 deficiency causes tooth decolourization due to iron transport disorder in enamel organ. *Genes Cells* 9, 641–651. doi: 10.1111/j.1356-9597.2004.00753.x

Yang, W. S., and Stockwell, B. R. (2008). Synthetic lethal screening identifies compounds activating iron-dependent, nonapoptotic cell death in oncogenic-RAS-harboring cancer cells. *Chem. Biol.* 15, 234–245. doi: 10.1016/j.chembiol.2008.02.010

Yauger, Y. J., Bermudez, S., Moritz, K. E., Glaser, E., Stoica, B., and Byrnes, K. R. (2019). Iron accentuated reactive oxygen species release by NADPH oxidase in activated microglia contributes to oxidative stress in vitro. *J. Neuroinflamm.* 16:41. doi: 10.1186/s12974-019-1430-7

Yu, C., Jiao, Y., Xue, J., Zhang, Q., Yang, H., Xing, L., et al. (2017). Metformin sensitizes non-small cell lung cancer cells to an epigallocatechin-3-Gallate (EGCG) treatment by suppressing the Nrf2/HO-1 Signaling Pathway. *Int. J. Biol. Sci.* 13, 1560–1569. doi: 10.7150/ijbs.18830

Yuan, H., Li, X., Zhang, X., Kang, R., and Tang, D. (2016). CISD1 inhibits ferroptosis by protection against mitochondrial lipid peroxidation. *Biochem. Biophys. Res. Commun.* 478, 838–844. doi: 10.1016/j.bbrc.2016.08.034

Zacharski, L. R., Chow, B. K., Howes, P. S., Shamayeva, G., Baron, J. A., Dalman, R. L., et al. (2008). Decreased cancer risk after iron reduction in patients with peripheral arterial disease: results from a randomized trial. *J. Natl. Cancer Inst.* 100, 996–1002. doi: 10.1093/jnci/djn209

Zhang, J., Zhao, H., Yao, G., Qiao, P., Li, L., and Wu, S. (2021). Therapeutic potential of iron chelators on osteoporosis and their cellular mechanisms. *Biomed. Pharmacother.* 137:111380. doi: 10.1016/j.biopha.2021.111380

Zhang, W., Hu, X., Shen, Q., and Xing, D. (2019). Mitochondria-specific drug release and reactive oxygen species burst induced by polyprodrug nanoreactors can enhance chemotherapy. *Nat. Commun.* 10:1704. doi: 10.1038/s41467-019-09566-3

Zhou, S., Ye, W., Duan, X., Zhang, M., and Wang, J. (2013). The noncytotoxic dose of sorafenib sensitizes Bel-7402/5-FU cells to 5-FU by down-regulating 5-FU-induced Nrf2 expression. *Dig. Dis. Sci.* 58, 1615–1626. doi: 10.1007/s10620-012-2537-1

Zimta, A. A., Cenariu, D., Irimie, A., Magdo, L., Nabavi, S. M., Atanasov, A. G., et al. (2019). The role of Nrf2 activity in cancer development and progression. *Cancers* 11:1755. doi: 10.3390/cancers11111755

Zong, W. X., Rabinowitz, J. D., and White, E. (2016). Mitochondria and Cancer. *Mol. Cell* 61, 667–676. doi: 10.1016/j.molcel.2016.02.011

Conflict of Interest: The authors declare that the research was conducted in the absence of any commercial or financial relationships that could be construed as a potential conflict of interest.

Publisher's Note: All claims expressed in this article are solely those of the authors and do not necessarily represent those of their affiliated organizations, or those of the publisher, the editors and the reviewers. Any product that may be evaluated in this article, or claim that may be made by its manufacturer, is not guaranteed or endorsed by the publisher.

frontiers in Cell and Developmental Biology

ORIGINAL RESEARCH
published: 06 October 2021
doi: 10.3389/fcell.2021.735013

Identification of the Prognostic Signature Associated With Tumor Immune Microenvironment of Uterine Corpus Endometrial Carcinoma Based on Ferroptosis-Related Genes

Jinhui Liu[1†], Yichun Wang[2†], Huangyang Meng[1†], Yin Yin[3†], Hongjun Zhu[4] and Tingting Ni[5*]*

[1] Department of Gynecology, The First Affiliated Hospital of Nanjing Medical University, Nanjing, China, [2] Department of Urology, The First Affiliated Hospital of Nanjing Medical University, Nanjing, China, [3] Department of Obstetrics and Gynecology, The First Affiliated Hospital of Nanjing Medical University, Nanjing, China, [4] Department of Oncology, Nantong Third People's Hospital Affiliated to Nantong University, Nantong, China, [5] Department of Oncology, Affiliated Tumor Hospital to Nantong University, Nantong, China

OPEN ACCESS

Edited by:
Maryam Mehrpour, Université Paris Descartes, France

Reviewed by:
Qingbin Cui, University of Toledo, United States
Eswari Dodagatta-Marri, University of California, San Francisco, United States

***Correspondence:**
Tingting Ni
nitt2007@163.com
Hongjun Zhu
zhj28254282@163.com

[†] These authors have contributed equally to this work

Specialty section:
This article was submitted to Molecular and Cellular Oncology, a section of the journal Frontiers in Cell and Developmental Biology

Received: *01 July 2021*
Accepted: *13 September 2021*
Published: *06 October 2021*

Citation:
Liu J, Wang Y, Meng H, Yin Y, Zhu H and Ni T (2021) Identification of the Prognostic Signature Associated With Tumor Immune Microenvironment of Uterine Corpus Endometrial Carcinoma Based on Ferroptosis-Related Genes. Front. Cell Dev. Biol. 9:735013. doi: 10.3389/fcell.2021.735013

Background: Uterine corpus endometrial carcinoma (UCEC) is the sixth most common cancer worldwide. Ferroptosis plays an important role in malignant tumors. However, the study of ferroptosis in the endometrial carcinoma remains blank.

Methods: First, we constructed a ferroptosis-related signature based on the expression profiles from The Cancer Genome Atlas database. Then, patients were divided into the high-risk and low-risk groups based on this signature. The signature was evaluated by Kaplan–Meier analysis and receiver operating characteristic (ROC) analysis. We further investigated the relationship between this signature and immune microenvironment via CIBERSORT algorithm, ImmuCellAI, MAF, MSI sensor algorithm, GSEA, and GDSC.

Results: This signature could be an independent prognostic factor based on multivariate Cox regression analysis. GSEA revealed that this signature was associated with immune-related phenotype. In addition, we indicated the different status of immune infiltration and response to the immune checkpoint between low-risk and high-risk groups. Patients in the low-risk group were more likely to present with a higher expression of immune checkpoint molecules and tumor mutation burden. Meanwhile, the low-risk patients showed sensitive responses to chemotherapy drugs.

Conclusion: In summary, the six ferroptosis-related genes signature could be used in molecular subgrouping and accurately predict the prognosis of UCEC.

Keywords: uterine corpus endometrial carcinoma, ferroptosis, prognostic signature, molecular subtypes, immune checkpoint, drug sensitivity

INTRODUCTION

Uterine corpus endometrial carcinoma (UCEC) is a huge threat to women's health, whose incidence is increasing year by year in the United States (Siegel et al., 2019). Most women diagnosed with highly differentiated endometrial histology tend to be diagnosed early and have a favorable prognosis (Amant et al., 2005). However, some patients have low-grade, early stage, well-differentiated endometrioid tumors, in which unexpected recurrence and poor prognosis have indeed occurred. For patients with relapsed or advanced tumors and clinically aggressive histological tumors, the clinical outcome will be greatly worsened (Siegel et al., 2018). Such a poor prognosis of endometrial cancer highlights the urgent need to understand the mechanism of tumorigenesis and develop more effective strategies for predicting patients' prognosis.

Ferroptosis is an iron-dependent regulation of cell death mediated by the fatal accumulation of lipid peroxides (Dixon et al., 2012). Artificial introduction of ferroptosis is considered a promising treatment for cancers resistant to traditional therapies (Hassannia et al., 2019; Liang et al., 2019). Ferroptosis has been reported to be a crucial process in human hepatocellular carcinoma, and CDGSH iron sulfur domain 1 (CISD1) (Yuan et al., 2016) and TP53 gene are known to be negative regulatory effective for ferroptosis (Jennis et al., 2016). In addition, other genes such as retinoblastoma (Rb), nuclear factor erythroid 2–related factor 2 (NRF2), and metallothionein (MT)-1G are reported to be associated with ferroptosis and protect liver cancer from induction of sorafenib (Louandre et al., 2015; Sun et al., 2016a,b). In 2021, researchers have revealed that ferroptosis process was aberrantly regulated in UCEC and an activator of ferroptosis can induce cell death in UCEC cells (Lopez-Janeiro et al., 2021; Zhang et al., 2021). However, the prognosis value of ferroptosis in the endometrial carcinoma still remains blank.

In the present study, expression profiles and clinical data of 511 UCEC patients from The Cancer Genome Atlas (TCGA) were used. We developed a ferroptosis-related prognostic signature. The prognostic role of the ferroptosis-related prognosis signature (FRPS) was identified by multi-faceted analysis. The relationships between the signature and immune cell type fractions, immune checkpoint modulators, mutation profile, consensus clustering, m6A regulators, mRNAsi, and functional analyses were further evaluated to explore underlying value of the FRPS.

MATERIALS AND METHODS

Data Collection

All these expression profiles and corresponding clinical data were obtained from TCGA[1]. Then, complete clinical data of 548 UCEC samples and 23 normal samples including survival time were filtered for further analysis. We integrated the transcriptome and complete clinical data to screen out 511 overall survival–related UCEC samples. Half of them (n = 256) were randomly split into training cohort. The entire patients (n = 511) were defined as testing cohort to verify the signature. The baseline information is exhibited in **Supplementary Table 1**. Then, 60 ferroptosis-related genes were retrieved from the gene list provided by previous literature (Liang et al., 2020). A total of 15 UCEC specimens and 15 adjacent tissues were obtained from the Affiliated Tumor Hospital of Nantong University. We obtained all the written informed consent from patients.

[1]http://cancergenome.nih.gov/

Development and Validation of Ferroptosis-Related Prognosis Signature

Firstly, we performed univariate Cox regression analysis to screen targeted ferroptosis-related genes with prognostic values. To reduce the risk of over-fitting, Lasso regression analysis, and univariate and multivariate Cox regression analysis were used to construct the prognosis model (Tibshirani, 1997). Lasso algorithm was used to select variables, and "glmnet" R package was used to shrink (Simon et al., 2011). The risk score of the FRPS was calculated according to the normalized expression level of each gene and its corresponding regression coefficient. The formula was FRPS risk score = Σ(the expression amount of each gene multiplied by the corresponding coefficient). According to the median risk score of the FRPS, we divided the patients into two groups. Then, principal component analysis (PCA) was performed by using "scatterplot3d" R package on the base of expression. The "survminer" R package was used for survival analysis of each gene. The R package "survival ROC" was used to evaluate the predictive ability of the signature.

Quantitative Real-Time-PCR

Total RNA from 15 UCEC samples and 15 adjacent tissues was extracted using TRIzol reagent (Invitrogen). The residual genomic DNA from total RNA was removed by 4 × gDNA wiper Mix (Vazyme R323-01). The complementary RNA was

TABLE 1 | The 17 significant prognostic genes revealed by univariate Cox regression.

Gene	Hazard ratio	95% CI	*P*-value
HMOX1	1.003	1.001–1.004	0.000
GOT1	1.023	1.010–1.037	0.001
SAT1	0.997	0.995–0.999	0.001
HSBP1	0.906	0.851–0.966	0.002
ATP5MC3	1.032	1.011–1.055	0.004
KEAP1	1.018	1.005–1.031	0.006
GPX4	0.995	0.991–0.999	0.007
AKR1C3	1.006	1.001–1.011	0.015
CISD1	1.096	1.017–1.182	0.016
ACSF2	1.067	1.012–1.124	0.017
CHAC1	1.028	1.003–1.053	0.025
GCLM	1.058	1.007–1.112	0.026
GCLC	1.034	1.003–1.067	0.031
AKR1C1	1.021	1.001–1.041	0.038
CBS	2.544	1.050–6.165	0.039
CS	1.038	1.001–1.076	0.042
HSPB1	0.999	0.998–1.000	0.047

synthesized using PrimeScript RT reagent kit. The SYBR Premix Ex Taq Kit (TaKaRa DRR041) was used to perform real-time quantification. The relative expression levels of target genes were normalized by GAPDH and estimated using the $2^{-\Delta\Delta Ct}$ method. The primers used in this research are listed in **Supplementary Table 2**.

Establishing and Validating a Nomogram for Prognosis Prediction

Nomogram involving prognostic clinicopathological factors (age, stage, histological type, grade, and FRPS) was carried out for prognosis prediction. In validation, we used the calibration plots for calibration of the nomogram. The "rms," "foreign," and "survival" package in R were used to establish and validate a nomogram (Park, 2018).

Assessment of Immune Cell Infiltration in Tumors

CIBERSORT algorithm was used to obtain the fraction of 22 immune cell types based on RNA-Seq data (Newman et al., 2015). The correlation between FRPS and these immune cells was analyzed by Spearman.

Immunotherapy Response Prediction

We used an online tool Immune Cell Abundance Identifier (ImmuCellAI) to estimate the abundance of 24 immune cells in UCEC (Miao et al., 2020). The datasets including RNA-Seq and

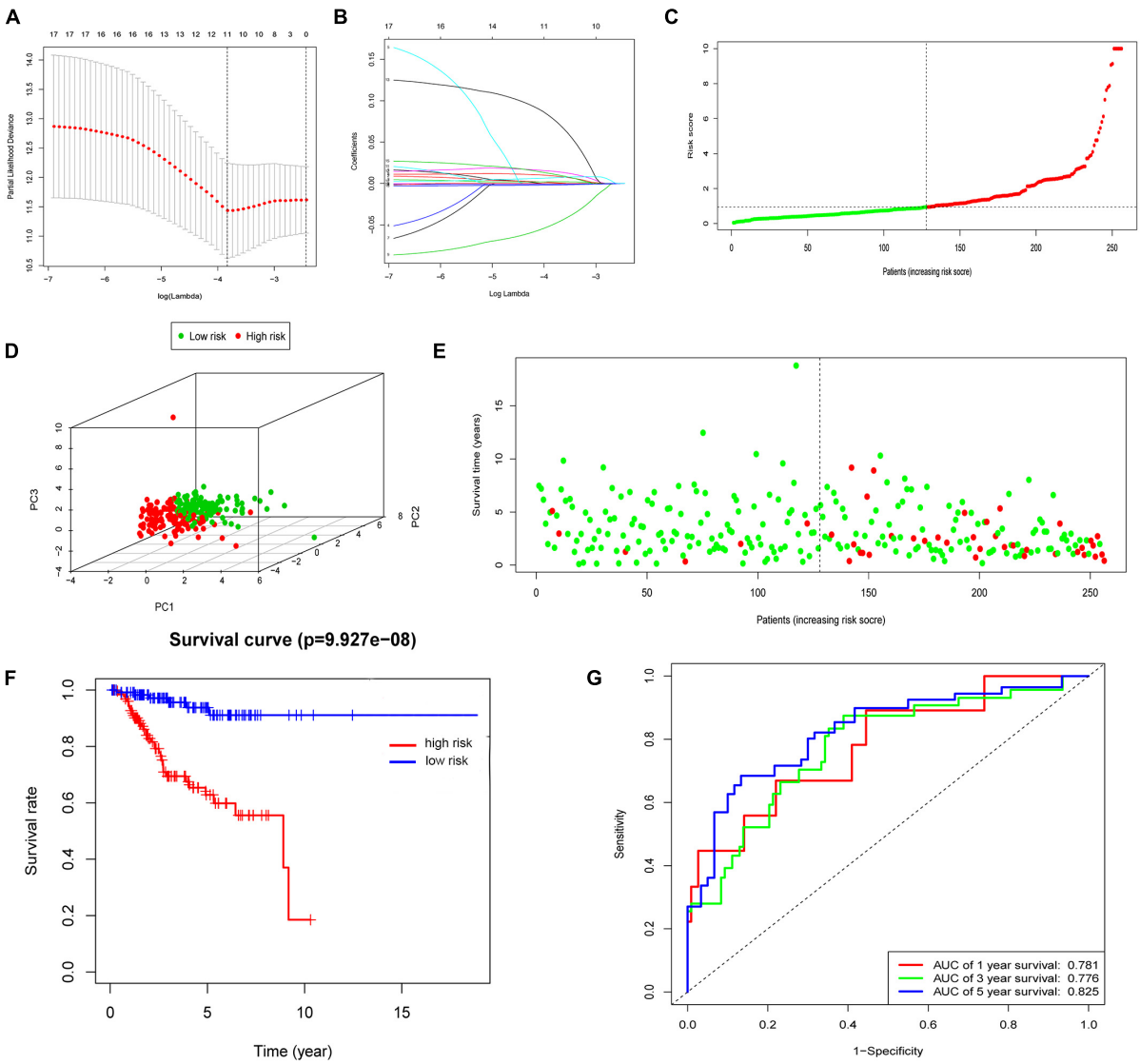

FIGURE 1 | Construction of the FRPS. **(A)** A cross-validation for tuning parameter selection in the LASSO model. **(B)** LASSO coefficient profiles of 17 prognostic immune-related genes. **(C–E)** The distribution of risk score, PCA and survival status in training set. **(F)** Kaplan-Meier survival curves of overall survival between high-risk and low-risk patients in training set. **(G)** 1-year, 3-year, and 5-year ROC curve of the predictive power of the FRPS in training set.

microarray data were used to predict the patient's response to an existing immune checkpoint blockade therapy.

mRNAsi, Mutation Analysis, and Functional Enrichment Analysis

The results of mRNAsi in TCGA-UCEC were obtained from a previous study (Malta et al., 2018). The mutation data of UCEC patients were downloaded from TCGA. The mutation annotation format (MAF) and MAF tool helped us to obtain somatic variation data (Mayakonda et al., 2018). The tumor mutation burden (TMB) score was obtained as follows: TMB = (total mutant bases/total covered bases) $\times$ 10^6 (Robinson et al., 2017). The functional enrichment analysis was conducted by single-sample gene set enrichment analysis (ssGSEA) using the infiltrating score of 16 immune cells and the activity of 13 immune-related pathways.

Microsatellite Instability Analysis

Microsatellite instability sensor algorithm is a program that can report the percentage of unstable microsatellites (Niu et al., 2014). We used this algorithm to obtain the MSI status for all cases based on somatic mutation data downloaded from TCGA. The relationship between FRPS and MSI was analyzed using Spearman's rank correlation coefficient.

Gene Set Enrichment Analysis

Gene set enrichment analysis is a method used to determine whether a set of marker genes can predict a statistically significant difference between two different cohorts. Here, we analyzed the significant difference in survival between the two cohorts in the entire TCGA cohort divided by the risk score. Normalized *p*-values less than 0.05 and false discovery rate (FDR) less than 0.05 are considered significantly enriched (Canzler and Hackermuller, 2020).

Prediction of Chemotherapy Response

To evaluate the response to chemotherapy drugs, we used public pharmacogenomics database Genomics of Drug Sensitivity in

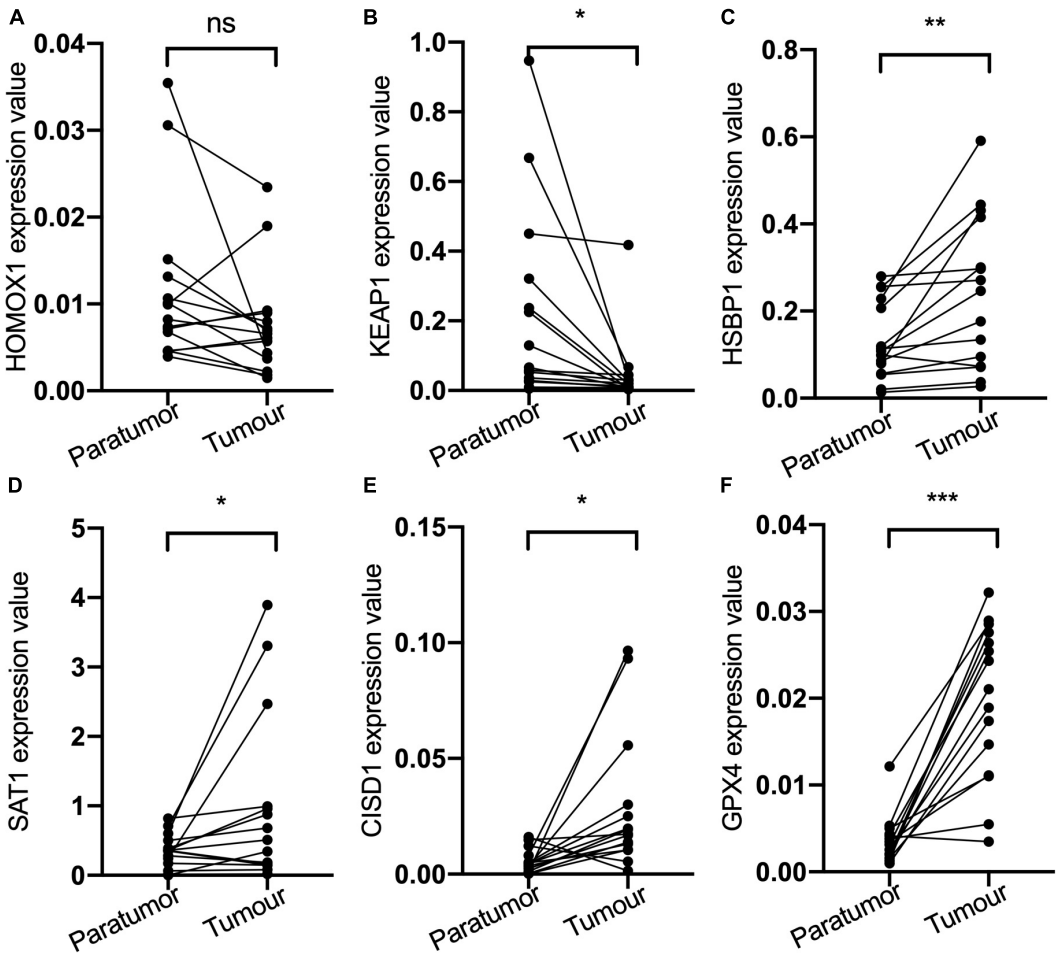

FIGURE 2 | (A) HOMOX1 expression level. **(B)** KEAP1 expression level. **(C)** HSBP1 expression level. **(D)** SAT1 expression level. **(E)** CIDS1 expression level. **(F)** GPX4 expression level. ns, not significant, $^*P < 0.05$, $^{**}P < 0.01$, $^{***}P < 0.001$.

Cancer (GDSC)[2]. The half-maximal inhibitory concentration (IC_{50}) is estimated by R package "pRRophetic" (Yang et al., 2013).

Consensus Clustering and Survival Analysis

To identify the molecular subtypes in endometrial cancer, the TCGA UCEC cohort was divided into different groups by R package "Consensus Cluster Plus, 1000 iterations and resampling rate of 80%" (Yu et al., 2015). We performed the log-rank test and Kaplan–Meier curve to assess the overall survival (OS) difference between different groups. Chi-square test was a good assistant helping us to compare the distribution of age, grade, stage, and histologic type between different clusters.

[2]https://www.cancerrxgene.org

Statistical Analysis

All statistics and figures were analyzed using R 3.6.2. Wilcoxon's test allowed us to evaluate the differential expression of genes related to ferroptosis between UCEC patients and controls. We used the χ^2 test to assess the relationship between FRPS and clinicopathological factors. P-value < 0.05 was considered to be statistically significant.

RESULTS

Construction of Ferroptosis-Related Prognosis Signature in the Cancer Genome Atlas Training Cohort

First, the expression profiles and survival data of UCEC patients in training cohort were filtered based on 60 ferroptosis-related genes through the univariate Cox regression analysis

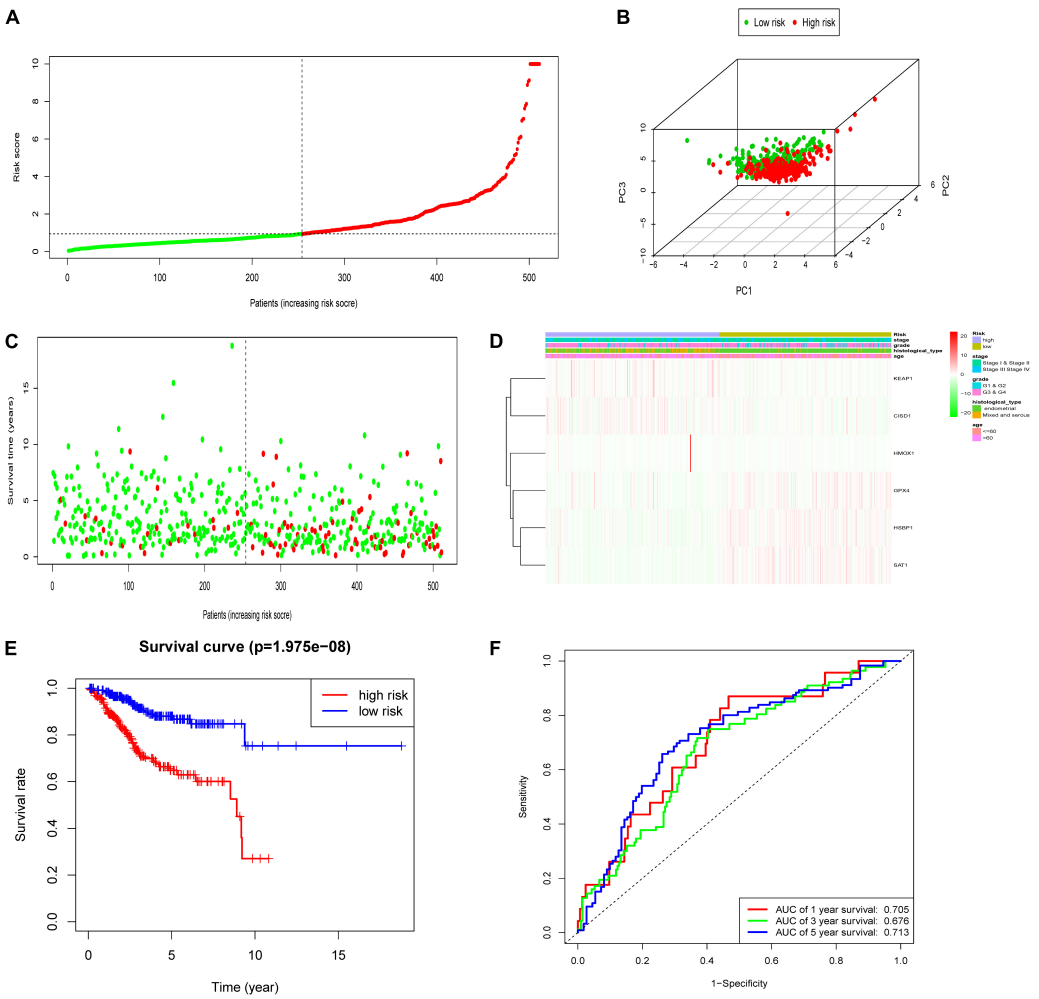

FIGURE 3 | Construction of the FRPS in the testing cohort. **(A)** The distribution of the risk score among patients. **(B)** PCA analysis confirmed that patients in two subgroups were distributed in discrete directions. **(C)** The distribution of the survival status among patients. **(D)** The distribution of stage, grade, histological type, age, and the expression of six genes in high-risk and low-risk groups. **(E)** Kaplan–Meier survival curves of overall survival between high-risk and low-risk patients in testing set. **(F)** 1-year, 3-year, and 5-year ROC curve of the predictive power of the FRPS in testing set.

TABLE 2 | Univariate and multivariate Cox regression analysis of the clinical factors and overall survival in different patient sets.

Variables	Univariable model			Multivariable mode		
	HR	95% CI	*P*-value	HR	95% CI	*P*-value
Train set						
Age	1.875	0.941–3.738	0.074			
Histological type	3.849	2.081–7.117	<0.001	2.665	1.377–5.160	0.004
Grade	4.237	1.024–17.542	0.046	1.645	0.367–7.370	0.515
Stage	4.714	2.540–8.746	<0.001	3.034	1.551–5.933	0.001
FRPS	1.029	1.017–1.042	<0.001	1.027	1.014–1.040	<0.001
Entire set						
Age	1.778	1.112–2.843	0.016	1.695	1.031–2.788	0.038
Histological type	3.044	2.003–4.624	<0.001	1.748	1.104–2.768	0.017
Grade	3.363	1.467–7.710	0.004	1.509	0.622–3.660	0.362
Stage	4.116	2.700–6.275	<0.001	3.286	2.078–5.194	<0.001
FRPS	1.024	1.014–1.034	<0.001	1.022	1.011–1.033	<0.001

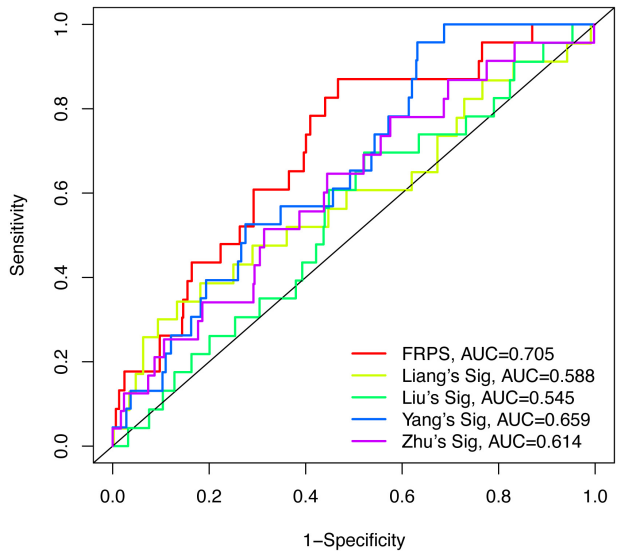

FIGURE 4 | The AUC for FRPS and the existing ferroptosis-related signatures.

and 17 genes were correlated with overall survival (**Table 1**). Then, LASSO analysis (**Figures 1A,B**), and univariate and multivariate Cox regression analysis narrowed the screened scope to six genes (HMOX1, KEAP1, HSBP1, SAT1, CISD1, and GPX4) (**Supplementary Material**). The risk score of FRPS for OS = (0.002907 × HMOX1) + (0.013486 × KEAP1) + (−0.089640 × HSBP1) + (−0.001665 × SAT1) + (0.148239 × CISD1) + (−0.003060 × GPX4). Meanwhile, patients in the training cohort were divided into high-risk and low-risk groups according to the median risk score of the FRPS (**Figure 1C**). PCA indicated the patients in different risk groups were distributed in two directions (**Figure 1D**). The distribution of FRPS and survival status of patients in OS signature are shown in **Figure 1E**. The OS of patients in the low-risk group was significantly longer than those in the high-risk group according to the Kaplan–Meier curve (**Figure 1F**). Besides, the 1-year, 3-year, and 5-year ROC curves based on training cohort are plotted as **Figure 1G**, suggesting satisfactory prognostic value of the signature.

Then, the mRNA expression of these genes was validated by qPCR using the samples from the Nantong Third People's Hospital Affiliated to Nantong University (**Figure 2**). The mRNA expression of KEAP1, HSBP1, SAT1, CISD1, and GPX4 were significantly different between tumor and the adjacent tissues. KEAP1 and HOMOX1 were low expressed in tumor than the para-carcinoma tissues, and the high expression of these two genes increased the risk of FRPS, which suggested the poor prognosis of patients. These results suggested the potential feasibility of this signature for clinical usage. Expression and Kaplan–Meier survival analysis of each gene in the signature were also performed and four genes were output significantly (**Supplementary Figure 1**).

Validation of Ferroptosis-Related Prognosis Signature in the Cancer Genome Atlas Testing Cohort

To test the robustness of the aforementioned signature, the entire TCGA patients were divided into high-risk and low-risk groups by the same risk score (**Figure 3A**). PCA confirmed the similar results obtained from the training cohort; the patients in the two subgroups were distributed in discrete directions (**Figure 3B**). Similarly, patients in the high-risk group showed worse prognosis (**Figure 3C**). The expression of six genes in the signature are exhibited in **Figure 3D**. Kaplan–Meier survival analysis claimed the reduced survival time of patients in the high-risk group compared with those in the low-risk group (**Figure 3E**). Furthermore, subgroup analyses in age, grade, stage, and histological type in the signature were performed, demonstrating that patients with high-risk scores shared shorter OS in all the subgroups ($p < 0.05$) (**Supplementary Figure 2**). Besides, the 1-year, 3-year, and 5-year AUC of signature was 0.705, 0.676, and 0.713, respectively (**Figure 3F**). According to the Cox regression analysis, the histological type, tumor stage, and this signature were independent prognostic factors (**Table 2**). We further compared the prediction value of this

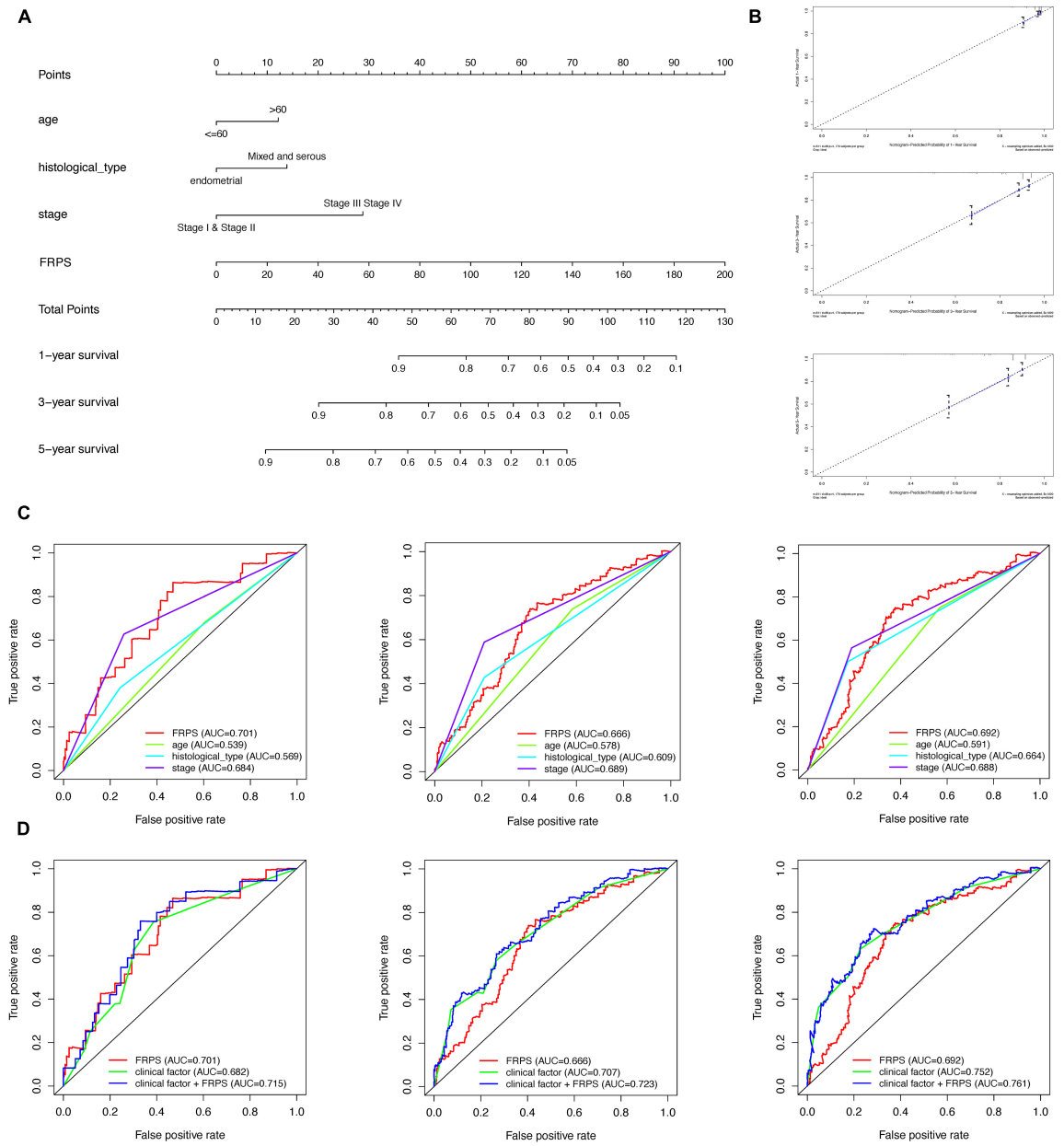

FIGURE 5 | Construction and validation of the nomogram. **(A)** Nomogram to predict the probability of 1-, 3-, and 5-year OS of UCEC patients. **(B)** Calibration curves of the nomogram to predict the probability of OS at 1, 3, and 5 years. **(C)** 1-, 3-, and 5-year ROC of FRPS and the other clinical characteristics. **(D)** 1-, 3-, and 5-year ROC of the combination of FRPS and clinical factors.

signature with other existing signatures. As shown in **Figure 4**, the AUC for this signature was 0.705, which was higher than the existing ferroptosis-related signatures. This result revealed that our established signature was superior to other signatures in predicting patient's survival information (Yu et al., 2015; Liu et al., 2021; Yang et al., 2021; Zhu et al., 2021).

Establishment of Nomogram

To better predict overall survival time, we integrated clinicopathological factors related to prognosis (age, stage, histological type, and FRPS) to establish a nomogram prediction model (**Figure 5A**). We compared the relationship between FRPS and clinicopathological factors (**Supplementary Table 3**). Quantifying the aforementioned variables as numerical points, 1-year, 3-year, and 5-year survival rates of UCEC patients can be calculated based on the total points of all risk factors. A calibration chart was also constructed to show the consensus of the predicted and observed results (**Figure 5B**). Meanwhile, ROC curve demonstrated the better predictive ability of FRPS in 1-year, 3-year, and 5-year OS than other clinical factors

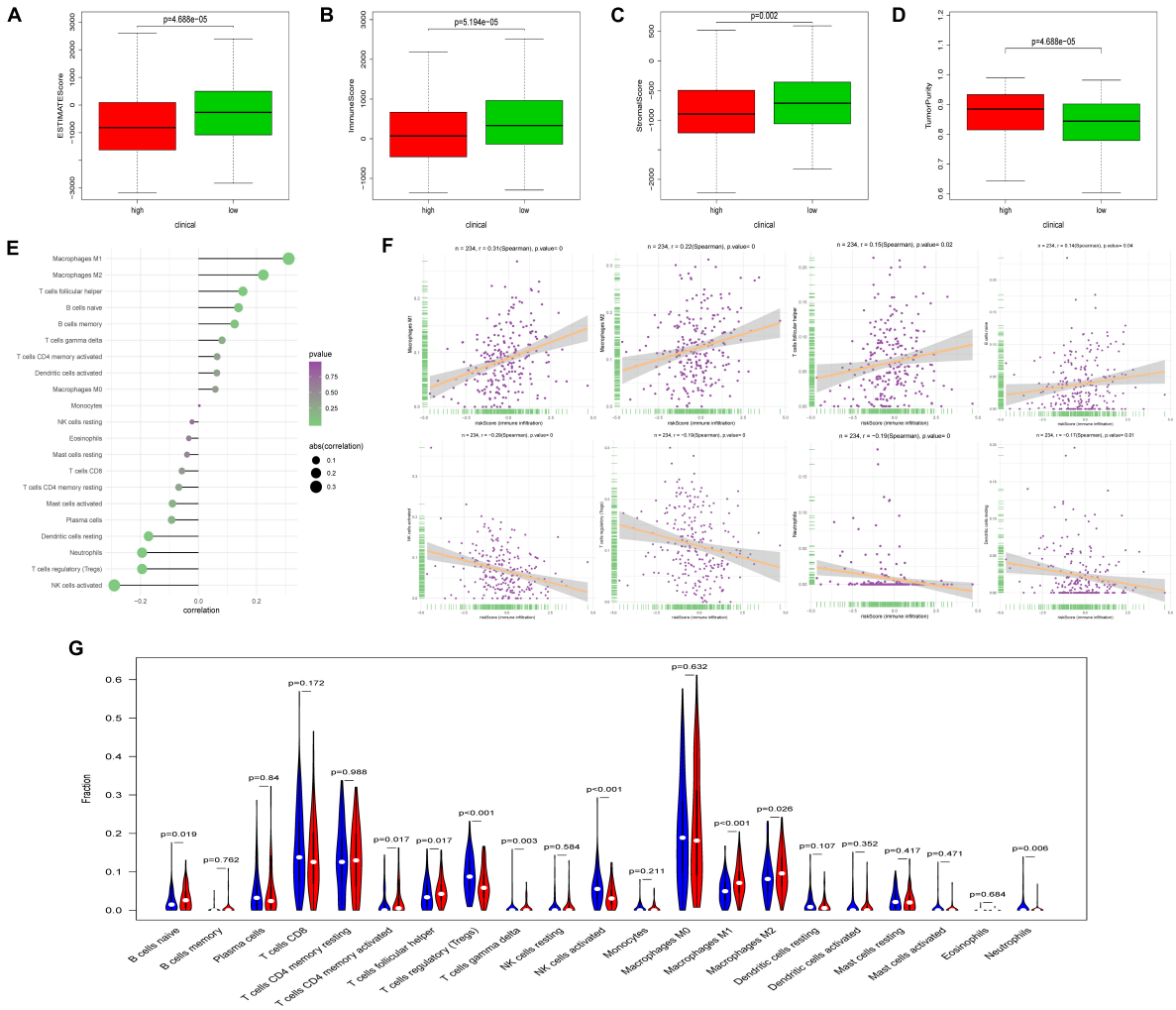

FIGURE 6 | Correlation between FRPS and immune cell infiltration. **(A–D)** The correlation between FRPS and **(A)** ESTIMATE Score, **(B)** Immune Score, **(C)** Stromal Score, and **(D)** Tumor Purity. **(E)** The association between FRPS and immune cell infiltration. **(F)** The association between IRPS and each type of immune cell. **(G)** The landscape of immune cell infiltration in low-risk and high-risk groups. The low-risk and high-risk groups are represented via blue and red violin, respectively.

(**Figure 5C**). Combining clinical factors and FRPS accessed optimal predicting effect in UCEC patients based on 1-year, 3-year, and 5-year OS (**Figure 5D**).

Ferroptosis-Related Prognosis Signature and Immune Cell Type Fractions

Using ESTIMATE algorithm, patients in the high-risk group were found to have lower immune scores, stromal scores, and ESTIMATE scores (**Figures 6A–C**). On the contrary, patients accessed higher tumor purity scores in the high-risk group (**Figure 6D**). The aforementioned findings suggested that the tumor immune microenvironment was closely associated with the FRPS in UCEC patients. To find the major immune cells between the high-risk groups and low-risk groups, CIBERSORT algorithm was employed. The results showed that macrophages M1, macrophages M2, T cell follicular helper, and B cells naive were positively correlated with FRPS while NK cells activated, T cells regulatory (Tregs), neutrophils, and dendritic cells resting were negatively correlated with FRPS (**Figure 6E**). The distribution of immune cells and scores for each patient is exhibited in **Figure 6F**. In the present research, we also focused on the tumor infiltrating cells between subgroups. We found that B cells naive, macrophages M1, macrophages M2, T cells CD4 memory activated, T cells follicular helper, T cells gamma delta, NK cells activated, T cells regulatory (Tregs), and neutrophils infiltrated differently in different groups (**Figure 6G**).

Ferroptosis-Related Prognosis Signature and Immune Checkpoint Modulators

Immune checkpoint proteins, playing important roles in the immune response, aroused our great interest to explore the relationship between FRPS and immune checkpoint modulators. The results demonstrated that CD40, PD-L1, and PD-L2 showed

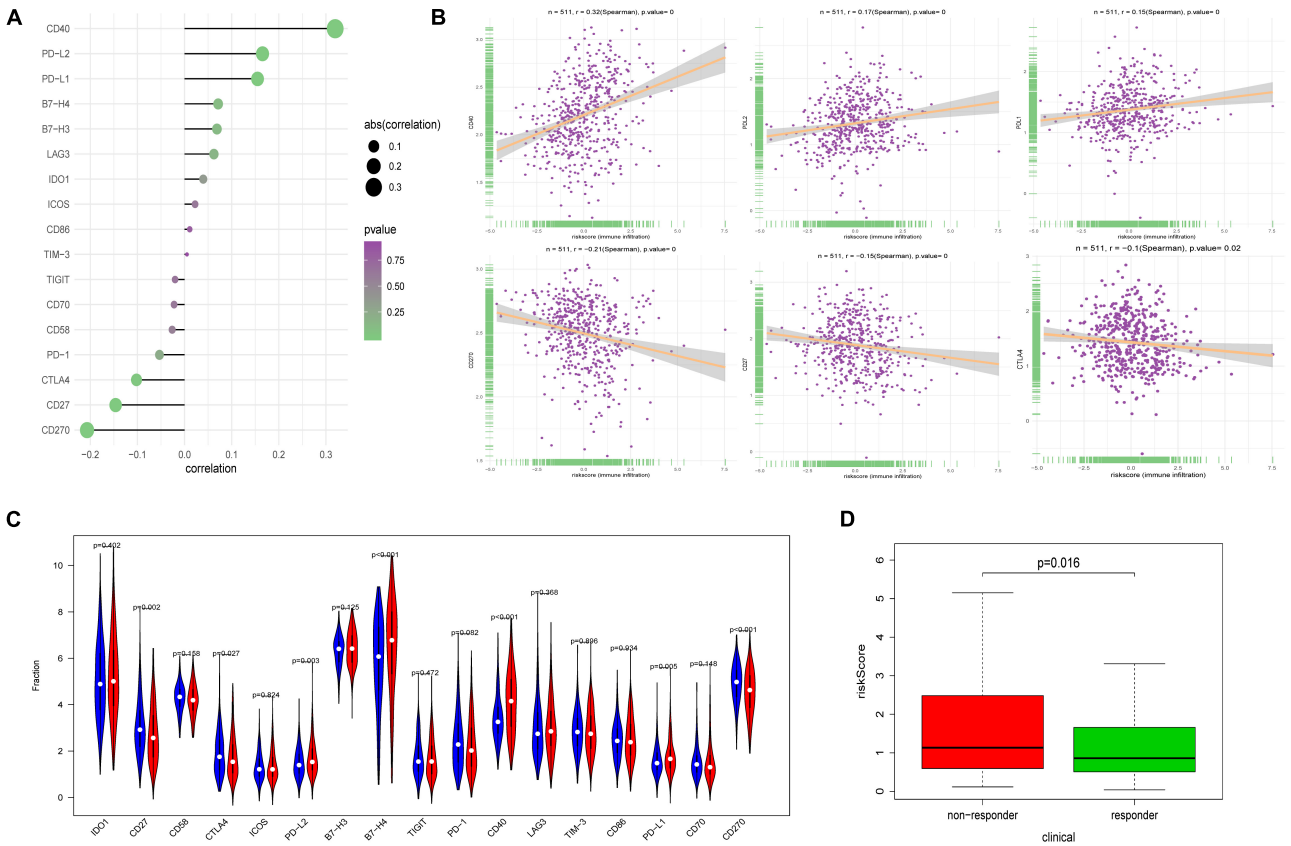

FIGURE 7 | Correlation between FRPS and immune checkpoint molecules and the predicted response to immunotherapy. **(A)** The association between FRPS and immune checkpoint molecules. **(B)** The association between FRPS and several immune checkpoint molecules in detail. **(C)** The landscape of the expression of immune checkpoint molecules in low-risk and high-risk groups. **(D)** The different immunotherapy response rates in low-risk and high-risk groups.

a positive correlation with FRPS while CD270, CD27, and CTLA4 were negatively related to FRPS (**Figure 7A**). The distribution of immune checkpoint proteins and risk scores for each patient is exhibited in **Figure 7B**. Immune checkpoint proteins between high-risk groups and low-risk groups were evaluated, and results demonstrated that CD27, CTLA4, PD-L2, B7-H4, CD40, PD-L1, and CD270 expressed differently between high- and low-risk groups (**Figure 7C**). Potential response to immunotherapy in each patient was further assessed by the online tool ImmuCellAI and patients in the low-risk group showed better reactivity to immunotherapy than those in the high-risk group (p = 0.016; **Figure 7D**).

Ferroptosis-Related Prognosis Signature and Mutation Profile

Tumor mutation burden (TMB) is an important cause of tumor occurrence and development, can be used to predict the efficacy of immune checkpoint blockade, and has been shown to be a biomarker for patients who benefit from immunotherapy. In this study, we declared that FRPS was negatively correlated with TMB (**Figure 8A**). Lower TMB was observed in the high-risk group (**Figure 8B**). In addition, the mutant genes that showed the most significant difference in their mutation frequency between the two groups are shown in **Figure 8C**. TP53 and PPP2R1A were found to have higher mutation frequency in the high-risk group, and the rest of the genes showed higher mutation frequency in the low-risk group. Therefore, somatic mutation data were used to assess the TMB of patients. The order of somatic mutation frequency in the high-risk group was TP53 > PTEN > PIK3CA > TTN > ARID1A > PIK3R1 > KMT2D > CHD4 > MUC16 > PPP2R1A (**Figure 8D**); in the low-risk group, PTEN > ARID1A > PIK3CA > TTN > CTCF > PIK3R1 > CTNNB1 > KMT2D > ZFHX3 > KRAS (**Figure 8E**).

Ferroptosis-Related Prognosis Signature and Microsatellite Instability

Several researches had illustrated that MSI can affect the effect of immunotherapy in several cancers. In this research, we also investigated the MSI status between groups. The results revealed that MSI status was negatively correlated with FRPS (**Figure 8F**). Besides, according to ImmuCellAI, higher immunotherapy response rate was observed in the low-risk group compared with patients in the high-risk group (**Figure 8G**), which implied that patients in the low-risk group might benefit from immunotherapy.

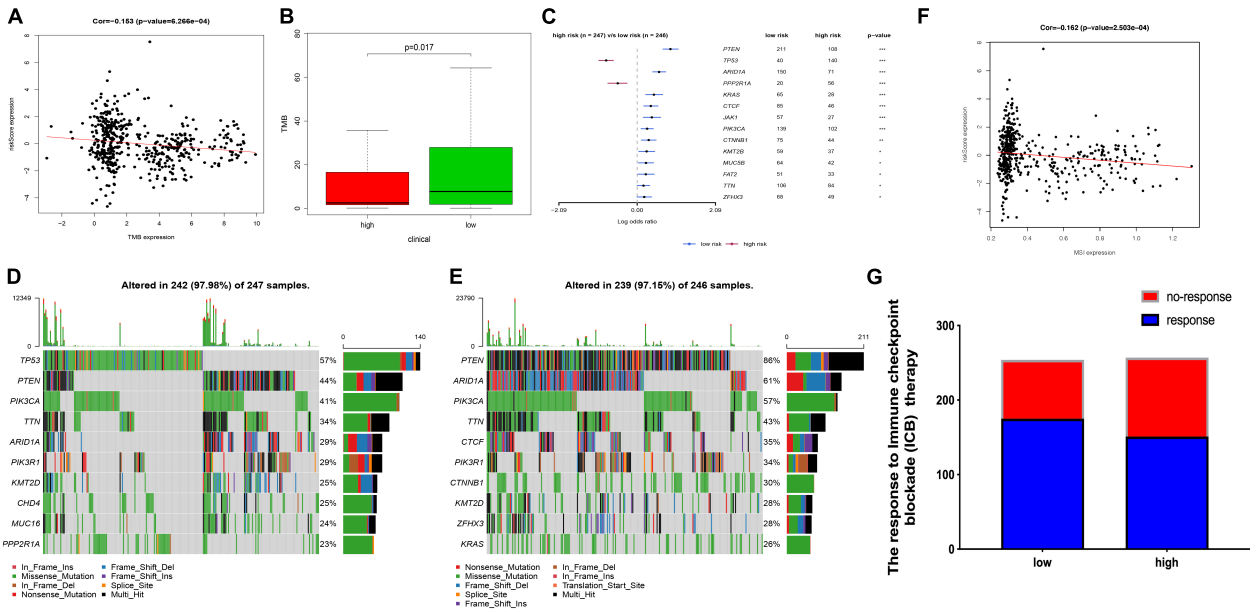

FIGURE 8 | The TMB, mutation profile, and MSI in high-risk and low-risk groups. **(A)** The correlation between TMB and FRPS. **(B)** The TMB status in high-risk and low-risk groups. **(C)** The most frequently mutated genes in high-risk and low-risk groups. **(D,E)** The top 10 mutated genes in high-risk and low-risk groups. **(F)** The relationship between MSI and FRPS. **(G)** The rate of response to immunotherapy in high-risk and low-risk groups. Red line to provide a brief tendency of association between TMB, MIS and riskscore. $^{*}P < 0.05$, $^{**}P < 0.01$, $^{***}P < 0.001$.

m6A Regulators, mRNAsi, and Functional Analyses in Two Groups

In recent years, the role of m6A methylation in cancer has attracted widespread attention. More and more evidence showed that the genetic changes and expression disorders of m6A RNA are associated with the tumor occurrence, progression, and treatment resistance. The expression levels of HNRNPC, YTHDC1, ZC3H13, YTHDF2, FTO, YTHDF1, YTHDF3, METTL14, RBM15, WTAP, KIAA1429, FMR1, and HNRNPA2B1 were dramatically higher in UCEC high-risk group ($p < 0.05$) (**Supplementary Figure 3A**). In addition, the expression levels of mRNAsi ($p = 3.52e\text{-}10$) and EREG-mRNAsi ($p = 0.032$) in high-risk group were also higher (**Supplementary Figure 3B**). To further explore the correlation between FRPS and immune status, we used ssGSEA to quantify the enrichment scores of various immune cell subgroups, related functions, or pathways (**Supplementary Figures 3C,D**). Interestingly, the antigen presentation process (aDC and iDC) was significantly different, and the enriched cytokine–cytokine receptor interaction in the KEGG analysis scored higher in the high-risk group ($p < 0.05$, **Supplementary Figure 3D**).

Gene Set Enrichment Analysis Identifies a Signaling Pathway Related With Ferroptosis-Related Prognosis Signature

In addition, GSEA analyzed the transcription information of patients in the high-risk and low-risk subgroups. Based on normalized p-value < 0.05, FDR < 0.05, and NES, we filtered the most significant enrichment biological approach. Representative KEGG pathways were related to some essential signaling pathways including cell cycle, DNA replication, mismatch repair, alpha linolenic acid metabolism, and ribosome and tyrosine metabolism (**Supplementary Figure 4**). The aforementioned results suggested the potential mechanism of the occurrence and development of UCEC.

Response to Chemotherapy in Two Groups

Using the pRRophetic algorithm, IC_{50} of 35 common chemotherapeutic agents was predicted in high- or low-risk group (PD.0332991, Nutlin.3a, X17.AAG, Bryostatin.1, PD.0325901, SB.216763, Bicalutamide, AZD6244, PF.02341066, LFM.A13, Temsirolimus, NVP.BEZ235, FTI.277, RDEA119, BMS.536924, MG.132, PF.562271, Roscovitine, AZ628, Vinblastine, EHT.1864, Tipifarnib, BMS.754807, Lapatinib, KIN001.135). All 25 drugs had higher IC_{50} in high-risk patients, indicating that the low-risk patients were more sensitive to these 25 drugs (Wilcoxon test, all $p < 0.05$; **Supplementary Figure 5**).

Ferroptosis-Related Prognosis Signature and Consensus Clustering

Consensus clustering was analyzed based on the expression levels of six targeted genes. We chose $K = 2$ as the most optimal clustering because the clustering was suboptimal when divided into more than two clusters (**Figures 9A–C**). UCEC patients in clusters 1 and 2 showed significant differences in age, stage, and histological type, but did not show any significant differences in grade (**Figures 9D,E**). Moreover, the OS was significantly shorter in the UCEC patients of cluster 1 based on Kaplan–Meier

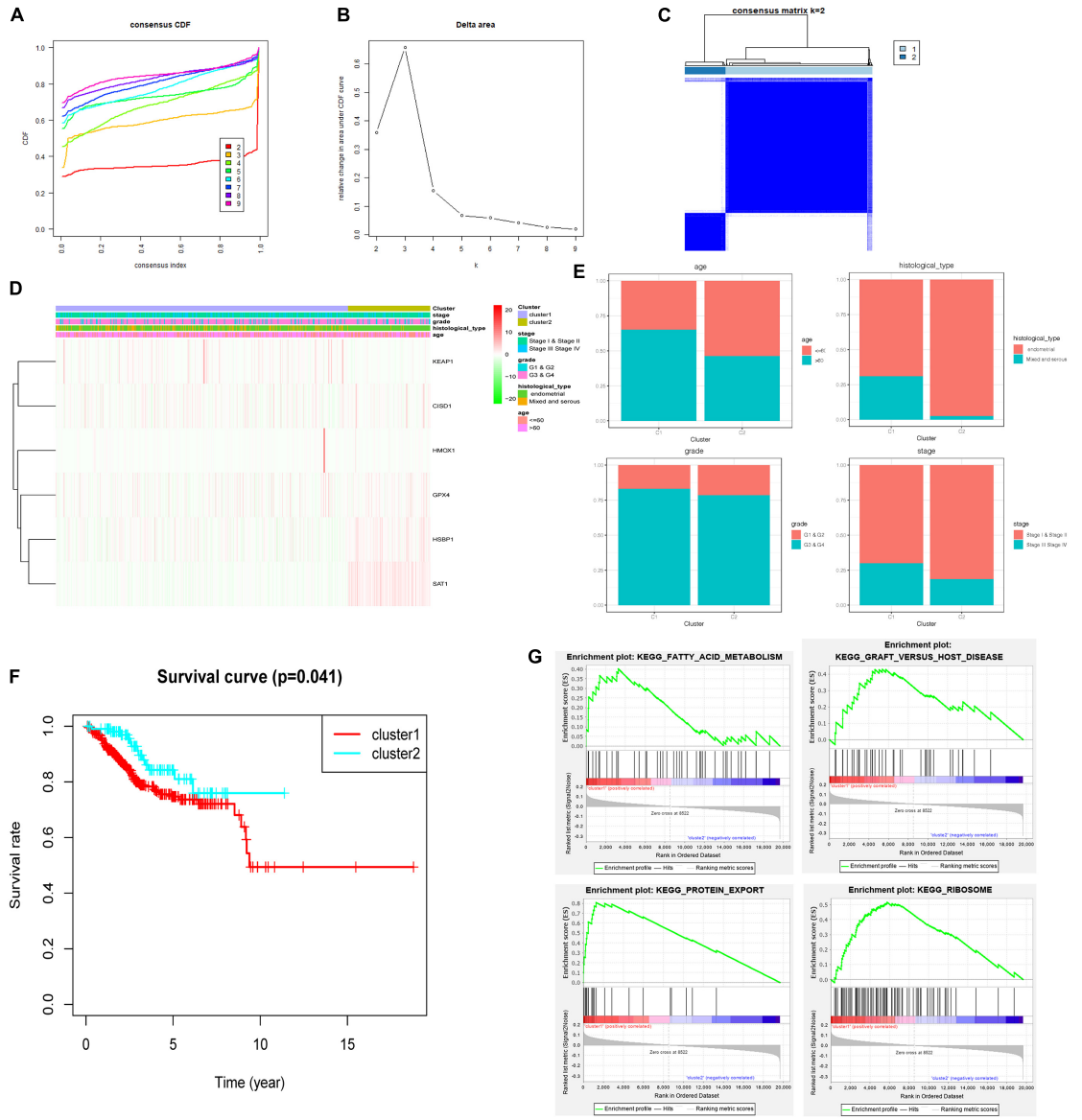

FIGURE 9 | Consensus clustering for ferroptosis-related genes in UCEC patients. **(A)** Consensus clustering CDF for $k = 2$ to $k = 9$. **(B)** Relative change in area under CDF curve for $k = 2$ to $k = 9$. **(C)** Consensus clustering matrix of UCEC samples from TCGA dataset for $k = 2$. **(D)** Heat map of two clusters defined by the six variable expression genes. **(E)** The proportion of clinical factors in two clusters. **(F)** K–M survival curve of patients in two clusters. **(G)** The significantly enriched KEGG pathways in two clusters.

curve compared with those of cluster 2 (**Figure 9F**). We also compared the significantly enriched KEGG pathways between two clusters; four pathways were identified, including fatty acid metabolism, graft-versus-host disease, protein export, and ribosome. These mechanisms may involve in the pathogenesis of UCEC (**Figure 9G**).

DISCUSSION

The incidence rate of uterine corpus endometrial carcinoma (UCEC) is increasing in recent years, becoming a global problem threatening women's health. To date, therapeutic regimens, such as immunological therapy and chemotherapy, are applied according to the clinical stages of the tumor. However, some patients cannot benefit from the current therapeutic regimens even if they are in the same clinical stage. To overcome this challenge, in this research, we developed a model for predicting the survival and therapeutic response of UCEC patients using ferroptosis-related genes.

Ferroptosis is emerging as an iron-dependent regulation of cell death mediated by the fatal accumulation of lipid peroxides. Previous studies had reported that several genes can serve as regulators of ferroptosis and plays a crucial role in HCC. In

this study, we systematically identified the expression of 60 ferroptosis-related genes and then filtered out six prognosis-related genes (HMOX1, KEAP1, HSBP1, SAT1, CISD1, and GPX4) to construct a signature for overall survival prediction in patients with UCEC. The AUC values of the training and testing cohort were greater than 0.7. The FRPS showed a higher prognostic value compared with other clinical factors.

This signature was constructed based on six HMOX1 prognosis-related genes (HMOX1, KEAP1, HSBP1, SAT1, CISD1, and GPX4). HMOX1 is a cell-protective enzyme that is important in maintaining the dynamic balance of REDOX and provides an effective antioxidant defense mechanism in response to cellular stress by breaking down toxic heme into carbon monoxide, biliverdin, and iron (Nath, 1999; Lever et al., 2016). Although HMOX1 expression is upregulated in the process of ferroptosis in cancer cells, it is not clear whether HMOX1 is induced in this context to enhance ferroptosis or as a protective response (Kwon et al., 2015). Based on our results, the imbalance of the expression of HMOX1 suggested the poor prognosis of patients. KEAP1, a component of Nrf2-Keap1 pathway, acts as a molecular switch to activate Nrf2, and KEAP1 senses and delivers the oxidizing challenge (Lau et al., 2008). Nrf2-Keap1 pathway can act as a switch for malignancy in gliomas promoting cell proliferation and resistance to cell death processes such as ferroptosis (Fan et al., 2017). HSBP1 is an evolutionarily conserved heat shock factor binding protein that can directly bind to the DNA of heat shock factor 1 (Hsf1) and inhibit its transcriptional activity (Satyal et al., 1998). There are no large data to prove the function of HSBP1 as a ferroptosis regulator. The transcriptional activation of SAT1 mediated by p53 is essential for ROS-induced ferroptosis because knocking out SAT1 can significantly eliminate the p53-induced ferroptosis under ROS stress (Ou et al., 2016). CISD1, also known as mitoNEET, is an iron-containing mitochondrial outer membrane protein with a size of 13 kDa (Geldenhuys et al., 2014). It was first identified as a target for the treatment of diabetes drug pioglitazone (Colca et al., 2004). Functionally, CISD1 regulates iron uptake and respiration in mitochondria (Wiley et al., 2007; Tamir et al., 2015). CISD1 deficiency leads to iron accumulation and subsequent oxidative damage in mitochondria, which are involved in fat and glucose metabolism (Kusminski et al., 2012). In addition to diabetes, CISD1 expression impairment is also associated with tumor growth (such as breast cancer and liver cancer) and has been considered as a potential chemotherapy target (Salem et al., 2012; Sohn et al., 2013). GPX4 has been determined as a central regulator of ferroptosis (Yang et al., 2014). In models where GPX4 deficiency leads to death or cell loss, iron prolapse is likely to occur. In fact, embryonic fibroblasts (MEF) in conditional Gpx4 knockout mice died of lipid peroxidation after Gpx4 deletion. Supplementation of vitamin E in the medium of the MEF saved cell death (Seiler et al., 2008). In normal cell physiology, the increase in lipid peroxidation caused by GPX4 inhibition raises the question of the origin of lipid peroxidation (Yang and Stockwell, 2008).

We further investigated the biological function of this FRPS. We found this signature was closely related to the tumor immune microenvironment. Several studies had demonstrated that tumor played important role in the developing and prognosing of tumor (Hinshaw and Shevde, 2019). Immune cells are important constituents of the tumor stroma and take part in this process. Immune cells like macrophages M1, macrophages M2, T cell follicular helper, and B cells naive were positively correlated with this signature while NK cells activated, T cells regulatory (Tregs), neutrophils, and dendritic cells resting were negatively correlated with this signature, which hinted the strong immunoreaction in patients from the low-risk group. Apart from the immune cell infiltration, results from the ImmuCellAI showed that patients in the low-risk group may exhibit sensitive response to immunotherapy, thus, may benefit from immunotherapy. This conclusion was also supported by the results from immune checkpoint modulators, TMB, and MSI. Meanwhile, chemotherapy was another important treatment for UCEC patients. According to the estimated IC_{50} results from the GDSC database, the patients in low-risk group were more sensitive to 25 chemotherapy drugs including bicalutamide, temsirolimus, roscovitine, vinblastine, tipifarnib, lapatinib, and other drugs.

However, this research also has several limitations. First, the research is conducted mainly based on online Public Database. To verify our model, the external data were necessary. Second, we mainly focused on the ferroptosis-related genes, and there might be more precise genes which can reflect patient's prognosis. Finally, the response to chemotherapy was predicted by online database, and some drugs were not the major drugs for UCEC, which should be verified in future search.

CONCLUSION

In summary, based on six selected ferroptosis-related genes, we constructed a prognostic signature possessing independent predictive value of UCEC patients in TCGA datasets. Through internal verification, the versatility of the signature was proven and the nomogram was showed to be suitable for clinical use. With the help of FRPS, clinical factors can predict a patient's response to immunotherapy and chemotherapy, which can provide valuable information on designing a therapeutic regimen.

DATA AVAILABILITY STATEMENT

The datasets presented in this study can be found in online repositories. The names of the repository/repositories and accession number(s) can be found in the article/**Supplementary Material**.

ETHICS STATEMENT

The studies involving human participants were reviewed and approved by the Affiliated Tumor Hospital to Nantong University. The patients/participants provided their written informed consent to participate in this study. Written informed consent was not obtained from the individual(s) for the publication of any potentially identifiable images or data included in this article.

AUTHOR CONTRIBUTIONS

TN and HZ conceived the study. JL, YW, HM, and YY participated in the design, analysis, and draft of the study. JL and YW plotted all figures in this article. HM and YY helped in the data analysis. All authors approved the final version of this article and agreed to be accountable for all aspects of the work.

ACKNOWLEDGMENTS

We would like to thank the researchers and study participants for their contributions.

SUPPLEMENTARY MATERIAL

The Supplementary Material for this article can be found online at: https://www.frontiersin.org/articles/10.3389/fcell.2021.735013/full#supplementary-material

Supplementary Figure 1 | The mRNA expression level of **(A)** CISD1, GPX4, HSBP1, SAT1, and their **(B)** Kaplan–Meier plot. $^{**}P < 0.01$ and $^{***}P < 0.001$.

Supplementary Figure 2 | Kaplan–Meier plot of the high- and low-risk groups under diverse situations by classifying the patients into different subgroups according to **(A)** age, **(B)** tumor grade, **(C)** tumor pathological pattern, and **(D)** stage.

Supplementary Figure 3 | m6A regulators, mRNAsi, and functional analyses in two groups. **(A)** The expression levels of HNRNPC, YTHDC1, ZC3H13, YTHDF2, FTO, YTHDF1, YTHDF3, METTL14, RBM15, WTAP, KIAA1429, FMR1, and HNRNPA2B1 were dramatically higher in UCEC high-risk group than in low-risk group. **(B)** The expression levels of mRNAsi and EREG-mRNAsi in high-risk and low-risk groups. **(C)** The correlation between the FRPS and scores of 16 immune cells determined by ssGSEA. **(D)** The enriched cytokine–cytokine receptor interaction determined by ssGSEA. The low-risk and high-risk groups are represented via blue and red violin, respectively.

Supplementary Figure 4 | Significantly enriched KEGG pathway related to FRPS identified by GSEA analysis.

Supplementary Figure 5 | The predicted chemotherapeutic response in the high-risk and low-risk groups.

Supplementary Table 1 | The basic clinical information of the involved patients in TCGA.

Supplementary Table 2 | Primers used in PCR application.

Supplementary Table 3 | The correlation between the signature and clinical factors.

REFERENCES

Amant, F., Moerman, P., Neven, P., Timmerman, D., Van Limbergen, E., and Vergote, I. (2005). Endometrial cancer. *Lancet* 366, 491–505. doi: 10.1016/S0140-6736(05)67063-8

Canzler, S., and Hackermuller, J. (2020). MultiGSEA: a GSEA-based pathway enrichment analysis for multi-omics data. *BMC Bioinformatics* 21:561. doi: 10.1186/s12859-020-03910-x

Colca, J. R., McDonald, W. G., Waldon, D. J., Leone, J. W., Lull, J. M., Bannow, C. A., et al. (2004). Identification of a novel mitochondrial protein ("mitoNEET") cross-linked specifically by a thiazolidinedione photoprobe. *Am. J. Physiol. Endocrinol. Metab.* 286, E252–E260. doi: 10.1152/ajpendo.00424.2003

Dixon, S. J., Lemberg, K. M., Lamprecht, M. R., Skouta, R., Zaitsev, E. M., Gleason, C. E., et al. (2012). Ferroptosis: an iron-dependent form of nonapoptotic cell death. *Cell* 149, 1060–1072. doi: 10.1016/j.cell.2012.03.042

Fan, Z., Wirth, A. K., Chen, D., Wruck, C. J., Rauh, M., Buchfelder, M., et al. (2017). Nrf2-Keap1 pathway promotes cell proliferation and diminishes ferroptosis. *Oncogenesis* 6:e371. doi: 10.1038/oncsis.2017.65

Geldenhuys, W. J., Leeper, T. C., and Carroll, R. T. (2014). MitoNEET as a novel drug target for mitochondrial dysfunction. *Drug Discov. Today* 19, 1601–1606. doi: 10.1016/j.drudis.2014.05.001

Hassannia, B., Vandenabeele, P., and Vanden, B. T. (2019). Targeting ferroptosis to iron out cancer. *Cancer Cell* 35, 830–849. doi: 10.1016/j.ccell.2019.04.002

Hinshaw, D. C., and Shevde, L. A. (2019). The tumor microenvironment innately modulates cancer progression. *Cancer Res.* 79, 4557–4566. doi: 10.1158/0008-5472.CAN-18-3962

Jennis, M., Kung, C. P., Basu, S., Budina-Kolomets, A., Leu, J. I., Khaku, S., et al. (2016). An African-specific polymorphism in the TP53 gene impairs p53 tumor suppressor function in a mouse model. *Genes Dev.* 30, 918–930. doi: 10.1101/gad.275891.115

Kusminski, C. M., Holland, W. L., Sun, K., Park, J., Spurgin, S. B., Lin, Y., et al. (2012). MitoNEET-driven alterations in adipocyte mitochondrial activity reveal a crucial adaptive process that preserves insulin sensitivity in obesity. *Nat. Med.* 18, 1539–1549. doi: 10.1038/nm.2899

Kwon, M. Y., Park, E., Lee, S. J., and Chung, S. W. (2015). Heme oxygenase-1 accelerates erastin-induced ferroptotic cell death. *Oncotarget* 6, 24393–24403. doi: 10.18632/oncotarget.5162

Lau, A., Villeneuve, N. F., Sun, Z., Wong, P. K., and Zhang, D. D. (2008). Dual roles of Nrf2 in cancer. *Pharmacol. Res.* 58, 262–270. doi: 10.1016/j.phrs.2008.09.003

Lever, J. M., Boddu, R., George, J. F., and Agarwal, A. (2016). Heme oxygenase-1 in kidney health and disease. *Antioxid. Redox. Signal.* 25, 165–183. doi: 10.1089/ars.2016.6659

Liang, C., Zhang, X., Yang, M., and Dong, X. (2019). Recent progress in ferroptosis inducers for cancer therapy. *Adv. Mater.* 31:e1904197. doi: 10.1002/adma.201904197

Liang, J. Y., Wang, D. S., Lin, H. C., Chen, X. X., Yang, H., Zheng, Y., et al. (2020). A novel ferroptosis-related gene signature for overall survival prediction in patients with hepatocellular carcinoma. *Int. J. Biol. Sci.* 16, 2430–2441. doi: 10.7150/ijbs.45050

Liu, Y., Guo, F., Guo, W., Wang, Y., Song, W., and Fu, T. (2021). Ferroptosis-related genes are potential prognostic molecular markers for patients with colorectal cancer. *Clin. Exp. Med.* 21, 467–477. doi: 10.1007/s10238-021-00697-w

Lopez-Janeiro, A., Ruz-Caracuel, I., Ramon-Patino, J. L., De Los, R. V., Villalba, E. M., Berjon, A., et al. (2021). Proteomic analysis of low-grade, early-stage endometrial carcinoma reveals new dysregulated pathways associated with cell death and cell signaling. *Cancers (Basel)* 13:794. doi: 10.3390/cancers13040794

Louandre, C., Marcq, I., Bouhlal, H., Lachaier, E., Godin, C., Saidak, Z., et al. (2015). The retinoblastoma (Rb) protein regulates ferroptosis induced by sorafenib in human hepatocellular carcinoma cells. *Cancer Lett.* 356(2 Pt B), 971–977. doi: 10.1016/j.canlet.2014.11.014

Malta, T. M., Sokolov, A., Gentles, A. J., Burzykowski, T., Poisson, L., Weinstein, J. N., et al. (2018). Machine learning identifies stemness features associated with oncogenic dedifferentiation. *Cell* 173, 338–354. doi: 10.1016/j.cell.2018.03.034

Mayakonda, A., Lin, D. C., Assenov, Y., Plass, C., and Koeffler, H. P. (2018). Maftools: efficient and comprehensive analysis of somatic variants in cancer. *Genome Res.* 28, 1747–1756. doi: 10.1101/gr.239244.118

Miao, Y. R., Zhang, Q., Lei, Q., Luo, M., Xie, G. Y., Wang, H., et al. (2020). ImmuCellAI: a unique method for comprehensive T-Cell subsets abundance prediction and its application in cancer immunotherapy. *Adv. Sci. (Weinh)* 7:1902880. doi: 10.1002/advs.201902880

Nath, K. A. (1999). Heme oxygenase-1: a redoubtable response that limits reperfusion injury in the transplanted adipose liver. *J. Clin. Invest.* 104, 1485–1486. doi: 10.1172/JCI8827

Newman, A. M., Liu, C. L., Green, M. R., Gentles, A. J., Feng, W., Xu, Y. et al. (2015). Robust enumeration of cell subsets from tissue expression profiles. *Nat. Methods* 12, 453–457.

Niu, B., Ye, K., Zhang, Q., Lu, C., Xie, M., McLellan, M. D., et al. (2014). MSIsensor: microsatellite instability detection using paired tumor-normal sequence data. *Bioinformatics* 30, 1015–1016. doi: 10.1093/bioinformatics/btt755

Ou, Y., Wang, S. J., Li, D., Chu, B., and Gu, W. (2016). Activation of SAT1 engages polyamine metabolism with p53-mediated ferroptotic responses. *Proc. Natl. Acad. Sci. U.S.A.* 113, E6806–E6812. doi: 10.1073/pnas.1607152113

Park, S. Y. (2018). Nomogram: an analogue tool to deliver digital knowledge. *J. Thorac. Cardiovasc. Surg.* 155:1793. doi: 10.1016/j.jtcvs.2017.12.107

Robinson, D. R., Wu, Y. M., Lonigro, R. J., Vats, P., Cobain, E., Everett, J., et al. (2017). Integrative clinical genomics of metastatic cancer. *Nature* 548, 297–303. doi: 10.1038/nature23306

Salem, A. F., Whitaker-Menezes, D., Howell, A., Sotgia, F., and Lisanti, M. P. (2012). Mitochondrial biogenesis in epithelial cancer cells promotes breast cancer tumor growth and confers autophagy resistance. *Cell Cycle* 11, 4174–4180. doi: 10.4161/cc.22376

Satyal, S. H., Chen, D., Fox, S. G., Kramer, J. M., and Morimoto, R. I. (1998). Negative regulation of the heat shock transcriptional response by HSBP1. *Genes Dev.* 12, 1962–1974. doi: 10.1101/gad.12.13.1962

Seiler, A., Schneider, M., Forster, H., Roth, S., Wirth, E. K., Culmsee, C., et al. (2008). Glutathione peroxidase 4 senses and translates oxidative stress into 12/15-lipoxygenase dependent- and AIF-mediated cell death. *Cell Metab.* 8, 237–248. doi: 10.1016/j.cmet.2008.07.005

Siegel, R. L., Miller, K. D., and Jemal, A. (2018). Cancer statistics, 2018. *CA Cancer J. Clin.* 68, 7–30. doi: 10.3322/caac.21442

Siegel, R. L., Miller, K. D., and Jemal, A. (2019). Cancer statistics, 2019. *CA Cancer J. Clin.* 69, 7–34. doi: 10.3322/caac.21551

Simon, N., Friedman, J., Hastie, T., and Tibshirani, R. (2011). Regularization Paths for Cox's Proportional Hazards Model via coordinate descent. *J. Stat. Softw.* 39, 1–13. doi: 10.18637/jss.v039.i05

Sohn, Y. S., Tamir, S., Song, L., Michaeli, D., Matouk, I., Conlan, A. R., et al. (2013). NAF-1 and mitoNEET are central to human breast cancer proliferation by maintaining mitochondrial homeostasis and promoting tumor growth. *Proc. Natl. Acad. Sci. U.S.A.* 110, 14676–14681. doi: 10.1073/pnas.1313198110

Sun, X., Niu, X., Chen, R., He, W., Chen, D., Kang, R., et al. (2016a). Metallothionein-1G facilitates sorafenib resistance through inhibition of ferroptosis. *Hepatology* 64, 488–500. doi: 10.1002/hep.28574

Sun, X., Ou, Z., Chen, R., Niu, X., Chen, D., Kang, R., et al. (2016b). Activation of the p62-Keap1-NRF2 pathway protects against ferroptosis in hepatocellular carcinoma cells. *Hepatology* 63, 173–184. doi: 10.1002/hep.28251

Tamir, S., Paddock, M. L., Darash-Yahana-Baram, M., Holt, S. H., Sohn, Y. S., Agranat, L., et al. (2015). Structure-function analysis of NEET proteins uncovers their role as key regulators of iron and ROS homeostasis in health and disease. *Biochi Biophy Acta* 1853, 1294–1315. doi: 10.1016/j.bbamcr.2014.10.014

Tibshirani, R. (1997). The lasso method for variable selection in the Cox model. *Stat. Med.* 16, 385–395. doi: 10.1002/(sici)1097-0258(19970228)16:4<385::aid-sim380<3.0.co;2-3

Wiley, S. E., Paddock, M. L., Abresch, E. C., Gross, L., van der Geer, P., Nechushtai, R., et al. (2007). The outer mitochondrial membrane protein mitoNEET contains a novel redox-active 2Fe-2S cluster. *J. Biol. Chem.* 282, 23745–23749. doi: 10.1074/jbc.C700107200

Yang, L., Tian, S., Chen, Y., Miao, C., Zhao, Y., Wang, R., et al. (2021). Ferroptosis-related gene model to predict overall survival of ovarian carcinoma. *J. Oncol.* 2021:6687391. doi: 10.1155/2021/6687391

Yang, W., Soares, J., Greninger, P., Edelman, E. J., Lightfoot, H., Forbes, S., et al. (2013). Genomics of Drug Sensitivity in Cancer (GDSC): a resource for therapeutic biomarker discovery in cancer cells. *Nucleic Acids Res.* 41, D955–D961. doi: 10.1093/nar/gks1111

Yang, W. S., SriRamaratnam, R., Welsch, M. E., Shimada, K., Skouta, R., Viswanathan, V. S., et al. (2014). Regulation of ferroptotic cancer cell death by GPX4. *Cell* 156, 317–331. doi: 10.1016/j.cell.2013.12.010

Yang, W. S., and Stockwell, B. R. (2008). Synthetic lethal screening identifies compounds activating iron-dependent, nonapoptotic cell death in oncogenic-RAS-harboring cancer cells. *Chem. Biol.* 15, 234–245. doi: 10.1016/j.chembiol.2008.02.010

Yu, Z., Chen, H., You, J., Liu, J., Wong, H. S., Han, G., et al. (2015). Adaptive fuzzy consensus clustering framework for clustering analysis of cancer data. *IEEE/ACM Trans. Comput. Biol. Bioinform.* 12, 887–901. doi: 10.1109/TCBB.2014.2359433

Yuan, H., Li, X., Zhang, X., Kang, R., and Tang, D. (2016). CISD1 inhibits ferroptosis by protection against mitochondrial lipid peroxidation. *Biochem. Biophys. Res. Commun.* 478, 838–844. doi: 10.1016/j.bbrc.2016.08.034

Zhang, Y. Y., Ni, Z. J., Elam, E., Zhang, F., Thakur, K., Wang, S., et al. (2021). Juglone, a novel activator of ferroptosis, induces cell death in endometrial carcinoma Ishikawa cells. *Food Funct.* 12, 4947–4959. doi: 10.1039/d1fo00790d

Zhu, L., Yang, F., Wang, L., Dong, L., Huang, Z., Wang, G., et al. (2021). Identification the ferroptosis-related gene signature in patients with esophageal adenocarcinoma. *Cancer Cell Int.* 21:124. doi: 10.1186/s12935-021-01821-2

Conflict of Interest: The authors declare that the research was conducted in the absence of any commercial or financial relationships that could be construed as a potential conflict of interest.

Publisher's Note: All claims expressed in this article are solely those of the authors and do not necessarily represent those of their affiliated organizations, or those of the publisher, the editors and the reviewers. Any product that may be evaluated in this article, or claim that may be made by its manufacturer, is not guaranteed or endorsed by the publisher.

frontiers in Cell and Developmental Biology

REVIEW
published: 29 October 2021
doi: 10.3389/fcell.2021.752426

Regulatory Roles of Six-Transmembrane Epithelial Antigen of the Prostate Family Members in the Occurrence and Development of Malignant Tumors

Wen-Jia Chen[1†], Hua-Tao Wu[2†], Chun-Lan Li[1], Yi-Ke Lin[2], Ze-Xuan Fang[1], Wen-Ting Lin[3] and Jing Liu[1]*

[1] Changjiang Scholar's Laboratory/Guangdong Provincial Key Laboratory for Diagnosis and Treatment of Breast Cancer/Department of Physiology, Shantou University Medical College, Shantou, China, [2] Department of General Surgery, The First Affiliated Hospital of Shantou University Medical College, Shantou, China, [3] Department of Pathology, Shantou University Medical College, Shantou, China

OPEN ACCESS

Edited by:
Ahmed Hamaï,
Institut National de la Santé et de la Recherche Médicale (INSERM), France

Reviewed by:
Young-Jun Jeon,
Sungkyunkwan University, South Korea
Niamh Buckley,
Queen's University Belfast, United Kingdom
Gao Chen,
Zhejiang University, China

***Correspondence:**
Jing Liu
jliu12@stu.edu.cn

[†] These authors have contributed equally to this work

Specialty section:
This article was submitted to Molecular and Cellular Oncology, a section of the journal Frontiers in Cell and Developmental Biology

Received: 03 August 2021
Accepted: 04 October 2021
Published: 29 October 2021

Citation:
Chen W-J, Wu H-T, Li C-L, Lin Y-K, Fang Z-X, Lin W-T and Liu J (2021) Regulatory Roles of Six-Transmembrane Epithelial Antigen of the Prostate Family Members in the Occurrence and Development of Malignant Tumors. Front. Cell Dev. Biol. 9:752426. doi: 10.3389/fcell.2021.752426

The human six-transmembrane epithelial antigen of the prostate (STEAP) proteins, which include STEAP1–4 and atypical STEAP1B, contain six transmembrane domains and are located in the cell membrane. STEAPs are considered archaeal metal oxidoreductases, based on their heme groups and F420H2:NADP+ oxidoreductase (FNO)-like structures, and play an important role in cell metal metabolism. Interestingly, STEAPs not only participate in biological processes, such as molecular transport, cell cycling, immune response, and intracellular and extracellular activities, but also are closely related to the occurrence and development of several diseases, especially malignant tumors. Up to now, the expression patterns of STEAPs have been found to be diverse in different types of tumors, with controversial participation in different aspects of malignancy, such as cell proliferation, migration, invasion, apoptosis, and therapeutic resistance. It is clinically important to explore the potential roles of STEAPs as new immunotherapeutic targets for the treatment of different malignant tumors. Therefore, this review focuses on the molecular mechanism and function of STEAPs in the occurrence and development of different cancers in order to understand the role of STEAPs in cancer and provide a new theoretical basis for the treatment of diverse cancers.

Keywords: STEAP, cancer, reductase, immunotherapy, biomarkers

INTRODUCTION

The six-transmembrane epithelial antigen of the prostate (STEAP) family proteins belong to a class of cellular transmembrane proteins. With five members so far, namely STEAP1–4 and STEAP1B, STEAP proteins possess a similar structure comprised of 4–6 transmembrane domains and intracellular amino- and carboxyl-terminal domains (Hubert et al., 1999; Rinaldy and Steiner, 1999; Zhang et al., 2001; Korkmaz et al., 2002, 2005; Grunewald et al., 2012a; Gomes et al., 2014b). Except for the highly homologous STEAP1 and STEAP1B, all other members have general metal reductase activity catalyzed by an F420H2:NADP+ oxidoreductase (FNO)-like domain

(Knutson, 2007). However, it has been reported that the intramembrane heme group in STEAP1 and STEAP1B can still be involved in metal metabolism, especially for the reduction and absorption of iron and copper (Ohgami et al., 2006).

Not surprisingly, STEAP family proteins have been reported to affect both intracellular oxidative stress and inflammation, by reducing extracellular Fe^{3+}/Cu^{2+} to Fe^{2+}/Cu^{+}, and cell uptake of Fe^{2+}/Cu^{+} through transferrin and copper transport proteins, as well as other cellular biological processes (Ohgami et al., 2005; Liao et al., 2020; Wu et al., 2020). In addition, the abnormal expression of STEAP family members in malignancies has been reported to be related to cell proliferation, migration, invasion, apoptosis, and prognosis by activating or suppressing different signaling pathways. Importantly, the location and function of STEAP family members in cells and their differential expression in tumor tissues raise awareness of the roles of STEAPs in tumorigenesis and development. This review focuses on the current literature, discusses the expression and functions of STEAP family members in different tumors, and describes their roles in tumors in order to propose therapeutic strategies for the treatment of malignant tumors.

STRUCTURAL CHARACTERISTICS OF SIX-TRANSMEMBRANE EPITHELIAL ANTIGEN OF THE PROSTATE

To better understand the basic characteristics of STEAP family, the information for each gene was obtained from the National Biotechnology Information Center (**Table 1**). STEAP1, usually referred to as STEAP, is the first reported STEAP protein and is located on chromosome 7q21.13. The STEAP1 gene has a total length of 10,359 bp and is comprised of 5 exons (Hubert et al., 1999). Only one mRNA transcript (NM_012449.3) has been recorded, is 1,219 nt in length, and encodes a 331-amino acid STEAP1 protein (NP_036581.1). The STEAP2 (also known as STAMP1) gene is also located on chromosome 7q21.13 and has a total length of 31,669 bp and 9 exons. The STEAP2 gene can be transcribed into six different mRNAs, the longest (NM_152999.4) of which is 6,871 nt in length and encodes the largest STEAP2 protein (NP_694544.2) at 490 amino acids. Other mRNA transcripts result in shorter encoded proteins. The gene for STEAP3, also known as pHyde, TSAP6, or STAMP3, is located on chromosome 2q14.2 and has a total length of 43,177 bp and 11 exons. The STEAP3 gene produces four mRNA transcripts of varying lengths, with the longest (NM_182915.3) being 4,259 nt and encoding the largest STEAP3 protein (NP_878919.2) at 498 amino acids. Other mRNA transcripts lack certain exons, resulting in shorter encoded proteins. Because the sequence of STEAP4 is similar to that of STAMP1 (STEAP2), it is also named STAMP2 and was identified in 2005 (Korkmaz et al., 2005). The STEAP4 gene is located on chromosome 7q21.12 and encodes a total length of 36,003 bp and 6 exons. Three different mRNA transcripts are produced by the STEAP4 gene. Among them, the main mRNA transcript (NM_024636.4) is 9,991 nt long, while the longest mRNA transcript (NM_001205315.2) contains additional exons compared with the principal transcript, but encodes the same 459-amino acid protein (NP_078912.2). Other mRNA transcripts lack specific coding exons, resulting in shorter encoded proteins. STEAP1B is a newly discovered member of the STEAP family and has 88% homology with STEAP1 (Grunewald et al., 2012a), but its structure is different from that of other family members. The gene for STEAP1B is located on chromosome 7p15.3 and has a total length of 80,839 bp and 6 exons. Transcription of the STEAP1B gene produces two mRNA transcripts. The longer one (NM_001164460.1), namely STEAP1B1, is comprised of 1,299 nt and encodes a protein of 342 amino acids (NP_001157932.1), while the shorter one (STEAP1B2, NM_207342.2) uses an alternate in-frame splice site in the 5′ coding region and an alternate 3′ exon with a distinct 3′ coding region and 3′UTR compared to the longer one. The resulting protein lacks an internal segment near the N-terminus and has a shorter and distinct C-terminus.

The structures of STEAP family proteins are similar. From the perspective of cell localization, all STEAP family proteins are located on the cell membrane and in the cytoplasm. The STEAP1–4 proteins located on the surface of the plasma membrane all have six potential transmembrane regions, as well as an intracellular hydrophilic amino and carboxyl-terminal, indicating that the STEAP proteins may function as a channel or transporter (Hubert et al., 1999). Furthermore, STEAP2 and STEAP4 are also located in vesicle-tubular structures of the trans-Golgi body network, plasma membrane, and cytoplasm, shuttle between the plasma membrane and Golgi body, and co-localize with early endosomal antigen 1 (EEA1), thereby participating in the secretion/endocytosis pathway (Korkmaz et al., 2005). STEAP3 is mainly located on the plasma and intracellular membranes (Valadi et al., 2007; Lespagnol et al., 2008). The protein structure of STEAP1 and STEAP2 contains at least one heme group, in the membrane, that may be related to the absorption of iron and copper (Finegold et al., 1996; Gomes et al., 2012). STEAP2, STEAP3, and STEAP4 have intrinsic metal reductase activity, endowed by its paleontological and bacterial FNO-like domain (Finegold et al., 1996), for transfer of electrons, which is necessary for iron and copper uptake (Passer et al., 2003; Ohgami et al., 2005). In addition, STEAP4 also has six-transmembrane domains, with the COOH end and the NH end containing dinucleotide binding regions, an NADP REDOX motif, and a pyrrolidine 5-carboxylate reductase motif, which may also be involved in the metal redox process (Korkmaz et al., 2005). However, different from other members, STEAP1 cannot reduce metals as it lacks the NADP+ oxidoreductase FNO-like domain homologous to paleontological and bacterial F420H2 (Ohgami et al., 2005). Nevertheless, it has been suggested that STEAP1 may be involved in iron metabolism, as it coexists with other iron uptake endosomal proteins, such as transferrin (Ohgami et al., 2006). The structure of STEAP1B is different from other proteins. STEAP1B has only four potential transmembrane regions and intracellular COOH and NH2 terminal regions (Gomes et al., 2014b). Without an NADPH oxidoreductase domain and a heme-binding site, STEAP1B is predicted to lack oxidoreductase activity (Grunewald et al., 2012a).

TABLE 1 | Members of the STEAP family.

Gene	Alternative names	Location	Size (bp)	Exons	Transcript* (nt)	Protein* (aa)
STEAP1	PRSS24 STEAP	7q21.13	10,359	5	NM_012449.3 (1,219)	NP_036581.1 (339)
STEAP2	STMP IPCA1 PUMPCn STAMP1 PCANAP1	7q21.13	31,669	9	NM_001244944.2 (6,948)	NP_001035755.1 (490)
					NM_152999.4 (6,871)	NP_001035756.1 (454)
					NM_001040665.2 (6,821)	NM_001244946.2 (451)
					NM_001040666.1 (2,230)	
					NM_001244945.2 (2,645)	
					NM_001244946.2 (2,267)	
STEAP3	STMP3 TSAP6 pHyde AHMIO2 Dudlin-2 Dudulin-2	2q14.2	43,177	11	NM_182915.3 (4,259)	NP_878919.1 (498)
					NM_018234.3 (3,912)	NP_001008410.1 (488)
					NM_001008410.2 (3,844)	NP_619543.1 (457)
					NM_138637.3 (4,076)	
STEAP4	TIARP STAMP2 SchLAH TNFAIP9	7q21.12	36,003	6	NM_024636.4 (9,991)	NP_001192244.1 (459)
					NM_024636.4 (10,090)	NP_001192245.1 (283)
					NM_024636.4 (9,463)	
STEAP1B	–	7p15.3	80,839	6	NM_001164460.1 (1,299)	NP_001157932.1 (342)
					NM_207342.2 (1,298)	NP_997225.1 (245)

**Gene information obtained from the National Center for Biotechnology Information.*

DIVERSE EXPRESSION PATTERNS OF SIX-TRANSMEMBRANE EPITHELIAL ANTIGEN OF THE PROSTATE AND THEIR REGULATORY MECHANISMS IN CANCERS

It is commonly found that STEAP1 is up-regulated in a variety of tumor tissues, especially in prostate cancer. Currently, investigations of STEAP1 mainly focus on prostate cancers and show that expression of STEAP1 is elevated compared with normal prostate tissue (Li et al., 2004; Challita-Eid et al., 2007; Wong and Abubakar, 2010; Hayashi et al., 2011; Gomes et al., 2013, 2014a, 2018; Ihlaseh-Catalano et al., 2013; Whiteland et al., 2014). The mutual regulation has been reported between STEAP1 and sex hormones. Gomes et al. (2013) showed that 5α-dihydrotestosterone (DHT) or 17β-estradiol (E2) treatment of prostate cancer cells suppresses the expression of STEAP1, but that this down-regulation of STEAP1 is AR-dependent and ER-independent. In addition, up-regulated STEAP1 expression has also been observed in renal cell carcinoma, bladder cancer, Ewing's sarcoma, breast cancer, colorectal cancer (CRC), gastric cancer, ovarian cancer, and lung cancer (Maia et al., 2008; Azumi et al., 2010; Grunewald et al., 2012b; Zhuang et al., 2015; Wu et al., 2018; Nakamura et al., 2019; Guo Q. et al., 2020; Jiang et al., 2020; Jiao et al., 2020; Tian et al., 2020). Phosphorylated eIF4E is required for peritoneal metastasis of gastric cancer *via* initiating the cap-dependent translation of STEAP1, providing phosphorylation of eIF4E as an effective therapeutic target for patients with peritoneal metastasis through translational control of STEAP1 (Jiang et al., 2020). Importantly, high STEAP1 levels are associated with low overall survival (OS) rates of patients with prostate cancer, CRC, lung cancer, ovarian cancer, diffuse large B-cell lymphoma, acute myeloid leukemia and multiple myeloma (Moreaux et al., 2012; Ihlaseh-Catalano et al., 2013; Lee et al., 2016; Guo Q. et al., 2020; Jiao et al., 2020), suggesting the prognostic value of STEAP1 as a biomarker of cancer. At present, the carcinogenic effect of STEAP1 in tumor progression is being studied intensely. However, certain investigations have also shown that STEAP1 also plays a role in inhibiting tumor growth. Xie et al. (2019) compared the expression of STEAP1 in normal breast tissue ($n = 40$), benign fibroadenoma ($n = 52$), and primary breast cancer ($n = 211$), and found a low level of STEAP1 in primary breast cancer tissues. In the MCF-7 breast cancer cell line, treatment with E2 also reduces the expression of STEAP1 but is mediated by membrane-bound ERalpha (mbERalpha) (Maia et al., 2008). It is speculated that the carcinogenic and anti-cancer effects of STEAP1 in diverse types of cancer may be related to different hormone levels and regulation of hormone receptor locally or throughout the body. Furthermore, Sun et al. (2019) also showed down-regulation of STEAP1 expression in endometrial carcinoma cell lines compared with normal endometrial cells, and low expression of STEAP1 has been related to poor prognosis of patients with Ewing's sarcoma, CRC, and breast cancer (Grunewald et al., 2012c; Lee et al., 2016; Xie et al., 2019). Although reports on down-regulation of STEAP1 expression in tumor tissues are limited, they evoke further studies to investigate a potential anti-cancer role of STEAP1 in cancers.

Studies on STEAP2 expression in cancers have also mainly focused on prostate cancers, although studies are limited. STEAP2 expression in prostate cancer was found to be significantly higher than that in normal tissues (Porkka et al., 2002; von Rozycki et al., 2004; Wang et al., 2010; Whiteland et al., 2014; Burnell et al., 2018, 2019). Specifically, Korkmaz et al. (2002) revealed that STEAP2 is highly expressed in androgen-sensitive, androgen receptor-positive prostate cancer cells, but not in androgen receptor-negative prostate cancer cells, suggesting that the regulation of STEAP2 expression may be related to sex hormone signaling. With regard to the

molecular mechanism of STEAP2 in prostate cancers, Gonen-Korkmaz et al. (2014) overexpressed STEAP2, in AR-negative DU145 prostate cancer cells, and showed an NFκB-mediated downregulation of STEAP2 expression following treatment with tumor necrosis factor-α (TNF-α). The authors showed that NFκB silencing increased anti-apoptotic STEAP2 expression, as well as inhibited p53 and MDM2 expression in TNF-α-treated, STEAP2-overexpressing DU145 cells, suggesting inhibition of NFκB for prostate cancer prevention in specific patients (Gonen-Korkmaz et al., 2014). Interestingly, Wang et al. (2010) found that activation of extracellular signal-regulated kinase, implicated in prostate cancer progression, increased ectopic expression of STEAP2 in AR-negative DU145 cells, but decreased STEAP2 levels in AR-positive LNCaP cells, suggesting a potential interaction between STEAP2 and sex hormones. The expression of STEAP2 was also found to be up-regulated in colon cancers (Bhatlekar et al., 2014). Similar to the expression pattern of STEAP1, STEAP2 also has been reported to play conflicting roles in prostate and breast cancers, Yang et al. (2020) proposed STEAP2 to be a tumor suppressor in breast cancers, based on its low expression in breast cancer. Through bioinformatics methods, Liu et al. (2021) also predicted that the expression of STEAP2 in glioblastoma was down-regulated compared with normal brain tissue. To construct a multiple RNA-based prediction model in patients with ovarian cancer, Zhang et al. (2020) used sequencing data from The Cancer Genome Atlas (TCGA) database and identified TM4SF1-AS1-miR-186-STEAP2 and LINC00536-miR-508-STEAP2 as new interaction axes to explain the possible functions of these RNAs in the prediction model for disease-free survival in patients with ovarian cancer. However, further investigation of these new axes is required for verification (Zhang et al., 2020).

STEAP3 was first found in prostate tissues and proposed as a candidate for prostate cancer immunotherapy (Machlenkin et al., 2005). Although the expression of STEAP3 in poorly differentiated prostate cancer is lower than that in well-differentiated and moderately differentiated prostate cancer, there is no difference in STEAP3 expression between benign prostatic hyperplasia and prostate cancer (Porkka et al., 2003). It was also found that the expression of STEAP3 is up-regulated in glioma, bladder cancer, and colon cancer (Isobe et al., 2011; Kim et al., 2016; Weston et al., 2016; Han et al., 2018; Zhang et al., 2019), whereas the expression of STEAP3 in hepatocellular carcinoma (HCC), breast cancer, and lung cancer is lower than that in normal tissues (Boelens et al., 2009; Caillot et al., 2009; Savci-Heijink et al., 2016; Cadiou et al., 2017). Han et al. (2018) reported that the expression of STEAP3 in gliomas is negatively correlated with patient OS, and multivariate Cox regression analysis showed that STEAP3 is an independent prognostic indicator. Zhang et al. (2019) used TCGA and GSE16011 online datasets to show that overexpression of STEAP3 is associated with poor prognosis in patients with glioblastoma. Research focused on the regulation of STEAP3 in cancers is limited. In a transcriptome analysis of a CRC series, an increased level of membrane copper transporter 1 protein (CTR1) accompanied increased STEAP3 transcription (Barresi et al., 2016). Yu et al. (2020) demonstrated that in pancreatic cancer, heat shock protein family B member 2 (HSPB2) could combine with mutant p53 to change the DNA binding site of mutant p53, resulting in an upregulated level of STEAP3 and leading to an inhibition of both cell proliferation and angiogenesis.

As a relatively new member of the STEAP family, STEAP4 was found to be increased in human prostate cancers compared with normal prostate tissues (Korkmaz et al., 2005; Jin et al., 2015), and is up-regulated in human colon cancer cells, predicting poor prognosis of patients with colon cancers (Xue et al., 2017). In CRC, interleukin-17 (IL-17) drives cellular uptake of copper through upregulation of STEAP4 expression, and the proinflammatory cytokines interleukin (IL)-6 and IL-1β can synergistically increase androgen-induced STEAP4 expression in prostate cancer cells, with knockdown of STEAP4 enhancing the ability of IL-6 and IL-1β to inhibit cell growth (Pihlstrom et al., 2021). In addition, IL-17 and TNF-α rely heavily on TNF receptor associated factor 4 (TRAF4) to up-regulate the expression of STEAP4 and thus play a role in airway epithelial cells (Jiang et al., 2021). Interestingly, although the up-regulated expression of STEAP4 was also detected in alcohol-induced breast cancer cells (Gelfand et al., 2017), Wu et al. (2020) found that the mRNA level of STEAP4 was decreased in tissues of ductal breast carcinoma compared with normal tissues. In bladder cancers, low STEAP4 expression was found in cancer tissues compared with normal, and the circular RNA circPICALM competed with STEAP4 for binding to miR-1265 to eliminate the enhancing effect of miR-1265 on invasion (Yan et al., 2019). Meanwhile, bioinformatics analysis has also revealed that the transcription level of STEAP4 in head and neck cancer tissues is reduced compared with normal tissues, and a low level of STEAP4 resulted in poor disease-free survival, progression-free survival and OS (Lan et al., 2021).

Currently, the research on STEAP1B in tumor is very limited. STEAP1B1 and STEAP1B2 mRNA are differentially expressed in prostate cell lines. Non-neoplastic prostate cells show little to no STEAP1B1 and STEAP1B2 mRNA expression. On the other hand, in malignant prostate cells, LNCaP and PC3, STEAP1B2 is highly expressed, whereas STEAP1B1 mRNA is mainly expressed on PNT2 and PC3 cells, and under-expressed on LNCaP cells (Gomes et al., 2014b).

BIOLOGICAL FUNCTIONS AND RELATED MOLECULAR MECHANISMS OF SIX-TRANSMEMBRANE EPITHELIAL ANTIGEN OF THE PROSTATE IN CANCERS

Based on the above summary of differential expression patterns of STEAP1 in a variety of tumors, dysregulated STEAP1 affects the occurrence and development of different types of cancers (**Figure 1**). Some investigations evoke an oncogenic role for STEAP1 in cancers. Yamamoto et al. (2013) found that in prostate cancer, STEAP1, as a cell surface membrane protein, is required for intercellular communication between tumor cells and adjacent tumor stromal cells to augment tumor growth. In androgen-dependent prostate cancers, Gomes et al. (2018)

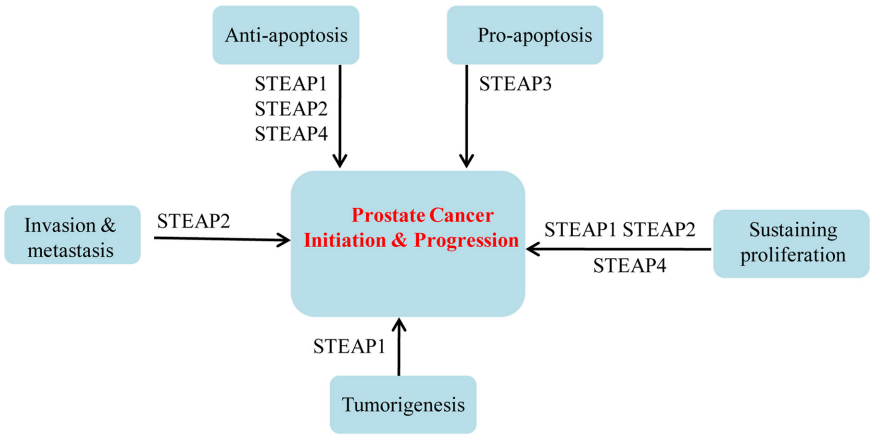

FIGURE 1 | Roles of STEAPs in prostate cancers.

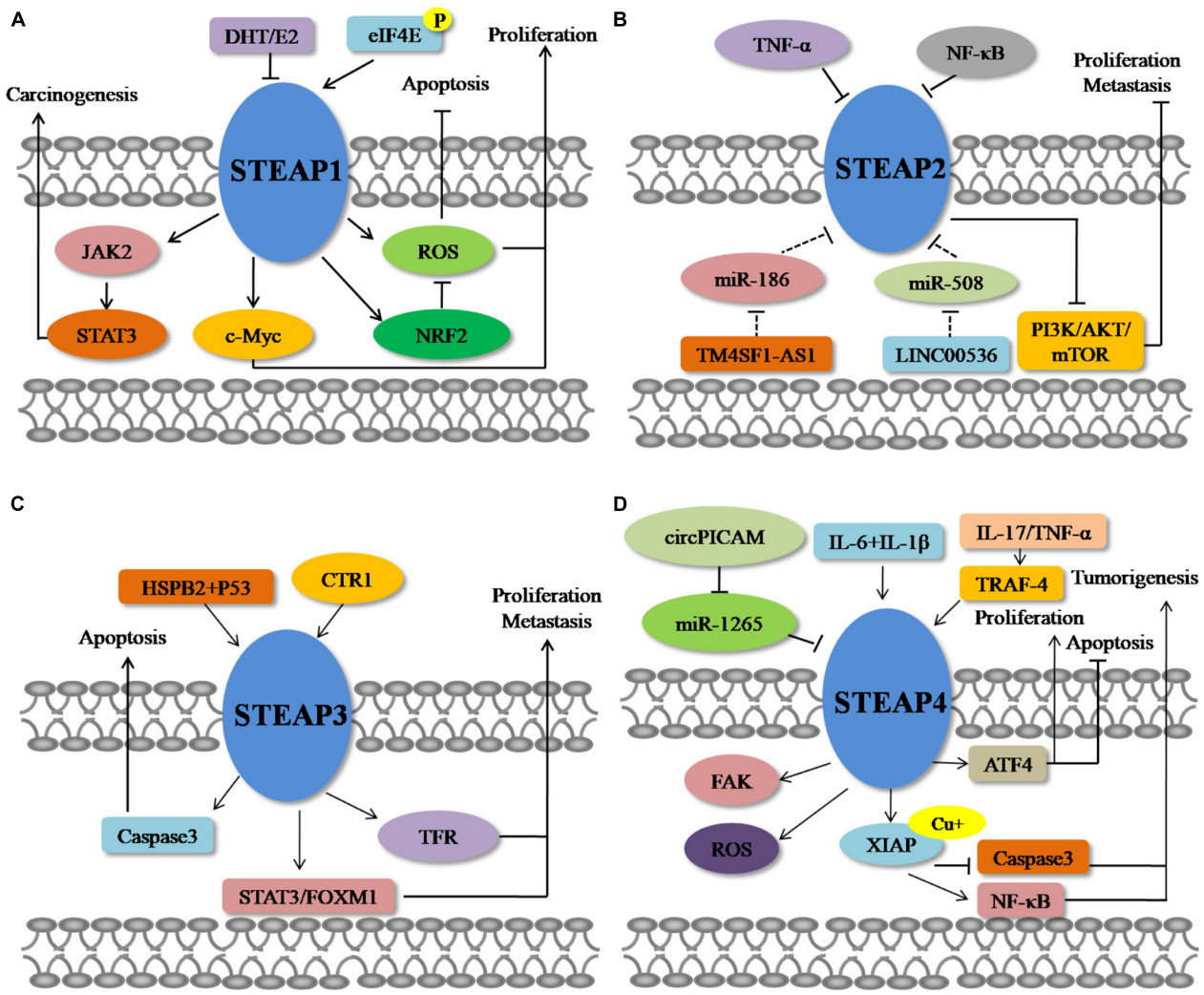

FIGURE 2 | Molecular mechanisms of STEAPs in cancer. **(A)** STEAP1. **(B)** STEAP2. **(C)** STEAP3. **(D)** STEAP4.

showed that knockdown of STEAP1 inhibits cell growth and induces apoptosis of LNCaP prostate cancer cells in a DHT-independent manner. In lung cancers, STEAP1 was found to affect endothelial cell migration and angiogenesis, and knockout of STEAP1 could inhibit the proliferation, migration, and invasion of tumor cells *via* the JAK2/STAT3 signaling pathway (Zhuang et al., 2015; Tian et al., 2020). Based on transcriptome and proteome analyses, Grunewald et al. (2012b) showed that STEAP1 levels correlate with oxidative stress responses and elevated reactive oxygen species (ROS), which regulate redox-sensitive and proinvasive genes to promote tumor proliferation and invasive behavior, and that knockout of STEAP1 reduces ROS levels and inhibits Ewing tumor proliferation, anchorage-independent colony formation, invasion *in vitro* and metastasis *in vivo*. Oxidative stress and ROS levels are also suppressed in CRC cells, by STEAP1 silencing, through regulation of the nuclear erythroid 2-related factor (NRF2) transcription factor, resulting in reduced cell growth and elevated apoptosis (Nakamura et al., 2019). In gastric cancers, STEAP1 was shown to promote peritoneal metastasis, and up-regulation of STEAP1 was found to promote tumor proliferation, migration, invasion, and tumorigenicity (Wu et al., 2018; Jiang et al., 2020). Silencing of STEAP1 suppressed c-Myc expression in hepatocarcinoma to arrest cancer cells in G1 phase and inhibit cell proliferation (Iijima et al., 2021). Jiao et al. (2020) found a relationship between high STEAP1 levels and epithelial-mesenchymal transition (EMT)-related genes, and demonstrated that STEAP1 promotes ovarian cancer metastasis by aiding EMT progression. Interestingly, down-regulation of STEAP1 in this study inhibited the invasion, migration, proliferation, clone formation, and EMT progression of human ovarian cancer cells and the growth of xenografts *in vivo*, but promoted apoptosis at the same time (Jiao et al., 2020). Although an oncogenic role of STEAP1 in tumors is commonly observed, a tumor suppressive function has also been reported. Recently, Xie et al. (2019) showed that knockdown of STEAP1 expression enhances breast cancer cell invasiveness and migration, and is accompanied by increased expression of EMT-related genes, MMP2, MMP9, MMP13, VIM, and CDH2, as well as decreased CDH1 expression. In a tumor of the female reproductive system, STEAP1 was restrictively expressed in endometrial carcinoma, and down-regulation of STEAP1 increased cancer cell proliferation, colony formation, migration, invasion, and EMT progression of endometrial carcinoma (Sun et al., 2019) (**Figure 2**).

An increased level of STEAP2 in prostate cancer suggests an oncogenic role. Wang et al. (2010) investigated STEAP2 function in prostate cancer and found that knockdown of STEAP2 dramatically retarded proliferation *in vitro* and *in vivo*, and interestingly, increased expression of STEAP2 was induced by the activation of extracellular signal-regulated kinase (ERK1/2). Whiteland et al. (2014) found that overexpression of STEAP2 resulted in the gain of ability to migrate and invade in normal prostate cells, and Burnell et al. (2018) showed that genes associated with STEAP2 enhancement of invasion were MMP3, MMP10, MMP13, FGFR4, IL-1β, KiSS1, and SERPINE1 in PC3 cells, and MMP7 in LNCaP cells, with altered CD82 in both. In contrast, in breast cancer, STEAP2 hinders cellular proliferation, invasion, and metastasis by inhibiting EMT through suppressing the PI3K/AKT/mTOR signaling pathway (Guo H. et al., 2020), predicting a tumor suppressor role in breast cancers.

The function of STEAP3 in tumors is also controversial. Zhang et al. (2001) first reported that STEAP3 induced apoptosis of prostate cells, based on a dose-dependent stimulation of endogenous caspase-3 expression. However, in glioblastoma, loss of STEAP3 attenuated the aggressive phenotype of glioma cells in regard to cell proliferation, invasion, sphere formation *in vitro*, and tumor growth *in vivo*, through suppressing mesenchymal transition, transferrin receptor expression and STAT3–FoxM2 signaling (Han et al., 2018). In biopsies from patients with HCC, decreased expression of STEAP3 was observed in cirrhotic tissues and related to decreased apoptosis, serving as a warning sign and predictive biomarker for the development of HCC (Caillot et al., 2009).

STEAP4, a relatively new STEAP, has been demonstrated to promote prostate cancer, based on its ability to increase cell growth and colony formation (Korkmaz et al., 2005). Jin et al. (2015) reported that STEAP4 increases ROS in prostate cancer cells through its iron reductase activity, and subsequently affects proliferation, colony formation, anchorage-independent growth, and apoptosis, involving a mechanism at least partly mediated by activating transcription factor 4 (ATF4). Recently, Orfanou et al. (2021) investigated the function of STEAP4 in breast cancer and demonstrated that knockdown of STEAP4 suppresses cell proliferation and enhances the inhibition of lapatinib in HER2-overexpressing breast cancer, predicting an oncogenic role for STEAP4 in breast cancer. On the contrary, STEAP4-mediated increases in intracellular copper levels result in activation of the E3 ligase X-linked inhibitor of apoptosis (XIAP), enhancing IL-17-induced NF-κB activation and inhibiting caspase-3 activity (Liao et al., 2020). However, in bladder cancer, the circular RNA circPICALM competed with STEAP4 for binding to miR-1265 and eliminated the ability of miR-1265 to enhance invasion (Yan et al., 2019).

Up to now, there are no relevant reports regarding the function of STEAP1B in cancer. However, considering the similar structural features of STEAP1B with other family members, STEAP1B may play a role in different cancers, but experimental proof is still required.

THERAPEUTIC IMPLICATIONS OF SIX-TRANSMEMBRANE EPITHELIAL ANTIGEN OF THE PROSTATE IN CANCERS

Considering their roles and location in the cell membrane, STEAPs are currently considered as promising therapeutic targets for cancers, especially prostate cancers. Therapeutic strategies have been discovered and developed during the last few years for targeting STEAP1, including monoclonal antibodies (mAbs),

antibody-drug conjugates, DNA vaccines, and small non-coding RNAs (ncRNAs) (Barroca-Ferreira et al., 2018).

Challita-Eid et al. (2007) first generated two mAbs that bind to cell surface STEAP1 epitopes, and both of them inhibited STEAP1-induced intercellular communication in a dose-dependent manner to suppress tumor growth *in vivo*. Subsequently, Esmaeili et al. (2018) developed a single-chain fragment variable (scFv) antibody, against a STEAP1 epitope, that successfully inhibited intercellular communication between prostate cancer cells by blocking gap junctions between cells, demonstrating a high potential for mAbs or single-chain antibodies as effective agents for prostate cancer immunotherapy. To combine the specificity of antibodies with cytotoxic potency of chemotherapeutic drugs, Boswell et al. (2011) designed and produced a synthetic antitumor drug involving humanized anti-STEAP1-monomethylauristatin E (MMAE) conjugates to increase hepatic uptake and reduce drug levels in other highly vascularized organs. Based on a high expression level of STEAP1, Yuan et al. (2019) established a novel contrast agent for ultrasound imaging by conjugating biotinylated STEAP1 monoclonal antibodies with streptavidin-coated SonoVue microbubbles, providing a prospective method to identify prostate tumors effectively *in vivo*. These experiments suggest that STEAP1 targeting may be an attractive and selective way to deliver drugs to cancer cells.

In addition, immunotherapy may provide an alternative treatment for cancer patients, especially for tumors with overexpressed antigens that can be recognized by immune cells. Azumi et al. (2010) used STEAP-derived epitope peptides to stimulate T cells, in the context of multiple major histocompatibility complex class II alleles, and induce STEAP-specific helper T lymphocytes in patients with renal cell or bladder cancers. These studies demonstrated the therapeutic potential of optimizing T cell-based immunotherapy for STEAP-expressing renal cells and bladder cancer (Azumi et al., 2010).

Producing an effective vaccine is one of the most important goals of tumor immunotherapy. It has been found that mouse STEAP (mSTEAP)-based vaccination can induce a specific CD8 T cell response to newly defined mSTEAP epitopes and prolong the survival rate of tumor-challenged mice, showing that vaccination against mSTEAP is a feasible option to delay tumor growth (Garcia-Hernandez Mde et al., 2007). Similarly, Cappuccini et al. (2016) constructed a simian adenovirus and modified a vaccinia Ankara virus, ChAdOx1-MVA, encoding STEAP1, to induce strong, sustained antigen-specific CD8+ T-cell responses in male C57BL/6 and BALB/c mice, which when combined with PD-1 blocking antibody, significantly improved the survival rate of animals, indicating that a ChAdOx1-MVA vaccination regimen for STEAP1 combined with PD-1 treatment may have high therapeutic potential in the clinic. Machlenkin et al. (2005) identified two novel immunogenic peptides derived from overexpressed prostate antigens, prostatic acid phosphatase (PAP) and STEAP1, and found that they could induce peptide-specific CTLs targeting human leukocyte antigen-A2.1^{+} LNCaP cells to inhibit tumor growth in adoptive immunotherapy, providing great potential as candidate vaccines for patients with prostate cancers.

A mAb targeting STEAP4 has been shown to promote caspase-dependent apoptosis and inhibit the proliferation of pre-adipocytes and glucose uptake without affecting lipogenesis and lipogenic differentiation (Qin et al., 2010). Since mAb binding to STEAPs appears to inhibit the function of STEAPs, it is easy to speculate that specific small molecules that may interfere with STEAP ion channels or their active sites may impair their carcinogenic function and may therefore also serve as targeted therapeutic agents.

Although the current therapeutic strategies for STEAPs have not been used in the clinic, their role in molecular transport and involvement in cancer progression makes them promising targets in the treatment of patients with prostate cancer, and even other types of cancers. Overall, future immunotherapeutic strategies are likely to include all members of the STEAP family.

CONCLUSION

Six-transmembrane epithelial antigen of the prostate family members are very similar in structure and, except for STEAP1, all serve as metal oxidoreductases in the absorption of copper and iron. STEAP family members in different cancers are irregularly expressed and participate in the proliferation, migration, invasion, apoptosis, and prognosis of cancer cells, although STEAP3 and STEAP4 may have tumor suppressor functions in cancers. All in all, current studies clearly indicate that the members of the STEAP family are likely to become biomarkers of cancer diseases. Although the mechanisms of the STEAPs in the progression of different cancers are still largely elusive, it is clear that the STEAP family is closely related to the occurrence and development of tumors. Therefore, further investigations are needed to clarify the role of STEAPs in tumor cell proliferation, cell cycling, apoptosis, invasion, and metastasis. In addition, more attention should be paid to the regulatory mechanisms of STEAP family members in different cancers. Future work must systematically analyze and describe the STEAP family based on molecular, cellular, animal and clinical data, and further explore their regulation and role in cancer pathophysiology, diagnosis, and treatment.

AUTHOR CONTRIBUTIONS

JL and W-JC: conceptualization. W-JC, H-TW, C-LL, Y-KL, Z-XF, and W-TL: organization of the database. W-JC, H-TW, C-LL, and Y-KL: searching the literature. W-JC and H-TW: writing – original draft preparation. JL, C-LL, Y-KL, Z-XF, and W-TL: writing – review and editing. JL: supervision and project administration. JL and H-TW: funding acquisition. All authors have read and agreed to the published version of the manuscript.

FUNDING

This work was supported by the National Natural Science Foundation of China (No. 81501539), the Natural Science

Foundation of Guangdong Province (Nos. 2021A1515012180 and 2016A030312008), 2021 Science and Technology Special Project of Guangdong Province, China (No. 210715216902829), Science and Technology Planning Project of Shantou, China (No. 200617105260368), Special Grant for Key Area Programs of Guangdong Department of Education (No. 2021ZDZX2004), and "Dengfeng Project" for the construction of high-level hospital in Guangdong Province – The First Affiliated Hospital of Shantou University College Supporting Funding (No. 202003-10).

ACKNOWLEDGMENTS

We are thankful to Stanley Lin for his critical and careful editing and proofreading of the manuscript.

REFERENCES

Azumi, M., Kobayashi, H., Aoki, N., Sato, K., Kimura, S., Kakizaki, H., et al. (2010). Six-transmembrane epithelial antigen of the prostate as an immunotherapeutic target for renal cell and bladder cancer. *J. Urol.* 183, 2036–2044. doi: 10.1016/j.juro.2009.12.094

Barresi, V., Trovato-Salinaro, A., Spampinato, G., Musso, N., Castorina, S., Rizzarelli, E., et al. (2016). Transcriptome analysis of copper homeostasis genes reveals coordinated upregulation of SLC31A1,SCO1, and COX11 in colorectal cancer. *FEBS Open Bio* 6, 794–806. doi: 10.1002/2211-5463.12060

Barroca-Ferreira, J., Pais, J. P., Santos, M. M., Goncalves, A. M., Gomes, I. M., Sousa, I., et al. (2018). Targeting STEAP1 protein in human cancer: current trends and future challenges. *Curr. Cancer Drug Targets* 18, 222–230. doi: 10.2174/1568009617666170427103732

Bhatlekar, S., Addya, S., Salunek, M., Orr, C. R., Surrey, S., Mckenzie, S., et al. (2014). Identification of a developmental gene expression signature, including HOX genes, for the normal human colonic crypt stem cell niche: overexpression of the signature parallels stem cell overpopulation during colon tumorigenesis. *Stem Cells Dev.* 23, 167–179. doi: 10.1089/scd.2013.0039

Boelens, M. C., Van Den Berg, A., Fehrmann, R. S., Geerlings, M., De Jong, W. K., Te Meerman, G. J., et al. (2009). Current smoking-specific gene expression signature in normal bronchial epithelium is enhanced in squamous cell lung cancer. *J. Pathol.* 218, 182–191. doi: 10.1002/path.2520

Boswell, C. A., Mundo, E. E., Zhang, C., Bumbaca, D., Valle, N. R., Kozak, K. R., et al. (2011). Impact of drug conjugation on pharmacokinetics and tissue distribution of anti-STEAP1 antibody-drug conjugates in rats. *Bioconjug. Chem.* 22, 1994–2004. doi: 10.1021/bc200212a

Burnell, S. E. A., Spencer-Harty, S., Howarth, S., Bodger, O., Kynaston, H., Morgan, C., et al. (2018). STEAP2 knockdown reduces the invasive potential of prostate cancer cells. *Sci. Rep.* 8:6252. doi: 10.1038/s41598-018-24655-x

Burnell, S. E. A., Spencer-Harty, S., Howarth, S., Bodger, O., Kynaston, H., Morgan, C., et al. (2019). Utilisation of the STEAP protein family in a diagnostic setting may provide a more comprehensive prognosis of prostate cancer. *PLoS One* 14:e0220456. doi: 10.1371/journal.pone.0220456

Cadiou, J. L., Pichat, S., Bondanese, V. P., Soulard, A., Fujii, T., Albarede, F., et al. (2017). Copper transporters are responsible for copper isotopic fractionation in eukaryotic cells. *Sci. Rep.* 7:44533. doi: 10.1038/srep44533

Caillot, F., Daveau, R., Daveau, M., Lubrano, J., Saint-Auret, G., Hiron, M., et al. (2009). Down-regulated expression of the TSAP6 protein in liver is associated with a transition from cirrhosis to hepatocellular carcinoma. *Histopathology* 54, 319–327. doi: 10.1111/j.1365-2559.2009.03224.x

Cappuccini, F., Stribbling, S., Pollock, E., Hill, A. V., and Redchenko, I. (2016). Immunogenicity and efficacy of the novel cancer vaccine based on simian adenovirus and MVA vectors alone and in combination with PD-1 mAb in a mouse model of prostate cancer. *Cancer Immunol. Immunother.* 65, 701–713. doi: 10.1007/s00262-016-1831-8

Challita-Eid, P. M., Morrison, K., Etessami, S., An, Z., Morrison, K. J., Perez-Villar, J. J., et al. (2007). Monoclonal antibodies to six-transmembrane epithelial antigen of the prostate-1 inhibit intercellular communication in vitro and growth of human tumor xenografts in vivo. *Cancer Res.* 67, 5798–5805. doi: 10.1158/0008-5472.CAN-06-3849

Esmaeili, S. A., Nejatollahi, F., and Sahebkar, A. (2018). Inhibition of intercellular communication between prostate cancer cells by a specific anti-STEAP-1 single chain antibody. *Anticancer Agents Med. Chem.* 18, 1674–1679. doi: 10.2174/1871520618666171208092115

Finegold, A. A., Shatwell, K. P., Segal, A. W., Klausner, R. D., and Dancis, A. (1996). Intramembrane bis-heme motif for transmembrane electron transport conserved in a yeast iron reductase and the human NADPH oxidase. *J. Biol. Chem.* 271, 31021–31024. doi: 10.1074/jbc.271.49.31021

Garcia-Hernandez Mde, L., Gray, A., Hubby, B., and Kast, W. M. (2007). In vivo effects of vaccination with six-transmembrane epithelial antigen of the prostate: a candidate antigen for treating prostate cancer. *Cancer Res.* 67, 1344–1351. doi: 10.1158/0008-5472.CAN-06-2996

Gelfand, R., Vernet, D., Bruhn, K. W., Sarkissyan, S., Heber, D., Vadgama, J. V., et al. (2017). Long-term exposure of MCF-7 breast cancer cells to ethanol stimulates oncogenic features. *Int. J. Oncol.* 50, 49–65. doi: 10.3892/ijo.2016.3800

Gomes, I. M., Maia, C. J., and Santos, C. R. (2012). STEAP proteins: from structure to applications in cancer therapy. *Mol. Cancer Res.* 10, 573–587. doi: 10.1158/1541-7786.MCR-11-0281

Gomes, I. M., Rocha, S. M., Gaspar, C., Alvelos, M. I., Santos, C. R., Socorro, S., et al. (2018). Knockdown of STEAP1 inhibits cell growth and induces apoptosis in LNCaP prostate cancer cells counteracting the effect of androgens. *Med. Oncol.* 35:40. doi: 10.1007/s12032-018-1100-0

Gomes, I. M., Santos, C. R., and Maia, C. J. (2014b). Expression of STEAP1 and STEAP1B in prostate cell lines, and the putative regulation of STEAP1 by post-transcriptional and post-translational mechanisms. *Genes Cancer* 5, 142–151. doi: 10.18632/genesandcancer.13

Gomes, I. M., Arinto, P., Lopes, C., Santos, C. R., and Maia, C. J. (2014a). STEAP1 is overexpressed in prostate cancer and prostatic intraepithelial neoplasia lesions, and it is positively associated with Gleason score. *Urol. Oncol.* 32, e23–e59. doi: 10.1016/j.urolonc.2013.08.028

Gomes, I. M., Santos, C. R., Socorro, S., and Maia, C. J. (2013). Six transmembrane epithelial antigen of the prostate 1 is down-regulated by sex hormones in prostate cells. *Prostate* 73, 605–613. doi: 10.1002/pros.22601

Gonen-Korkmaz, C., Sevin, G., Gokce, G., Arun, M. Z., Yildirim, G., Reel, B., et al. (2014). Analysis of tumor necrosis factor alpha-induced and nuclear factor kappaB-silenced LNCaP prostate cancer cells by RT-qPCR. *Exp. Ther. Med.* 8, 1695–1700. doi: 10.3892/etm.2014.2032

Grunewald, T. G., Bach, H., Cossarizza, A., and Matsumoto, I. (2012a). The STEAP protein family: versatile oxidoreductases and targets for cancer immunotherapy with overlapping and distinct cellular functions. *Biol. Cell* 104, 641–657. doi: 10.1111/boc.201200027

Grunewald, T. G., Diebold, I., Esposito, I., Plehm, S., Hauer, K., Thiel, U., et al. (2012b). STEAP1 is associated with the invasive and oxidative stress phenotype of Ewing tumors. *Mol. Cancer Res.* 10, 52–65. doi: 10.1158/1541-7786.MCR-11-0524

Grunewald, T. G., Ranft, A., Esposito, I., Da Silva-Buttkus, P., Aichler, M., Baumhoer, D., et al. (2012c). High STEAP1 expression is associated with improved outcome of Ewing's sarcoma patients. *Ann. Oncol.* 23, 2185–2190. doi: 10.1093/annonc/mdr605

Guo, H., He, J., Yang, X., Zheng, W., and Yao, W. (2020). Responses of intestinal morphology and function in offspring to heat stress in primiparous sows during late gestation. *J. Therm. Biol.* 89:102539. doi: 10.1016/j.jtherbio.2020.102539

Guo, Q., Ke, X. X., Liu, Z., Gao, W. L., Fang, S. X., Chen, C., et al. (2020). Evaluation of the prognostic value of STEAP1 in lung adenocarcinoma and insights into its potential molecular pathways via bioinformatic analysis. *Front. Genet.* 11:242. doi: 10.3389/fgene.2020.00242

Han, M., Xu, R., Wang, S., Yang, N., Ni, S., Zhang, Q., et al. (2018). Six-transmembrane epithelial antigen of prostate 3 predicts poor prognosis and

promotes glioblastoma growth and invasion. *Neoplasia* 20, 543–554. doi: 10.1016/j.neo.2018.04.002

Hayashi, T., Oue, N., Sakamoto, N., Anami, K., Oo, H. Z., Sentani, K., et al. (2011). Identification of transmembrane protein in prostate cancer by the *Escherichia coli* ampicillin secretion trap: expression of CDON is involved in tumor cell growth and invasion. *Pathobiology* 78, 277–284. doi: 10.1159/000329588

Hubert, R. S., Vivanco, I., Chen, E., Rastegar, S., Leong, K., Mitchell, S. C., et al. (1999). STEAP: a prostate-specific cell-surface antigen highly expressed in human prostate tumors. *Proc. Natl. Acad. Sci. U. S. A.* 96, 14523–14528. doi: 10.1073/pnas.96.25.14523

Ihlaseh-Catalano, S. M., Drigo, S. A., De Jesus, C. M., Domingues, M. A., Trindade Filho, J. C., and De Camargo, J. L. (2013). STEAP1 protein overexpression is an independent marker for biochemical recurrence in prostate carcinoma. *Histopathology* 63, 678–685. doi: 10.1111/his.12226

Iijima, K., Nakamura, H., Takada, K., Hayasaka, N., Kubo, T., Umeyama, Y., et al. (2021). Six-transmembrane epithelial antigen of the prostate 1 accelerates cell proliferation by targeting c-Myc in liver cancer cells. *Oncol. Lett.* 22:546. doi: 10.3892/ol.2021.12807

Isobe, T., Baba, E., Arita, S., Komoda, M., Tamura, S., Shirakawa, T., et al. (2011). Human STEAP3 maintains tumor growth under hypoferric condition. *Exp. Cell Res.* 317, 2582–2591. doi: 10.1016/j.yexcr.2011.07.022

Jiang, C., Wu, B., Xue, M., Lin, J., Hu, Z., Nie, X., et al. (2021). Inflammation accelerates copper-mediated cytotoxicity through induction of six-transmembrane epithelial antigens of prostate 4 expression. *Immunol. Cell Biol.* 99, 392–402. doi: 10.1111/imcb.12427

Jiang, J. N., Wu, Y. Y., Fang, X. D., and Ji, F. J. (2020). EIF4E regulates STEAP1 expression in peritoneal metastasis. *J. Cancer* 11, 990–996. doi: 10.7150/jca.29105

Jiao, Z., Huang, L., Sun, J., Xie, J., Wang, T., Yin, X., et al. (2020). Six-transmembrane epithelial antigen of the prostate 1 expression promotes ovarian cancer metastasis by aiding progression of epithelial-to-mesenchymal transition. *Histochem. Cell Biol.* 154, 215–230. doi: 10.1007/s00418-020-01877-7

Jin, Y., Wang, L., Qu, S., Sheng, X., Kristian, A., Maelandsmo, G. M., et al. (2015). STAMP2 increases oxidative stress and is critical for prostate cancer. *EMBO Mol. Med.* 7, 315–331. doi: 10.15252/emmm.201404181

Kim, S. H., Ho, J. N., Jin, H., Lee, S. C., Lee, S. E., Hong, S. K., et al. (2016). Upregulated expression of BCL2, MCM7, and CCNE1 indicate cisplatin-resistance in the set of two human bladder cancer cell lines: T24 cisplatin sensitive and T24R2 cisplatin resistant bladder cancer cell lines. *Investig. Clin. Urol.* 57, 63–72. doi: 10.4111/icu.2016.57.1.63

Knutson, M. D. (2007). Steap proteins: implications for iron and copper metabolism. *Nutr. Rev.* 65, 335–340.

Korkmaz, C. G., Korkmaz, K. S., Kurys, P., Elbi, C., Wang, L., Klokk, T. I., et al. (2005). Molecular cloning and characterization of STAMP2, an androgen-regulated six transmembrane protein that is overexpressed in prostate cancer. *Oncogene* 24, 4934–4945. doi: 10.1038/sj.onc.1208677

Korkmaz, K. S., Elbi, C., Korkmaz, C. G., Loda, M., Hager, G. L., and Saatcioglu, F. (2002). Molecular cloning and characterization of STAMP1, a highly prostate-specific six transmembrane protein that is overexpressed in prostate cancer. *J. Biol. Chem.* 277, 36689–36696. doi: 10.1074/jbc.M202414200

Lan, G., Yu, X., Sun, X., Li, W., Zhao, Y., Lan, J., et al. (2021). Comprehensive analysis of the expression and prognosis for TNFAIPs in head and neck cancer. *Sci. Rep.* 11:15696. doi: 10.1038/s41598-021-95160-x

Lee, C. H., Chen, S. L., Sung, W. W., Lai, H. W., Hsieh, M. J., Yen, H. H., et al. (2016). The prognostic role of STEAP1 expression determined via immunohistochemistry staining in predicting prognosis of primary colorectal cancer: a survival analysis. *Int. J. Mol. Sci.* 17:592. doi: 10.3390/ijms17040592

Lespagnol, A., Duflaut, D., Beekman, C., Blanc, L., Fiucci, G., Marine, J. C., et al. (2008). Exosome secretion, including the DNA damage-induced p53-dependent secretory pathway, is severely compromised in TSAP6/Steap3-null mice. *Cell Death Differ.* 15, 1723–1733. doi: 10.1038/cdd.2008.104

Li, L., Li, J., Shen, Z., Liu, W., and Chen, Z. (2004). [Clinical significance of six-transmembrane epithelial antigen of the prostate expressed in prostatic carcinoma]. *Zhonghua Nan Ke Xue* 10, 351–354.

Liao, Y., Zhao, J., Bulek, K., Tang, F., Chen, X., Cai, G., et al. (2020). Inflammation mobilizes copper metabolism to promote colon tumorigenesis via an IL-17-STEAP4-XIAP axis. *Nat. Commun.* 11:900. doi: 10.1038/s41467-020-14698-y

Liu, Z., Zhang, H., Hu, H., Cai, Z., Lu, C., Liang, Q., et al. (2021). A novel six-mRNA signature predicts survival of patients with glioblastoma multiforme. *Front. Genet.* 12:634116. doi: 10.3389/fgene.2021.634116

Machlenkin, A., Paz, A., Bar Haim, E., Goldberger, O., Finkel, E., Tirosh, B., et al. (2005). Human CTL epitopes prostatic acid phosphatase-3 and six-transmembrane epithelial antigen of prostate-3 as candidates for prostate cancer immunotherapy. *Cancer Res.* 65, 6435–6442. doi: 10.1158/0008-5472.CAN-05-0133

Maia, C. J., Socorro, S., Schmitt, F., and Santos, C. R. (2008). STEAP1 is over-expressed in breast cancer and down-regulated by 17beta-estradiol in MCF-7 cells and in the rat mammary gland. *Endocrine* 34, 108–116. doi: 10.1007/s12020-008-9113-7

Moreaux, J., Kassambara, A., Hose, D., and Klein, B. (2012). STEAP1 is overexpressed in cancers: a promising therapeutic target. *Biochem. Biophys. Res. Commun.* 429, 148–155. doi: 10.1016/j.bbrc.2012.10.123

Nakamura, H., Takada, K., Arihara, Y., Hayasaka, N., Murase, K., Iyama, S., et al. (2019). Six-transmembrane epithelial antigen of the prostate 1 protects against increased oxidative stress via a nuclear erythroid 2-related factor pathway in colorectal cancer. *Cancer Gene Ther.* 26, 313–322. doi: 10.1038/s41417-018-0056-8

Ohgami, R. S., Campagna, D. R., Greer, E. L., Antiochos, B., Mcdonald, A., Chen, J., et al. (2005). Identification of a ferrireductase required for efficient transferrin-dependent iron uptake in erythroid cells. *Nat. Genet.* 37, 1264–1269. doi: 10.1038/ng1658

Ohgami, R. S., Campagna, D. R., Mcdonald, A., and Fleming, M. D. (2006). The steap proteins are metalloreductases. *Blood* 108, 1388–1394. doi: 10.1182/blood-2006-02-003681

Orfanou, I. M., Argyros, O., Papapetropoulos, A., Tseleni-Balafouta, S., Vougas, K., and Tamvakopoulos, C. (2021). Discovery and pharmacological evaluation of STEAP4 as a novel target for HER2 overexpressing breast cancer. *Front. Oncol.* 11:608201. doi: 10.3389/fonc.2021.608201

Passer, B. J., Nancy-Portebois, V., Amzallag, N., Prieur, S., Cans, C., Roborel De Climens, A., et al. (2003). The p53-inducible TSAP6 gene product regulates apoptosis and the cell cycle and interacts with Nix and the Myt1 kinase. *Proc. Natl. Acad. Sci. U. S. A.* 100, 2284–2289. doi: 10.1073/pnas.0530298100

Pihlstrom, N., Jin, Y., Nenseth, Z., Kuzu, O. F., and Saatcioglu, F. (2021). STAMP2 expression mediated by cytokines attenuates their growth-limiting effects in prostate cancer cells. *Cancers* 13:1579. doi: 10.3390/cancers13071579

Porkka, K. P., Helenius, M. A., and Visakorpi, T. (2002). Cloning and characterization of a novel six-transmembrane protein STEAP2, expressed in normal and malignant prostate. *Lab. Invest.* 82, 1573–1582. doi: 10.1097/01.LAB.0000038554.26102.C6

Porkka, K. P., Nupponen, N. N., Tammela, T. L., Vessella, R. L., and Visakorpi, T. (2003). Human pHyde is not a classical tumor suppressor gene in prostate cancer. *Int. J. Cancer* 106, 729–735. doi: 10.1002/ijc.11278

Qin, D. N., Kou, C. Z., Ni, Y. H., Zhang, C. M., Zhu, J. G., Zhu, C., et al. (2010). Monoclonal antibody to the six-transmembrane epithelial antigen of prostate 4 promotes apoptosis and inhibits proliferation and glucose uptake in human adipocytes. *Int. J. Mol. Med.* 26, 803–811. doi: 10.3892/ijmm_00000528

Rinaldy, A. R., and Steiner, M. S. (1999). Application of an improved cDNA competition technique to identify prostate cancer-associated gene. *DNA Cell Biol.* 18, 829–836. doi: 10.1089/104454999314827

Savci-Heijink, C. D., Halfwerk, H., Koster, J., and Van De Vijver, M. J. (2016). A novel gene expression signature for bone metastasis in breast carcinomas. *Breast Cancer Res. Treat.* 156, 249–259. doi: 10.1007/s10549-016-3741-z

Sun, J., Ji, G., Xie, J., Jiao, Z., Zhang, H., and Chen, J. (2019). Six-transmembrane epithelial antigen of the prostate 1 is associated with tumor invasion and migration in endometrial carcinomas. *J. Cell Biochem.* 120, 11172–11189. doi: 10.1002/jcb.28393

Tian, Y. X., Huo, S. F., Shang, W. L., Yu, M., Ren, X. P., Wen, H. X., et al. (2020). STEAP1 facilitates metastasis and epithelial-mesenchymal transition of lung adenocarcinoma via the JAK2/STAT3 signaling pathway. *Biosci. Rep.* 40:BSR20193169. doi: 10.1042/BSR20193169

Valadi, H., Ekstrom, K., Bossios, A., Sjostrand, M., Lee, J. J., and Lotvall, J. O. (2007). Exosome-mediated transfer of mRNAs and microRNAs is a novel mechanism of genetic exchange between cells. *Nat. Cell Biol.* 9, 654–659. doi: 10.1038/ncb1596

von Rozycki, T., Yen, M. R., Lende, E. E., and Saier, M. H. Jr. (2004). The YedZ family: possible heme binding proteins that can be fused to transporters and electron carriers. *J. Mol. Microbiol. Biotechnol.* 8, 129–140. doi: 10.1159/000085786

Wang, L., Jin, Y., Arnoldussen, Y. J., Jonson, I., Qu, S., Maelandsmo, G. M., et al. (2010). STAMP1 is both a proliferative and an antiapoptotic factor in prostate cancer. *Cancer Res.* 70, 5818–5828. doi: /10.1158/0008-5472.CAN-09-4697

Weston, C., Klobusicky, J., Weston, J., Connor, J., Toms, S. A., and Marko, N. F. (2016). Aberrations in the iron regulatory gene signature are associated with decreased survival in diffuse infiltrating gliomas. *PLoS One* 11:e0166593. doi: 10.1371/journal.pone.0166593

Whiteland, H., Spencer-Harty, S., Morgan, C., Kynaston, H., Thomas, D. H., Bose, P., et al. (2014). A role for STEAP2 in prostate cancer progression. *Clin. Exp. Metastasis* 31, 909–920. doi: 10.1007/s10585-014-9679-9

Wong, P. F., and Abubakar, S. (2010). Comparative transcriptional study of the effects of high intracellular zinc on prostate carcinoma cells. *Oncol. Rep.* 23, 1501–1516. doi: 10.3892/or_00000789

Wu, H. T., Chen, W. J., Xu, Y., Shen, J. X., Chen, W. T., and Liu, J. (2020). The tumor suppressive roles and prognostic values of STEAP family members in breast cancer. *Biomed. Res. Int.* 2020:9578484. doi: 10.1155/2020/9578484

Wu, Y. Y., Jiang, J. N., Fang, X. D., and Ji, F. J. (2018). STEAP1 regulates tumorigenesis and chemoresistance during peritoneal metastasis of gastric cancer. *Front. Physiol.* 9:1132. doi: 10.3389/fphys.2018.01132

Xie, J., Yang, Y., Sun, J., Jiao, Z., Zhang, H., and Chen, J. (2019). STEAP1 inhibits breast cancer metastasis and is associated with epithelial-mesenchymal transition procession. *Clin. Breast Cancer* 19, e195–e207. doi: 10.1016/j.clbc.2018.08.010

Xue, X., Bredell, B. X., Anderson, E. R., Martin, A., Mays, C., Nagao-Kitamoto, H., et al. (2017). Quantitative proteomics identifies STEAP4 as a critical regulator of mitochondrial dysfunction linking inflammation and colon cancer. *Proc. Natl. Acad. Sci. U. S. A.* 114, E9608–E9617. doi: 10.1073/pnas.1712946114

Yamamoto, T., Tamura, Y., Kobayashi, J., Kamiguchi, K., Hirohashi, Y., Miyazaki, A., et al. (2013). Six-transmembrane epithelial antigen of the prostate-1 plays a role for in vivo tumor growth via intercellular communication. *Exp. Cell Res.* 319, 2617–2626. doi: 10.1016/j.yexcr.2013.07.025

Yan, D., Dong, W., He, Q., Yang, M., Huang, L., Kong, J., et al. (2019). Circular RNA circPICALM sponges miR-1265 to inhibit bladder cancer metastasis and influence FAK phosphorylation. *EBioMedicine* 48, 316–331. doi: 10.1016/j.ebiom.2019.08.074

Yang, Q., Ji, G., and Li, J. (2020). STEAP2 is down-regulated in breast cancer tissue and suppresses PI3K/AKT signaling and breast cancer cell invasion in vitro and in vivo. *Cancer Biol. Ther.* 21, 278–291. doi: 10.1080/15384047.2019.1685290

Yu, Z., Wang, H., Fang, Y., Lu, L., Li, M., Yan, B., et al. (2020). Molecular chaperone HspB2 inhibited pancreatic cancer cell proliferation via activating p53 downstream gene RPRM. BAI1, and TSAP6. *J. Cell Biochem.* 121, 2318–2329. doi: 10.1002/jcb.29455

Yuan, Y., Liu, Y., Zhu, X. M., Hu, J., Zhao, C. Y., and Jiang, F. (2019). Six-transmembrane epithelial antigen of the prostate-1 (STEAP-1)-targeted ultrasound imaging microbubble improves detection of prostate cancer in vivo. *J. Ultrasound Med.* 38, 299–305. doi: 10.1002/jum.14689

Zhang, M., Lv, X., Jiang, Y., Li, G., and Qiao, Q. (2019). Identification of aberrantly methylated differentially expressed genes in glioblastoma multiforme and their association with patient survival. *Exp. Ther. Med.* 18, 2140–2152. doi: 10.3892/etm.2019.7807

Zhang, X., Steiner, M. S., Rinaldy, A., and Lu, Y. (2001). Apoptosis induction in prostate cancer cells by a novel gene product, pHyde, involves caspase-3. *Oncogene* 20, 5982–5990. doi: 10.1038/sj.onc.1204831

Zhang, Y., Ye, Q., He, J., Chen, P., Wan, J., Li, J., et al. (2020). Recurrence-associated multi-RNA signature to predict disease-free survival for ovarian cancer patients. *Biomed. Res. Int.* 2020:1618527. doi: 10.1155/2020/1618527

Zhuang, X., Herbert, J. M., Lodhia, P., Bradford, J., Turner, A. M., Newby, P. M., et al. (2015). Identification of novel vascular targets in lung cancer. *Br. J. Cancer* 112, 485–494. doi: 10.1038/bjc.2014.626

Conflict of Interest: The authors declare that the research was conducted in the absence of any commercial or financial relationships that could be construed as a potential conflict of interest.

Publisher's Note: All claims expressed in this article are solely those of the authors and do not necessarily represent those of their affiliated organizations, or those of the publisher, the editors and the reviewers. Any product that may be evaluated in this article, or claim that may be made by its manufacturer, is not guaranteed or endorsed by the publisher.

frontiers in Cell and Developmental Biology

ORIGINAL RESEARCH
published: 29 October 2021
doi: 10.3389/fcell.2021.666025

Identifying a Ferroptosis-Related Gene Signature for Predicting Biochemical Recurrence of Prostate Cancer

Zhengtong Lv[1,2], Jianlong Wang[1], Xuan Wang[1], Miao Mo[3], Guyu Tang[3], Haozhe Xu[3], Jianye Wang[1,2], Yuan Li[4] and Ming Liu[1,2]**

[1] Department of Urology, Beijing Hospital, National Center of Gerontology, Institute of Geriatric Medicine, Chinese Academy of Medical Sciences, Beijing, China, [2] Graduate School of Peking Union Medical College and Chinese Academy of Medical Sciences, Beijing, China, [3] Department of Urology, Xiangya Hospital, Central South University, Changsha, China, [4] Department of Urology, The Second Xiangya Hospital, Central South University, Changsha, China

Ferroptosis induced by lipid peroxidation is closely related to cancer biology. Prostate cancer (PCa) is not only a malignant tumor but also a lipid metabolic disease. Previous studies have identified ferroptosis as an important pathophysiological pathway in PCa development and treatment, but its role in the prognosis of PCa is less well known. In this study, we constructed a nine-ferroptosis-related gene risk model that demonstrated strong prognostic and therapeutic predictive power. The higher risk score calculated by the model was significantly associated with a higher ferroptosis potential index, higher Ki67 expression, higher immune infiltration, higher probability of biochemical recurrence, worse clinicopathological characteristics, and worse response to chemotherapy and antiandrogen therapy in PCa. The mechanisms identified by the gene set enrichment analysis suggested that this signature can accurately distinguish high- and low-risk populations, which is possibly closely related to variations in steroid hormone secretion, regulation of endocrine processes, positive regulation of humoral immune response, and androgen response. Results of this study were confirmed in two independent PCa cohorts, namely, The Cancer Genome Atlas cohort and the MSK-IMPACT Clinical Sequencing Cohort, which contributed to the body of scientific evidence for the prediction of biochemical recurrence in patients with PCa. In addition, as the main components of this signature, the effects of the *AIFM2* and *NFS1* genes on ferroptosis were evaluated and verified by *in vivo* and *in vitro* experiments, respectively. The above findings provided new insights and presented potential clinical applications of ferroptosis in PCa.

Keywords: prostate cancer, TCGA, MSKCC, ferroptosis, prognosis, biochemical recurrence

OPEN ACCESS

Edited by:
Ahmed Hamaï, Institut National de la Santé et de la Recherche Médicale (INSERM), France

Reviewed by:
Tang-Long Shen, National Taiwan University, Taiwan
Sushant Kachhap, Johns Hopkins Medicine, United States

***Correspondence:**
Ming Liu
liumingbjh@126.com
Yuan Li
yuanlixy@csu.edu.cn

Specialty section:
This article was submitted to Molecular and Cellular Oncology, a section of the journal Frontiers in Cell and Developmental Biology

Received: *09 February 2021*
Accepted: *27 September 2021*
Published: *29 October 2021*

Citation:
Lv Z, Wang J, Wang X, Mo M, Tang G, Xu H, Wang J, Li Y and Liu M (2021) Identifying a Ferroptosis-Related Gene Signature for Predicting Biochemical Recurrence of Prostate Cancer. Front. Cell Dev. Biol. 9:666025. doi: 10.3389/fcell.2021.666025

INTRODUCTION

The latest cancer statistics show that prostate cancer (PCa) has surpassed lung cancer, as it becomes the malignant tumor with the highest incidence in men and ranks second to lung cancer in terms of mortality rate (Siegel et al., 2020). Radical prostatectomy, external-beam radiation therapy, and brachytherapy are recommended interventions for localized PCa (Mottet et al., 2020).

Although these radical treatments can control the disease chronically, several patients (20–25%) still experienced biochemical recurrence (BCR) during the follow-up period (Pound et al., 1999; Simmons et al., 2007; Van den Broeck et al., 2019). Patients with BCR who did not receive secondary therapy will develop clinical progression within 5–8 years, and 32–45% will die of the disease within 15 years (Brockman et al., 2015). Therefore, identifying new biomarkers is crucial to predict high-risk PCa patients with high BCR risk.

Ferroptosis is a new kind of regulated cell death (RCD) and is different from apoptosis, necrosis, and autophagy in terms of morphology, biochemistry, and genetics (Stockwell et al., 2017). In the last 8 years, the complex relationship between ferroptosis and cancer has incited widespread concern (Tang D. et al., 2020). Changes in iron metabolism not only promote the growth and proliferation of tumor cells by increasing iron reserves (Manz et al., 2016) but also induce excessive iron concentration that can cause lipid peroxidation in the tumor cell membrane and lead to ferroptosis. Over the past 5 years, basic and clinical researchers have shown a growing interest in the role of ferroptosis in the pathogenesis of cancer (Chen et al., 2021). At present, triggering ferroptosis, as a new method of treating cancer, has received high expectations and has been an area of active research (Hassannia et al., 2019; Liang et al., 2019).

Numerous studies have demonstrated the critical role of ferroptosis in the development and treatment of PCa. For example, enzalutamide was found to induce lipid uptake and remodeling, which in turn induces ferroptosis hypersensitivity (Tousignant et al., 2020). Flubendazole can induce potent antitumor effects by targeting P53 and promoting ferroptosis in castration-resistant PCa (CRPC) (Zhou et al., 2021). Erastin is a classical inducer of ferroptosis and can suppress the transcriptional activities of both the full-length and splice variants of androgen receptors (AR) in CRPC (Yang Y. et al., 2021). Qin et al. (2021) designed and synthesized an isothiocyanate-containing hybrid AR antagonist that can efficiently downregulate AR/AR splice variant and induce ferroptosis in CRPC cells combined with glutathione (GSH) synthesis inhibitor. There was a suggestion that the induction of ferroptosis is a new therapeutic strategy for advanced PCa, which can be used as a monotherapy or as a combination therapy with second-generation antiandrogens (Ghoochani et al., 2021). However, the effect of ferroptosis on the prognosis of PCa has rarely been reported.

This study identified ferroptosis-related genes associated with long-term BCR of PCa and finally constructed a prognostic signature based on nine ferroptosis-related genes, which can accurately identify patients with high-risk PCa. The findings provide evidence on the key role of ferroptosis in PCa development.

MATERIALS AND METHODS

Data Acquisition

This study included two independent PCa cohorts. Data of the PCa patient cohort were downloaded from The Cancer Genome Atlas (TCGA) database and used as the training set (2021.03.01), which included 483 patients with comprehensive transcriptome (FPKM standardized data) and clinical information[1]. Data of the MSK-IMPACT Clinical Sequencing Cohort (MSKCC) PCa cohort were obtained from the Cbioportal database[2] and used as the validation set, which included 138 patients with complete expression profile (normalized log2 mRNA expression data) and clinicopathological information. In addition, several Gene Expression Omnibus (GEO) datasets were selected to verify our results, including GSE54460, GSE70769, GSE104749, GSE88808, GSE70768, GSE69223, GSE68555, GSE55945, GSE46602, GSE38241, GSE35988, GSE32571, GSE32448, GSE6919, and GSE3325[3]. The 84 ferroptosis-related genes were taken from a previous study (Liang et al., 2020) and the "WP_FERROPTOSIS" gene set, which was obtained from the Molecular Signatures Database[4]. The clinicopathological features of the two cohorts are summarized in **Table 1**.

Construction of the Ferroptosis-Related Prognostic Signature

The risk prognostic model was constructed based on the TCGA cohort. The "Limma" package was used to obtain differentially expressed ferroptosis-related genes between PCa tissues and normal tissues, with a false discovery rate (FDR) of <0.05 as the

[1]https://portal.gdc.cancer.gov/

[2]https://www.cbioportal.org/, or GSE21032.

[3]https://www.ncbi.nlm.nih.gov/geo/

[4]https://www.gsea-msigdb.org/gsea/msigdb/

TABLE 1 | The basic characteristics of the two cohorts of PCa.

Clinical characteristics	Classification	TCGA (*n* = 472)	MSKCC (*n* = 138)
Age		60.87 ± 6.80	58.03 ± 6.63
PSA		10.86 ± 11.67	12.14 ± 44.08
Gleason score	6	44 (9.32%)	41 (29.71%)
	7	237 (50.21%)	77 (55.80%)
	8	57 (12.08%)	10 (7.25%)
	9	131 (27.75%)	10 (7.25%)
	10	3 (0.64%)	0 (0%)
WHO ISUP	1	44 (9.32%)	41 (29.71%)
	2	142 (30.08%)	53 (38.41%)
	3	95 (20.13%)	24 (17.39%)
	4	57 (12.08%)	10 (7.25%)
	5	134 (28.39%)	10 (7.25%)
T stage	T2a	12 (2.54%)	8 (5.80%)
	T2b	10 (2.12%)	48 (34.78%)
	T2c	158 (33.47%)	29 (21.01%)
	T3a	152 (32.20%)	29 (21.01%)
	T3b	130 (27.54%)	13 (9.42%)
	T3c	0 (0.00%)	4 (2.90%)
	T4	10 (2.12%)	7 (5.07%)
Biochemical recurrence	Yes	87 (18.43%)	35 (25.36%)
	No	385 (81.57%)	103 (74.64%)

PCa, prostate cancer; TCGA, The Cancer Genome Atlas; MSKCC, MSK-IMPACT Clinical Sequencing Cohort; PSA, prostate-specific antigen.

boundary. Univariate Cox regression analysis was employed to identify the ferroptosis-related genes associated with the BCR of PCa. The genes contained in the intersection of the above two analyses were used as the core genes to construct the protein interaction network based on the STRING database[5] and the expression correlation network based on the expressions of these core genes. Lasso regression was employed to avoid overfitting of the final prediction model. The calculation formula of the model is as follows: $Risk\ score = \sum_{m=1}^{n} Coef_m \times Exp_m$, where $Coef_m$ is the risk coefficient and Exp_m is the relative mRNA expression of each ferroptosis-related gene. The median risk score was used as a cutoff to distinguish patients with high- and low-risk PCa.

Evaluation and Validation of the Prognostic Signature

The TCGA and MSKCC cohorts were used to evaluate and verify the prognosis model separately, and the same statistical methods were applied in both cohorts. Log-rank and Kaplan–Meier (K–M) tests were used to visualize the difference in the biochemical relapse-free survival (bRFS) between the two risk groups. The sensitivity and specificity of survival prediction were tested by the receiver operating characteristic (ROC) analysis. An area under the ROC curve (AUC) was calculated as an index of the prediction accuracy, and "vegan" and "stats" packages were used for the principal component analysis (PCA) to explore the distribution among groups. Univariate and multivariate Cox regression analyses were used to investigate whether the risk score can be used as an independent prognostic factor in PCa. The correlation between the risk score and other clinicopathological features was shown by a heat map.

Gene Set Enrichment Analysis

Hallmark and Gene Ontology (GO) gene sets were downloaded for the gene set enrichment analysis (GSEA) to determine which gene sets were significantly different between the high- and low-risk groups. A total of 1,000 gene set permutations were performed to finally obtain the normalized enrichment score, normalized *p*-value, and FDR. The ferroptosis potential index (FPI) was calculated according to the methods of Liu et al. (2020c) by subtracting the enrichment score of the negative- from the positive-core machine components through single-sample GSEA (ssGSEA) by using the "GSVA" package.

Immune Infiltration and Tumor Microenvironment

Single-sample GSEA was also used to quantify the immune infiltration level (Rooney et al., 2015). The annotated gene set file was derived from the study of Liang et al. (2020). Finally, the enrichment levels of 16 immune cells and 13 immune-related pathways in each PCa sample were quantified, and the results were expressed by box plots. Moreover, we predicted the TME of PCa by using the "ESTIMATE" package to calculate the immune/stromal/ESTIM/tumor purity score (Yoshihara et al., 2013).

[5]https://string-db.org/

Prediction of Antiandrogenic Therapy and Immunotherapy Responses

The response of each patient with PCa in both cohorts to bicalutamide and docetaxel was obtained from the Genomics of Drug Sensitivity in Cancer[6] using the "pRRophetic" R package (Geeleher et al., 2014). Half-maximal inhibitory concentration (IC50) was used to measure the response of tumor cells to drugs.

Cell Culture

Human prostate and PCa cell lines (PWR1E and DU145) were obtained from the American Type Culture Collection (Manassas, VA, United States) and the Shanghai Institute of Biochemistry and Cell Biology, Chinese Academy of Sciences (Shanghai, China), which were cultured in keratinocyte serum-free medium containing 50 μg/ml bovine pituitary extract and 5 ng/ml epidermal growth factor for PWR1E and RPMI-1640 medium supplemented with 2 mM L-Glutamine, 10% fetal bovine serum, 1% penicillin/streptomycin for DU145. These cells were grown at 37°C with 5% CO_2 in a humidified incubator. The lentiviral vector carrying AIFM2 shRNA or NFS1 shRNA and the corresponding control shRNA were synthesized and purchased from GenePharma and GenScript (China), respectively.

Cell Viability Assay

Cell viability was assessed using the MTT assay to evaluate the effects of different concentrations of erastin on cell viability. PWR1E or DU145 cell lines at 2×10^3 cells/well were incubated in 96-well plates for 24 h. An MTT solution (5 mg/ml) was cultured for 4 h. The cells were then treated with 150 μl of dimethylsulfoxide. Cell viability was determined by enzyme-linked immunosorbent assay at 570 nm.

Ferroptosis-Related Analysis

Various cell biological methods were used to evaluate ferroptosis. Lipid peroxidation was assessed using the BODIPY^{TM} 581/591 C11 (D3861, Thermo Fisher Scientific), and oxidation of the polyunsaturated butadienyl portion of the dye results in the shifting of the fluorescence emission peak from ∼590 (red) to ∼510 nm (green). PWR1E or DU145 cell lines were incubated with 10 μM erastin for 24 h. Then 1 μg/ml of Hoechst 33342 and 1 μm of BODIPY^{TM} 581/591 C11 were added to the culture medium for living cell imaging at the last hour of incubation. Ferroptosis-related indexes, including the levels of Fe^{2+} release, malondialdehyde (MDA), reactive oxygen species (ROS), and GSH, were determined using the Iron Assay Kit (ab83366, Abcam, United Kingdom), lipid peroxidation (MDA) assay (ab118970, Abcam), DCF ROS/RNS Assay (ab238535, Abcam), and GSH/GSSG Ratio Detection Assay Kit II (ab205811, Abcam), respectively.

Real-Time Quantitative Polymerase Chain Reaction Analysis and Western Blotting

Total RNA was extracted from the cells using Trizol reagent (Invitrogen, Waltham, MA, United States). Approximately

[6]https://www.cancerrxgene.org

500 ng of RNA was used for the reverse transcription reaction with PrimeScript RT Master Mix [Takara Biotechnology (Dalian) Co., Ltd., Japan]. Then, with GAPDH as the internal control, real-time quantitative polymerase chain reaction (RT-qPCR) was performed using Premix Ex Taq^{TM} II [Takara Biotechnology (Dalian) Co., Ltd.] with the Roche Light Cycler 480 Real-Time PCR system. The sequence of primers is as follows: AIFM2 forward: TTACAAGCCAGAGACTGACCAA, reverse: ACAAGGCCTGTCACTGAAGAG; NFS1 forward: CA CTCCCGGACACATGCTTAT, reverse: TGTCTGGGTGGTGAT CAAGTG; GAPDH forward: ATCATCAGCAATGCCTCCTG, reverse: ATGGACTGTGGTCATGAGTC.

Protein samples (50 μg) were separated by sodium dodecyl sulfate–polyacrylamide gel electrophoresis in 4–12% gel and transferred to nitrocellulose membranes for reaction with antibodies against target genes. Secondary antibodies, i.e., horseradish peroxidase-conjugated rabbit anti-goat and rabbit anti-mouse IgG, were detected by using SuperSignal Chemiluminescent substrate (Pierce Biotechnology, Rockford, IL, United States).

Immunohistochemistry

Tumors and adjacent normal tissues of 52 patients with PCa who underwent radical prostatectomy at the Beijing Hospital, Xiangya Hospital, and the Second Xiangya Hospital were examined by immunohistochemistry (IHC). Sections were incubated with anti-AIFM2 and anti-NFS1 (1:100 dilution). The sections were scored for staining intensity according to the following scale: negative, no staining; weak, weak staining (light yellow); moderate, moderate staining (yellowish brown); and strong, strong staining (brown). The experiments were reviewed and approved by the Ethics Committee of the Beijing Hospital (2018BJYYEC-085-03). The patients provided their written informed consent to participate in this study.

Colony Formation Assay

Prostate cancer cells in the logarithmic growth stage were put into six-well plates. The culture continued for 1–3 weeks, during which the solution was changed every 3 days, and the cell status was observed every day until the number of cells in most single clones was greater than 50. Then the cells were cleaned with phosphate-buffered saline buffer, made in methanol approximately 30 min, and stained with crystal violet dye at a dose of 1%. Thereafter, the number of colonies was calculated.

Tumorigenicity in Nude Mice

All animal experiments were approved by the Institutional Ethics Committee of Xiangya Hospital, Central South University. A subcutaneous xenograft model was established by subcutaneously injecting male nude mice with 1×10^6 DU145 cells on the right side. The tumor volume was measured with calipers and repeatedly measured every 7 days (length × width^2)/2. At 28 days following implantation, the mice were euthanized by cervical dislocation. Then, the xenografts were removed, fixed, weighed, photographed, and preserved.

Statistical Analysis

All data sorting and analyses were completed by the R 3.6.1 software. For continuous variables with normal distribution and homogeneity of variance, an independent sample *t*-test was used; otherwise, Wilcoxon rank-sum test was selected. Pearson correlation coefficient test was used to analyze the correlation. A value of $p < 0.05$ was considered significant. Based on the results of the multivariate Cox proportional hazards analysis, a nomogram was developed to predict 1-, 3-, and 5-year bRFS rates. To evaluate the prediction performance of the nomogram, the consistency index (C index), ROC, and calibration curve were used to evaluate the nomogram.

RESULTS

Development of the Prognostic Ferroptosis-Related Signature of Patients With Prostate Cancer

Figure 1 shows the flow diagram of this study. Among 84 ferroptosis-related genes, 31 were underexpressed, and 27 were highly expressed in tumor tissues compared with the corresponding normal tissues in the TCGA cohort (FDR < 0.05) (**Figure 2A** and **Supplementary Table 1**). To identify prognostic genes associated with the bRFS, the univariate Cox regression analysis suggested that 22 ferroptosis-related genes correlated with the prognosis of PCa (**Supplementary Table 2**). Only four genes serve as protective factors, while the other 18 genes were risk factors (**Figure 2B**). Taking the intersection of the two lists of genes, 17 ferroptosis-related genes were identified as candidate genes for the subsequent construction of a prognostic model (**Figure 2C**). The expression of these genes in tumor tissues and adjacent normal tissues is shown in **Figure 2D**.

These 17 bRFS-related genes were uploaded to STRING to construct a protein–protein interaction (PPI) network (**Figure 3A**). The correlation analysis also showed that these genes were strongly correlated at the transcriptional level (**Figure 3B**). To screen the colinearity of these 17 genes, the LASSO Cox regression analysis was performed to determine the real bRFS-affecting factors and finally identified a prognostic panel of 9 ferroptosis-related genes (**Figures 3C,D**). The following formula was used to calculate the risk assessment score: risk score = *AIFM2* × (0.19867) + *AKR1C1* × (0.05148) + *AKR1C2* × (0.04941) + *CBS* × (0.02658) + *FANCD2* × (0.00202) + *FTH1* × (0.00027) + *G6PD* × (0.00189) + *NFS1* × (0.13708) + *SLC1A5* × (-0.00602).

Evaluation and Validation of the Prognostic Signature

Based on the signature calculation formula, all patients in the TCGA cohort were divided into high- and low-risk groups according to their median risk score. The K-M curve showed that the high-risk group had a higher probability of BCR ($p < 0.001$) (**Figure 4A**). When evaluating bRFS prediction, the 1-, 3-, and 5-year AUCs of the developed gene signature were 0.680, 0.738,

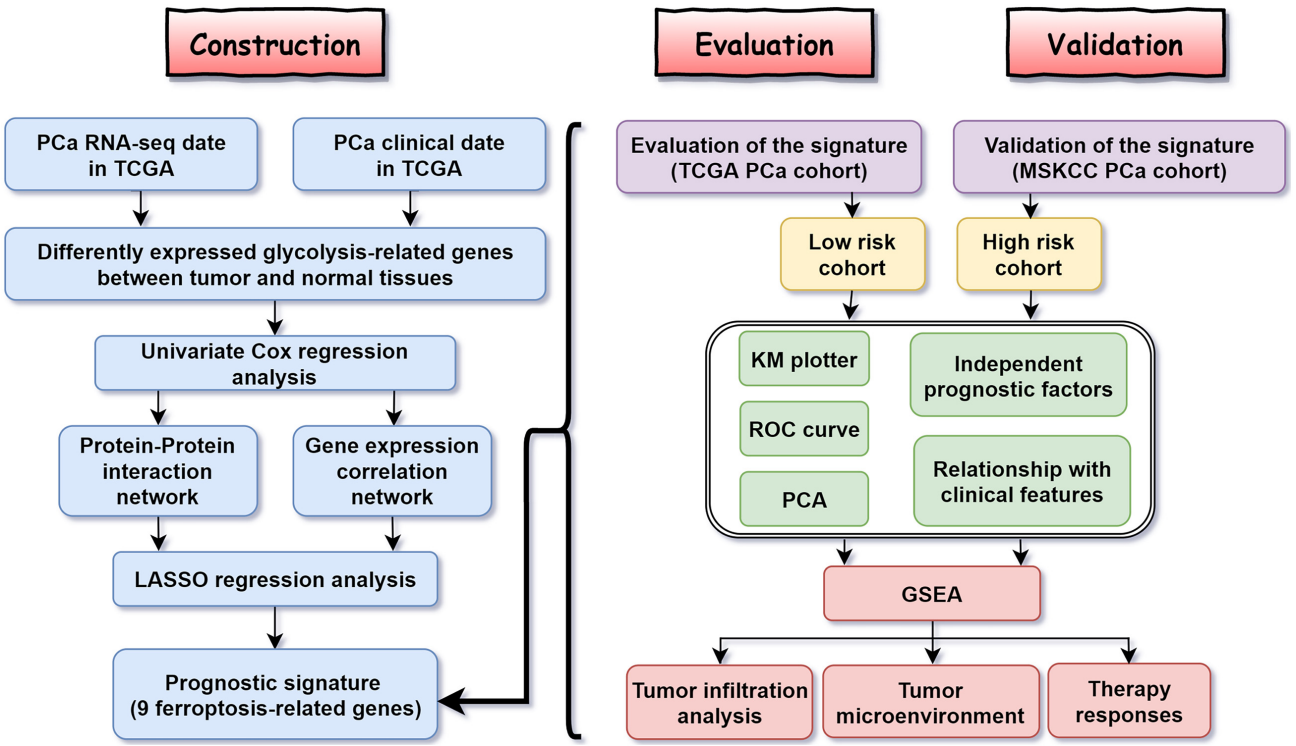

FIGURE 1 | The flow diagram of the study.

and 0.767, respectively (**Figure 4B**). PCA demonstrated that patients in various risk groups showed different two-dimensional spatial distributions ($p < 0.001$) (**Figure 4C**). When all patients were ranked according to their risk scores, the proportion of patients with BCR in the high-risk group was significantly higher than that in the low-risk group (**Figure 4D**). Univariate and multivariate Cox regression analyses were implemented to evaluate whether the model was an independent predictor among other clinical factors such as age, prostate-specific antigen (PSA), Gleason score (GS), and staging. We found that the risk score remained independently associated with bRFS not only at the univariate but also at the multivariate analysis when combined with all the clinical features ($p < 0.05$) (**Figures 4E,F** and **Supplementary Table 3**).

This study evaluated the MSKCC to verify the predictive robustness of this model. To avoid false positives caused by information bias, the same statistical methods were used. Surprisingly, the validation results were highly consistent with that in the TCGA cohort. Survival analysis also demonstrated that a high-risk score was associated with the poor bRFS of patients with PCa (**Figure 5A**). The AUC values for the prognostic model for bRFS were 0.766 at 1 year, 0.729 at 3 years, and 0.726 at 5 years (**Figure 5B**). The PCA results also suggested that different risk subgroups showed significant discrete tendency directly in the two-dimensional plane (**Figure 5C**). The BCR rate in the high-risk group was significantly higher than that in the low-risk group (**Figure 5D**). The risk score was still an independent prognostic factor in the MSKCC (**Figures 5E,F** and **Supplementary Table 3**).

Correlation Between Prognostic Risk Signature and Clinical Features

To test the predictive power of the prognostic risk model for clinical features, we correlated the risk score with the clinical features (i.e., age, BCR state, PSA, GS, WHO ISUP classification, and T-staging). The risk grouping system showed a significant correlation with the BCR state, GS, WHO ISUP classification, and T-staging but not with age and PSA in both cohorts. The high-risk group showed a higher percentage of BCR and higher WHO ISUP classification, GS, and T-staging than the low-risk group. The heat map of gene expression showed that risk factors *AIFM2*, *AKR1C1*, *AKR1C*, *CBS*, *FANCD2*, *FTH1*, *G6PD*, and *NFS1* were highly expressed in the high-risk group, while only *SLC1A5*, as a protective factor, was highly expressed in the low-risk group in both cohorts (**Figure 6** and **Supplementary Table 4**).

Exploration of Potential Mechanism

To explore the mechanism of this risk model, GSEA was used to analyze the potential biological processes and pathways. GSEA results showed that "steroid hormone secretion," "regulation of endocrine processes," and "positive regulation of humoral immune response" were significantly enriched in the high-risk group (**Figures 7A–C**), while the low-risk group was significantly enriched in "androgen response" (**Figure 7D**). In addition, the levels of Ki67 expression were compared between the high- and low-risk groups, which revealed that the level of Ki67 expression was higher in the high-risk group (**Figure 7E**). The

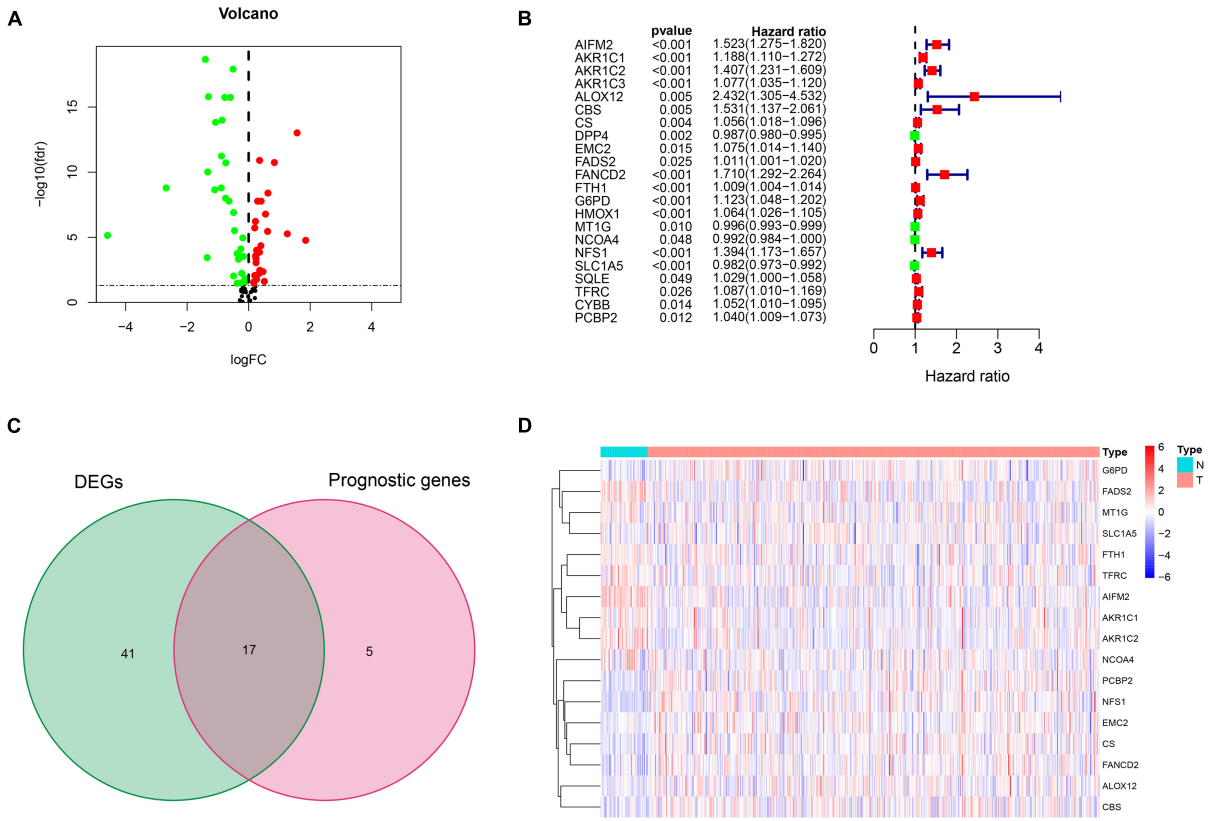

FIGURE 2 | Initial screening of potential prognostic ferroptosis-related genes in The Cancer Genome Atlas (TCGA) cohort. **(A)** Volcano plot of differential expression of ferroptosis-related genes between prostate cancer (PCa) tissues and normal tissues. **(B)** Twenty-two ferroptosis-related genes associated with biochemical recurrence (BCR) of PCa patients through univariate Cox regression analysis. **(C)** Identification of 17 prognostic genes by intersection. **(D)** Heat map of the expression of 17 prognostic genes between PCa and normal tissues.

FPI model constructed by Liu et al. (2020c) showed that a high FPI predicts poor prognosis in various tumors, and it was associated with many important metastasis and immune-related pathways. Therefore, the relationship between the risk score of our prognostic model and FPI was explored. Similarly, the FPI of the high-risk group was significantly higher than that of the low-risk group (**Figure 7F**). Notably, all the presented results are consistent in the TCGA and MSKCC cohorts (**Supplementary Table 5**).

Immune Infiltration and Tumor Microenvironment

Given the above GSEA results and results of previous studies that iron death may be associated with immune cells, immune function, and immune microenvironment, we compared the differences in immune-related parameters between high- and low-risk groups in terms of the infiltration of 16 immune cells and activity of 13 immune-related pathways. In this study, most immune cell and immune function scores were higher in the high-risk group than in the low-risk group (**Figure 8**). In particular, aDCs, Tfh, TIL, APC co-inhibition, checkpoint, cytolytic activity, T-cell co-inhibition, and T-cell co-stimulation scores were significantly enriched in the high-risk group (**Supplementary Table 6**). We used the "ESTIMATE" package to evaluate TME and obtained similar results. With the increase in the risk score, the immune/stromal/ESTIM scores as a predictor of TME also increased, and the purity of the tumor decreased (**Figure 9A** and **Supplementary Table 7**).

Prediction of Antiandrogenic Therapy and Immunotherapy Responses

Alongside radical surgery and radiotherapy, drug therapy, including endocrine therapy and chemotherapy, is an important treatment of PCa. In the GSEA, "androgen response" was significantly enriched in the low-risk group, so we explored whether patients in the high- and low-risk groups responded differently to bicalutamide. The estimated IC50 value demonstrated that the low-risk group in both cohorts had a better response to bicalutamide ($p < 0.0001$) (**Figure 9B**). Similarly, the level of Ki67 expression was higher in the high-risk group than in the low-risk group, suggesting that the high-risk group had more active tumor cell proliferation, faster tumor growth, and worse tissue differentiation than the low-risk group. This also raises the question on whether the response to chemotherapy is different between the high- and low-risk groups. Docetaxel, the most classic chemotherapy drug for PCa,

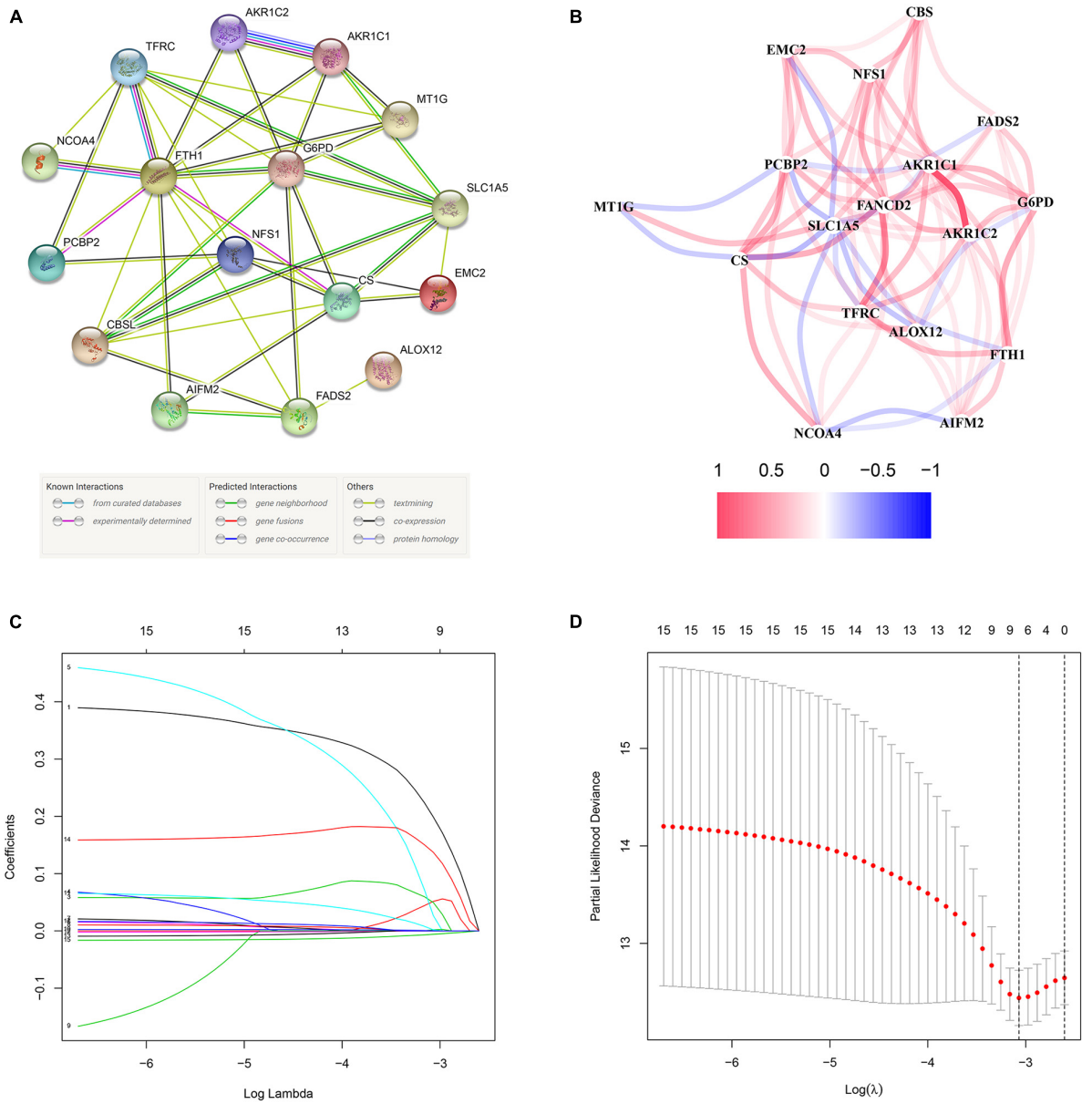

FIGURE 3 | The network of candidate genes and construction of the signature in TCGA cohort. **(A)** The construction of protein–protein interaction (PPI) network by STRING. **(B)** The gene expression correlation network. **(C,D)** A nine-mRNA signature was constructed by LASSO Cox regression.

was also found to have a better response in the low-risk group of the two cohorts, but the difference was not significant in the MSKCC cohort ($p = 0.15$) (**Figure 9C**).

Nomogram for Biochemical Relapse-Free Survival Prediction

To improve the accuracy of the risk score model in predicting bRFS, we combined the risk scores of the two cohorts and constructed a nomogram with conventional clinicopathological features (**Figure 10A**). The C-index (0.751) showed good predictive accuracy for the nomogram. The calibration curves had good linearity for the 1-, 3-, and 5-year bRFS (**Figure 10B**). The nomogram scores achieved a higher AUC–ROC than all other clinicopathological parameters in predicting 1-, 3-, and 5-year bRFS (AUC at 1 year, 0.774; AUC at 3 years, 0.768; AUC at 5 years, 0.789) (**Figure 10C**).

AIFM2 and *NFS1* Were Differentially Expressed in Prostate Cancer Tissues and Were Associated With Poor Outcome

To further explore the mechanisms involved in the risk signature, we focused on the nine ferroptosis-related genes. The coefficients

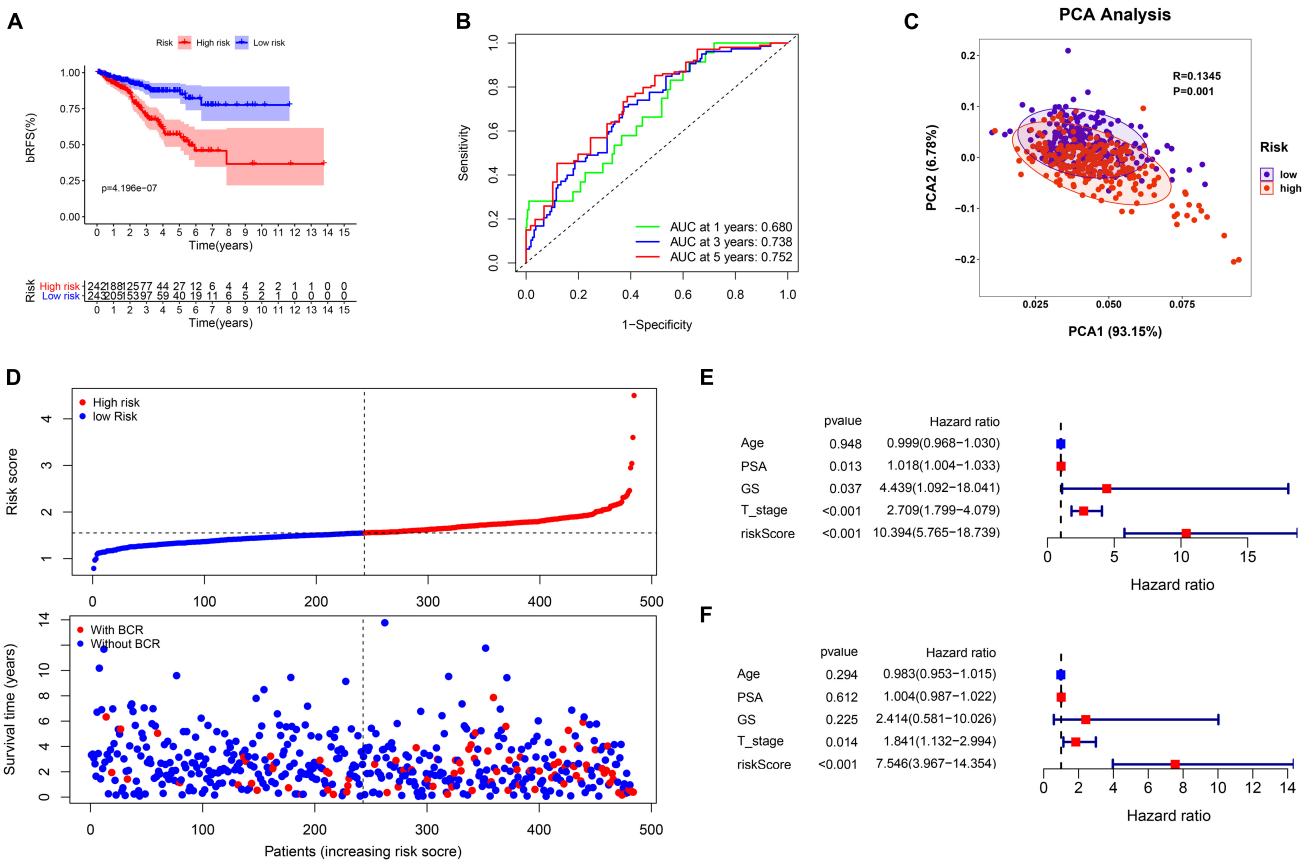

FIGURE 4 | The evaluation of prognostic signature in TCGA cohort. **(A)** The biochemical relapse-free survival (bRFS) analysis of the two subgroups stratified based on the median of risk scores calculated by the risk model. **(B)** Receiver operating characteristic (ROC) curve of model and clinical characteristics predicting 1-, 3-, and 5-year bRFS. **(C)** The two risk groups were distinguished by principal component analysis (PCA). **(D)** The curve of risk score and BCR status of the patients. **(E,F)** Univariate and multivariate Cox regression analyses showed that the risk score had prominent prognostic values.

of *AIFM2* and *NFS1* genes were significantly higher than those of the other seven genes involved in the construction of the signature, and a larger weight often indicates that the gene is more prognostically important (**Figure 11A**). Therefore, *AIFM2* and *NFS1* became the focus of the subsequent research. First, we evaluated the differential expression of *AIFM2* and *NFS1* between the tumor tissues and corresponding normal tissues in multiple datasets. The results of a meta-analysis after combining 15 independent datasets showed that the expression of *AIFM2* in the tumor was lower than that in normal tissues, while opposite results were obtained in *NFS1* ($p < 0.001$) (**Figure 11B**). Furthermore, we found that patients with a high expression of *AIFM2* or *NFS1* had earlier onset of biochemical relapse and that a high expression of *AIFM2* or *NFS1* was associated with higher GS and WHO ISUP grade, poorer clinicopathological stage, and higher positive rate of the surgical margin, but some of the results were not significant because of the small sample size (**Figure 11C**). To verify these findings, IHC of these two genes was performed in 52 pairs of tumor tissues and corresponding normal tissues after radical prostatectomy. The actual results were consistent with the expected results. The expression of *AIFM2* was lower in tumor tissues than in normal tissues, but the high expression of *AIFM2* tended to have higher GS ($p < 0.01$). *NFS1* is highly expressed in tumors; likewise, highly expressed *NFS1* tends to have higher GS ($p < 0.001$) (**Figure 12A**).

Prostate Cancer Cells Are More Sensitive to Ferroptosis Than Normal Prostate Cells

We assessed the sensitivity of PCa cells (DU145) to ferroptosis. Erastin (ferroptosis inducer) treatment decreased the viability of DU145 cells in a dose-dependent manner. Compared with normal human prostate cells (PWR1E), the activities of DU145 cells were significantly decreased at any concentrations of erastin ($p < 0.001$) (**Figure 12B**). By using BODIPY^{TM} 581/591 C11 as a lipid peroxidation probe, we confirmed that the DU145 cell lines induced by erastin produced more lipid peroxidations (green) than the PWR1E cell lines (**Figure 12C**). In addition, the levels of Fe^{2+} release, MDA, DCF, and GSH in DU145 cells were measured for 24 h under different treatment conditions. After induction by erastin, Fe^{2+}, MDA, and DCF levels in DU145 cells were significantly increased, while the GSH level was significantly

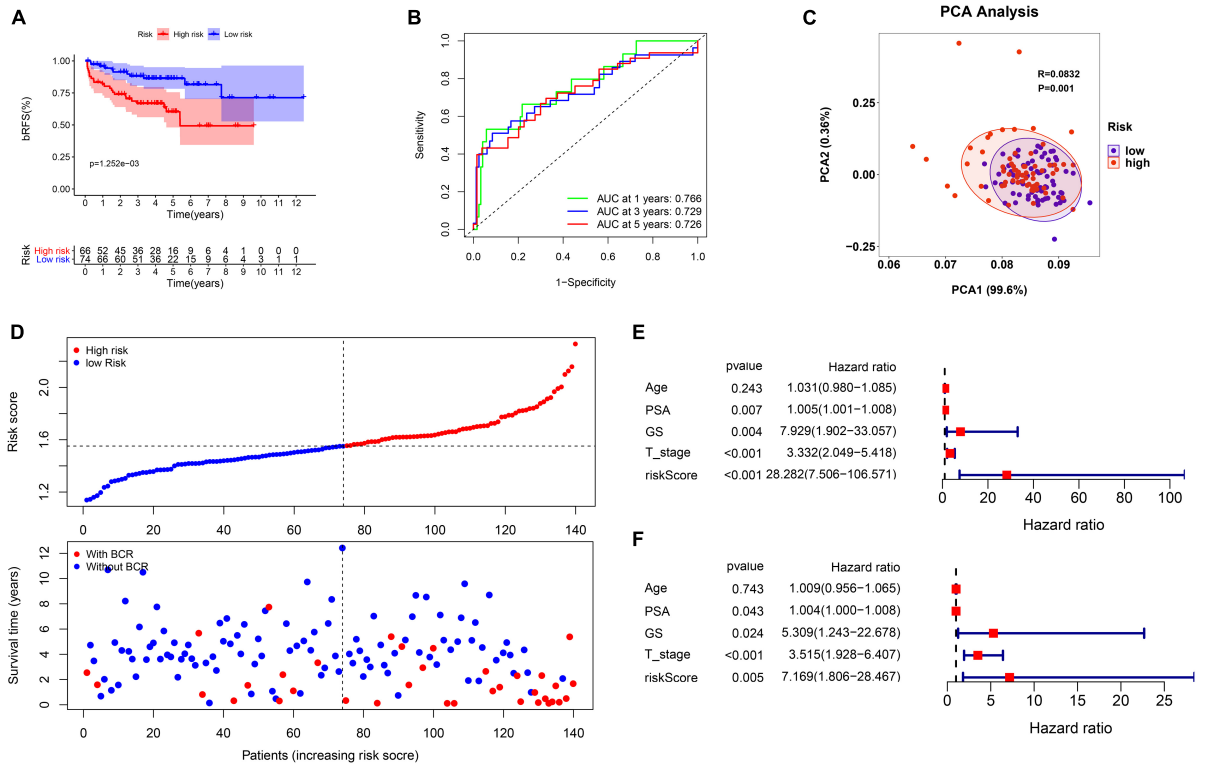

FIGURE 5 | The validation of prognostic signature in MSK-IMPACT Clinical Sequencing Cohort (MSKCC) cohort. **(A)** The bRFS analysis of the two subgroups stratified based on the median of risk scores calculated by the risk model. **(B)** ROC curve of model and clinical characteristics predicting 1-, 3-, and 5-year bRFS. **(C)** The two risk groups were distinguished by PCA. **(D)** The curve of risk score and BCR status of the patients. **(E,F)** Univariate and multivariate Cox regression analyses showed that the risk score had prominent prognostic values.

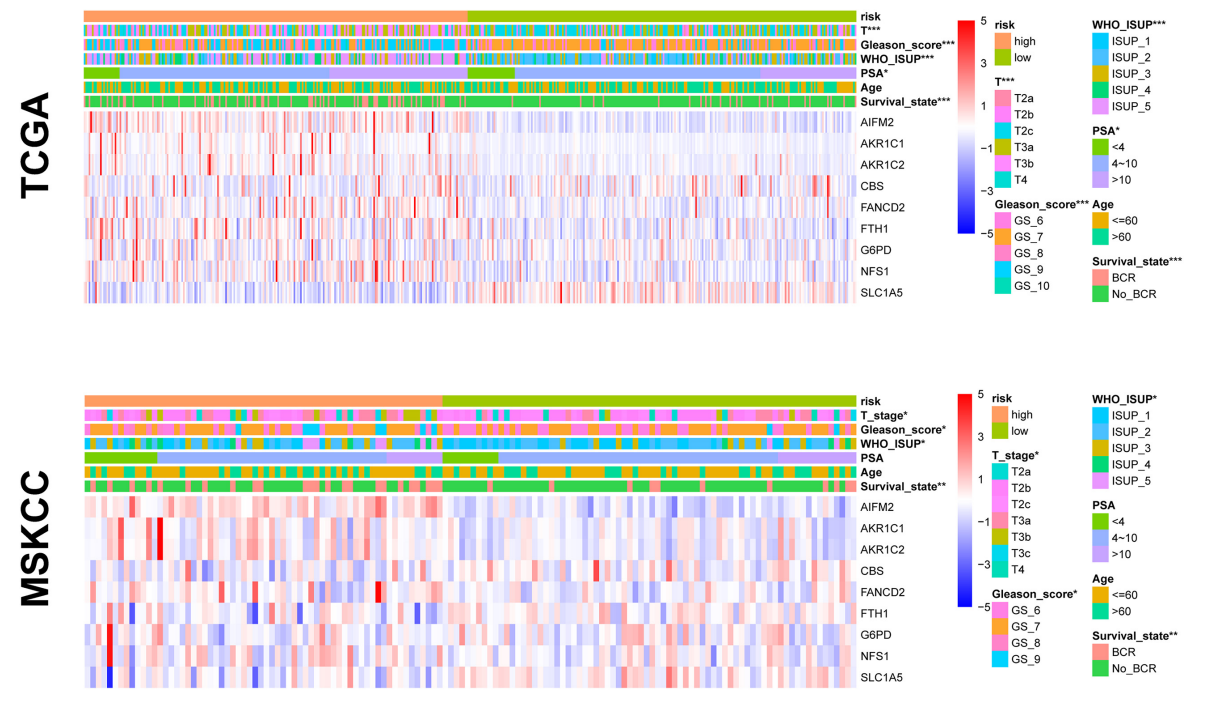

FIGURE 6 | The relationship between prognosis and clinicopathological parameters in two cohorts (*$p < 0.05$; **$p < 0.01$; ***$p < 0.001$).

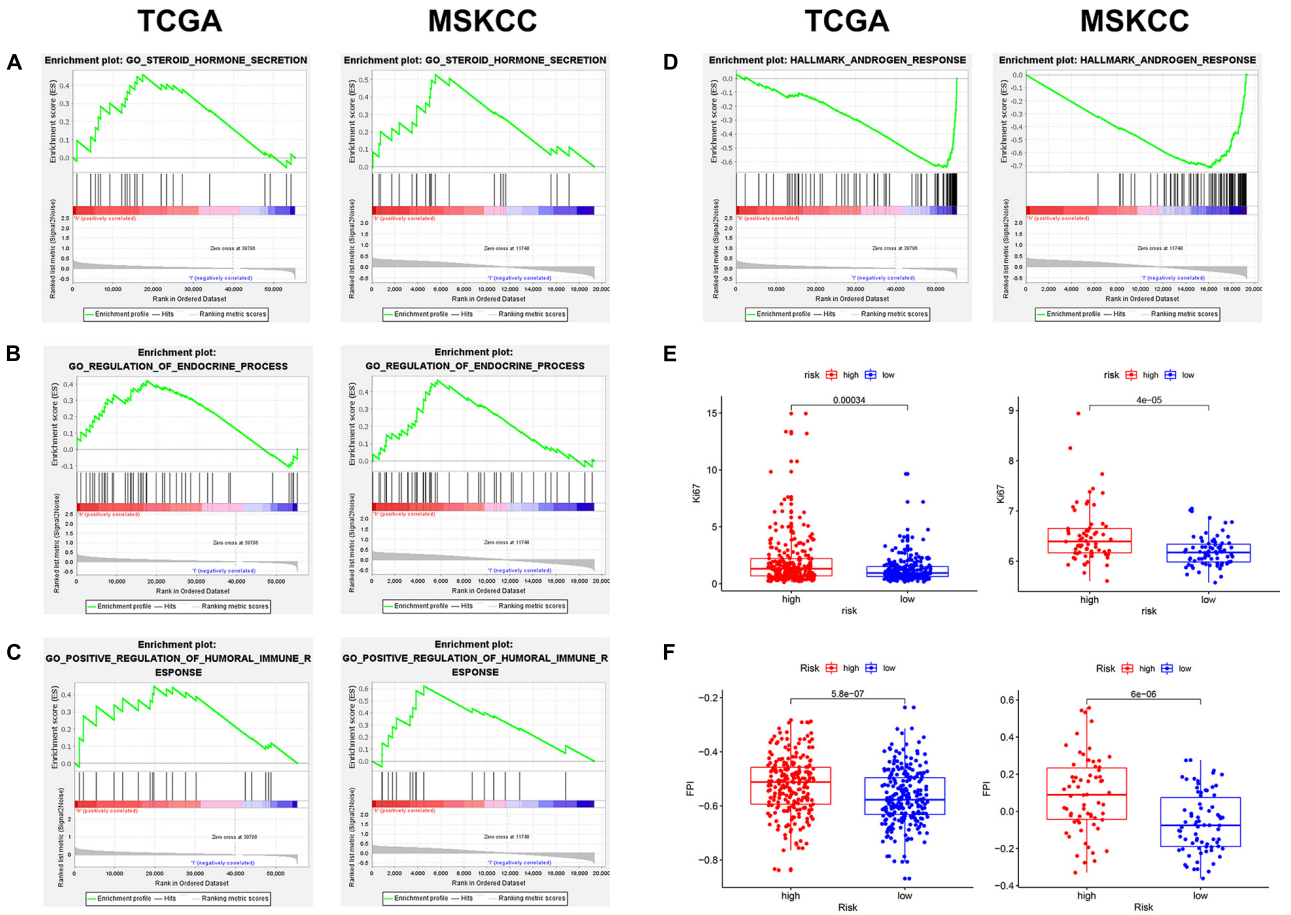

FIGURE 7 | The exploration of potential mechanism about the prognostic signature in two cohorts. **(A–D)** Gene set enrichment analysis (GSEA) results of the high- and low-risk groups. **(E)** The Ki67 expression level was higher in high-risk patients. **(F)** The ferroptosis potential index (FPI) level was higher in high-risk patients.

decreased. This trend can be partially rescued by ferrostatin-1, a ferroptosis inhibitor (**Figure 12D**).

AIFM2 and *NFS1* Knockdowns Promote Ferroptosis and Suppress Proliferation *in vitro* and *in vivo*

Moreover, we detected a difference in the expressions of the *AIFM2* or *NFS1* genes between PCa cell lines and normal cell lines, which was consistent with the analysis results of the tissue samples (**Figure 13A**). To evaluate the potential role of *AIFM2* and *NFS1* in the regulation of PCa ferroptosis, human PCa DU145 cells were treated with control shRNA or target genes shRNA (**Figure 13A**). Erastin-induced lipid peroxidation measured with BODIPY^{TM} 581/591 C11 could be promoted by sh-AIFM2 and sh-NFS1 (**Figure 13B**). As expected, *AIFM2* and *NFS1* knockdowns by shRNA notably increased the levels of Fe^{2+}, MDA, and DCF, but decreased the level of GSH (but not significantly) (**Figure 13C**). The above results indicated that *AIFM2* or *NFS1* knockdown could promote the ferroptosis of PCa cell lines. To date, the phospholipid hydroperoxide-reducing enzyme glutathione peroxidase 4 (*GPX4*) has been known to be the main enzyme that protects against ferroptosis (Stockwell et al., 2017), and Acyl-CoA synthetase long-chain family member 4 (*ACSL4*) is also a key contributor and regulator of ferroptosis, which determines the sensitivity of ferroptosis (Yuan et al., 2016; Doll et al., 2017). Therefore, we tried to explore whether the *AIFM2* and *NFS1* knockdowns affect ferroptosis by affecting the expressions of *GPX4* and *ACSL4* proteins. However, we did not observe significantly positive results (**Figure 13D**), which suggests the involvement of other pathways. In addition, colony formation assays indicated that *AIFM2* or *NFS1* knockdown significantly inhibited cell colony formation. However, it is unclear whether the reduced clonogenic capacity is due to the increase in ferroptosis sensitivity or the decrease in tumor cell proliferation. Therefore, ferrostatin-1 was added after *NFS1*/*AIFM2* knockdown to inhibit ferroptosis. The addition of ferrostatin-1 partially rescued the reduced clonogenic capacity in both sh-*AIFM2* and sh-*NFS1* cells (**Figure 13E**). This illustrated the decreased ability to form colonies after *NFS1*/*AIFM2* knockdown, on the one hand, by promoting ferroptosis, and on the other, by inhibiting cell proliferation ability. This was indeed confirmed by subsequent detection of proliferation markers *Ki67* and proliferating cell nuclear

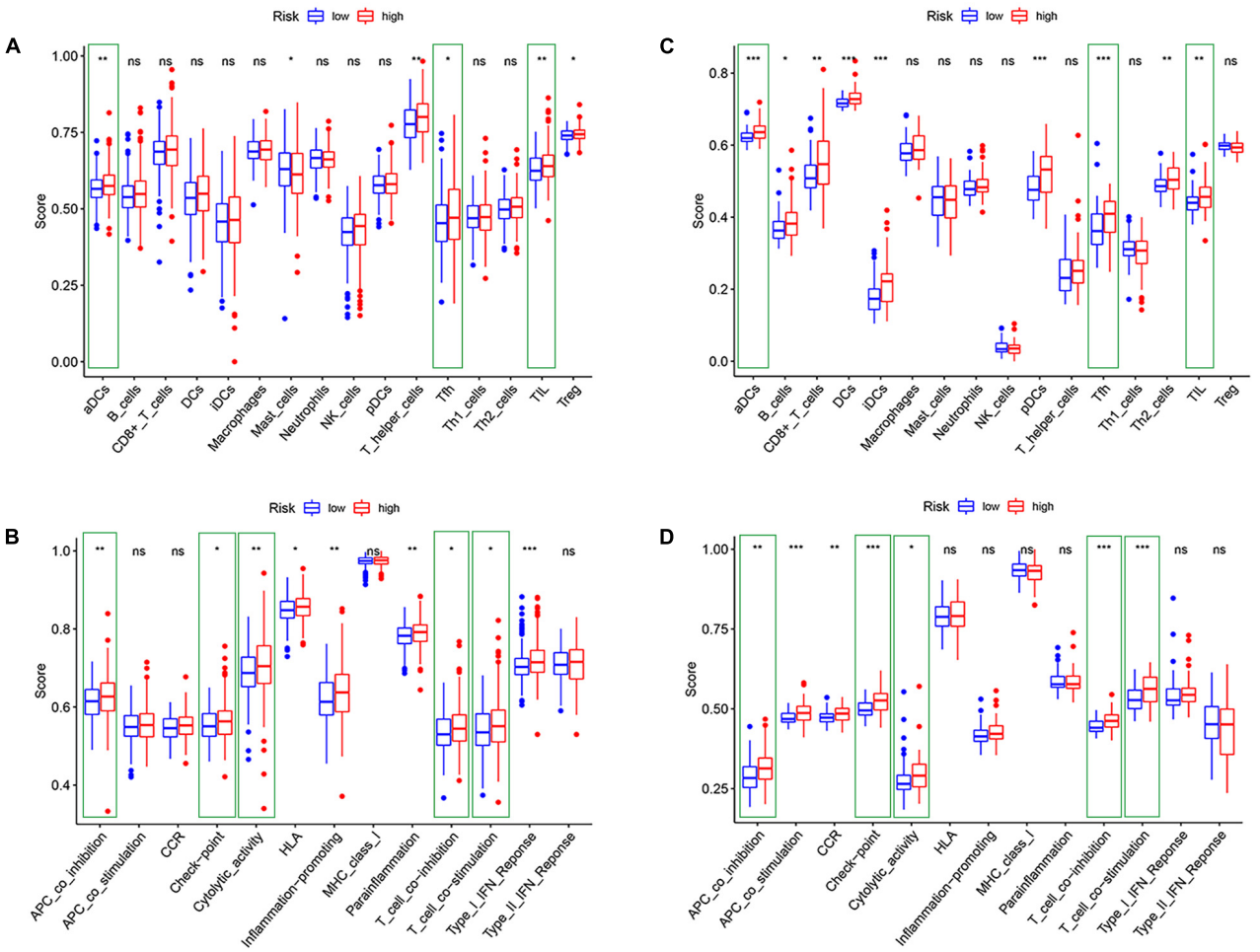

FIGURE 8 | The comparison of immune cells and immune function by single-sample GSEA (ssGSEA) in the two cohorts. **(A,C)** Enrichment results of immune cell score in the two cohorts. **(B,D)** Enrichment results of immune function score in the two cohorts (*$p < 0.05$; **$p < 0.01$; ***$p < 0.001$).

antigen (*PCNA*), which were significantly downregulated in both sh-*AIFM2* and sh-*NFS1* cells (**Figure 13F**). Finally, we further explored the effects of *AIFM2* and *NFS1* on the development of PCa *in vivo*. We found that *AIFM2* and *NFS1* knockdowns both suppressed PCa cell tumorigenicity (**Figure 13G**).

DISCUSSION

Ferroptosis, as a newly discovered form of RCD, regulates cells to death by accumulating iron-dependent extensive lipid peroxidation. This concept was first proposed by Dixon et al. (2012), and its research has grown exponentially in the past few years. Although ferroptosis is still a mysterious veil in physiology, its role in the human pathological state, especially in cancer, has been extensively studied (Jiang et al., 2021). Many studies have recently identified ferroptosis as a natural mechanism of tumor inhibition and have shown that inactivation of ferroptosis can promote tumor development, just like inactivation of apoptosis (Jiang et al., 2015; Zhang et al., 2018). Ferroptosis is also important in the systematic treatment, radiotherapy, and immunotherapy of cancer (Chen et al., 2021). Therapies that rely on ferroptosis provided a new field of cancer treatment (Conrad et al., 2021). Therefore, ferroptosis may become a new marker and a potential prognostic indicator of malignant tumors.

As we suspected, ferroptosis and its related gene signature are closely related to the prognosis of various cancers. Liu et al. (2020a) and Zhuo et al. (2020) constructed ferroptosis-related gene signatures, which were significantly correlated with the diagnosis and prognosis of gliomas. Liang et al. (2020) and Liu et al. (2020b) also developed novel gene signatures associated with ferroptosis, which can be used to predict the prognosis of hepatocellular carcinoma. Tang R. et al. (2020) reported that the ferroptosis pathway is mainly involved in the prognosis of pancreatic cancer and proposed that the combination of immunotherapy and chemotherapy with ferroptosis inducer may

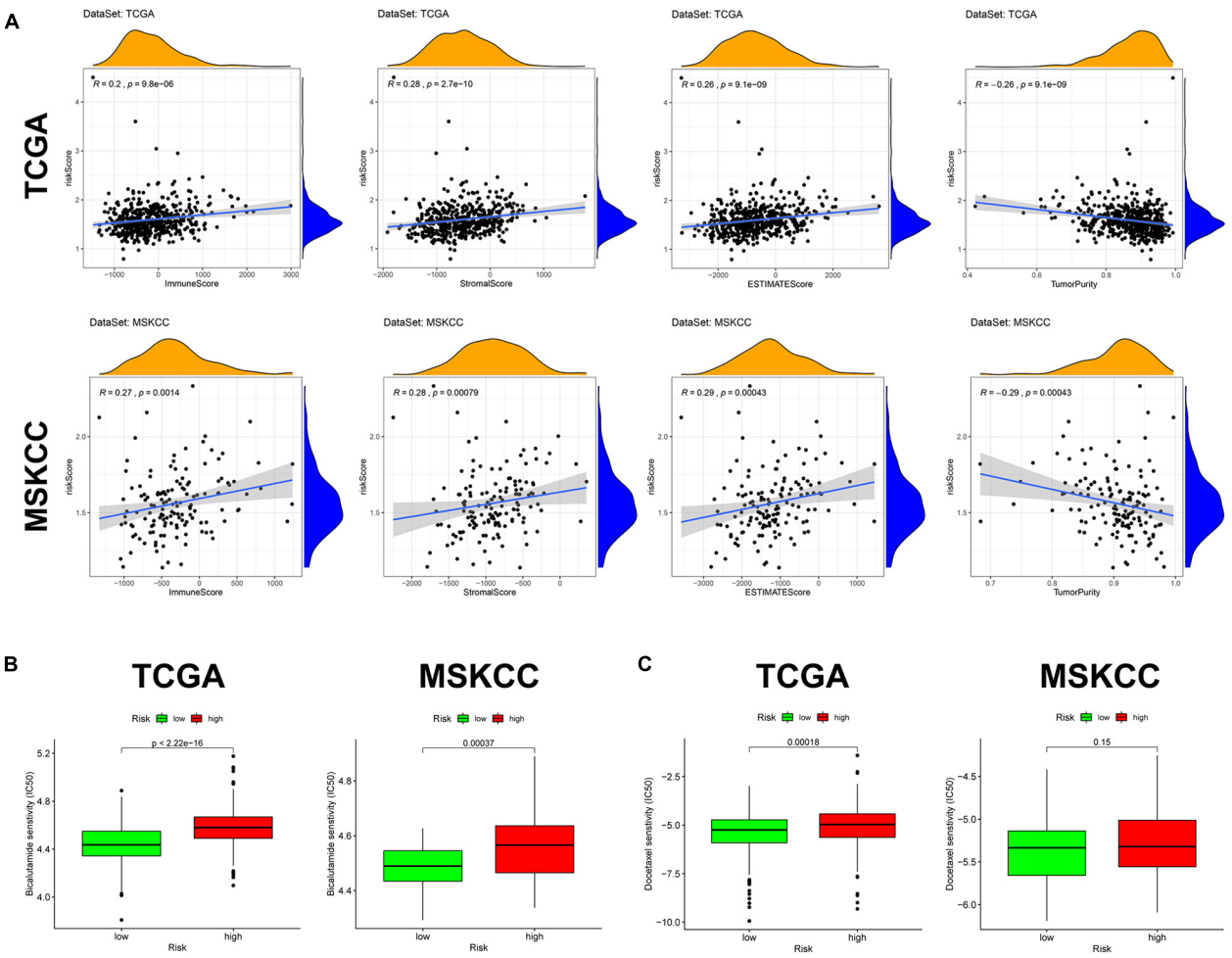

FIGURE 9 | Tumor microenvironment and prediction of therapeutic response in the two cohorts. **(A)** Tumor microenvironment in the two cohorts. **(B)** Sensitivity to bicalutamide in different risk groups. **(C)** Sensitivity to docetaxel in different risk groups.

be a feasible treatment of pancreatic cancer. Similar research results can also be found in lung adenocarcinoma, ovarian carcinoma, and uveal melanoma (Gao et al., 2021; Luo and Ma, 2021; Yang L. et al., 2021). However, no studies have attempted to construct a ferroptosis-related prognostic model of PCa. PCa mainly relies on lipid metabolism to obtain energy (Liu, 2006). The overexpression of lipid metabolism-related genes and proteins has been found in its early and late stages, even in metastatic lesions (Swinnen et al., 2002; Ettinger et al., 2004; Chen et al., 2018; Iglesias-Gato et al., 2018; Zadra and Loda, 2018). These observations suggest that PCa, as a lipid metabolic tumor, may be sensitive to ferroptosis. Ghoochani et al. (2021) used erastin and RSL3, which are ferroptosis inducers, to significantly reduce the growth and migration of PCa cells *in vitro* and significantly delayed the growth of drug-resistant prostate tumors *in vivo* without noticeable side effects. Similarly, Zhou et al. (2020) used flubendazole to elicit valid antitumor effects by promoting ferroptosis in CRPC. Their results are sufficient to confirm that PCa is closely related to ferroptosis, which provides an opportunity to develop a ferroptosis-related prognosis model.

High-throughput gene sequencing technology for biological samples enables large-scale omics research. In this study, we tried to explore a genetic marker based on ferroptosis to predict the BCR of PCa. First, we obtained 17 ferroptosis-related genes potentially associated with the BCR of PCa based on the difference analysis between tumor tissue and normal tissue and results of the univariate Cox regression analysis. Both the protein interaction and gene expression correlation networks suggested that these 17 genes had significant functional and expression correlations. Thus, based on these 17 genes, Lasso regression analysis was adopted to finally construct a nine-ferroptosis-related gene prognosis signature. bRFS analysis showed that the signature could strongly predict the BCR of PCa. Univariate and multivariate Cox regression analyses showed that the calculated risk score was an independent risk factor for the BCR of PCa. In addition, the risk score was positively correlated with poor clinicopathological features, including BCR state, GS, WHO ISUP classification, and T-staging. Mechanism exploration results showed that a high-risk score was associated with steroid secretion, endocrine process, and humoral immune

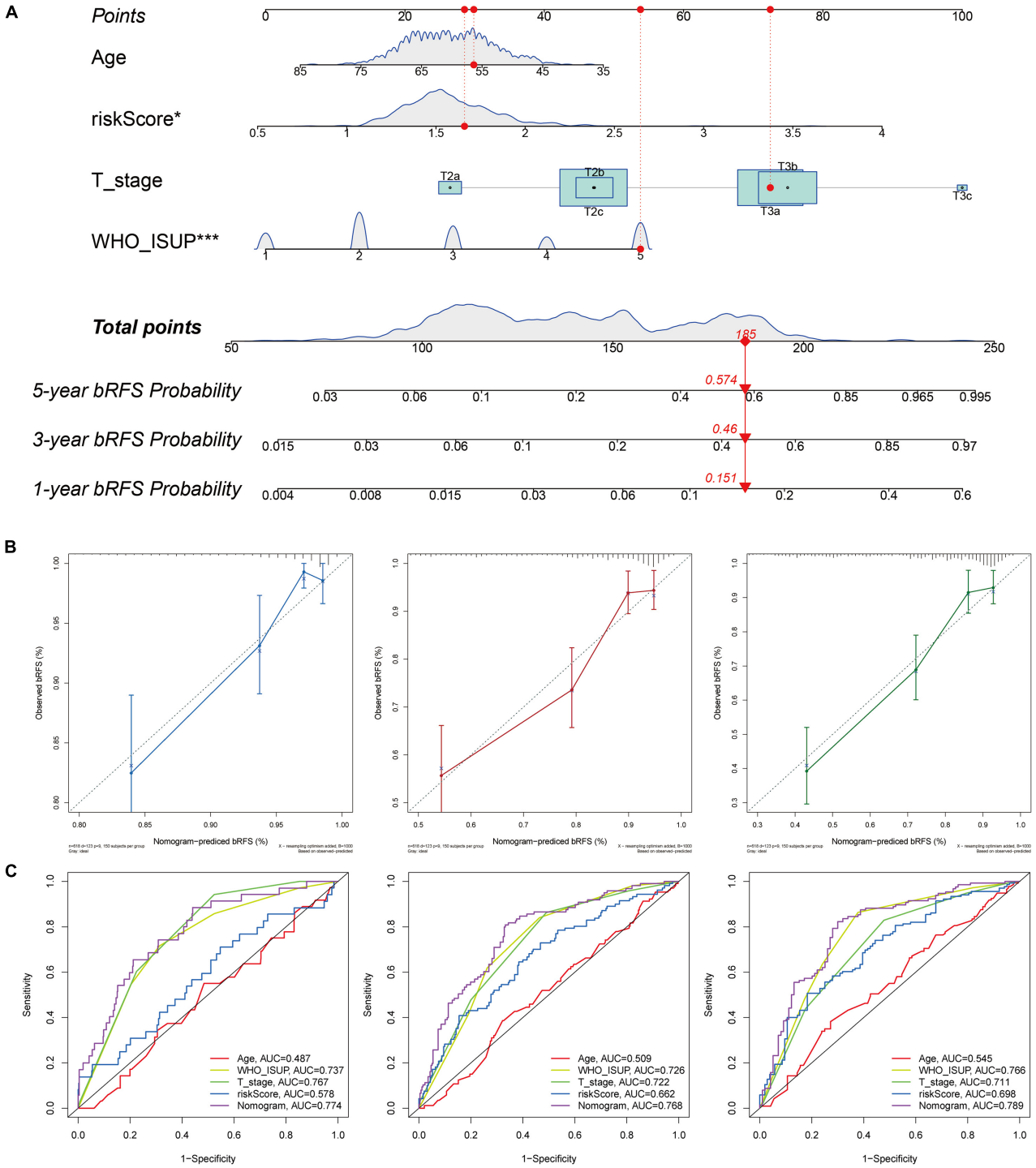

FIGURE 10 | Nomogram for bRFS prediction. **(A)** A prognostic nomogram including signature risk score and other clinical factors. For example, a patient with an age of 56.37, WHO ISUP of 5, a T stage of T3a, and a signature score of 1.6597 had a total nomogram score of 185, implying the 1-, 3-, and 5-year bRFS probability of 15.1, 46, and 57.4%, respectively. **(B)** The calibration curves of the 1-, 3-, and 5-year bRFS. **(C)** ROC curve used to evaluate the 1-, 3-, and 5-year bRFS predictive efficiency.

response, while a low-risk score was associated with androgen response. Metabolic recombination and immune evasion are two distinct characteristics of cancer, but recent studies have shown a close relationship between them (Chang et al., 2015; Hao et al., 2019). The metabolic competition between tumor and immune cells may lead to tumor immunosuppression (Chang et al., 2015).

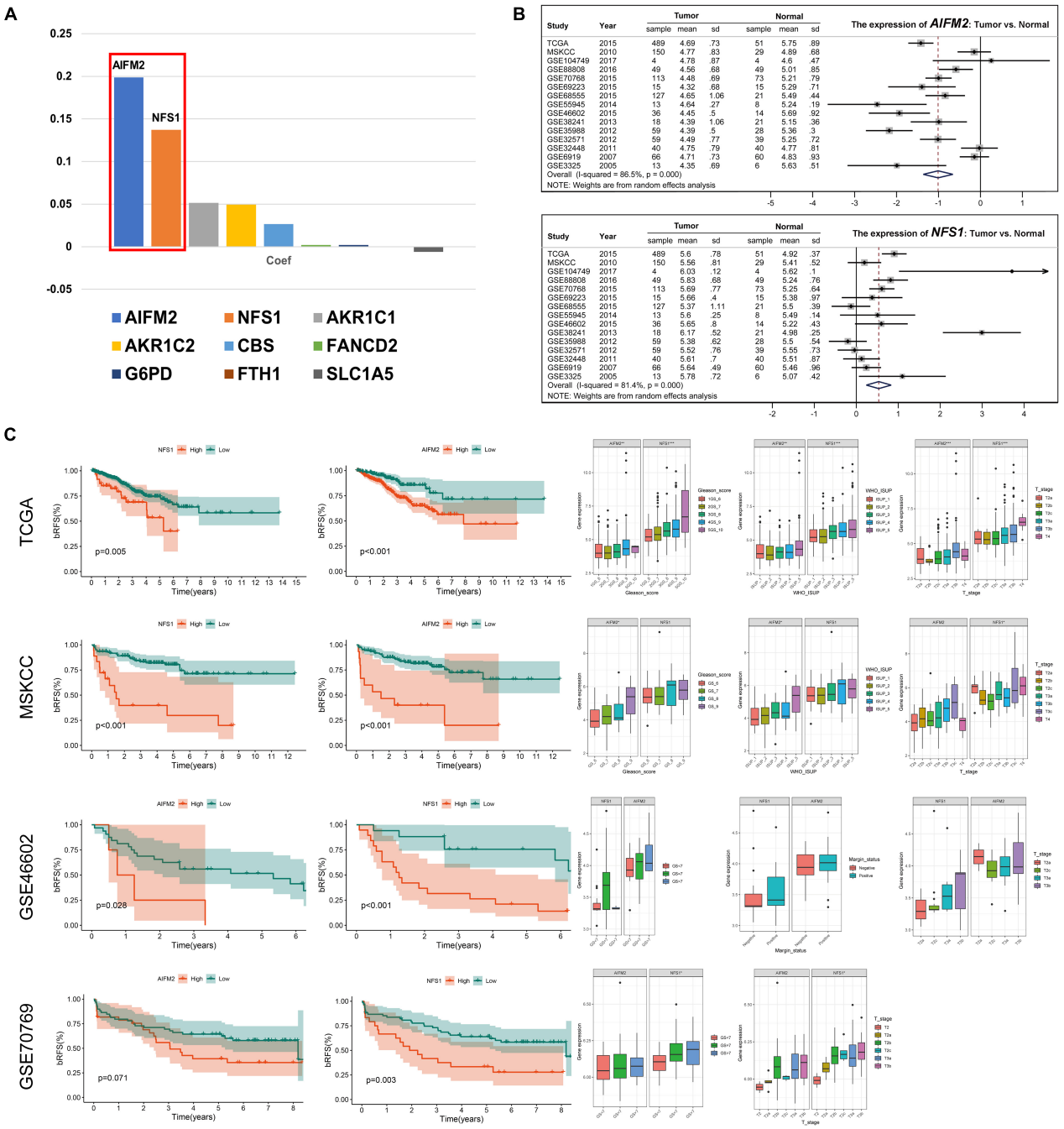

FIGURE 11 | *AIFM2* and *NFS1* were differentially expressed in PCa tissues and were associated with poor outcome. **(A)** The weight coefficient of each component in the signature. **(B)** The differential expression of *AIFM2* and *NFS1* in tumor and normal tissues based on multiple datasets. **(C)** *AIFM2* and *NFS1* were significantly associated with prognosis based on multiple datasets (*$p < 0.05$; **$p < 0.01$; ***$p < 0.001$).

We confirmed that the higher the risk score, the higher the degree of immune cell infiltration, the more active the immune-related function, and the higher the immune/stromal/ESTIM scores. Owing to the different expressions of Ki67 and different responses to androgen in high- and low-risk groups, we explored whether the signature could predict the response of patients to chemotherapy and endocrine therapy. Predictably, patients in the low-risk group responded better to docetaxel and bicalutamide than those in the high-risk group. Notably, all the above results were confirmed in two independent PCa cohorts (TCGA and MSKCC).

In our analysis of the nine-gene model, among the most important predictors of the model, we found that *AIFM2* and *NFS1* genes account for more than half of the weight of the

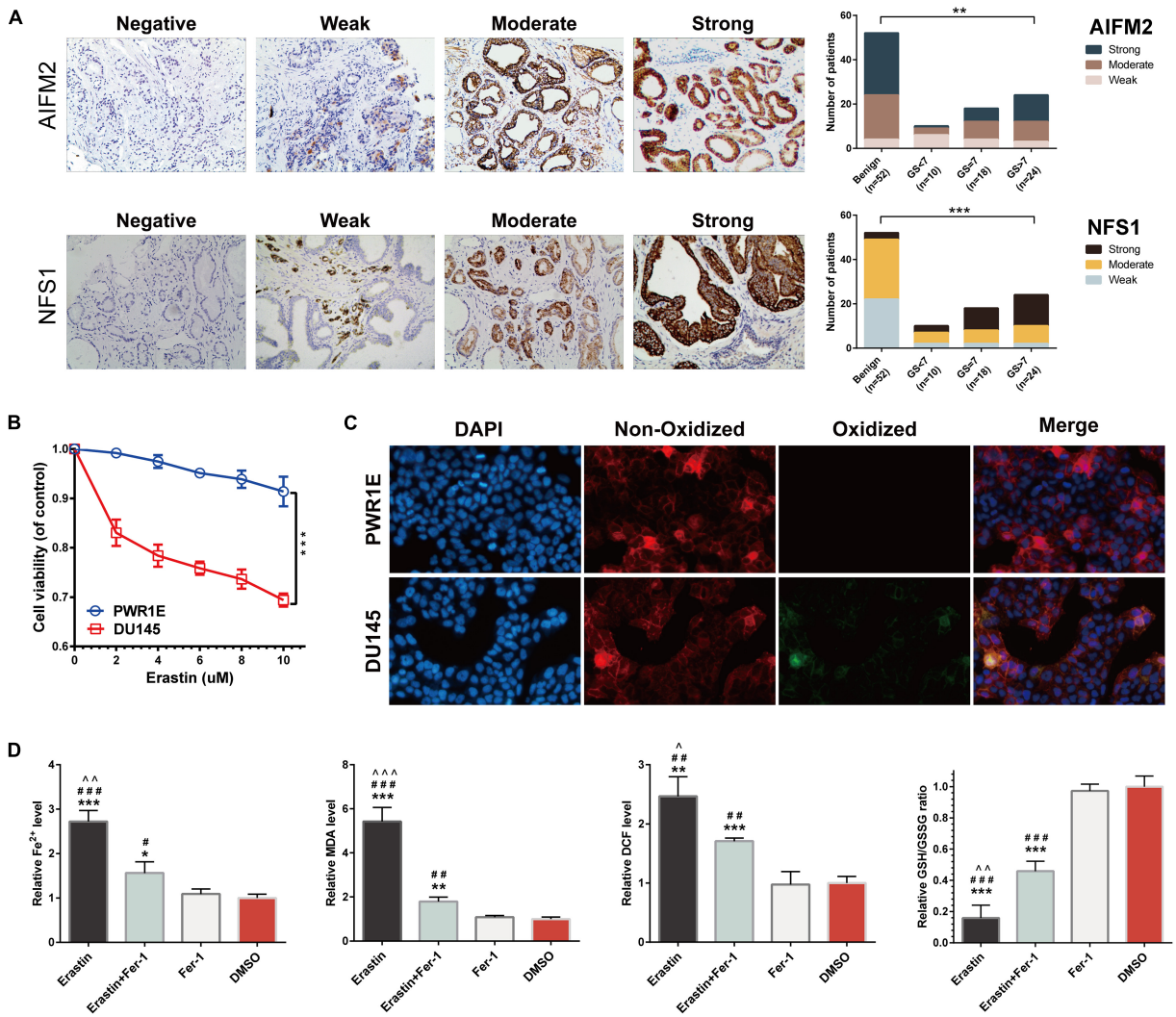

FIGURE 12 | Immunohistochemistry (IHC) verification of *AIFM2* and *NFS1* and sensitivity verification of PCa cells to ferroptosis. **(A)** The protein expression of *AIFM2* and *NFS1* in tumor and normal tissues by IHC. **(B)** Cell viability was assessed following exposure of DU145 cells and PWR1E cells to different concentrations of erastin. **(C)** Immunofluorescence staining of oxidized lipid reactive oxygen species (ROS) (green color) and reduced lipid ROS (red color) formation in DU145 and PWR1E cells treated with erastin for 24 h. **(D)** Fe^{2+} release, malondialdehyde (MDA), DCF, and glutathione (GSH) levels detected by Assay Kit in DU145 cells incubated with erastin, ferrostatin-1, both, and DMSO for 24 h (*$p < 0.05$; **$p < 0.01$; ***$p < 0.001$; #$p < 0.05$; ##$p < 0.01$; ###$p < 0.001$; ^$p < 0.05$; ^^$p < 0.01$; ^^^$p < 0.001$).

model, which mainly determines the risk score of the patients. In our review of existing studies, *AIFM2*, also called ferroptosis suppressor protein 1, can catalyze CoQ10 regeneration by NAD(P)H. As a lipophilic radical-trapping antioxidant, CoQ10 can halt the propagation of lipid peroxides and prevent the damage of the plasma membrane from peroxide. *AIFM2* protects tumor cells by catalyzing the continuous regeneration of CoQ10 and improving the ability to trap lipid peroxyl radicals to inhibit ferroptosis. The above findings were completed almost simultaneously by two research teams and published back-to-back in the famous journal *Nature* (Bersuker et al., 2019; Doll et al., 2019). Alvarez et al. (2017) found that *NFS1* was generally highly expressed in lung cancer tissues and cell lines. Further experiments showed that *NSF1* collected more sulfur elements from cysteine to produce iron–sulfur clusters, which reduced the release of iron from cells and significantly alleviated hyperoxia-induced ferroptosis. In animal experiments, the tumor formation time was significantly prolonged after *NSF1* knockdown, suggesting a positive selection for *NSF1* during the development of lung cancer to overcome cell ferroptosis. These findings were also published in *Nature*. Subsequently, we conducted *in vivo* and *in vitro* experiments to evaluate the prognostic significance of these two genes in PCa and to explore their influence on ferroptosis, and the results were widely validated.

In addition to *AIFM2* and *NFS1*, the remaining seven genes in the signature were also associated with cancer in both basic and clinical research fields. *AKR1C1* and *AKR1C2* were prognostic

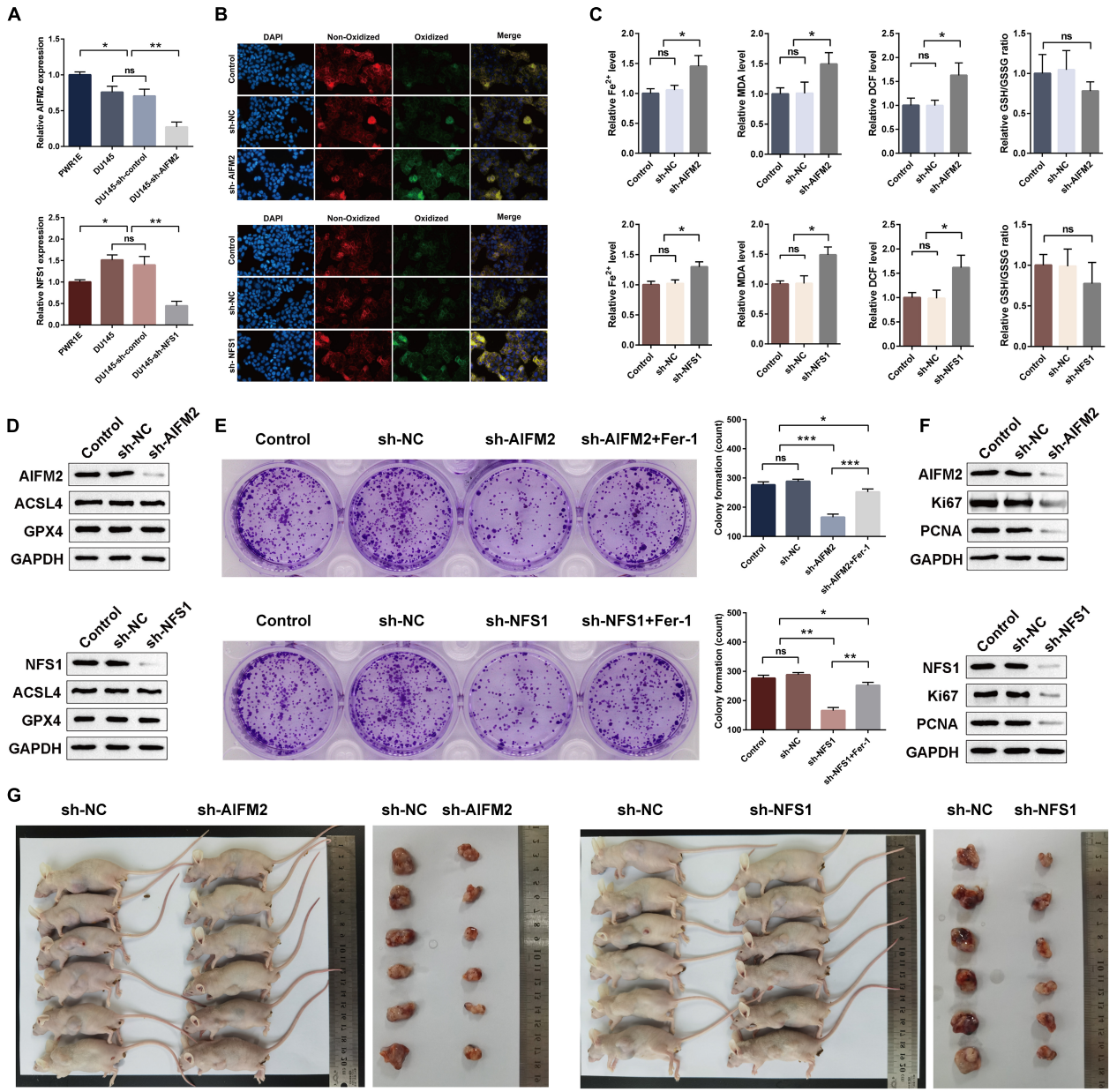

FIGURE 13 | *AIFM2* and *NFS1* knockdowns promote ferroptosis and suppress proliferation *in vitro* and *in vivo*. **(A)** The real-time quantitative polymerase chain reaction (RT-qPCR) analysis of *AIFM2* and *NFS1* expression levels in PWR1E, DU145, DU145 sh-control, and DU145 sh-*AIFM2/NFS1*. **(B)** Immunofluorescence staining of oxidized lipid ROS (green color) and reduced lipid ROS (red color) formation in DU145 after *AIFM2/NFS1* knockdown. **(C)** Fe^{2+} release, MDA, DCF, and GSH levels detected by Assay Kit in DU145 cells after *AIFM2/NFS1* knockdown. **(D)** The Western blot analysis of *ACSL4* and *GPX4* expression levels after *AIFM2/NFS1* knockdown. **(E)** Colony formation assays were constructed in *AIFM2/NFS1* knockdown DU145 cells. **(F)** The Western blot analysis of *Ki67* and *PCNA* expression levels after AIFM2/NFS1 knockdown. **(G)** Xenograft tumors in nude mouse models (*$p < 0.05$; **$p < 0.01$; ***$p < 0.001$).

factors of breast cancer (Wenners et al., 2016), and selective loss of these genes may help enhance endocrine therapy in breast cancer (Ji et al., 2004). Moreover, the overexpression of *AKR1C1/AKR1C2* may serve as a biomarker of chemoresistance in non-small cell lung cancer cells (Wang et al., 2007). Recent studies have shown that CBS promotes the growth of colon and ovarian cancer in preclinical models (Zhu et al., 2018), and CBS blockers have the potential as adjuvants in the treatment of breast cancer to reduce the ability of cancer cells to resist oxidative stress induced by many chemotherapeutic drugs (Sen et al., 2015). *FANCD2* was a sensitive and independent prognostic factor for breast cancer (Fagerholm et al., 2013), and its overexpression is a reliable indicator of lymph node metastasis in colorectal cancer (Ozawa et al., 2010). *FTH1* was highly expressed in primary liver tumors, and its lower expression was associated with better survival (Muhammad et al., 2020). FTH1 pseudogenes, as

competitive endogenous RNAs, play various roles in oncology, particularly in PCa (Chan et al., 2018; Di Sanzo et al., 2020). Blocking the glycosylation of G6PD, the rate-limiting enzyme of the pentose phosphate pathway, can reduce the proliferation of cancer cells *in vitro* and tumor growth *in vivo* (Rao et al., 2015). *SLC1A5* plays an important role in glutamine transport by controlling the metabolism, growth, and survival of lung cancer cells (Hassanein et al., 2013), and its variant is a mitochondrial glutamine transporter for cancer metabolic reprogramming (Yoo et al., 2020).

This study has some limitations. First, the results were based on retrospective public datasets that need to be verified in a prospective cohort in the future. Second, owing to the inherent intratumoral heterogeneity and the technical noise caused by cross-platform sequencing, how to correctly standardize the expression data is the ultimate challenge for the clinical application of this nine-gene signature. Therefore, the RNA-seq data of the patients need data preprocessing, such as scaling and normalization, in future clinical applications. It is even possible to develop a standardized and commercial gene detection kit based on these nine genes, which can automatically calculate the risk score for risk grouping. Finally, the underlying biological mechanisms of this signature, in particular, how *AIFM2* and *NFS1* influence the ferroptosis process in PCa, remain unknown. At present, research on the two genes is still in the embryonic stage, so further research is needed.

In summary, we constructed a nine-gene signature associated with ferroptosis, which can accurately predict the BCR of PCa. The higher the risk score, the higher the probability of developing BCR, the worse the clinicopathological characteristics, and the worse the response to chemotherapy and antiandrogen therapy. This signature can be used as a novel tool for distinguishing high- and low-risk PCa populations and help in understanding the mechanism of cellular ferroptosis in the carcinogenesis and development of PCa.

DATA AVAILABILITY STATEMENT

Publicly available datasets were analyzed in this study. This data can be found here: All raw data can be downloaded from the TCGA Research Network (https://www.cancer.gov/tcga), Cbioportal database (https://www.cbioportal.org/), Gene Expression Omnibus repository (https://www.ncbi.nlm.nih.gov/geo/), and the MSigDB (https://www.gsea-msigdb.org/gsea/msigdb/).

ETHICS STATEMENT

The studies involving human participants were reviewed and approved by the Ethics Committee of the Beijing Hospital. The patients/participants provided their written informed consent to participate in this study. The animal study was reviewed and approved by the Institutional Ethics Committee of Xiangya Hospital, Central South University.

AUTHOR CONTRIBUTIONS

ZL developed the methodology, performed the formal analysis, and wrote the original draft. JLW supervised the study and acquired the funding. XW was in charge of the data curation and acquired the funding. MM acquired the funding. GT was in charge of the software and validation. HX investigated and validated the study. JYW was in charge of the project administration. YL acquired the funding and resources. ML acquired the funding and wrote, reviewed, and edited the manuscript. All authors contributed to the article and approved the submitted version.

FUNDING

This work was supported by the Beijing Hospital Clinical Research 121 Project (BJ-2018-090 and BJ-2020-171), the Fundamental Research Funds for the Central Universities (3332019122 and 3332020069), and the National Natural Science Foundation of China (81874094, 82172878, and 82103639).

SUPPLEMENTARY MATERIAL

The Supplementary Material for this article can be found online at: https://www.frontiersin.org/articles/10.3389/fcell.2021.666025/full#supplementary-material

REFERENCES

Alvarez, S. W., Sviderskiy, V. O., Terzi, E. M., Papagiannakopoulos, T., Moreira, A. L., Adams, S., et al. (2017). NFS1 undergoes positive selection in lung tumours and protects cells from ferroptosis. *Nature* 551, 639–643. doi: 10.1038/nature24637

Bersuker, K., Hendricks, J. M., Li, Z., Magtanong, L., Ford, B., Tang, P. H., et al. (2019). The CoQ oxidoreductase FSP1 acts parallel to GPX4 to inhibit ferroptosis. *Nature* 575, 688–692. doi: 10.1038/s41586-019-1705-2

Brockman, J. A., Alanee, S., Vickers, A. J., Scardino, P. T., Wood, D. P., Kibel, A. S., et al. (2015). Nomogram predicting prostate cancer-specific mortality for men with biochemical recurrence after radical prostatectomy. *Eur. Urol.* 67, 1160–1167. doi: 10.1016/j.eururo.2014.09.019

Chan, J. J., Kwok, Z. H., Chew, X. H., Zhang, B., Liu, C., Soong, T. W., et al. (2018). A FTH1 gene:pseudogene:microRNA network regulates tumorigenesis in prostate cancer. *Nucleic Acids Res.* 46, 1998–2011. doi: 10.1093/nar/gkx1248

Chang, C. H., Qiu, J., O'Sullivan, D., Buck, M. D., Noguchi, T., Curtis, J. D., et al. (2015). Metabolic competition in the tumor microenvironment is a driver of cancer progression. *Cell* 162, 1229–1241. doi: 10.1016/j.cell.2015.08.016

Chen, M., Zhang, J., Sampieri, K., Clohessy, J. G., Mendez, L., Gonzalez-Billalabeitia, E., et al. (2018). An aberrant SREBP-dependent lipogenic program promotes metastatic prostate cancer. *Nat. Genet.* 50, 206–218. doi: 10.1038/s41588-017-0027-2

Chen, X., Kang, R., Kroemer, G., and Tang, D. (2021). Broadening horizons: the role of ferroptosis in cancer. *Nat. Rev. Clin. Oncol.* 18, 280–296. doi: 10.1038/s41571-020-00462-0

Conrad, M., Lorenz, S. M., and Proneth, B. (2021). Targeting ferroptosis: new hope for as-yet-incurable diseases. *Trends Mol. Med.* 27, 113–122. doi: 10.1016/j.molmed.2020.08.010

Di Sanzo, M., Quaresima, B., Biamonte, F., Palmieri, C., and Faniello, M. C. (2020). FTH1 pseudogenes in cancer and cell metabolism. *Cells* 9:554. doi: 10.3390/cells9122554

Dixon, S. J., Lemberg, K. M., Lamprecht, M. R., Skouta, R., Zaitsev, E. M., Gleason, C. E., et al. (2012). Ferroptosis: an iron-dependent form of nonapoptotic cell death. *Cell* 149, 1060–1072. doi: 10.1016/j.cell.2012.03.042

Doll, S., Freitas, F. P., Shah, R., Aldrovandi, M., da Silva, M. C., Ingold, I., et al. (2019). FSP1 is a glutathione-independent ferroptosis suppressor. *Nature* 575, 693–698. doi: 10.1038/s41586-019-1707-0

Doll, S., Proneth, B., Tyurina, Y. Y., Panzilius, E., Kobayashi, S., Ingold, I., et al. (2017). ACSL4 dictates ferroptosis sensitivity by shaping cellular lipid composition. *Nat. Chem. Biol.* 13, 91–98. doi: 10.1038/nchembio.2239

Ettinger, S. L., Sobel, R., Whitmore, T. G., Akbari, M., Bradley, D. R., Gleave, M. E., et al. (2004). Dysregulation of sterol response element-binding proteins and downstream effectors in prostate cancer during progression to androgen independence. *Cancer Res.* 64, 2212–2221. doi: 10.1158/0008-5472.can-2148-2

Fagerholm, R., Sprott, K., Heikkinen, T., Bartkova, J., Heikkila, P., Aittomaki, K., et al. (2013). Overabundant FANCD2, alone and combined with NQO1, is a sensitive marker of adverse prognosis in breast cancer. *Ann. Oncol.* 24, 2780–2785. doi: 10.1093/annonc/mdt290

Gao, X., Tang, M., Tian, S., Li, J., and Liu, W. (2021). A ferroptosis-related gene signature predicts overall survival in patients with lung adenocarcinoma. *Future Oncol.* 17, 1533–1544. doi: 10.2217/fon-2020-1113

Geeleher, P., Cox, N., and Huang, R. S. (2014). pRRophetic: an R package for prediction of clinical chemotherapeutic response from tumor gene expression levels. *PLoS One* 9:e107468. doi: 10.1371/journal.pone.0107468

Ghoochani, A., Hsu, E. C., Aslan, M., Rice, M. A., Nguyen, H. M., Brooks, J. D., et al. (2021). Ferroptosis inducers are a novel therapeutic approach for advanced prostate cancer. *Cancer Res.* 81, 1583–1594. doi: 10.1158/0008-5472.CAN-20-3477

Hao, Y., Li, D., Xu, Y., Ouyang, J., Wang, Y., Zhang, Y., et al. (2019). Investigation of lipid metabolism dysregulation and the effects on immune microenvironments in pan-cancer using multiple omics data. *BMC Bioinform.* 20(Suppl. 7):195. doi: 10.1186/s12859-019-2734-4

Hassanein, M., Hoeksema, M. D., Shiota, M., Qian, J., Harris, B. K., Chen, H., et al. (2013). SLC1A5 mediates glutamine transport required for lung cancer cell growth and survival. *Clin. Cancer Res.* 19, 560–570. doi: 10.1158/1078-0432.CCR-12-2334

Hassannia, B., Vandenabeele, P., and Vanden Berghe, T. (2019). Targeting ferroptosis to iron out cancer. *Cancer Cell* 35, 830–849. doi: 10.1016/j.ccell.2019.04.002

Iglesias-Gato, D., Thysell, E., Tyanova, S., Crnalic, S., Santos, A., Lima, T. S., et al. (2018). The proteome of prostate cancer bone metastasis reveals heterogeneity with prognostic implications. *Clin. Cancer Res.* 24, 5433–5444. doi: 10.1158/1078-0432.CCR-18-1229

Ji, Q., Aoyama, C., Nien, Y. D., Liu, P. I., Chen, P. K., Chang, L., et al. (2004). Selective loss of AKR1C1 and AKR1C2 in breast cancer and their potential effect on progesterone signaling. *Cancer Res.* 64, 7610–7617. doi: 10.1158/0008-5472.CAN-04-1608

Jiang, L., Kon, N., Li, T., Wang, S. J., Su, T., Hibshoosh, H., et al. (2015). Ferroptosis as a p53-mediated activity during tumour suppression. *Nature* 520, 57–62. doi: 10.1038/nature14344

Jiang, X., Stockwell, B. R., and Conrad, M. (2021). Ferroptosis: mechanisms, biology and role in disease. *Nat. Rev. Mol. Cell. Biol.* 22, 266–282. doi: 10.1038/s41580-020-00324-8

Liang, C., Zhang, X., Yang, M., and Dong, X. (2019). recent progress in ferroptosis inducers for cancer therapy. *Adv. Mater* 31:e1904197. doi: 10.1002/adma.201904197

Liang, J. Y., Wang, D. S., Lin, H. C., Chen, X. X., Yang, H., Zheng, Y., et al. (2020). A novel ferroptosis-related gene signature for overall survival prediction in patients with hepatocellular carcinoma. *Int. J. Biol. Sci.* 16, 2430–2441. doi: 10.7150/ijbs.45050

Liu, Y. (2006). Fatty acid oxidation is a dominant bioenergetic pathway in prostate cancer. *Prostate Cancer Prostatic Dis.* 9, 230–234. doi: 10.1038/sj.pcan.4500879

Liu, Y., Xu, Z., Jin, T., Xu, K., Liu, M., and Xu, H. (2020a). Ferroptosis in low-grade glioma: a new marker for diagnosis and prognosis. *Med. Sci. Monit.* 26:e921947. doi: 10.12659/MSM.921947

Liu, Y., Zhang, X., Zhang, J., Tan, J., Li, J., and Song, Z. (2020b). Development and validation of a combined ferroptosis and immune prognostic classifier for hepatocellular carcinoma. *Front. Cell Dev. Biol.* 8:596679. doi: 10.3389/fcell.2020.596679

Liu, Z., Zhao, Q., Zuo, Z. X., Yuan, S. Q., Yu, K., Zhang, Q., et al. (2020c). Systematic analysis of the aberrances and functional implications of ferroptosis in cancer. *iScience* 23:101302. doi: 10.1016/j.isci.2020.101302

Luo, H., and Ma, C. (2021). A novel ferroptosis-associated gene signature to predict prognosis in patients with uveal melanoma. *Diagnostics* 11:219. doi: 10.3390/diagnostics11020219

Manz, D. H., Blanchette, N. L., Paul, B. T., Torti, F. M., and Torti, S. V. (2016). Iron and cancer: recent insights. *Ann. N.Y. Acad. Sci.* 1368, 149–161. doi: 10.1111/nyas.13008

Mottet, N., van den Bergh, R. C. N., Briers, E., Van den Broeck, T., Cumberbatch, M. G., De Santis, M., et al. (2020). EAU-EANM-ESTRO-ESUR-SIOG guidelines on prostate cancer-2020 update. part 1: screening, diagnosis, and local treatment with curative intent. *Eur. Urol.* 79, 243–262. doi: 10.1016/j.eururo.2020.09.042

Muhammad, J. S., Bajbouj, K., Shafarin, J., and Hamad, M. (2020). Estrogen-induced epigenetic silencing of FTH1 and TFRC genes reduces liver cancer cell growth and survival. *Epigenetics* 15, 1302–1318. doi: 10.1080/15592294.2020.1770917

Ozawa, H., Iwatsuki, M., Mimori, K., Sato, T., Johansson, F., Toh, H., et al. (2010). FANCD2 mRNA overexpression is a bona fide indicator of lymph node metastasis in human colorectal cancer. *Ann. Surg. Oncol.* 17, 2341–2348. doi: 10.1245/s10434-010-1002-7

Pound, C. R., Partin, A. W., Eisenberger, M. A., Chan, D. W., Pearson, J. D., and Walsh, P. C. (1999). Natural history of progression after PSA elevation following radical prostatectomy. *JAMA* 281, 1591–1597. doi: 10.1001/jama.281.17.1591

Qin, Z., Ou, S., Xu, L., Sorensen, K., Zhang, Y., Hu, D. P., et al. (2021). Design and synthesis of isothiocyanate-containing hybrid androgen receptor (AR) antagonist to downregulate AR and induce ferroptosis in GSH-Deficient prostate cancer cells. *Chem. Biol. Drug. Des.* 97, 1059–1078. doi: 10.1111/cbdd.13826

Rao, X., Duan, X., Mao, W., Li, X., Li, Z., Li, Q., et al. (2015). O-GlcNAcylation of G6PD promotes the pentose phosphate pathway and tumor growth. *Nat. Commun.* 6:8468. doi: 10.1038/ncomms9468

Rooney, M. S., Shukla, S. A., Wu, C. J., Getz, G., and Hacohen, N. (2015). Molecular and genetic properties of tumors associated with local immune cytolytic activity. *Cell* 160, 48–61. doi: 10.1016/j.cell.2014.12.033

Sen, S., Kawahara, B., Gupta, D., Tsai, R., Khachatryan, M., Roy-Chowdhuri, S., et al. (2015). Role of cystathionine beta-synthase in human breast cancer. *Free Radic Biol. Med.* 86, 228–238. doi: 10.1016/j.freeradbiomed.2015.05.024

Siegel, R. L., Miller, K. D., and Jemal, A. (2020). Cancer statistics, 2020. *CA Cancer J. Clin.* 70, 7–30. doi: 10.3322/caac.21590

Simmons, M. N., Stephenson, A. J., and Klein, E. A. (2007). Natural history of biochemical recurrence after radical prostatectomy: risk assessment for secondary therapy. *Eur. Urol.* 51, 1175–1184. doi: 10.1016/j.eururo.2007.01.015

Stockwell, B. R., Friedmann Angeli, J. P., Bayir, H., Bush, A. I., Conrad, M., Dixon, S. J., et al. (2017). Ferroptosis: a regulated cell death nexus linking metabolism, redox biology, and disease. *Cell* 171, 273–285. doi: 10.1016/j.cell.2017.09.021

Swinnen, J. V., Roskams, T., Joniau, S., Van Poppel, H., Oyen, R., Baert, L., et al. (2002). Overexpression of fatty acid synthase is an early and common event in the development of prostate cancer. *Int. J. Cancer* 98, 19–22. doi: 10.1002/ijc.10127

Tang, D., Chen, X., Kang, R., and Kroemer, G. (2020). Ferroptosis: molecular mechanisms and health implications. *Cell Res.* 31, 107–125. doi: 10.1038/s41422-020-00441-1

Tang, R., Hua, J., Xu, J., Liang, C., Meng, Q., Liu, J., et al. (2020). The role of ferroptosis regulators in the prognosis, immune activity and gemcitabine resistance of pancreatic cancer. *Ann. Transl. Med.* 8:1347. doi: 10.21037/atm-20-2554a

Tousignant, K. D., Rockstroh, A., Poad, B. L. J., Talebi, A., Young, R. S. E., Taherian Fard, A., et al. (2020). Therapy-induced lipid uptake and remodeling

underpin ferroptosis hypersensitivity in prostate cancer. *Cancer Metab.* 8:11. doi: 10.1186/s40170-020-00217-6

Van den Broeck, T., van den Bergh, R. C. N., Arfi, N., Gross, T., Moris, L., Briers, E., et al. (2019). Prognostic value of biochemical recurrence following treatment with curative intent for prostate cancer: a systematic review. *Eur. Urol.* 75, 967–987. doi: 10.1016/j.eururo.2018.10.011

Wang, H. W., Lin, C. P., Chiu, J. H., Chow, K. C., Kuo, K. T., Lin, C. S., et al. (2007). Reversal of inflammation-associated dihydrodiol dehydrogenases (AKR1C1 and AKR1C2) overexpression and drug resistance in nonsmall cell lung cancer cells by wogonin and chrysin. *Int. J. Cancer* 120, 2019–2027. doi: 10.1002/ijc.22402

Wenners, A., Hartmann, F., Jochens, A., Roemer, A. M., Alkatout, I., Klapper, W., et al. (2016). Stromal markers AKR1C1 and AKR1C2 are prognostic factors in primary human breast cancer. *Int. J. Clin. Oncol.* 21, 548–556. doi: 10.1007/s10147-015-0924-2

Yang, L., Tian, S., Chen, Y., Miao, C., Zhao, Y., Wang, R., et al. (2021). Ferroptosis-related gene model to predict overall survival of ovarian carcinoma. *J. Oncol.* 2021:6687391. doi: 10.1155/2021/6687391

Yang, Y., Liu, T., Hu, C., Xia, H., Liu, W., Chen, J., et al. (2021). Ferroptosis inducer erastin downregulates androgen receptor and its splice variants in castrationresistant prostate cancer. *Oncol. Rep.* 45:7976. doi: 10.3892/or.2021.7976

Yoo, H. C., Park, S. J., Nam, M., Kang, J., Kim, K., Yeo, J. H., et al. (2020). A variant of SLC1A5 is a mitochondrial glutamine transporter for metabolic reprogramming in cancer cells. *Cell Metab.* 31, 267–283.e212. doi: 10.1016/j.cmet.2019.11.020

Yoshihara, K., Shahmoradgoli, M., Martinez, E., Vegesna, R., Kim, H., Torres-Garcia, W., et al. (2013). Inferring tumour purity and stromal and immune cell admixture from expression data. *Nat. Commun.* 4:2612. doi: 10.1038/ncomms3612

Yuan, H., Li, X., Zhang, X., Kang, R., and Tang, D. (2016). Identification of ACSL4 as a biomarker and contributor of ferroptosis. *Biochem. Biophys. Res. Commun.* 478, 1338–1343. doi: 10.1016/j.bbrc.2016.08.124

Zadra, G., and Loda, M. (2018). Metabolic vulnerabilities of prostate cancer: diagnostic and therapeutic opportunities. *Cold Spring Harb. Perspect. Med.* 8:a030569. doi: 10.1101/cshperspect.a030569

Zhang, Y., Shi, J., Liu, X., Feng, L., Gong, Z., Koppula, P., et al. (2018). BAP1 links metabolic regulation of ferroptosis to tumour suppression. *Nat. Cell Biol.* 20, 1181–1192. doi: 10.1038/s41556-018-0178-0

Zhou, X., Zou, L., Chen, W., Yang, T., Luo, J., Wu, K., et al. (2020). Flubendazole, FDA-approved anthelmintic, elicits valid antitumor effects by targeting P53 and promoting ferroptosis in castration-resistant prostate cancer. *Pharmacol. Res.* 164:105305.

Zhou, X., Zou, L., Chen, W., Yang, T., Luo, J., Wu, K., et al. (2021). Flubendazole, FDA-approved anthelmintic, elicits valid antitumor effects by targeting P53 and promoting ferroptosis in castration-resistant prostate cancer. *Pharmacol. Res.* 164:105305. doi: 10.1016/j.phrs.2020.105305

Zhu, H., Blake, S., Chan, K. T., Pearson, R. B., and Kang, J. (2018). Cystathionine beta-synthase in physiology and cancer. *Biomed. Res. Int.* 2018:3205125. doi: 10.1155/2018/3205125

Zhuo, S., Chen, Z., Yang, Y., Zhang, J., Tang, J., and Yang, K. (2020). Clinical and biological significances of a ferroptosis-related gene signature in glioma. *Front. Oncol.* 10:590861. doi: 10.3389/fonc.2020.590861

Conflict of Interest: The authors declare that the research was conducted in the absence of any commercial or financial relationships that could be construed as a potential conflict of interest.

Publisher's Note: All claims expressed in this article are solely those of the authors and do not necessarily represent those of their affiliated organizations, or those of the publisher, the editors and the reviewers. Any product that may be evaluated in this article, or claim that may be made by its manufacturer, is not guaranteed or endorsed by the publisher.

frontiers in Cell and Developmental Biology

ORIGINAL RESEARCH
published: 01 November 2021
doi: 10.3389/fcell.2021.739011

Prognostic Value of a Ferroptosis-Related Gene Signature in Patients With Head and Neck Squamous Cell Carcinoma

*Dongsheng He, Shengyin Liao, Linlin Xiao, Lifang Cai, Mengxing You, Limei He and Weiming Huang**

Department of Medical Oncology, The First Hospital of Putian, Teaching Hospital, Fujian Medical University, Putian, China

OPEN ACCESS

Edited by:
Zhi-Xiang Xu,
The University of Alabama at Birmingham, United States

Reviewed by:
Jinhui Liu,
Nanjing Medical University, China
Feilong Yang,
Peking University Third Hospital, China

***Correspondence:**
Weiming Huang
Huangweiming1039@ptu.edu.cn

Specialty section:
This article was submitted to Molecular and Cellular Oncology, a section of the journal Frontiers in Cell and Developmental Biology

Received: *09 July 2021*
Accepted: *29 September 2021*
Published: *01 November 2021*

Citation:
He D, Liao S, Xiao L, Cai L, You M, He L and Huang W (2021) Prognostic Value of a Ferroptosis-Related Gene Signature in Patients With Head and Neck Squamous Cell Carcinoma. Front. Cell Dev. Biol. 9:739011. doi: 10.3389/fcell.2021.739011

Background: Ferroptosis is an iron-dependent programmed cell death (PCD) form that plays a crucial role in tumorigenesis and might affect the antitumor effect of radiotherapy and immunotherapy. This study aimed to investigate distinct ferroptosis-related genes, their prognostic value and their relationship with immunotherapy in patients with head and neck squamous cell carcinoma (HNSCC).

Methods: The differentially expressed ferroptosis-related genes in HNSCC were filtered based on multiple public databases. To avoid overfitting and improve clinical practicability, univariable, least absolute shrinkage and selection operator (LASSO) and multivariable Cox algorithms were performed to construct a prognostic risk model. Moreover, a nomogram was constructed to forecast individual prognosis. The differences in tumor mutational burden (TMB), immune infiltration and immune checkpoint genes in HNSCC patients with different prognoses were investigated. The correlation between drug sensitivity and the model was firstly analyzed by the Pearson method.

Results: Ten genes related to ferroptosis were screened to construct the prognostic risk model. Kaplan-Meier (K-M) analysis showed that the prognosis of HNSCC patients in the high-risk group was significantly lower than that in the low-risk group ($P < 0.001$), and the area under the curve (AUC) of the 1-, 3- and 5-year receiver operating characteristic (ROC) curve increased year by year (0.665, 0.743, and 0.755). The internal and external validation further verified the accuracy of the model. Then, a nomogram was build based on the reliable model. The C-index of the nomogram was superior to a previous study (0.752 vs. 0.640), and the AUC (0.729 vs. 0.597 at 1 year, 0.828 vs. 0.706 at 3 years and 0.853 vs. 0.645 at 5 years), calibration plot and decision curve analysis (DCA) also shown the satisfactory predictive capacity. Furthermore, the TMB was revealed to be positively correlated with the risk score in HNSCC patients ($R = 0.14$; $P < 0.01$). The differences in immune infiltration and immune checkpoint genes were significant

($P < 0.05$). Pearson analysis showed that the relationship between the model and the sensitivity to antitumor drugs was significant ($P < 0.05$).

Conclusion: Our findings identified potential novel therapeutic targets, providing further potential improvement in the individualized treatment of patients with HNSCC.

Keywords: HNSCC, ferroptosis, prognosis, nomogram, immunotherapy

INTRODUCTION

Head and neck cancer is the sixth most common malignancy that leads to considerable mortality, with >450,000 deaths reported worldwide in 2020 (International Agency for Research on Cancer, and World Health Organization, 2021). The incidence rate of head and neck squamous cell carcinoma (HNSCC), which is the most common type of head and neck cancer, is approximately 20 per 100000 people in the regions of South America, China, Europe, the Indian subcontinent, and among African Americans in the United States (Stenson, 2021). The well-known risk factors for HNSCC are chronic exposure to alcohol, smoking, different forms of chewing tobacco (such as betel palm), chronic oral trauma, and HPV infection (Gillison et al., 2015). Currently, surgical resection, radiotherapy, chemotherapy, targeted therapy, and immunotherapy have been developed to comprehensively treat HNSCC patients. However, the 5-year overall survival (OS) of HNSCC patients has remained at 50%, which has not significantly improved in the past decade (Torre et al., 2015; Bray et al., 2018). Moreover, mounting evidence highlights that the percentage of locoregional failure is approximately 40–50%, while distant failure is 20–30% in locoregionally advanced HNSCC patients (Samra et al., 2018; Muzaffar et al., 2021). Therefore, studies exploring novel therapeutic targets and developing novel prognostic models to identify patients with different prognoses are urgently required for HNSCC patients.

Iron is an important transition metal for maintaining the rapid proliferation and growth of cancer cells (Zhou et al., 2018). Moreover, iron participates in several important biological processes, such as oxygen transport, DNA synthesis, and ATP generation. However, excess intracellular iron accumulation can trigger reactive oxygen species (ROS), which cause lipid peroxidation and ferroptosis, a unique form of cell death (Bogdan et al., 2016; Fanzani and Poli, 2017). Ferroptosis is defined as an iron-dependent programmed cell death (PCD) that is dependent on ROS accumulation and lipid peroxidation, and the mechanism and morphology of PCD are distinct from other PCDs, such as autophagy, apoptosis, and necroptosis (Dixon et al., 2012; Stockwell et al., 2017). In recent decades, research on ferroptosis in tumors has rapidly increased, and this PCD has been indicated to be correlated with tumor origin, development, and treatment (Liang et al., 2019; Stockwell and Jiang, 2019). Ferroptosis regulatory genes, such as P53, DPP4, and GPX4, have been shown to be correlated with tumorigenesis and progression (Junttila and Evan, 2009; Liu et al., 2018; Enz et al., 2019). Moreover, ferroptosis has been suggested to regulate the sensitivity of tumor cells to radiotherapy and immunotherapy. Radiotherapy has been suggested to induce ferroptosis, which plays a crucial role in radiotherapy-mediated anticancer effects, and improve the sensitivity of tumor cells to ferroptosis inducers (Lang et al., 2019). Furthermore, interferon-gamma and T cells may sensitize tumor cells to ferroptosis (Wang et al., 2019). After treatment of tumor models with immune checkpoint inhibitors, ROS levels were significantly increased, while tumor size was significantly reduced (Mou et al., 2019). Radiotherapy and immunotherapy have been shown to promote lipid oxidation and ferroptosis in tumor cells owing to a synergistic effect (Lang et al., 2019). Nevertheless, the prognostic value and relationship of distinct ferroptosis-related genes with immunotherapy in HNSCC remain predominantly unknown.

In this study, we first integrated The Cancer Genome Atlas (TCGA), Genotype-Tissue Expression (GTEx), and ArrayExpress databases to construct and validate a novel prognostic risk model based on ferroptosis-related messenger RNA (mRNA). Moreover, internal and external validations were first used to assess the risk model accuracy compared with a previous study (He et al., 2021). To the best of our knowledge, the prognostic risk model and nomogram based on the model showed the best prognostic effect in the present study of risk models based on ferroptosis-related mRNA (He et al., 2021). In addition, the values of the model used to predict prognosis with other clinical parameters and immunotherapy of HNSCC patients were further explored. The correlation between the prognostic risk model and drug sensitivity in cancers was first analyzed.

MATERIALS AND METHODS

Patients and Clinical Data Acquisition

In this study, mRNA sequencing data (fragments per kilobase million) of HNSCC patients were obtained from TCGA database[1] (44 normal head and neck samples and 501 HNSCC samples). To further strengthen the reliability, the sequencing data of 55 salivary gland samples in the GTEx[2] database were obtained using the UCSC Xena tool and integrated with HNSCC sequencing data from TCGA database (Cao et al., 2019). The integrated data were normalized and processed using the Limma R package (Ritchie et al., 2015). Moreover, the clinical data of HNSCC patients were downloaded from TCGA database.

[1]https://portal.gdc.cancer.gov/
[2]https://gtexportal.org/home/

Acquisition of Differentially Expressed Ferroptosis-Related Genes in HNSCC Patients

The Limma package was used to screen the differentially expressed genes (DEGs) in HNSCC patients with a false discovery rate (FDR) <0.05, and fold change > 2 (Wu et al., 2020). Ferroptosis-related gene sets (driver, suppressor, and marker) were downloaded from FerrDb, the first manually curated database of ferroptosis regulators and markers and ferroptosis-disease associations. The database provides up-to-date and comprehensive ferroptosis-related genes (Zhou and Bao, 2020). Moreover, a ferroptosis-related gene set (WP_FERROPTOSIS) in the Molecular Signature Database v7.2 (MSigDB) was downloaded (Liberzon et al., 2015). The ferroptosis-related genes were identified after removing the overlapping genes. Differentially expressed ferroptosis-related genes were identified by intersecting ferroptosis-related genes with DEGs.

Construction and Assessment of the Risk Score Prognostic Model

The differentially expressed ferroptosis-related genes in HNSCC patients were matched with the corresponding survival time and status (n = 498) after excluding missing data. HNSCC patients were then randomly separated into training and testing groups using the caret package at a ratio of 7:3 (Zhang et al., 2020). A univariate Cox regression algorithm was employed to screen for ferroptosis-related genes associated with OS in the training group ($P < 0.05$). The least absolute shrinkage and selection operator (LASSO) logistic regression algorithm was used to avoid overfitting. Finally, a multivariable Cox regression analysis was conducted to construct a prognostic risk score model. HNSCC patients were divided into high- and low-risk groups based on the median risk score as the cutoff value. The Kaplan-Meier (K-M) method and receiver operating characteristic (ROC) curves were used to validate model feasibility.

Internal and External Validation of the Risk Score Prognostic Model

HNSCC patients in the testing cohort were divided into high- and low-risk groups based on the median risk score in the training cohort. The K-M method and ROC curve were used to test the feasibility of internal validation. Moreover, the prognostic capability of the risk score model was externally validated in the entire cohort and the ArrayExpress database[3]. The mRNA sequencing data and corresponding clinical information of HNSCC (n = 108) were obtained from the E-MTAB-8588 dataset in the ArrayExpress database. The risk score was calculated for HNSCC patients using the prognostic model in the training cohort, and the "sva" R package was utilized to eliminate different dataset biases (Leek et al., 2012).

[3]https://www.ebi.ac.uk/arrayexpress/

Functional Enrichment Analysis of the 10-Gene Signature

Gene Ontology (GO) analysis is a major bioinformatics tool for annotating genes and gene functions (Gaudet et al., 2017). The Kyoto Encyclopedia of Genes and Genomes (KEGG) is a collection of databases that contain information regarding genomes, biological pathways, diseases, and chemical substances (Kanehisa et al., 2017). The "clusterProfiler" R package was employed to explore the gene function and pathway of the 10 genes (Liu M. et al., 2021). Differences were considered statistically significant at FDR < 0.05.

Construction and Assessment of the Nomogram for HNSCC Patients

To further assess the capability of the risk score prognostic model to be an independent prognostic factor, the risk score of HNSCC patients was integrated with the clinical parameters of HNSCC patients in the training group. The inclusion criteria for HNSCC patients were as follows: (1) pathological type was squamous cell carcinoma, (2) complete follow-up data, (3) received chemotherapy or radiotherapy, and (4) clear pathological stage. A univariate Cox regression algorithm was used to screen out the OS-related characteristics in HNSCC patients ($P < 0.05$), and multivariable Cox regression analyses were used to identify independent prognostic parameters. Subsequently, a nomogram was constructed to predict an individual's OS based on the independent prognostic parameters, and the concordance index (C-index), ROC curve, calibration plot, and decision curve analysis (DCA) were used to determine the prognostic ability of the nomogram from multiple perspectives. The nomogram was further validated in the testing, entire, and external groups.

Analysis of the Relationship Between the Immune Microenvironment and Risk Score Model in HNSCC Patients

The single nucleotide variant (SNV) data of HNSCC patients were obtained from TCGA database, and tumor mutational burden (TMB) was calculated for each HNSCC patient. The correlation analysis between risk score and TMB was conducted using Spearman's algorithm, and the difference in TMB between the high- and low-risk groups was explored. Moreover, the "Cell Type Identification by Estimating Relative Subsets of RNA Transcripts (CIBERSORT)" deconvolution algorithm with 1,000 permutations was applied to quantify 22 tumor-infiltrating lymphocyte types in the microenvironment of high- and low-risk HNSCC patients (Becht et al., 2016). Statistical significance was set at $P < 0.05$.

Exploration of Drug Sensitivity Based on the Prognostic Model

To explore the anticancer drugs targeted to the prognostic model, the sensitivity information of anticancer drugs approved by the United States Food and Drug Administration for use in the clinic, and RNA sequencing data in the NCI 60 platform were

downloaded from the CellMiner database[4] (Foy et al., 2017). The correlation between ferroptosis-related genes to construct a prognostic model and drug sensitivity in cancers was analyzed using Pearson analysis (Reinhold et al., 2019).

RESULTS

Identification of Ferroptosis-Related Genes in HNSCC

A total of 8655 DEGs were screened out in HNSCC based on TCGA and GTEx databases (**Figure 1A**). After overlapping genes were filtered, 275 ferroptosis-related genes were screened based on the FerrDb and MSigDB (**Figure 1B**). Next, 175 differentially expressed ferroptosis-related genes in HNSCC were identified by intersecting the DEGs and ferroptosis-related genes (**Figure 1C**).

Construction and Assessment of the Risk Score Prognostic Model

After the survival data were integrated with the expression profile of 175 ferroptosis-related genes, HNSCC patients were randomly divided into training (n = 350) and testing cohorts (n = 148) at a ratio of 7:3. Univariate Cox regression analysis was performed to screen 25 genes related to the OS of HNSCC patients in the training cohort (**Supplementary Table 1**). The 25 filtered genes were further included in the LASSO logistic regression algorithm to avoid overfitting (**Figure 2A**), and cross-validation was conducted, which filtered out 13 prognostic signatures (**Figure 2B**). Next, 10 gene signatures were screened to construct the following prognostic risk model by multivariable Cox regression analyses (**Supplementary Figure 1**): Risk score = (−0.191 × MAP1LC3A expression level) + (0.189 × SLC7A5 expression level) + (0.525 × OTUB1 expression level) + (0.399 × PRDX6 expression level) + (−0.374 × MAP3K5 expression level) + (−0.258 × SOCS1 expression level) + (0.555 × ATG5 expression level) + (0.227 × DDIT4 expression level) + (0.406 × ACSL3 expression level) + (0.602 × PRKAA2 expression level; **Figure 2C**). The correlation network of the 10 genes is shown in **Figure 2D**. Training group HNSCC patients were divided into high- (n = 175) and low-risk groups (n = 175) based on the median risk score. The OS in the low-risk group was significantly better than that in the high-risk group according to the K-M analysis (P < 0.001; **Figure 3A**). As shown in **Figures 3B–D**, the area under the curve (AUC) values for the ROC curves at 1, 3, and 5 years are 0.665, 0.743, and 0.755, respectively, increasing annually.

To further verify the predictive capability of the model in the training cohort, the testing cohort was used for internal validation, and the entire cohort and E-MTAB-8588 dataset were used for external validation. HNSCC patients in the testing cohort were divided into high- (n = 65) and low-risk (n = 83) groups based on the risk model in the training cohort. The OS of the two groups differed significantly in the K-M analysis (P < 0.01; **Supplementary Figure 2A**), and the AUC values at 1, 3, and 5 years were 0.648, 0.688, and 0.659, respectively (**Supplementary Figures 2D–F**). Similar to internal validation, external validation further strengthens model reliability during training. As shown in **Supplementary Figures 2B,C,K-M** analysis shows a significant difference between the high- and low-risk groups in the entire group (P < 0.001) and MTAB-8588 dataset (P = 0.03). The AUC values at 1, 3, and 5 years were 0.660, 0.718, and 0.713, respectively, for the entire cohort, and 0.632, 0.687, and 0.647, respectively, for the MTAB-8588 dataset (**Supplementary Figures 2G–L**). Overall, the accuracy increased as the sample size increased.

Functional Enrichment Analysis of the 10 Ferroptosis-Related Genes

The most highly enriched functions of the 10 screened genes were cellular response to chemical stress, starvation, nutrient levels, and oxidative stress (**Supplementary Figure 3A**). Moreover, KEGG pathway analysis demonstrated that the 10 genes might participate in ferroptosis via autophagy or mTOR signaling pathways (**Supplementary Figure 3B**). The involvement of these potential pathways in ferroptosis has been previously reported (Liu et al., 2020; Yi et al., 2020).

Construction and Assessment of the Nomogram for HNSCC Patients

The risk score for each HNSCC patient in the training cohort was integrated with age, sex, grade, stage, margin status, radiotherapy, and chemotherapy (n = 243). Five clinical characteristics, namely sex, stage, margin status, radiotherapy, and risk, were found by univariate Cox regression analysis to be correlated with prognosis (**Supplementary Figure 4A**). A multivariable Cox algorithm was used to identify the five independent prognostic parameters of HNSCC patients (**Supplementary Figure 4B**). A nomogram with a satisfactory C-index (0.752) was constructed based on independent prognostic parameters (**Figure 4A**). Moreover, ROC curve analysis was employed to determine the nomogram accuracy for predicting the 1-, 3-, and 5-year OS of individuals, and the AUC values revealed optimal values (0.729, 0.828, and 0.853, respectively), increasing annually (**Figures 4B–D**). The actual curve was similar to the ideal curve in the calibration plot (**Figures 4E–G**). DCA further confirmed the creditability of the prognostic effect of the nomogram, and the risk and combined curves were superior to other factors in forecasting individual prognosis (**Figures 4H–J**).

To validate the prognostic value of the nomogram, the risk score of the testing cohort was integrated with the corresponding clinical information for internal validation, and the entire cohort and E-MTAB-8588 dataset were integrated with the corresponding clinical parameters for external validation. In the testing cohort, the C-index was 0.629, and the AUC values at 1, 3, and 5 years were 0.645, 0.693, and 0.717, respectively, increasing annually (**Supplementary Figures 5A–C**). In the entire cohort (n = 361), the C-index was 0.721, and the AUC values at 1, 3, and 5 years were 0.738, 0.770, and 0.820, respectively, increasing annually (**Supplementary Figures 5D–F**). In the E-MTAB-8588

[4]https://discover.nci.nih.gov/cellminer/

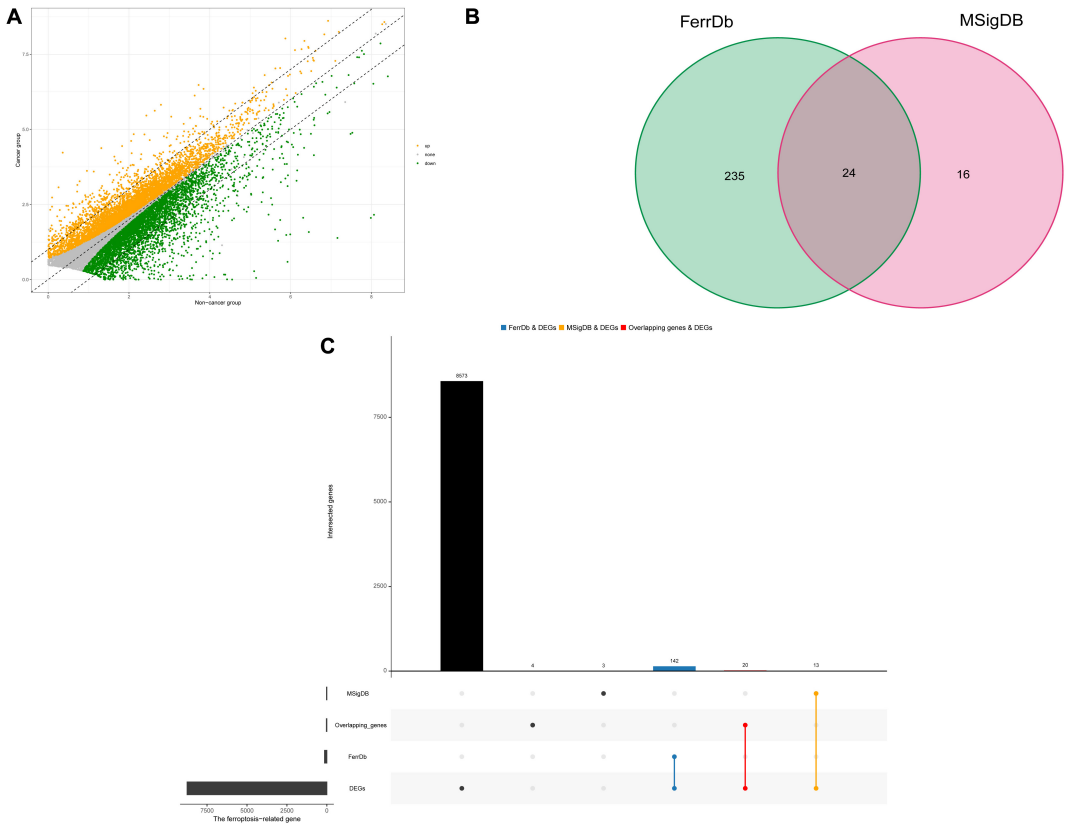

FIGURE 1 | Identification of differential expressed ferroptosis-related genes in HNSCC. **(A)** Differential expressed genes (DEGs) of head and neck squamous cell carcinoma (HNSCC). **(B)** Venn diagram of ferroptosis-related gene sets. **(C)** The blue and orange bars represents the unique DEGs related to ferroptosis in HNSCC in the FerrDb and MSigDB, respectively, and the red bar represents the overlapping DEGs related to ferroptosis in HNSCC between the FerrDb and MSigDB.

dataset (n = 107), the C-index was 0.600, and the AUC values at 1, 3, and 5 years were 0.604, 0.641, and 0.611, respectively, when margin status data were missing (**Supplementary Figures 5G–I**). Together, the internal and external validations strengthened the creditability of the nomogram. Internal and external validation suggested that the prognostic effect of the risk score model and the model-based nomogram reliable. Moreover, the risk score differed significantly in the T stage, N stage, lymphovascular invasion, and perineural invasion (**Supplementary Figure 6**).

Analysis of the Relationship Between the Immune Microenvironment and Risk Score Model in HNSCC Patients

To investigate the relationship between risk model-related ferroptosis and TMB, the risk score was integrated with SNV in HNSCC patients, and the TMB was significantly different in the high- and low-risk groups (**Figures 5A–C**). Moreover, the correlation analysis indicated that TMB was positively correlated with the risk score (R = 0.14, $P < 0.01$; **Figure 5D**). However, a high TMB might fail to predict the immune checkpoint blockade response across all cancer types.

To further explore the individual immune microenvironment and develop individualized treatment, immune infiltration and immune checkpoint genes in high- and low-risk HNSCC patients were further investigated (**Figures 6A,B**). Compared to the high-risk patients, the low-risk HNSCC patients had higher marker expression of naive B cells ($P < 0.001$), plasma cells ($P < 0.05$), CD8 T cells ($P < 0.001$), follicular helper T cells ($P < 0.01$), regulatory T cells (Tregs, $P < 0.001$), gamma delta T cells ($P < 0.01$), resting mast cells ($P < 0.05$), and neutrophils ($P < 0.001$), however, lower marker expression of resting NK cells ($P < 0.01$), M0 macrophages ($P < 0.05$), M2 macrophages $P < 0.05$), activated mast cells ($P < 0.05$), and eosinophils ($P < 0.01$; **Supplementary Figure 7**). Moreover, differences in immune checkpoint genes in high- and low-risk HNSCC patients were identified. The expression levels of IL10, CTLA4, PD1, TNFRSF14, BTLA, LGALS9, TIGIT, LAG3, EDNRB, and IDO1 were higher in the low-risk group than those in the high-risk group. Contrastingly, the high-risk group had higher MICA and MICB expressions compared to that of the low-risk group (**Supplementary Figure 8**). The corresponding correlations between the immune checkpoint genes and risk scores are shown in **Supplementary Figure 9**.

The above results suggest that the ability of TMB to predict the response to immunotherapy in HNSCC patients is related to the target genes of immunotherapy. Furthermore, the use of various immune checkpoint inhibitors for HNSCC patients with different

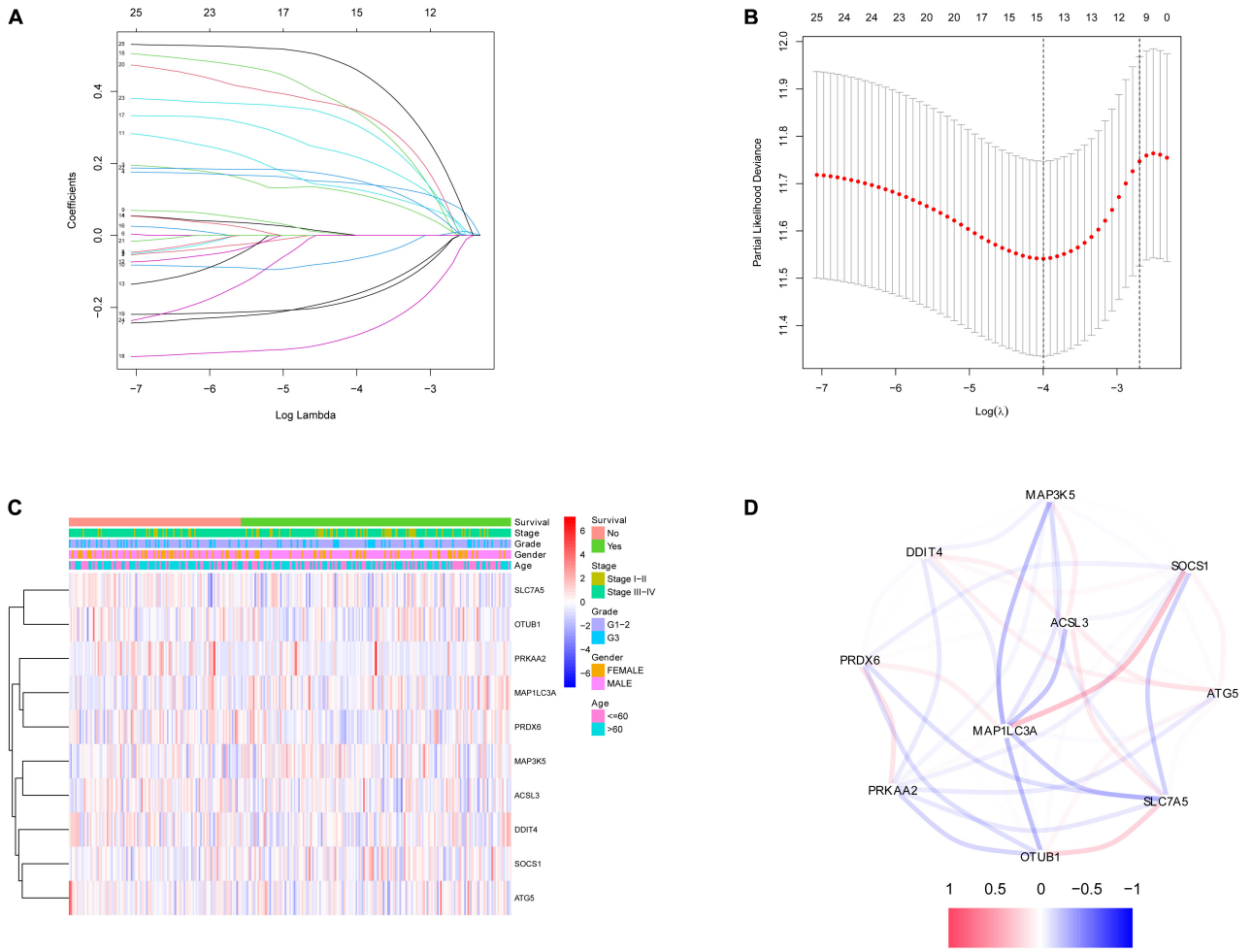

FIGURE 2 | Identification of ferroptosis-related signatures by LASSO regression algorithm in HNSCC. **(A)** LASSO coefficient profiles of the 25 ferroptosis-related genes. **(B)** Cross-validation for tuning parameter selection in the proportional hazards model. **(C)** The heatmap of the 10 ferroptosis-related genes. **(D)** The correlation of the 10 ferroptosis-related genes.

risks based on differences in immune infiltration and immune checkpoint genes may be more beneficial to patients.

Exploration of Drug Sensitivity Based on the Prognostic Model

The reliability of the risk score prognostic model and nomogram based on the model was validated by multiple methods, and it is necessary to reduce the risk of HNSCC. **Figure 7** exhibits that, in the representative 16 correction analysis, ACSL3 expression is positively correlated with the sensitivity of cancer patients to ARRY-162 (MEK162), and SOCS1 expression is negatively correlated with the sensitivity of cancer patients to cobimetinib (isomer 1), thereby promoting novel research on targeted drugs.

DISCUSSION

Excluding communicable diseases, approximately 30% of premature deaths are attributable to cancer in adults aged approximately 30–69 years (WHO, 2020). As a malignant tumor with increasing incidence, the OS of HNSCC patients is unsatisfactory with the currently available treatments, and HNSCC recurrence with a 50% ratio in locally advanced disease further reduces the 5-year survival rate (Muzaffar et al., 2021). Therefore, identifying HNSCC patients with poor prognosis and developing more effective treatments to promote individualized treatment and improve clinical outcomes are urgently required.

Ferroptotic cell death, a relatively novel cell death mechanism, has been shown to improve the curative effect of radiotherapy and immunotherapy in cancer (Lang et al., 2019). However, few studies have investigated the relationship between ferroptosis-related genes and OS in HNSCC patients. In this study, a novel prognostic risk model for HNSCC was first built based on ferroptosis-related genes, and a clinical prognostic model was constructed to assess patient prognosis.

In the present study, we systematically investigated the correlation between ferroptosis-related genes and HNSCC. A total of 175 differentially expressed ferroptosis-related genes

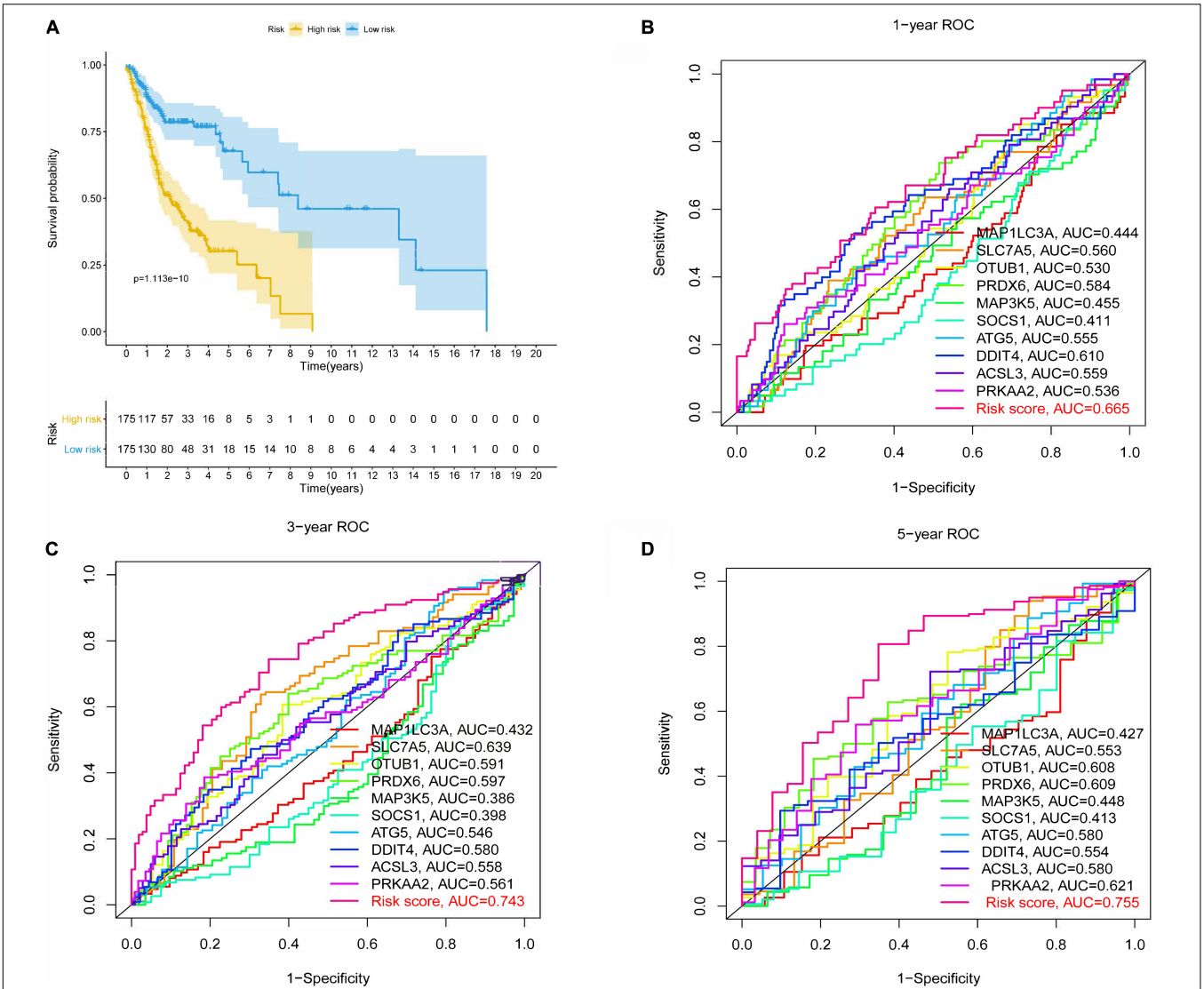

FIGURE 3 | Kaplan-Meier (K-M) survival analysis and receiver operating characteristic (ROC) curves of risk prognostic model in HNSCC patients. **(A)** K-M survival analysis of risk prognostic model of HNSCC patients in training cohort. **(B–D)** ROC curves analysis of risk prognostic model of HNSCC patients at 1, 3, and 5 years in training cohort.

were identified in HNSCC based on TCGA, GTEx, FerrDb, and MSigDB, which provided a reliable foundation for future exploration. The 10 independent prognostic genes were screened to construct the risk score model based on univariate, LASSO, and multivariable logistic regression algorithms, which avoided overfitting and improved the clinical practicability of the model.

In the 10 ferroptosis-related genes, the coefficients of MAP1LC3A, MAP3K5, and SOCS1 were negatively correlated with the prognostic risk score, suggesting that these 3 genes might induce ferroptosis in HNSCC. However, the coefficients of the other 7 genes were positively correlated with the prognostic risk score, suggesting that these 7 genes might inhibit ferroptosis in HNSCC. Moreover, the potential gene functions and pathways of these 10 genes were further explored. Several results have been suggested to be correlated with ferroptosis in the top 10 KEGG and GO enrichment analyses. The top 10 results of GO analysis were primarily enriched in biological processes related to cellular responses to chemical stress, starvation, nutrient levels, and oxidative stress. Previous studies suggested that chemotherapeutic agents, such as sulfasalazine and cisplatin, might induce ferroptosis by acting on system xc- or GSH, which play a key role in ferroptosis development (Mou et al., 2019). Oxidative stress, as an important characteristic, has been identified as a crucial factor in ferroptosis induction (Mou et al., 2019). Moreover, the top 10 gene functions in the GO analysis are related to the cell response to nutrients and starvation, suggesting that deregulating cellular energetics might participate in ferroptosis. Energy stress has been reported to inhibit lipid peroxidation and ferroptosis (Lee et al., 2020). For the KEGG enrichment analysis, the top result was ferroptosis,

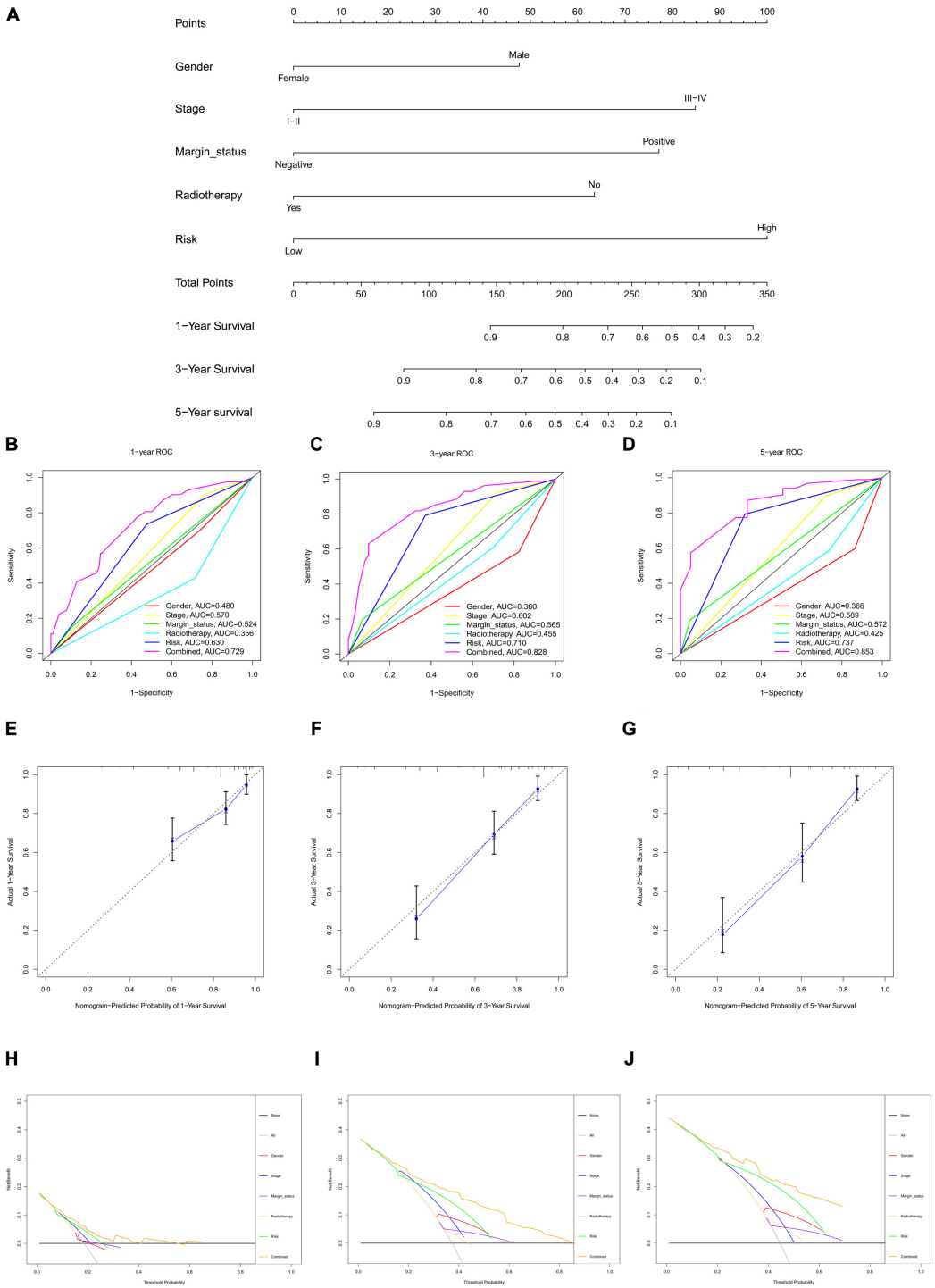

FIGURE 4 | Nomogram to predict 1-, 3-, and 5-year overall survival (OS) and its validation in HNSCC patients. **(A)** Nomogram to predict 1-, 3-, and 5-year OS of HNSCC patients. **(B–D)** ROC curves to assess nomogram accuracy to predict 1-, 3-, and 5-year OS in HNSCC patients. **(E–G)** Calibration plot analysis to assess nomogram accuracy of to predict 1-, 3-, and 5-year OS in HNSCC patients. **(H–J)** Decision curve analysis to assess nomogram accuracy to predict 1-, 3-, and 5-year OS in HNSCC patients.

which further suggested that the 10 genes might participate in ferroptosis and HNSCC development. Autophagy may promote ferroptotic death by ferritinophagy, lipophagy, or clockophagy (Liu et al., 2020). Moreover, cell sensitivity to ferroptosis might be affected by mTOR pathway regulation (Yi et al., 2020). In summary, the most significant gene functions and pathways from

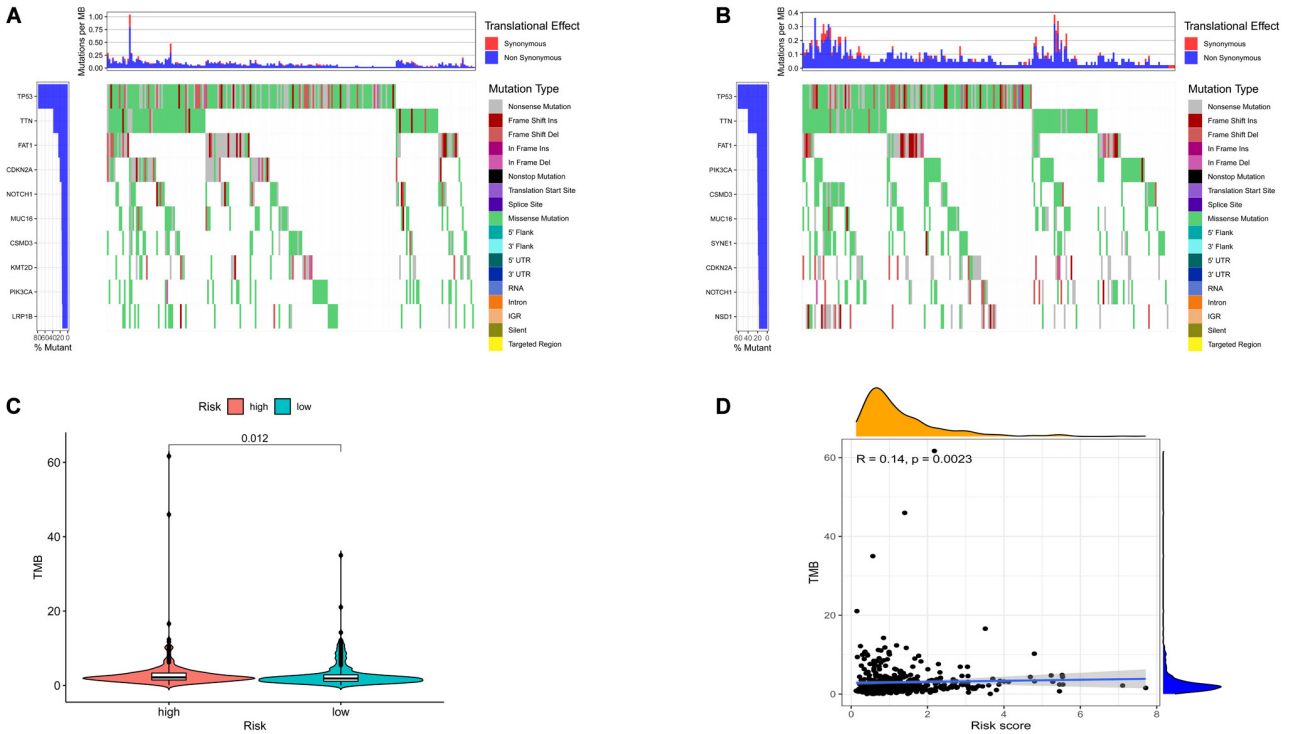

FIGURE 5 | The differences of tumor mutational burden (TMB) in high- and low-risk HNSCC patients. **(A)** The TMB in high-risk HNSCC patients. **(B)** The TMB in low-risk HNSCC patients. **(C)** The difference of TMB was significant in HNSCC patients with different risk. **(D)** The TMB was positively correlated with the risk score in HNSCC patients.

GO and KEGG analyses indicated that the mechanism of the 10 genes might be correlated with ferroptosis.

The majority of the 10 signature genes in the prognostic model have been shown to be involved in multiple cancers. However, the role of several genes in HNSCC prognosis remains to be explored. Ovarian tumor domain-containing ubiquitin aldehyde binding protein 1 (OTUB1) is an important deubiquitinating enzyme (DUB) that inhibits the ubiquitination of E2s following cleavage of the ubiquitin chains in target proteins (Wiener et al., 2012). OTUB1 has complex functions in various cancers, promotes tumor migration, and is a tumor suppressor that induces cell apoptosis and cell growth by regulating the DNA damage response (Sun et al., 2012; Herhaus et al., 2013; Kato et al., 2014). Moreover, OTUB1 may influence immune factor production. OTUB1 deletion downregulates the synthesis of the protective chemokine INF-γ, which is secreted by NK cells (Mulas et al., 2021). In addition, OTUB1 participates in metabolic reprogramming, which is an essential mechanism for activated T cell function (Pearce et al., 2013). Acyl-coenzyme A (CoA) synthetase long-chain family member 3 (ACSL3) regulates fatty acid metabolism and is a substrate for both β-oxidation and lipid synthesis after converting free long-chain fatty acids into fatty acyl-CoA esters (Coleman et al., 2002). Lipid metabolic reprogramming is one of the most prominent metabolic changes in cancer cells and has received increasing attention. As an important component of lipid metabolism, fatty acid deregulation might disturb the curative effect of radiotherapy and chemotherapy and affect immunotherapy for cancer patients (Wu et al., 2009; Han et al., 2019; Corn et al., 2020). ACSL enzymes, including ACSL3, have been suggested to induce apoptosis in a subset of TP53-deficient cancer cells (Yamashita et al., 2000; Mashima et al., 2005). Moreover, ACSL3 has been shown to be essential for mutant KRAS lung cancer tumorigenesis (Padanad et al., 2016). Mitogen-activated protein kinase 5 (MAP3K5) has been suggested to be involved in multiple biological activities, including stress-induced apoptosis and cell differentiation (Subramanian et al., 2004; Mizumura et al., 2006). As an important apoptosis signal-regulating kinase, MAP3K5 catalytic activity leads to differentially regulated apoptosis by inducing DNA damage, ROS, and tumor necrosis factor (Nagai et al., 2007). Moreover, MAP3K5 has been shown to play an important role in innate immune responses through the production of proinflammatory cytokine production (Matsuzawa et al., 2005). In general, ferroptosis-related genes are correlated with the human immune system, prompting subsequent analysis of immune function based on the present model.

After the model was constructed, K-M analysis and ROC curves were used to determine the effect of the model to identify HNSCC patients at different risks, and the test method revealed a satisfactory effect in predicting HNSCC patient prognosis.

The K-M analysis of our model showed a more optimistic trend; the difference in survival curve in the high- and low-risk groups was more significant compared with that of the previous study (He et al., 2021). Moreover, the prognostic risk model of

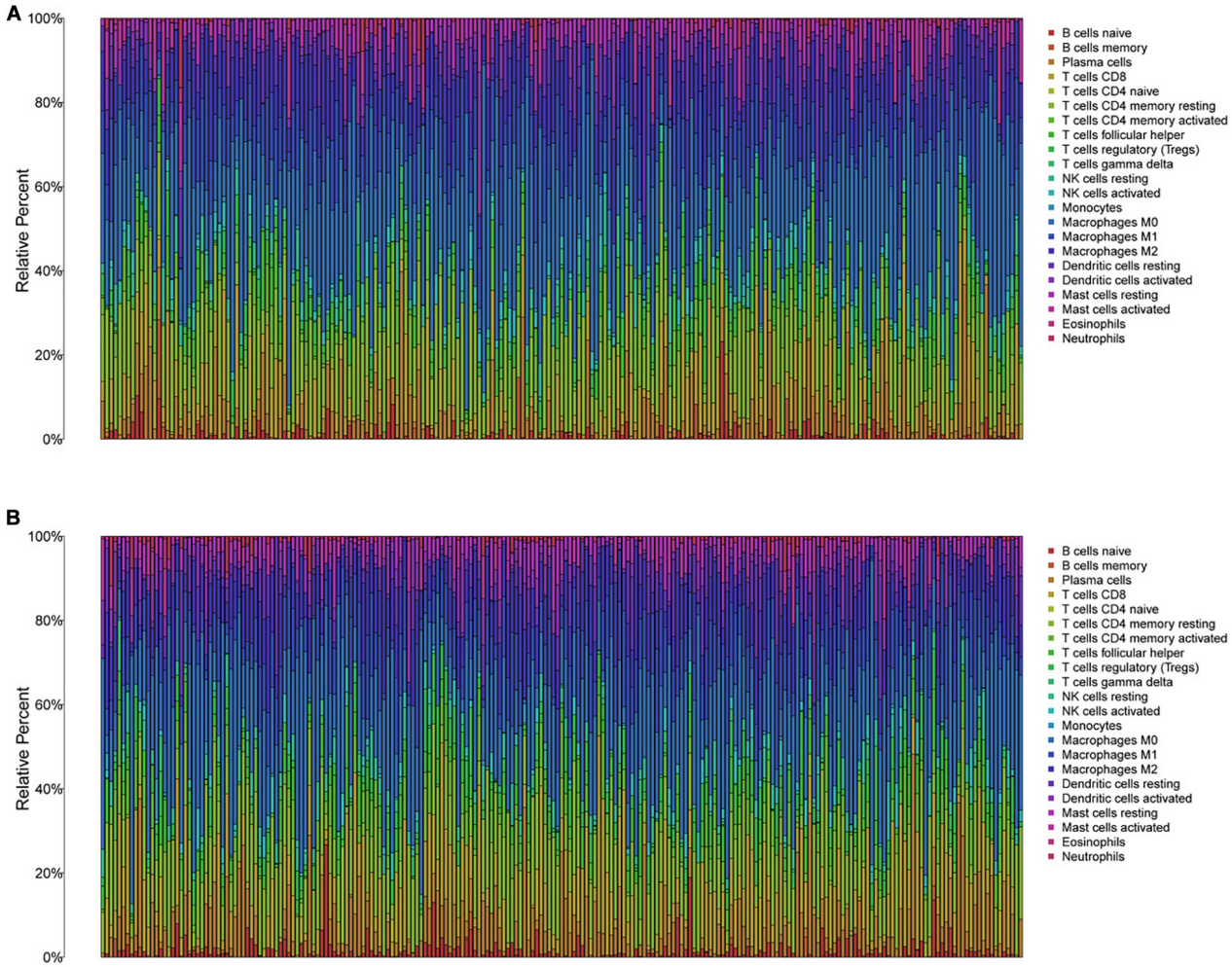

FIGURE 6 | The immune infiltration of 22 immune cell types in high- and low-risk HNSCC patients. **(A)** The immune infiltration of 22 immune cell types in high-risk HNSCC patients. **(B)** The immune infiltration of 22 immune cell types in low-risk HNSCC patients.

HNSCC patients was more accurate than the models reported in certain previous studies with a preferable AUC for 1 (0.665 vs. 0.634 and 0.663), 3 (0.743 vs. 0.672 and 0.686), and 5 years (0.755 vs. 0.642 and 0.622) (Yang et al., 2020; Liu B. et al., 2021). Interestingly, the AUC values of our model increased annually, which further strengthened the prognostic effect of the model. Moreover, the internal validation in the test cohort and external validation in the entire cohort and the MTAB-8588 dataset further improved model stringency. Overall, the practicability of the model was validated using multiple methods.

To further explore the clinical value of the model in HNSCC patients, the risk score was integrated with the clinical parameters of HNSCC patients. The risk score based on the model was an independent prognostic parameter that had synergistic effects with other independent prognostic characteristics to further improve the value of the nomogram to calculate individual prognoses, which were validated by the C-index, ROC curve, calibration plot, and DCA. The nomogram designed to predict HNSCC patient prognosis was more accurate than the models reported in a previous study with a superior C-index (0.752 vs. 0.640) and AUC for 1 (0.729 vs. 0.597), 3 (0.828 vs. 0.706), and 5 years (0.853 vs. 0.645) (He et al., 2021). Surprisingly, the AUC values of the nomogram at 1, 3, and 5 years increased annually, and the trend was consistent with the AUC values of the risk score model, which further strengthened the reliability of the risk score model and nomogram. Moreover, internal and external validation revealed optimistic effects for the nomogram.

Recently, tumor immunotherapy has been considered a breakthrough in oncotherapy. However, the response to immunotherapy differs between cancers and within cohorts with the same cancer (Ventola, 2017). Thus, the TMB level was developed to predict the response to immunotherapy in cancer patients, and high TMB has been shown to be positively correlated with the curative effect of immunotherapy (Galuppini et al., 2019). However, it has been reported that a high TMB fails to predict the immune checkpoint blockade response across all cancers (McGrail et al., 2021).

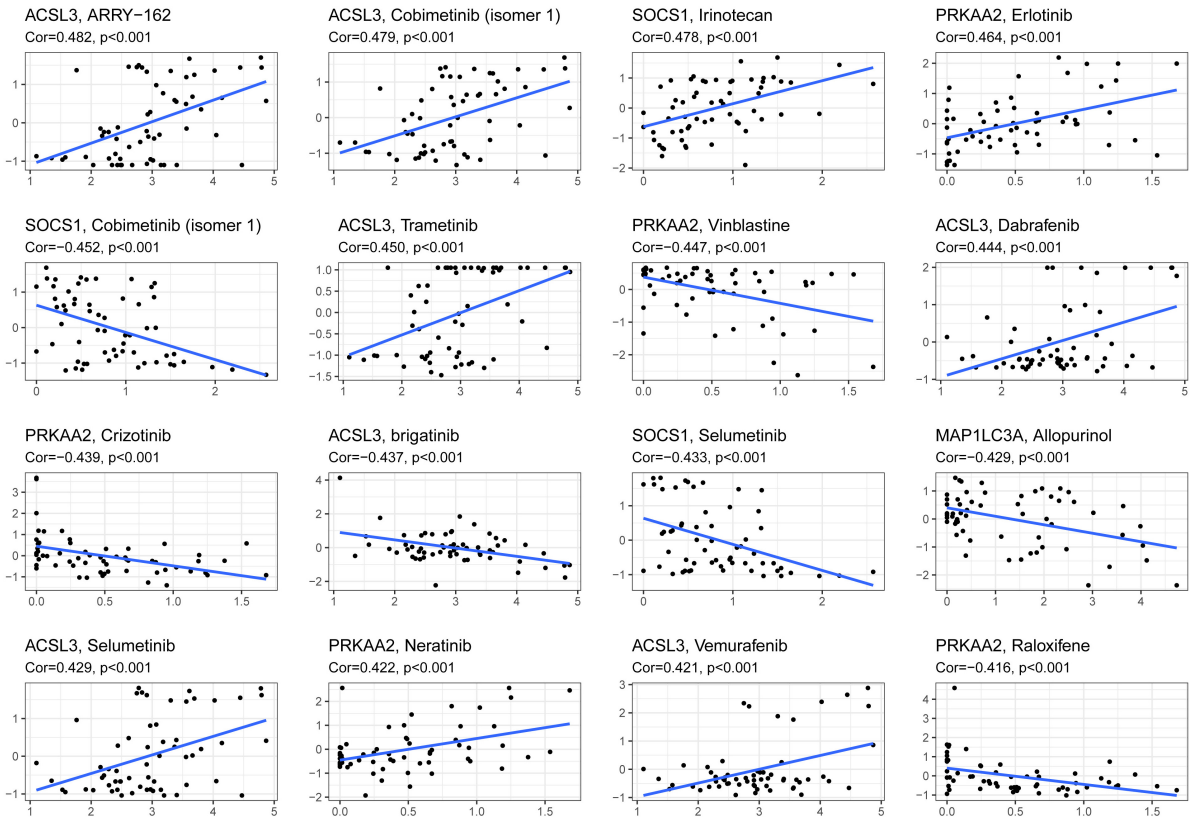

FIGURE 7 | The correlation between ferroptosis-related genes to construct the prognostic model and drug sensitivity.

After analyzing the correlation between the risk score and TMB in HNSCC patients, immune cell infiltration in the tumor microenvironment and the differences in immune checkpoints of high- and low-risk HNSCC patients were further investigated to explore the curative effect of immunotherapy based on the risk score model. The relationship between ferroptosis and the immune microenvironment is complicated. Cancer cells with ferroptosis can increase immunogenicity by releasing immune-stimulating signals, which allow immune cells, such as macrophages and dendritic cells (DCs), to locate the cancer cell site (Friedmann Angeli et al., 2019; Tang et al., 2021). Early ferroptotic cancer cells can elicit a vaccination-like effect by promoting phenotypic DC maturation (Efimova et al., 2020). The increased immunogenicity of cancer cells may enhance the efficacy of immune checkpoint inhibitors. Moreover, immune cells, such as CD8 + cells, can trigger lipid peroxidation and cause ferroptosis in tumor cells, which suggests that immune checkpoint inhibitors targeting CD8 + cells might act synergistically with ferroptosis (Wang et al., 2019). In addition to predicting HNSCC patient prognosis, differences in the immune microenvironment based on the prognostic risk model might be beneficial for developing individualized immunotherapy and improving the curative effect of HNSCC patients.

Moreover, the analysis of drug sensitivity based on the model suggested the possibility of targeting the 10 gene risk signatures and reducing the prognostic risk of HNSCC patients. The drugs might regulate the ferroptosis level of cancer cells by targeting the 10 ferroptosis-related genes. ACSL3 was found to contribute the most to drug sensitivity. ARRY-162 (MEK162), as the drug with the greatest correlation with ACSL3, is a highly selective MEK1/2 inhibitor that could offer a new combination therapy with ferroptosis and immunotherapy (Erkes et al., 2020; Gagliardi et al., 2020).

The present study has several limitations. Certain *in vitro* and *in vivo* experiments, such as the in-depth molecular mechanisms of the ferroptosis-related genes, needed to construct the prognostic model require further verification in experimental studies. Moreover, the study was based only on research data from public databases, which might have contributed to the selection bias. Thus, a multicenter and large-scale study is required to further validate the clinical utility of our model.

CONCLUSION

In summary, the present study systematically investigated the correlation between ferroptosis-related genes and HNSCC patient prognosis, and a novel prognostic model of HNSCC patients based on 10 ferroptosis-related genes was established and validated. Furthermore, the values of the model to be

used in predicting prognosis with other clinical parameters, immunotherapy, and drug sensitivity of HNSCC patients were positive, indicating that the novel ferroptosis-related gene signatures might be beneficial in developing individualized treatments, thereby improving the OS of HNSCC patients.

DATA AVAILABILITY STATEMENT

The datasets used and analysed for this study were obtained from TCGA 487 (https://portal.gdc.cancer.gov/) and ArrayExpress database 488 (https://www.ebi.ac.uk/arrayexpress/).

AUTHOR CONTRIBUTIONS

DH and WH: conceptualization and project administration. SL and LX: methodology and investigation. SL, LX, LH, and LC: formal analysis. DH: writing – original draft preparation. WH: writing – review and editing and supervision. DH, LH, and MY: visualization. MY and SL: funding acquisition. All authors support publishing, contributed to the article, and approved the submitted version.

FUNDING

This work was supported by grants from the youth scientific research project of Fujian Provincial Health and Family Planning Commission (No. 2017-2-80) and the project of Putian Science and Technology department (No. 2020SY006). The funding body had no role in the design of the study and collection, analysis, and interpretation of data and in writing the manuscript.

SUPPLEMENTARY MATERIAL

The Supplementary Material for this article can be found online at: https://www.frontiersin.org/articles/10.3389/fcell.2021.739011/full#supplementary-material

Supplementary Figure 1 | Multivariable Cox regression analysis to construct a prognostic risk score model.

Supplementary Figure 2 | K-M survival analysis and ROC curves of risk prognostic model in internal and external validation. **(A–C)** K-M survival analysis of risk prognostic model of HNSCC patients in internal, entire, and external validated cohorts. **(D–L)** ROC curves analysis of risk prognostic model of HNSCC patients at 1, 3, and 5 years in internal, entire, and external validated cohorts.

Supplementary Figure 3 | Representative results of GO and KEGG analyses. **(A)** The GO analysis of the 10 screened genes. **(B)** The potential signaling pathway of the 10 screened genes.

Supplementary Figure 4 | Independent prognostic parameter identification in HNSCC patients. **(A)** The univariate Cox regression analysis of clinical parameters in HNSCC patients. **(B)** The multivariate Cox regression analysis of clinical parameters in HNSCC patients.

Supplementary Figure 5 | The validation of nomogram in internal and external cohorts. **(A–C)** ROC curves to assess nomogram accuracy to predict 1-, 3-, and 5-year OS in internal cohort. **(D–F)** ROC curves to assess nomogram accuracy to predict 1-, 3-, and 5-year OS in entire cohort. **(G–I)** ROC curves to assess nomogram accuracy to predict 1-, 3-, and 5-year OS in external cohort.

Supplementary Figure 6 | The analysis between risk score and different clinical parameters in HNSCC patients. **(A)** The difference of risk score is significant in HNSCC patients with different stage. **(B)** The difference of risk score is significant in HNSCC patients with different N stage. **(C)** The difference of risk score is significant in HNSCC patients with different lymphovascular invasion. **(D)** The difference of risk score is significant in HNSCC patients with different perineural invasion.

Supplementary Figure 7 | The different immune infiltration in the high- and low-risk HNSCC patients. **(A,B)** The expression of eight immune cell types is higher in the low-risk group compared with that of the high-risk group. **(C)** The expression of four cell types is higher in the high-risk group compared with that of the low-risk group.

Supplementary Figure 8 | The different immune checkpoint genes in the high- and low-risk HNSCC patients. **(A,B)** The expression of 10 immune checkpoint gene types is higher in the low-risk group compared with that of the high-risk group. **(C)** The expression of two immune checkpoint gene types is higher in the high-risk compared with that of the low-risk group.

Supplementary Figure 9 | The correlations between the immune checkpoint genes and risk score. **(A–J)** The immune checkpoint genes were negatively correlated with the risk score in HNSCC patients. **(K,L)** The immune checkpoint genes were positively correlated with the risk score in HNSCC patients.

Supplementary Table 1 | Univariate COX regression analysis of differentially expressed ferroptosis-related genes in HNSCC patients.

REFERENCES

Becht, E., Giraldo, N. A., Lacroix, L., Buttard, B., Elarouci, N., Petitprez, F., et al. (2016). Estimating the population abundance of tissue-infiltrating immune and stromal cell populations using gene expression. *Genome Biol.* 17:218. doi: 10.1186/s13059-016-1070-5

Bogdan, A. R., Miyazawa, M., Hashimoto, K., and Tsuji, Y. (2016). Regulators of iron homeostasis: new players in metabolism, cell death, and disease. *Trends Biochem. Sci.* 41, 274–286. doi: 10.1016/j.tibs.2015.11.012

Bray, F., Ferlay, J., Soerjomataram, I., Siegel, R. L., Torre, L. A., and Jemal, A. (2018). Global cancer statistics 2018: GLOBOCAN estimates of incidence and mortality worldwide for 36 cancers in 185 countries. *CA Cancer J. Clin.* 68, 394–424. doi: 10.3322/caac.21492

Cao, T., Pan, W., Sun, X., and Shen, H. (2019). Increased expression of TET3 predicts unfavorable prognosis in patients with ovarian cancer-a bioinformatics integrative analysis. *J. Ovarian Res.* 12:101. doi: 10.1186/s13048-019-0575-4

Coleman, R. A., Lewin, T. M., Van Horn, C. G., and Gonzalez-Baró, M. R. (2002). Do long-chain acyl-CoA synthetases regulate fatty acid entry into synthetic versus degradative pathways? *J. Nutr.* 132, 2123–2126. doi: 10.1093/jn/132.8.2123

Corn, K. C., Windham, M. A., and Rafat, M. (2020). Lipids in the tumor microenvironment: from cancer progression to treatment. *Prog. Lipid Res.* 80:101055. doi: 10.1016/j.plipres.2020.101055

Dixon, S. J., Lemberg, K. M., Lamprecht, M. R., Skouta, R., Zaitsev, E. M., Gleason, C. E., et al. (2012). Ferroptosis: an iron-dependent form of nonapoptotic cell death. *Cell* 149, 1060–1072. doi: 10.1016/j.cell.2012.03.042

Efimova, I., Catanzaro, E., Van der Meeren, L., Turubanova, V. D., Hammad, H., Mishchenko, T. A., et al. (2020). Vaccination with early ferroptotic cancer cells induces efficient antitumor immunity. *J. Immunother. Cancer* 8:e001369. doi: 10.1136/jitc-2020-001369

Enz, N., Vliegen, G., De Meester, I., and Jungraithmayr, W. (2019). CD26/DPP4 – a potential biomarker and target for cancer therapy. *Pharmacol. Ther.* 198, 135–159. doi: 10.1016/j.pharmthera.2019.02.015

Erkes, D. A., Cai, W., Sanchez, I. M., Purwin, T. J., Rogers, C., Field, C. O., et al. (2020). Mutant BRAF and MEK inhibitors regulate the tumor immune microenvironment via pyroptosis. *Cancer Discov.* 10, 254–269. doi: 10.1158/2159-8290.CD-19-0672

Fanzani, A., and Poli, M. (2017). Iron, oxidative damage and ferroptosis in rhabdomyosarcoma. *Int. J. Mol. Sci.* 18:1718. doi: 10.3390/ijms18081718

Foy, J. P., Bazire, L., Ortiz-Cuaran, S., Deneuve, S., Kielbassa, J., Thomas, E., et al. (2017). A 13-gene expression-based radioresistance score highlights the heterogeneity in the response to radiation therapy across HPV-negative HNSCC molecular subtypes. *BMC Med.* 15:165. doi: 10.1186/s12916-017-0929-y

Friedmann Angeli, J. P., Krysko, D. V., and Conrad, M. (2019). Ferroptosis at the crossroads of cancer-acquired drug resistance and immune evasion. *Nat. Rev. Cancer* 19, 405–414. doi: 10.1038/s41568-019-0149-1

Gagliardi, M., Saverio, V., Monzani, R., Ferrari, E., Piacentini, M., and Corazzari, M. (2020). Ferroptosis: a new unexpected chance to treat metastatic melanoma? *Cell Cycle* 19, 2411–2425. doi: 10.1080/15384101.2020.1806426

Galuppini, F., Dal Pozzo, C. A., Deckert, J., Loupakis, F., Fassan, M., and Baffa, R. (2019). Tumor mutation burden: from comprehensive mutational screening to the clinic. *Cancer Cell Int.* 19:209. doi: 10.1186/s12935-019-0929-4

Gaudet, P., Škunca, N., Hu, J. C., and Dessimoz, C. (2017). Primer on the gene ontology. *Methods Mol. Biol.* 1446, 25–37. doi: 10.1007/978-1-4939-3743-1_3

Gillison, M. L., Chaturvedi, A. K., Anderson, W. F., and Fakhry, C. (2015). Epidemiology of human papillomavirus-positive head and neck squamous cell carcinoma. *J. Clin. Oncol.* 33, 3235–3242. doi: 10.1200/JCO.2015.61.6995

Han, S., Wei, R., Zhang, X., Jiang, N., Fan, M., Huang, J. H., et al. (2019). CPT1A/2-mediated FAO enhancement-a metabolic target in radioresistant breast cancer. *Front. Oncol.* 9:1201. doi: 10.3389/fonc.2019.01201

He, F., Chen, Z., Deng, W., Zhan, T., Huang, X., Zheng, Y., et al. (2021). Development and validation of a novel ferroptosis-related gene signature for predicting prognosis and immune microenvironment in head and neck squamous cell carcinoma. *Int. Immunopharmacol.* 98:107789. doi: 10.1016/j.intimp.2021.107789

Herhaus, L., Al-Salihi, M., Macartney, T., Weidlich, S., and Sapkota, G. P. (2013). OTUB1 enhances TGFβ signalling by inhibiting the ubiquitylation and degradation of active SMAD2/3. *Nat. Commun.* 4:2519. doi: 10.1038/ncomms3519

International Agency for Research on Cancer, and World Health Organization (2021). *Cancer Today*. Available online at: https:// https://gco.iarc.fr/ (accessed March 10, 2021).

Junttila, M. R., and Evan, G. I. (2009). p53–a Jack of all trades but master of none. *Nat. Rev. Cancer* 9, 821–829. doi: 10.1038/nrc2728

Kanehisa, M., Furumichi, M., Tanabe, M., Sato, Y., and Morishima, K. (2017). KEGG: new perspectives on genomes, pathways, diseases and drugs. *Nucleic Acids Res.* 45, D353–D361. doi: 10.1093/nar/gkw1092

Kato, K., Nakajima, K., Ui, A., Muto-Terao, Y., Ogiwara, H., and Nakada, S. (2014). Fine-tuning of DNA damage-dependent ubiquitination by OTUB2 supports the DNA repair pathway choice. *Mol. Cell* 53, 617–630. doi: 10.1016/j.molcel.2014.01.030

Lang, X., Green, M. D., Wang, W., Yu, J., Choi, J. E., Jiang, L., et al. (2019). Radiotherapy and immunotherapy promote tumoral lipid oxidation and ferroptosis via synergistic repression of SLC7A11. *Cancer Discov.* 9, 1673–1685. doi: 10.1158/2159-8290

Lee, H., Zandkarimi, F., Zhang, Y., Meena, J. K., Kim, J., Zhuang, L., et al. (2020). Energy-stress-mediated AMPK activation inhibits ferroptosis. *Nat. Cell Biol.* 22, 225–234. doi: 10.1038/s41556-020-0461-8

Leek, J. T., Johnson, W. E., Parker, H. S., Jaffe, A. E., and Storey, J. D. (2012). The sva package for removing batch effects and other unwanted variation in high-throughput experiments. *Bioinformatics* 28, 882–883. doi: 10.1093/bioinformatics/bts034

Liang, C., Zhang, X., Yang, M., and Dong, X. (2019). Recent progress in ferroptosis inducers for cancer therapy. *Adv. Mater.* 31:e1904197. doi: 10.1002/adma.201904197

Liberzon, A., Birger, C., Thorvaldsdóttir, H., Ghandi, M., Mesirov, J. P., and Tamayo, P. (2015). The molecular signatures database (MSigDB) hallmark gene set collection. *Cell Syst.* 1, 417–425. doi: 10.1016/j.cels.2015.12.004

Liu, B., Su, Q., Ma, J., Chen, C., Wang, L., Che, F., et al. (2021). Prognostic value of eight-gene signature in head and neck squamous carcinoma. *Front. Oncol.* 11:657002. doi: 10.3389/fonc.2021.657002

Liu, H., Schreiber, S. L., and Stockwell, B. R. (2018). Targeting dependency on the GPX4 lipid peroxide repair pathway for cancer therapy. *Biochemistry* 57, 2059–2060. doi: 10.1021/acs.biochem.8b00307

Liu, J., Kuang, F., Kroemer, G., Klionsky, D. J., Kang, R., and Tang, D. (2020). Autophagy-dependent ferroptosis: machinery and regulation. *Cell Chem. Biol.* 27, 420–435. doi: 10.1016/j.chembiol.2020.02.005

Liu, M., Li, F., Liu, B., Jian, Y., Zhang, D., Zhou, H., et al. (2021). Profiles of immune cell infiltration and immune-related genes in the tumor microenvironment of esophageal squamous cell carcinoma. *BMC Med. Genomics* 14:75. doi: 10.1186/s12920-021-00928-9

Mashima, T., Oh-hara, T., Sato, S., Mochizuki, M., Sugimoto, Y., Yamazaki, K., et al. (2005). p53-defective tumors with a functional apoptosome-mediated pathway: a new therapeutic target. *J. Natl. Cancer Inst.* 97, 765–777. doi: 10.1093/jnci/dji133

Matsuzawa, A., Saegusa, K., Noguchi, T., Sadamitsu, C., Nishitoh, H., Nagai, S., et al. (2005). ROS-dependent activation of the TRAF6-ASK1-p38 pathway is selectively required for TLR4-mediated innate immunity. *Nat. Immunol.* 6, 587–592. doi: 10.1038/ni1200

McGrail, D. J., Pilié, P. G., Rashid, N. U., Voorwerk, L., Slagter, M., Kok, M., et al. (2021). High tumor mutation burden fails to predict immune checkpoint blockade response across all cancer types. *Ann. Oncol.* 32, 661–672. doi: 10.1016/j.annonc.2021.02.006

Mizumura, K., Takeda, K., Hashimoto, S., Horie, T., and Ichijo, H. (2006). Identification of Op18/stathmin as a potential target of ASK1-p38 MAP kinase cascade. *J. Cell. Physiol.* 206, 363–370. doi: 10.1002/jcp.20465

Mou, Y., Wang, J., Wu, J., He, D., Zhang, C., Duan, C., et al. (2019). Ferroptosis, a new form of cell death: opportunities and challenges in cancer. *J. Hematol. Oncol.* 12:34. doi: 10.1186/s13045-019-0720-y

Mulas, F., Wang, X., Song, S., Nishanth, G., Yi, W., Brunn, A., et al. (2021). The deubiquitinase OTUB1 augments NF-κB-dependent immune responses in dendritic cells in infection and inflammation by stabilizing UBC13. *Cell. Mol. Immunol.* 18, 1512–1527. doi: 10.1038/s41423-020-0362-6

Muzaffar, J., Bari, S., Kirtane, K., and Chung, C. H. (2021). Recent advances and future directions in clinical management of head and neck squamous cell carcinoma. *Cancers* 13:338. doi: 10.3390/cancers13020338

Nagai, H., Noguchi, T., Takeda, K., and Ichijo, H. (2007). Pathophysiological roles of ASK1-MAP kinase signaling pathways. *J. Biochem. Mol. Biol.* 40, 1–6. doi: 10.5483/bmbrep.2007.40.1.001

Padanad, M. S., Konstantinidou, G., Venkateswaran, N., Melegari, M., Rindhe, S., Mitsche, M., et al. (2016). Fatty acid oxidation mediated by Acyl-CoA synthetase long chain 3 is required for mutant KRAS lung tumorigenesis. *Cell Rep.* 16, 1614–1628. doi: 10.1016/j.celrep.2016.07.009

Pearce, E. L., Poffenberger, M. C., Chang, C. H., and Jones, R. G. (2013). Fueling immunity: insights into metabolism and lymphocyte function. *Science* 342:1242454. doi: 10.1126/science.1242454

Reinhold, W. C., Varma, S., Sunshine, M., Elloumi, F., Ofori-Atta, K., Lee, S., et al. (2019). RNA sequencing of the NCI-60: integration into CellMiner and CellMiner CDB. *Cancer Res.* 79, 3514–3524. doi: 10.1158/0008-5472.CAN-18-2047

Ritchie, M. E., Phipson, B., Wu, D., Hu, Y., Law, C. W., Shi, W., et al. (2015). limma powers differential expression analyses for RNA-sequencing and microarray studies. *Nucleic Acids Res.* 43:e47. doi: 10.1093/nar/gkv007

Samra, B., Tam, E., Baseri, B., and Shapira, I. (2018). Checkpoint inhibitors in head and neck cancer: current knowledge and perspectives. *J. Investig. Med.* 66, 1023–1030. doi: 10.1136/jim-2018-000743

Stenson, K. M. (2021). *Epidemiology and Risk Factors for Head and Neck Cancer*. Available online at: https://www.uptodate.com/contents/epidemiology-and-risk-factors-for-head-and-neck-cancer (accessed March 10, 2021).

Stockwell, B. R., and Jiang, X. (2019). A physiological function for ferroptosis in tumor suppression by the immune system. *Cell Metab.* 30, 14–15. doi: 10.1016/j.cmet.2019.06.012

Stockwell, B. R., Friedmann Angeli, J. P., Bayir, H., Bush, A. I., Conrad, M., Dixon, S. J., et al. (2017). Ferroptosis: a regulated cell death nexus linking metabolism, redox biology, and disease. *Cell* 171, 273–285. doi: 10.1016/j.cell.2017.09.021

Subramanian, R. R., Zhang, H., Wang, H., Ichijo, H., Miyashita, T., and Fu, H. (2004). Interaction of apoptosis signal-regulating kinase 1 with isoforms of 14-3-3 proteins. *Exp. Cell Res.* 294, 581–591. doi: 10.1016/j.yexcr.2003.12.009

Sun, X. X., Challagundla, K. B., and Dai, M. S. (2012). Positive regulation of p53 stability and activity by the deubiquitinating enzyme Otubain 1. *EMBO J.* 31, 576–592. doi: 10.1038/emboj.2011.434

Tang, D., Chen, X., Kang, R., and Kroemer, G. (2021). Ferroptosis: molecular mechanisms and health implications. *Cell Res.* 31, 107–125. doi: 10.1038/s41422-020-00441-1

Torre, L. A., Bray, F., Siegel, R. L., Ferlay, J., Lortet-Tieulent, J., and Jemal, A. (2015). Global cancer statistics, 2012. *CA Cancer J. Clin.* 65, 87–108. doi: 10.3322/caac.21262

Ventola, C. L. (2017). Cancer immunotherapy part 3: challenges and future trends. *P T* 42, 514–521.

Wang, W., Green, M., Choi, J. E., Gijón, M., Kennedy, P. D., Johnson, J. K., et al. (2019). CD8(+) T cells regulate tumour ferroptosis during cancer immunotherapy. *Nature* 569, 270–274. doi: 10.1038/s41586-019-1170-y

WHO (2020). *WHO Report on Cancer: Setting Priorities, Investing Wisely and Providing Care for All*. Geneva: World Health Organization.

Wiener, R., Zhang, X., Wang, T., and Wolberger, C. (2012). The mechanism of OTUB1-mediated inhibition of ubiquitination. *Nature* 483, 618–622. doi: 10.1038/nature10911

Wu, D., Zhang, P., Li, F., Shen, Y., Chen, H., and Feng, Y. (2020). CD138(-) multiple myeloma cells express high level of CHK1 which correlated to overall survival in MM patient. *Aging* 12, 23067–23081. doi: 10.18632/aging.104066

Wu, Y., Fabritius, M., and Ip, C. (2009). Chemotherapeutic sensitization by endoplasmic reticulum stress: increasing the efficacy of taxane against prostate cancer. *Cancer Biol. Ther.* 8, 146–152. doi: 10.4161/cbt.8.2.7087

Yamashita, Y., Kumabe, T., Cho, Y. Y., Watanabe, M., Kawagishi, J., and Yoshimoto, T. (2000). Fatty acid induced glioma cell growth is mediated by the acyl-CoA synthetase 5 gene located on chromosome 10q25.1-q25.2, a region frequently deleted in malignant gliomas. *Oncogene* 19, 5919–5925. doi: 10.1038/sj.onc.1203981

Yang, C., Mei, H., Peng, L., Jiang, F., Xie, B., and Li, J. (2020). Prognostic correlation of an autophagy-related gene signature in patients with head and neck squamous cell carcinoma. *Comput. Math. Methods Med.* 2020:7397132. doi: 10.1155/2020/7397132

Yi, J., Zhu, J., Wu, J., Thompson, C. B., and Jiang, X. (2020). Oncogenic activation of PI3K-AKT-mTOR signaling suppresses ferroptosis via SREBP-mediated lipogenesis. *Proc. Natl. Acad. Sci. U.S.A.* 117, 31189–31197. doi: 10.1073/pnas.2017152117

Zhang, M., Wang, X., Chen, X., Zhang, Q., and Hong, J. (2020). Novel immune-related gene signature for risk stratification and prognosis of survival in lower-grade glioma. *Front. Genet.* 11:363. doi: 10.3389/fgene.2020.00363

Zhou, L., Zhao, B., Zhang, L., Wang, S., Dong, D., Lv, H., et al. (2018). Alterations in cellular iron metabolism provide more therapeutic opportunities for cancer. *Int. J. Mol. Sci.* 19:1545. doi: 10.3390/ijms19051545

Zhou, N., and Bao, J. (2020). FerrDb: a manually curated resource for regulators and markers of ferroptosis and ferroptosis-disease associations. *Database* 2020:baaa021. doi: 10.1093/database/baaa021

Conflict of Interest: The authors declare that the research was conducted in the absence of any commercial or financial relationships that could be construed as a potential conflict of interest.

Publisher's Note: All claims expressed in this article are solely those of the authors and do not necessarily represent those of their affiliated organizations, or those of the publisher, the editors and the reviewers. Any product that may be evaluated in this article, or claim that may be made by its manufacturer, is not guaranteed or endorsed by the publisher.

frontiers in Cell and Developmental Biology

ORIGINAL RESEARCH
published: 04 November 2021
doi: 10.3389/fcell.2021.777215

A Novel Prognostic Model Based on the Serum Iron Level for Patients With Early-Stage Triple-Negative Breast Cancer

*Xin Hua†, Fangfang Duan†, Jiajia Huang†, Xiwen Bi, Wen Xia, Chenge Song, Li Wang, Chang Jiang and Zhongyu Yuan**

Department of Medical Oncology, The State Key Laboratory of Oncology in South China, Collaborative Innovation Center for Cancer Medicine, Sun Yat-sen University Cancer Center, Guangzhou, China

The dysregulation of iron homeostasis has been explored in malignancies. However, studies focusing on the association between the serum iron level and prognosis of patients with early-stage triple-negative breast cancer (TNBC) are scarce. Accordingly, in current study, 272 patients with early-stage TNBC treated at Sun Yat-sen University Cancer Center (SYSUCC) between September 2005 and October 2016 were included as a training cohort, another 86 patients from a previous randomized trial, SYSUCC-001, were analyzed as a validation cohort (SYSUCC-001 cohort). We retrospectively collected their clinicopathological data and tested the serum iron level using blood samples at the diagnosis. In the training cohort, patients were divided into low-iron and high-iron groups according to the serum iron level cut-off of 17.84 μmol/L determined by maximally selected rank statistics. After a median follow-up of 87.10 months, patients with a low iron had a significantly longer median disease-free survival (DFS) of 89.13 [interquartile range (IQR): 66.88–117.38] months and median overall survival (OS) of 92.85 (IQR: 68.83–117.38) months than those in the high-iron group (median DFS: 75.25, IQR: 39.76–105.70 months, $P = 0.015$; median OS: 77.17, IQR: 59.38–110.28 months, $P = 0.015$). Univariate and multivariate Cox analysis demonstrated the serum iron level to be an independent predictor for DFS and OS. Then, a prognostic nomogram incorporating the serum iron level, T stage and N stage was developed for individualized prognosis predictions. It had good discriminative ability with a C-index of DFS (0.729; 95% CI 0.666–0.792) and OS (0.739; 95% CI 0.666–0.812), respectively. Furtherly, we validated the predictive model in the SYSUCC-001 cohort, which also showed excellent predictive performance with a C-index of DFS (0.735; 95% CI 0.614–0.855) and OS (0.722; 95% CI 0.577–0.867), respectively. All these suggested that the serum iron level might be a potential prognostic biomarker for patients with early-stage TNBC, the predictive model based on it might be served as a practical tool for individualized survival predictions.

Keywords: serum iron level, early-stage triple-negative breast cancer, predictive model, nomogram, survival

OPEN ACCESS

Edited by:
Chang Gong,
Sun Yat-sen University, China

Reviewed by:
Jian Zhang,
Fudan University, China
Shu Wang,
Peking University People's Hospital, China

***Correspondence:**
Zhongyu Yuan
yuanzhy@sysucc.org.cn

†These authors share first authorship

Specialty section:
This article was submitted to Molecular and Cellular Oncology, a section of the journal Frontiers in Cell and Developmental Biology

Received: *15 September 2021*
Accepted: *11 October 2021*
Published: *04 November 2021*

Citation:
Hua X, Duan F, Huang J, Bi X, Xia W, Song C, Wang L, Jiang C and Yuan Z (2021) A Novel Prognostic Model Based on the Serum Iron Level for Patients With Early-Stage Triple-Negative Breast Cancer. Front. Cell Dev. Biol. 9:777215. doi: 10.3389/fcell.2021.777215

INTRODUCTION

Triple-negative breast cancer (TNBC), lacking the expression of estrogen receptor (ER), progesterone receptor (PR), and human epidermal growth factor receptor 2 (HER-2), accounts for about 10–15% and is the most aggressive molecular subtype of all breast tumors (Sung et al., 2021; Wang et al., 2021). Due to its invasiveness, early relapse, strong heterogeneity and limited therapeutic options, TNBC patients usually have distant metastasis at the diagnosis and worse long-term clinical outcomes compared with patients with other subtypes of breast cancer (Gadi and Davidson, 2017; Vagia et al., 2020). In recent years, advances in the landscape of diagnosis and treatment have elicited survival benefits for patients with TNBC. Nevertheless, TNBC remains a huge threat to life due to its recurrence and relatively high mortality (Dent et al., 2007; Bianchini et al., 2016; Garrido-Castro et al., 2019). Thus, identification of novel, accurate biomarkers, and exploration of individualized therapeutic targets for women with TNBC is very necessary.

Iron is a critical trace element for the activity of many proteins and enzymes. Iron is involved in cell respiration, oxygen transport, energy metabolism, DNA repair, and different signaling pathways (Torti et al., 2018). It is essential for human health, but excess iron or iron overload due to disorders of iron metabolism can induce severe toxicity even tumorigenesis in humans (Wu et al., 2004; Adams, 2015).

Increasing studies have demonstrated an association between consumption of red meat, intake of heme iron, or dietary intake of iron and initiation of breast cancer (Ferrucci et al., 2009; Guo J. et al., 2015; Inoue-Choi et al., 2016). Also, dysregulation of systemic iron homeostasis is a risk factor for the initiation, growth, progression, and metastasis of tumor cells (Bingham et al., 2002; Radulescu et al., 2012; Guo W. et al., 2015). Besides, iron accumulation has an important role in multiple cell-death pathways, including iron-dependent cell death, i.e., ferroptosis, which suggests a potential therapeutic target to inhibit tumor development in cancer patients (Dixon et al., 2012; Basuli et al., 2017). Several preclinical/clinical studies have explored the anti-tumor activity and safety of depleting iron overload in tumors by means of iron chelators (Nutting et al., 2009; Yamasaki et al., 2011; List et al., 2012; Neufeld et al., 2012; Kalinowski et al., 2016). Targeting an increased iron level instead of iron chelators could also be a novel treatment option (Stockwell et al., 2017; von Hagens et al., 2017). Usually, researchers obtain values for iron by measuring circulating levels of iron-bound proteins (e.g., transferrin, ferritin) (Hambidge, 2003; Fonseca-Nunes et al., 2014; Morales and Xue, 2021). However, direct measurement of iron is more accurate to reflect the iron level in the body, but is poorly understood.

Thus, we explored the association between the baseline serum iron level at the diagnosis and clinical prognosis of women with early-stage TNBC. We aimed to establish a model on basis of direct measurement of the serum iron level for individualized prognosis predictions and treatment guidance.

MATERIALS AND METHODS

Study Design and Patient Eligibility

We retrospectively analyzed the prognostic value of the serum iron level in women newly diagnosed with TNBC between September 2005 and October 2016 at Sun Yat-sen University Cancer Center (SYSUCC) in Guangzhou, China. Approval for our study protocol was obtained from the Ethics Committees of SYSUCC (2021-FXY-140). The requirement for written

TABLE 1 | Characteristics of eligible patients.

Characteristic	ALL	Training cohort	SYSUCC-001
	N = 358	*N* = 272	*N* = 86
Age (years), median (IQR)	46.8 (39.3–56.0)	48.0 (41.0–49.2)	43.5 (37.3–50.8)
Age at the diagnosis (years)			
< 50	208 (58.1%)	149 (54.8%)	59 (68.6%)
≥ 50	150 (41.9%)	123 (45.2%)	27 (31.4%)
T stage [a]			
T1	121 (33.8%)	92 (33.8%)	29 (33.7%)
T2	204 (57.0%)	151 (55.5%)	53 (61.7%)
T3	25 (7.0%)	23 (8.5%)	2 (2.3%)
T4	8 (2.2%)	6 (2.2%)	2 (2.3%)
N stage [a]			
N0	208 (58.1%)	156 (57.4%)	52 (60.5%)
N1	82 (22.9%)	63 (23.2%)	19 (22.1%)
N2	34 (9.5%)	28 (10.3%)	6 (6.9%)
N3	34 (9.5%)	25 (9.1%)	9 (10.5%)
Menopausal status			
Premenopausal	242 (67.6%)	174 (63.8%)	68 (79.1%)
Postmenopausal	116 (32.4%)	98 (36.2%)	18 (20.9%)
Pathological grade [b]			
1	6 (1.7%)	5 (1.84%)	1 (1.1%)
2	130 (36.3%)	114 (41.9%)	16 (18.6%)
3	213 (59.5%)	153 (56.2%)	60 (69.8%)
4	9 (2.5%)	0 (0.0%)	9 (10.5%)
Ki-67 Index [c]			
< 30%	75 (20.9%)	63 (23.2%)	12 (14.0%)
≥ 30%	283 (79.1%)	209 (76.8%)	74 (86.0%)
Lymphovascular invasion			
No	284 (79.4%)	213 (78.3%)	71 (82.6%)
Yes	74 (20.6%)	59 (21.7%)	15 (17.4%)
Serum iron (μmol/L) [d], median (IQR)	14.7 (10.9–18.8)	14.7 (11.1–18.9)	14.6 (10.6–18.9)
Serum iron (μmol/L) [d]			
High	114 (31.8%)	88 (32.4%)	26 (30.2%)
Low	244 (68.2%)	184 (67.6%)	60 (69.8%)

[a] *Diagnosed based on the AJCC 2010 criteria (seventh edition).*
[b] *Histological grade at the diagnosis was based on the degree of tumor differentiation.*
[c] *The Ki-67 index at the diagnosis indicates DNA synthetic activity as measured using immunocytochemistry.*
[d] *The cut-off value was determined by means of maximally selected rank statistics. IQR, interquartile range.*

informed consent from patients were waived due to the retrospective nature of our study. We processed all personal data anonymously following the Helsinki Declaration 1964 and its later amendments.

The inclusion criteria were: (i) age ≥ 18 years; (ii) breast cancer diagnosed by pathology; (iii) hormone receptor-negative [<1% or 0 by immunohistochemical (IHC) staining in nuclei] according to American Society of Clinical Oncology (ASCO)/College of American Pathologists (CAP) guideline (Allison et al., 2020) and HER2-negative (scored as 0, 1 +, or 2 + by IHC analyses without amplification of the ERBB2 gene on fluorescence *in situ* hybridization) disease; (iv) patients were restaged at T1-4N0-3M0 according to the seventh version of the American Joint Committee on Cancer (AJCC 2010); (v) complete clinicopathological information and blood samples obtained within 1 week of the diagnosis.

Patients were excluded if they met the following criteria: (i) local relapse or distant metastasis at the diagnosis (i.e., brain, lung, bone, liver); (ii) pregnancy; (iii) previous malignancy including breast cancer; (iv) severe or uncontrolled complications.

Data Collection and Measurement of Serum Iron Level

We retrieved the clinicopathological information of enrolled patients from the electronic medical records system of SYSUCC. We obtained their blood samples within 1 week of initiation of any anti-cancer treatment from the Tumor Resource Library of SYSUCC. Measurement of the serum iron level of participants was conducted using the Iron (Fe) Assay Kit (PAESA Chromogenic Method) of the Cobas 8000 system (Roche Diagnostics, Basel, Switzerland).

Follow-Up and Endpoints

Follow-up data were obtained using the outpatient electronic records of SYSUCC or telephone interviews. Patients were evaluated every 3 months within 2 years of the diagnosis, then every 6 months until 5 years and, subsequently, annually. The assessment comprised routine hematology and laboratory tests, menopausal status, ultrasound (breast, abdomen) or computed tomography. Radiography and bone scintigraphy were undertaken annually.

The primary endpoint was disease-free survival (DFS), which was defined as the time from the diagnosis to the first disease progression or death due to any cause. The second endpoint was overall survival (OS), which was defined as the time from the diagnosis to death due to any cause.

Statistical Analysis

Age is shown as the median with interquartile range (IQR). Categorical variables are listed as frequencies with percentages. The cutoff for the serum iron level was determined by maximally selected rank statistics using the "maxstat" plugin (R Institute of Statistical Computing, Vienna, Austria). We stratified patients with early-stage TNBC into low- and high-iron groups. Survival curves of these two groups were estimated by the Kaplan–Meier method and compared using the log-rank test. If $P < 0.05$ was achieved in the univariate Cox regression model, factors could be analyzed further in the multivariate Cox proportional hazards

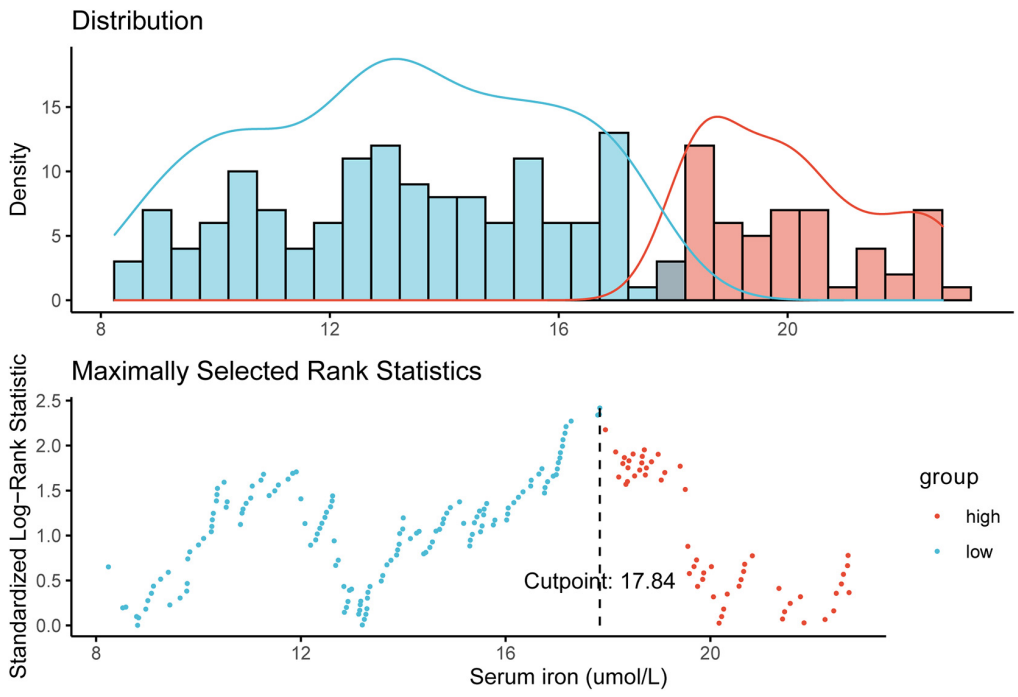

FIGURE 1 | Definition of the cutoff of 17.84 μmol/L for the serum iron level according to maximally selected log-rank statistics.

analysis. Factors were examined according to the Schoenfeld residuals (Wileyto et al., 2013), and their corresponding hazard ratios with 95% confidence interval (CIs) were estimated. Subsequently, a prognostic nomogram incorporating the serum iron level with other independent clinicopathological indicators was developed. The discrimination performance of the predictive nomogram was assessed by the Concordance Index (C- index), calibration curves, and time-dependent receiver operating

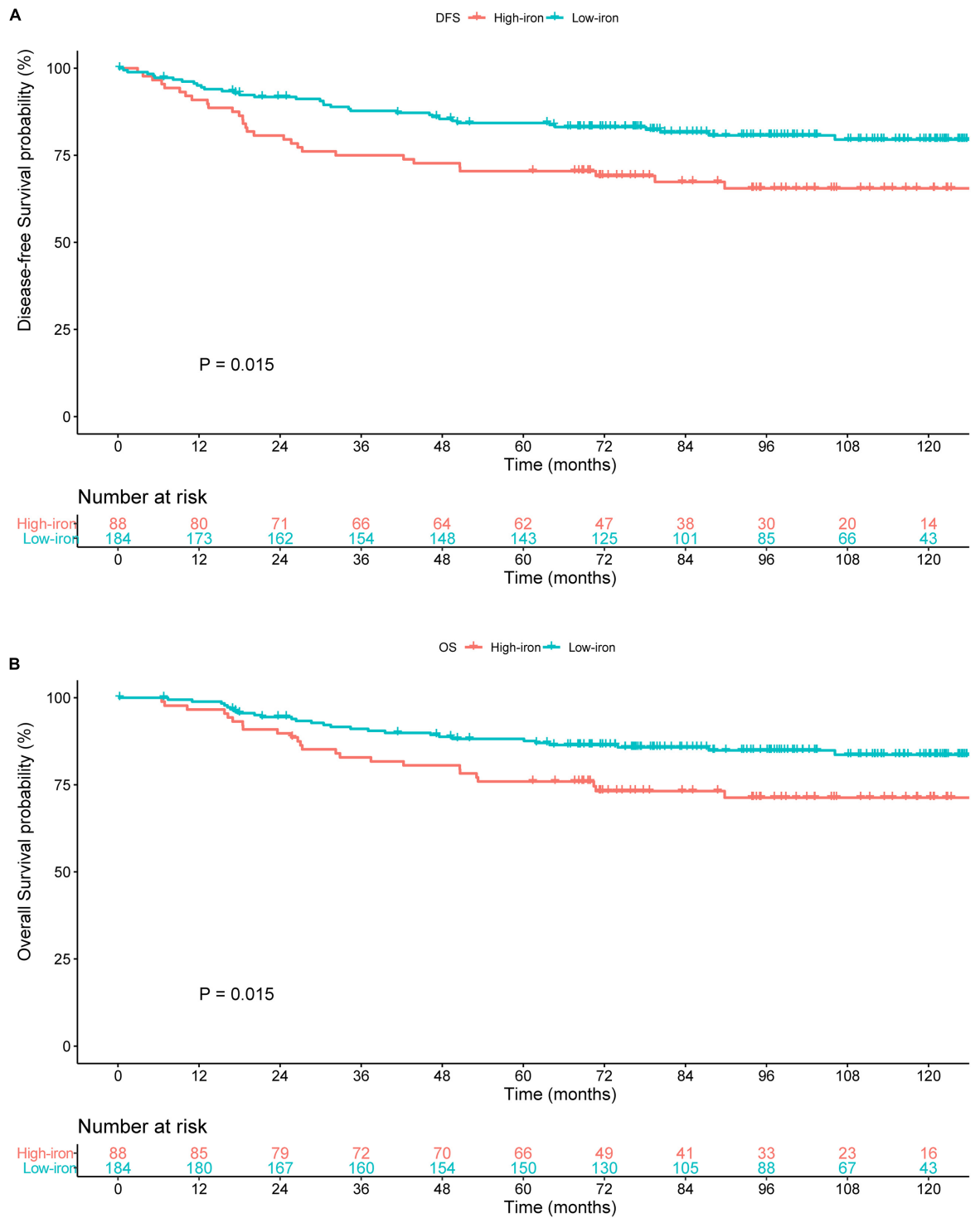

FIGURE 2 | Survival curves estimated by the Kaplan–Meier method and compared with log-rank tests in different groups of serum iron level in the training cohort. **(A)** Disease-free survival (DFS) curve. **(B)** Overall survival (OS) curve. Low iron: ≤ 17.84 μmol/L; high iron: > 17.84 μmol/L.

characteristic (ROC) curves in the training cohort and validation (SYSUCC-001) cohort. $P < 0.05$ (two-sided) was considered significant. Statistical analyses were conducted using R 4.0.1.

RESULTS

Patients Clinicopathologic Characteristics in the Training Cohort

After excluding 75 women due to incomplete data (30 without the Ki67 Index; 38 without the histology grade; four without lymphovascular invasion; three without the T stage). Finally, a total of 358 patients with early-stage TNBC were eligible: 272 in the training cohort and 86 in the SYSUCC-001 cohort. The clinicopathological characteristics of patients are listed in **Table 1**.

In the training cohort, the median age was 48.0 (IQR 41.0–49.2) years. A total of 174 (63.8%) women were premenopausal and 98 (36.2%) were postmenopausal. Most patients (76.8%) had Ki-67 Index ≥ 30%. Also, 92 (33.8%), 151 (55.5%), 23 (8.5%), and 6 (2.2%) patients had a pathological stage of T1, T2, T3, and T4, respectively. In addition, 156 (57.4%) had the N0 stage, whereas N1, N2, and N3 stages accounted for 63 (23.2%), 28 (10.3%), and 25 (9.1%), respectively.

Optimal Cut-Off Value of Serum Iron Level in the Training Cohort

We defined 17.84 μmol/L as the optimal cutoff of the serum iron level to stratify patients into two different iron groups according to maximally selected rank statistics (**Figure 1**). Eighty-eight (32.4%) women were classified into the high-iron group with serum iron > 17.84 μmol/L, and the other 184 (67.6%) patients had serum iron ≤ 17.84 μmol/L (**Table 1**).

Survival Outcomes in the Training Cohort

The median duration of follow-up was 87.10 months. In the training cohort, compared with patients with a low serum iron level, patients with early-stage TNBC in the high-iron group achieved significantly shorter median DFS (89.13, IQR: 66.88–117.38 months vs. 75.25, IQR: 39.76–105.70 months, $P = 0.015$) (**Figure 2A**) and median OS (92.85, IQR: 68.83–117.38 months vs. 77.17, IQR: 59.38–110.28 months, $P = 0.015$) (**Figure 2B**), respectively.

Development of the Prognostic Model

Table 2 shows results of the univariate Cox analysis for DFS in the training cohort. Variates achieved the predetermined significance ($P < 0.05$) in the univariate Cox regression model. Hence, age, menopausal status, lymphovascular invasion, T stage, N stage, and serum iron level were entered into the multivariate Cox analysis. The latter demonstrated that the N stage and serum iron level continued to be related significantly to DFS in patients with early-stage TNBC (**Figure 3A**). Then, a prognostic model incorporating the T stage, N stage, and serum iron level was established to predict DFS individually (**Figure 4A**).

Age, menopausal status, lymphovascular invasion, T stage, N stage, and serum iron level were recognized as independent predictors of OS for patients with early-stage TNBC (**Table 2**). Subsequently, the T stage, N stage, and serum iron level continued to be independent indicators for OS in patients with early-stage TNBC according to the multivariate Cox regression model (**Figure 3B**). On basis of the three independent prognostic factors stated above, we developed a model for individualized prediction of OS (**Figure 5A**).

Evaluation of Predictive Performance of the Prognostic Model

The discriminative accuracy and prognostic ability of the prognostic nomogram of DFS were very good. It achieved a good C-index of 0.729 (95%CI 0.666–0.792) in the training cohort and 0.735 (95%CI 0.614–0.855) in the SYSUCC-001 cohort, respectively. Calibration plots for 1−, 3−, and 5-year DFS showed satisfactory consistency between the actual DFS and nomogram-predicted DFS in the training cohort and SYSUCC-001 cohort (**Figures 4B,C**). Time-dependent ROC curves suggested that the prognostic value of this

A

Variable		Hazard ratio	p
Serum iron	High	Reference	
	Low	0.53 (0.32, 0.89)	0.015*
Menopausal status	1	Reference	
	2	0.91 (0.37, 2.22)	0.836
Age	< 50	Reference	
	≥ 50	1.40 (0.59, 3.35)	0.450
Lymphovascular invasion	0	Reference	
	1	1.63 (0.90, 2.98)	0.110
T stage	T1	Reference	
	T2	0.81 (0.46, 1.41)	0.453
	T3	0.75 (0.28, 2.00)	0.563
	T4	2.69 (0.88, 8.22)	0.083
N stage	N0	Reference	
	N1	2.24 (1.17, 4.29)	0.015*
	N2	3.33 (1.57, 7.08)	0.002*
	N3	4.43 (2.00, 9.81)	<0.001*

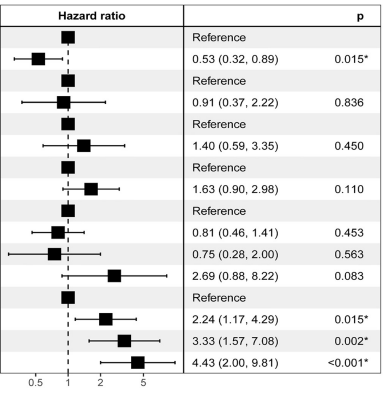

B

Variable		Hazard ratio	p
Serum iron	High	Reference	
	Low	0.45 (0.26, 0.80)	0.006
Lymphovascular invasion	0	Reference	
	1	1.74 (0.89, 3.39)	0.104
T stage	T1	Reference	
	T2	0.75 (0.40, 1.41)	0.365
	T3	0.78 (0.29, 2.09)	0.625
	T4	4.50 (1.46, 13.81)	0.009
N stage	N0	Reference	
	N1	1.65 (0.77, 3.51)	0.196
	N2	3.38 (1.47, 7.78)	0.004
	N3	5.08 (2.19, 11.79)	<0.001

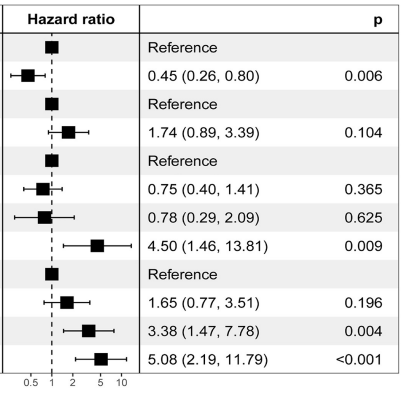

FIGURE 3 | Results of stepwise multivariate Cox models in the training cohort are showed as forest plots. **(A)** Forest plot of disease-free survival (DFS). **(B)** Forest plot of overall survival (OS).

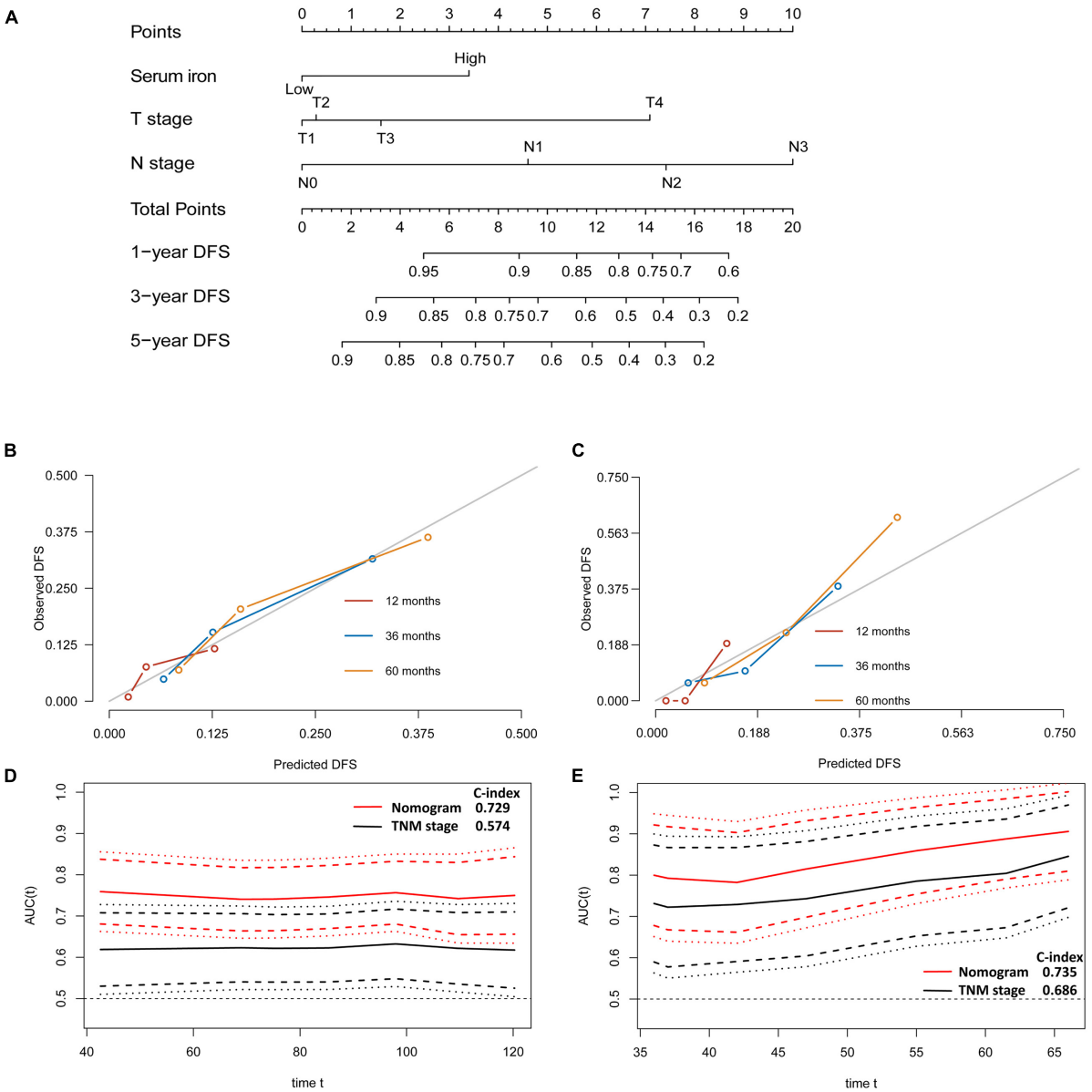

FIGURE 4 | Establishment and validation of a model for individualized prediction of disease-free survival (DFS). **(A)** Nomogram of this predictive model for patients with early-stage triple-negative breast cancer. **(B)** Calibration plots of 1−, 3−, and 5-year DFS predictions in the training cohort. **(C)** Calibration plots of 1−, 3−, and 5-year DFS predictions in the SYSUCC-001 validation cohort. **(D)** Time-dependent receiver operating characteristic (ROC) curves in the training cohort. **(E)** Time-dependent ROC curves in the SYSUCC-001 cohort.

nomogram for DFS was much better than that using the traditional tumor-node-metastasis (TNM) staging system in the training cohort (**Figure 4D**) and SYSUCC-001 cohort, respectively (**Figure 4E**).

The predictive nomogram of OS also had good discrimination with a satisfactory C Index of 0.739 (95%CI 0.666–0.812) in the training cohort and 0.722 (95%CI 0.577–0.867) in the SYSUCC-001 cohort, respectively. Good agreement between the observed 1−, 3−, and 5-year OS and nomogram-predicted 1−, 3−, and 5-year OS was documented in the calibration plot (**Figures 5B,C**). Moreover, compared with traditional TNM staging, the prognostic accuracy of this predictive nomogram in OS was more accurate based on the time-dependent ROC curves in the training cohort (**Figure 5D**) and SYSUCC-001 cohort, respectively (**Figure 5E**).

DISCUSSION

In this study, we determined a cut-off value of 17.84 μmol/L for the serum iron level to stratify heterogeneous female with early-stage TNBC into low- and high-iron groups according

TABLE 2 | Univariate Cox regression analysis of overall survival and disease-free survival in women with breast cancer in the training cohort.

Characteristics	Overall survival		Disease-free survival	
	Hazard ratio (95%CI)	*P*	Hazard ratio (95%CI)	*P*
Age (year)				
< 50	Reference		Reference	
≥ 50	**2.039 (1.162–3.579)**	**0.013***	**1.732 (1.060–2.830)**	**0.029***
Menopausal status				
Premenopausal	Reference		Reference	
Postmenopausal	**1.826 (1.054–3.163)**	**0.032***	**1.625 (0.998–2.647)**	**0.051**
Histological grade [a]				
½	Reference		Reference	
3	1.246 (0.734–2.116)	0.415	1.098 (0.670–1.723)	0.685
Lymphovascular invasion				
No	Reference		Reference	
Yes	**2.752 (1.555–4.870)**	**0.001***	**2.513 (1.491–4.236)**	**0.001***
Ki-67 index at diagnosis < 30% [b]				
No	Reference		Reference	
Yes	1.272 (0.637–2.539)	0.496	1.085 (0.606–1.943)	0.783
T stage[c]				
1	Reference		Reference	
2	0.854 (0.459–1.590)	0.619	0.826 (0.483–1.412)	0.484
3	1.412 (0.560–3.601)	0.419	1.062 (0.432–2.610)	0.896
4	**5.034 (1.691–14.990)**	**0.004***	**3.496 (1.206–10.132)**	**0.021***
N stage [c]				
0	Reference		Reference	
1	1.882 (0.899–3.941)	0.094*	**2.416 (1.283–4.546)**	**0.006***
2	**3.571 (1.634–7.804)**	**0.001***	**3.582 (1.761–7.284)**	**<0.001***
3	**6.669 (3.174–14.014)**	**<0.001***	**6.767 (3.419–13.393)**	**<0.001***
Serum iron level (μmol/L) [d]				
High	Reference		Reference	
Low	**2.560 (1.363–4.811)**	**0.017***	**0.550 (0.337–0.897)**	**0.017***

**P<0.05.*

[a] *Histological grade at the diagnosis was based on the degree of tumor differentiation.*

[b] *The Ki-67 index at the diagnosis indicates DNA synthetic activity as measured using immunocytochemistry.*

[c] *Diagnosed based on the AJCC 2010 criteria (seventh edition).*

[d] *The cut-off value was determined by maximally selected rank statistics.*

The bold values represents that features reach to the predetermined significance threshold (P < 0.05) in the univariate Cox regression model.

to maximally selected rank statistics. Patients in the high-iron group had a significantly shorter median survival than those in the low-iron group. Multivariate Cox regression analysis revealed that a high serum iron level continued to be an independent predicator of poor survival in patients with early-stage TNBC. Then, a prognostic model combining the serum iron level and two clinicopathological factors (T stage, N stage) was established and represented graphically as a nomogram. The latter showed satisfactory discriminative accuracy and good predictive consistency between the actual survival probability and nomogram-predicted clinical outcome in the training cohort and SYSUCC-001 cohort, respectively.

Iron is essential for the activity or inhibition of various proteins and enzymes involved in many biological processes (Adams, 2015; Torti et al., 2018). However, iron also contributes to oxidative stress, which can result in damage to DNA. Increasing numbers of studies have demonstrated that homeostatic dysregulation of iron metabolism and changes in distribution of iron in serum are found in different types of cancers, including breast cancer (Galaris and Pantopoulos, 2008; Torti et al., 2018). Excess iron or iron overload due to dysregulation of iron homeostasis can promote the development, progression, and metastasis of tumor cells (Bingham et al., 2002; Radulescu et al., 2012; Guo W. et al., 2015).

The main source of biologically available iron comes from dietary intake. More and more studies have explored a positive relationship between the intake of red meat, heme iron, and initiation of breast tumors (Ferrucci et al., 2009; Guo J. et al., 2015; Inoue-Choi et al., 2016). Also, iron accumulation might have a significant role in multiple pathways of programmed cell death, including apoptosis, necroptosis, ascorbate-mediated death, and ferroptosis (Dixon et al., 2012; Basuli et al., 2017; Torti et al., 2018). Therefore, iron chelators, because of depleting iron levels in the body, have been investigated as a potential therapeutic strategy with promising outcomes for cancer patients (Nutting et al., 2009;

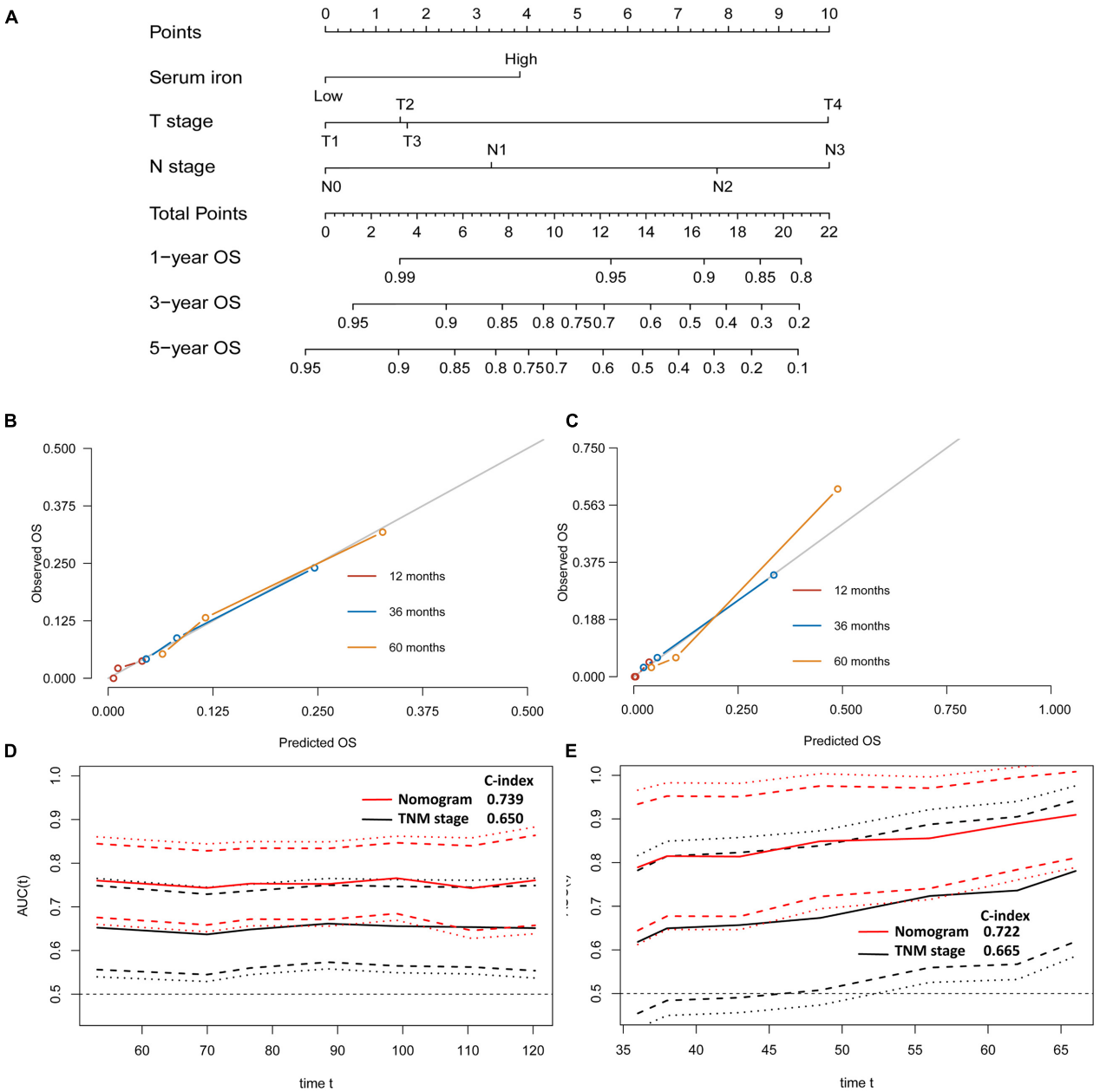

FIGURE 5 | Establishment and validation of a model for individualized prediction of overall survival (OS). **(A)** Nomogram of this predictive model for patients with early-stage triple-negative breast cancer. **(B)** Calibration plots for predicting OS at 1−, 3−, and 5-year in the training cohort. **(C)** Calibration plots for predicting OS at 1−, 3−, and 5-year in the SYSUCC-001 validation cohort. **(D)** Time-dependent receiver operating characteristic (ROC) curves in the training cohort. **(E)** Time-dependent ROC curves in the SYSUCC-001 cohort.

Yamasaki et al., 2011; List et al., 2012; Neufeld et al., 2012; Kalinowski et al., 2016).

Excess iron can lead to lipid peroxidation, DNA/protein damage, as well as the initiation and progression of tumors (Galaris and Pantopoulos, 2008; Radulescu et al., 2012; Guo W. et al., 2015; Torti et al., 2018). Conversely, the toxicity of iron accumulation can promote lethal damage to tumor cells by peroxidation of membrane lipids, subsequently, contribute to interruption of tumorigenesis and tumor development (Wang et al., 2018; Chang et al., 2019). Hence, iron overload or iron depletion might provide potential targets for anti-tumor treatment. Therefore, exploring the relationship between iron levels in the body and cancer is a rational approach.

Most studies have assessed iron levels in the body by measuring circulating levels of iron-bound proteins (e.g., transferrin, ferritin) (Hambidge, 2003; Fonseca-Nunes et al., 2014; Morales and Xue, 2021). However, this strategy might generate errors in reflecting the actual iron level, and few studies

have measured the iron level directly (Torti et al., 2018). In current study, we creatively measured the serum iron level rather than levels of transferrin or ferritin to represent the iron level in the body, and explored the prognostic value of serum iron levels, on which researches remain not to reach a consensus up to date. Feng et al. evaluated trace element levels in serum for patients with different types of cancer, they failed to find a significant difference of serum iron between liver, kidney tumors and normal tissues (Yang et al., 2021). Others researchers demonstrated that, compared with normal cells, tumor cells were more dependent upon iron, and that they remodeled iron-metabolism pathways to acquire, store, and efflux iron during their development and replication (Wang et al., 2018). Patients with cancer suffering from anemia due to cachexia or therapeutic drugs tend to have a low serum iron level. This phenomenon has been explored in several tumor types, including breast cancer (Torti et al., 2018; Yang et al., 2021). In this study, we collected baseline blood samples < 1 week of the diagnosis, and defined an optimal cutoff of 17.84 μmol/L for the serum iron level. Based on the latter, we stratified patients with early-stage TNBC into two groups with significantly different survival outcomes.

Based on classification of the serum iron level, a prognostic model incorporating the serum iron level as well as the traditional T stage and N stage was developed. The common 21-gene recurrence score, 70-gene MammaPrint Assay, and the PAM50 prognostic model are limited to a specific subtype or lymph node-negative breast cancer or patients at high clinical risk from breast cancer with limited predictive accuracy of the C-index (Gnant et al., 2015; Wallden et al., 2015; Ibraheem et al., 2020; Poorvu et al., 2020). Our predictive nomogram was accurate, cost-efficient, convenient, and readily available in hospitals in developing countries. The TNM staging system is used commonly for risk stratification and therapeutic recommendations. However, TNM criteria are based on a limited number of clinical factors, and their discriminative accuracy is limited due to differences between patients (Bareche et al., 2018; Grosselin et al., 2019). According to our time-dependent ROC curves, the predictive accuracy of our prognostic model was higher than that of the traditional TNM staging system in the training cohort and SYSUCC-001 cohort, which suggests that our nomogram might be a potential supplement to the traditional TNM staging system. Besides, except from the TNM staging system, a series of prognostic models based on inflammatory status, tumor marker, stromal tumor-infiltrating lymphocytes, and kinds of gene signature have been explored with C-index ranging 0.69–0.77 (Shi et al., 2019; Yang et al., 2019; Zheng et al., 2020), compared with them, our prognostic models achieved a comparative predictive accuracy, and was more cost-efficient and convenient. As far as we know, our study is the first to propose a predictive model integrating the impact of trace element iron with clinicopathological features. But it should be noted that a further exploration about the preliminary mechanisms is warrant.

Our study had three main limitations. First, a retrospective study will have a selection bias. Nevertheless, we tried our best to enroll all eligible TNBC patients to minimize a selection bias, and validated our prognostic models in a cohort from previous randomized trial SYSUCC-001. Second, we measured only the baseline serum iron level at the diagnosis. It would have been preferable to monitor the dynamic change in the serum iron level during therapy and adjust the therapeutic strategy. Third, we included early-stage TNBC patients only from China. Hence, the availability and predictive accuracy of our prognostic nomogram to women from other geographic regions are required to be warrant in future study.

CONCLUSION

We proposed a cutoff of the serum iron level to stratify patients with early-stage TNBC into high- and low-iron groups. On basis of the serum iron level, we established a predictive model for individualized survival prediction and validated it in the SYSUCC-001 cohort. The prognostic nomogram showed good predictive performance and satisfactory consistency compared with the actual clinical outcome.

DATA AVAILABILITY STATEMENT

The raw data supporting the conclusions of this article will be made available by the authors, without undue reservation.

ETHICS STATEMENT

The studies involving human participants were reviewed and approved by the Ethics Committee of Sun Yat-sen University Cancer Center. The ethics committee waived the requirement of written informed consent for participation.

AUTHOR CONTRIBUTIONS

ZY designed this study. XH, FD, and JH collected, primarily analyzed, and interpreted data. XH, FD, JH, CS, LW, and CJ participated in the drafting of the manuscript. XH, FD, JH, WX, XB, and ZY contributed to administrative, technical, or material support. All authors revised this manuscript and approved the final submitted version.

FUNDING

This study was funded by the Natural Science Foundation of Guangdong Province (No. 2019A151011781), the Sci-Tech Project Foundation of Guangzhou City (No. 202002020033), and the cultivation foundation for the junior teachers in Sun Yat-sen University (No. 20ykpy164).

ACKNOWLEDGMENTS

We would like to thank patients and their family for all their help in enabling completion of this study.

REFERENCES

Adams, P. C. (2015). Epidemiology and diagnostic testing for hemochromatosis and iron overload. *Int. J. Lab. Hematol.* 37, 25–30. doi: 10.1111/ijlh.12347

Allison, K. H., Hammond, M. E. H., Dowsett, M., McKernin, S. E., Carey, L. A., Fitzgibbons, P. L., et al. (2020). Estrogen and Progesterone Receptor Testing in Breast Cancer: ASCO/CAP Guideline Update. *J. Clin. Oncol.* 38, 1346–1366. doi: 10.1200/JCO19.02309

Bareche, Y., Venet, D., Ignatiadis, M., Aftimos, P., Piccart, M., Rothe, F., et al. (2018). Unravelling triple-negative breast cancer molecular heterogeneity using an integrative multiomic analysis. *Anna. Oncol.* 29, 895–902. doi: 10.1093/annonc/mdy024

Basuli, D., Tesfay, L., Deng, Z., Paul, B., Yamamoto, Y., Ning, G., et al. (2017). Iron addiction: a novel therapeutic target in ovarian cancer. *Oncogene* 36, 4089–4099. doi: 10.1038/onc.2017.11

Bianchini, G., Balko, J. M., Mayer, I. A., Sanders, M. E., and Gianni, L. (2016). Triple negative breast cancer: challenges and opportunities of a heterogeneous disease. *Nat. Rev. Clin. Oncol.* 13, 674–690. doi: 10.1038/nrclinonc.2016.66

Bingham, S. A., Hughes, R., and Cross, A. J. (2002). Effect of white versus red meat on endogenous N-nitrosation in the human colon and further evidence of a dose response. *J. Nutr.* 132, 3522s–3525s. doi: 10.1093/jn/132.11.3522S

Chang, V. C., Cotterchio, M., and Khoo, E. (2019). Iron intake, body iron status, and risk of breast cancer: a systematic review and meta-analysis. *BMC Cancer* 19:543. doi: 10.1186/s12885-019-5642-0

Dent, R., Trudeau, M., Pritchard, K. I., Hanna, W. M., Kahn, H. K., Sawka, C. A., et al. (2007). Triple-negative breast cancer: clinical features and patterns of recurrence. *Clin. Cancer Res.* 13, 4429–4434. doi: 10.1158/1078-0432.CCR-06-3045

Dixon, S. J., Lemberg, K. M., Lamprecht, M. R., Skouta, R., Zaitsev, E. M., Gleason, C. E., et al. (2012). Ferroptosis: an iron-dependent form of nonapoptotic cell death. *Cell* 149, 1060–1072. doi: 10.1016/j.cell.2012.03.042

Ferrucci, L. M., Cross, A. J., Graubard, B. I., Brinton, L. A., McCarty, C. A., Ziegler, R. G., et al. (2009). Intake of meat, meat mutagens, and iron and the risk of breast cancer in the Prostate, Lung, Colorectal, and Ovarian Cancer Screening Trial. *Br. J. Cancer* 101, 178–184. doi: 10.1038/sj.bjc.660511

Fonseca-Nunes, A., Jakszyn, P., and Agudo, A. (2014). Iron and cancer risk–a systematic review and meta-analysis of the epidemiological evidence. *Cancer Epidemiol. Biomarkers Prev.* 23, 12–31. doi: 10.1158/1055-9965.EPI-13-0733

Gadi, V. K., and Davidson, N. E. (2017). Practical Approach to Triple-Negative Breast Cancer. *J. Oncol. Pract.* 13, 293–300. doi: 10.1200/JOP.2017.022632

Galaris, D., and Pantopoulos, K. (2008). Oxidative stress and iron homeostasis: mechanistic and health aspects. *Crit. Rev. Clin. Lab. Sci.* 45, 1–23. doi: 10.1080/10408360701713104

Garrido-Castro, A. C., Lin, N. U., and Polyak, K. (2019). Insights into Molecular Classifications of Triple-Negative Breast Cancer: Improving Patient Selection for Treatment. *Cancer Discov.* 9, 176–198. doi: 10.1158/2159-8290.CD-18-1177

Gnant, M., Sestak, I., Filipits, M., Dowsett, M., Balic, M., Lopez-Knowles, E., et al. (2015). Identifying clinically relevant prognostic subgroups of postmenopausal women with node-positive hormone receptor-positive early-stage breast cancer treated with endocrine therapy: a combined analysis of ABCSG-8 and ATAC using the PAM50 risk of recurrence score and intrinsic subtype. *Anna. Oncol.* 26, 1685–1691. doi: 10.1093/annonc/mdv215

Grosselin, K., Durand, A., Marsolier, J., Poitou, A., Marangoni, E., Nemati, F., et al. (2019). High-throughput single-cell ChIP-seq identifies heterogeneity of chromatin states in breast cancer. *Nat. Genet.* 51, 1060–1066. doi: 10.1038/s41588-019-0424-9

Guo, J., Wei, W., and Zhan, L. (2015). Red and processed meat intake and risk of breast cancer: a meta-analysis of prospective studies. *Breast Cancer Res. Treat.* 151, 191–198. doi: 10.1007/s10549-015-3380-9

Guo, W., Zhang, S., Chen, Y., Zhang, D., Yuan, L., Cong, H., et al. (2015). An important role of the hepcidin-ferroportin signaling in affecting tumor growth and metastasis. *Acta Biochim. Biophys. Sin.* 47, 703–715. doi: 10.1093/abbs/gmv063

Hambidge, M. (2003). Biomarkers of trace mineral intake and status. *J. Nutr.* 133, 948s–955s. doi: 10.1093/jn/133.3.948S

Ibraheem, A., Olopade, O. I., and Huo, D. (2020). Propensity score analysis of the prognostic value of genomic assays for breast cancer in diverse populations using the National Cancer Data Base. *Cancer* 126, 4013–4022. doi: 10.1002/cncr.32956

Inoue-Choi, M., Sinha, R., Gierach, G. L., and Ward, M. H. (2016). Red and processed meat, nitrite, and heme iron intakes and postmenopausal breast cancer risk in the NIH-AARP Diet and Health Study. *Int. J. Cancer* 138, 1609–1618. doi: 10.1002/ijc.29901

Kalinowski, D. S., Stefani, C., Toyokuni, S., Ganz, T., Anderson, G. J., Subramaniam, N. V., et al. (2016). Redox cycling metals: Pedaling their roles in metabolism and their use in the development of novel therapeutics. *Biochim. Biophys. Acta* 1863, 727–748. doi: 10.1016/j.bbamcr.2016.01.026

List, A. F., Baer, M. R., Steensma, D. P., Raza, A., Esposito, J., Martinez-Lopez, N., et al. (2012). Deferasirox reduces serum ferritin and labile plasma iron in RBC transfusion-dependent patients with myelodysplastic syndrome. *J. Clin. Oncol.* 30, 2134–2139. doi: 10.1200/JCO.2010.34.1222

Morales, M., and Xue, X. (2021). Targeting iron metabolism in cancer therapy. *Theranostics* 11, 8412–8429. doi: 10.7150/thno.59092

Neufeld, E. J., Galanello, R., Viprakasit, V., Aydinok, Y., Piga, A., Harmatz, P., et al. (2012). A phase 2 study of the safety, tolerability, and pharmacodynamics of FBS0701, a novel oral iron chelator, in transfusional iron overload. *Blood* 119, 3263–3268. doi: 10.1182/blood-2011-10-386268

Nutting, C. M., van Herpen, C. M., Miah, A. B., Bhide, S. A., Machiels, J. P., Buter, J., et al. (2009). Phase II study of 3-AP Triapine in patients with recurrent or metastatic head and neck squamous cell carcinoma. *Ann. Oncol.* 20, 1275–1279. doi: 10.1093/annonc/mdn775

Poorvu, P. D., Gelber, S. I., Rosenberg, S. M., Ruddy, K. J., Tamimi, R. M., Collins, L. C., et al. (2020). Prognostic Impact of the 21-Gene Recurrence Score Assay Among Young Women With Node-Negative and Node-Positive ER-Positive/HER2-Negative Breast Cancer. *J. Clin. Oncol.* 38, 725–733. doi: 10.1200/JCO.19.01959

Radulescu, S., Brookes, M. J., Salgueiro, P., Ridgway, R. A., McGhee, E., Anderson, K., et al. (2012). Luminal iron levels govern intestinal tumorigenesis after Apc loss in vivo. *Cell Rep.* 2, 270–282. doi: 10.1016/j.celrep.2012.07.003

Shi, H., Wang, X. H., Gu, J. W., and Guo, G. L. (2019). Development and Validation of Nomograms for Predicting the Prognosis of Triple-Negative Breast Cancer Patients Based on 379 Chinese Patients. *Cancer Manag. Res.* 11, 10827–10839. doi: 10.2147/CMAR.S234926

Stockwell, B. R., Friedmann Angeli, J. P., Bayir, H., Bush, A. I., Conrad, M., Dixon, S. J., et al. (2017). Ferroptosis: A Regulated Cell Death Nexus Linking Metabolism, Redox Biology, and Disease. *Cell* 171, 273–285. doi: 10.1016/j.cell2017.09.021

Sung, H., Ferlay, J., Siegel, R. L., Laversanne, M., Soerjomataram, I., Jemal, A., et al. (2021). Global Cancer Statistics 2020: GLOBOCAN Estimates of Incidence and Mortality Worldwide for 36 Cancers in 185 Countries. *CA Cancer J. Clin.* 71, 209–249. doi: 10.3322/caac.21660

Torti, S. V., Manz, D. H., Paul, B. T., Blanchette-Farra, N., and Torti, F. M. (2018). Iron and Cancer. *Annu. Rev. Nutr.* 38, 97–125. doi: 10.1146/annurev-nutr-082117-051732

Vagia, E., Mahalingam, D., and Cristofanilli, M. (2020). The Landscape of Targeted Therapies in TNBC. *Cancers* 12:916. doi: 10.3390/cancers12040916

von Hagens, C., Walter-Sack, I., Goeckenjan, M., Osburg, J., Storch-Hagenlocher, B., Sertel, S., et al. (2017). Prospective open uncontrolled phase I study to define a well-tolerated dose of oral artesunate as add-on therapy in patients with metastatic breast cancer (ARTIC M33/2). *Breast Cancer Res. Treat.* 164, 359–369. doi: 10.1007/s10549-017-4261-1

Wallden, B., Storhoff, J., Nielsen, T., Dowidar, N., Schaper, C., Ferree, S., et al. (2015). Development and verification of the PAM50-based Prosigna breast cancer gene signature assay. *BMC Med. Genom.* 8:54. doi: 10.1186/s12920-015-0129-6

Wang, X., Wang, S. S., Huang, H., Cai, L., Zhao, L., Peng, R. J., et al. (2021). Effect of Capecitabine Maintenance Therapy Using Lower Dosage and Higher Frequency vs Observation on Disease-Free Survival Among Patients With Early-Stage Triple-Negative Breast Cancer Who Had Received Standard Treatment: The SYSUCC-001 Randomized Clinical Trial. *JAMA* 325, 50–58. doi: 10.1001/jama.2020.23370

Wang, Y., Yu, L., Ding, J., and Chen, Y. (2018). Iron Metabolism in Cancer. *Int. J. Mole. Sci.* 20:95. doi: 10.3390/ijms20010095

Wileyto, E., Li, Y., Chen, J., and Heitjan, D. (2013). Assessing the fit of parametric cure models. *Biostatistics* 14, 340–350. doi: 10.1093/biostatistics/kxs043

Wu, T., Sempos, C. T., Freudenheim, J. L., Muti, P., and Smit, E. (2004). Serum iron, copper and zinc concentrations and risk of cancer mortality in US adults. *Ann. Epidemiol.* 14, 195–201. doi: 10.1016/S1047-2797(03)00119-4

Yamasaki, T., Terai, S., and Sakaida, I. (2011). Deferoxamine for advanced hepatocellular carcinoma. *N. Engl. J. Med.* 365, 576–578. doi: 10.1056/NEJMc1105726

Yang, Y., Wang, Y., Deng, H., Tan, C., Li, Q., He, Z., et al. (2019). Development and validation of nomograms predicting survival in Chinese patients with triple negative breast cancer. *BMC Cancer* 19:541. doi: 10.1186/s12885-019-5703-4

Yang, Y. W., Dai, C. M., Chen, X. H., and Feng, J. F. (2021). The Relationship between Serum Trace Elements and Oxidative Stress of Patients with Different Types of Cancer. *Oxidat. Med. Cell. Long.* 2021:4846951. doi: 10.1155/2021/4846951

Zheng, S., Zou, Y., Liang, J. Y., Xiao, W., Yang, A., Meng, T., et al. (2020). Identification and validation of a combined hypoxia and immune index for triple-negative breast cancer. *Mol. Oncol.* 14, 2814–2833. doi: 10.1002/1878-0261.12747

Conflict of Interest: The authors declare that the research was conducted in the absence of any commercial or financial relationships that could be construed as a potential conflict of interest.

Publisher's Note: All claims expressed in this article are solely those of the authors and do not necessarily represent those of their affiliated organizations, or those of the publisher, the editors and the reviewers. Any product that may be evaluated in this article, or claim that may be made by its manufacturer, is not guaranteed or endorsed by the publisher.

frontiers in Cell and Developmental Biology

ORIGINAL RESEARCH
published: 08 November 2021
doi: 10.3389/fcell.2021.746696

A Prognostic Model of Pancreatic Cancer Based on Ferroptosis-Related Genes to Determine Its Immune Landscape and Underlying Mechanisms

Xiao Yu[1,2,3,4†], *Qingyuan Zheng*[1,2,3,4†], *Menggang Zhang*[1,2,3,4], *Qiyao Zhang*[1,2,3,4], *Shuijun Zhang*[1,2,3,4], *Yuting He*[1,2,3,4*] and *Wenzhi Guo*[1,2,3,4*]

[1]Department of Hepatobiliary and Pancreatic Surgery, The First Affiliated Hospital of Zhengzhou University, Zhengzhou, China, [2]Key Laboratory of Hepatobiliary and Pancreatic Surgery and Digestive Organ Transplantation of Henan Province, The First Affiliated Hospital of Zhengzhou University, Zhengzhou, China, [3]Open and Key Laboratory of Hepatobiliary and Pancreatic Surgery and Digestive Organ Transplantation at Henan Universities, Zhengzhou, China, [4]Henan Key Laboratory of Digestive Organ Transplantation, Zhengzhou, China

OPEN ACCESS

Edited by:
Chang Gong,
Sun Yat-sen University, China

Reviewed by:
Xinwei Han,
Zhengzhou University, China
Mingyi Zhao,
Central South University, China

***Correspondence:**
Wenzhi Guo
fccguowz@zzu.edu.cn
Yuting He
fccheyt1@zzu.edu.cn

[†]These authors have contributed equally to this work

Specialty section:
This article was submitted to Molecular and Cellular Oncology, a section of the journal Frontiers in Cell and Developmental Biology

Received: 24 July 2021
Accepted: 26 October 2021
Published: 08 November 2021

Citation:
Yu X, Zheng Q, Zhang M, Zhang Q, Zhang S, He Y and Guo W (2021) A Prognostic Model of Pancreatic Cancer Based on Ferroptosis-Related Genes to Determine Its Immune Landscape and Underlying Mechanisms. Front. Cell Dev. Biol. 9:746696. doi: 10.3389/fcell.2021.746696

Pancreatic cancer is one of the malignant tumors with the worst prognosis in the world. As a new way of programmed cell death, ferroptosis has been proven to have potential in tumor therapy. In this study, we used the TCGA-PAAD cohort combined with the previously reported 60 ferroptosis-related genes to construct and validate the prognosis model and in-depth analysis of the differences in the function and immune characteristics of different RiskTypes. The results showed that the six-gene signature prognostic model that we constructed has good stability and effectiveness. Further analysis showed that the upregulated genes in the high-risk group were mainly enriched in extracellular matrix receptor-related pathways and other tumor-related pathways and the infiltration of immune cells, such as B, T, and NK cells, was suppressed. In short, our model shows good stability and effectiveness. Further studies have found that the prognostic differences between different RiskTypes may be due to the changes in the ECM-receptor pathway and activation of the immune system. Additionally, ICI drugs can treat pancreatic cancer in high-risk groups.

Keywords: pancreatic cancer, ferroptosis, prognostic, immune, ECM

INTRODUCTION

Pancreatic adenocarcinoma (PAAD) is one of the most aggressive and malignant tumors in humans. The prognosis of PAAD patients is inferior, with a median survival time of less than 6 months (Maisonneuve, 2019). Although pancreatic cancer is not common, owing to its high mortality rate, PAAD has become the seventh leading cause of cancer-related death worldwide, and the incidence of PAAD increases yearly (Rahib et al., 2014; Guarneri et al., 2019). Although surgical treatment, radiotherapy, and chemotherapy have made significant progress in decades, the prognosis of PAAD patients is still not optimistic because the molecular mechanism of this cancer has not been studied clearly (Jeune et al., 2019; Springfeld et al., 2019). Therefore, it is urgent to explore the pathogenic mechanism of PAAD from the molecular and genetic level and to find new therapeutic targets.

Ferroptosis is a new type of iron-dependent programmed cell death that is different from apoptosis, necrosis, and autophagy (Dixon et al., 2012). The primary mechanism of ferroptosis is that under the action of divalent iron or esteroxygenase, unsaturated fatty acids highly expressed on the cell membrane undergo liposomal peroxidation, thereby inducing cell death (Stockwell et al., 2017; Hassannia et al., 2019). Because of the unique role of ferroptosis in controlling programmed cell death, the role of ferroptosis in cancer and cancer treatment has been intensively investigated (Yuan et al., 2016; Liang et al., 2019). Studies have reported that the depletion of the intracellular iron storage prevents the oxidative stress induced by sorafenib in HCC cells, thus affecting the antitumor effect of sorafenib (Louandre et al., 2013; Louandre et al., 2015). Additionally, Sun *et al.* proved that heat shock protein β-1 (HSPB1) is a negative regulator of ferroptosis in cancer cells. Heat shock pretreatment and HSPB1 overexpression inhibited erastin-induced ferroptosis. In short, the unique role of ferroptosis in cancer is widely accepted by researchers (Friedmann Angeli et al., 2019). Dozens of genes related to ferroptosis have been identified (Louandre et al., 2015; Sun et al., 2016). However, the overall role of these genes in the progression of PAAD and their effect on prognosis are still unclear.

This study collected 60 ferroptosis-related genes (FRGs) previously reported in the literature and used the TCGA-PAAD cohort to construct a prognostic model of FRGs. A validation of internal and external datasets confirms the validity and stability of our model. Subsequently, various functional enrichment analyses were conducted to determine the underlying mechanism of the ferroptosis gene in PAAD. Additionally, we analyzed immune differences in models and explored the role of immunity in the differential prognosis caused by ferroptosis. Thus, we believe that this study plays a unique role in fully understanding the role of FRGs in PAAD and finding potential therapeutic targets.

MATERIALS AND METHODS

Source of Expression Profile Data

The latest RNA-Seq data and clinical follow-up information were from the TCGA-PAAD cohort, and the download time was January 30, 2021. The GEO data were downloaded from Gene Expression Omnibus (GEO). GSE57495 and GSE71729 chip datasets with survival time were selected. The download time was January 30, 2021.

Data Preprocessing

We processed the RNA-Seq data of TCGA-PAAD in the following steps:

1) Remove samples without clinical follow-up information, 2) remove samples without survival time, 3) remove samples without survival status, 4) convert Ensembl to gene symbol, and 5) take the median expression of genes with multiple gene symbols.

The following steps were processed for the GEO dataset:

1) Remove samples without clinical follow-up information, 2) remove samples without survival time and survival status, 3) convert the probe to gene symbol, 4) if one probe corresponds to multiple genes, remove the probe needle, and 5) take the median expression of genes with multiple gene symbols.

After preprocessing the three sets of data, we obtained 176 samples in TCGA-PAAD, 123 samples in the GSE71729 dataset, and 63 samples in GSE57495.

Construction of a Prognostic Risk Model Based on Ferroptosis-Related Gene

We divide the 176 samples in TCGA-PAAD into a training set and validation set. To avoid the bias of random allocation affecting the stability of subsequent modeling, we prerandomize all samples 100 times without replacement and proceed according to the ratio of the training set: validation set = 1:1. The most suitable training set and validation set were selected according to the following conditions: 1) The two groups were similar in age distribution, gender, follow-up time, and the proportion of patient deaths; 2) after clustering the gene expression profiles of the two randomly grouped datasets. The number of samples in the two categories is close. Finally, we determined the best training set (n = 88) and validation set (n = 88). The sample information of the training set and the validation set was tested using the chi-square test (**Table 1**). The results showed that our grouping was reasonable, and there was no significant difference between the groups ($p > 0.05$). Subsequently, the single-factor and LASSO analysis of the training set was conducted. On the basis of the risk score, we constructed a risk model.

Functional Enrichment Analysis

Differentially expressed genes were determined on the basis of the limma package. KEGG pathway analysis and GO functional enrichment analysis were conducted using R software package WebGestaltR (v.0.4.2), and the Gene set enrichment analysis (GSEA) analysis was based on the R software package GSVA for a single sample. GSVA is a popular R package, which was extensively utilized in cancer-related studies (Liu et al., 2021a; Liu et al., 2021b). All steps are shown in **Supplementary Figure S1**.

RESULTS

Identification of Differentially Expressed FRGs With Prognostic Differences

We collected existing literature on ferroptosis and obtained 60 FRGs (**Supplementary file S1**) (Stockwell et al., 2017; Bersuker et al., 2019; Doll et al., 2019; Hassannia et al., 2019). Subsequently, for each FRG, the training set and survival data were used to construct a univariate Cox proportional hazard regression model using the R package survival coxph function, and $p < 0.05$ was considered a significant difference. As a result, seven differentially expressed FRGs with prognostic significance were identified: CD44, FANCD2, MT1G, PTGS2, SAT1, TFRC, and STEAP3.

TABLE 1 | Differences in clinical characteristics between training set and validation set.

Clinical features		TCGA-PAAD train	TCGA-PAAD text	P	Clinical features		TCGA-PAAD train	TCGA-PAAD text	P
OS	0	39	45	0.4505	Stage	I	7	14	0.3832
	1	49	43			II	75	70	
T stage	T1	5	2	0.09		III	1	2	
	T2	7	17			IV	3	1	
	T3	73	67			X	2	1	
	T4	1	2		Grade	G1	14	16	0.5703
	TX	2	0			G2	46	48	
N stage	N0	23	26	0.812		G3	27	21	
	N1	62	60			G4	0	2	
	NX	3	2			GX	1	1	
M stage	M0	35	44	0.2791	Gender	Male	47	49	0.8797
	M1	3	1			Female	41	39	
	MX	50	43		Age	≤65	47	46	1
						>65	41	42	

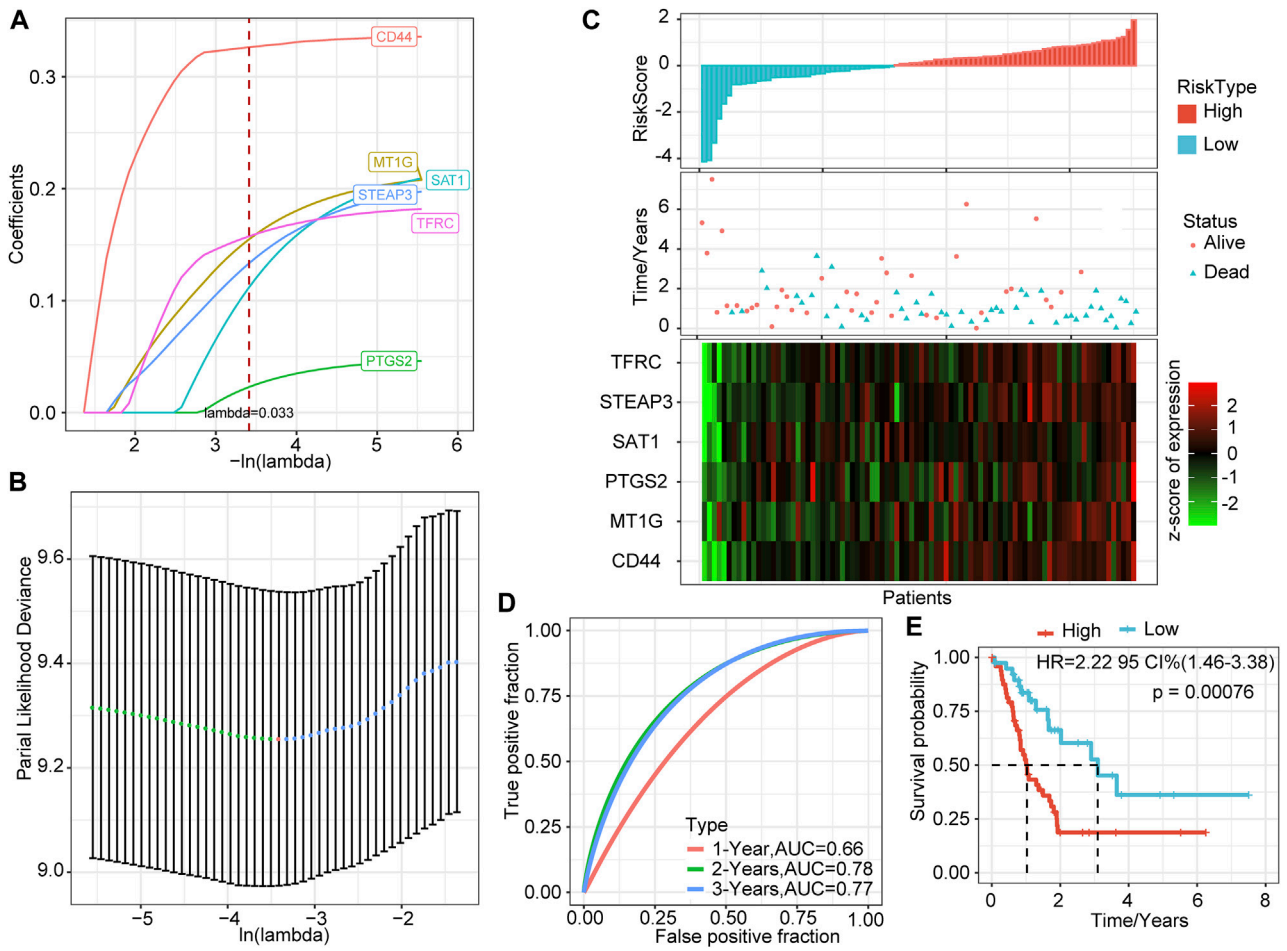

FIGURE 1 | LASSO based on ferroptosis-related genes and prediction effect in the training set. **(A)** The changing trajectory of each independent variable; the horizontal axis represents the log value of the independent variable lambda, and the vertical axis represents the coefficient of the independent variable. **(B)** The confidence interval of each lambda. **(C)** RiskScore, survival time and status, and six-gene expression trend in the training set. **(D)** ROC curve of the prognostic model. **(E)** KM survival curve of the six-gene signature model in the training set.

Regression Analysis of Least Absolute Shrinkage and Selection Operator

The above seven genes were identified as related to the prognosis of PAAD patients. To further screen for key genes associated with the development and prognosis of PAAD, LASSO regression analysis was used to screen the above seven FRGs using the R software package "glmnet." The trajectory of the coefficient of each gene with a value of −ln (lambda) is shown in **Figure 1A**. With the gradual increase in the lambda value, the number of coefficients of FRGs tending to 0 also gradually increased. We built the model by fivefold cross-validation, and the confidence interval under each lambda is shown in **Figure 1B**. The model was optimal when lambda = 0.033. Thus, we chose six genes when lambda = 0.033 as the model's gene signature. Multifactor COX analysis on six genes was performed, and it calculated the risk coefficient of each gene and obtained the risk score calculation formula as follows:

$$\begin{aligned} \textit{RiskScore} = {} & \mathbf{0.340} \times \textit{CD44} + \mathbf{0.216} \times \textit{MT1G} + \mathbf{0.050} \times \textit{PTGS2} \\ & + \mathbf{0.225} \times \textit{SAT1} + \mathbf{0.186} \times \textit{TFRC} + \mathbf{0.207} \\ & \times \textit{STEAP3} \end{aligned}$$

Construction of a Prognostic Model Based on LASSO

We calculated the risk score of each sample based on the expression levels of the six genes identified by LASSO and plotted the distribution of risk scores (**Figure 1C**). Most samples in the training set had high-risk scores. The distribution of the survival status also showed that higher risk scores were associated with more death events. Interestingly, as the risk score increased, the expression levels of these six genes had a significant upward trend. Combined with the above formula, these results verified the tumor-promoting effect of FRGs in PAAD and the effectiveness of the six genes that we screened.

Further, we used the R software package timeROC to perform ROC analysis of prognostic predictions on the risk scores of the training set. The classification efficiency of prognostic predictions of 1, 2, and 3 years was analyzed (**Figure 1D**). The prediction performance of the classification model reached 0.66 (1 year), 0.78 (2 years), and 0.77 (3 years), which shows that our model had good classification performance.

To verify further the effectiveness of our model, we performed Z-score on risk score, divided the training set samples into high-risk groups (risk score >0) and low-risk groups (risk score <0), and showed the survival curve between the groups (**Figure 1E**). The results showed that the high-risk group had a significantly lower survival probability (p = 0.00076).

The Validation Set in TCGA Verifies the Robustness of the Prognostic Model

To verify the robustness of the six-gene signature model, we calculated the risk score of each sample in the TCGA verification set based on the same model and coefficients as the training set and plotted the RiskScore distribution. Similar to the training set, higher risk scores correspond to more death events. The expression trends of these six genes were consistent with the training set (**Figure 2A**). ROC analysis showed that the model's 1-, 2-, and 3-years AUCs in the validation set were 0.62, 0.6, and 0.79, respectively (**Figure 2B**). Finally, the prognosis of the high-risk group was significantly worse than that of the low-risk group (p = 0.036, **Figure 2C**).

We verified the above results in all samples of the TCGA-PAAD cohort. As we expected, as the risk score increased, the deaths of patients increased, and the expression levels of the six signature genes increased consistently (**Figure 2D**). The 1-, 2-, and 3-years AUCs of this model in all samples were 0.66, 0.69, and 0.77, respectively, showing an excellent long-term survival rate prediction (**Figure 2E**). The prognosis of the high-risk group was significantly worse than that of the low-risk group (p = 0.0032, **Figure 2F**). 106 samples were classified as high-risk groups, and 70 samples were classified as low-risk groups.

External Dataset Verifies the Robustness of the Six-Gene Signature Model

To determine further the validity and stability of our model, we conducted model verification on the GSE57495 and GSE71729 datasets. All parameters and tools were consistent with those in the training set. The RiskScore distribution of the independent verification dataset GSE57495 is shown in **Figure 3A**. Like the TCGA-PAAD cohort, most samples have high-risk scores, and these high-scoring samples have more death events and higher expression of the six signature genes. ROC analysis showed that the 1-, 2-, and 3-years AUCs of this model in GSE57495 were 0.55, 0.57, and 0.83, respectively, showing a good long-term survival prediction performance (**Figure 3B**). Survival analysis showed that consistent with the above results, there was a significant prognostic difference between the two groups (**Figure 3C**).

Subsequently, we conducted the above analysis in the GSE71729 dataset. The analysis results showed that the survival status of PAAD patients had an obvious relationship with the risk score, and the expression trends of the six signature genes have a strong consistency (**Figure 3D**). ROC analysis indicated that the 1-, 2-, and 3-years AUCs in the GSE71729 dataset were 0.7, 0.65, and 0.6, respectively (**Figure 3E**). Meanwhile, the survival analysis of the high-risk group and the low-risk group also showed significant differences. Like the performance in other datasets, the prognosis of the high-risk group was significantly worse (**Figure 3F**). However, most patients in this dataset had low-risk scores, perhaps due to the batch effect.

Correlation Between Risk Score and Clinical Characteristics

To explore further the characteristics of the risk score, we conducted an exploratory analysis of the risk score and clinical

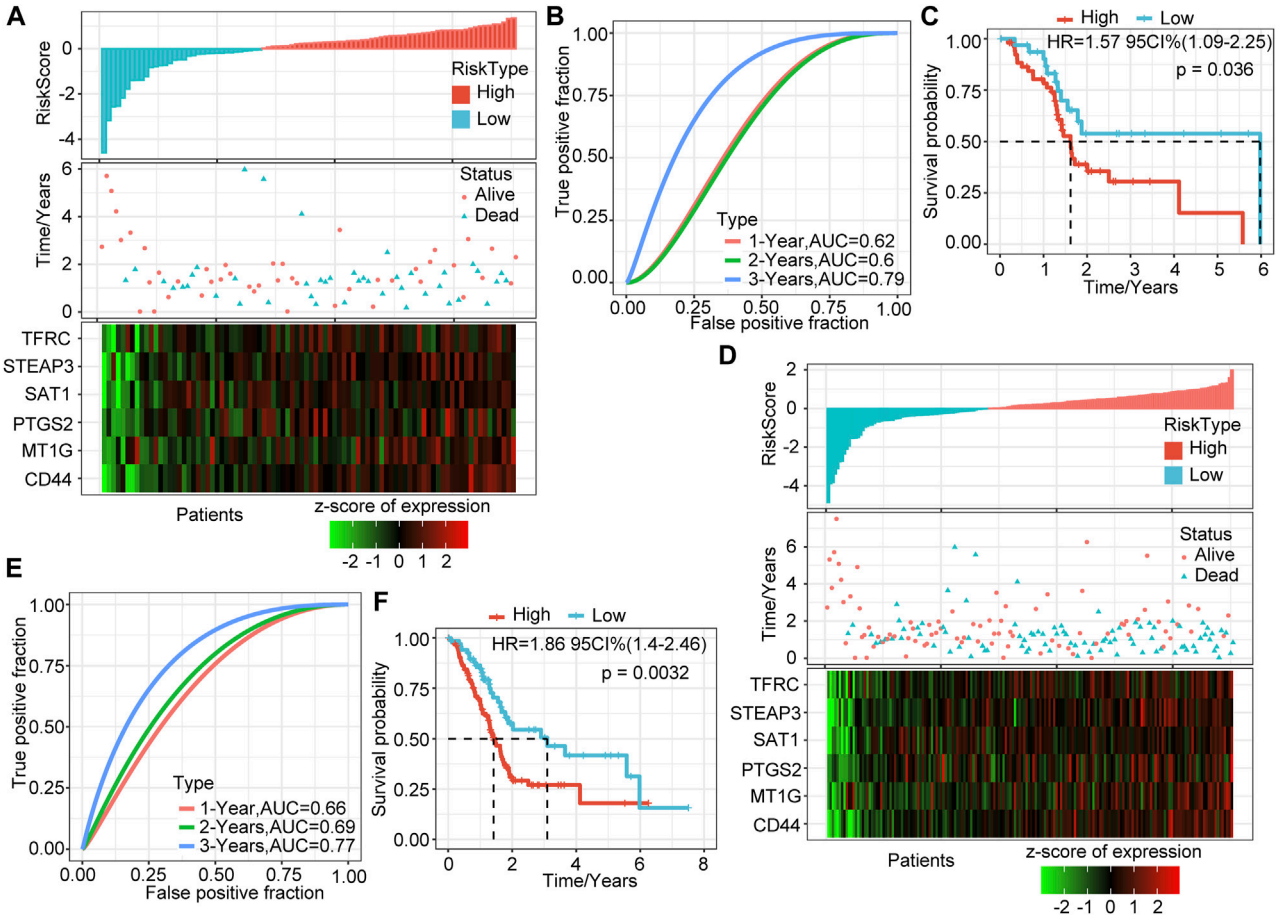

FIGURE 2 | Validation of the prognostic model of the internal dataset. **(A)** RiskScore, survival time and status, and six-gene expression trend in the validation set. **(B)** ROC curve of the prognostic model in the validation set. **(C)** KM survival curve of the six-gene signature model in the validation set. **(D)** RiskScore, survival time and status, and six-gene expression trend in all sample sets (TCGA, 176 samples). **(E)** ROC curve of the prognosis model in all samples. **(F)** KM survival curve of the six-gene signature model in all samples.

features. The results showed that there was no significant relationship between the risk score and T stage, M stage, gender, and age, and patients with different N stage, Stage, and grade have significantly different risk scores (**Figures 4A–G**). There was a clear trend here: higher risk scores were associated with a higher stage, and more differentiated samples have higher risk scores. Stage III and Grade 4 are inconsistent with other stages mainly because of the small sample size of these two stages, which results in large deviations.

Single-Factor and Multivariate Analysis of Six-Gene Signature

To identify the independence of the six-gene signature model in clinical application, we performed single-factor and multifactor Cox regression analysis based on the clinical follow-up information of the TCGA database. These clinical indicators include age, gender, T stage, N stage, M stage, stage, grade, and our RiskType grouping information. Single-factor cox analysis results showed that T stage, N stage, and RiskType (p = 0.004, HR = 1.95) were significant risk factors for prognosis (**Figure 4H**). Multifactor Cox regression analysis showed that RiskType was an independent risk factor for prognosis (p = 0.01, HR = 1.52, **Figure 4I**). The above results indicate that our model has good predictive power in predicting the clinical prognosis of PAAD patients.

Identification of Differentially Expressed Genes and Functional Enrichment Analysis

We identified DEGs between the groups to understand the underlying mechanism of high- and low-risk groups with different prognoses. A total of 1,287 upregulated genes and 42 downregulated genes were identified in the high-risk group (**Figure 5A**). DEGs in the high-risk group were mainly upregulated expressed genes.

Subsequently, functional enrichment analysis on DEGs was performed using the R software package WebGestaltR (v0.4.2).

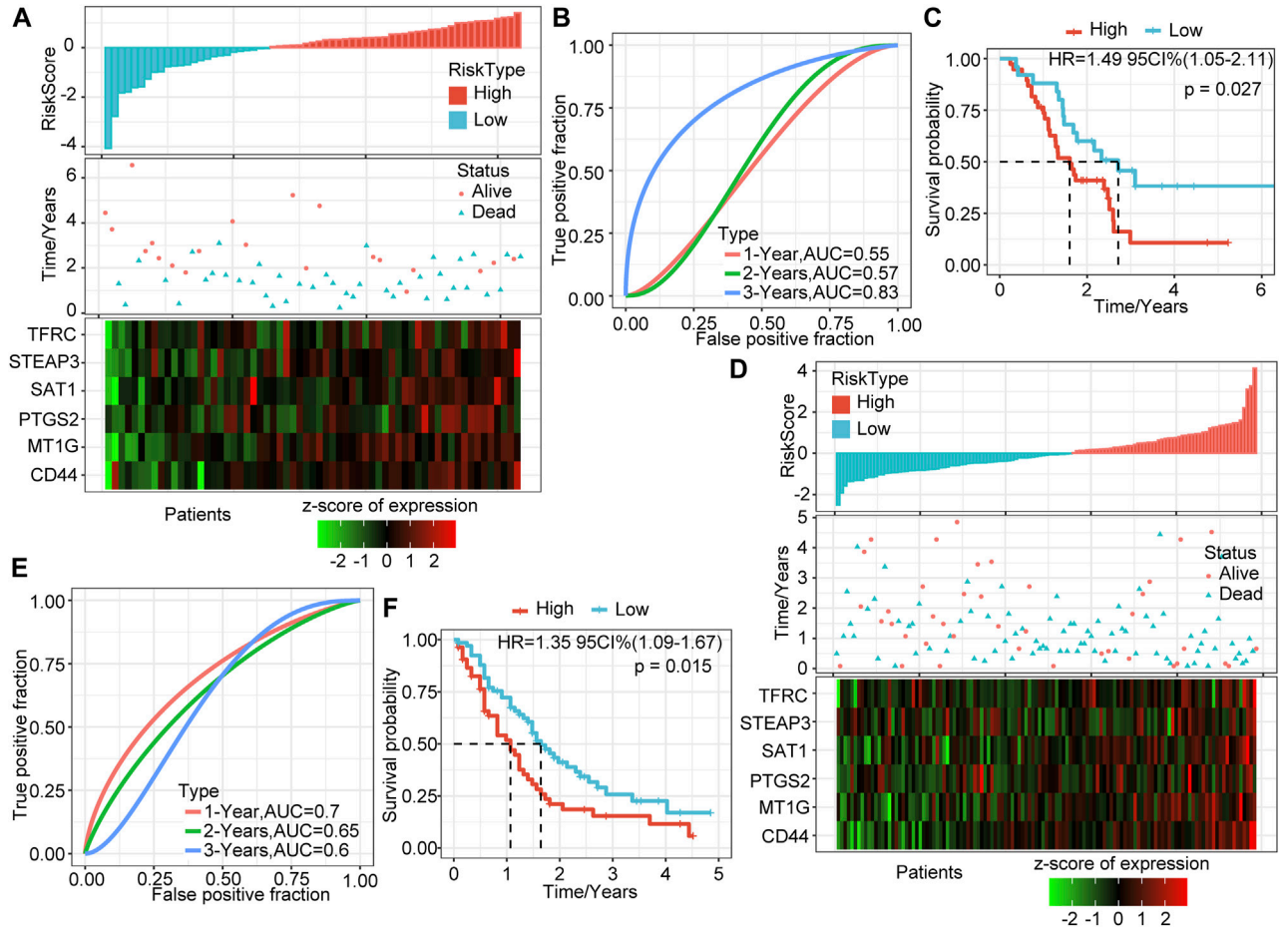

FIGURE 3 | Validation of the prognostic model of the external dataset. **(A)** RiskScore, survival time and status, and six-gene expression trend in GSE57495. **(B)** ROC curve of prognosis model 1, 2, and 3 years. **(C)** KM survival curve of the six-gene signature model in GSE57495. **(D)** RiskScore, survival time and status, and six-gene expression trend in GSE71729. **(E)** ROC curve of prognosis model 1, 2, and 3 years. **(F)** KM survival curve of the six-gene signature model in GSE71729.

With FDR <0.05 as the threshold, 1057 GO terms were annotated to biological processes (BP), 62 terms were annotated to molecular functions (MF), and 126 terms were annotated to cellular components (CC). The results showed that multiple pathways related to cell migration and tumor progression were enriched, including angiogenesis and epidermal development. Interestingly, pathways such as cell–cell and cell–substrate junctions were enriched in multiple categories. This may mean that the connection between tumor cells and cells or tissues is disturbed, which affects the tumor's ability to migrate. Additionally, KEGG pathway enrichment analysis results showed that tumor-related pathways such as ECM-receptor interaction, focal adhesion, and PI3K-Akt signaling pathway were significant. We respectively showed the 10 most significantly enriched terms in each category (**Figures 5B–E**).

GSEA of DEGs

We performed GSEA on the high-risk and low-risk groups, and the thresholds for the enrichment pathway selection were $p < 0.05$ and FDR <0.25 (**Figure 6A**). As we expected, multiple tumor-related pathways were enriched in the high-risk group, such as MISMATCH_REPAIR, NOTCH_SIGNALING_PATHWAY, CELL_CYCLE, and PANCREATIC_CANCER, which may imply that the poor prognosis of the high-risk group was a combination of multiple tumor pathways.

Gene Expression Difference in Tumor-Related Pathways Between Groups

Furthermore, we performed a single-sample GSEA on the TCGA-PAAD cohort samples and calculated the ssGSEA score of each sample on different pathways. Correlation analysis of ssGSEA and risk scores was performed, and pathways with a correlation coefficient >0.5 were displayed (**Figure 6B**). A total of 32 pathways were screened, of which the ssGSEA of 29 pathways was positively correlated with the risk score, and the remaining three pathways were negatively correlated with the risk score. After consulting related literature, we found that multiple tumor-

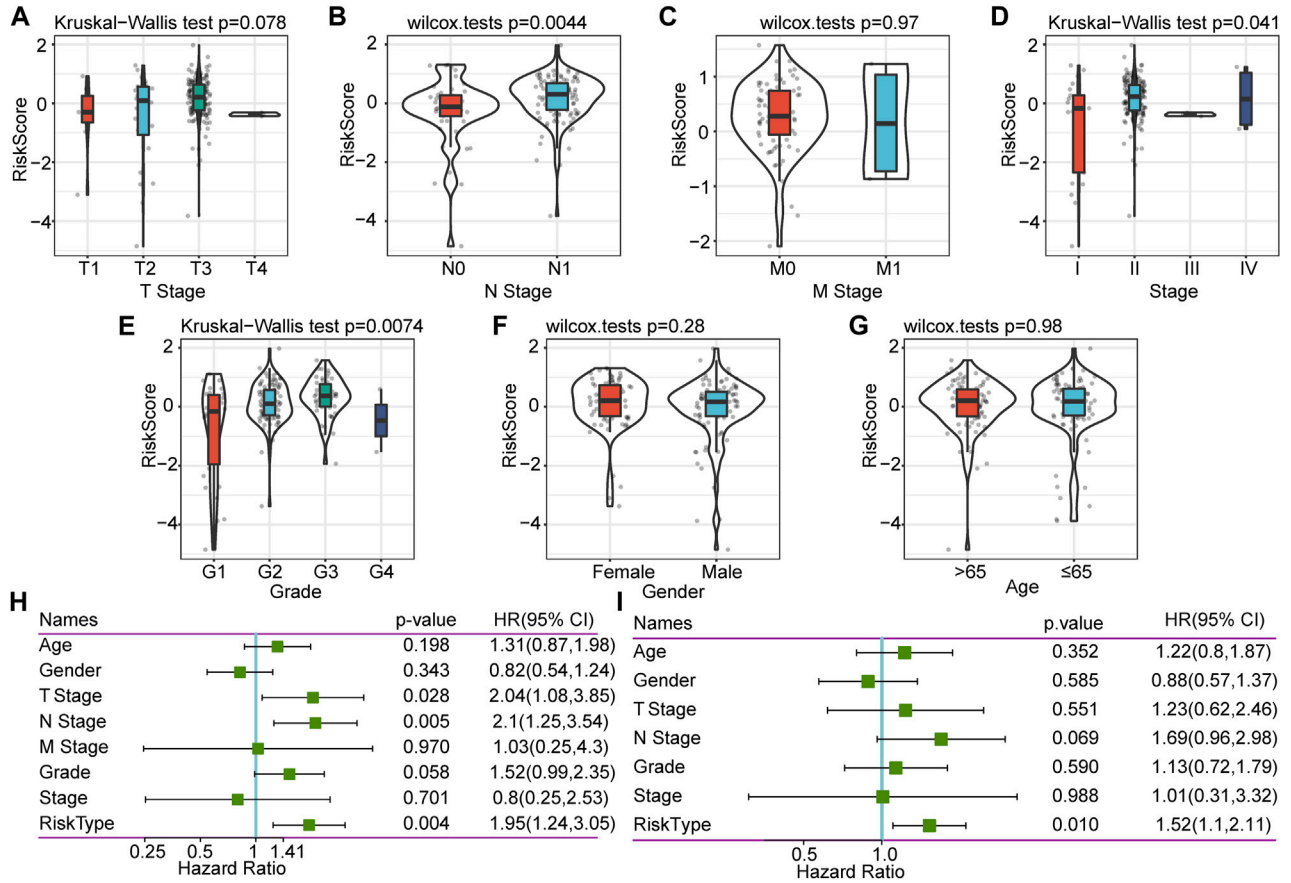

FIGURE 4 | Correlation between RiskScore and clinical characteristics, and single-factor and multifactor analysis. **(A)** Correlation between RiskScore and T. stage. **(B)** Correlation between RiskScore and N. stage. **(C)** Correlation between RiskScore and M. stage. **(D)** Correlation between RiskScore and Stage. **(E)** Correlation between RiskScore and Grade. **(F)** Correlation between RiskScore and Gender. **(G)** Correlation between RiskScore and Age. **(H)** Clinical features and RiskScore's single-factor analysis results. **(I)** Clinical features and RiskScore's multivariate analysis results.

related pathways, including KEGG_PROSTATE_CANCER, KEGG_ECM_RECEPTOR_INTERACTION, and KEGG_FOCAL_ADHESIO, increased with the increase of RiskScore score whereas KEGG_SNARE_INTERACTIONS_IN_VESICULAR_TRANSPORT, KEGG_OLFACTORY_TRANSDUCTION, and KEGG_CARDIAC_MUSCLE_CONTRACTION had an opposite trend. Interestingly, the ECM-receptor pathway has been identified in multiple functional enrichment analyses. The expression of related genes in this pathway tended to increase as the risk score increased. Thus, the ECM-receptor pathway may be potentially linked to FRGs.

Differences in Immune Infiltration Between Groups

To explore the differences in immune infiltration between the high-risk and low-risk groups that we identified, we assessed the differences in overall immune infiltration and immune cells using ESTIMATE, MCPcounter, and CIBERSORT tools. The results showed no significant differences in Stromal Score, Immune Score, and ESTIMATE Score between groups (**Figure 7A**). However, in the MCP method, monotypic lineage and neutrophils were significantly increased in the high-risk group ($p < 0.05$), which implies that the high-risk group has a stronger inflammatory response (**Figure 7B**). In the results of CIBERSORT, native B cells, activated NK cells, and Tregs infiltrate in the high-risk group were lower than those in the low-risk group, which implies that compared to low-risk group, the specific and nonspecific immune responses of the high-risk group were suppressed (**Figure 7C**).

Subsequently, we compared the expression differences in some immune checkpoints in the high- and low-risk groups. As we expected, almost all immune checkpoint genes were upregulated in the high-risk group. CD274, CD276, CD44, CD80, IDO1, and PDCD1LG2 had significant statistical differences (**Figure 7D**). This indicates that immune checkpoint-related pathways play an essential role in the poor prognosis of the high-risk group, suggesting that immune checkpoint inhibitors (ICIs) are effective for this type of pancreatic cancer.

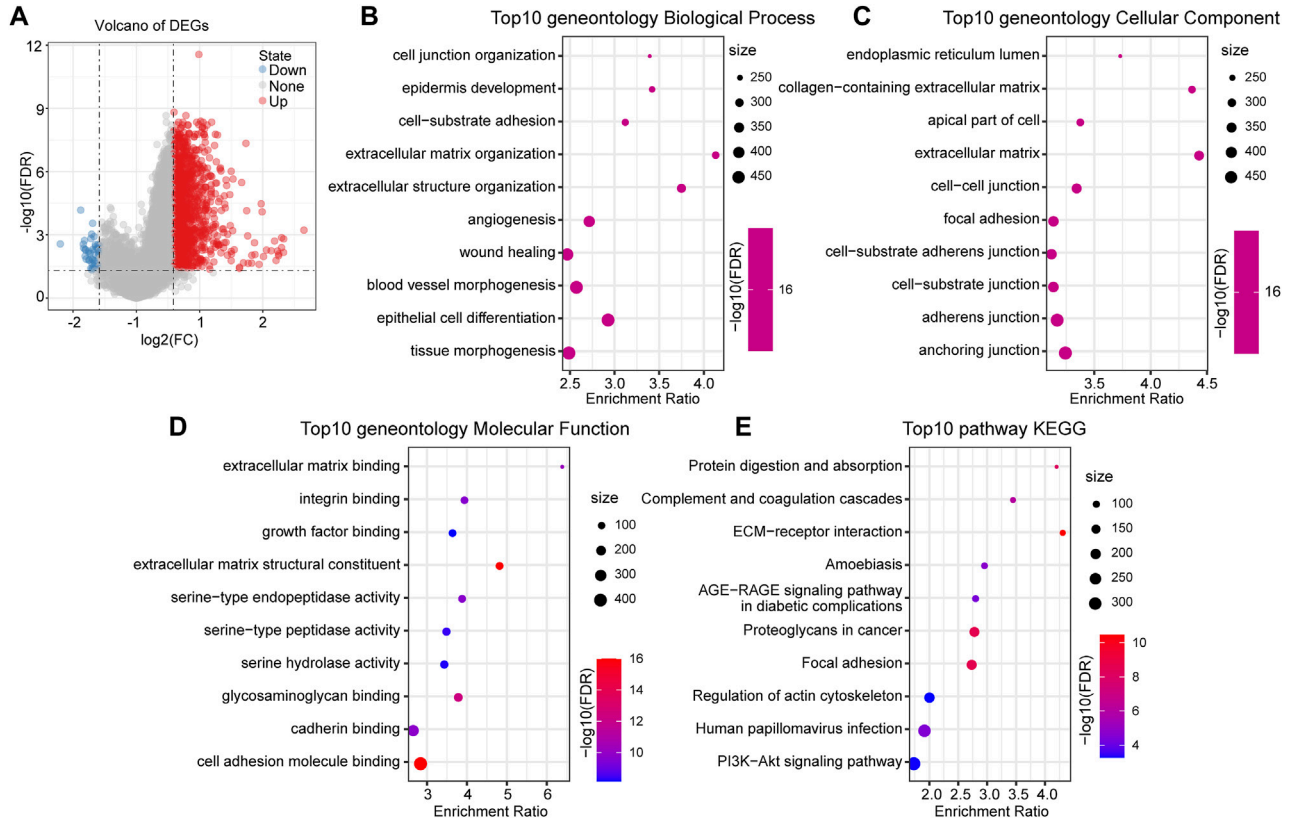

FIGURE 5 | Functional enrichment analysis between RiskTypes. **(A)** Volcano plot of differentially expressed genes between high- and low-risk groups; the red dots represent upregulated genes in the high-risk group. **(B)** Top 10 BP terms of differentially upregulated genes between RiskTypes. **(C)** Top 10 CC terms of differentially upregulated genes between RiskTypes. **(D)** Top 10 MF terms of differentially upregulated genes between RiskTypes. **(E)** Top 10 KEGG pathways of differentially upregulated genes between RiskTypes.

Comparison of Risk Models and Existing Models

To verify further the effectiveness of our model, by consulting relevant literature, we compared the predictive performance of three prognostic-related risk models (seven-gene signature (Cheng), six-gene signature (Stratford), and nine-gene signature (Xu)) and our model. To make the models comparable, we calculated the Z-score risk score of each PAAD sample based on the signature genes in these three models using the same method and divided the samples into the high-risk (risk score >0) and low-risk (risk score <0) groups. The ROC results of the seven-gene signature (Cheng) risk model showed that the 1-, 2-, and 3-years AUCs of the model were 0.72, 0.68, and 0.68, respectively (**Figure 8A**) (Cheng et al., 2019). The AUCs of the six-gene signature (Stratford) risk model were 0.61, 0.67, and 0.73, respectively (**Figure 8C**), and the AUCs of the nine-gene signature (Xu) risk model were 0.67, 0.69, and 0.74, respectively (**Figure 8E**) (Stratford et al., 2010; Xu et al., 2021). The prognosis of the three models is significantly different between the groups (**Figures 8B,D,F**). We found that the 1-, 2-, and 3-years AUCs of these three models on the TCGA data were lower than those of our model, indicating that our model had a good predictive performance.

DISCUSSION

Owing to the unique cell death mechanism of ferroptosis and its potential therapeutic prospects in cancer, ferroptosis has attracted the attention of many researchers (Yang et al., 2014; Conrad et al., 2016). Although the execution of ferroptosis requires the oxidation of polyunsaturated fatty acids, the underlying mechanism of the sensitivity of carcinogenic mutations and other noncarcinogenic cancer-related states to ferroptosis remains largely unclear. The latest research suggests that the tumor suppressor genes p53 and BCRA may be associated with increased sensitivity to ferroptosis (Li et al., 2012; Jiang et al., 2015; Wang et al., 2016). Additionally, Liu *et al.* found that in clear cell renal cell carcinoma, the deletion of the von-Hippel-Lindau gene makes this type of tumor sensitive to ferroptosis caused by

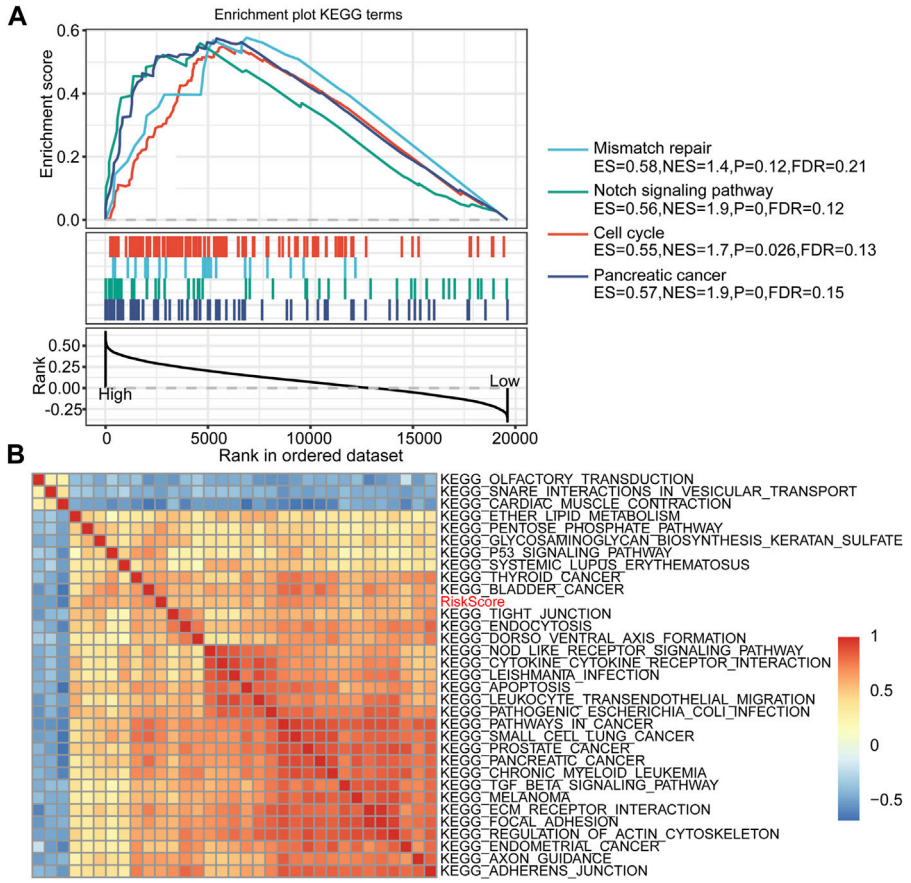

FIGURE 6 | RiskScore-related pathways and GSEA results. **(A)** GSEA results between high-risk and low-risk groups. **(B)** Clustering correlation coefficients between the KEGG pathway and RiskScore with correlation >0.5.

glutathione depletion (Yang et al., 2014; Miess et al., 2018). Additionally, reports have pointed out that ferrophilic cancer cells may release immunomodulatory signals, such as lipid mediators, to attract immune cells, such as macrophages, for effective phagocytosis (Elliott and Ravichandran, 2016; Kloditz and Fadeel, 2019; Liu et al., 2021c). Although we have made positive progress in the mechanism that drives ferroptosis, ferroptosis in tumors and its regulatory mechanism are still contradictory (Friedmann Angeli et al., 2019). It is necessary to identify further the difference between ferroptosis that inhibits tumor growth and ferroptosis that drives cancer progression.

In this study, we used the TCGA-PAAD cohort to perform univariate cox regression combined with the previously reported 60 FRGs and identified seven prognostic-related ferroptosis genes. Subsequently, the LASSO algorithm was used to reduce dimensionality and construct a six-gene signature prognostic model. We verified the effectiveness of the model in the training set, the validation set, and all samples. The model's long-term prognosis predicted that AUC reached 0.79. Additionally, to verify the stability of the model on different sequencing platforms, we confirmed it in GSE57495 and GSE71729. The results showed that whether it is an internal dataset or an external dataset, the model showed convincing stability and effectiveness. Subsequently, we analyzed the correlation between different risk groups and clinical characteristics. There were significant differences in N stage, Stage, and Grade between the risk groups. Additionally, there was a trend that the high-risk group has a higher degree of differentiation. Both univariate and multivariate COX regression analyses showed that RiskType was significantly related to prognosis. To validate further the prognostic model, three pre-existing PAAD prognostic models were compared with our model. The 1-, 3-, and 5-years AUCs of these three models on the same dataset were lower than those of our model. This also verifies that our model has prognostic prediction ability.

Further functional enrichment analysis showed that the ECM-receptor pathway and the cell–cell and cell–matrix connection pathways were enriched by multiple categories. The extracellular matrix (ECM) is composed of a complex mixture of structural and functional macromolecules and

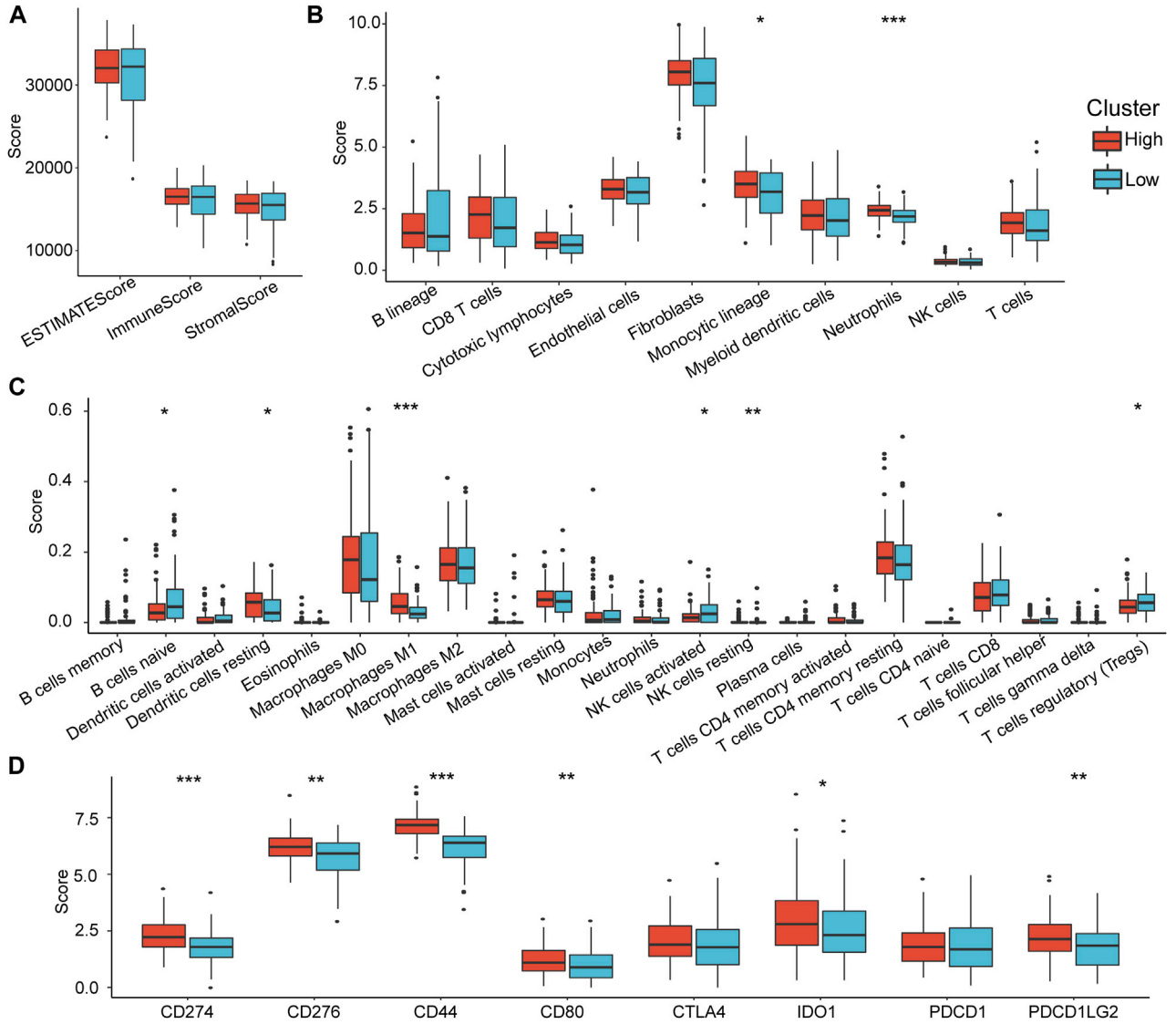

FIGURE 7 | Differences in immune infiltration characteristics between RiskTypes. **(A)** Differences in Stromal Score, Immune Score, and ESTIMATE Score among RiskTypes. **(B)** Differences in 10 immune cells assessed by MCPcounter among RiskTypes. **(C)** The difference of 22 immune cell scores between RiskTypes using COBERSORT. **(D)** Differences in immune checkpoint genes between high- and low-risk groups.

plays a vital role in the formation of tissues and organs and the maintenance of the structure and function of cells and tissues (Mohan et al., 2020). Cells interact with ECM through ECM receptors to control cell migration, differentiation, and apoptosis (Eble and Niland, 2019; Mohan et al., 2020). A study by Brown *et al.* found that ECM detachment is an essential factor in triggering the ferroptosis of cancer cells (Buchheit et al., 2014; Brown et al., 2017; Dixon, 2017). The activation of Src mediated by α6β4 contributes to resistance to ferroptosis. In the absence of α6β4, cell ECM detachment is prone to ferroptosis. Our research results corroborate this conclusion. However, there is also evidence that ECM detachment can increase intracellular reactive oxygen species (ROS) and cause ROS-dependent cell death (Schafer et al., 2009). It is essential to determine the difference between apoptosis and ferroptosis, which may determine the outcome of the cell, which requires more rigorous experiments.

Additionally, ferroptosis regulates the antitumor response of the immune system. There is evidence that different types of ferritic cancer cells can release HMGB1, a damage-related molecule, in a ferroptosis-dependent manner, and can then obtain the characteristics of immune stimulation and act as an adjuvant (Yamazaki et al., 2014; Yu et al., 2015; Wen et al., 2019). This molecule can promote the activation of innate and

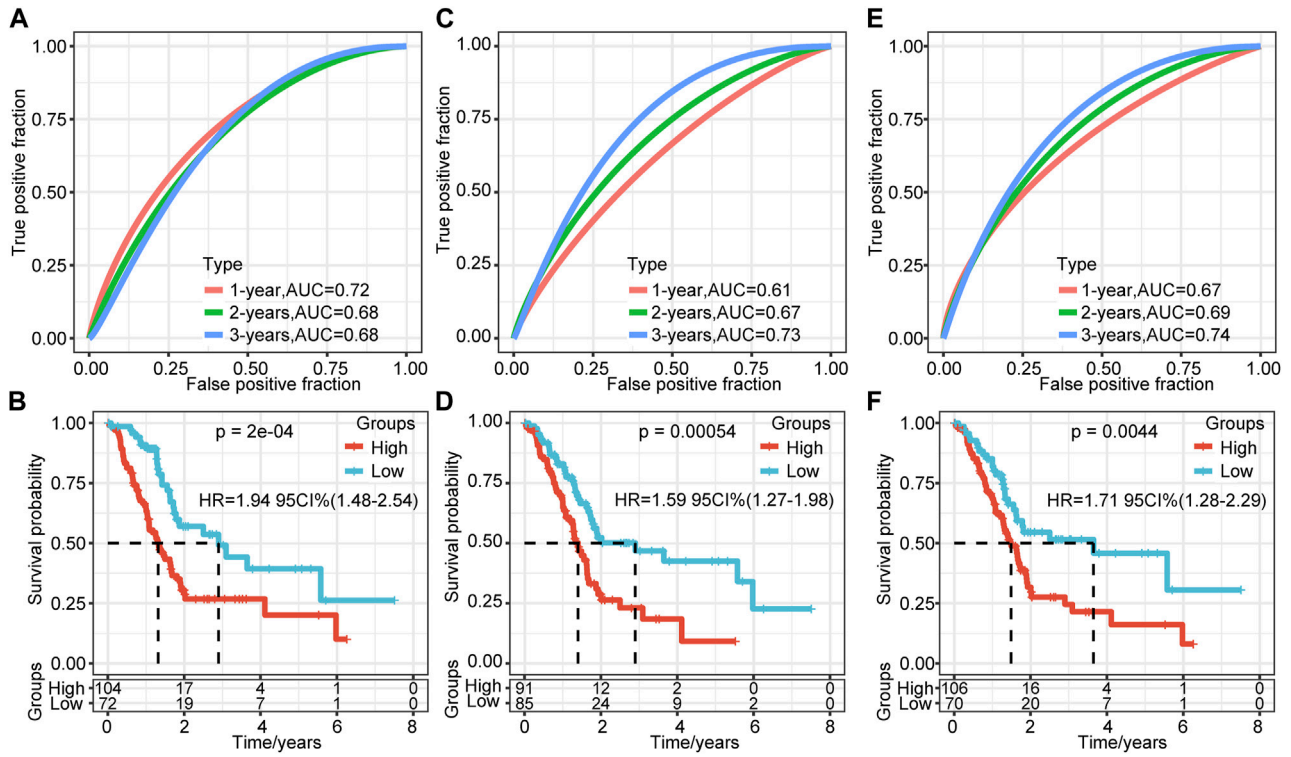

FIGURE 8 | Comparison of the risk model and existing model. **(A–B)** ROC of seven-gene signature (Cheng) risk model and KM curve of high/low RiskTypes (Cheng). **(C–D)** ROC of the six-gene signature (Stratford) risk model and KM curve of high/low RiskTypes. **(E–F)** ROC of the nine-gene signature (Xu) risk model and KM curve of high/low RiskTypes.

adaptive immune systems by binding with pattern recognition receptors. This conclusion is consistent with our research results (Liu et al., 2021d). We found that various immune cells, including B cells, helper T cells, and NK cells, were upregulated in the low-risk group. This implied that compared to the high-risk group, samples from the low-risk group could activate the specific and non-specific immune systems through the above pathways, then stimulate the anti-tumor response of immune system. Interestingly, we found a significant difference in the expression of immune checkpoints between the high-risk group and the low-risk group. Almost all immune checkpoint genes were upregulated in the high-risk group. This may mean that pancreatic cancer in the high-risk group suppresses the immune response by "hijacking" the immune checkpoint pathway to obtain immune escape (Liu et al., 2021e). This suggests that ICIs is an effective treatment for this type of pancreatic cancer with a worse prognosis.

Although many studies have explored the mechanism of ferroptosis and the biological processes that it causes, it cannot be ignored that ferroptosis is a kind of programmed cell death induced by multifactorial stress. We should explain this phenomenon from multiple perspectives. In our pancreatic cancer research, FRGs are involved in various tumor-related pathways. The differential prognosis of our model is the result of multiple tumor-related pathways, including the ECM-receptor pathway and tumor immune regulation. These results lay the foundation for further exploration of the role and mechanism of ferroptosis in pancreatic cancer.

CONCLUSION

We constructed a six-gene signature prognostic model based on FRGs. After extensive verification, this model has been proven to be stable and effective in predicting the prognosis of pancreatic cancer. Further research showed that the prognostic differences between different RiskTypes may be due to the changes in the ECM-receptor pathway and activation of the immune system. ICI drugs can treat pancreatic cancer in the high-risk group in our model.

DATA AVAILABILITY STATEMENT

Publicly available datasets were analyzed in this study, these can be found in The Cancer Genome Atlas (https://portal.gdc.cancer.gov/) and Gene Expression Omnibus (GSE57495, and GSE71729).

AUTHOR CONTRIBUTIONS

SZ, WG and YH designed the study. XY and QZe drafted the manuscript and collected the references. QZa and ZW analyzed the data. MZ revised the manuscript. All authors read and approved the final manuscript.

FUNDING

This work was supported by the Youth Talent Lifting Project of Henan Province (2021HYTP059), and Key Scientific Research Project of Henan Higher Education Institutions of China (21A320026).

ACKNOWLEDGMENTS

We thank the patients and investigators who participated in TCGA and GEO for providing data.

SUPPLEMENTARY MATERIAL

The Supplementary Material for this article can be found online at: https://www.frontiersin.org/articles/10.3389/fcell.2021.746696/full#supplementary-material

Supplementary Figure S1 | Research flowchart of ferroptosis-related genes in the prognostic model of pancreatic cancer.

REFERENCES

Bersuker, K., Hendricks, J. M., Li, Z., Magtanong, L., Ford, B., Tang, P. H., et al. (2019). The CoQ Oxidoreductase FSP1 Acts Parallel to GPX4 to Inhibit Ferroptosis. *Nature* 575 (7784), 688–692. doi:10.1038/s41586-019-1705-2

Brown, C. W., Amante, J. J., Goel, H. L., and Mercurio, A. M. (2017). The α6β4 Integrin Promotes Resistance to Ferroptosis. *J. Cel Biol.* 216 (12), 4287–4297. doi:10.1083/jcb.201701136

Buchheit, C. L., Weigel, K. J., and Schafer, Z. T. (2014). Cancer Cell Survival during Detachment from the ECM: Multiple Barriers to Tumour Progression. *Nat. Rev. Cancer* 14 (9), 632–641. doi:10.1038/nrc3789

Cheng, Y., Wang, K., Geng, L., Sun, J., Xu, W., Liu, D., et al. (2019). Identification of Candidate Diagnostic and Prognostic Biomarkers for Pancreatic Carcinoma. *EBioMedicine* 40, 382–393. doi:10.1016/j.ebiom.2019.01.003

Conrad, M., Angeli, J. P. F., Vandenabeele, P., and Stockwell, B. R. (2016). Regulated Necrosis: Disease Relevance and Therapeutic Opportunities. *Nat. Rev. Drug Discov.* 15 (5), 348–366. doi:10.1038/nrd.2015.6

Dixon, S. J. (2017). Ferroptosis: Bug or Feature? *Immunol. Rev.* 277 (1), 150–157. doi:10.1111/imr.12533

Dixon, S. J., Lemberg, K. M., Lamprecht, M. R., Skouta, R., Zaitsev, E. M., Gleason, C. E., et al. (2012). Ferroptosis: an Iron-dependent Form of Nonapoptotic Cell Death. *Cell* 149 (5), 1060–1072. doi:10.1016/j.cell.2012.03.042

Doll, S., Freitas, F. P., Shah, R., Aldrovandi, M., da Silva, M. C., Ingold, I., et al. (2019). FSP1 Is a Glutathione-independent Ferroptosis Suppressor. *Nature* 575 (7784), 693–698. doi:10.1038/s41586-019-1707-0

Eble, J. A., and Niland, S. (2019). The Extracellular Matrix in Tumor Progression and Metastasis. *Clin. Exp. Metastasis* 36 (3), 171–198. doi:10.1007/s10585-019-09966-1

Elliott, M. R., and Ravichandran, K. S. (2016). The Dynamics of Apoptotic Cell Clearance. *Develop. Cel* 38 (2), 147–160. doi:10.1016/j.devcel.2016.06.029

Friedmann Angeli, J. P., Krysko, D. V., and Conrad, M. (2019). Ferroptosis at the Crossroads of Cancer-Acquired Drug Resistance and Immune Evasion. *Nat. Rev. Cancer* 19 (7), 405–414. doi:10.1038/s41568-019-0149-1

Guarneri, G., Gasparini, G., Crippa, S., Andreasi, V., and Falconi, M. (2019). Diagnostic Strategy with a Solid Pancreatic Mass. *La Presse Méd.* 48 (3 Pt 2), e125–e145. doi:10.1016/j.lpm.2019.02.026

Hassannia, B., Vandenabeele, P., and Vanden Berghe, T. (2019). Targeting Ferroptosis to Iron Out Cancer. *Cancer Cell* 35 (6), 830–849. doi:10.1016/j.ccell.2019.04.002

Jeune, F., Coriat, R., Prat, F., Dousset, B., Vaillant, J.-C., and Gaujoux, S. (2019). Pancreatic Cancer Surgical Management. *La Presse Méd.* 48 (3 Pt 2), e147–e158. doi:10.1016/j.lpm.2019.02.027

Jiang, L., Kon, N., Li, T., Wang, S.-J., Su, T., Hibshoosh, H., et al. (2015). Ferroptosis as a P53-Mediated Activity during Tumour Suppression. *Nature* 520 (7545), 57–62. doi:10.1038/nature14344

Klöditz, K., and Fadeel, B. (2019). Three Cell Deaths and a Funeral: Macrophage Clearance of Cells Undergoing Distinct Modes of Cell Death. *Cel Death Discov.* 5, 65. doi:10.1038/s41420-019-0146-x

Li, T., Kon, N., Jiang, L., Tan, M., Ludwig, T., Zhao, Y., et al. (2012). Tumor Suppression in the Absence of P53-Mediated Cell-Cycle Arrest, Apoptosis, and Senescence. *Cell* 149 (6), 1269–1283. doi:10.1016/j.cell.2012.04.026

Liang, C., Zhang, X., Yang, M., and Dong, X. (2019). Recent Progress in Ferroptosis Inducers for Cancer Therapy. *Adv. Mater.* 31 (51), 1904197. doi:10.1002/adma.201904197

Liu, Z., Lu, T., Wang, Y., Jiao, D., Li, Z., Wang, L., et al. (2021a). Establishment and Experimental Validation of an Immune miRNA Signature for Assessing Prognosis and Immune Landscape of Patients with Colorectal Cancer. *J. Cel Mol. Med.* 25 (14), 6874–6886. doi:10.1111/jcmm.16696

Liu, Z., Wang, L., Guo, C., Liu, L., Jiao, D., Sun, Z., et al. (2021b). TTN/OBSCN 'Double-Hit' Predicts Favourable Prognosis, 'immune-hot' Subtype and Potentially Better Immunotherapeutic Efficacy in Colorectal Cancer. *J. Cel Mol. Med.* 25 (7), 3239–3251. doi:10.1111/jcmm.16393

Liu, Z., Wang, L., Liu, L., Lu, T., Jiao, D., Sun, Y., et al. (2021c). The Identification and Validation of Two Heterogenous Subtypes and a Risk Signature Based on Ferroptosis in Hepatocellular Carcinoma. *Front. Oncol.* 11, 619242. doi:10.3389/fonc.2021.619242

Liu, Z., Zhang, Y., Dang, Q., Wu, K., Jiao, D., Li, Z., et al. (2021d). Genomic Alteration Characterization in Colorectal Cancer Identifies a Prognostic and Metastasis Biomarker: FAM83A|IDO1. *Front. Oncol.* 11, 632430. doi:10.3389/fonc.2021.632430

Liu, Z., Zhang, Y., Shi, C., Zhou, X., Xu, K., Jiao, D., et al. (2021e). A Novel Immune Classification Reveals Distinct Immune Escape Mechanism and Genomic Alterations: Implications for Immunotherapy in Hepatocellular Carcinoma. *J. Transl. Med.* 19 (1), 5. doi:10.1186/s12967-020-02697-y

Louandre, C., Ezzoukhry, Z., Godin, C., Barbare, J.-C., Mazière, J.-C., Chauffert, B., et al. (2013). Iron-dependent Cell Death of Hepatocellular Carcinoma Cells Exposed to Sorafenib. *Int. J. Cancer* 133 (7), 1732–1742. doi:10.1002/ijc.28159

Louandre, C., Marcq, I., Bouhlal, H., Lachaier, E., Godin, C., Saidak, Z., et al. (2015). The Retinoblastoma (Rb) Protein Regulates Ferroptosis Induced by Sorafenib in Human Hepatocellular Carcinoma Cells. *Cancer Lett.* 356 (2 Pt B), 971–977. doi:10.1016/j.canlet.2014.11.014

Maisonneuve, P. (2019). Epidemiology and burden of Pancreatic Cancer. *La Presse Méd.* 48 (3 Pt 2), e113–e123. doi:10.1016/j.lpm.2019.02.030

Miess, H., Dankworth, B., Gouw, A. M., Rosenfeldt, M., Schmitz, W., Jiang, M., et al. (2018). The Glutathione Redox System Is Essential to Prevent Ferroptosis Caused by Impaired Lipid Metabolism in clear Cell Renal Cell Carcinoma. *Oncogene* 37 (40), 5435–5450. doi:10.1038/s41388-018-0315-z

Mohan, V., Das, A., and Sagi, I. (2020). Emerging Roles of ECM Remodeling Processes in Cancer. *Semin. Cancer Biol.* 62, 192–200. doi:10.1016/j.semcancer.2019.09.004

Rahib, L., Smith, B. D., Aizenberg, R., Rosenzweig, A. B., Fleshman, J. M., and Matrisian, L. M. (2014). Projecting Cancer Incidence and Deaths to 2030: the Unexpected burden of Thyroid, Liver, and Pancreas Cancers in the United States. *Cancer Res.* 74 (11), 2913–2921. doi:10.1158/0008-5472.CAN-14-0155

Schafer, Z. T., Grassian, A. R., Song, L., Jiang, Z., Gerhart-Hines, Z., Irie, H. Y., et al. (2009). Antioxidant and Oncogene rescue of Metabolic Defects Caused by Loss of Matrix Attachment. *Nature* 461 (7260), 109–113. doi:10.1038/nature08268

Springfeld, C., Jäger, D., Büchler, M. W., Strobel, O., Hackert, T., Palmer, D. H., et al. (2019). Chemotherapy for Pancreatic Cancer. *La Presse Méd.* 48 (3 Pt 2), e159–e174. doi:10.1016/j.lpm.2019.02.025

Stockwell, B. R., Friedmann Angeli, J. P., Bayir, H., Bush, A. I., Conrad, M., Dixon, S. J., et al. (2017). Ferroptosis: A Regulated Cell Death Nexus Linking Metabolism, Redox Biology, and Disease. *Cell* 171 (2), 273–285. doi:10.1016/j.cell.2017.09.021

Stratford, J. K., Bentrem, D. J., Anderson, J. M., Fan, C., Volmar, K. A., Marron, J. S., et al. (2010). A Six-Gene Signature Predicts Survival of Patients with Localized Pancreatic Ductal Adenocarcinoma. *Plos Med.* 7 (7), e1000307. doi:10.1371/journal.pmed.1000307

Sun, X., Ou, Z., Chen, R., Niu, X., Chen, D., Kang, R., et al. (2016). Activation of the P62-Keap1-NRF2 Pathway Protects against Ferroptosis in Hepatocellular Carcinoma Cells. *Hepatology* 63 (1), 173–184. doi:10.1002/hep.28251

Wang, S.-J., Li, D., Ou, Y., Jiang, L., Chen, Y., Zhao, Y., et al. (2016). Acetylation Is Crucial for P53-Mediated Ferroptosis and Tumor Suppression. *Cel Rep.* 17 (2), 366–373. doi:10.1016/j.celrep.2016.09.022

Wen, Q., Liu, J., Kang, R., Zhou, B., and Tang, D. (2019). The Release and Activity of HMGB1 in Ferroptosis. *Biochem. Biophys. Res. Commun.* 510 (2), 278–283. doi:10.1016/j.bbrc.2019.01.090

Xu, D., Wang, Y., Liu, X., Zhou, K., Wu, J., Chen, J., et al. (2021). Development and Clinical Validation of a Novel 9-gene Prognostic Model Based on Multi-Omics in Pancreatic Adenocarcinoma. *Pharmacol. Res.* 164, 105370. doi:10.1016/j.phrs.2020.105370

Yamazaki, T., Hannani, D., Poirier-Colame, V., Ladoire, S., Locher, C., Sistigu, A., et al. (2014). Defective Immunogenic Cell Death of HMGB1-Deficient Tumors: Compensatory Therapy with TLR4 Agonists. *Cell Death Differ.* 21 (1), 69–78. doi:10.1038/cdd.2013.72

Yang, W. S., SriRamaratnam, R., Welsch, M. E., Shimada, K., Skouta, R., Viswanathan, V. S., et al. (2014). Regulation of Ferroptotic Cancer Cell Death by GPX4. *Cell* 156 (1-2), 317–331. doi:10.1016/j.cell.2013.12.010

Yu, Y., Xie, Y., Cao, L., Yang, L., Yang, M., Lotze, M. T., et al. (2015). The Ferroptosis Inducer Erastin Enhances Sensitivity of Acute Myeloid Leukemia Cells to Chemotherapeutic Agents. *Mol. Cell Oncol.* 2 (4), e1054549. doi:10.1080/23723556.2015.1054549

Yuan, H., Li, X., Zhang, X., Kang, R., and Tang, D. (2016). CISD1 Inhibits Ferroptosis by protection against Mitochondrial Lipid Peroxidation. *Biochem. Biophys. Res. Commun.* 478 (2), 838–844. doi:10.1016/j.bbrc.2016.08.034

Conflict of Interest: The authors declare that the research was conducted in the absence of any commercial or financial relationships that could be construed as a potential conflict of interest.

The reviewer XH declared a shared affiliation with the authors to the handling editor at time of review.

Publisher's Note: All claims expressed in this article are solely those of the authors and do not necessarily represent those of their affiliated organizations, or those of the publisher, the editors and the reviewers. Any product that may be evaluated in this article, or claim that may be made by its manufacturer, is not guaranteed or endorsed by the publisher.

frontiers in Cell and Developmental Biology

ORIGINAL RESEARCH
published: 08 November 2021
doi: 10.3389/fcell.2021.766978

Vitamin D-Mediated Anti-cancer Activity Involves Iron Homeostatic Balance Disruption and Oxidative Stress Induction in Breast Cancer

Khuloud Bajbouj[1,2], Lina Sahnoon[2], Jasmin Shafarin[2], Abeer Al-Ali[2], Jibran Sualeh Muhammad[1,2], Asima Karim[1,2], Salman Y. Guraya[1,2] and Mawieh Hamad[2,3]**

[1] College of Medicine, University of Sharjah, Sharjah, United Arab Emirates, [2] Research Institute for Medical and Health Sciences, University of Sharjah, Sharjah, United Arab Emirates, [3] College of Health Sciences, University of Sharjah, Sharjah, United Arab Emirates

OPEN ACCESS

Edited by:
Ahmed Hamai, Institut National de la Santé et de la Recherche Médicale (INSERM), France

Reviewed by:
Bandana Chakravarti, Sanjay Gandhi Postgraduate Institute of Medical Sciences (SGPGI), India
Keith R. Laderoute, Consultant, Redwood City, CA, United States

***Correspondence:**
Khuloud Bajbouj
kbajbouj@sharjah.ac.ae
Mawieh Hamad
mabdelhaq@sharjah.ac.ae

Specialty section:
This article was submitted to Molecular and Cellular Oncology, a section of the journal Frontiers in Cell and Developmental Biology

Received: *30 August 2021*
Accepted: *05 October 2021*
Published: *08 November 2021*

Citation:
Bajbouj K, Sahnoon L, Shafarin J, Al-Ali A, Muhammad JS, Karim A, Guraya SY and Hamad M (2021) Vitamin D-Mediated Anti-cancer Activity Involves Iron Homeostatic Balance Disruption and Oxidative Stress Induction in Breast Cancer. Front. Cell Dev. Biol. 9:766978. doi: 10.3389/fcell.2021.766978

Background: Vitamin D deficiency associates with high risk of breast cancer (BRCA) and increased cellular iron. Vitamin D exerts some of its anti-cancer effects by regulating the expression of key iron regulatory genes (IRGs). The association between vitamin D and cellular iron content in BRCA remains ambiguous. Herein, we addressed whether vitamin D signaling exerts a role in cellular iron homeostasis thereby affecting survival of breast cancer cells.

Methods: Expression profile of IRGs in vitamin D-treated breast cancer cells was analyzed using publicly available transcriptomic datasets. After treatment of BRCA cell lines MCF-7 and MDA-MB-231 with the active form of vitamin D, labile iron content, IRGs protein levels, oxidative stress, and cell survival were evaluated.

Results: Bioinformatics analysis revealed several IRGs as well as cellular stress relates genes were differentially expressed in BRCA cells. Vitamin D treatment resulted in cellular iron depletion and differentially affected the expression of key IRGs protein levels. Vitamin D treatment exerted oxidative stress induction and alteration in the cellular redox balance by increasing the synthesis of key stress-related markers. Collectively, these effects resulted in a significant decrease in BRCA cell survival.

Conclusion: These findings suggest that vitamin D disrupts cellular iron homeostasis leading to oxidative stress induction and cell death.

Keywords: vitamin D, breast cancer, iron, oxidative stress, cell death

INTRODUCTION

It is well-established that potent forms of vitamin D, mainly 1,25-dihydroxycholecalciferol, play important roles in human development and physiology, especially in bone metabolism and the regulation of calcium and phosphorus levels. Moreover, numerous studies elaborated that vitamin D has a role in the development, progression, and treatment of numerous disease states including cardiovascular diseases, autoimmunity, and cancer (Jeon and Shin, 2018). Previous work showed

that deficiency of vitamin D is highly associated with a high risk of breast cancer (BRCA) development (Eliassen et al., 2016; Iqbal and Khan, 2017) as it has anti-neoplastic effects against the disease (Eliassen et al., 2016). It was previously reported that there is a strong negative correlation between vitamin D levels and BRCA incidence in postmenopausal women (Abbas et al., 2009; Edlich et al., 2009). Moreover, patients with BRCA were shown to have lower vitamin D levels relative to healthy individuals (Hatse et al., 2012). When the level of vitamin D in BRCA patients is < 20 ng/mL, it is often associated with poor prognosis, metastasis (>90% of cases), and death (>70% of cases) (Imtiaz et al., 2012). Vitamin D and its mechanism of action as an anti-cancer agent were supported by different studies (Honma et al., 1983; Krishnan et al., 2012; Miseta et al., 2015). For example, it was reported that vitamin D can upregulate the expression of p21WAF 1/Cip 1 and p27Kip 1 which are the cell cycle regulators thus limiting the proliferative potential of cancer cells (Gartel and Tyner, 2002; Audo et al., 2003). It was also reported to prompt retinoblastoma (Rb) protein dephosphorylation leading to cell cycle arrest in multiple cancer cells *in vitro* (Audo et al., 2003). *In vitro* studies stated that vitamin D has the ability of BRCA cell lines inhibition as well as induction of apoptosis by upregulating the expression of p21WAF1/Cip, p53, and Bax (caspase activator) genes and by reducing the expression of Bcl-2 (anti-apoptotic mediator) (Calvert et al., 1998; Gartel and Tyner, 2002; Audo et al., 2003).

Iron is an essential nutrient that is intricately involved in the various metabolic processes including cellular respiration and bioenergetics and cell growth and proliferation among others (Winterbourn, 1995). Although iron availability is essential for cells and organisms, excess iron could result in the production and propagation of reactive oxygen species (ROS) by Fenton chemistry (Dixon et al., 2012; Miseta et al., 2015). That would lead to cell damage, generation of oxidative stress, and death by apoptosis and ferroptosis (Mancias et al., 2014; Yang et al., 2014; Hou et al., 2016). Increased cellular iron content in BRCA has been previously reported to associate with poor prognosis and chemoresistance (Habashy et al., 2010). Differential expression of key iron regulatory genes (IRGs) including HAMP, ferroportin (FPN; SLC40A1), and transferrin receptor 1 (TFRC; CD71) has been widely reported as significant biomarkers in BRCA (Pinnix et al., 2010). For example, reduction in the expression of FPN, high ferritin, hepcidin, transferrin receptor (TfR1; CD71) expression, and high labile iron content (LIP) are consistent with the findings associated with breast cancer (Habashy et al., 2010; Pinnix et al., 2010).

Vitamin D was previously reported to reverse iron-mediated oxidative stress (Uberti et al., 2016) and to differentially alter HAMP expression in a tumor type-specific manner (Welsh et al., 2002). Vitamin D treatment in hepatocellular carcinoma was reported to reduce hepcidin and ferritin production and increase in FPN (Bacchetta et al., 2014). Additionally, previous reports have indicated that vitamin D can exert some of its anti-cancer effects by regulating the IRGs expression (Zughaier et al., 2014), suggesting that the treatment effectiveness of BRCA cellular iron metabolism with vitamin D remains ambiguous. In this context, previous work also suggested that vitamin D could exert an anti-growth effect on BRCA cells by modulating several metabolic pathways (Swami et al., 2003). Additionally, preliminary *in silico* data seems to suggest that treatment with calcitriol resulted in a significant decrease in the viability of BRCA cells. In relation to these findings, we have hypothesized that treatment with vitamin D may enhance cell death in BRCA cells by reducing cellular iron content. To address this issue, labile iron content, expression of IRGs at the protein level, oxidative stress, and cell survival were evaluated in both MCF-7 and MDA-MB-231 cells post-vitamin D treatment.

MATERIALS AND METHODS

Bioinformatics Analysis of Publicly Available Transcriptomic Data Resources

We searched for transcriptomic datasets available from National Center for Biotechnology Information (NCBI0 Gene Expression Omnibus (GEO),[1] which is a free public genomics database. The search terms Vitamin D/Cholecalciferol/Calcitriol and breast cancer cells were used to identify datasets for human breast cancer cell lines treated with vitamin D. We selected the dataset GSE53975, which included MCF-7 and MDA-MB-231 cells treated with calcitriol or DMSO ($n = 3$ for each group; $n = 6$ per cell line and $n = 12$ in total) using the Affymetrix Human Exon 1.0 ST platform. The gene expression profiles were downloaded, and the raw data were processed using R statistical software (version 3.5.1). According to the expression profiling data, relative mRNA expression in calcitriol-treated samples vs. DMSO-treated controls was identified using the Limma package (available at http://www.bioconductor.org/packages/release/bioc/html/limma.html) in Bioconductor package version 1.0.2. A log2 fold-change (log2FC) was calculated to present differentially expressed genes (DEGs) and an adjusted p-value < 0.05 using classical t-test was applied. Gene set enrichment analysis was performed using several ontologies resources on DEGs to identify the underlying pathways using pathfinder tool. Gene ontology (GO) terms with a p-value < 0.01, a minimum count of 3, and an enrichment factor > 1.5 (the enrichment factor is the ratio between the observed counts and the counts expected by chance) were collected and grouped into clusters based on their membership similarities.

Cells and Treatment Protocols

In this study, both MCF-7 and MDA-MB-231 human BRCA cell lines were used from American Type Culture Collection (Manassas, VA, United States). Dulbecco's Modified Eagle's Medium (DMEM) was used to maintain the cells at 37°C and 5% CO_2 as it was supplemented with 4 mM glutamine, 2 μg/mL insulin, 10% fetal calf serum, 1 mM of sodium pyruvate, 1 mM of non-essential amino acids, and penicillin/streptomycin antibiotics. Cells at 0.5–1 × 105 cells/mL were seeded using 25 cm flasks and the treatment with different concentrations of calcitriol (25 hydroxyvitamin D; the active form of vitamin

[1]https://www.ncbi.nlm.nih.gov/geo/

D) from (Abcam) was performed at a confluency of ∼70% for different time points. Control cells were left untreated or treated with DMSO.

Calcitriol Treatment and MTT Cell Viability Assay

Cell viability was determined in cells treated with vitamin by using a colorimetric assay MTT (3-(4,5-dimethylthiazol-2-yl)-2,5-diphenyltetrazolium bromide (Sigma-Aldrich), 104 cells of vitamin D treated and untreated control cells were grown in 96-well plates with 0.2 mL culture media and were cultured for 24, 48, and 72 h. After that MTT salt was added and mixed with the cells then kept for 2 h incubation in a humidified incubator at 37°C and 5% CO_2. Product of MTT formazan was dissolved in DMSO and then reading of absorbance was taken at 570 nm using a microplate reader.

Quantitative Real-Time PCR

The cDNA was synthesized from 1 μg of total RNA using the QuantiTect Reverse Transcription Kit (Qiagen) according to the manufacturer's protocol. qPCR was performed using 1:l of complementary DNA (cDNA), specific primers for each genes as listed, SYBR® Green I, and an iCycler Thermal Cycler. Expression levels of target human genes: hepcidin gene expression were (forward: 5′-CTGTTTTCCCACAACAGACG-3′, reverse: 5′-CAGCACATCCCACACTTTGA-3′) and ferroportin (forward: 5′-CAGTTAACCAACATCTTAGC-3′, reverse: 5′-AAGCTCATGGATGTTAGAG-3′) were normalized to GAPDH expression (forward: 5′-CCAGGTGGTCTCCTCTGACTTC-3′, reverse: 5′-TCATACCCAGGAAATGAGCTTGACA-3′).

Western Blot Analysis

Post-vitamin D treatment both MCF-7 and MDA-MB-231 cells were collected and lysed using NP-40 lysis buffer (1.0% NP-40, 150 mM of NaCl, 50 mM of Tris–Cl, pH 8.0) containing protease cocktail inhibitor tablets (Sigma, Germany). Protein quantification was performed using the standard Bradford method. After that protein lysates were separated on 12% sodium dodecyl sulfate–polyacrylamide gel electrophoresis (SDS-PAGE), proteins were transferred into nitrocellulose membrane using semi-dray and/or wet transfer method. Membranes were blocked in 5% skimmed milk for 1 h at room temperature. Proteins of interests were detected using the following different types of primary monoclonal antibodies (anti-TfR1, anti-TfR2, anti-hepcidin, anti-survivin, and anti-HIf1-α all from Abcam, United Kingdom, anti-γH2AX from Millipore, Billerica, MA, United States, and anti-FTH1 from LSBio, United States) diluted at 1:1,000 and kept overnight at 4°C on the shaker. For oxidative stress enzymes, we used anti-HO-1 (Thermo Fisher Scientific, United States), anti-catalase (Abcam, United Kingdom). Secondary labeled anti-mouse and anti-rabbit antibodies from (Cell Signaling) were reacted with the membrane for 1 h at room temperature. Detection of chemiluminescence was performed using an ECL kit (Bio-Rad, United States). Bio-Rad Image Lab software (ChemiDoc^{TM} Touch Gel and Western Blot Imaging System; Bio-Rad) was used to quantify protein bands and β-actin was used as the normalization control. Control sample values were defined as 1.00 and the protein level changes of treated samples were quantified relative to the control.

Labile Iron Measurement

Labile iron content was measured and assessed as it was previously described but a slight modification was performed where deferoxamine was used as a chelator instead of deferiprone (Prus and Fibach, 2008). In brief, cells were washed two times with PBS then 0.5 × 106 was incubated with 0.125 μM calceinacetoxymethyl ester (Cat. No. 56496, Sigma Aldrich) for 15 min at 37°C. Two times washing was performed, and cells were kept for 15 min incubation with 100 mM DFO. Flow cytometry analysis was performed (The BD FACSAria^{TM} III, Becton-Dickinson) applying a 488-nm laser beam for excitation. As a minimum number of events was 50,000 that were collected/sample and percentage of positively stained cells was computed to the 99% level of confidence. Mean fluorescence intensity (MIF) was presented and as it represents the geometric mean fluorescence intensity of a log-normal distribution of fluorescence signals. MFI level increases as the content of free iron decrease; ΔMFI is a qualitative measurement of LIP changes (MFICA-AM/DFO-MFICA-AM alone). If $\Delta MFI > 0$, this would indicate LIP availability while $\Delta MFI < 0$ indicates depletion of LIP.

Reactive Oxygen Species Measurement

Antioxidant related enzymes were measured using the ROS-Glo H_2O_2 Assay Kit (Promega, Cat No. G8820, United States) in both MDMBA-321 and MCF-7 cells, 5,500 cells/well were seeded using a 96-well plate and treated with calcitriol substrate as per manufacturer's instructions to assess ROS production for 3 and 6 h; cells that were plated and left untreated before ROS quantification served as controls.

Proteome Profiler Array

Human Cell Stress Array Kit (R&D system, Cat No. ARY018, United States) was used to detect 26 different cell stress related proteins in both cell lines. After protein quantification by using the standard Bradford method, four nitrocellulose membranes, each containing 26 different capture antibodies, were blocked for 1 h by Array Buffer 6 at room temperature on a shaker. Cell lysate that contains 300 μg of protein was prepared with Array Buffer 4 and 20 μL of detection antibody cocktail. Samples were loaded onto the membrane overnight at 2–8°C. Chemiluminescence was detected by Streptavidin-HRP methods using the dilution factor suggested by the manufacturer. A Bio-Rad Image Lab software (ChemiDoc^{TM} Touch Gel and Western Blot Imaging System; Bio-Rad) was used for protein dot quantification. Reference spots were used as a normalization control and control sample values were defined as 1.00 and the values of treated samples were quantified relative to the control.

Cell Cycle Progression Analysis

Analysis of a cell cycle progression was performed by using Propidium Iodide Flow Cytometry Kit (Abcam,

United Kingdom). Briefly, cells were seeded at a density of 1 × 106 cells/mL. After indicated treatment time points, cells were harvested and washed with PBS, cells were then resuspended in 0.5 mL ice-cold PBS and fixed for 48 h with 4 mL of ice-cold 70% ethanol at −20°C. The cell pellet was washed again twice with ice-cold PBS, resuspended, and incubated with 0.2 mL of staining buffer that is supplemented with stain solution containing RNase and propidium iodide (PI) at room temperature in the dark. Phases of the cell cycle with different DNA contents were determined by performing flow cytometry (The BD FACSAria^{TM} III; Becton Dickinson and Company). The cell cycle platform of the FlowJo software was used to analyze the distribution of the cell cycle and percentage of cells in sub-G1, G1, S, and G2/M phases in addition to the Watson pragmatic model (Tree Star).

Annexin-V Staining for Apoptosis Detection

Cell apoptosis was performed using Annexin V-FITC Apoptosis Staining/Detection Kit protocol from (Abcam, United States). In brief, 1 × 106 cells/mL were seeded, treated, and harvested then washed with PBS two times. Cells were kept for 20 min with 0.2 mL staining buffer annexin-V/PI in the dark at room temperature. Cell apoptosis was analyzed using flow cytometry (The BD FACSAria III; Becton Dickinson and Company) with an excitation wavelength of 488 nm; a 530/30 nm band pass filter for fluorescein detection and a long pass filter of 670 nm was used. Apoptotic and necrotic cells were analyzed as the following: PI only positive cells were counted and indicated necrosis, cells which were counted as annexin V positive and PI negative were indicated as early apoptotic cells, and cells which were counted as annexin V positive and PI positive were indicated as late apoptotic cells. FlowJo software with the Watson pragmatic model (Tree Star, Ashland OR, United States) was used for data analysis of the flow results.

Statistical Analysis

Graph prism Pad 5 software (GraphPad Software Inc., La Jolla, CA, United States) was used for data analysis of cell viability and iron regulation. Other data paired *t*-test was used for *p*-values generation to compare between groups in each data set.

RESULTS

Subsection

Vitamin D Differentially Alters the Expression Profile of Iron Regulatory Genes

To investigate the effect of vitamin D on breast cancer cells, we first performed *in silico* analysis of a publicly available expression array dataset of breast cancer cells treated with 40–50 μM of calcitriol. Both breast cancer cell types, MCF-7, and MDA-MB-231, showed more than 5000 DEGs (**Figure 1A**, significantly up/downregulated, $p < 0.05$). Disruption of iron metabolism and

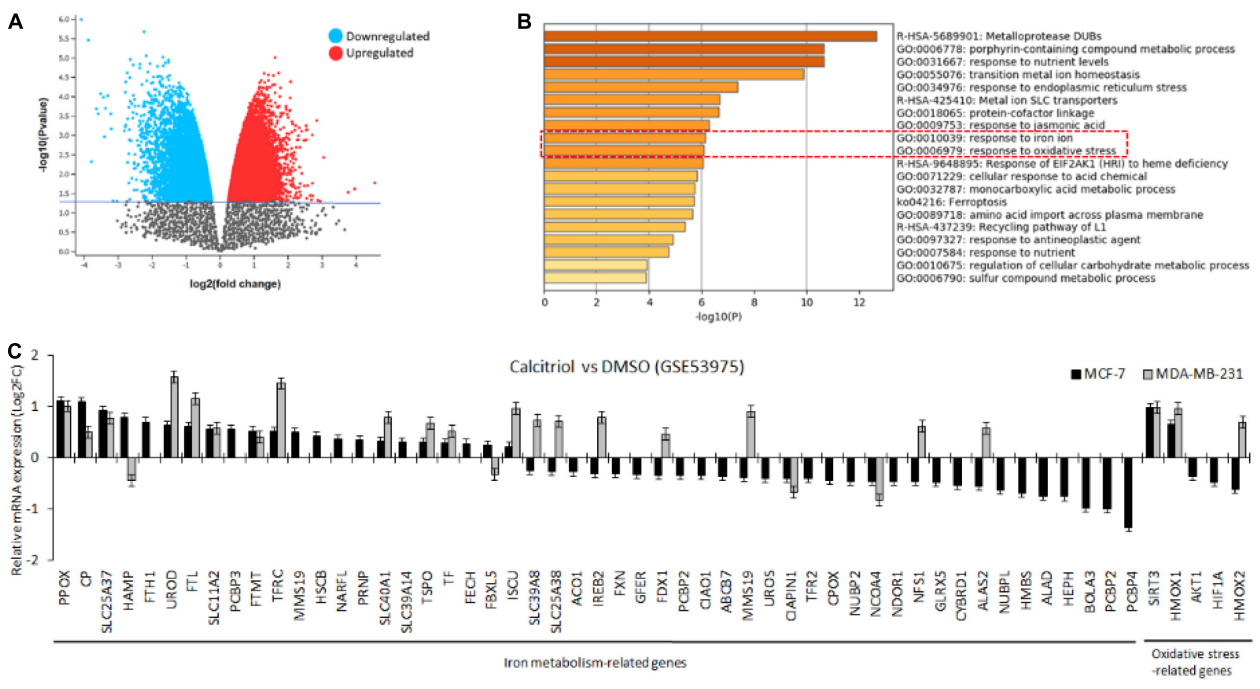

FIGURE 1 | *In silico* analysis to investigate the effect of vitamin D treatment on breast cancer cells. **(A)** Volcano plot showing more than 5,000 genes were significantly up-/downregulated in MCF-7 and MDA-MB-231 cells. **(B)** Pathway analysis of differentially expressed genes showing enrichment of pathways related to the response to iron ion and oxidative stress. **(C)** Bar graph plot showing the mean expression values of iron metabolism and oxidative stress-related genes for both cell lines treated with calcitriol compared with DMSO-treated cells.

induction of oxidative stress is known to induce a deleterious effect on cancer cells. Therefore, we aimed to explore if the DEGs in vitamin D-treated breast cancer cells included iron metabolism-related and oxidative stress-related genes. Utilizing the DEGs common to both MCF-7 and MDA-MB-231 cell lines treated with vitamin D, we performed pathway enrichment analysis. The results showed a significant enrichment of GO pathways related to response to iron ion and response to

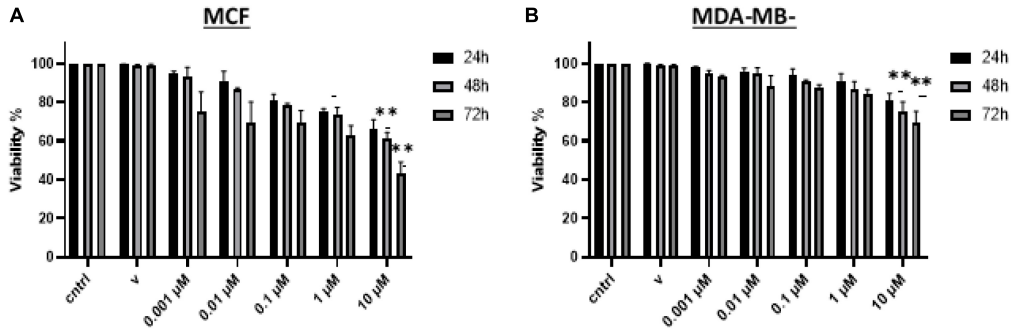

FIGURE 2 | Assessment of BRCA cell viability following vitamin D treatment. Percentage cell viability of **(A)** MCF-7 and **(B)** MDA-MB-231 cells treated with 0.001, 0.01, 0.1, 1, and 10 μM vitamin D for 24, 48, and 72 h as measured by the MTT assay. **Represents statistically significant change ($P < 0.01$) in cell survival between calcitriol-treated and untreated controls at each time point tested.

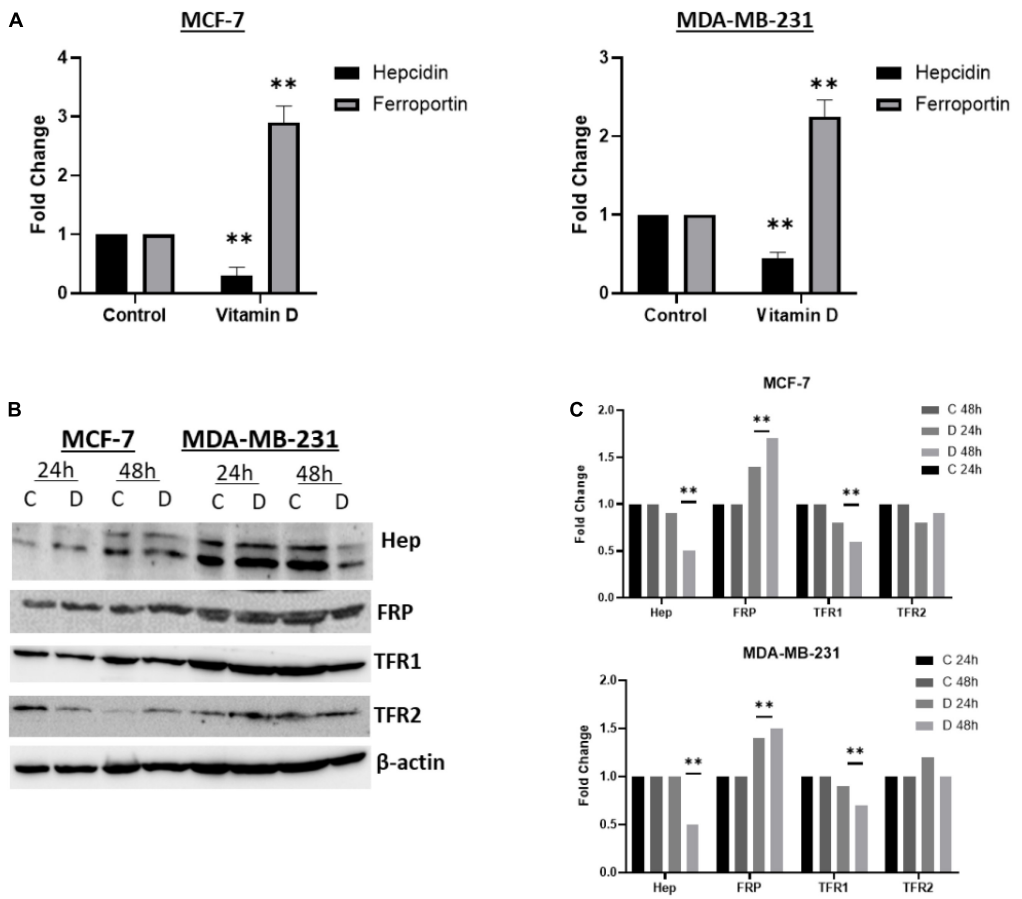

FIGURE 3 | Vitamin D disrupts cellular iron metabolism in BRCA cells. The status of hepcidin, FPN, TfR1, and TfR2 in vitamin D treated MCF-7 and MDA-MB-231 cells. **(A)** Gene expression was analyzed in from MCF-7 and MDA-MB-231 cells treated with vitamin D 10 μM and cultured for 6 h. **(B)** Cell lysates were prepared from MCF-7 and MDA-MB-231 cells treated with vitamin D 10 μM and cultured for 24 and 48 h. Shown data are representative of three separate experiments. **(C)** Quantitative analysis of relative protein band density after normalization to β-actin and compared to the control. **Represents statistically significant change ($P < 0.01$).

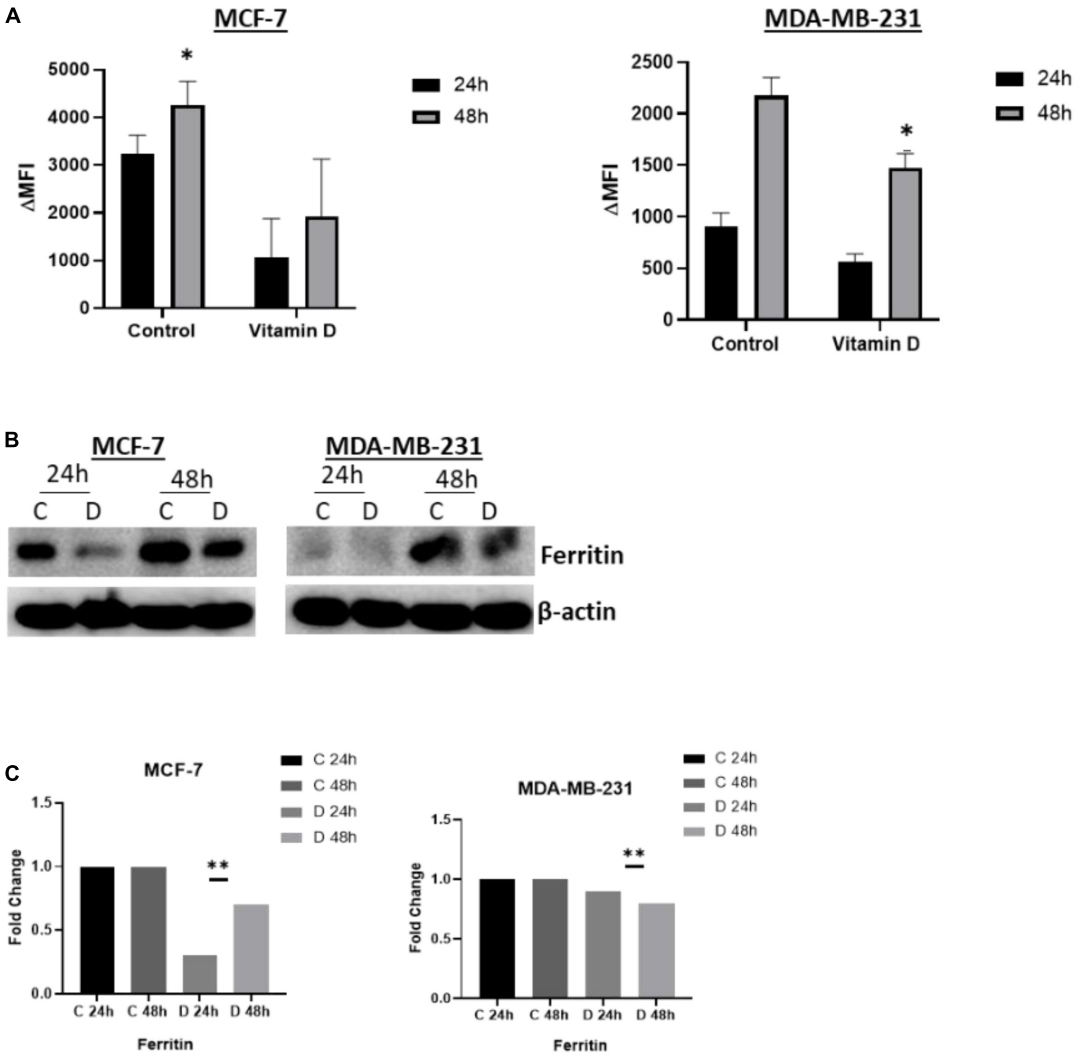

FIGURE 4 | Vitamin D depletes labile cellular iron in BRCA cells. **(A)** Calcein-based flow cytometry method was used to assess labile iron pool (LIP) content in MCF-7 and MD-MBA-231 cells treated with 10 μM vitamin D. Difference in mean fluorescence intensity (ΔMFI) between calcein + chelator and calcein only is an indirect measurement of LIP content; the smaller the ΔMFI value, the lower the LIP content. **(B)** Ferritin expression was assessed in cell lysates of MCF-7 and MDA-MB-231 cells at 24 and 48 h post vitamin D treatment; untreated cells served as controls. The data shown are the mean MFI ± SEM of four separate experiments. **(C)** Quantitative analysis of relative protein band density after normalization to β-actin and compared to the control. *Represents statistically significant change ($P < 0.05$) and **Represents statistically significant change ($P < 0.01$).

oxidative stress (**Figure 1B**, GO:001039, GO:0006979, $p < 0.01$). Other significantly enriched genes set in these treated breast cancer cells included metalloproteases, porphyrin-containing compound metabolic process, and response to nutrient levels.

Next, the mean expression values were plotted of those genes for both cell lines treated with calcitriol compared with DMSO-treated cells. We found that 56 genes related to iron metabolism and oxidative stress were significantly dysregulated in MCF-7 cells but only 26 of those genes were dysregulated in MDA-MB-231 cells (**Figure 1C**). Few of the critical IRGs, such as CP, FTH1, SLC11A2, SLC40A1, and SLC39A14, were upregulated, and TFR2 was downregulated upon calcitriol treatment in both types of cell lines. Additionally, SIRT3 and HMOX, key oxidative stress markers, were also found upregulated in both calcitriol-treated cell lines. Nevertheless, only a few other key IRGs, such as HAMP and FTL, were upregulated only in calcitriol-treated MCF-7 cells. This suggested us to further investigate the protein expression of few of these iron metabolism and oxidative stress on cancer cell survival in vitamin D-treated breast cancer cells.

Vitamin D Reduces Breast Cancer Cell Viability

BRCA cell viability was examined post-treatment to test the effect of vitamin D in both MCF-7 and MDA-MB-231 by using the MTT assay. In **Figure 2**, it is shown that cell viability was significantly reduced in cultures that were treated with 0.001, 0.01, 0.1, 1, and 10 μM of vitamin D for 24, 48, and 72 h; this was true for MCF-7 and MDA-MB-231 cells. There is a significant

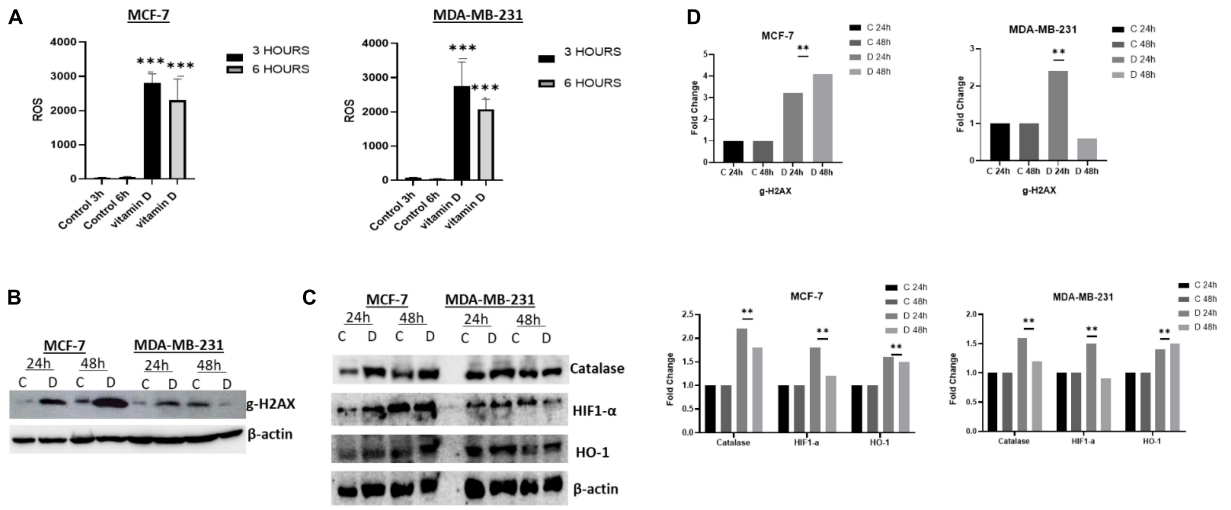

FIGURE 5 | Vitamin D alters the redox balance in BRCA cells in favor of oxidative stress. **(A)** ROS level expression following 3 and 6 h post vitamin D treatment. Expression of **(B)** the DNA damage sensor, g-H2AX, and **(C)** the redox balance regulators proteins catalase, Hif-1α and OH-1 levels in MCF-7 and MDA-MB-231 cells following at 24 and 48 h post-treatment with vitamin D. The data shown are representative of three separate experiments. **(D)** Quantitative analysis of relative protein band density after normalization to β-actin and compared to the control. **Represents statistically significant change ($P < 0.01$) and ***Represents statistically significant change ($P < 0.001$).

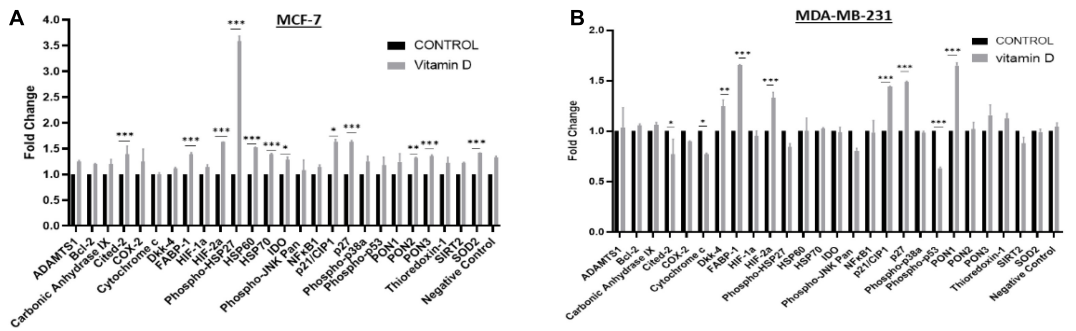

FIGURE 6 | Proteome profiling of cell stress regulators in vitamin D-treated BRCA cells. Expression status of key cell stress regulators in **(A)** MCF-7 and **(B)** MDA-MB-231 cells using cell lysates prepared from cells at 24 h post-treatment with vitamin D. *Denotes the presence of statistically significant changes ($p < 0.05$) in protein expression in treated vs. control samples. **Represents statistically significant change ($P < 0.01$), ***Represents statistically significant change ($P < 0.001$).

reduction in cell viability at 24 (72%), 48 (65%), and 72 (50%) h treatment of MCF-7 cells with 10 μM vitamin D as is shown in **Figure 2A**. There was more pronounced reduction in MDA-MB-231 cell viability when treated with 10 μM vitamin D for 72 h (79%; **Figure 2B**).

Vitamin D Differentially Disrupts Cellular Iron Metabolism in Breast Cancer Cells

A significant depletion of cellular iron was observed in the treatment of MCF-7 and MDA-MB-231 with 10 μM vitamin D and it differentially affected key IRGs expression. After calcitriol treatment, both MCF-7 and MDA-MD-231 cells showed reduction in hepcidin gene expression and protein levels (**Figures 3A,B**), and there was a significant increase of FPN levels in both cell types (**Figures 3A,B**). Additionally, in MCF-7 cells TFR1 expression showed a drop at 24 and 48 h post-treatment and in MDA-MB-231 cells at 48 h (**Figure 3B**). Changes were not significant in TFR2 expression following vitamin D treatment (**Figure 3B**). LIP content was tested in both MCF-7 and MDA-MB-231 cells following treatment with 10 μM vitamin D for 24 and 48 h to test if the reduction in hepcidin and increase in FPN would result in increased cellular iron efflux. As shown in **Figure 4A**, depletion of LIP ($\Delta MFI < 0$) was evident in both cell types post-treatment with vitamin D; MCF-7 at 24 h and MDA-MB-231 at 48 h. Lysates were obtained from control and treated cells to evaluate ferritin expression. As shown in **Figures 4B,C**, significant changes in ferritin protein synthesis were observed in MCF-7 following vitamin D treatment at 24 h; no clear change in ferritin synthesis was evident in vitamin D-treated MDA-MB-231 cells at 24 or 48 h post-treatment.

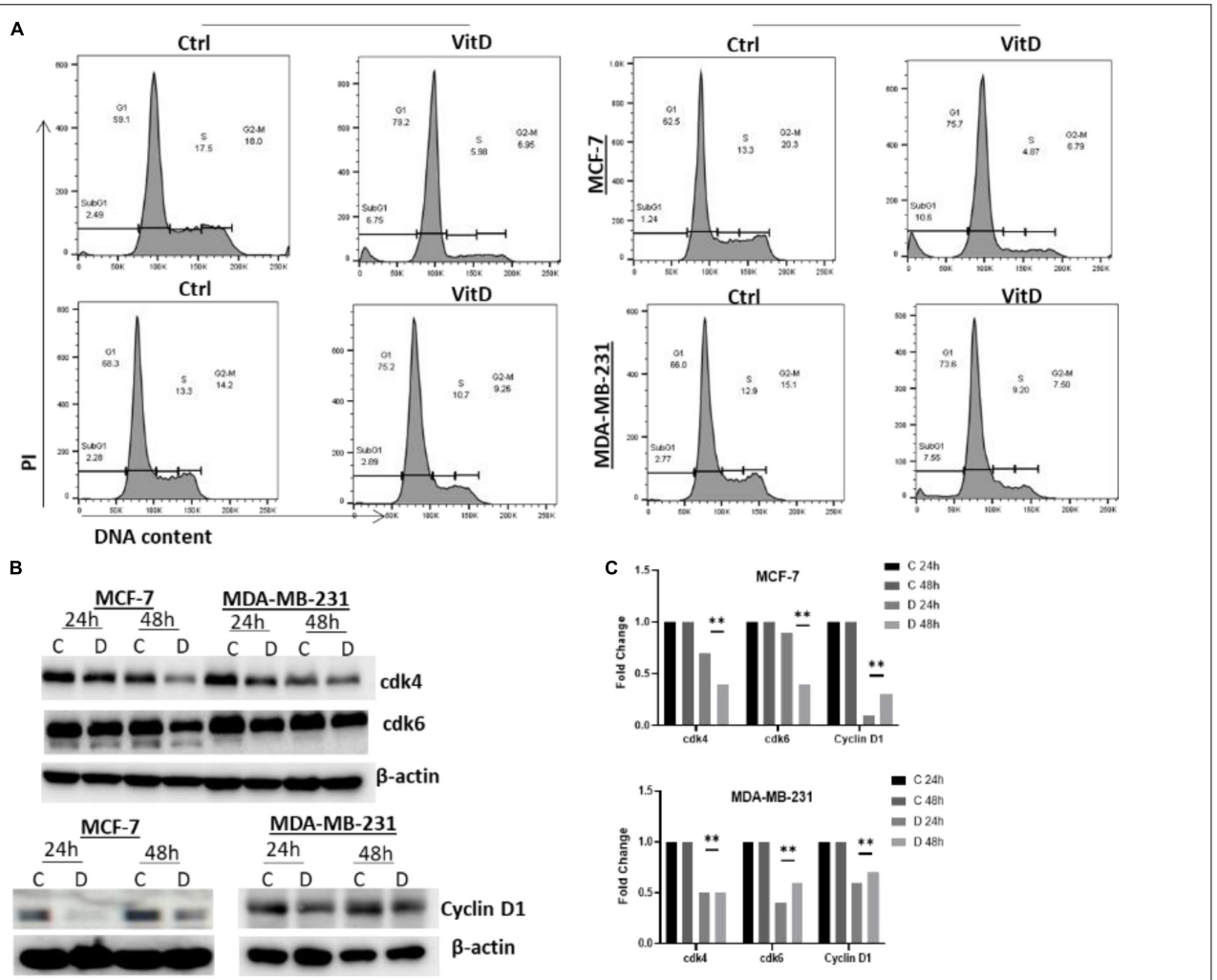

FIGURE 7 | Vitamin D treatment leads to cell cycle arrest at G1/S phase arrests in BRCA cells. **(A)** Cells treated with 10 μM vitamin D for 24 and 48 h as well as PI stain were used for untreated controls and analyzed. **(B)** cdk4 (U/mg protein), cdk6 (U/mg protein), and cyclin D1 (U/mg protein) were assayed for control, and MCF-7 and MDA-MB-231 cells treated with 10 μM of vitamin D for 24 and 48 h. **(C)** Quantitative analysis of relative protein band density after normalization to β-actin and compared to the control. **Represents statistically significant change ($P < 0.01$).

Vitamin D Induces Oxidative Stress and Alters the Redox Balance in Breast Cancer Cells

The observation that vitamin D disrupts cellular iron homeostasis raised the possibility that this could consequently influence the oxidative stress status in treated cells. To address this issue, we examined the ROS level in vitamin D-treated MCF-7 and MDA-MB-231 cells as shown in **Figure 5A** which indicate a significant increase in both cell lines post 3 and 6 h vitamin D treatment. Furthermore, we confirmed redox balance disturbance by assaying for the expression of several stress-related markers including catalase, γ-H2AX, HIF-1α, and HO-1. A significant increase of γ-H2AX was observed in MCF-7 treated at 24 and 48 h and in MDA-MB-231 treated at 24 h (**Figure 5B**, top panel). Likewise, catalase activity in vitamin D-treated MCF-7 cells at 24 and 48 h and in MDA-MB-231 cells at 24 h was significantly increased (**Figures 5C,D**, first panel from top). Compared to the control, HIF-1α was highly increased in MCF-7 and MDA-MB-231 (**Figure 5C**, second panel from top). The expression level of Heme Oxygenase 1 (HO-1) protein was significantly upregulated in both cell lines at both time points following vitamin D treatment (**Figure 5C**, third panel from top).

Oxidative stress/redox balance was further investigated in treated cells, the proteome profiler for human cell stress markers was employed. In **Figure 6A**, MCF-7 cells treated at 24 h show that there is a significant increase in phosphor-HSP27, Cited-2, FABP-1, HIF-2α, HSP60, HSP70, p27, PON3, and SOD2. A significant increase in FABP-1, HIF-2α, p21/CIP-1, p27, and PON1 stress markers was observed in MDA-MB-231 at 24 h after treatment with vitamin D (**Figure 6B**).

Vitamin D Disrupts Cell-Cycling in MCF-7 and MDA-MB-231 Cells

Treatment of vitamin D resulted in a significant disruption in cellular iron metabolism and cell redox balance, we next

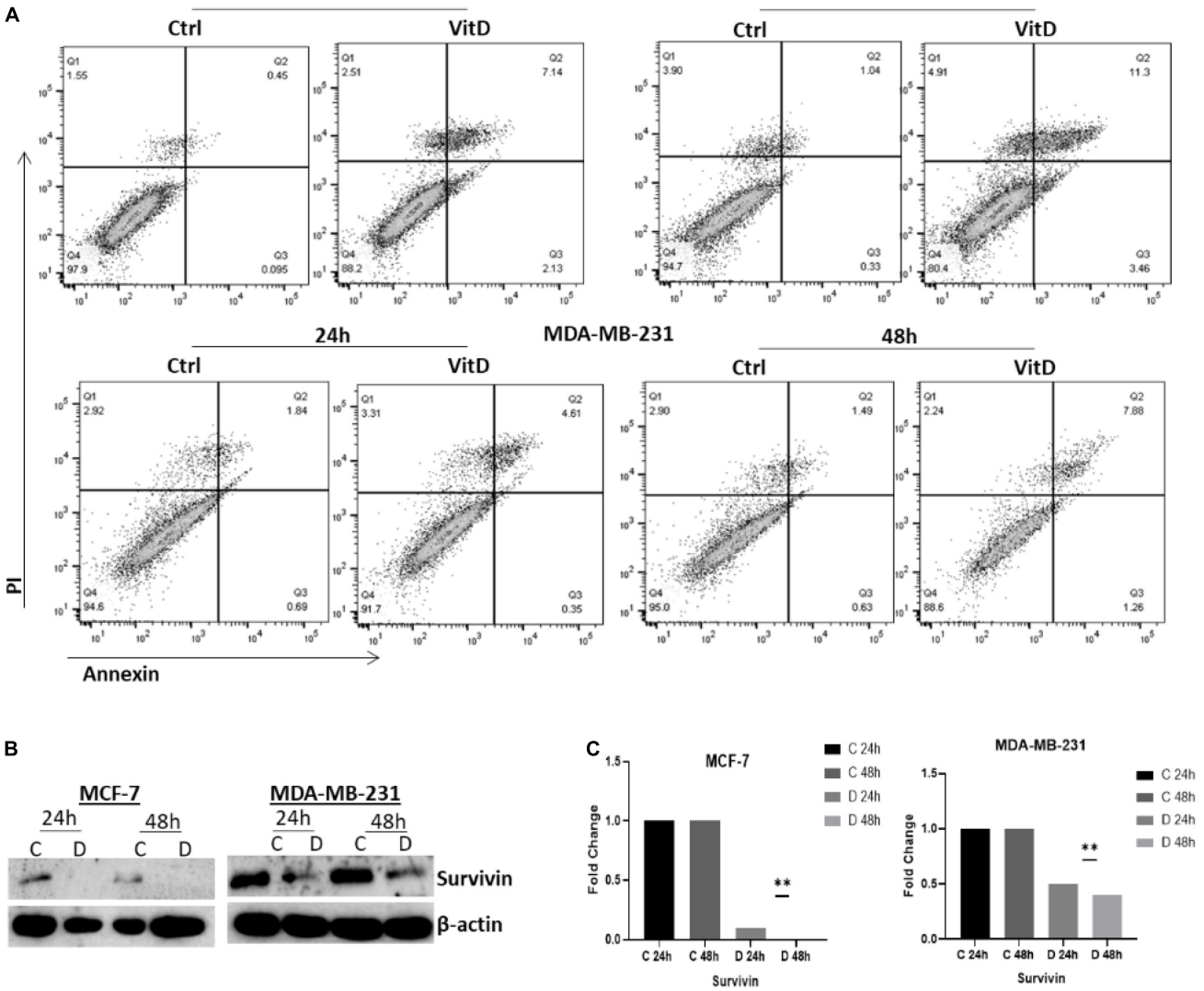

FIGURE 8 | Vitamin D effect on apoptosis and cell survival in BRCA cells. **(A)** The Annexin V/PI flow cytometry-based method used to assess the percentage of apoptotic and pro-apoptotic in MCF-7 and MDA-MB-231 cells treated with 10 μM of vitamin D for 24 or 48 h. **(B)** Survivin expression was assessed in 10 μM of vitamin D-treated cell lysates and from untreated controls at 24 and 48 h post-culture. **(C)** Quantitative analysis of relative protein band density after normalization to β-actin and compared to the control. **Represents statistically significant change ($P < 0.01$).

measured the percentage of cells/cell cycle phases in vitamin D-treated vs. control cells to evaluate the treatment effects on cell cycling. Treatment of MCF-7 with vitamin D for 48 h resulted in a G1/S phase arrest prior to cell cycle analysis (**Figure 7**). At both 24 and 48 h MCF-7 treated cells, the percentage of G1 phase was higher in relative to untreated controls (79.2% vs. 59.1%) and 48 h (75.7% vs. 62.5%);% of treated vs. untreated MDA-MB-231 at G1 phase was (75.2% vs. 66.3%) at 24 h and (73.6% vs. 66%) at 48 h. Moreover, the expression of cyclin D1 in MCF-7 and MDA-MB-231 at 24 and 48 h post-treatment was significantly downregulated. These findings notwithstanding, a significant decrease in cdk4 and cdk6 in vitamin D-treated MCF-7 and MDA-MB-231 cells at 48 h post-treatment (**Figure 7B**).

Vitamin D Induces Apoptosis and Decreases Cell Growth Potential in Breast Cancer Cells

Annexin V/PI flow cytometry-based method was used to assess the rate of cells growth; percentage of apoptotic cells MCF-7 and MDA-MB-231 treated with vitamin D was significantly increased relative to controls, especially at 48 h where it was 11.3% vs. 1.04% in MCF-7 cells and 7.88% vs. 1.49% in MDA-MB-231 (**Figure 8A**). Moreover, the expression levels of antiapoptotic protein surviving were assessed in cell lysates of both vitamin D-treated cells and untreated controls by western blotting. Survivin expression showed a significant reduction in MCF-7 and MDA-MB-231 treated cells at 24 and 48 h (**Figure 8B**).

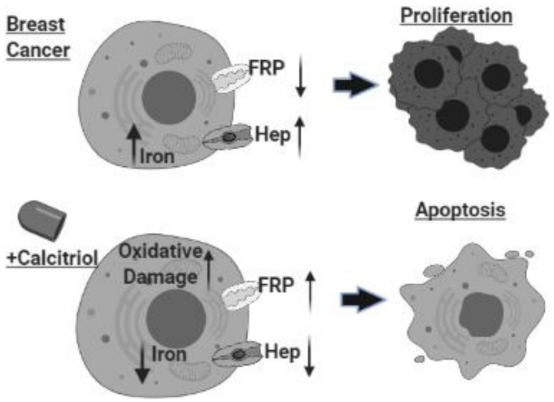

FIGURE 9 | Schematic illustration of study conclusion. Created with BioRender.com.

DISCUSSION

Data presented here clearly show that vitamin D precipitates significant anti-cancer effects in BRCA cells. This effect is based on disruption of cellular iron metabolism, increasing in oxidative stress, induction of cell cycle arrest, enhancement of apoptosis, and reduction in cell growth potential in two distinct BRCA cell lines, MCF-7 and MDA-MB-231. Our data showed that the expression of key IRGs was modulated after vitamin D by causing a disruption in cellular iron metabolism, vis-à-vis reducing hepcidin synthesis, increasing HIF-1α and FPN expression, and decreasing TFR1 expression. Moreover, vitamin D treatment resulted in a transient LIP and FT depletion. Collectively, this suggests that vitamin D treatment induces an iron release phenotype in BRCA cells. The expression of high HIF-1α protein after vitamin D treatment is in positive agreement with previously published data (Jiang et al., 2010). Moreover, reduction of hepcidin synthesis and increasing of HIF-1α expression is in agreement with the other findings. HIF-1α can negatively regulate the synthesis of hepcidin to enhance cellular iron export to increase systemic demand for iron (Nemeth et al., 2004). A previous study observed that vitamin D binding to the vitamin D receptor reduces hepcidin mRNA expression levels in PBMC monocytes and this is consistent with our finding of vitamin D ability to reduce hepcidin synthesis, THP1 cells, and HepG2 cells (Bacchetta et al., 2014). Proinflammatory cytokines and hepcidin were reported to be significantly downregulated in vitamin D THP-1 treated cells (Zughaier et al., 2014) and to significantly reduce plasma hepcidin concentrations in healthy adults (Smith et al., 2017). Together, these findings are consistent with our results of vitamin D treated breast cancer cells have low hepcidin expression (**Figure 3**).

Our data showed that reduced hepcidin synthesis paralleled a significant increase in FPN expression. This is consistent with the negative impact of hepcidin on FPN expression and the fact that reduced hepcidin synthesis maintains FPN integrity (Zughaier et al., 2014). Given that TfR1 is a key player in iron import to cells (Wan et al., 2019), suppressed TfR1 expression following vitamin D treatment would likely result in reduced cellular iron content or LIP. Collectively, therefore, reduced hepcidin and TfR1 expression along with increased FPN expression are all consistent with an iron release phenotype as evidenced by decreased LIP content (Δ MFI < 0).

Interestingly and perhaps surprisingly, vitamin D treatment disrupted the redox balance as demonstrated by the high levels of ROS and the increased expression of stress-related markers like γ-H2AX, HIF-1α, and HO-1. This is indicative that vitamin D treatment decreased cellular LIP content, which would be expected to reduce rather than increase oxidative stress. Increasing oxidative stress in treated cells was confirmed by the overexpression of the antioxidant HO-1 (Abo El-Magd and Eraky, 2020) and increased expression of HIF-1α. The ability of vitamin D to inhibit cell growth in BRCA cells by generating ROS and causing DNA damage was observed in previous research (Marchionatti et al., 2009; Bohl et al., 2017). Our findings are consistent with the ability of vitamin D-treated cells to induce DNA disruption as proven by the transitory increased expression of γ-H2AX (**Figure 6**).

Proteome profiling, which further probed the oxidative stress status in vitamin D-treated cells and which revealed overexpression of cell cycle modulators p21 and p2, may help explain suppressed BRCA growth and proliferation following vitamin treatment. Previous work has reported that calcitriol increases the levels of p21WAF 1/Cip1 and p27Kip1 cell cycle regulators which inhibits the ability of cancer cells to proliferate (Gartel and Tyner, 2002; Audo et al., 2003). Our results also demonstrated a significant increase in catalase expression in vitamin D-treated BRCA. Given that the catalase enzyme is an antioxidant that catalyzes hydrogen peroxide neutralization, its increase further suggests that vitamin D treatment puts cells under significant oxidative stress which triggers antioxidant systems like catalase as means of oxidative stress and cellular damage. It is worth noting here that high metabolic rates in tumor cells associate with increased production of ROS and oxidative stress (Marklund et al., 1982; Sandstrom and Buttke, 1993; Glorieux and Calderon, 2017). Therefore, the ability of vitamin D to target and capitalize on this precarious pathway in cancer cells merits further examination as a potential therapeutic target. In this context, our data showed that vitamin D induced G1/S phase cell cycle arrest associating with downregulated cdk4, cdk6, and cyclin D1 expression (**Figure 7**) and induced apoptosis which is associated with reduced expression of survivin (**Figure 8**). These findings are consistent with previous research that further founded that vitamin D supplementation inhibited cell proliferation throughout multipotent mesenchymal cells and arresting cell cycling (Artaza et al., 2010). Additionally, previously published data have suggested that vitamin D induced apoptosis in different types of cancers including breast cancer, colon cancer, and glioma cell lines (Welsh, 1994; Sergeev, 2014). Increasing evidence suggests an important antiproliferative and apoptotic effects of vitamin D in cancer. Importantly, however, new treatment strategies are needed to reverse the multidrug resistance in many cancer types by using vitamin D in combination with different drugs and investigating the related pathways.

CONCLUSION

In conclusion, as shown in **Figure 9**, our findings highlighted the complex relationship between vitamin D and cellular iron metabolism suggesting that vitamin D could have significant anti-cancer effects by disrupting cellular iron homeostasis. The molecular pathway of vitamin D ability to alter the expression of key IRGs requires additional conformational work.

DATA AVAILABILITY STATEMENT

The original contributions presented in the study are included in the article/supplementary material, further inquiries can be directed to the corresponding author/s.

AUTHOR CONTRIBUTIONS

KB and MH: conceptualization and funding acquisition. KB, LS, JS, AA-A, AK, JM, and SG: visualization, methodology, and validation. JS: software. KB and LS: formal analysis. KB, LS, JS, AA-A, AK, and JM: investigation. KB, LS, JS, AA-A, and JM: data curation. KB, LS, and MH: writing—original draft preparation. KB, LS, and MH: writing—review and editing. KB: supervision and project administration. All authors have read and agreed to the published version of the manuscript.

FUNDING

This work was supported by the University of Sharjah Seed grant, Ref. no. 1901090150. The abstract of this manuscript was presented at the American Association for Cancer Research (AACR) Annual virtual meeting, April 2021, United States, as an online abstract with interim findings. The abstract was published in "e-Abstracts planner" supplement in the AACR annual meeting website, https://www.abstractsonline.com/pp8/#!/9325/presentation/3354.

ACKNOWLEDGMENTS

We acknowledge the support of the Sharjah Institute for Medical Research (SIMR), University of Sharjah, United Arab Emirates. We agree to be accountable for all aspects of the work.

REFERENCES

Abbas, S., Chang-Claude, J., and Linseisen, J. (2009). Plasma 25-hydroxyvitamin D and premenopausal breast cancer risk in a German case-control study. *Int. J. Cancer* 124, 250–255. doi: 10.1002/ijc.23904

Abo El-Magd, N. F., and Eraky, S. M. (2020). The molecular mechanism underlining the preventive effect of vitamin D against hepatic and renal acute toxicity through the NrF2/ BACH1/ HO-1 pathway. *Life Sci.* 244:117331. doi: 10.1016/j.lfs.2020.117331

Artaza, J. N., Sirad, F., Ferrini, M. G., and Norris, K. C. (2010). 1,25(OH)2vitamin D3 inhibits cell proliferation by promoting cell cycle arrest without inducing apoptosis and modifies cell morphology of mesenchymal multipotent cells. *J. Steroid Biochem. Mol. Biol.* 119, 73–83. doi: 10.1016/j.jsbmb.2010.01.001

Audo, I., Darjatmoko, S. R., Schlamp, C. L., Lokken, J. M., Lindstrom, M. J., Albert, D. M., et al. (2003). Vitamin D analogues increase p53, p21, and apoptosis in a xenograft model of human retinoblastoma. *Invest. Ophthalmol. Vis. Sci.* 44, 4192–4199. doi: 10.1167/iovs.02-1198

Bacchetta, J., Zaritsky, J. J., Sea, J. L., Chun, R. F., Lisse, T. S., Zavala, K., et al. (2014). Suppression of iron-regulatory hepcidin by vitamin D. *J. Am. Soc. Nephrol.* 25, 564–572. doi: 10.1681/ASN.2013040355

Bohl, L., Guizzardi, S., Rodríguez, V., Hinrichsen, L., Rozados, V., Cremonezzi, D., et al. (2017). Combined calcitriol and menadione reduces experimental murine triple negative breast tumor. *Biomed. Pharmacother.* 94, 21–26. doi: 10.1016/j.biopha.2017.07.058

Calvert, P., Yao, K. S., Hamilton, T. C., and O'Dwyer, P. J. (1998). Clinical studies of reversal of drug resistance based on glutathione. *Chem. Biol. Interact.* 111-112, 213–224. doi: 10.1016/s0009-2797(98)00008-8

Dixon, S. J., Lemberg, K. M., Lamprecht, M. R., Skouta, R., Zaitsev, E. M., Gleason, C. E., et al. (2012). Ferroptosis: an iron-dependent form of nonapoptotic cell death. *Cell* 149, 1060–1072. doi: 10.1016/j.cell.2012.03.042

Edlich, R., Mason, S. S., Chase, M. E., Fisher, A. L., Gubler, K., Long, W. B. III, et al. (2009). Scientific documentation of the relationship of vitamin D deficiency and the development of cancer. *J. Environ. Pathol. Toxicol. Oncol.* 28, 133–141. doi: 10.1615/jenvironpatholtoxicoloncol.v28.i2.50

Eliassen, A. H., Warner, E. T., Rosner, B., Collins, L. C., Beck, A. H., Quintana, L. M., et al. (2016). Plasma 25-hydroxyvitamin D and risk of breast cancer in women followed over 20 years. *Cancer Res.* 76, 5423–5430. doi: 10.1158/0008-5472.CAN-16-0353

Gartel, A. L., and Tyner, A. L. (2002). The role of the cyclin-dependent kinase inhibitor p21 in apoptosis. *Mol. Cancer Ther.* 1, 639–649.

Glorieux, C., and Calderon, P. B. (2017). Catalase, a remarkable enzyme: targeting the oldest antioxidant enzyme to find a new cancer treatment approach. *Biol. Chem.* 398, 1095–1108. doi: 10.1515/hsz-2017-0131

Habashy, H., Powe, D., and Staka, C. (2010). Transferrin receptor (CD71) is a marker of poor prognosis in breast cancer and can predict response to tamoxifen. *Breast Cancer Res. Treat.* 119, 283–293. doi: 10.1007/s10549-009-0345-x

Hatse, S., Lambrechts, D., and Verstuy, A. (2012). Vitamin D status at breast cancer diagnosis: correlation with tumor characteristics, disease outcome, and genetic determinants of vitamin D insufficiency. *Carcinogenesis* 33, 1319–1326. doi: 10.1093/carcin/bgs187

Honma, Y., Hozumi, M., Abe, E., Konno, K., Fukushima, M., Hata, S., et al. (1983). 1 alpha,25-Dihydroxyvitamin D3 and 1 alpha-hydroxyvitamin D3prolong survival time of mice inoculated with myeloid leukemia cells. *Proc. Natl. Acad. Sci. U.S.A.* 80, 201–204. doi: 10.1073/pnas.80.1.201

Hou, W., Xie, Y., Song, X., Sun, X., Lotze, M. T., Zeh, H. J. III, et al. (2016). Autophagy promotes ferroptosis by degradation of ferritin. *Autophagy* 12, 1425–1428. doi: 10.1080/15548627.2016.1187366

Imtiaz, S., Siddiqui, N., Raza, S. A., Loya, A., and Muhammad, A. (2012). Vitamin D deficiency in newly diagnosed breast cancer patients. *Indian J. Endocrinol. Metab.* 16, 409–413. doi: 10.4103/2230-8210.95684

Iqbal, M. U. N., and Khan, T. A. (2017). Association between vitamin D receptor (Cdx2, Fok1, Bsm1, Apa1, Bgl1, Taq1, and Poly (A)) gene polymorphism and breast cancer. *Tumour. Biol.* 39, 721–739. doi: 10.1177/1010428317731280

Jeon, S. M., and Shin, E. A. (2018). Exploring vitamin D metabolism and function in cancer. *Exp. Mol. Med.* 50, 1–14. doi: 10.1038/s12276-018-0038-9

Jiang, Y., Zheng, W., and Teegarden, D. (2010). 1α, 25-Dihydroxyvitamin D regulates hypoxia-inducible factor-1α in untransformed and Harvey-ras transfected breast epithelial cells. *Cancer Lett.* 298, 159–166. doi: 10.1016/j.canlet.2010.06.014

Krishnan, A. V., Swami, S., and Feldman, D. (2012). The potential therapeutic benefits of vitamin D in the treatment of estrogen receptor positive breast cancer. *Steroids* 77, 1107–1112. doi: 10.1016/j.steroids.2012.06.005

Mancias, J., Wang, X., Gygi, S. P., Wade Harper, J., and Kimmelman, A. C. (2014). Quantitative proteomics identifies NCOA4 as the cargo receptor mediating ferritinophagy. *Nature* 509, 105–109. doi: 10.1038/nature13148

Marchionatti, A. M., Picotto, G., Narvaez, C. J., Welsh, J., and Tolosa de Talamoni, N. G. (2009). Antiproliferative action of menadione and 1,25(OH)2D3 on breast cancer cells. *J. Steroid Biochem. Mol. Biol.* 113, 227–232. doi: 10.1016/j.jsbmb.2009.01.004

Marklund, S. L., Westman, N. G., Lundgren, E., and Roos, G. (1982). Copper- and zinc-containing superoxide dismutase, manganese-containing superoxide dismutase, catalase, and glutathione peroxidase in normal and neoplastic human cell lines and normal human tissues. *Cancer Res.* 42, 1955–1961.

Miseta, A., Nagy, J., Nagy, T., Soma Poór, V., Fekete, Z., and Sipos, K. (2015). Hepcidin and its potential clinical utility. *Cell Biol. Int.* 39, 1191–1202. doi: 10.1002/cbin.10505

Nemeth, E., Tuttle, M. S., Powelson, J., Vaughn, M. B., Donovan, A., Ward, D. M., et al. (2004). Hepcidin regulates cellular iron efflux by binding to ferroportin and inducing its internalization. *Science* 306, 2090–2093. doi: 10.1126/science.1104742

Pinnix, Z. K., Miller, L. D., Wang, W., D'Agostino, R. Jr., Kute, T., Willingham, M. C., et al. (2010). Ferroportin and iron regulation in breast cancer progression and prognosis. *Sci. Transl. Med.* 2:43ra56. doi: 10.1126/scitranslmed.3001127

Prus, E., and Fibach, E. (2008). Flow cytometry measurement of the labile iron pool in human hematopoietic cells. *Cytometry A* 73, 22–27. doi: 10.1002/cyto.a.20491

Sandstrom, P. A., and Buttke, T. M. (1993). Autocrine production of extracellular catalase prevents apoptosis of the human CEM T-cell line in serum-free medium. *Proc. Natl. Acad. Sci. U.S.A.* 90, 4708–4712. doi: 10.1073/pnas.90.10.4708

Sergeev, I. N. (2014). Vitamin D-mediated apoptosis in cancer and obesity. *Horm. Mol. Biol. Clin. Investig.* 20, 43–49.

Smith, E. M., Alvarez, J. A., Kearns, M. D., Hao, L., Sloan, J. H., Konrad, R. J., et al. (2017). High-dose vitamin D3 reduces circulating hepcidin concentrations: a pilot, randomized, double-blind, placebo-controlled trial in healthy adults. *Clin. Nutr.* 36, 980–985. doi: 10.1016/j.clnu.2016.06.015

Swami, S., Raghavachari, N., Muller, U. R., Bao, Y. P., and Feldman, D. (2003). Vitamin D growth inhibition of breast cancer cells: gene expression patterns assessed by cDNA microarray. *Breast Cancer Res. Treat.* 80, 49–62. doi: 10.1023/A:1024487118457

Uberti, F., Morsanuto, V., Lattuada, D., Colciaghi, B., Cochis, A., Bulfoni, A., et al. (2016). Protective effects of vitamin D3 on fimbrial cells exposed to catalytic iron damage. *J. Ovarian Res.* 9:34. doi: 10.1186/s13048-016-0243-x

Wan, Q., Liao, Z., Rao, Y., Yang, C., Ji, J., Chen, X., et al. (2019). Transferrin receptor 1-associated iron accumulation and oxidative stress provides a way for grass carp to fight against reovirus infection. *Int. J. Mol. Sci.* 20:5857. doi: 10.3390/ijms20235857

Welsh, J. (1994). Induction of apoptosis in breast cancer cells in response to vitamin D and antiestrogens. *Biochem. Cell Biol.* 72, 537–545. doi: 10.1139/o94-072

Welsh, J., Wietzke, J. A., Zinser, G. M., Smyczek, S., Romu, S., Tribble, E., et al. (2002). Impact of the Vitamin D3 receptor on growth-regulatory pathways in mammary gland and breast cancer. *J. Steroid Biochem. Mol. Biol.* 83, 85–92. doi: 10.1016/s0960-0760(02)00277-7

Winterbourn, C. C. (1995). Toxicity of iron and hydrogen peroxide: the Fenton reaction. *Toxicol. Lett.* 82-83, 969–974. doi: 10.1016/0378-4274(95)03532-x

Yang, W. S., SriRamaratnam, R., Welsch, M. E., Shimada, K., Skouta, R., Viswanathan, V. S., et al. (2014). Regulation of ferroptotic cancer cell death by GPX4. *Cell* 156, 317–331. doi: 10.1016/j.cell.2013.12.010

Zughaier, S. M., Alvarez, J. A., Sloan, J. H., Konrad, R. J., and Tangpricha, V. (2014). The role of vitamin D in regulating the iron-hepcidin-ferroportin axis in monocytes. *J. Clin. Transl. Endocrinol.* 1, 19–25. doi: 10.1016/j.jcte.2014.01.003

Conflict of Interest: The authors declare that the research was conducted in the absence of any commercial or financial relationships that could be construed as a potential conflict of interest.

Publisher's Note: All claims expressed in this article are solely those of the authors and do not necessarily represent those of their affiliated organizations, or those of the publisher, the editors and the reviewers. Any product that may be evaluated in this article, or claim that may be made by its manufacturer, is not guaranteed or endorsed by the publisher.

frontiers in Oncology

REVIEW
published: 10 November 2021
doi: 10.3389/fonc.2021.778492

The Role of Iron in Cancer Progression

Qianqian Guo[1†], Liwen Li[3†], Shanshan Hou[4], Ziqiao Yuan[5], Chenhui Li[3], Wenzhou Zhang[1], Lufeng Zheng[3*] and Xiaoman Li[2*]*

[1] Department of Pharmacy, Affiliated Cancer Hospital of Zhengzhou University, Henan Cancer Hospital, Zhengzhou, China, [2] Jiangsu Key Laboratory for Pharmacology and Safety Evaluation of Chinese Materia Medica, School of Pharmacy, Nanjing University of Chinese Medicine, Nanjing, China, [3] School of Life Science and Technology, Jiangsu Key Laboratory of Carcinogenesis and Intervention, School of Basic Medicine and Clinical Pharmacy, China Pharmaceutical University, Nanjing, China, [4] Department of Pharmacy, Zhejiang Pharmaceutical College, Ningbo, China, [5] School of Pharmaceutical Sciences, Zhengzhou University, Zhengzhou, China

Iron is an essential trace element for the human body, and its deficiency or excess can induce a variety of biological processes. Plenty of evidences have shown that iron metabolism is closely related to the occurrence and development of tumors. In addition, iron plays an important role in cell death, which is very important for the development of potential strategies for tumor treatment. Here, we reviewed the latest research about iron metabolism disorders in various types of tumors, the functions and properties of iron in ferroptosis and ferritinophagy, and new opportunities for iron-based on treatment methods for tumors, providing more information regarding the prevention and treatment of tumors.

Keywords: iron, cancer, ferroptosis, ferritinophagy, prognostic, therapy

OPEN ACCESS

Edited by:
Maryam Mehrpour, Université Paris Descartes, France

Reviewed by:
Richard Possemato, NYU Grossman School of Medicine, United States
Keith R. Laderoute, Consultant, Redwood City, CA, United States

****Correspondence:***
Wenzhou Zhang
hnzzzwzx@sina.com
Xiaoman Li
lixm@njucm.edu.cn
Lufeng Zheng
zhlf@cpu.edu.cn

[†]These authors have contributed equally to this work

Specialty section:
This article was submitted to Molecular and Cellular Oncology, a section of the journal Frontiers in Oncology

Received: *17 September 2021*
Accepted: *15 October 2021*
Published: *10 November 2021*

Citation:
Guo Q, Li L, Hou S, Yuan Z, Li C, Zhang W, Zheng L and Li X (2021) The Role of Iron in Cancer Progression. Front. Oncol. 11:778492. doi: 10.3389/fonc.2021.778492

INTRODUCTION

Iron (Fe) is one of the most abundant elements in the earth's crust (1). The oxidation-reduction reaction mainly involves electron transfer between two chemicals. Iron, as a transition-metal, can exhibit a wide range of oxidation states, which makes it a multifunctional participant in redox reactions. Therefore, iron is an indispensable trace element to maintain life (2). This element plays a vital role in various cellular processes, such as cellular respiration (e.g., cytochrome c oxidase, ferredoxin, cytochrome, and Rieske protein), energy metabolism (e.g., aconitase, citrate synthase, succinate dehydrogenase, and isocitrate dehydrogenase), DNA replication, DNA synthesis and nucleic acid repair (e.g., the catalytic subunit of replicative DNA polymerases, DNA helicase and ribonucleotide reductase), and iron-dependent signaling (3, 4). Iron is also used in the synthesis of heme and iron–sulfur clusters (ISC), which are incorporated into proteins that carry out the citric acid cycle, oxidative phosphorylation, and many other essential functions (5, 6). However, although

Abbreviations: DCYTB, duodenal cytochrome B; DMT1, divalent metal transporter 1; HO-1, heme oxygenase-1; FPN1, ferroportin; HEPH, hephaestin; TF, transferrin; TFR1, transferrin receptor; STEAP3, six-transmembrane prostate epithelial antigen 3; LIP, labile iron pool; IRPs, iron-responsive element binding proteins; IRE, iron responsive element; mRNA, messenger RNA; BMP6, bone morphogenetic protein; ROS, reactive oxygen species; DFO, Desferoxamine; IREB2, Iron responsive element binding protein 2 gene; ISC, iron-sulfur cluster; GSSG, glutathione disulphide; GSH, glutathione; L-OHs, lipid alcohols; L-OOHs, lipid hydroperoxides; PUFA, polyunsaturated fatty acids; GPX4, glutathione peroxidase 4; NCOA4, nuclear receptor coactivator 4; FTH1, ferritin heavy chain 1; FTL, ferritin light chain.

iron is essential for the normal physiological function of the human body, it may also be toxic in that it generates a large number of free radicals in the presence of hydrogen peroxide (7). For example, in the well-known Fenton reaction, ferrous iron (Fe^{2+}) reacts with hydrogen peroxide to be oxidized to ferric iron (Fe^{3+}) while generating hydroxyl radicals. When superoxide is present, the Fe^{3+} produced by the Fenton reaction can be reduced to Fe^{2+}, and then the Fenton reaction will proceed again, which called Haber-Weiss reaction (8). Both the Fenton reaction and Haber-Weiss reaction can produce a large number of hydroxyl radicals. Hydroxyl radical is one of the most important oxidant found in human body, which can lead to peroxidation and apoptosis by attacking protein, lipids, nucleic acids, and carbohydrates (9, 10). In addition, excessive free radicals in the human body can lead to cell and tissue organ damage, and these processes are closely related to tumorigenesis.

Therefore, iron is not only an essential nutrient element, but also potentially toxic. Both aspects play important roles in the occurrence and development of tumors. This article mainly discusses iron metabolism disorders in tumors, ferroptosis, ferritinophagy, and the role of iron in tumor treatment.

PHYSIOLOGICAL MECHANISMS OF IRON REGULATION

Homeostasis of iron metabolism is a physiological process that needs to be strictly controlled. Iron is mainly present in the oxidized state (Fe^{3+}) and is divided into dietary iron and environmental iron. Dietary iron primarily exists as either nonheme bound iron or heme (11). Heme iron has a higher absorption rather than nonheme bound iron. Iron in the diet is mainly reduced to Fe^{2+} in the duodenum by duodenal cytochrome B (DCYTB) and absorbed into intestinal epithelial cells under the synergistic effect of divalent metal transporter 1 (DMT1) (1). Heme iron is also absorbed by intestinal cells through an unknown mechanism and is metabolized by heme oxygenase-1 (HO-1) to release Fe^{2+}. Heme iron is absorbed by intestinal cells through an unknown mechanism and degraded by heme oxygenase-1 (HO-1), releasing Fe^{2+}, which is transported out of the cells by the iron efflux pump ferroportin (FPN1) on the basal side of the intestinal epithelial cells, and consequently oxidized into Fe^{3+} by hephaestin (HEPH) (1); then Fe^{3+} binds to transferrin (TF) and enters the circulation through the portal vein. Each transferrin in blood can bind two Fe^{3+} to form TF- $[Fe^{3+}]_2$ complex, which binds to transferrin receptor (TFR1) on the cell surface and is absorbed into cells to form endosome (12). Subsequently, it is reduced to Fe^{2+} by six-transmembrane prostate epithelial antigen 3 (STEAP3), which is then transported into cytoplasm by DMT1 to exert physiological functions or constitute the cytoplasmic labile iron pool (LIP) (1, 13). LIP can be taken up by non-hematopoietic cells causing parenchymal iron deposition which can result in free radical damage (14) (**Figure 1**).

Intracellular iron homeostasis is mainly regulated through an iron-dependent protein network including iron-responsive

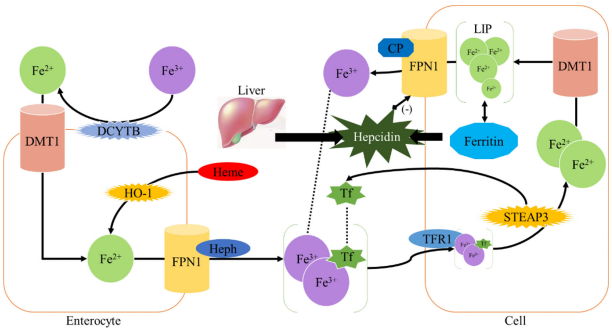

FIGURE 1 | Iron metabolism.

element binding proteins (IRPs), in which both IRP1 and IRP2 are important components (15). It is noteworthy that thioredoxin family proteins are important mediators in iron metabolism since these proteins regulate the expression of IRPs (5). To ensure iron homeostasis, IRP binds to the corresponding iron responsive element (IRE) on the untranslated region of messenger RNA encoding the protein essential for cellular iron regulation (TFR1, DMT1), thereby participating in iron uptake (TFR1), storage (FT), redistribution, and efflux (FPN1) (2). In the absence of intracellular iron, IRP can inhibit the translation of FPN1 and FT, but increase the protein synthesis of TFR1. In contrast, when the intracellular iron is abundant, the synthesis of FPN1 and FT is increased due to the instability of IRP, while the degradation of TFR1 is promoted (16). IRP1/2 are key iron regulators for the maintenance of cellular iron homeostasis. IRP1 is cytosolic aconitase, an enzyme containing a [4Fe-4S] cluster. When absence of intracellular iron, there is insufficient iron for Fe-S biogenesis leaving an incomplete [3Fe-4S] cluster. The enzymatic activity of aconitase is lost and this protein then initiates its IRP activity, as IRP1. When the protein contains the [3Fe-4S] cluster it can bind to IREs (17, 18). Through these mechanisms, IRP can not only meet the metabolic needs of cellular iron, but also minimize the toxic effects of excessive iron (**Figure 2**).

The excess iron is mainly stored in liver, which also acts as an iron-sensing organ and controls systemic iron through the secretion of the peptide hormone hepcidin (19). Hepcidin is a 25-amino acid short peptide produced by the liver and encoded by the *HAMP* (20). FPN1, which is mainly expressed in the cell membrane and cytoplasm, is the only known 571-amino acid transmembrane protein in vertebrates that transports iron from intracellular to extracellular (21). When the intracellular or circulating iron level is relatively high, Hepcidin is generated from hepatocytes and secreted into the circulation system through a bone morphogenetic protein (BMP6) - mediated pathway (1, 22). Hepcidin can trigger the internalization and subsequent lysosomal degradation of FPN1 *via* binding to the basal side of the intestinal epithelium and to the FPN1 on the macrophage surface, preventing iron absorption from the digestive tract and iron circulation from the body, respectively (23). Conversely, the reduction of iron modulators causes FPN1

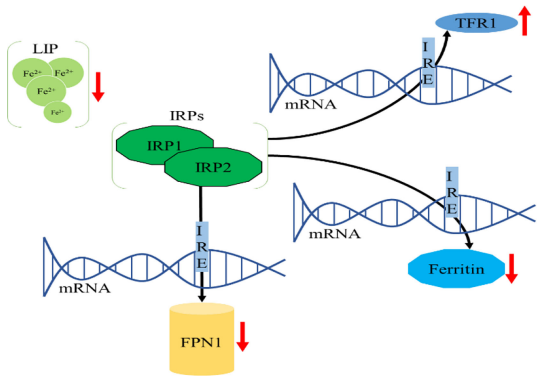

FIGURE 2 | Cellular iron metabolism. **(A)** When the cellular iron levels are low, IRPs bind to the 5' IREs of FPN1 and FT mRNA, resulting in translation repression. Additionally, IRPs bind to 3' IREs in TFR1 mRNA to stabilize the DMT1 mRNA and increase TFR1 protein synthesis. These two effects can increase intracellular iron. **(B)** When the cellular iron levels are high, IRP1 converts to cytosolic aconitase and IRP2 is degraded, preventing IRP1 and IRP2 from binding to the IREs of these mRNAs. This permits unimpeded translation of FPN1 and FT and fosters degradation of DMT1 and TFR1 mRNA, leading to decreased cytosolic iron.

to absorb iron and increases systemic iron levels (24) (**Figure 1**). Therefore, FPN1 and ferritin are essential for maintaining iron homeostasis in the body.

IRON METABOLISM IN CANCER

A large number of studies have shown that abnormal iron homeostasis is one of the markers of cancer (**Table 1**). As the metabolism and proliferation rate of tumor cells are generally higher than that of normal cells, so their demand for iron is also significantly higher than that of normal cells, this leading to the exceeding oxidative stress; however, tumor cells can exert a concomitant upregulation of antioxidant defenses for survival, such as activating antioxidant transcription factors and promoting the expression of various antioxidant genes (57). Conversely, since tumor cells are strongly dependent on iron for their growth/proliferation, they are more sensitive to iron depletion than normal cells. This imbalance in cancer is mainly manifested as increased iron metabolism, iron affinity, iron input, and inhibition of its output, thereby completing iron accumulation.

Iron Uptake

TFR1

As early as 1980, studies have shown that *TFR1* is significantly up-regulated in breast cancer (27). Subsequent studies have confirmed that *TFR1* is highly expressed in various cancers such as glioma, leukemia, breast cancer, and ovarian cancer (25, 26, 28, 29). Recent studies have shown that Beclin 1 inhibits the proliferation of breast cancer cells by regulating the endocytosis transport and degradation of EGFR and TFR1 (58). Bajbouj et al. found that estrogen inhibited the synthesis of ferritin and enhanced the efflux of intracellular iron. Meanwhile, combining with doxorubicin, estrogen significantly reduced TFR1 expression and enhanced the sensitivity of breast cancer cells to doxorubicin (59). Using Gene Expression Profiling Interactive Analysis (GEPIA) database analysis, Xiao et al. found that TFR1 was significantly up-regulated in hepatocellular carcinoma tissues and hepatocellular carcinoma stem cells (31), and knocking down TFR1 reduced iron accumulation, reactive oxygen species (ROS) accumulation induced by erastin, and maintained mitochondrial function, thereby inhibiting tumor development (31). Additionally, a higher expression of *TFR1* is closely related to the activation of ERK signaling pathway in thyroid cancer, leading to the disorder of genes involved in abnormal accumulation of intracellular free iron and drug resistance (33).

Other studies have shown that targeting TFR1 can suppress tumor progression, such as MiR-107 can inhibit the proliferation, migration, and invasion of SW620 cells by targeting TFR1 (34); MiR-148a could reduce the proliferation of liver cancer cells by targeting TFR1 (32); EGFR regulates cellular iron homeostasis by regulating the redistribution of TFR1, and promotes the development of non-small cell lung cancer (60). Similarly, knock-down of *ST6GALNACIII* can down-regulate TFR1 and delay A549 cell proliferation (61). And Hui et al. found that TFR1 level was significantly up-regulated in non-small-cell lung cancer (NSCLC) by Fusaricide, which is a novel iron chelating agent and can efficiently inhibit the proliferation of a variety of human NSCLC cell lines (62). In addition, TFR1 is highly expressed in activated lymphocytes and malignant cells, and TFR1 antibody *ch128.1/IgG1* effectively inhibits the activation, growth, and immortalization of EBV^+ human B cells as well as the development of these cells into lymphoma-like tumors in immunodeficient mice (63). Chlorogenic acid inhibits the growth of pancreatic ductal adenocarcinoma cells by targeting the c-Myc-TFR1 axis, perhaps chlorogenic acid is a promising compound for pancreatic ductal adenocarcinoma therapy (64). However, although *TFR1* is highly expressed in colorectal cancer tissues, the authors demonstrated that down-regulation of *TFR1* promoted rectal cell migration and invasion through the JAK/STAT pathway (35). These results demonstrate that TFR1 might hold tumor-specific roles.

DMT1

DMT1 is highly expressed in various cancers, such as colorectal cancer and ovarian cancer (30, 38). Q. Wang et al. found that DMT1, TFR1, and ferritin were highly expressed in ovarian cancer cell spheres, and overexpression of DMT1 promoted the progression of ovarian tumor (30). In SDHB-Mutated Pheochromocytoma, iron accumulation caused by significant up-regulation of iron transport-related proteins, such as DMT1, TF, TFR2, can increase oxidative stress to some extent (37). In colorectal cancer, DMT1 can be induced through hypoxia-inducible factor 2α-dependent transcription (38). However, in hepatocellular carcinoma, patients with a lower expression of DMT1 displayed a worse disease-free survival, this effect was more significant in patients with advanced

TABLE 1 | Iron regulators in cancer.

Altered Player	Cancer	Regulation	Ref.
TFR1	glioblastoma	up	(25)
TFR1	leukemia	up	(26)
TFR1	breast cancer	up	(27,28)
TFR1	ovarian cancer	up	(29,30)
TFR1	hepatic carcinoma	up	(31,32)
TFR1	thyroid cancer	up	(33)
TFR1	colorectal cancer	up	(34–36)
DMT1	ovarian cancer	up	(30)
DMT1	pheochromocytoma	up	(37)
DMT1	colorectal cancer	up	(38)
STEAP3	glioblastoma	up	(39)
STEAP3	kidney renal clear cell carcinoma	up	(39)
STEAP3	Liver Hepatocellular Carcinoma	down	(28)
IRP2	colorectal cancer	up	(36)
IREB2	lung cancer	up	(40,41)
FPN	pancreatic cancer	down	(42)
FPN	multiple myeloma	down	(43)
FPN	thyroid cancer	down	(44)
Hepcidin	breast cancer	up	(45)
Hepcidin	colorectal cancer	up	(46)
Hepcidin	prostate cancer	up	(47,48)
Hepcidin	thyroid cancer	up	(44)
Hepcidin	breast cancer	up	(49)
Hepcidin	multiple myeloma	up	(50,51)
Hepcidin	non-Hodgkin's lymphoma	up	(52)
Hepcidin	UUTUC	up	(53)
Hepcidin	Renal Cell Carcinoma	up	(53)
Hepcidin	hepatocellular carcinoma	down	(54)
HAMP	hepatocellular carcinoma	down	(55)
HAMP	cholangiocarcinoma	down	(56)

hepatocellular carcinoma (65). Notably, the carcinogenic activity of DMT1 is tightly correlated with its iron-transport activity, which is characterized by the evidence that tumor in DMT1-knocked out mice was weakened when being fed with a high-iron diet. Additionally, Desferoxamine (DFO) increases iron concentration by up-regulating the expression of DMT1 and TFR1, thereby promoting the migration of breast cancer cells (66). Similarly, the latest research by Chen et al. has revealed that the up-regulation of DMT1 and TFR1 is related to the activation of the IL-6/PI3K/AKT signaling pathway in triple-negative breast cancer cells, and enhance iron absorption (67). Consistently, targeting DMT1 can be used to potentially suppress tumor progression. For example, DMT1 inhibitors can selectively target stem cells in primary cancer cells and circulating tumor cells to inhibit the occurrence and development of tumors (68); Propofol, which is widely used in clinical practice for intraoperative general anesthesia and postoperative sedation, regulates DMT1 expression by modifying Ca2+-permeable α-amino-3-hydroxyl-5-methylisoxazole-4-propionic acid receptors (CPARs), thereby inhibiting tumor oxidative stress and glioma tumor growth (69).

STEAPs

The expression STEAPs also exhibits an upregulation in tumors and they can promote tumor cell proliferation as well as suppress apoptosis (70–73), for example, STEAP3 promotes glioma cell proliferation, invasion, and spheroid formation by inducing mesenchymal transformation, promoting TFR1 expression, and activating the STAT3-FoxM1 axis (39); In colorectal cancer, STEAP3 expression is significantly higher in tumor than that in colonic mucosa (74). However, they recently found that silencing lncRNA STEAP3-AS1(the antisense transcript of *STEAP3*) inhibited the proliferation, migration, and arrested colon cancer cells at the G0–G1 phase cancer cells through upregulation STEAP3 (75). Additionally, Z. Wang et al. found that among Burkitt's lymphoma, the rarely studied iron reductase CYB561A3 was essential for Burkitt proliferation, but lymphoblastoid B cells with the EBV latency III program depended on STEAP3 iron reductase instead (76). Similarly, STEAP2 accelerates prostate cancer progression by promoting proliferation, migration, and invasion by regulating the transcriptional profiles of some genes involved in metastasis. And Burnell et al. proved that reducing the expression of STEAP2 inhibited the proliferation, migration, and invasion in prostate cancer cells (77).

Intracellular Iron Regulation

IRP1 or IRP2 can increase intracellular iron and abnormal activation of them is closely related to many cancers. Compared with normal colonic mucosa, IRP2 is overexpressed in colorectal cancer, and is positively correlated with TFR1 expression. In addition, the expression of IRP2 is associated with mutations of BRAF, which primarily occur in the early stages of colorectal cancer and are often associated with poor

prognosis (36). IRP1 and IRP2 are strictly regulated in tumors, and preferably modulate tumor progression in an iron-engaged signaling pathways, such as IRP2 is regulated by ubiquitin ligase FBXL5, which mediated IRP2 ubiquitination and degradation under the condition of sufficient iron; Dysregulation of FBXL5 has been associated with a poor prognosis of human hepatocellular carcinoma (78); A recent study demonstrated that FBXL5 is stabilized and increases iron levels when iron is at low levels, facilitating the production of [2Fe2S] cluster, which can serve as an FBXL5 cofactor, and by incorporating into the C-terminal LRR domain of FBXL5, and only when oxygen level is high enough to maintain the [2Fe2S] cluster in its oxidized $[2Fe2S]^{2+}$ state could the SCF^{FBXL5} E3 ligase recruits IRP2 as a substrate for polyubiquination and degradation. This IRP2-FBXL5 interaction might help release IRP2 from IREs to alter the translation of iron metabolism genes (79). IRP2 is also regulated by the deubiquitinating enzyme OTUD1, which promotes TFR1-mediated iron transport *via* deubiquitinating and stabilizing IRP2, leading to increased ROS production, and the downregulation of OTUD1 has been found to be highly correlated with poor prognosis of colorectal cancer (80); A study linking a clinical trial of JBR.10 (n = 131) with a sample of patients from the University of Toronto Health Network (n = 181) indicated that the effect of the 15q25 mutation on lung cancer risk was associated with increased expression of *IREB2 (*40); Another large-scale case-control study confirmed that the miRNA binding site SNP rs1062980 in the *IREB2* 3' UTR might potentially alter *IREB2* expression to reduce the risk of lung cancer by regulating the binding of miR-29a (41). Additionally, the specific cause of dysregulation of IRP1/2 may be related to inhibition of TAp63 and activation of MDM2 (81, 82).Notably, chemotherapy and targeted-therapy may work together to disrupt IRP-mediated iron regulation, like Horniblow et al. found that the MEK inhibitor trimetinib consistently inhibited IRP2 expression in four colorectal cell lines, resulting in decreased TFR1 expression and increased ferritin expression (83); Miyazawa et al. found that cisplatin bound to Cys512 and Cys516 of human IRP2 and destroyed its function, based on which DFO combined with cisplatin resulted in increased iron consumption and reduced tumor growth in a mouse xenograft model of colonic adenocarcinoma (84); Yao et al. confirmed that erastin and RSL3 increased the expression of IRP1 and IRP2, knockdown of which conversely inhibited erastin- or RSL3-induce cell death, and IRP2 could enhance the promoting effect of IRP1 in melanoma cells (85).

Iron Efflux in Cancer

Ferroportin

FPN1, the only iron export protein, is involved in the regulation of intracellular iron concentration, and its abnormal downregulation is also observed in most tumors (29, 47, 86, 87). The suppressive roles of FPN1 have been established in tumors, such as in prostate cancer cell lines, a low FPN1 level caused by up-regulation of ferritin promoted proliferation, migration, and apoptotic resistance, and overexpression of FPN1 induced p53 and autophagy, and reduced tumor growth *in vivo* (42); Overexpression of FPN1 decreased proliferation, colony formation, and tumor growth, as well as liver metastasis in breast cancer (88). In consistent, various studies have indicated that FPN1 regulates tumor progression *via* destroying iron homeostasis, as a study demonstrated that cadmium (Cd)-induced MDA-MB-231 cell proliferation, EMT, and migration were caused by inhibiting FPN1 expression and associated with destruction of iron homeostasis (89), and hepcidin secreted by thyroid cancer cells could decrease FPN1 and retain intracellular iron, thereby promoting cancer proliferation (44); another study showed that FPN1-mediated iron metabolism might play a role in chemosensitivity and treatment outcome of acute myeloid leukemia (90); Similarly, overexpression of ZNF217 promoted prostate cancer growth by inhibiting FPN1-conducted iron efflux (91); Xue et al. found that Nrf2, a transcription factor of *FPN1*, inhibited the proliferation and metastasis of prostate cancer cells by up-regulating FPN1, which was also related to the reduction of intracellular ferritin content (92), and Nrf2 was able to inhibit myeloma cell proliferation by promoting *FPN1* transcription (43). Additionally, Geng et al. demonstrated that knockdown of FPN1 accelerated erastin-induced suppression of neuroblastoma by increasing the accumulation of iron-dependent lipid ROS, and FPN1 inhibitors might provide a new approach for the chemosensitization of neuroblastoma (93); Tang et al. verified that USP35 could maintain the stability of its protein by deubiquitinating FPN1, and reduce the iron disorder triggered by erastin/RSL3, thereby promoting lung cancer cell growth and tumor progression. Meanwhile, knockdown of USP35 enhanced the sensitivity of lung cancer cells to cisplatin and paclitaxel by targeting FPN1 in lung cancer (94). However, a study showed that matrix/macrophage expression of Lcn-2 was associated with tumor onset, lung metastasis, and recurrence, whereas FPN1 was not by analyzing the expression profiles of *lipocalin-2* (*Lcn-2*) and *FPN1* through a model of T-oncogene (PyMT) breast cancer in spontaneous polymerases and mining publicly available TCGA and GEO database from gene expression synthesis (95). Macrophages provide iron for the microenvironment of breast tumors *via* forcing secretion of Lcn-2-bound iron and increasing expression of FPN1 (95). Nevertheless, the reason why the matrix/macrophage expression of FPN1 is not associated with tumor onset, lung metastasis, and recurrence requires further investigation.

Hepcidin

Disorders of iron modulators in cancer cause changes in iron homeostasis. Hepcidin, a negative regulator of FPN1, is significantly up-regulated in various tumors, such as breast, colorectal, and prostate cancer (45–47). And numerous studies have shown the promoting effects of hepcidin on tumor progression, for example, Schwartz et al. found that compared with wild-type littermates, mice lacking hepcidin in colonic tumor epithelium significantly reduced the number, tumor burden and size in the sporadic model of colorectal cancer, whereas lacking of FPN1 led to intracellular iron accumulation and promoted tumor occurrence (96); Lopes et al. found that acute myeloid leukemia had a unique iron component,

mainly manifested as a low expression of transferrin, and high expression of ferritin and hepcidin; notably, these characteristics were not related to inflammation or blood transfusion (50); Zhao et al. confirmed that hepcidin enhanced the proliferation, migration, and anti-apoptotic capabilities of prostate cancer cells by reducing the expression of FPN1 and increasing intracellular iron level (48); Additionally, Zhou et al. identified that the synthesis of hepcidin is regulated by SOSTDC1, the BMP4/7 antagonist, providing a new mechanism for cellular iron dysfunction *via* the E4BP4/G9a/SOSTDC1/hepcidin pathway in the thyroid gland, which can inhibit the secretion of hepcidin and proliferation of thyroid cancer cells (44).

In addition to the iron modulators synthesized by cancer cells, systemic iron disorders in cancer patients can also be observed (88, 97, 98). Serum hepcidin is elevated in many cancer patients, including prostate cancer, breast cancer, multiple myeloma, and non-Hodgkin's lymphoma (48, 49, 51, 52).A study of 456 cases of primary gastric adenocarcinoma and 900 matched controls with an average of 11 years of follow-up showed a significant negative correlation between gastric cancer risk and serum hepcidin level, which was mainly caused by ferritin level (99). Additionally, treatment with morotinib was found to decrease serum hepcidin and improve iron metabolism and erythropoiesis in a Phase 2 clinical trial of morotinib for bone marrow fibrosis (100). Similarly, a retrospective study, including 38 patients suffering from upper urinary tract urothelial carcinoma (UUTUC), 94 patients Suffering from Renal Cell Carcinoma (RCC), and 21 patients without infections or cancer, showed that serum hepcidin level was significant increased compared to sera of controls in patients with UUTUC and RCC, and high serum hepcidin was associated with cancer recurrence and metastasis (53).

Interestingly, liver cancers showed a drastic reduction of hepcidin expression compared to benign liver tissues (101, 102). Furthermore, in patients of the White race with no history of alcohol consumption, down-regulation of hepcidin is associated with rapid cancer progression and poor disease-specific survival. Hepcidin expression is positively correlated with BMP6/interleukin -6 (IL6) cytokines and cytotoxic immune infiltration in liver cancer tissues (54). In addition, blocking hepcidin with its antagonist furthiomine could moderately reduce sorafenib-induced apoptosis in HepG2 and Huh7 cells (54). In consistent, *HAMP*, the coding gene for hepcidin is mainly expressed in benign liver tissues but significantly reduced in hepatocellular carcinoma tissues (54, 55). Similarly, Z. Wang et al. found that *HAMP* was decreased and associated with the chemokine CCL16 in Cholangiocarcinoma (CHOL), the second common malignant tumor in the liver, indicating that *HAMP* may contribute to the immune activation in CHOL microenvironment (56).

Heme has been indicated to promote cell proliferation in leukemia and lung cancer, and increase HO-1 activity promotes invasion and migration of breast cancer cells (103–105). Up-regulation of BMP, which induces cancer cells to secrete hepcidin, has also been observed in various tumors, including breast, prostate, and bladder cancers (47, 106, 107).

In conclusion, cancer cells usually increase the input of iron and inhibit its output, thereby achieving iron accumulation. However, it is not entirely clear how they respond to the increased instability.

IRON AND CELL DEATH

Iron and Ferroptosis

In recent years, non-apoptotic cell death has attracted a widespread attention in tumor therapy, among which ferroptosis is defined as iron-dependent regulatory necrosis caused by membrane damage mediated by massive lipid peroxidation (108–110) (**Figure 3**). Upon being experienced ferroptosis, cells show unique signs such as cell membrane rupture, cytoplasmic swelling, cytoplasmic organelle swelling, mitochondrial membrane density increase, mitochondrial cristae reduction/disappearance, mitochondrial outer membrane rupture, *etc*. Ferroptosis can occur through two main pathways: the external or transporter-dependent pathway, and the internal or enzyme-regulated pathway (111). Ferroptosis is caused by the redox imbalance between the production of oxidants and antioxidants, which is driven by the abnormal expression and activity of numerous redox active enzymes that produce or detoxify free radicals and lipid oxidation products (109, 111).

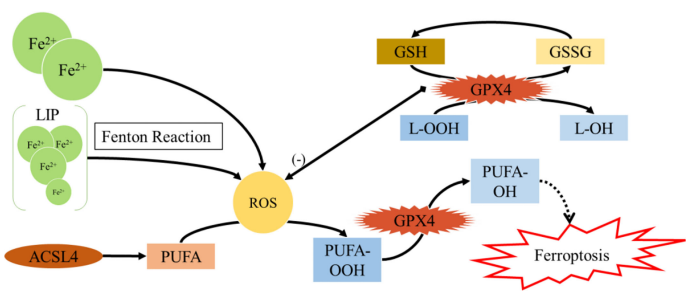

FIGURE 3 | Ferroptosis.

As the center of metabolism, mitochondria are an important source of ROS in most mammalian cells. Earlier studies showed that mitochondrial-mediated ROS production was not necessary for ferroptosis (108). However, recent studies have shown that mitochondrial-mediated ROS production, DNA stress, and metabolic reprogramming are necessary for lipid peroxidation and induction of ferroptosis (112–114). Readers can obtain a more comprehensive understanding of ferroptosis by referring to other relevant documents (111, 115–118). Here we focus on recent research, aiming to clarify the possible novel mechanisms of ferroptosis in cancer.

The previous study suggested that the stability of IRP2 protein was mainly regulated by E3 ubiquitin ligase FBXL5 (78), while Terzi et al. confirmed a new regulatory mechanism of IRP2, which senses the absence of ISC synthesis, and ISC defects could enhance the binding of IRP2 to target mRNA ignoring the changes in IRP1, IRP2, and FBXL5 protein levels. ISC are made up of iron and sulfur ions to form [1Fe-0S], [2Fe-2S], [3Fe-4S] and [4Fe-4S] clusters (6, 119). Suppressing ISC synthesis can activate IRP2 and promote ferroptosis sensitivity (120); in line with this finding, insufficient ISC maintenance has been shown to robustly activate the iron-starvation response and trigger ferroptosis (121). Notably, inorganic sulfur is first produced from the cysteine by the cysteine desulfurase NFS1 and ISC is formed on the ISC assembly enzyme (ISCU) with the help of frataxin (FXN) (122),Which was indicated to be localized in the mitochondrial matrix and participated in the biosynthesis of ISC and FXN deficiency accelerates erastin-activated ferroptosis (123). Furthermore, overexpression of ISCU significantly attenuated Dihydroartemisinin-induced ferroptosis by regulating iron metabolism, rescuing the mitochondrial function and increasing the level of GSH (124). Additionally, FXN could activate NFS1 and accelerate a rate-limiting sulfur transfer step of ISC assembly, and suppression of NFS1 make cancer cell be sensitive to ferroptosis (121, 125). Besides, Chafe et al. identified a novel synthetic lethal interaction between carbonic anhydrase IX (CAIX) and NFS1 by elucidating the important role of CAIX in redox homeostasis and the prevention of ferroptosis through pH regulation, which may facilitate researchers to develop new strategies for the treatment of solid tumors (126).

The latest research provides more possibilities that targeting ferroptosis may be a new strategy for tumor treatment. For example, Mao et al. identified a ferroptosis-defensive mechanism mediated by Dihydroorotate dehydrogenase (DHODH) in the mitochondria, which works with mitochondrial glutathione peroxidase 4 (GPX4) to reduce ubiquinone to panthenol, thereby inhibiting ferroptosis in mitochondrial inner membrane, while Brequinar (a DHODH inhibitor) selectively inhibits the proliferation of tumor cells with low GPX4 expression by inducing ferroptosis, thus it can occur synergistically to induce ferroptosis and inhibit the growth of tumor cells with high GPX4 expression by the combined use of Brequinar and sulfasalazine (ferroptosis inducers) (127); Subsequently, Ding et al. demonstrated that DMOCPTL induced ferroptosis and apoptosis primarily through GPX4 ubiquitination in triple-negative breast cancer cells (128); Additionally, D. Chen et al. confirmed that IPLA2β inhibited ferroptosis by cleaving through lipid peroxide for detoxify without depending on GPX4, and that the absence of iPLA2β had no significant effect on the normal development or cell viability of normal tissues, thus, iPLA2β may become a new target for ferroptosis-targeted therapy for tumor (129); Furthermore, X. Wang et al. demonstrated that SOX2 promoted *SLC7A11* transcription by binding to *SLC7A11* promoter, and oxidation at *Cys265* of SOX2 inhibited its activity and decreased the self-renewal capacity of lung cancer stem cell-like cells. This suggests that oxidation of SOX2 could be a potential target for ferroptosis-targeted treatment for cancer (130). Moreover, as cell density-dependent E-cadherin and Merlin/Neurofibromin (NF2) loss can induce ferroptosis, Bao et al. found that NF2-inactivated meningioma cells were sensitive to Erastin-induced ferroptosis by analyzing 35 meningioma samples (10 *NF2* loss and 25 *NF2* wildtype), and further confirmed that myoenhancer factor 2C (*MEF2C)* acted as a promoter of *NF2* and *CDH1*, thereby inhibiting ferroptosis-related lipid peroxidation and meningioma cell death (131). Notably, Kremer et al. indicated that aspartate aminotransferase (GOT1) could damage mitochondrial oxidative phosphorylation and promote catabolism, resulting in the increase of unstable iron pool and susceptibility to ferroptosis, this effect suggests that inhibiting GOT1 could destroy the redox balance and proliferation in pancreatic ductal carcinoma, and establishes a biochemical link between GOT1 and ferroptosis (132). Few studies reported the direct crosstalk between ferroptosis and antitumor immunity, until Wang et al. reported that $CD8^+$ T cells induce ferroptosis in tumor cells, which is the direct evidence of the connection between ferroptosis and antitumor immunity (133). They found that interferon gamma (IFNγ) released from $CD8^+$ T cells downregulated the expression of SLC3A2 and SLC7A11, impaired the uptake of cystine by tumour cells, and promoted ferroptosis. Thus, T cell-promoted tumour ferroptosis is an anti-tumour mechanism, and targeting this pathway in combination with checkpoint blockade is a potential therapeutic approach.

Furthermore, studies also demonstrated that activating ferroptosis and apoptosis immensely increased chemotherapy sensitivity, which might provide strategies for the combination therapy for cancers. For example, Ye et al. found that the synergy of apoptotic activator and ferroptosis inducer could significantly enhance the cytotoxic effect of gemcitabine in pancreatic cancer, providing a new strategy for pancreatic cancer treatment (134); Hong et al. unveiled a novel treatment strategy for ovarian cancer through a combined use of Poly (ADP-ribose) polymerase S (PARP) inhibitor and ferroptosis inducer (135); Sun et al. identified that QSOX1 (Quiescin sulfhydryl oxidase 1) enhanced sorafenib-induced ferroptosis by promoting the ubiquitination degradation of EGFR and inhibiting EGFR activation and thus inhibiting NRF2, providing QSOX1 as a new candidate target for a sorafenib-based combination therapy in advanced hepatocellular carcinoma or EGFR-dependent tumor types (136).

There are also some new discoveries focusing on the relationship between lipid peroxidation and ferroptosis. Tan et al. found a hypoxia-inducible factor-dependent adipokine chemerin, which could prevent fatty acid oxidation and lead to escape from ferroptosis, and targeting chemerin reduced lipid storage and tumor growth (137); Lang et al. demonstrated that supplementing unsaturated fatty acids while inhibiting the biogenesis of lipid droplets could induce ferroptosis in acidic cancer cells (138); Additionally, Dierge et al. found that a diet rich in n-3 long-chain unsaturated fatty acids significantly inhibited tumor growth in mice, indicating that supplementation of dietary unsaturated fatty acids can serve as a selective adjuvant anti-tumor approach (139); Furthermore, supplementation of dietary unsaturated fatty acids may serve as a selective adjuvant anti-tumor approach. W. Liu et al. verified that dyslipidemia affected the occurrence and development of tumors by selectively resisting ferroptosis, which primarily due to the continued expression of GPX4 in the metabolism of 27-hydroxycholesterol-resistant cells (140); In consistent, Beatty et al. identified conjugated linoleic acids, including α-eleostearic acid (αESA), acted as inducers of ferroptosisby acyl coenzyme a synthetase long-chain isomer 1 and interfering with the biosynthesis of triglycerides inhibited αESA-induced ferroptosis, but not GPX4-inhibited ferroptosis (141).

Notably, many extracts from plants and herbs also exhibit anti-tumor effects by inducing ferroptosis. Z.X.Wang et al. found that quercetin could promote the degradation of lysosomal-dependent ferritin and the release of free iron, this effect and quercetin-induced ROS production synergistically led to lipid peroxidation and ferroptosis (142). C.Y. Wu et al. found that *Dihydroisotanshinone I* (*Radix Salviae Miltiorrhizae* extract) could induce ferroptosis in lung cancer cells by blocking the expression of GPX4 protein (143). And Wen et al. confirmed that 18-β-glycyrrhetinic acid could promote the production of ROS and RNS by activating NADPH oxidase and iNOS, and reducing GSH and GPX activities in triple-negative breast cancer cells, thereby accelerating lipid peroxidation and leading to ferroptosis (144).

Iron and Ferritinophagy

Ferritinophagy is a type of cell selective autophagy, in which the ferritin (mainly ferritin heavy chain 1) is degraded in autophagosomes mediated by nuclear receptor coactivator 4 (NCOA4), leading to the ferritin-bound iron to be released as free iron (145, 146) (**Figure 4**). Ferritinophagy contributes to the initiation of ferroptosis through degradation of ferritin, which triggers labile iron overload (IO), lipid peroxidation, membrane damage, and cell death (147), and plays a certain role in tumorigenesis.

Ferritin is a complex that can hold 4,500 Fe^{3+} and is widely present in mammalian cells. The ferritin complex is assembled by the heavy chain (*ferritin heavy chain 1, FTH1*) and the light chain *(ferritin light chain, FTL)* (148). *FTH1* has a ferrous oxidase activity and can catalyze the oxidation of Fe^{2+} to Fe^{3+}, thereby reducing a large number of Fe^{2+}-produced free radicals participating in the Fenton reaction, and the damage of free radicals to tissues and organs (149, 150). Iron combines with each other through ferritin iron pores and Fe^{2+} is further oxidized to Fe^{3+} by *FTH1* in the ferritin cage, resulting in the inert deposition of Fe^{3+}, which cannot use or generate ROS in cells (151).The main way of ferritin to release iron is selective autophagy mediated by NCOA4, which binds to ferritin and is transported to lysosomes, where ferritin is degraded and iron is released for cell use (145). NCOA4 selectively interacts with *FTH1* subunit of ferritin through its conserved C-terminal domain and key residues on *FTH1* (152). Notably, NCOA4 is regulated by HECT and the RLD domain containing E3 ubiquitin protein ligase2 (HERC2) (153).

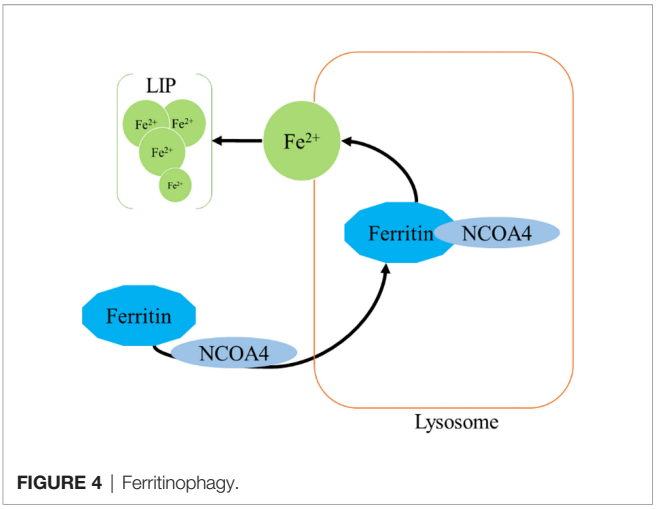

FIGURE 4 | Ferritinophagy.

Mechanistically, when cellular iron level is high, NCOA4 and HERC2 have an iron-dependent effect, resulting in the degradation of NCOA4 through ubiquitin proteasome system, thereby reducing the release of iron and facilitating the storage of ferritin. On the contrary, under low cellular iron conditions, the interaction between NCOA4 and HERC2 is reduced, leading to an increase of NCOA4 level, which increases the degradation of ferritin and iron autophagy flux to supplement cellular iron (154, 155). Thus, a proper amount of ferritinophagy can maintain the balance of iron in cells. However, an excessive activation of ferritinophagy can lead to disease induced by iron overload. Importantly, studies have found that there is a close link between iron release caused by ferritinophagy and ROS damage in ferroptosis (115, 156, 157). Under certain conditions, iron release caused by ferritinophagy is a component of ferroptosis, and may be a direct driving factor of ferroptosis (115, 156, 157). The role of ferritinophagy-related genes in cancer progression has been confirmed (158–164). Here, we focus on clarifying the new discovers of NCOA4 and *FTH1* in cancer.

The expression of NCOA4 is lower in Clear cell renal cell carcinoma (ccRCC) tissues compared with normal tissues, and low NCOA4 expression is closely related to high-grade malignant tumors and advanced TNM staging (165, 166). Some studies have indicated the critical role of NCOA4-mediated ferritinophagy in tumor progression, such as knockdown of *COPZ1* leads to an increase in NCOA4, resulting in the degradation of ferritin, and ultimately ferroptosis in glioblastoma (167); Vara-Pérez et al. found that

melanoma cells lacking BNIP3 showed increased intracellular iron levels caused by NCOA4-mediated increase in ferritinophagy (168). Nevertheless, NCOA4-mediated ferritinophagy is not effective in all tumors as Hasan et al. found that the destruction of ferritinophagy by NCOA4 knockout resulted in minor differences in growth under basal and iron-restricted conditions in colon cancer cells; Additionally, NCOA4 does not engage in cell death induced by 5-fluorouracil and erastin (169).

Furthermore, *FTH1* is also another important gene involved in ferritinophagy. Hayashima et al. demonstrated that in glioblastoma cells, cystine deprivation rather than L-buthionine sulfoximine treatment caused ferroptosis, although they both lead to depletion of cellular GSH, and NCOA4-mediated degradation of *FTH1* was observed in cystine-deprived cells but not in L-buthionine sulfoximine -treated cells. Besides, inhibition of *FTH1* degradation suppressed cystine deprivation-induced ferroptosis. This suggests that cystine deprivation-induced ferroptosis required not only GSH depletion, but also intracellular iron accumulation, and ferritinophagy plays an essential role in cystine deprivation-induced ferroptosis (170). Notably, due to insufficient *FTH1*, Erastin or RSL3 induces ferroptosis in neuroblastoma N2A cells, but fails to induce normal nerve cell death, indicating that ferroptosis may be a promising therapeutic target for neuroblastoma (171).

IRON IN CANCER THERAPEUTICS

Iron in Cancer Prognosis

Because iron is essential at all stages of tumor development, survival, proliferation, and metastasis, we analyzed the prognostic value of iron and iron regulatory genes. It has shown that serum ferritin has prognostic value in various cancers, and elevated serum FT levels are associated with poor prognosis (46, 172–175). However, the increase of serum ferritin are not necessarily associated with upregulated iron level in the body, this means that iron level is regulated by other stimuli, such as inflammation (2). Therefore, we hereby summarize the association between factors related to iron metabolism and prognosis (**Table 2**).

In view of the important role of TFR1 in iron uptake, TFR1 has been identified as a prognostic marker for many tumors, such as TFR1 expression in ER^- tissue was significantly higher than that in ER^+ tissue (188); Compared with adjacent non-cancer tissues, the mRNA expression level of *TFR1* in hepatocellular carcinoma tissues is remarkably increased, and the expression of *TFR1* and *TFR2* is negatively correlated with tumor differentiation (176, 177); Furthermore, patients with a high TFR1 expression have a high risk of recurrence and death after hepatectomy (177); Similarly, TFR1 is significantly overexpressed in ovarian cancer and glioblastoma, and TFR1 expression may be related to tumor staging, progression or the short survival time (29, 180). Additionally, the activation of EGFR induces cell redistribution of TFR1, and the highly expressed TFR1 is closely related to the progression of lung cancer (178). The assessment of 178 gastric cancer tissues revealed a negative correlation between TFR1 expression and patient prognosis, and the TFR1 positive sorting cells showed a strong proliferative capacity; however, the TFR1-negative cells showed a more aggressive tumor features (179). In contrast, although TFR2 is also significantly up-regulated in glioblastoma, but its up-regulation predicts a good prognosis for glioblastoma (181). Notably, in colorectal cancer, patients with a low expression of TFR1 have a shorter survival compared with patients with positive TFR1 expression (182). These results suggest that the roles of TFR1/2 in tumor prognosis might be tumor-specific.

TABLE 2 | Iron regulators in cancer prognosis.

Altered Player	Cancer	Regulation	prognosis	Ref.
TFR1	hepatic carcinoma	up	poor	(176,177)
TFR1	ovarian cancer	up	poor	(29)
TFR1	lung cancer	up	poor	(178)
TFR1	gastric cancer	up	poor	(179)
TFR1	glioblastoma	up	poor	(180)
TFR2	glioblastoma	up	good	(181)
TFR1	colorectal cancer	up	good	(182)
FPN1	breast cancer	down	poor	(45)
FPN1	lung cancer	down	poor	(178)
FPN1	adrenocortical carcinoma	down	poor	(183)
FPN1	multiple myeloma	down	poor	(43)
FPN1	clear cell renal cell carcinoma	down	poor	(184)
STEAP3	glioblastoma	up	poor	(39)
STEAP1	breast cancer	up	good	(185)
STEAP2	breast cancer	up	good	(185)
STEAP4	breast cancer	up	good	(185)
Hepcidin	breast cancer	up	poor	(186)
FTL	ovarian cancer	up	poor	(187)
DMT1	ovarian cancer	up	poor	(187)
HAMP	ovarian cancer	up	poor	(187)
DMT1	hepatocellular carcinoma	low	poor	(65)

Similarly, *FPN1* has been identified as a favorable prognostic marker for many tumors (189). In a gene expression profile of approximately 800 breast cancer patients, it was reported that decreased *FPN1* expression was significantly associated with reduced metastasis-free and disease-free survival (45). And *FPN1* mRNA and protein expression are significantly down-regulated, and patients with a low *FPN1* expression have a poor prognosis in lung cancer and adrenocortical carcinoma (ACC) (178, 183). Additionally, a similar effect was observed in multiple myeloma and ccRCC (43, 184). Furthermore, STEAP3 is highly expressed in glioblastoma and is closely related to the decreased overall survival rate (39); however, a survival analysis showed that breast cancer patients with high levels of STEAP1, STEAP2, and STEAP4 had an overall good prognosis (185).

Higher hepcidin is also reported to be associated with a shorter recurrence time of distant breast cancer, and hepcidin may be associated with a poor prognosis for breast cancer in obese women (186). Survival analysis showed that ovarian cancer patients with a high expression of *FTL*, DMT1 and *HAMP* showed a poor overall survival rate (190). IL-6 and BMP control hepcidin secretion in cancer and IL-6 level is elevated in lung cancer patients with poor prognosis (187).

The progression of breast cancer is negatively correlated with hemoglobin (Hb) and positively correlated with ferritin levels (191). Compared with the high-DMT1 group, liver cancer patients with a low DMT1 expression have a worse disease-free survival rate, which is particularly obvious in patients with advanced liver cancer (65).

Iron in Cancer Therapy

Many approaches have been constructed to treat cancer against intracellular iron metabolism disorders: one strategy is to deplete iron of tumor cells, such as iron chelator; another important one is to generate cytotoxic level of ROS or ferroptosis through excess iron in tumor cells (**Table 3**).

TABLE 3 | Iron in Cancer Therapy.

Name	Mechanism	Ref.
Cyst(e)inase	degrading cysteine	(133,192,193)
DFO	iron depletion	(194)
DFO	iron depletion	(195)
Triapine	iron depletion	(196)
Dp44mT	iron depletion	
Fusaricide	iron depletion	(62)
Ga	iron depletion	(197)
Tris (8-quinolinolato) Gallium (III) (KP46)	iron depletion	(198)
Gallium Mallotate	iron depletion	(198)
Ferrocene derivatives	elevated iron levels	(199)
Ferumoxytol	elevated iron levels	(200)
ascorbic acid	ferroptosis	(201–205)
salinomycin derivatives	ferroptosis inducers	(206)
DMT1 inhibitor	target DMT1	(68)
HFn-PTX	target TFR1	(207)
DOX-FTH	target TFR1	(179,208)
miR-375	target *SLC7A11*	(209)
miR-148a	targeting *TFR1*	(32)
miR-184	targeting *HAMP*	(210)
miR-200b	targeting ferritin	(211)

Iron Depletion

Iron chelators can change the metabolism of tumor cells by reducing the intake of iron. It has also been demonstrated that iron chelators inhibit ribonucleotide reductase activity and play important roles in various signaling pathways associated with tumor progression and metastasis (212, 213). In a study of patients with advanced hepatocellular carcinoma, 20% of patients responded to treatment with DFO (194); In another study of nine patients with neuroblastoma, seven patients had reduced bone marrow infiltration after DFO treatment (195). However, iron chelators appear to be effective only in specific tumors. Other studies have shown that DFO is ineffective in the treatment of hormone-reducing refractory prostate cancer and recurrent neuroblastoma (214, 215). Notably, other chelating agents, such as Triapine and Dp44mT, have entered clinical experiments (216, 217). After receiving Triapine treatment, 76% of patients with advanced hematological malignancies had a 50% reduction in white blood cell count (196). However, Triapine only showed the smallest overall response rate in metastatic renal cell carcinoma and recurrent and metastatic head and neck squamous cell carcinoma (218, 219). Additionally, Hui et al. confirmed that Fusaricide, a novel iron chelating agent, could induce apoptosis by activating Caspase-3 (62). Furthermore, iron chelators have been shown to alter macrophage polarization, and immune signaling. Prill et al. showed that DFO administration led to high iron efflux by decreasing ferritin expression in the tumor-associated macrophages (220). EC1 (a thiosemicarbazone chelator) treatment reversed the positive effect of macrophage-conditioned media on the proliferation and migration of cancer cells (221). Moreover, the safety and efficacy of iron chelators as cancer therapeutics have been tested in clinical trials, gastrointestinal symptoms and fatigue appear to be the most prevalent toxicities (194, 219, 222, 223).

The use of iron chelators in combination therapy has also been partially investigated. DFO was combined with many different chemotherapeutic drugs, such as cyclophosphamide, etoposide, cisplatin, carboplatin, and thiotepa (190, 224, 225). In a cohort of patients with advanced neuroblastoma and primitive neuroectodermal tumors, DFO was effective in combination with cyclophosphamide, etoposide, carboplatin, and thiotepa (224). In another study of 37 patients with accelerated myeloproliferative tumors and secondary acute myeloid leukemia, the combination of Triapine and fludarabine (a DNA synthesis inhibitor) showed 49% overall response rate and 24% complete response rate (226).

Gallium salts, which belong to the group IIIa metals and have common chemical properties with iron, are variants of the iron depletion strategy in tumor therapy. Therefore, gallium (Ga) is used to disrupt iron metabolism to mimic the behavior of iron. Gallium can be incorporated into protein and enzymes that use iron as a cofactor, such as ribonucleotide reductase, which inactivates enzymes that require iron to function and lead to an increase in mitochondrial reactive oxygen species (197). Thus, the gallium-based compound exhibits antitumor activity by disrupting iron-dependent tumor metabolism. The spectrum antineoplastic activity of gallium nitrate in the clinic was evaluated in Phase II clinical trials. Among a number of cancers examined, gallium nitrate displayed promising

antineoplastic activity in patients with nonHodgkin's lymphoma and bladder cancer (198, 227–229).The anti-cancer activity of newer gallium-ligands have been developed and are being undergone clinical evaluation, such as Tris (8-quinolinolato) Gallium (III) (KP46) and Gallium Mallotate, which may be more effective than the nitrate salt used in the original clinical formulation of gallium (198, 230).

Elevated Iron Levels

The strategy in contrast to iron depletion is to supply cells with excess iron. Excess iron combines with high levels of unstable iron in tumor cells to produce large amounts of ROS to eliminate tumor cells. For example, the metal-containing drugs Ferrocene derivatives are stable and exhibit favorable redox properties, inhibiting proliferative activity of tumor cell lines (199). Additionally, Ferumoxytol is an iron oxide nanoparticle approved by the FDA for the treatment of clinical iron deficiency, and studies have shown that ferumoxytol can produce excessive amounts of free iron, the reactive oxygen species produced by which can cause cell death, increase oxidative stress, and reduce tumor burden cells in mouse leukemia models and patients (200).

What's more, ascorbic acid therapy is a variant of cancer treatment strategy by affecting the oxidation state of iron and increasing LIP levels, which is indicated for various tumors (201–203). Multiple clinical trials of this therapy are currently being pursued. Such as NCT02344355, NCT02420314, NCT02905578, NCT02905591, NCT03508726, NCT03602235, and NCT03799094 (https://clinicaltrials.gov/) (204, 205). However, it must be noted that if a large amount of divalent iron is oxidized to trivalent iron, you will suffer from methemoglobinemia. Furthermore, high levels of iron in the blood reduce our healthy years of life, and keeping these levels in check could prevent age-related damage (231).

Ferroptosis Inducers

The ferroptosis inducers can target the treatment of tumor by increasing the iron level of the tumor cells. Conversely, targeting ferroptosis inhibitors also have been shown to suppress tumor progression, for example, depletion of cystine or cystine by cyst (e)inase (an engineered enzyme that degrades both cystine and cysteine) in combination with checkpoint blockade synergistically enhances T cell-mediated anti-tumour immunity and induces ferroptosis in tumor cells (133); Cyst(e)inase also can synergize with thioredoxin reductase inhibition for suppression of pancreatic tumor growth (192); Additionally, administration of cyst(e)inase induces tumor-selective ferroptosis and inhibited pancreatic tumor growth (193). IFN-γ derived from immunotherapy-activated $CD8^+$ T cells synergizing with radiotherapy-activated ataxia-telangiectasia mutated (ATM) suppresses SLC7A11, to induce cystine uptake, enhance tumor lipid oxidation and ferroptosis in human fibrosarcoma and melanoma cells (232). Notably, as we and others previously showed that that ferroptosis inducers target tumor stem cells to inhibit tumor proliferation and reduce metastasis (205, 233, 234). Several US Food and Drug Administration (FDA)-approved drugs have been shown to induce ferroptosis in tumor cells in preclinical models, but the clinical utility of these ferroptosis inducers require further investigation (2). Another study has shown that salinomycin derivatives can trigger the ferroptosis pathway in cancer stem cells (206). Furthermore, Andreea L Turcu et al. developed a DMT1 inhibitor that selectively targets cancer stem cells by blocking lysosomal iron translocation, leading to lysosomal iron accumulation, ROS production, and ferroptosis (68). However, it must be noted that ferroptosis inducers have potentially harmful side effects, mainly manifested as DNA damage and cell death in normal bone marrow cells and various tissues (235, 236).

In addition to the above two strategies, another strategy is to directly target proteins related to iron homeostasis disorders. Such as methods that target TFR1, which is commonly overexpressed in tumor cell species. W. Liu et al. developed endogenous human ferritin heavy-chain nanocages (HFn) to serve as the carrier of paclitaxel (PTX), which can specifically bind to blood-brain barrier and TFR1 widely overexpressed in glioma cells, and showed that HFn-PTX showed the best anti-tumor effect, and the median survival time was significantly longer than that of free PTX (207); additionally, doxorubicin-loaded ferritin heavy chain (DOX-FTH) can be taken up and induce apoptosis of cancer cells overexpressing TFR1 (208); and Cheng et al. indicated that HFn-Dox treatment could significantly improve the therapeutic effect of doxorubicin on gastric cancer, and increase overall survival rate of tumor-bearing mice (179).

Another possible new treatment strategy is to target miRNAs that regulate iron metabolism or to use miRNA in combination with chemotherapeutic drugs. Such as, our laboratory observed that miR-375 can trigger the ferroptosis through targeting *SLC7A11*, which is essential for miR-375-mediated inhibition on gastric cancer cell stemness (209); Overexpression of miR-148a can inhibit the proliferation of liver cancer cells by targeting *TFR1* (32); MiR-184 can inhibit the occurrence and development of liver cancer by regulating the expression of *HAMP* (210); And overexpression of miR-200b can reduce ferritin levels *in vitro* and increase the sensitivity of cancer cells to doxorubicin (211).

PERSPECTIVES AND FUTURE DIRECTIONS

Iron is necessary for normal cell metabolism, while as a redox active metal, iron can also produce active oxygen, which is a potentially toxic substance. In recent years, there has been an exPLoSive growth in the research of iron homeostasis in normal cells and iron metabolism disorders in cancer. In most tumors, cancer cells retain iron metabolism pathways similar to those of normal cells, but the levels of many proteins and enzyme activities are changed, which indicates that reprogramming of iron metabolism is an important aspect of tumor cell survival. The increase of iron levels in cancer cells promotes the activity of iron-dependent proteins, while avoids the damage caused by iron overload and achieves the "adjusted iron homeostasis" in line with tumor metabolism. However, the specific mechanism is not yet fully understood, such as is the iron metabolism of different types of tumor cells

consistent? How to quantify the level of iron so as to specifically target tumor cells without harming normal cells?

It may be helpful to solve these problems by developing powerful quantitative methods to measure the metabolizable iron in the cytoplasm and organelles, as well as developing iron chelating agents for organelles. Additionally, currently, the main treatment is to trigger the apoptotic death of tumor cells with anticancer drugs. However, due to the intrinsic and acquired resistance of tumor cells to apoptosis, the therapeutic effect is limited, and drug resistance is still the main limiting factor for the cure of tumor patients. Therefore, using other forms of non-apoptotic cell death provides a new therapeutic strategy. Importantly, abnormal lipid metabolism, ROS accumulation, and iron addiction are the physiological differences between malignant tumor cells and normal cells, and these differences happen to be the key regulatory factors of ferroptosis. Therefore, compared with normal cells, tumor cells are more sensitive to ferroptosis. From our own perspectives, ferroptosis inducers could have a worthwhile therapeutic index. However, based on different metabolic states and expression levels of key regulatory proteins, different tumor cells might have different sensitivity and response to ferroptosis. Notably, increasing evidences showed that combined use of ferroptosis inducer and other treatments, such as chemotherapy, radiotherapy, and immunotherapy, is a good treatment strategy, especially for cancer stem cells and drug-resistant cells. Thus, it is expected that cancer cell iron addiction will be successfully used as an effective cancer treatment in the next few years, such as: introducing drugs that induce ferroptosis into the clinic, transforming the unique iron metabolism characteristics of cancer stem cells into therapeutic advantages, and developing more targeted and effective anti-cancer iron chelating agents.

AUTHOR CONTRIBUTIONS

QG, SH, and ZY reviewed the literature and drafted the article. LL, XL, CL, WZ, and LZ finalized the paper and provided suggestions to improve it. All authors participated in designing the concept of this manuscript. All authors contributed to the article and approved the submitted version.

FUNDING

This work was supported by the National Natural Science Foundation of China (no. 81903857), the Science and Technology Research Project of Henan Province (no. 202102310158); the Medical Science and Technology Research Project of Henan Province (no. LHGJ20190675); the Medical Science and Technology Research Project of Henan Province (no. SBGJ202003010); the 2019 Ningbo Natural Science Foundation (2019A610311); the Doctoral Research Start-up Foundation of Henan Cancer Hospital, and the Priority Academic Program Development (PAPD) of Jiangsu Higher Education Institutions.

REFERENCES

1. Vogt AS, Arsiwala T, Mohsen M, Vogel M, Manolova V, Bachmann MF. On Iron Metabolism and Its Regulation. *Int J Mol Sci* (2021) 22(9):4591. doi: 10.3390/ijms22094591
2. Torti SV, Manz DH, Paul BT, Blanchette-Farra N, Torti FM. Iron and Cancer. *Annu Rev Nutr* (2018) 38:97–125. doi: 10.1146/annurev-nutr-082117-051732
3. Torti SV, Torti FM. Iron and Cancer: More Ore to be Mined. *Nat Rev Cancer* (2013) 13(5):342–55. doi: 10.1038/nrc3495
4. Jung M, Mertens C, Tomat E, Brüne B. Iron as a Central Player and Promising Target in Cancer Progression. *Int J Mol Sci* (2019) 20(2):273. doi: 10.3390/ijms20020273
5. Seco-Cervera M, González-Cabo P, Pallardó FV, Romá-Mateo C, García-Giménez JL. Thioredoxin and Glutaredoxin Systems as Potential Targets for the Development of New Treatments in Friedreich's Ataxia. *Antioxid (Basel Switzerland)* (2020) 9(12):1257. doi: 10.3390/antiox9121257
6. Tifoun N, De Las Heras JM, Guillaume A, Bouleau S, Mignotte B, Le Floch N. Insights Into the Roles of the Sideroflexins/SLC56 Family in Iron Homeostasis and Iron-Sulfur Biogenesis. *Biomedicines* (2021) 9(2):103. doi: 10.3390/biomedicines9020103
7. Jomova K, Valko M. Advances in Metal-Induced Oxidative Stress and Human Disease. *Toxicology* (2011) 283(2-3):65–87. doi: 10.1016/j.tox.2011.03.001
8. Filipovic MR, Koppenol WH. The Haber-Weiss Reaction - The Latest Revival. *Free Radical Biol Med* (2019) 145:221–2. doi: 10.1016/j.freeradbiomed.2019.09.017
9. Lipinski B. Hydroxyl Radical and Its Scavengers in Health and Disease. *Oxid Med Cell Longevity* (2011) 2011:809696. doi: 10.1155/2011/809696
10. Reiter RJ, Mayo JC, Tan DX, Sainz RM, Alatorre-Jimenez M, Qin L. Melatonin as an Antioxidant: Under Promises But Over Delivers. *J Pineal Res* (2016) 61(3):253–78. doi: 10.1111/jpi.12360
11. Abbaspour N, Hurrell R, Kelishadi R. Review on Iron and Its Importance for Human Health. *J Res Med Sci* (2014) 19(2):164–74.
12. Kawabata H. Transferrin and Transferrin Receptors Update. *Free Radical Biol Med* (2019) 133:46–54. doi: 10.1016/j.freeradbiomed.2018.06.037
13. Bogdan AR, Miyazawa M, Hashimoto K, Tsuji Y. Regulators of Iron Homeostasis: New Players in Metabolism, Cell Death, and Disease. *Trends Biochem Sci* (2016) 41(3):274–86. doi: 10.1016/j.tibs.2015.11.012
14. Ginzburg YZ. Hepcidin-Ferroportin Axis in Health and Disease. *Vitamins Hormones* (2019) 110:17–45. doi: 10.1016/bs.vh.2019.01.002
15. Zhang DL, Ghosh MC, Rouault TA. The Physiological Functions of Iron Regulatory Proteins in Iron Homeostasis - An Update. *Front Pharmacol* (2014) 5:124. doi: 10.3389/fphar.2014.00124
16. Anderson CP, Shen M, Eisenstein RS, Leibold EA. Mammalian Iron Metabolism and Its Control by Iron Regulatory Proteins. *Biochim Biophys Acta* (2012) 1823(9):1468–83. doi: 10.1016/j.bbamcr.2012.05.010
17. Hentze MW, Muckenthaler MU, Galy B, Camaschella C. Two to Tango: Regulation of Mammalian Iron Metabolism. *Cell* (2010) 142(1):24–38. doi: 10.1016/j.cell.2010.06.028
18. Petronek MS, Spitz DR, Buettner GR, Allen BG. Linking Cancer Metabolic Dysfunction and Genetic Instability Through the Lens of Iron Metabolism. *Cancers* (2019) 11(8):1077. doi: 10.3390/cancers11081077
19. Anderson GJ, Frazer DM. Hepatic Iron Metabolism. *Semin Liver Dis* (2005) 25(4):420–32. doi: 10.1055/s-2005-923314
20. Rishi G, Subramaniam VN. The Liver in Regulation of Iron Homeostasis. *Am J Physiol Gastrointest Liver Physiol* (2017) 313(3):G157–g65. doi: 10.1152/ajpgi.00004.2017
21. Qiao B, Sugianto P, Fung E, Del-Castillo-Rueda A, Moran-Jimenez MJ, Ganz T, et al. Hepcidin-Induced Endocytosis of Ferroportin Is Dependent on Ferroportin Ubiquitination. *Cell Metab* (2012) 15(6):918–24. doi: 10.1016/j.cmet.2012.03.018

22. Andriopoulos BJr., Corradini E, Xia Y, Faasse SA, Chen S, Grgurevic L, et al. BMP6 Is a Key Endogenous Regulator of Hepcidin Expression and Iron Metabolism. *Nat Genet* (2009) 41(4):482–7. doi: 10.1038/ng.335
23. Pietrangelo A. Ferroportin Disease: Pathogenesis, Diagnosis and Treatment. *Haematologica* (2017) 102(12):1972–84. doi: 10.3324/haematol.2017.170720
24. Gao G, Li J, Zhang Y, Chang YZ. Cellular Iron Metabolism and Regulation. *Adv Exp Med Biol* (2019) 1173:21–32. doi: 10.1007/978-981-13-9589-5_2
25. Prior R, Reifenberger G, Wechsler W. Transferrin Receptor Expression in Tumours of the Human Nervous System: Relation to Tumour Type, Grading and Tumour Growth Fraction. *Virchows Archiv A Pathol Anat Histopathol* (1990) 416(6):491–6. doi: 10.1007/BF01600299
26. Das Gupta A, Shah VI. Correlation of Transferrin Receptor Expression With Histologic Grade and Immunophenotype in Chronic Lymphocytic Leukemia and Non-Hodgkin's Lymphoma. *Hematol Pathol* (1990) 4(1):37–41.
27. Faulk WP, Hsi BL, Stevens PJ. Transferrin and Transferrin Receptors in Carcinoma of the Breast. *Lancet (Lond Engl)* (1980) 2(8191):390–2. doi: 10.1016/S0140-6736(80)90440-7
28. Zhang S, Chang W, Wu H, Wang YH, Gong YW, Zhao YL, et al. Pan-Cancer Analysis of Iron Metabolic Landscape Across the Cancer Genome Atlas. *J Cell Physiol* (2020) 235(2):1013–24. doi: 10.1002/jcp.29017
29. Basuli D, Tesfay L, Deng Z, Paul B, Yamamoto Y, Ning G, et al. Iron Addiction: A Novel Therapeutic Target in Ovarian Cancer. *Oncogene* (2017) 36(29):4089–99. doi: 10.1038/onc.2017.11
30. Wang Q, Gu T, Ma L, Bu S, Zhou W, Mao G, et al. Efficient Iron Utilization Compensates for Loss of Extracellular Matrix of Ovarian Cancer Spheroids. *Free Radical Biol Med* (2021) 164:369–80. doi: 10.1016/j.freeradbiomed.2021.01.001
31. Xiao C, Fu X, Wang Y, Liu H, Jiang Y, Zhao Z, et al. Transferrin Receptor Regulates Malignancies and the Stemness of Hepatocellular Carcinoma-Derived Cancer Stem-Like Cells by Affecting Iron Accumulation. *PLoS One* (2020) 15(12):e0243812. doi: 10.1371/journal.pone.0243812
32. Babu KR, Muckenthaler MU. miR-148a Regulates Expression of the Transferrin Receptor 1 in Hepatocellular Carcinoma. *Sci Rep* (2019) 9 (1):1518. doi: 10.1038/s41598-018-35947-7
33. Campisi A, Bonfanti R, Raciti G, Bonaventura G, Legnani L, Magro G, et al. Gene Silencing of Transferrin-1 Receptor as a Potential Therapeutic Target for Human Follicular and Anaplastic Thyroid Cancer. *Mol Ther Oncol* (2020) 16:197–206. doi: 10.1016/j.omto.2020.01.003
34. Fu Y, Lin L, Xia L. MiR-107 Function as a Tumor Suppressor Gene in Colorectal Cancer by Targeting Transferrin Receptor 1. *Cell Mol Biol Lett* (2019) 24:31. doi: 10.1186/s11658-019-0155-z
35. Xue X, Ramakrishnan SK, Weisz K, Triner D, Xie L, Attili D, et al. Iron Uptake *via* DMT1 Integrates Cell Cycle With JAK-STAT3 Signaling to Promote Colorectal Tumorigenesis. *Cell Metab* (2016) 24(3):447–61. doi: 10.1016/j.cmet.2016.07.015
36. Sideris M, Adams K, Moorhead J, Diaz-Cano S, Bjarnason I, Papagrigoriadis S. BRAF V600E Mutation in Colorectal Cancer Is Associated With Right-Sided Tumours and Iron Deficiency Anaemia. *Anticancer Res* (2015) 35 (4):2345–50.
37. Liu Y, Pang Y, Zhu B, Uher O, Caisova V, Huynh TT, et al. Therapeutic Targeting of SDHB-Mutated Pheochromocytoma/Paraganglioma With Pharmacologic Ascorbic Acid. *Clin Cancer Res* (2020) 26(14):3868–80. doi: 10.1158/1078-0432.CCR-19-2335
38. Xue X, Taylor M, Anderson E, Hao C, Qu A, Greenson JK, et al. Hypoxia-Inducible Factor-2α Activation Promotes Colorectal Cancer Progression by Dysregulating Iron Homeostasis. *Cancer Res* (2012) 72(9):2285–93. doi: 10.1158/0008-5472.CAN-11-3836
39. Han M, Xu R, Wang S, Yang N, Ni S, Zhang Q, et al. Six-Transmembrane Epithelial Antigen of Prostate 3 Predicts Poor Prognosis and Promotes Glioblastoma Growth and Invasion. *Neoplasia (New York NY)* (2018) 20 (6):543–54. doi: 10.1016/j.neo.2018.04.002
40. Zhang L, Ye Y, Tu H, Hildebrandt MA, Zhao L, Heymach JV, et al. MicroRNA-Related Genetic Variants in Iron Regulatory Genes, Dietary Iron Intake, microRNAs and Lung Cancer Risk. *Ann Oncol* (2017) 28 (5):1124–9. doi: 10.1093/annonc/mdx046
41. Fehringer G, Liu G, Pintilie M, Sykes J, Cheng D, Liu N, et al. Association of the 15q25 and 5p15 Lung Cancer Susceptibility Regions With Gene Expression in Lung Tumor Tissue. *Cancer Epidemiol Biomarkers Prev* (2012) 21(7):1097–104. doi: 10.1158/1055-9965.EPI-11-1123-T
42. Deng Z, Manz DH, Torti SV, Torti FM. Effects of Ferroportin-Mediated Iron Depletion in Cells Representative of Different Histological Subtypes of Prostate Cancer. *Antioxid Redox Signaling* (2019) 30(8):1043–61. doi: 10.1089/ars.2017.7023
43. Kong Y, Hu L, Lu K, Wang Y, Xie Y, Gao L, et al. Ferroportin Downregulation Promotes Cell Proliferation by Modulating the Nrf2-miR-17-5p Axis in Multiple Myeloma. *Cell Death Dis* (2019) 10(9):624. doi: 10.1038/s41419-019-1854-0
44. Zhou Q, Chen J, Feng J, Wang J. E4BP4 Promotes Thyroid Cancer Proliferation by Modulating Iron Homeostasis Through Repression of Hepcidin. *Cell Death Dis* (2018) 9(10):987. doi: 10.1038/s41419-018-1001-3
45. Pinnix ZK, Miller LD, Wang W, D'Agostino RJr., Kute T, Willingham MC, et al. Ferroportin and Iron Regulation in Breast Cancer Progression and Prognosis. *Sci Trans Med* (2010) 2(43):43ra56. doi: 10.1126/scitranslmed.3001127
46. Sornjai W, Nguyen Van Long F, Pion N, Pasquer A, Saurin JC, Marcel V, et al. Iron and Hepcidin Mediate Human Colorectal Cancer Cell Growth. *Chemico-Biol Interact* (2020) 319:109021. doi: 10.1016/j.cbi.2020.109021
47. Tesfay L, Clausen KA, Kim JW, Hegde P, Wang X, Miller LD, et al. Hepcidin Regulation in Prostate and Its Disruption in Prostate Cancer. *Cancer Res* (2015) 75(11):2254–63. doi: 10.1158/0008-5472.CAN-14-2465
48. Zhao B, Li R, Cheng G, Li Z, Zhang Z, Li J, et al. Role of Hepcidin and Iron Metabolism in the Onset of Prostate Cancer. *Oncol Lett* (2018) 15(6):9953–8. doi: 10.3892/ol.2018.8544
49. El-Mahdy RI, Zakhary MM, Maximous DW, Mokhtar AA, El Dosoky MI. Circulating Osteocyte-Related Biomarkers (Vitamin D, Sclerostin, Dickkopf-1), Hepcidin, and Oxidative Stress Markers in Early Breast Cancer: Their Impact in Disease Progression and Outcome. *J Steroid Biochem Mol Biol* (2020) 204:105773. doi: 10.1016/j.jsbmb.2020.105773
50. Lopes M, Duarte TL, Teles MJ, Mosteo L, Chacim S, Aguiar E, et al. Loss of Erythroblasts in Acute Myeloid Leukemia Causes Iron Redistribution With Clinical Implications. *Blood Adv* (2021) 5(16):3102–12. doi: 10.1182/bloodadvances.2021004373
51. Maes K, Nemeth E, Roodman GD, Huston A, Esteve F, Freytes C, et al. In Anemia of Multiple Myeloma, Hepcidin Is Induced by Increased Bone Morphogenetic Protein 2. *Blood* (2010) 116(18):3635–44. doi: 10.1182/blood-2010-03-274571
52. Hara M, Ando M, Tsuchiya K, Nitta K. Serum Hepcidin-25 Level Linked With High Mortality in Patients With Non-Hodgkin Lymphoma. *Ann Hematol* (2015) 94(4):603–8. doi: 10.1007/s00277-014-2255-1
53. Traeger L, Ellermann I, Wiethoff H, Ihbe J, Gallitz I, Eveslage M, et al. Serum Hepcidin and GDF-15 Levels as Prognostic Markers in Urothelial Carcinoma of the Upper Urinary Tract and Renal Cell Carcinoma. *BMC Cancer* (2019) 19(1):74. doi: 10.1186/s12885-019-5278-0
54. Wang J, Liu W, Li JC, Li M, Li B, Zhu R. Hepcidin Downregulation Correlates With Disease Aggressiveness And Immune Infiltration in Liver Cancers. *Front Oncol* (2021) 11:714756. doi: 10.3389/fonc.2021.714756
55. Shen Y, Li X, Su Y, Badshah SA, Zhang B, Xue Y, et al. HAMP Downregulation Contributes to Aggressive Hepatocellular Carcinoma *via* Mechanism Mediated by Cyclin4-Dependent Kinase-1/STAT3 Pathway. *Diagn (Basel Switzerland)* (2019) 9(2):48. doi: 10.3390/diagnostics9020048
56. Wang Z, Du Y. Identification of a Novel Mutation Gene Signature HAMP for Cholangiocarcinoma Through Comprehensive TCGA and GEO Data Mining. *Int Immunopharmacol* (2021) 99:108039. doi: 10.1016/j.intimp.2021.108039
57. Schieber M, Chandel NS. ROS Function in Redox Signaling and Oxidative Stress. *Curr Biol CB* (2014) 24(10):R453–62. doi: 10.1016/j.cub.2014.03.034
58. Matthew-Onabanjo AN, Janusis J, Mercado-Matos J, Carlisle AE, Kim D, Levine F, et al. Beclin 1 Promotes Endosome Recruitment of Hepatocyte Growth Factor Tyrosine Kinase Substrate to Suppress Tumor Proliferation. *Cancer Res* (2020) 80(2):249–62. doi: 10.1158/0008-5472.CAN-19-1555
59. Bajbouj K, Shafarin J, Hamad M. Estrogen-Dependent Disruption of Intracellular Iron Metabolism Augments the Cytotoxic Effects of Doxorubicin in Select Breast and Ovarian Cancer Cells. *Cancer Manage Res* (2019) 11:4655–68. doi: 10.2147/CMAR.S204852
60. Wang B, Zhang J, Song F, Tian M, Shi B, Jiang H, et al. EGFR Regulates Iron Homeostasis to Promote Cancer Growth Through Redistribution of

Transferrin Receptor 1. *Cancer Lett* (2016) 381(2):331–40. doi: 10.1016/j.canlet.2016.08.006
61. Jung SY, Lee HK, Kim H, Kim S, Kim JS, Kang JG, et al. Depletion of ST6GALNACIII Retards A549 Non-Small Cell Lung Cancer Cell Proliferation by Downregulating Transferrin Receptor Protein 1 Expression. *Biochem Biophys Res Commun* (2021) 575:78–84. doi: 10.1016/j.bbrc.2021.08.055
62. Hui Y, Tang T, Wang J, Zhao H, Yang HY, Xi J, et al. Fusaricide Is a Novel Iron Chelator That Induces Apoptosis Through Activating Caspase-3. *J Natural Products* (2021) 84(8):2094–103. doi: 10.1021/acs.jnatprod.0c01322
63. Martínez LE, Daniels-Wells TR, Guo Y, Magpantay LI, Candelaria PV, Penichet ML, et al. Targeting TfR1 With the Ch128.1/IgG1 Antibody Inhibits EBV-Driven Lymphomagenesis in Immunosuppressed Mice Bearing EBV(+) Human Primary B-Cells. *Mol Cancer Ther* (2021) 20(9):1592–602. doi: 10.1158/1535-7163.MCT-21-0074
64. Yang H, Said AM, Huang H, Papa APD, Jin G, Wu S, et al. Chlorogenic Acid Depresses Cellular Bioenergetics to Suppress Pancreatic Carcinoma Through Modulating C-Myc-TFR1 Axis. *Phytother Res PTR* (2021) 35(4):2200–10. doi: 10.1002/ptr.6971
65. Hoki T, Katsuta E, Yan L, Takabe K, Ito F. Low DMT1 Expression Associates With Increased Oxidative Phosphorylation and Early Recurrence in Hepatocellular Carcinoma. *J Surg Res* (2019) 234:343–52. doi: 10.1016/j.jss.2018.11.008
66. Chen C, Wang S, Liu P. Deferoxamine Enhanced Mitochondrial Iron Accumulation and Promoted Cell Migration in Triple-Negative MDA-MB-231 Breast Cancer Cells Via a ROS-Dependent Mechanism. *Int J Mol Sci* (2019) 20(19):4952. doi: 10.3390/ijms20194952
67. Chen C, Liu P, Duan X, Cheng M, Xu LX. Deferoxamine-Induced High Expression of TfR1 and DMT1 Enhanced Iron Uptake in Triple-Negative Breast Cancer Cells by Activating IL-6/PI3K/AKT Pathway. *OncoTargets Ther* (2019) 12:4359–77. doi: 10.2147/OTT.S193507
68. Turcu AL, Versini A, Khene N, Gaillet C, Cañeque T, Müller S, et al. DMT1 Inhibitors Kill Cancer Stem Cells by Blocking Lysosomal Iron Translocation. *Chem (Weinheim an der Bergstrasse Germany)* (2020) 26(33):7369–73. doi: 10.1002/chem.202000159
69. Yang C, Xia Z, Li T, Chen Y, Zhao M, Sun Y, et al. Antioxidant Effect of Propofol in Gliomas and Its Association With Divalent Metal Transporter 1. *Front Oncol* (2020) 10:590931. doi: 10.3389/fonc.2020.590931
70. Grunewald TG, Bach H, Cossarizza A, Matsumoto I. The STEAP Protein Family: Versatile Oxidoreductases and Targets for Cancer Immunotherapy With Overlapping and Distinct Cellular Functions. *Biol Cell* (2012) 104(11):641–57. doi: 10.1111/boc.201200027
71. Chen H, Xu C, Yu Q, Zhong C, Peng Y, Chen J, et al. Comprehensive Landscape of STEAP Family Functions and Prognostic Prediction Value in Glioblastoma. *J Cell Physiol* (2021) 236(4):2988–3000. doi: 10.1002/jcp.30060
72. Burnell SEA, Spencer-Harty S, Howarth S, Bodger O, Kynaston H, Morgan C, et al. Utilisation of the STEAP Protein Family in a Diagnostic Setting may Provide a More Comprehensive Prognosis of Prostate Cancer. *PLoS One* (2019) 14(8):e0220456. doi: 10.1371/journal.pone.0220456
73. Valenti MT, Dalle Carbonare L, Donatelli L, Bertoldo F, Giovanazzi B, Caliari F, et al. STEAP mRNA Detection in Serum of Patients With Solid Tumours. *Cancer Lett* (2009) 273(1):122–6. doi: 10.1016/j.canlet.2008.07.037
74. Isobe T, Baba E, Arita S, Komoda M, Tamura S, Shirakawa T, et al. Human STEAP3 Maintains Tumor Growth Under Hypoferric Condition. *Exp Cell Res* (2011) 317(18):2582–91. doi: 10.1016/j.yexcr.2011.07.022
75. Na H, Li X, Zhang X, Xu Y, Sun Y, Cui J, et al. lncRNA STEAP3-AS1 Modulates Cell Cycle Progression *via* Affecting CDKN1C Expression Through STEAP3 in Colon Cancer. *Mol Ther Nucleic Acids* (2020) 21:480–91. doi: 10.1016/j.omtn.2020.06.011
76. Wang Z, Guo R, Trudeau SJ, Wolinsky E, Ast T, Liang JH, et al. CYB561A3 Is the Key Lysosomal Iron Reductase Required for Burkitt B-Cell Growth and Survival. *Blood* (2021) 2021011079. doi: 10.1182/blood.2021011079
77. Burnell SEA, Spencer-Harty S, Howarth S, Bodger O, Kynaston H, Morgan C, et al. STEAP2 Knockdown Reduces the Invasive Potential of Prostate Cancer Cells. *Sci Rep* (2018) 8(1):6252. doi: 10.1038/s41598-018-24655-x
78. Jiao Q, Du X, Wei J, Li Y, Jiang H. Oxidative Stress Regulated Iron Regulatory Protein IRP2 Through FBXL5-Mediated Ubiquitination-Proteasome Way in SH-SY5Y Cells. *Front Neurosci* (2019) 13:20. doi: 10.3389/fnins.2019.00020
79. Wang H, Shi H, Rajan M, Canarie ER, Hong S, Simoneschi D, et al. FBXL5 Regulates IRP2 Stability in Iron Homeostasis *via* an Oxygen-Responsive [2fe2s] Cluster. *Mol Cell* (2020) 78(1):31–41.e5. doi: 10.1016/j.molcel.2020.02.011
80. Song J, Liu T, Yin Y, Zhao W, Lin Z, Yin Y, et al. The Deubiquitinase OTUD1 Enhances Iron Transport and Potentiates Host Antitumor Immunity. *EMBO Rep* (2021) 22(2):e51162. doi: 10.15252/embr.202051162
81. Zhang Y, Feng X, Zhang J, Chen X. Iron Regulatory Protein 2 Exerts Its Oncogenic Activities by Suppressing TAp63 Expression. *Mol Cancer Res MCR* (2020) 18(7):1039–49. doi: 10.1158/1541-7786.MCR-19-1104
82. Zhang J, Kong X, Zhang Y, Sun W, Xu E, Chen X. Mdm2 is a Target and Mediator of IRP2 in Cell Growth Control. *FASEB J* (2020) 34(2):2301–11. doi: 10.1096/fj.201902278RR
83. Horniblow RD, Bedford M, Hollingworth R, Evans S, Sutton E, Lal N, et al. BRAF Mutations Are Associated With Increased Iron Regulatory Protein-2 Expression in Colorectal Tumorigenesis. *Cancer Sci* (2017) 108(6):1135–43. doi: 10.1111/cas.13234
84. Miyazawa M, Bogdan AR, Tsuji Y. Perturbation of Iron Metabolism by Cisplatin Through Inhibition of Iron Regulatory Protein 2. *Cell Chem Biol* (2019) 26(1):85–97.e4. doi: 10.1016/j.chembiol.2018.10.009
85. Yao F, Cui X, Zhang Y, Bei Z, Wang H, Zhao D, et al. Iron Regulatory Protein 1 Promotes Ferroptosis by Sustaining Cellular Iron Homeostasis in Melanoma. *Oncol Lett* (2021) 22(3):657. doi: 10.3892/ol.2021.12918
86. Pan X, Lu Y, Cheng X, Wang J. Hepcidin and Ferroportin Expression in Breast Cancer Tissue and Serum and Their Relationship With Anemia. *Curr Oncol (Toronto Ont)* (2016) 23(1):e24–6. doi: 10.3747/co.23.2840
87. Babu KR, Muckenthaler MU. miR-20a Regulates Expression of the Iron Exporter Ferroportin in Lung Cancer. *J Mol Med (Berlin Germany)* (2016) 94(3):347–59. doi: 10.1007/s00109-015-1362-3
88. Guo W, Zhang S, Chen Y, Zhang D, Yuan L, Cong H, et al. An Important Role of the Hepcidin-Ferroportin Signaling in Affecting Tumor Growth and Metastasis. *Acta Biochim Biophys Sin* (2015) 47(9):703–15. doi: 10.1093/abbs/gmv063
89. Shan Z, Wei Z, Shaikh ZA. Suppression of Ferroportin Expression by Cadmium Stimulates Proliferation, EMT, and Migration in Triple-Negative Breast Cancer Cells. *Toxicol Appl Pharmacol* (2018) 356:36–43. doi: 10.1016/j.taap.2018.07.017
90. Gasparetto M, Pei S, Minhajuddin M, Stevens B, Smith CA, Seligman P. Low Ferroportin Expression in AML Is Correlated With Good Risk Cytogenetics, Improved Outcomes and Increased Sensitivity to Chemotherapy. *Leukemia Res* (2019) 80:1–10. doi: 10.1016/j.leukres.2019.02.011
91. Jiang X, Zhang C, Qi S, Guo S, Chen Y, Du E, et al. Elevated Expression of ZNF217 Promotes Prostate Cancer Growth by Restraining Ferroportin-Conducted Iron Egress. *Oncotarget* (2016) 7(51):84893–906. doi: 10.18632/oncotarget.12753
92. Xue D, Zhou C, Shi Y, Lu H, Xu R, He X. Nuclear Transcription Factor Nrf2 Suppresses Prostate Cancer Cells Growth and Migration Through Upregulating Ferroportin. *Oncotarget* (2016) 7(48):78804–12. doi: 10.18632/oncotarget.12860
93. Geng N, Shi BJ, Li SL, Zhong ZY, Li YC, Xua WL, et al. Knockdown of Ferroportin Accelerates Erastin-Induced Ferroptosis in Neuroblastoma Cells. *Eur Rev Med Pharmacol Sci* (2018) 22(12):3826–36. doi: 10.26355/eurrev_201806_15267
94. Tang Z, Jiang W, Mao M, Zhao J, Chen J, Cheng N. Deubiquitinase USP35 Modulates Ferroptosis in Lung Cancer *via* Targeting Ferroportin. *Clin Trans Med* (2021) 11(4):e390. doi: 10.1002/ctm2.390
95. Mertens C, Schnetz M, Rehwald C, Grein S, Elwakeel E, Weigert A, et al. Iron-Bound Lipocalin-2 From Tumor-Associated Macrophages Drives Breast Cancer Progression Independent of Ferroportin. *Metabolites* (2021) 11(3):108. doi: 10.3390/metabo11030180
96. Schwartz AJ, Goyert JW, Solanki S, Kerk SA, Chen B, Castillo C, et al. Hepcidin Sequesters Iron to Sustain Nucleotide Metabolism and Mitochondrial Function in Colorectal Cancer Epithelial Cells. *Nat Metab* (2021) 3(7):969–82. doi: 10.1038/s42255-021-00406-7
97. Abdel-Razeq H, Hashem H. Recent Update in the Pathogenesis and Treatment of Chemotherapy and Cancer Induced Anemia. *Crit Rev Oncol/Hematol* (2020) 145:102837. doi: 10.1016/j.critrevonc.2019.102837

98. Manz DH, Blanchette NL, Paul BT, Torti FM, Torti SV. Iron and Cancer: Recent Insights. *Ann New York Acad Sci* (2016) 1368(1):149–61. doi: 10.1111/nyas.13008
99. Jakszyn P, Fonseca-Nunes A, Lujan-Barroso L, Aranda N, Tous M, Arija V, et al. Hepcidin Levels and Gastric Cancer Risk in the EPIC-EurGast Study. *Int J Cancer* (2017) 141(5):945–51. doi: 10.1002/ijc.30797
100. Oh ST, Talpaz M, Gerds AT, Gupta V, Verstovsek S, Mesa R, et al. ACVR1/JAK1/JAK2 Inhibitor Momelotinib Reverses Transfusion Dependency and Suppresses Hepcidin in Myelofibrosis Phase 2 Trial. *Blood Adv* (2020) 4 (18):4282–91. doi: 10.1182/bloodadvances.2020002662
101. Tseng HH, Chang JG, Hwang YH, Yeh KT, Chen YL, Yu HS. Expression of Hepcidin and Other Iron-Regulatory Genes in Human Hepatocellular Carcinoma and Its Clinical Implications. *J Cancer Res Clin Oncol* (2009) 135(10):1413–20. doi: 10.1007/s00432-009-0585-5
102. Kijima H, Sawada T, Tomosugi N, Kubota K. Expression of Hepcidin mRNA Is Uniformly Suppressed in Hepatocellular Carcinoma. *BMC Cancer* (2008) 8:167. doi: 10.1186/1471-2407-8-167
103. Tsiftsoglou AS, Tsamadou AI, Papadopoulou LC. Heme as Key Regulator of Major Mammalian Cellular Functions: Molecular, Cellular, and Pharmacological Aspects. *Pharmacol Ther* (2006) 111(2):327–45. doi: 10.1016/j.pharmthera.2005.10.017
104. Kalainayakan SP, FitzGerald KE, Konduri PC, Vidal C, Zhang L. Essential Roles of Mitochondrial and Heme Function in Lung Cancer Bioenergetics and Tumorigenesis. *Cell Biosci* (2018) 8:56. doi: 10.1186/s13578-018-0257-8
105. Tracey N, Creedon H, Kemp AJ, Culley J, Muir M, Klinowska T, et al. HO-1 Drives Autophagy as a Mechanism of Resistance Against HER2-Targeted Therapies. *Breast Cancer Res Treat* (2020) 179(3):543–55. doi: 10.1007/s10549-019-05489-1
106. Zhang S, Chen Y, Guo W, Yuan L, Zhang D, Xu Y, et al. Disordered Hepcidin-Ferroportin Signaling Promotes Breast Cancer Growth. *Cell Signal* (2014) 26(11):2539–50. doi: 10.1016/j.cellsig.2014.07.029
107. Martínez VG, Rubio C, Martínez-Fernández M, Segovia C, López-Calderón F, Garín MI, et al. BMP4 Induces M2 Macrophage Polarization and Favors Tumor Progression in Bladder Cancer. *Clin Cancer Res* (2017) 23(23):7388–99. doi: 10.1158/1078-0432.CCR-17-1004
108. Dixon SJ, Lemberg KM, Lamprecht MR, Skouta R, Zaitsev EM, Gleason CE, et al. Ferroptosis: An Iron-Dependent Form of Nonapoptotic Cell Death. *Cell* (2012) 149(5):1060–72. doi: 10.1016/j.cell.2012.03.042
109. Tang D, Chen X, Kang R, Kroemer G. Ferroptosis: Molecular Mechanisms and Health Implications. *Cell Res* (2021) 31(2):107–25. doi: 10.1038/s41422-020-00441-1
110. Hirschhorn T, Stockwell BR. The Development of the Concept of Ferroptosis. *Free Radical Biol Med* (2019) 133:130–43. doi: 10.1016/j.freeradbiomed.2018.09.043
111. Jiang X, Stockwell BR, Conrad M. Ferroptosis: Mechanisms, Biology and Role in Disease. *Nat Rev Mol Cell Biol* (2021) 22(4):266–82. doi: 10.1038/s41580-020-00324-8
112. Gao M, Yi J, Zhu J, Minikes AM, Monian P, Thompson CB, et al. Role of Mitochondria in Ferroptosis. *Mol Cell* (2019) 73(2):354–63.e3. doi: 10.1016/j.molcel.2018.10.042
113. Li C, Zhang Y, Liu J, Kang R, Klionsky DJ, Tang D. Mitochondrial DNA Stress Triggers Autophagy-Dependent Ferroptotic Death. *Autophagy* (2021) 17(4):948–60. doi: 10.1080/15548627.2020.1739447
114. Lee H, Zandkarimi F, Zhang Y, Meena JK, Kim J, Zhuang L, et al. Energy-Stress-Mediated AMPK Activation Inhibits Ferroptosis. *Nat Cell Biol* (2020) 22(2):225–34. doi: 10.1038/s41556-020-0461-8
115. Zhou B, Liu J, Kang R, Klionsky DJ, Kroemer G, Tang D. Ferroptosis Is a Type of Autophagy-Dependent Cell Death. *Semin Cancer Biol* (2020) 66:89–100. doi: 10.1016/j.semcancer.2019.03.002
116. Chen X, Yu C, Kang R, Kroemer G, Tang D. Cellular Degradation Systems in Ferroptosis. *Cell Death Differ* (2021) 28(4):1135–48. doi: 10.1038/s41418-020-00728-1
117. Mou Y, Wang J, Wu J, He D, Zhang C, Duan C, et al. Ferroptosis, a New Form of Cell Death: Opportunities and Challenges in Cancer. *J Hematol Oncol* (2019) 12(1):34. doi: 10.1186/s13045-019-0720-y
118. Friedmann Angeli JP, Krysko DV, Conrad M. Ferroptosis at the Crossroads of Cancer-Acquired Drug Resistance and Immune Evasion. *Nat Rev Cancer* (2019) 19(7):405–14. doi: 10.1038/s41568-019-0149-1
119. Lill R, Mühlenhoff U. Maturation of Iron-Sulfur Proteins in Eukaryotes: Mechanisms, Connected Processes, and Diseases. *Annu Rev Biochem* (2008) 77:669–700. doi: 10.1146/annurev.biochem.76.052705.162653
120. Terzi EM, Sviderskiy VO, Alvarez SW, Whiten GC, Possemato R. Iron-Sulfur Cluster Deficiency can be Sensed by IRP2 and Regulates Iron Homeostasis and Sensitivity to Ferroptosis Independent of IRP1 and FBXL5. *Sci Adv* (2021) 7(22):eabg430. doi: 10.1126/sciadv.abg4302
121. Alvarez SW, Sviderskiy VO, Terzi EM, Papagiannakopoulos T, Moreira AL, Adams S, et al. NFS1 Undergoes Positive Selection in Lung Tumours and Protects Cells From Ferroptosis. *Nature* (2017) 551(7682):639–43. doi: 10.1038/nature24637
122. Rouault TA. Biogenesis of Iron-Sulfur Clusters in Mammalian Cells: New Insights and Relevance to Human Disease. *Dis Models Mech* (2012) 5 (2):155–64. doi: 10.1242/dmm.009019
123. Du J, Zhou Y, Li Y, Xia J, Chen Y, Chen S, et al. Identification of Frataxin as a Regulator of Ferroptosis. *Redox Biol* (2020) 32:101483. doi: 10.1016/j.redox.2020.101483
124. Du J, Wang T, Li Y, Zhou Y, Wang X, Yu X, et al. DHA Inhibits Proliferation and Induces Ferroptosis of Leukemia Cells Through Autophagy Dependent Degradation of Ferritin. *Free Radical Biol Med* (2019) 131:356–69. doi: 10.1016/j.freeradbiomed.2018.12.011
125. Patra S, Barondeau DP. Mechanism of Activation of the Human Cysteine Desulfurase Complex by Frataxin. *Proc Natl Acad Sci USA* (2019) 116 (39):19421–30. doi: 10.1073/pnas.1909535116
126. Chafe SC, Vizeacoumar FS, Venkateswaran G, Nemirovsky O, Awrey S, Brown WS, et al. Genome-Wide Synthetic Lethal Screen Unveils Novel CAIX-NFS1/xCT Axis as a Targetable Vulnerability in Hypoxic Solid Tumors. *Sci Adv* (2021) 7(35):eabj0364. doi: 10.1126/sciadv.abj0364
127. Mao C, Liu X, Zhang Y, Lei G, Yan Y, Lee H, et al. DHODH-Mediated Ferroptosis Defence Is a Targetable Vulnerability in Cancer. *Nature* (2021) 593(7860):586–90. doi: 10.1038/s41586-021-03539-7
128. Ding Y, Chen X, Liu C, Ge W, Wang Q, Hao X, et al. Identification of a Small Molecule as Inducer of Ferroptosis and Apoptosis Through Ubiquitination of GPX4 in Triple Negative Breast Cancer Cells. *J Hematol Oncol* (2021) 14 (1):19. doi: 10.1186/s13045-020-01016-8
129. Chen D, Chu B, Yang X, Liu Z, Jin Y, Kon N, et al. Ipla2β-Mediated Lipid Detoxification Controls P53-Driven Ferroptosis Independent of GPX4. *Nat Commun* (2021) 12(1):3644. doi: 10.1038/s41467-021-23902-6
130. Wang X, Chen Y, Wang X, Tian H, Wang Y, Jin J, et al. Stem Cell Factor SOX2 Confers Ferroptosis Resistance in Lung Cancer *via* Upregulation of SLC7A11. *Cancer Res* (2021) 81(20):5217–29. doi: 10.1158/0008-5472.CAN-21-0567
131. Bao Z, Hua L, Ye Y, Wang D, Li C, Xie Q, et al. MEF2C Silencing Downregulates NF2 and E-Cadherin and Enhances Erastin-Induced Ferroptosis in Meningioma. *Neuro-oncology* (2021), noab114. doi: 10.1093/neuonc/noab114
132. Kremer DM, Nelson BS, Lin L, Yarosz EL, Halbrook CJ, Kerk SA, et al. GOT1 Inhibition Promotes Pancreatic Cancer Cell Death by Ferroptosis. *Nat Commun* (2021) 12(1):4860. doi: 10.1038/s41467-021-24859-2
133. Wang W, Green M, Choi JE, Gijón M, Kennedy PD, Johnson JK, et al. CD8 (+) T Cells Regulate Tumour Ferroptosis During Cancer Immunotherapy. *Nature* (2019) 569(7755):270–4. doi: 10.1038/s41586-019-1170-y
134. Ye Z, Zhuo Q, Hu Q, Xu X, Mengqi L, Zhang Z, et al. FBW7-NRA41-SCD1 Axis Synchronously Regulates Apoptosis and Ferroptosis in Pancreatic Cancer Cells. *Redox Biol* (2021) 38:101807. doi: 10.1016/j.redox.2020.101807
135. Hong T, Lei G, Chen X, Li H, Zhang X, Wu N, et al. PARP Inhibition Promotes Ferroptosis *via* Repressing SLC7A11 and Synergizes With Ferroptosis Inducers in BRCA-Proficient Ovarian Cancer. *Redox Biol* (2021) 42:101928. doi: 10.1016/j.redox.2021.101928
136. Sun J, Zhou C, Zhao Y, Zhang X, Chen W, Zhou Q, et al. Quiescin Sulfhydryl Oxidase 1 Promotes Sorafenib-Induced Ferroptosis in Hepatocellular Carcinoma by Driving EGFR Endosomal Trafficking and Inhibiting NRF2 Activation. *Redox Biol* (2021) 41:101942. doi: 10.1016/j.redox.2021.101942
137. Tan SK, Mahmud I, Fontanesi F, Puchowicz M, Neumann CKA, Griswold AJ, et al. Obesity-Dependent Adipokine Chemerin Suppresses Fatty Acid Oxidation to Confer Ferroptosis Resistance. *Cancer Discovery* (2021) 11 (8):2072–93. doi: 10.1158/2159-8290.CD-20-1453
138. Lange M, Olzmann JA. Ending on a Sour Note: Lipids Orchestrate Ferroptosis in Cancer. *Cell Metab* (2021) 33(8):1507–9. doi: 10.1016/j.cmet.2021.07.011

139. Dierge E, Debock E, Guilbaud C, Corbet C, Mignolet E, Mignard L, et al. Peroxidation of N-3 and N-6 Polyunsaturated Fatty Acids in the Acidic Tumor Environment Leads to Ferroptosis-Mediated Anticancer Effects. *Cell Metab* (2021) 33(8):1701–15.e5. doi: 10.1016/j.cmet.2021.05.016
140. Liu W, Chakraborty B, Safi R, Kazmin D, Chang CY, McDonnell DP. Dysregulated Cholesterol Homeostasis Results in Resistance to Ferroptosis Increasing Tumorigenicity and Metastasis in Cancer. *Nat Commun* (2021) 12(1):5103.doi: 10.1038/s41467-021-25354-4
141. Beatty A, Singh T, Tyurina YY, Tyurin VA, Samovich S, Nicolas E, et al. Ferroptotic Cell Death Triggered by Conjugated Linolenic Acids Is Mediated by ACSL1. *Nat Commun* (2021) 12(1):2244. doi: 10.1038/s41467-021-22471-y
142. Wang ZX, Ma J, Li XY, Wu Y, Shi H, Chen Y, et al. Quercetin Induces P53-Independent Cancer Cell Death Through Lysosome Activation by the Transcription Factor EB and Reactive Oxygen Species-Dependent Ferroptosis. *Br J Pharmacol* (2021) 178(5):1133–48. doi: 10.1111/bph.15350
143. Wu CY, Yang YH, Lin YS, Chang GH, Tsai MS, Hsu CM, et al. Dihydroisotanshinone I Induced Ferroptosis and Apoptosis of Lung Cancer Cells. *BioMed Pharmacother* (2021) 139:111585. doi: 10.1016/j.biopha.2021.111585
144. Wen Y, Chen H, Zhang L, Wu M, Zhang F, Yang D, et al. Glycyrrhetinic Acid Induces Oxidative/Nitrative Stress and Drives Ferroptosis Through Activating NADPH Oxidases and iNOS, and Depriving Glutathione in Triple-Negative Breast Cancer Cells. *Free Radical Biol Med* (2021) 173:41–51. doi: 10.1016/j.freeradbiomed.2021.07.019
145. Mancias JD, Wang X, Gygi SP, Harper JW, Kimmelman AC. Quantitative Proteomics Identifies NCOA4 as the Cargo Receptor Mediating Ferritinophagy. *Nature* (2014) 509(7498):105–9. doi: 10.1038/nature13148
146. Tang M, Chen Z, Wu D, Chen L. Ferritinophagy/ferroptosis: Iron-Related Newcomers in Human Diseases. *J Cell Physiol* (2018) 233(12):9179–90. doi: 10.1002/jcp.26954
147. Ajoolabady A, Aslkhodapasandhokmabad H, Libby P, Tuomilehto J, Lip GYH, Penninger JM, et al. Ferritinophagy and Ferroptosis in the Management of Metabolic Diseases. *Trends Endocrinol Metabol: TEM* (2021) 32(7):444–62. doi: 10.1016/j.tem.2021.04.010
148. Finazzi D, Arosio P. Biology of Ferritin in Mammals: An Update on Iron Storage, Oxidative Damage and Neurodegeneration. *Arch Toxicol* (2014) 88 (10):1787–802. doi: 10.1007/s00204-014-1329-0
149. Zarjou A, Jeney V, Arosio P, Poli M, Zavaczki E, Balla G, et al. Ferritin Ferroxidase Activity: A Potent Inhibitor of Osteogenesis. *J Bone Mineral Res* (2010) 25(1):164–72. doi: 10.1359/jbmr.091002
150. Timoshnikov VA, Kobzeva TV, Polyakov NE, Kontoghiorghes GJ. Inhibition of Fe(2+)- and Fe(3+)- Induced Hydroxyl Radical Production by the Iron-Chelating Drug Deferiprone. *Free Radical Biol Med* (2015) 78:118–22. doi: 10.1016/j.freeradbiomed.2014.10.513
151. Philpott CC. The Flux of Iron Through Ferritin in Erythrocyte Development. *Curr Opin Hematol* (2018) 25(3):183–8. doi: 10.1097/MOH.0000000000000417
152. Dowdle WE, Nyfeler B, Nagel J, Elling RA, Liu S, Triantafellow E, et al. Selective VPS34 Inhibitor Blocks Autophagy and Uncovers a Role for NCOA4 in Ferritin Degradation and Iron Homeostasis In Vivo. *Nat Cell Biol* (2014) 16(11):1069–79. doi: 10.1038/ncb3053
153. Mancias JD, Pontano Vaites L, Nissim S, Biancur DE, Kim AJ, Wang X, et al. Ferritinophagy *via* NCOA4 Is Required for Erythropoiesis and Is Regulated by Iron Dependent HERC2-Mediated Proteolysis. *eLife* (2015) 4:e10308. doi: 10.7554/eLife.10308
154. Bellelli R, Federico G, Matte A, Colecchia D, Iolascon A, Chiariello M, et al. NCOA4 Deficiency Impairs Systemic Iron Homeostasis. *Cell Rep* (2016) 14 (3):411–21. doi: 10.1016/j.celrep.2015.12.065
155. Asano T, Komatsu M, Yamaguchi-Iwai Y, Ishikawa F, Mizushima N, Iwai K. Distinct Mechanisms of Ferritin Delivery to Lysosomes in Iron-Depleted and Iron-Replete Cells. *Mol Cell Biol* (2011) 31(10):2040–52. doi: 10.1128/MCB.01437-10
156. Bai Y, Meng L, Han L, Jia Y, Zhao Y, Gao H, et al. Lipid Storage and Lipophagy Regulates Ferroptosis. *Biochem Biophys Res Commun* (2019) 508 (4):997–1003. doi: 10.1016/j.bbrc.2018.12.039
157. Yang M, Chen P, Liu J, Zhu S, Kroemer G, Klionsky DJ, et al. Clockophagy is a Novel Selective Autophagy Process Favoring Ferroptosis. *Sci Adv* (2019) 5 (7):eaaw2238. doi: 10.1126/sciadv.aaw2238
158. Liu NQ, De Marchi T, Timmermans AM, Beekhof R, Trapman-Jansen AM, Foekens R, et al. Ferritin Heavy Chain in Triple Negative Breast Cancer: A Favorable Prognostic Marker That Relates to a Cluster of Differentiation 8 Positive (CD8+) Effector T-Cell Response. *Mol Cell Proteomics MCP* (2014) 13(7):1814–27. doi: 10.1074/mcp.M113.037176
159. Funauchi Y, Tanikawa C, Yi Lo PH, Mori J, Daigo Y, Takano A, et al. Regulation of Iron Homeostasis by the P53-ISCU Pathway. *Sci Rep* (2015) 5:16497. doi: 10.1038/srep16497
160. Wu X, Chen F, Sahin A, Albarracin C, Pei Z, Zou X, et al. Distinct Function of Androgen Receptor Coactivator ARA70α and ARA70β in Mammary Gland Development, and in Breast Cancer. *Breast Cancer Res Treat* (2011) 128(2):391–400. doi: 10.1007/s10549-010-1131-5
161. Chan JJ, Kwok ZH, Chew XH, Zhang B, Liu C, Soong TW, et al. A FTH1 Gene:Pseudogene:microRNA Network Regulates Tumorigenesis in Prostate Cancer. *Nucleic Acids Res* (2018) 46(4):1998–2011. doi: 10.1093/nar/gkx1248
162. Yang ND, Tan SH, Ng S, Shi Y, Zhou J, Tan KS, et al. Artesunate Induces Cell Death in Human Cancer Cells *via* Enhancing Lysosomal Function and Lysosomal Degradation of Ferritin. *J Biol Chem* (2014) 289(48):33425–41. doi: 10.1074/jbc.M114.564567
163. Xu Z, Feng J, Li Y, Guan D, Chen H, Zhai X, et al. The Vicious Cycle Between Ferritinophagy and ROS Production Triggered EMT Inhibition of Gastric Cancer Cells was Through P53/AKT/mTor Pathway. *Chemico-biol Interact* (2020) 328:109196. doi: 10.1016/j.cbi.2020.109196
164. Santana-Codina N, Mancias JD. The Role of NCOA4-Mediated Ferritinophagy in Health and Disease. *Pharm (Basel Switzerland)* (2018) 11(4):114. doi: 10.3390/ph11040114
165. Mou Y, Wu J, Zhang Y, Abdihamid O, Duan C, Li B. Low Expression of Ferritinophagy-Related NCOA4 Gene in Relation to Unfavorable Outcome and Defective Immune Cells Infiltration in Clear Cell Renal Carcinoma. *BMC Cancer* (2021) 21(1):18. doi: 10.1186/s12885-020-07726-z
166. Chang K, Yuan C, Liu X. Ferroptosis-Related Gene Signature Accurately Predicts Survival Outcomes in Patients With Clear-Cell Renal Cell Carcinoma. *Front Oncol* (2021) 11:649347. doi: 10.3389/fonc.2021.649347
167. Zhang Y, Kong Y, Ma Y, Ni S, Wikerholmen T, Xi K, et al. Loss of COPZ1 Induces NCOA4 Mediated Autophagy and Ferroptosis in Glioblastoma Cell Lines. *Oncogene* (2021) 40(8):1425–39. doi: 10.1038/s41388-020-01622-3
168. Vara-Pérez M, Rossi M, Van den Haute C, Maes H, Sassano ML, Venkataramani V, et al. BNIP3 Promotes HIF-1α-Driven Melanoma Growth by Curbing Intracellular Iron Homeostasis. *EMBO J* (2021) 40 (10):e106214. doi: 10.15252/embj.2020106214
169. Hasan M, Reddy SM, Das NK. Ferritinophagy is Not Required for Colon Cancer Cell Growth. *Cell Biol Int* (2020) 44(11):2307–14. doi: 10.1002/cbin.11439
170. Hayashima K, Kimura I, Katoh H. Role of Ferritinophagy in Cystine Deprivation-Induced Cell Death in Glioblastoma Cells. *Biochem Biophys Res Commun* (2021) 539:56–63. doi: 10.1016/j.bbrc.2020.12.075
171. Lu R, Jiang Y, Lai X, Liu S, Sun L, Zhou ZW. A Shortage of FTH Induces ROS and Sensitizes RAS-Proficient Neuroblastoma N2A Cells to Ferroptosis. *Int J Mol Sci* (2021) 22(16):8898. doi: 10.3390/ijms22168898
172. Marcus DM, Zinberg N. Measurement of Serum Ferritin by Radioimmunoassay: Results in Normal Individuals and Patients With Breast Cancer. *J Natl Cancer Inst* (1975) 55(4):791–5. doi: 10.1093/jnci/55.4.791
173. Lee S, Eo W, Jeon H, Park S, Chae J. Prognostic Significance of Host-Related Biomarkers for Survival in Patients With Advanced Non-Small Cell Lung Cancer. *J Cancer* (2017) 8(15):2974–83. doi: 10.7150/jca.20866
174. Koyama S, Fujisawa S, Watanabe R, Itabashi M, Ishibashi D, Ishii Y, et al. Serum Ferritin Level Is a Prognostic Marker in Patients With Peripheral T-Cell Lymphoma. *Int J Lab Hematol* (2017) 39(1):112–7. doi: 10.1111/ijlh.12592
175. Khanna V, Karjodkar F, Robbins S, Behl M, Arya S, Tripathi A. Estimation of Serum Ferritin Level in Potentially Malignant Disorders, Oral Squamous Cell Carcinoma, and Treated Cases of Oral Squamous Cell Carcinoma. *J Cancer Res Ther* (2017) 13(3):550–5. doi: 10.4103/0973-1482.181182
176. Shen Y, Li X, Dong D, Zhang B, Xue Y, Shang P. Transferrin Receptor 1 in Cancer: A New Sight for Cancer Therapy. *Am J Cancer Res* (2018) 8 (6):916–31.
177. Adachi M, Kai K, Yamaji K, Ide T, Noshiro H, Kawaguchi A, et al. Transferrin Receptor 1 Overexpression Is Associated With Tumour De-

Differentiation and Acts as a Potential Prognostic Indicator of Hepatocellular Carcinoma. *Histopathology* (2019) 75(1):63–73. doi: 10.1111/his.13847
178. Liu B, Song Z, Fan Y, Zhang G, Cao P, Li D, et al. Downregulation of FPN1 Acts as a Prognostic Biomarker Associated With Immune Infiltration in Lung Cancer. *Aging* (2021) 13(6):8737–61. doi: 10.18632/aging.202685
179. Cheng X, Fan K, Wang L, Ying X, Sanders AJ, Guo T, et al. TfR1 Binding With H-Ferritin Nanocarrier Achieves Prognostic Diagnosis and Enhances the Therapeutic Efficacy in Clinical Gastric Cancer. *Cell Death Dis* (2020) 11 (2):92. doi: 10.1038/s41419-020-2272-z
180. Rosager AM, Sørensen MD, Dahlrot RH, Hansen S, Schonberg DL, Rich JN, et al. Transferrin Receptor-1 and Ferritin Heavy and Light Chains in Astrocytic Brain Tumors: Expression and Prognostic Value. *PLoS One* (2017) 12(8):e0182954. doi: 10.1371/journal.pone.0182954
181. Calzolari A, Larocca LM, Deaglio S, Finisguerra V, Boe A, Raggi C, et al. Transferrin Receptor 2 Is Frequently and Highly Expressed in Glioblastomas. *Trans Oncol* (2010) 3(2):123–34. doi: 10.1593/tlo.09274
182. Cui C, Cheng X, Yan L, Ding H, Guan X, Zhang W, et al. Downregulation of TfR1 Promotes Progression of Colorectal Cancer *via* the JAK/STAT Pathway. *Cancer Manage Res* (2019) 11:6323–41. doi: 10.2147/CMAR.S198911
183. Zhu B, Zhi Q, Xie Q, Wu X, Gao Y, Chen X, et al. Reduced Expression of Ferroportin1 and Ceruloplasmin Predicts Poor Prognosis in Adrenocortical Carcinoma. *J Trace Elements Med Biol* (2019) 56:52–9. doi: 10.1016/j.jtemb.2019.07.009
184. Park CK, Heo J, Ham WS, Choi YD, Shin SJ, Cho NH. Ferroportin and FBXL5 as Prognostic Markers in Advanced Stage Clear Cell Renal Cell Carcinoma. *Cancer Res Treat* (2021) 53(4):1174–83. doi: 10.4143/crt.2021.031
185. Wu HT, Chen WJ, Xu Y, Shen JX, Chen WT, Liu J. The Tumor Suppressive Roles and Prognostic Values of STEAP Family Members in Breast Cancer. *BioMed Res Int* (2020) 2020:9578484. doi: 10.1155/2020/9578484
186. Jerzak KJ, Lohmann AE, Ennis M, Nemeth E, Ganz T, Goodwin PJ. Prognostic Associations of Plasma Hepcidin in Women With Early Breast Cancer. *Breast Cancer Res Treat* (2020) 184(3):927–35. doi: 10.1007/s10549-020-05903-z
187. Kuang Y, Wang Q. Iron and Lung Cancer. *Cancer Lett* (2019) 464:56–61. doi: 10.1016/j.canlet.2019.08.007
188. Yu H, Yang C, Jian L, Guo S, Chen R, Li K, et al. Sulfasalazine–induced Ferroptosis in Breast Cancer Cells Is Reduced by the Inhibitory Effect of Estrogen Receptor on the Transferrin Receptor. *Oncol Rep* (2019) 42(2):826–38. doi: 10.3892/or.2019.7189
189. Lelièvre P, Sancey L, Coll JL, Deniaud A, Busser B. Iron Dysregulation in Human Cancer: Altered Metabolism, Biomarkers for Diagnosis, Prognosis, Monitoring and Rationale for Therapy. *Cancers* (2020) 12(12):3524. doi: 10.3390/cancers12123524
190. Wang L, Li X, Mu Y, Lu C, Tang S, Lu K, et al. The Iron Chelator Desferrioxamine Synergizes With Chemotherapy for Cancer Treatment. *J Trace Elements Med Biol* (2019) 56:131–8. doi: 10.1016/j.jtemb.2019.07.008
191. George A, Bobby Z, Dubashi B. Utility of Ferritin and Inflammatory Biomarkers in the Diagnosis of Different Stages of Breast Cancer. *Saudi Med J* (2021) 42(8):825–31. doi: 10.15537/smj.2021.42.8.20210244
192. Kshattry S, Saha A, Gries P, Tiziani S, Stone E, Georgiou G, et al. Enzyme-Mediated Depletion of L-Cyst(E)Ine Synergizes With Thioredoxin Reductase Inhibition for Suppression of Pancreatic Tumor Growth. *NPJ Precis Oncol* (2019) 3:16. doi: 10.1038/s41698-019-0088-z
193. Badgley MA, Kremer DM, Maurer HC, DelGiorno KE, Lee HJ, Purohit V, et al. Cysteine Depletion Induces Pancreatic Tumor Ferroptosis in Mice. *Sci (New York NY)* (2020) 368(6486):85–9. doi: 10.1126/science.aaw9872
194. Yamasaki T, Terai S, Sakaida I. Deferoxamine for Advanced Hepatocellular Carcinoma. *New Engl J Med* (2011) 365(6):576–8. doi: 10.1056/NEJMc1105726
195. Donfrancesco A, Deb G, Dominici C, Pileggi D, Castello MA, Helson L. Effects of a Single Course of Deferoxamine in Neuroblastoma Patients. *Cancer Res* (1990) 50(16):4929–30.
196. Giles FJ, Fracasso PM, Kantarjian HM, Cortes JE, Brown RA, Verstovsek S, et al. Phase I and Pharmacodynamic Study of Triapine, a Novel Ribonucleotide Reductase Inhibitor, in Patients With Advanced Leukemia. *Leukemia Res* (2003) 27(12):1077–83. doi: 10.1016/S0145-2126(03)00118-8
197. Chitambar CR. Gallium Complexes as Anticancer Drugs. *Metal ions Life Sci* (2018) 18:281–302. doi: 10.1515/9783110470734-010
198. Chitambar CR. The Therapeutic Potential of Iron-Targeting Gallium Compounds in Human Disease: From Basic Research to Clinical Application. *Pharmacol Res* (2017) 115:56–64. doi: 10.1016/j.phrs.2016.11.009
199. Najlaoui F, Pigeon P, Aroui S, Pezet M, Sancey L, Marrakchi N, et al. Anticancer Properties of Lipid and Poly(ε-Caprolactone) Nanocapsules Loaded With Ferrocenyl-Tamoxifen Derivatives. *J Pharm Pharmacol* (2018) 70(11):1474–84. doi: 10.1111/jphp.12998
200. Trujillo-Alonso V, Pratt EC, Zong H, Lara-Martinez A, Kaittanis C, Rabie MO, et al. FDA-Approved Ferumoxytol Displays Anti-Leukaemia Efficacy Against Cells With Low Ferroportin Levels. *Nat Nanotechnol* (2019) 14 (6):616–22. doi: 10.1038/s41565-019-0406-1
201. Ma Y, Chapman J, Levine M, Polireddy K, Drisko J, Chen Q. High-Dose Parenteral Ascorbate Enhanced Chemosensitivity of Ovarian Cancer and Reduced Toxicity of Chemotherapy. *Sci Trans Med* (2014) 6(222):222ra18. doi: 10.1126/scitranslmed.3007154
202. Welsh JL, Wagner BA, van't Erve TJ, Zehr PS, Berg DJ, Halfdanarson TR, et al. Pharmacological Ascorbate With Gemcitabine for the Control of Metastatic and Node-Positive Pancreatic Cancer (PACMAN): Results From a Phase I Clinical Trial. *Cancer Chemother Pharmacol* (2013) 71 (3):765–75. doi: 10.1007/s00280-013-2070-8
203. Schoenfeld JD, Sibenaller ZA, Mapuskar KA, Wagner BA, Cramer-Morales KL, Furqan M, et al. O(2)(·-) and H(2)O(2)-Mediated Disruption of Fe Metabolism Causes the Differential Susceptibility of NSCLC and GBM Cancer Cells to Pharmacological Ascorbate. *Cancer Cell* (2017) 32(2):268. doi: 10.1016/j.ccell.2017.07.008
204. Allen BG, Bodeker KL, Smith MC, Monga V, Sandhu S, Hohl R, et al. First-In-Human Phase I Clinical Trial of Pharmacologic Ascorbate Combined With Radiation and Temozolomide for Newly Diagnosed Glioblastoma. *Clin Cancer Res* (2019) 25(22):6590–7. doi: 10.1158/1078-0432.CCR-19-0594
205. Torti SV, Torti FM. Iron and Cancer: 2020 Vision. *Cancer Res* (2020) 80 (24):5435–48. doi: 10.1158/0008-5472.CAN-20-2017
206. Mai TT, Hamaï A, Hienzsch A, Cañeque T, Müller S, Wicinski J, et al. Salinomycin Kills Cancer Stem Cells by Sequestering Iron in Lysosomes. *Nat Chem* (2017) 9(10):1025–33. doi: 10.1038/nchem.2778
207. Liu W, Lin Q, Fu Y, Huang S, Guo C, Li L, et al. Target Delivering Paclitaxel by Ferritin Heavy Chain Nanocages for Glioma Treatment. *J Controlled Release* (2020) 323:191–202. doi: 10.1016/j.jconrel.2019.12.010
208. Inoue I, Chiba M, Ito K, Okamatsu Y, Suga Y, Kitahara Y, et al. One-Step Construction of Ferritin Encapsulation Drugs for Cancer Chemotherapy. *Nanoscale* (2021) 13(3):1875–83. doi: 10.1039/D0NR04019C
209. Ni H, Qin H, Sun C, Liu Y, Ruan G, Guo Q, et al. MiR-375 Reduces the Stemness of Gastric Cancer Cells Through Triggering Ferroptosis. *Stem Cell Res Ther* (2021) 12(1):325. doi: 10.1186/s13287-021-02394-7
210. Wu M, Sun T, Xing L. Circ_0004913 Inhibits Cell Growth, Metastasis, and Glycolysis by Absorbing miR-184 to Regulate HAMP in Hepatocellular Carcinoma. *Cancer Biother Radiopharm* (2020). doi: 10.1089/cbr.2020.3779
211. Shpyleva SI, Tryndyak VP, Kovalchuk O, Starlard-Davenport A, Chekhun VF, Beland FA, et al. Role of Ferritin Alterations in Human Breast Cancer Cells. *Breast Cancer Res Treat* (2011) 126(1):63–71. doi: 10.1007/s10549-010-0849-4
212. Lui GY, Kovacevic Z, Richardson V, Merlot AM, Kalinowski DS, Richardson DR. Targeting Cancer by Binding Iron: Dissecting Cellular Signaling Pathways. *Oncotarget* (2015) 6(22):18748–79. doi: 10.18632/oncotarget.4349
213. Steinbrueck A, Sedgwick AC, Brewster JT2nd, Yan KC, Shang Y, Knoll DM, et al. Transition Metal Chelators, Pro-Chelators, and Ionophores as Small Molecule Cancer Chemotherapeutic Agents. *Chem Soc Rev* (2020) 49 (12):3726–47. doi: 10.1039/C9CS00373H
214. Dreicer R, Kemp JD, Stegink LD, Cardillo T, Davis CS, Forest PK, et al. A Phase II Trial of Deferoxamine in Patients With Hormone-Refractory Metastatic Prostate Cancer. *Cancer Invest* (1997) 15(4):311–7. doi: 10.3109/07357909709039731
215. Blatt J. Deferoxamine in Children With Recurrent Neuroblastoma. *Anticancer Res* (1994) 14(5b):2109–12.

216. Kunos CA, Ivy SP. Triapine Radiochemotherapy in Advanced Stage Cervical Cancer. *Front Oncol* (2018) 8:149. doi: 10.3389/fonc.2018.00149
217. Merlot AM, Kalinowski DS, Kovacevic Z, Jansson PJ, Sahni S, Huang ML, et al. Exploiting Cancer Metal Metabolism Using Anti-Cancer Metal-Binding Agents. *Curr Med Chem* (2019) 26(2):302–22. doi: 10.2174/0929867324666170705120809
218. Knox JJ, Hotte SJ, Kollmannsberger C, Winquist E, Fisher B, Eisenhauer EA. Phase II Study of Triapine in Patients With Metastatic Renal Cell Carcinoma: A Trial of the National Cancer Institute of Canada Clinical Trials Group (NCIC IND.161). *Invest New Drugs* (2007) 25(5):471–7. doi: 10.1007/s10637-007-9044-9
219. Nutting CM, van Herpen CM, Miah AB, Bhide SA, Machiels JP, Buter J, et al. Phase II Study of 3-AP Triapine in Patients With Recurrent or Metastatic Head and Neck Squamous Cell Carcinoma. *Ann Oncol* (2009) 20(7):1275–9. doi: 10.1093/annonc/mdn775
220. Prill S, Rebstock J, Tennemann A, Körfer J, Sönnichsen R, Thieme R, et al. Tumor-Associated Macrophages and Individual Chemo-Susceptibility Are Influenced by Iron Chelation in Human Slice Cultures of Gastric Cancer. *Oncotarget* (2019) 10(46):4731–42. doi: 10.18632/oncotarget.27089
221. Schnetz M, Meier JK, Rehwald C, Mertens C, Urbschat A, Tomat E, et al. The Disturbed Iron Phenotype of Tumor Cells and Macrophages in Renal Cell Carcinoma Influences Tumor Growth. *Cancers* (2020) 12(3):530. doi: 10.3390/cancers12030530
222. Minden MD, Hogge DE, Weir SJ, Kasper J, Webster DA, Patton L, et al. Oral Ciclopirox Olamine Displays Biological Activity in a Phase I Study in Patients With Advanced Hematologic Malignancies. *Am J Hematol* (2014) 89(4):363–8. doi: 10.1002/ajh.23640
223. Neufeld EJ, Galanello R, Viprakasit V, Aydinok Y, Piga A, Harmatz P, et al. A Phase 2 Study of the Safety, Tolerability, and Pharmacodynamics of FBS0701, A Novel Oral Iron Chelator, in Transfusional Iron Overload. *Blood* (2012) 119(14):3263–8. doi: 10.1182/blood-2011-10-386268
224. Donfrancesco A, Deb G, Angioni A, Maurizio C, Cozza R, Jenkner A, et al. D-CECaT: A Breakthrough for Patients With Neuroblastoma. *Anti-Cancer Drugs* (1993) 4(3):317–21. doi: 10.1097/00001813-199306000-00004
225. Shinoda S, Kaino S, Amano S, Harima H, Matsumoto T, Fujisawa K, et al. Deferasirox, an Oral Iron Chelator, With Gemcitabine Synergistically Inhibits Pancreatic Cancer Cell Growth *In Vitro* and *In Vivo*. *Oncotarget* (2018) 9(47):28434–44. doi: 10.18632/oncotarget.25421
226. Zeidner JF, Karp JE, Blackford AL, Smith BD, Gojo I, Gore SD, et al. A Phase II Trial of Sequential Ribonucleotide Reductase Inhibition in Aggressive Myeloproliferative Neoplasms. *Haematologica* (2014) 99(4):672–8. doi: 10.3324/haematol.2013.097246
227. Straus DJ. Gallium Nitrate in the Treatment of Lymphoma. *Semin Oncol* (2003) 30(2 Suppl 5):25–33. doi: 10.1016/S0093-7754(03)00173-8
228. Einhorn L. Gallium Nitrate in the Treatment of Bladder Cancer. *Semin Oncol* (2003) 30(2 Suppl 5):34–41. doi: 10.1016/S0093-7754(03)00174-X
229. Chitambar CR. Gallium Nitrate for the Treatment of Non-Hodgkin's Lymphoma. *Expert Opin Invest Drugs* (2004) 13(5):531–41. doi: 10.1517/13543784.13.5.531
230. Timerbaev AR. Advances in Developing Tris(8-Quinolinolato)Gallium(Iii) as an Anticancer Drug: Critical Appraisal and Prospects. *Metallomics Integr Biometal Sci* (2009) 1(3):193–8. doi: 10.1039/b902861g
231. Timmers P, Wilson JF, Joshi PK, Deelen J. Multivariate Genomic Scan Implicates Novel Loci and Haem Metabolism in Human Ageing. *Nat Commun* (2020) 11(1):3570. doi: 10.1038/s41467-020-17312-3
232. Lang X, Green MD, Wang W, Yu J, Choi JE, Jiang L, et al. Radiotherapy and Immunotherapy Promote Tumoral Lipid Oxidation and Ferroptosis *via* Synergistic Repression of SLC7A11. *Cancer Discov* (2019) 9(12):1673–85. doi: 10.1158/2159-8290.CD-19-0338
233. Shi Z, Zhang L, Zheng J, Sun H, Shao C. Ferroptosis: Biochemistry and Biology in Cancers. *Front Oncol* (2021) 11:579286. doi: 10.3389/fonc.2021.579286
234. Yang Y, Li X, Wang T, Guo Q, Xi T, Zheng L. Emerging Agents That Target Signaling Pathways in Cancer Stem Cells. *J Hematol Oncol* (2020) 13(1):60. doi: 10.1186/s13045-020-00901-6
235. Zhang X, Xing X, Liu H, Feng J, Tian M, Chang S, et al. Ionizing Radiation Induces Ferroptosis in Granulocyte-Macrophage Hematopoietic Progenitor Cells of Murine Bone Marrow. *Int J Radiat Biol* (2020) 96(5):584–95. doi: 10.1080/09553002.2020.1708993
236. Lei G, Zhang Y, Koppula P, Liu X, Zhang J, Lin SH, et al. The Role of Ferroptosis in Ionizing Radiation-Induced Cell Death and Tumor Suppression. *Cell Res* (2020) 30(2):146–62. doi: 10.1038/s41422-019-0263-3

Conflict of Interest: The authors declare that the research was conducted in the absence of any commercial or financial relationships that could be construed as a potential conflict of interest.

frontiers in Cell and Developmental Biology

ORIGINAL RESEARCH
published: 25 November 2021
doi: 10.3389/fcell.2021.709180

Development and Validation of a Robust Ferroptosis-Related Gene Panel for Breast Cancer Disease-Specific Survival

Pei Li[1,2†], *Benlong Yang*[1,2†], *Bingqiu Xiu*[1,2], *Yayun Chi*[1,2], *Jingyan Xue*[1,2*] *and Jiong Wu*[1,2,3*]

[1]*Department of Breast Surgery, Fudan University Shanghai Cancer Center, Shanghai, China,* [2]*Department of Breast Surgery, Key Laboratory of Breast Cancer in Shanghai, Fudan University Shanghai Cancer Center, Shanghai, China,* [3]*Collaborative Innovation Center for Cancer Medicine, Shanghai, China*

OPEN ACCESS

Edited by:
Maryam Mehrpour,
Université Paris Descartes, France

Reviewed by:
Binghao Zhao,
Peking Union Medical College Hospital (CAMS), China
Yi Jin,
Central South University, China

****Correspondence:***
Jingyan Xue
xuejy@163.com
Jiong Wu
wujiong1122@vip.sina.com

[†]These authors have contributed equally to this work and share first authorship

Specialty section:
This article was submitted to Molecular and Cellular Oncology, a section of the journal Frontiers in Cell and Developmental Biology

Received: *13 May 2021*
Accepted: *02 November 2021*
Published: *25 November 2021*

Citation:
Li P, Yang B, Xiu B, Chi Y, Xue J and Wu J (2021) Development and Validation of a Robust Ferroptosis-Related Gene Panel for Breast Cancer Disease-Specific Survival. Front. Cell Dev. Biol. 9:709180. doi: 10.3389/fcell.2021.709180

Background: New biomarker combinations have been increasingly developed to improve the precision of current diagnostic and therapeutic modalities. Recently, researchers have found that tumor cells are more vulnerable to ferroptosis. Furthermore, ferroptosis-related genes (FRG) are promising therapeutic targets in breast cancer patients. Therefore, this study aimed to identify FRG that could predict disease-specific survival (DSS) in breast cancer patients.

Methods: Gene expression matrix and clinical data were downloaded from public databases. We included 960, 1,900, and 234 patients from the TCGA, METABRIC, and GSE3494 cohorts, respectively. Data for FRG were downloaded from the FerrDb website. Differential expression of FRG was analyzed by comparing the tumors with adjacent normal tissues. Univariate Cox analysis of DSS was performed to identify prognostic FRG. The TCGA-BRCA cohort was used to generate a nine-gene panel with the LASSO cox regression. The METABRIC and GSE3494 cohorts were used to validate the panel. The panel's median cut-off value was used to divide the patients into high- or low-risk subgroups. Analyses of immune microenvironment, functional pathways, and clinical correlation were conducted *via* GO and KEGG analyses to determine the differences between the two subgroups.

Results: The DSS of the low-risk subgroup was longer than that of the high-risk subgroup. The panel's predictive ability was confirmed by ROC curves (TCGA cohort AUC values were 0.806, 0.695, and 0.669 for 2, 3, and 5 years respectively, and the METABRIC cohort AUC values were 0.706, 0.734, and 0.7, respectively for the same periods). The panel was an independent DSS prognostic indicator in the Cox regression analyses. (TCGA cohort: HR = 3.51, 95% CI = 1.792–6.875, $p < 0.001$; METABRIC cohort: HR = 1.76, 95% CI = 1.283–2.413, $p < 0.001$). Immune-related pathways were enriched in the high-risk subgroup. The two subgroups that were stratified by the nine-gene panel were also associated with histology type, tumor grade, TNM stage, and Her2-positive and TNBC subtypes. The patients in the high-risk subgroup, whose CTLA4 and PD-1 statuses were both positive or negative, demonstrated a substantial clinical benefit from combination therapy with anti-CTLA4 and anti-PD-1.

Conclusion: The new gene panel consisting of nine FRG may be used to assess the prognosis and immune status of patients with breast cancer. A precise therapeutic approach can also be possible with risk stratification.

Keywords: breast cancer, ferroptosis, prognosis model, immune status, disease-specific survival

INTRODUCTION

Breast cancer (BRCA) has entered the era of precision treatment at the molecular level. The molecular hallmarks of BRCA, including ER, PR, HER2, Ki-67, and PD-1, and PD-L1, have been employed for personalized and individualized treatment (Harbeck et al., 2019; Waks and Winer, 2019). For instance, the endocrine therapy, HER2 targeted therapy, and immune checkpoint therapy are employed for ER/PR-positive, Her2-positive, and PD-1/PD-L1-positive BRCA tumors, respectively[2].

Since the advancement of microarray and high-throughput sequencing, multi-gene prediction, such as the PAM50 signature (Cheang et al., 2015), 70-gene assay, and 21-gene recurrence score[2], has been widely used to guide decision making in the therapeutic approach for various BRCA subtypes. Multi-gene prediction has been commonly used to predict the benefits of chemotherapy or to estimate patient's prognosis. Thus, new biomarker combinations have been developed to improve the precision of current diagnostic and therapeutic modalities. Currently, researchers are looking for new therapeutic targets and biomarkers for BRCA treatment. Moreover, there is still an insurmountable therapeutic challenge for triple negative breast cancer (TNBC) because therapeutic targets and biomarkers have not yet been identified. A few previous studies found that several ferroptosis-related genes (FRG) could be promising therapeutic targets in BRCA (Hangauer et al., 2017; Zhang et al., 2019), especially for the TNBC subtype (Chen et al., 2017; Zhu et al., 2020; Ding et al., 2021; Zhang et al., 2021). Therefore, it is necessary to develop a panel involving FRG biomarkers for risk stratification and identification of new targets.

Ferroptosis refers to cell death resulting from iron-mediated lipid peroxidation and is characterized by intracellular accumulation of reactive oxygen species (ROS) (**Supplementary Figure S3**) (Dixon et al., 2012). According to preliminary data, ferroptosis inhibits tumor development and proliferation; hence, ferroptosis can be targeted for cancer therapy (Stockwell et al., 2017). Correspondingly, researchers have increasingly focused on the role of ferroptosis in BRCA, especially in TNBC and Her2-positive BRCA. Due to the high recurrence and metastatic rate, TNBC and Her2-positive BRCA have been regarded as refractory and aggressive BRCA subtypes (Foulkes et al., 2010; Cesca et al., 2020). Ma et al. (Dixon et al., 2012) found that siramesine and lapatinib induced ferroptosis more than other canonical ferroptotic reagents did, implying that lapatinib participated in modulating ferroptosis without targeting EGFR and HER2 (Ma et al., 2016). Moreover, a recent study discovered that neoadjuvant neratinib induced ferroptosis and prevented brain metastasis in Her2-positive BRCA (Nagpal et al., 2019). Furthermore, several studies reported that ferroptosis could be a useful therapeutic target in the treatment of TNBC (Chen et al., 2017; Zhu et al., 2020; Ding et al., 2021; Zhang et al., 2021). It has been found that through the stimulated GCN2-eIF2-ATF4 pathway, CHAC1 degradation of GSH increases cystine-starvation-induced ferroptosis in TNBC cells (Chen et al., 2017). The anti-TNBC impact of DMOCPTL was demonstrated in a cell death method test by triggering ferroptosis *via* GPX4 ubiquitination (Ding et al., 2021). Chen et al. found that treatment of TNBC cells with holo-Lf increased total iron concentration, boosted ROS production, increased the lipid peroxidation end product malondialdehyde, and improved ferroptosis (Zhang et al., 2021). In addition, chemotherapy, radiotherapy, and immunotherapy were all influenced by ferroptosis; thus, targeting both ferroptosis and the identified biomarkers could be an effective treatment strategy for BRCA (Chen et al., 2021).

The aim of this research was to develop a panel consisting of FRG that could be used to predict the disease-specific survival (DSS) of patients with BRCA and to develop a risk stratification system that could aid diagnosis and provide novel therapeutic strategies.

MATERIALS AND METHODS

An overview of our methodology is summarized in **Figure 1**.

Acquisition of the Gene, miRNA, and Genome Mutation Data; FRG; and Clinical Data

On January 30, 2021, 1,068 patients with BRCA were identified. Their gene, miRNA, genome mutation data (containing somatic mutations and copy number variations (CNV)), and clinical information were downloaded from the TCGA website. On the same day, the gene expression matrix and clinical data of 1,906 patients with BRCA were downloaded from the cBioPortal website. The patients whose data were obtained from both websites were the same patients involved in the Molecular Taxonomy of BRCA International Consortium (METABRIC) project. Since the data from both websites were open to the public, this study was exempted from obtaining the approval of the local ethics committee. The GSE3494 dataset were downloaded from the Gene Expression Omnibus (GEO) database. The current study adhered to the TCGA, METABRIC, and GEO data access and publishing policies. The exclusion criteria were as follows: male sex, incomplete clinical and gene expression data, and less than 30 days of DSS follow-up. Finally, we included 960, 1,900, and 234 patients from the TCGA, METABRIC, and GSE3494 cohorts, respectively. The baseline features of the three cohorts are presented in **Table 1**.

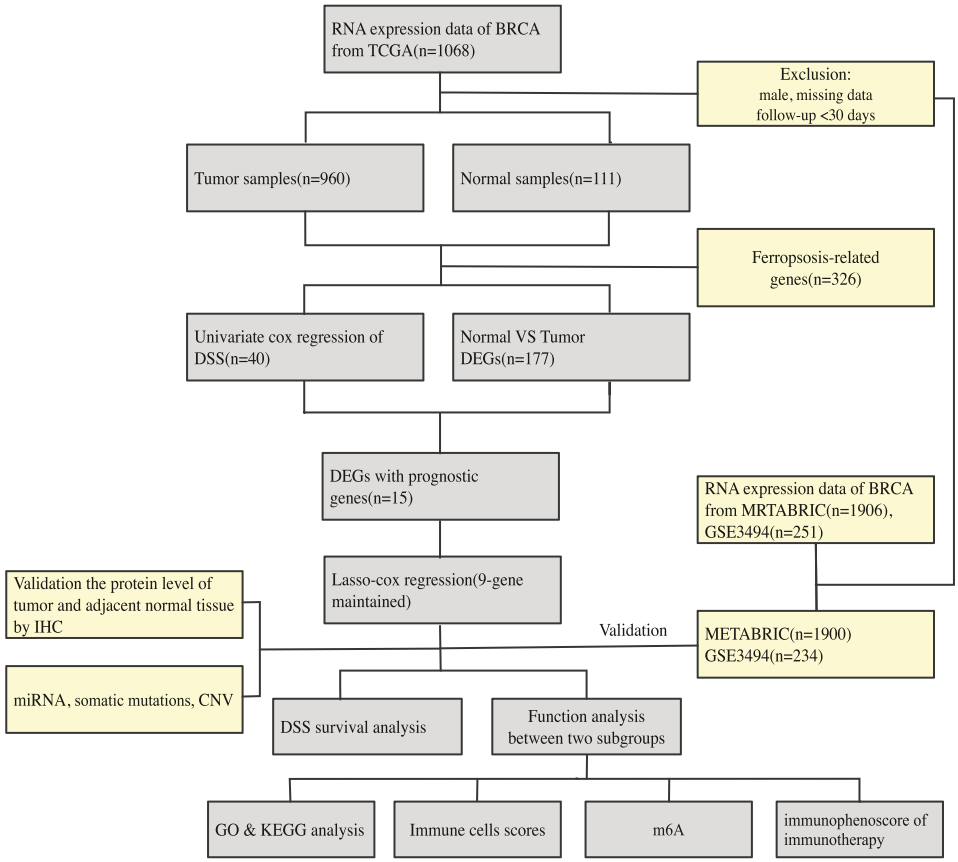

FIGURE 1 | An overview of our methodology is summarized.

The list of FRG was downloaded from the FerrDb website. The website divided FRG into three categories: drivers, which stimulate ferroptosis, suppressors, which prevent ferroptosis, and biomarkers, which reveal the presence of ferroptosis (Zhou and FerrDb, 2020). We reviewed the existing literature to identify these genes, and we subsequently ruled out unrelated genes and added newly discovered genes that were related to this study. The immunohistochemistry (IHC) image data of prognostic ferroptotic proteins were downloaded from the Human Protein Atlas (HPA) database.

Identification of Differentially Expressed and Prognostic Genes

Running the "Limma" R package, the TCGA cohort was used to identify differently expressed FRG by comparing the expression levels in tumor and adjacent normal tissues (log FC > 0.5, FDR <0.05). We subsequently used univariate Cox analysis of DSS to identify prognostic FRG. For survival outcomes, DSS event was defined as death due to BRCA, while no event was defined as death due to causes other than BRCA or a living status. The intersect gene set was identified as the FRG that were both differentially expressed and prognostic. The LASSO process was used to pick and shrink the important variables in the regression panel by running the "glmnet" R package (Tibshirani, 1997; Wang and Liu, 2020). The DSS statuses of the TCGA cohort patients were the response variables in the regression, with the matrix of the intersect gene set as the independent variable. The panel's penalty parameter was calculated using the cross validation, which was multiplied by ten, and the optimal parameter was the λ value that corresponded to the lowest deviation. The patients' risk scores were calculated using each of the selected gene expressing values, which were multiplied by their coefficients. The formula was as follows:

$$\begin{aligned} &the\ risk\ score\ formula \\ &\quad = coefficients * expressing\ values\ of\ A\ gene + coefficients \\ &\quad * expressing\ values\ of\ B\ gene \ldots \ldots + \end{aligned}$$

The patients were classified into the high- or low-risk subgroups according to the median cut-off value of the developed panel. PCA and t-SNE were used to investigate the distribution of the two subgroups by running the "Rtsne" R package. The optimal cut-off expressing values for each gene were determined by running the "survminer" R package. The "ggalluvial" R package was used to portray the Sankey map. The predictive ability of the developed panel was determined by time-dependent receiver operating characteristic (ROC) curves by running the R "timeROC" package. The area under curve (AUC) of the ROC curve was determined to show the sensitivity and specificity of the panel in providing a

TABLE 1 | The baseline features of the TCGA, METABRIC and GSE3494 cohorts.

Characteristics	TCGA	METABRIC	GSE3494
Number	**n = 960**	**n = 1900**	**n = 234**
Age(average)	58	61.1	62.7
Race(%)			
White	666 (69.4)		—
Black	168 (17.5)	—	-
Asian and other	52 (5.4)	—	—
NA	74 (7.7)	—	—
Tumor grade(%)			
G1	—	164 (8.6)	62 (2.5)
G2	—	740 (38.9)	120 (51.3)
G3	—	925 (48.7)	50 (21.4)
NA	—	71 (3.7)	2 (0.9)
Histological type(%)			
IDC	704 (73.3)	1450 (76.3)	—
ILC	191 (19.9)	142 (7.5)	—
Other	65 (6.8)	308 (16.2)	
Menopause status(%)			
Pre	209 (21.8)	411 (21.6)	—
Post	616 (64.2)	1489 (78.4)	—
Peri	37 (3.9)	—	—
NA	98 (10.2)	—	—
ER status (%)			
Positive	716 (74.6)	1457 (76.7)	200 (87)
Negative		443 (23.3)	30 (13)
NA	41 (4.3)		—
PR status (%)			
Positive	624 (65)	1007 (53)	178 (76.1)
Negative		893 (47)	56 (23.9)
NA	43 (4.5)	0	—
HER2 status (%)			
Positive	169 (17.6)	236 (12.4)	—
Negative	672 (70)	1667 (87.7)	—
NA	122 (12.7)	0	—
Molecular subtype			
HR+/Her2-	535 (56)	1378 (73)	—
HR+/Her2+	132 (14)	104 (5)	—
HR-/Her2+	33 (3)	132 (7)	—
TNBC	135 (14)	299 (16)	—
NA	125 (13)	—	—
TNM stage(%)			
0	—	4 (0.2)	—
I	166 (17.3)	473 (24.9)	—
II	545 (56.8)	800 (42.1)	—
III	211 (22)	115 (6.1)	—
IV	18 (1.9)	9 (0.5)	—
NA	20 (2.1)	499 (26.3)	—
follow up state(%)			
alive	883 (92)	1279 (67.3)	180 (76.9)
dead	77 (8)	621 (32.7)	54 (23.1)
DSS years (median)	2.5	9.5	10.2

IDC: invasive ductal carcinoma, ILC: invasive lobular carcinoma.

prognostic efficiency, which varied from 0.5–1. Values that were closer to 1 indicated a good prognostic ability.

To establish the miRNA-FRG regulatory network in BRCA. We put the FRG into the starBase database to identify potential miRNAs (Li et al., 2013). We then conducted an analysis in TCGA-BRCA and adjacent normal tissue to identify the different miRNAs. In addition, we sought candidate miRNAs that were only shared by the two databases to enhance the veracity of the prediction. Finally, the network was visualized using Cytoscape. (**Supplementary Figure S2**).

The "maftools" and "Rcircos" R packages were used for somatic mutations identification and CNV, respectively.

We looked for publications on m6A methylation regulators in the literature and found 23 of them, with 8 writers (METTL3, METTL14, METTL16, RBM15, RBM15B, WTAP, ZC3H13, VIRMA), 2 erasers (FTO and ALKBH5), and 13 readers (YTHDC1, YTHDC2, YTHDF1, YTHDF3, HNRNPC, FMR1, IGFBP3, RBMX, IGFBP1, YTHDF2, HNRNPA2B1, LRPPRC, and KIAA1429).

Function Enrichment Analysis, single-sample Gene Set Enrichment Analysis (ssGSEA), and immunophenoscore (IPS)

Based on the differentially expressed genes between the two stratified subgroups, Gene Ontology (GO) and Kyoto Encyclopedia of Genes and Genomes (KEGG) analyses were performed by running.

the "clusterProfiler" R package. Differentially expressed genes between the high- and low-risk subgroups were identified (| log2FC| > 1, FDR <0.05). The Benjamini-Hochberg (BH) method was used to adjust the p values.

The "GSVA" R package was used to measure the infiltrating score of 16 immune cells and the activity of 13 immune-related pathways with ssGSEA (Rooney et al., 2015). The Wilcoxon test was also used to look at intergroup variations in putative immunological checkpoints, such as PD-L1, PD-1, and CTLA4. Furthermore, to predict the efficacy of immunotherapy, we downloaded an IPS file of immune checkpoint inhibitors (ICIs) from the Cancer Immunome database; the IPS is a good predictor for responsiveness to CTLA4 and PD-1, and predicts the intergroup differences in response to immunotherapy using CTLA4 and PD-1 blockers (Charoentong et al., 2017).

Statistical Analyses

The gene matrix of tumor and adjacent normal tissues was compared using the Student's t-test. The X^2 test was used to compare the proportional differences. The ssGSEA scores of immune cells or pathways were compared between the high- and low-risk subgroups using the Mann-Whitney test with p values that were adjusted by the BH method. The log-rank test was used to compare the DSS of different subgroups using the Kaplan-Meier analysis. The univariate and multivariate Cox regression tests were used to identify independent predictors of DSS. The R program (version 3.6.3) or Statistical Package for the Social Sciences (SPSS), version 20 was used for all statistical analyses. A p value of less than 0.05 was deemed statistically significant, unless otherwise stated, and all p values were two-tailed.

RESULTS

Identification of 177 Differentially Expressed FRG and 40 DSS Prognostic FRG

There were 177 FRG, which were differentially expressed between the tumor and adjacent normal tissues (all FDR <0.05, log FC > 0.5,

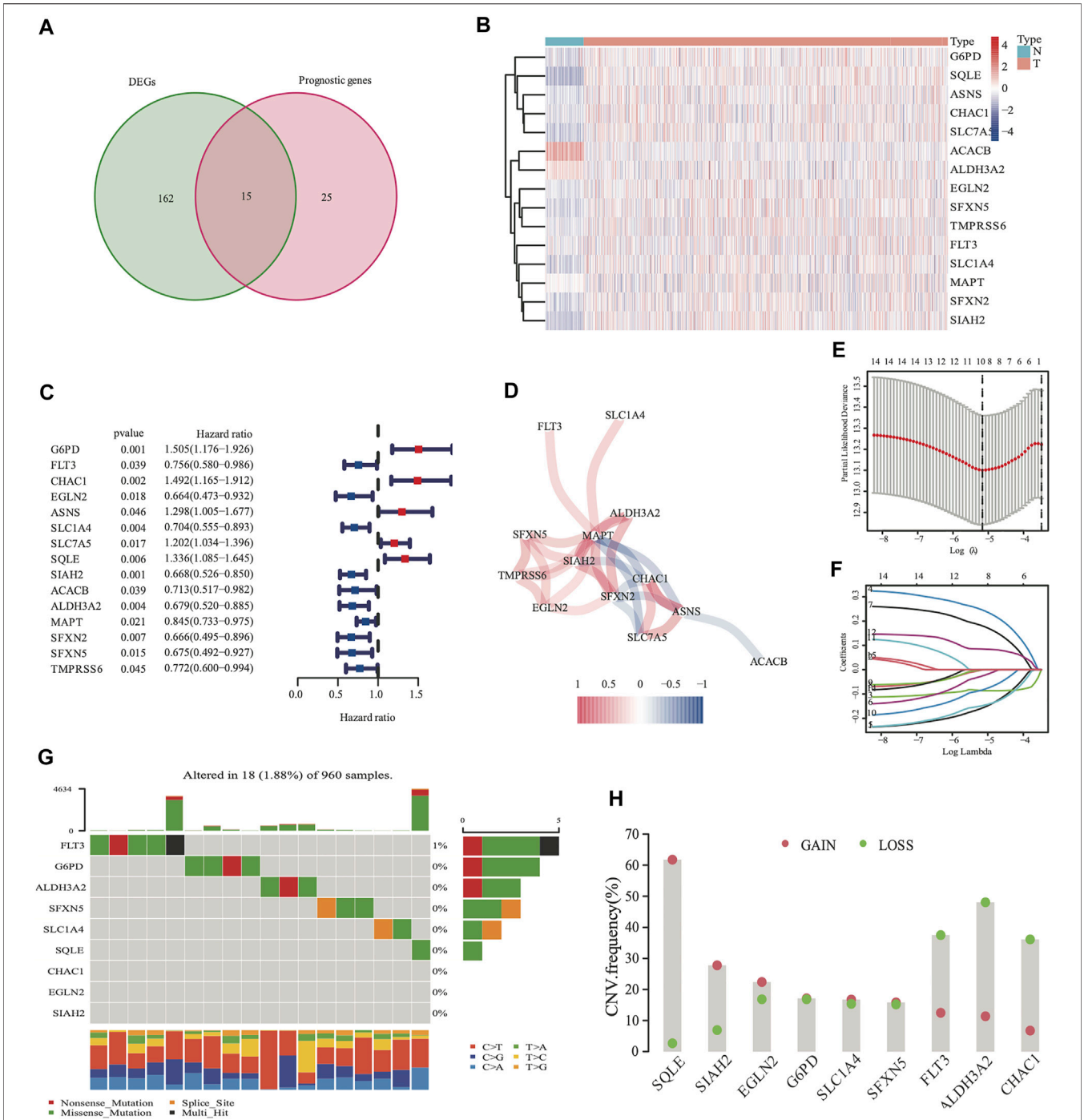

FIGURE 2 | Identification of 177 differentially expressed genes (DEGs) and 40 DSS prognostic FRG. A venn diagram was used to identify overlapping genes **(A)**. Heatmap showed that 15 FRG were differentially expressed in breast cancer tissues and non-cancer tissues **(B)** Forest plots demonstrated the hazard ratio of the univariate cox analyses in DSS **(C)**. The correlation link of the selected genes in TCGA cohort **(D)**. Lasso regression analysis reduced variable **(E, F)**. Somatic mutations on a query of FRG from TCGA cohort **(G)** The CNV frequency of FRG from the TCGA cohort **(H)**, red dots represent CNV amplification, while green dots represent CNV deletion.

Figure 2A). In addition, there were 40 FRG, which were associated with DSS (**Figure 2A**) in the univariate Cox regression study. Moreover, 15 genes were maintained in the intersection of the 177 differentially expressed and 40 prognostic FRG genes. Most of them were upregulated, except for the following genes: *ACACB* and *ALDH3A2* (**Figure 2B**). *CHAC1, SIAH2, MAPT, SFXN2*, and *ASNS* were identified to be the hub genes in the interaction network among these genes. **Figure 2D** shows the relationship among these genes.

TABLE 2 | Clinical features in different risk subgroups.

Characteristics	TCGA-BRCA			METABRIC-BRCA			GSE3494-BRCA		
	High risk	Low risk	*p* Value	High risk	Low risk	*p* Value	High risk	Low risk	*p* Value
number(%)	960			1900			234		
	480 (50)	480 (50)		1252 (65.9)	648 (34.1)		70 (30)	164 (70)	
Age (%)			0.003			<0.001			0.309
<60y	283 (29.5)	237 (24.7)		598 (31.5)	241 (12.7)		31 (13.2)	61 (26.1)	
≥60y	197 (20.5)	243 (25.3)		654 (34.4)	407 (21.4)		39 (16.7)	103 (44)	
Race(%)			<0.001						
White	289 (30.1)	377 (39.3)	—	—	—		—	—	
Black	117 (12.2)	51 (5.3)		—			—	—	
Asian and other	36 (3.7)	16 (1.7)		—	—		—	—	
NA	38 (4)	36 (3.8)		—	—		—	—	
Tumor grade(%)			—			<0.001			<0.001
G1	—	—		54 (2.8)	110 (5.8)		7 (3)	55 (23.5)	
G2	—	—		370 (19.5)	370 (19.5)		28 (12)	92 (39.3)	
G3	—	—		788 (41.5)	137 (7.2)		35 (15)	15 (6.4)	
NA	—	—		40 (2.1)	31 (1.6)		—	2 (0.9)	
Histological type(%)			<0.001			<0.001			
IDC	430 (44.8)	274 (28.5)		1028 (54.1)	422 (22.2)		—	—	
ILC	28 (2.9)	163 (16.9)		64 (3.4)	78 (4.1)		—	—	
Other	22 (2.2)	43 (4.5)		161 (8.4)	148 (7.8)		—	—	
Menopause status(%)			0.723			<0.001			
Pre	106	103		301 (15.8)	110 (5.8)		—	—	
Post	302	314		951 (50.1)	538 (28.3)		—	—	
Peri	18	19		—	—		—	—	
NA	54	44		—	—		—	—	
ER status(%)			<0.001			<0.001			<0.001
Positive	274 (28.5)	442 (46)		814 (42.8)	643 (33.8)		51 (22.2)	149 (93.1)	
Negative	188 (19.6)	15 (1.6)		438 (23.1)	5 (0.3)		19 (8.3)	11 (4.8)	
NA	18 (1.9)	23 (2.4)		—	—				
PR status(%)			<0.001	—	—	<0.001			<0.001
Positive	224 (23.3)	400 (41.7)		496 (26.1)	511 (26.9)		40 (17.1)	138 (59)	
Negative	239 (24.9)	54 (5.6)		756 (39.8)	137 (7.2)		30 (12.8)	26 (11.1)	
NA	17 (1.78)	26 (2.7)		—	—		—	—	
HER2 status(%)			<0.001	—	—	<0.001			
Positive	114 (11.9)	55 (5.7)		227 (11.9)	9 (0.5)		—	—	
Negative	306 (31.9)	366 (38.1)		1027 (54.1)	640 (33.7)		—	—	
NA	63 (6.6)	59 (6.1)					—	—	
Molecular subtype			<0.001			<0.001			
HR+/Her2-	182 (19)	353 (60)		732 (38.5)	646 (33.4)		—	—	
HR+/Her2+	77 (16)	55 (11.5)		96 (7.7)	8 (1.2)		—	—	
HR-/Her2+	33 (3.4)	0		131 (6.9)	1 (0.1)		—	—	
TNBC	123 (12.8)	12 (1.3)		295 (15.5)	4 (1.3)		—	—	
NA	65 (6.8)	60 (12.5)		—	—		—	—	
TNM stage(%)			0.045			<0.001			
0				3 (0.2)	1 (0.1)		—	—	
I	67 (7)	99 (10.3)		263 (13.8)	210 (11.1)		—	—	
II	279 (29.1)	266 (27.7)		560 (29.5)	240 (12.6)		—	—	
III	113 (11.8)	98 (10.2)		98 (5.2)	17 (0.9)		—	—	
IV	12 (1.3)	6 (0.6)		7 (0.4)	2 (0.1)		—	—	
NA	9 (0.9)	11 (1.1)		321 (16.9)	178 (9.4)		—	—	
Follow up state(%)									
Alive	428 (44.6)	455 (47.4)		776 (40,8)	503 (26.5)		48 (20.5)	132 (56.4)	
Dead	52 (5.4)	25 (2.6)		476 (25.1)	145 (7.6)		22 (9.4)	32 (13.7)	
DSS years (median)	2.4	2.5		8.7	10.6		9.9	10.4	

Development of a Prognostic Panel With the TCGA Cohort, and Analysis of Nine FRG Genome Mutations

The expression values of the 15 overlapped genes were used to create a prognostic panel with the LASSO regression analysis. The following formula was used to measure the risk score. The optimum value of λ was used to identify a nine-gene signature (**Figures 2E,F**).

$$= risk\ score = 0.181*expression\ values\ of\ (EV)SQLE + 0.247*EV\ of\ G6PD + 0.085 *EV\ of\ CHAC1 - 0.158*EV\ of\ ALDH3A2 - 0.086*EV\ of\ SIAH2 - 0.149 *EV\ of\ SLC1A4 - 0.026*EV\ of\ FLT3 - 0.001*EV\ of\ EGLN2 - 0.084 *EV\ of\ SFXN5$$

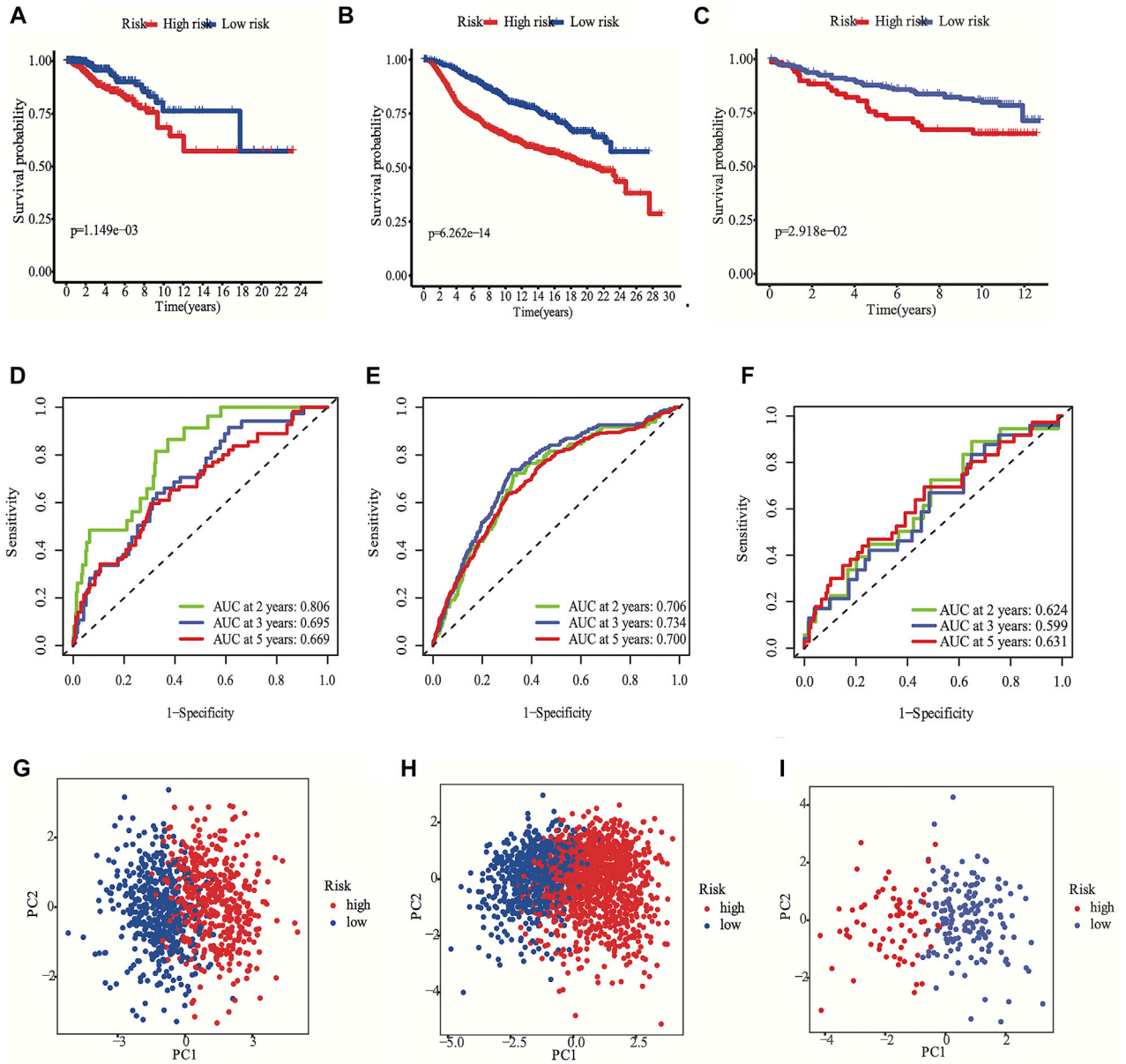

FIGURE 3 | Development the prognostic FRG panel in TCGA cohort **(A, D, G)**. Validation the prognostic FRG panel in METABRIC cohort **(B, E, H)** and GSE3494 cohort **(C, F, I)**. The Kaplan-Meier curve showed that the DSS of the high-risk subgroup was substantially shorter than that of the low-risk subgroup **(A, B, C)**. AUC time-dependent ROC curves for DSS **(D, E, F)**.

According to the median cut-off value of the nine-gene panel, patients were classified into the high- (n = 480) and low-risk (n = 480) subgroups. In the TCGA cohort, the risk score was associated with the histological type; HER2, ER, and PR statuses; TNM stage, and molecular subtype (**Table 2**). Moreover, the high-risk subgroup was positively associated with an advanced TNM stage and Her2-positive and TNBC subtypes (**Table 2**; **Figure 4C**). All of these indicators were related to an unfavorable prognosis in BRCA patients (Waks and Winer, 2019). The PCA and t-SNE showed that the patients of these two subgroups were distributed in two directions (**Figure 3G** and **Supplementary Figure S1G**). The risk score of patients were positively associated with a higher death toll (**Supplementary Figures S1A, 1D**). The Kaplan-Meier curve consistently showed that the DSS of the high-risk subgroup was substantially shorter than that of the low-risk subgroup (**Figure 3A**, p = 0.001). The DSS predictive performance of the nine-gene panel was assessed by ROC curves, and the values of the AUC were 0.806, 0.695, and 0.669 in 2, 3, and 5 years, respectively, in the TCGA cohort (**Figure 3D**). The IHC staining results also provided the levels of seven (including *G6PD, SQLE, CHAC1, ALDH3A2, SIAH2, SLC1A4*, and *SFXN5*) of nine prognostic ferroptotic proteins between

BRCA and adjacent normal tissues, consistent with the mRNA expression data (**Figure 7**).

Analysis of Nine FRG Genome Mutations and Establishing the miRNA-Nine-FRG Regulatory Network

The somatic mutations and CNV of nine FRG in breast cancer were initially summarized. Only 18 of the 960 patients (1.88%) had mutations in the nine FRG, and the mutation frequencies were zero in eight of nine except *FLT3* (1%; **Figure 2G**). We found that higher frequencies of CNV deletions were in *ALDH3A2, FLT3* and *CHAC1*; conversely, higher probabilities of CNV amplification were in *SQLE, SIAH2* and *EGLN2* (**Figure 2H**). Cytoscape showed that the network contains four hub miRNAs (hsa-miR-23a-3p, hsa-miR-378a-3p, hsa-miR-146a-5p, and hsa-miR-146b-5p). (**Supplementary Figure S2**).

Validation of the Nine-Gene Panel With the METABRIC and GSE3494 Cohorts

The METABRIC and GES3494 cohorts were used to robustly validate the nine-gene panel using the same formula as that used for the construction of the panel using the TCGA cohort. Correspondingly, the nine-gene panel was also associated with the histological type, tumor grade; HER2, ER, and PR statuses; and TNM stage (**Table 2**). Similarly, the high-risk subgroup was positively associated with a high tumor grade; an advanced TNM stage; and Her2-positive and TNBC subtypes (**Table 2**). All of the above indicators were related to an unfavorable prognosis in patients with BRCA (**Table 2**). The death toll of the high-risk subgroup was also more than that of the low-risk subgroup (**Figures 3B,C**). The PCA and t-SNE analyses also indicated that the two subgroups were spread in discrete directions, which was consistent with the findings obtained from the TCGA cohort (**Figures 3H,I** and **Supplementary Figures S1H, I**). Patients in the high-risk subgroup consistently died from the tumor much sooner than those in the low-risk subgroup (**Figures 3B,C**), as determined by the Kaplan-Meier curve. Furthermore, the AUC of the ROC curve for the nine-gene panel was 0.706 after 2 years, 0.734 after 3 years, and 0.7 after 5 years in the METABRIC and were respectively 0.624, 0.599, and 0.631 in the GSE3494 cohort (**Figures 3E,F**).

The Nine-Gene Panel has an Independent Prognostic Significance

We conducted univariate and multivariate Cox analyses to test if the nine-gene panel was an independent predictor of DSS. The univariate Cox regression analysis was conducted to reveal obvious linkages between the nine-gene panel and DSS in both the TCGA and METABRIC cohorts (TCGA cohort: HR = 3.555, 95% confidence interval [CI] = 2.253–5.611, $p < 0.001$; METABRIC cohort: HR = 2.511, 95% CI = 2.075–3.04, $p < 0.001$; **Figure 4A**). After controlling other confounding variables in the multivariate cox regression study, the nine-gene panel remained an independent indicator of DSS (TCGA cohort: HR = 3.51, 95% CI = 1.792–6.875, $p < 0.001$; METABRIC cohort: HR = 1.76, 95% CI = 1.283–2.413, $p < 0.001$) (**Figure 4B**). The panel had a high predictive accuracy for DSS and was even better than the statuses of ER, PR, HER2, tumor size, and lymph nodes. It offered a more reliable predictor of 2 years DSS in the TCGA (AUC = 0.806) and the METABRIC cohorts (AUC = 0.706) (**Figures 3D,E**). As a result, the panel had an outstanding prognostic benefit for patients with BRCA.

Functional Studies Between the Stratified Subgroups

To explore the preliminary function of the nine-gene panel, KEGG pathway enrichment and GO function analyses were performed to compare the two stratified subgroups by running the ClusterProfiler R package (adjust $p < 0.05$, $|\log FC| > 1$). The GO analysis showed that the genes were significantly enriched in immune-related functions (**Figures 5A,B**), such as humoral immune response, circulating immunoglobulin-mediated human immune response, complement activation, and classical pathways. These pathways functioned in antigen binding, immunoglobulin receptor binding, and chemokine activity. Furthermore, the KEGG analyses showed that the genes were enriched in the IL−17 signaling pathway, viral protein interaction with cytokine and cytokine receptor, and PPAR signaling pathway. IL−17 signaling transduction could regulate PD-1/PD-L1 and the infiltration of $CD8^+$ T cells in patients with BRCA (Shuai et al., 2020), while the PPAR signaling pathway is activated in patients with TNBC (Lin et al., 2021). The PPAR pathway genes from KEGG analysis differentially expressed between two subgroups. Compared with the low risk subgroup, the expression of *MMP1, FABP5, FADS2, FABP7*, and *ME1* were upregulated, *UCP1, PLIN5, ADIPOQ, PLIN4, FABP4*, and *SLC27A2* were downregulated in high risk subgroup (**Supplementary Figure S4**). Study found that activating *MMP1* expression could increases multi-drug resistance in breast cancer (Shen et al., 2017). The *FADS2* activity associated with the aromatase drug letrozole in breast cancer cells (Park et al., 2021). The GO and KEGG analyses both showed that all pathways were immune-related.

Analysis of Immune Cell Enrichment

ssGSEA was used to quantify the scores of various immune cell subpopulations that corresponded to functions and pathways to further investigate the relationship between the nine-gene panel and immune status. Our findings revealed that the types of immune cells were significantly different between the two subgroups (**Figures 6A,B**). The high-risk subgroup had a significantly higher score than did the low-risk subgroup for most immune cells, including aDCs, $CD8^+$ T, B, dendritic cells, natural killer cells, macrophages, plasmacytoid dendritic cells, T helper, Tfh, Th1 cells, Th2, TIL, and Treg cells, except for the score of mast cells, which was lower (**Figures 6A,B**). Furthermore, the high-risk subgroup had significantly higher scores for immune functions than did the low-risk subgroup. The immune functions were the check point, type I interferon response, T cell co-stimulation/inhibition, major histocompatibility class I, inflammation promotion, HLA,

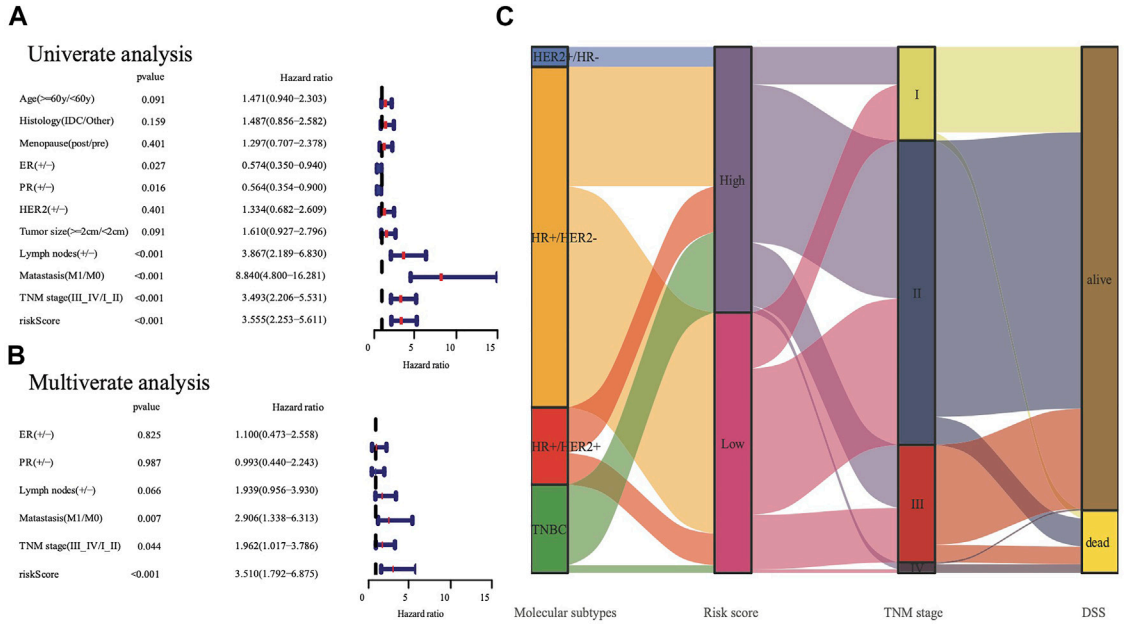

FIGURE 4 | The analysis nine gene panel of FRG based on TCGA. The hazard ratio of univariate and multivariate Cox regression analysis **(A,B)**, (+/ -) means (positive/negative). A Sankey map demonstrated the relationship between FRG risk score and molecular subtypes **(C)**.

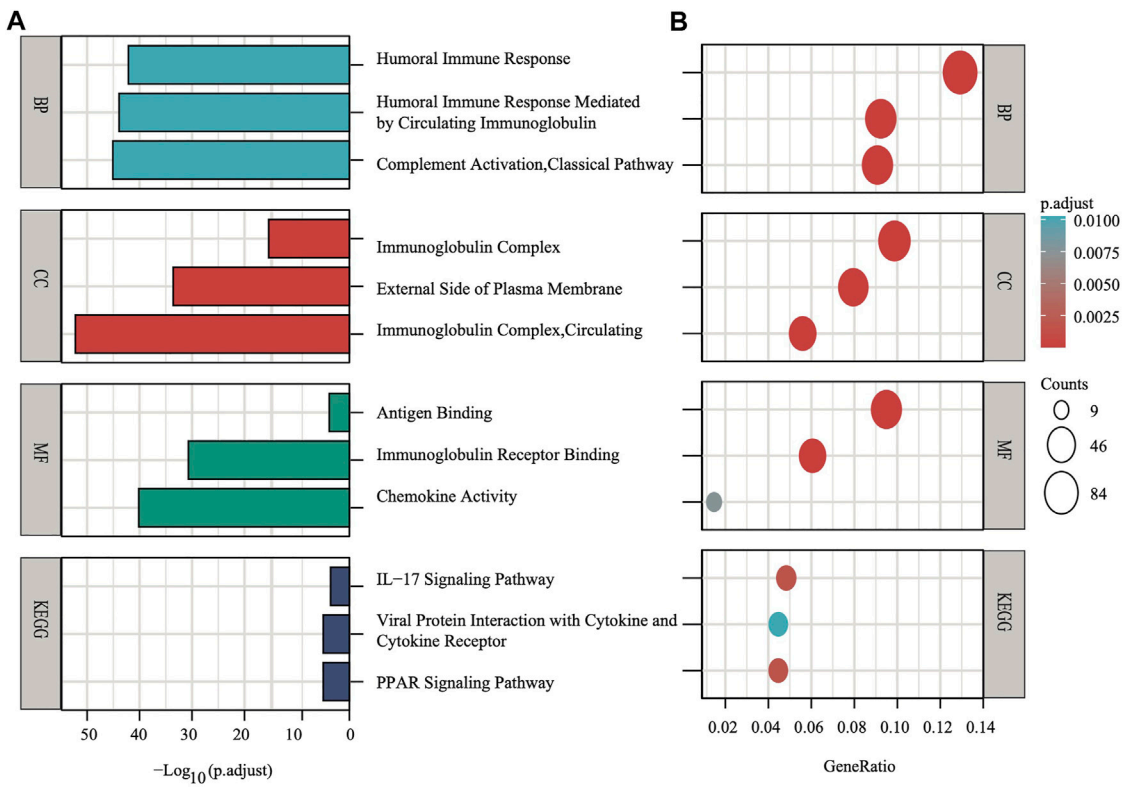

FIGURE 5 | The *X*-axis depicts adjust *p* values, whereas the *Y*-axis depicts the enriched mechanism or pathway **(A)**. The *X*-axis depicts the gene ratio in the overall number of differential expression genes between two subgroups, whereas the *Y*-axis depicts the enriched mechanism or pathway **(B)**.

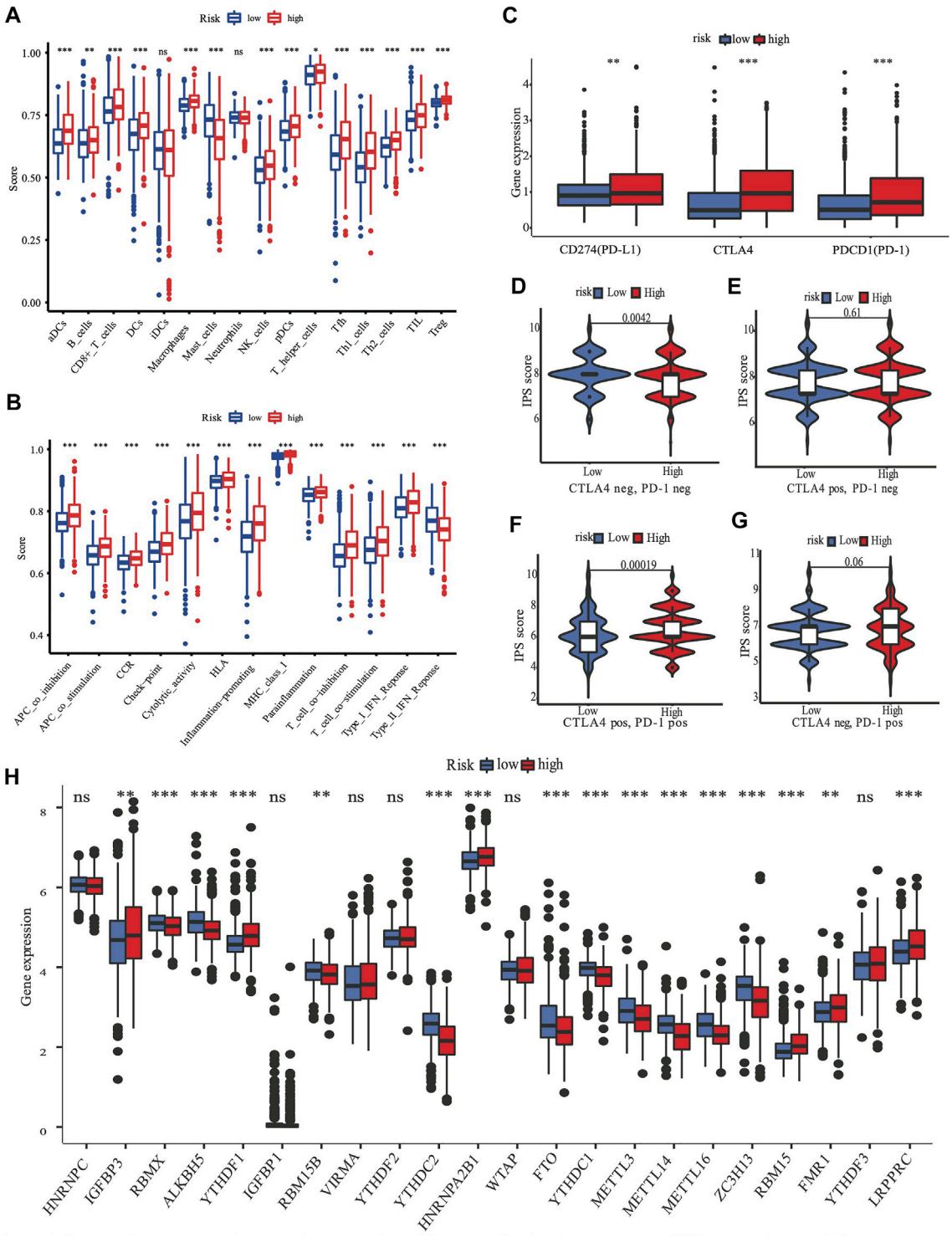

FIGURE 6 | The role of nine-gene panel in immunotherapy based on TCGA cohort. Boxplots depict the scores of 16 immune cells **(A)** and 13 immune-related roles **(B)** in high and low risk subgroup by"ssGSEA". Expression of immune checkpoints among high and low subgroups, such as CTLA4, PD-L1, PD-1 **(C)**; The immunophenoscore (IPS) distribution was also compared between high and low risk subgroups **(D–G)**. The gene expression levels of 22 m6A from TCGA cohort between two subgroups **(H)**. (ns, not significant; *$p < 0.05$; **$p < 0.01$; ***$p < 0.001$; pos means positive; neg means negative).

cytolytic activity, cytokine-cytokine receptor, parainflammation, and antigen presenting cell co-inhibition/stimulation ($p < 0.05$, **Figures 6A,B**). Analyses of both the TCGA and the METABRIC cohorts demonstrated that the results of the ssGSEA, GO, and KEGG analyses were consistent with the different immune functions and pathways of the two subgroups.

Analysis of m6A Methylation Regulators

A review summarized m6A methylation (Zaccara et al., 2019) regulators that we used for analysis, with 8 writers (*VIRMA, ZC3H13, WTAP, METTL14, METTL16, METTL3, RBM15B,* and *RBM15*), two erasers (*ALKBH5* and *FTO*), and 13 readers (*YTHDC1, YTHDC2, YTHDF1, YTHDF3, HNRNPC, FMR1, IGFBP3, RBMX, IGFBP1, YTHDF2, HNRNPA2B1, LRPPRC,* and *KIAA1429*). We found substantial variations in the expression of m6A regulators between high and low risk subgroups (**Figure 6H**). Compared with the low risk subgroup, the expression of *IGFBP3,YTHDF1, HNRNPA2B1, RBM15, FMR1,* and *LRPPRC* were upregulated, *RBMX, ALKBH5, RBM15B, YTHDC2, FTO, YTHDC1, METTL3, METTL14, METTL16,* and *ZC3H13* were downregulated in the high risk subgroup.

The Risk Score Was Characterized by Distinct Immunotherapy Landscapes Circumstance

Targeting the immunological checkpoints CTLA4, PD-L1, and PD-1, has made significant progress in recent years in Her2-positive and TNBC patients. Our results showed that the high-risk subgroup was closely associated with Her2-positive and TNBC subtypes (**Figure 4C**; **Table 2**). As a result, we looked at the differences in immunological checkpoint expression between the two subgroups. The results showed that patients in the high-risk subgroup displayed a high abundance of PD-1, CTLA4, and PD-L1 (**Figure 6C**). Given the significant connection between the risk subgroups and immunological response, the response to ICIs treatment represented by CTLA4/PD-1 inhibitors was further examined in terms of immunotherapy across the two subgroups. Patients in the high-risk subgroup showed higher ICIs scores than those in the low-risk subgroup, when the CTLA4 and PD-1 statuses were both positive or negative (**Figures 6D–F**). This indicated that patients in the high-risk subgroup, whose CTLA4 and PD-1statuses were both positive or negative, demonstrated a substantial clinical benefit from combination therapy with anti-CTLA4 and anti-PD-1. Our results, taken together, clearly indicate that the nine-FRG panel is linked to immunotherapy response.

DISCUSSION

Cell death plays an essential role in the homeostasis of the body. An advantage of cell death is the prevention of the uncontrolled growth and proliferation of cancer cells, which have excessive energy demands to maintain their infinite self-renewal potential. Cancer is associated with alterations in energy metabolism, antioxidants, and intake of iron (Stockwell et al., 2017). Therefore, tumor cells are more vulnerable to iron-induced necrosis, which is also known as ferroptosis, due to their iron-dependent growth mechanism (Dixon et al., 2012).

A few study developed a similar model to predict BRCA prognosis and validated the FRG expression level using cell lines (Zhu et al., 2021a; Wu et al., 2021). However, it did not consider the molecular subtype and was not based on DSS. Further, only three genes in that model (*G6PD, FLT3*, and *SLC1A4*) overlapped with those in our DSS model. After the multivariate Cox regression analysis, the ferroptosis-related nine-gene panel that we discovered demonstrated an excellent prognostic prediction capability in the TCGA, METABRIC, and GSE3494 cohorts. The high-risk subgroup was significantly associated with a high tumor grade, an advanced TNM stage, and TNBC and Her2-positive subtypes, which were all related to poor survival and refractory treatment response. Conversely, the low-risk subgroup was positively associated with positive statuses of ER and PR and a negative HER2 status (**Table2**), which all corresponded to favorable survival outcomes in the traditional classification. Due to the high recurrence and metastatic rate, Her2-positive BRCA and TNBC have been regarded as refractory and aggressive subtypes (Foulkes et al., 2010; Cesca et al., 2020). Hence, researchers are focusing on exploring more therapeutic methods to fill this gap. Several studies suggested that targeting ferroptosis may be a useful therapeutic approach in the treatment of TNBC and Her2-positive BRCA (Chen et al., 2017; Nagpal et al., 2019; Zhu et al., 2020; Ding et al., 2021; Zhang et al., 2021).

The predictive capability of the nine-gene panel was more significant than those of traditional indicators (**Figure 4A**) in terms of tumor size, lymph node metastasis, and ER/PR and HER2 statuses, especially for TNBC and Her2-positive BRCA subtypes. This finding suggested that treatment could be escalated or de-escalated depending on patients' risk stratification combined with canonical methods. However, the relationship between the nine genes and ferroptosis needs further exploration. The median follow-up of the TCGA was 2.5 years when the events was only 8% (**Table 1**), while METABRIC and GSE3494 cohorts were about 10 years, resulting in the AUC value for 3 years and 5 years DSS prediction is lower than the 2 years in TCGA. The nine-gene panel was a more reliable predictor of 2 years DSS in the TCGA (AUC = 0.806), METABRIC (AUC = 0.706), and GSE3494 cohorts (AUC = 0.624) (**Figures 3D–F**) because it had a high predictive accuracy for DSS, which was even better than those of the statuses of ER, PR, HER2, and lymph nodes as well as tumor size (**Figures 4A,B**).

A total of nine FRG constituted our panel. These FRG were *ALDH3A2, SIAH2, G6PD, SLC1A4, FLT3, SQLE, EGLN2, SFXN5*, and *CHAC1*. *G6PD, SQLE*, and *CHAC1* were unfavorable genes for BRCA prognosis in this gene panel, and they were significantly overexpressed in the tumor compared with levels in the adjacent tissues (**Figures 2B**, **7**). Contrastingly, the other genes were protective. A few studies have discovered that these nine genes are all associated with ferroptosis. The *SQLE* gene

encodes squalene epoxidase to catalyze the oxidation of squalene that could change the lipid profile of tumor cells and protect them from ferroptosis (Garcia-Bermudez et al., 2019). In addition, it is one of the most significantly upregulated genes in many tumors, especially in BRCA (Xu et al., 2020). Moreover, Qin et al. (Shen et al., 2017) found that *SQLE* mRNA is stabilized by lnc030 in collaboration with poly (rC) binding protein 2(PCBP2), resulting in an increase in cholesterol synthesis. They suggested that targeting *SQLE* might be a potential mechanism of terbinafine in the treatment of BRCA (Qin et al., 2021). The *G6PD* gene encodes glucose-6-phosphate dehydrogenase, which produces NADPH to keep the glutathione (GSH) in balance to inhibit ferroptosis. In addition, *G6PD* eliminates ROS (Hao et al., 2018). Hence, the upregulation of *G6PD* facilitates cancer development and is thus associated with a poor prognosis in many forms of carcinomas (Ju et al., 2017; Chen et al., 2018; Zhu et al., 2021b). Likewise, the upregulated expression of *CHAC1* could prognosticate unfavorable outcomes in BRCA (Goebel et al., 2012; Li et al., 2021). Additionally, *CHAC1* has been discovered to decease intracellular GSH levels, enhancing tumor cell ferroptosis (Chen et al., 2017). Moreover, *FLT3, ALDH3A2,* and *SIAH2* gene depletion or deficiency can result in ferroptosis (Kang et al., 2014; Hassannia et al., 2019; Chillappagari et al., 2020). A loss in *ALDH3A2* triggers ferroptosis and cooperates with *GPX4* inhibition (Yusuf et al., 2020). *SIAH2*-deficient cells exhibit increased vulnerability to ferroptosis, and re-expression of *GPX4* can rescue these cells from ferroptosis (Chillappagari et al., 2020). Equally, *EGLN2* knockdown inhibited ferroptosis in mice, researchers validated the mRNA level of prostaglandin-endoperoxide synthase two b y qPCR, it is as a marker for assessing ferroptosis *in vivo*; and *EGLN2* gene could mediate *HIF1A* downregulation to promote ferroptosis (Yang et al., 2019). Only few researches have focused on *SLC1A4* and *SFXN5*. However, they did not find an association between these genes and ferroptosis. Nonetheless, *SLC1A4* may promote ferroptosis and may function as a marker of ferroptosis, according to the FerrDb website data. Moreover, *SFXN5* may be involved in cellular iron ion homeostasis (Tifoun et al., 2021). These two genes need further study to confirm their relationship with ferroptosis. Further, these genes are all linked to the promotion or prevention of ferroptosis in various cancers *via* multiple mechanisms (**Supplementary Figure S3**); however, it is unclear whether these genes influence the prognosis of BRCA patients through ferroptosis.

Recently, researchers have been exploring the role of ferroptosis in tumor therapy. However, the possible regulation of tumor immunity and ferroptosis remains a mystery. The idea that immunity stimulates or inhibits cancer cells is widely known, and targeting the immune checkpoint has become a promising and potential therapeutic approach in recent years. Studies that involved the TCGA and METABRIC cohorts revealed that the majority of the types of immune cells in the high-risk subgroup had higher immune scores than did those in the low-risk subgroup, except for mast cells (**Figure 6A**). Furthermore, the high-risk subgroup also had excessively higher scores for most immune functions (**Figure 6B**). There may be a crosstalk between the ferroptosis of cancer cells and those of infiltrating immune cells. One theory is that ferroptotic cancer cells emit distinct signals, which cause phagocytosis and induce antigen presentation by dendritic cells (Friedmann Angeli et al., 2019). Meanwhile, the suppression of ferroptotic activity impairs the capacity of $CD8^+$ T and natural killer cells to destroy cells *in vivo* (Wang et al., 2019).

The results of the GO analysis suggested that many immune-related pathways and biological processes, such as humoral immune response, circulating immunoglobulin-mediated human immune response, complement activation, and classical pathways were enriched. The enriched KEGG pathways were the IL−17 signaling pathway and the PPAR signaling pathway (**Figures 5A,B**). The IL−17 signaling transduction regulated the infiltration of $CD8^+$ T cells and PD-1/PD-L1 in BRCA patients (Shuai et al., 2020), while the PPAR signaling pathway was activated in TNBC patients (Lin et al., 2021). Our results demonstrated that the TNBC subtypes (91% in TCGA, 98.7% in METABRIC, **Figure 4C**) were mostly found in the high-risk subgroup (**Table2**). The clinical trial of combination anti-PD-1/PD-L1 showed that the progression-free survival was significantly improved in TNBC patients with metastasis (Cortes et al., 2020). The mechanism of anti-PD-L1 antibodies was to trigger ferroptosis, which subsequently enhanced the efficacy of immunotherapy (Wang et al., 2019). The resistance to anti-PD-1/PD-L1 in TNBC cells inhibited ferroptosis and changed the proportion of macrophage cells (Jiang et al., 2021). Therefore, ferroptosis may be induced through changes in the immune system. According to our panel, BRCA patients are stratified into the high- and low-risk subgroups. The patients in the high risk subgroup, whose CTLA4 and PD-1statuses were both positive or negative, demonstrated a substantial clinical benefit from combination therapy with anti-CTLA4 and anti-PD-1 (**Figures 6D,F**). Therefore, the high-risk subgroup should be administered intensive treatment or immunotherapies, whereas the low-risk subgroup should be administered de-escalated treatment. The relationship between immunity and ferroptosis has not been thoroughly clarified. However, there might be a strong relationship between the immune microenvironment of the tumor and ferroptosis in BRCA patients. Thus, further research is needed to validate the above findings.

Our study has several limitations. First, since ferroptosis research is a new and rapidly expanding field, more FRG are likely to be discovered in the future. Second, because of the observed heterogeneity between different populations, the findings of this retrospective and cross-cohort research need validation by further prospective reviews involving multicenter cohorts. Third, since the data were downloaded from public databases, several important clinical details were not accessible. These inaccessible data included chemotherapy regimens, drug information, and tumor burden, and the lack of these data limited a more in-depth comparison among the TCGA, METABRIC, and GSE3494 data. Finally, since the results are based on RNA sequence, verification of protein expression in terms of immunohistochemistry is needed to conveniently apply our findings in clinical practice.

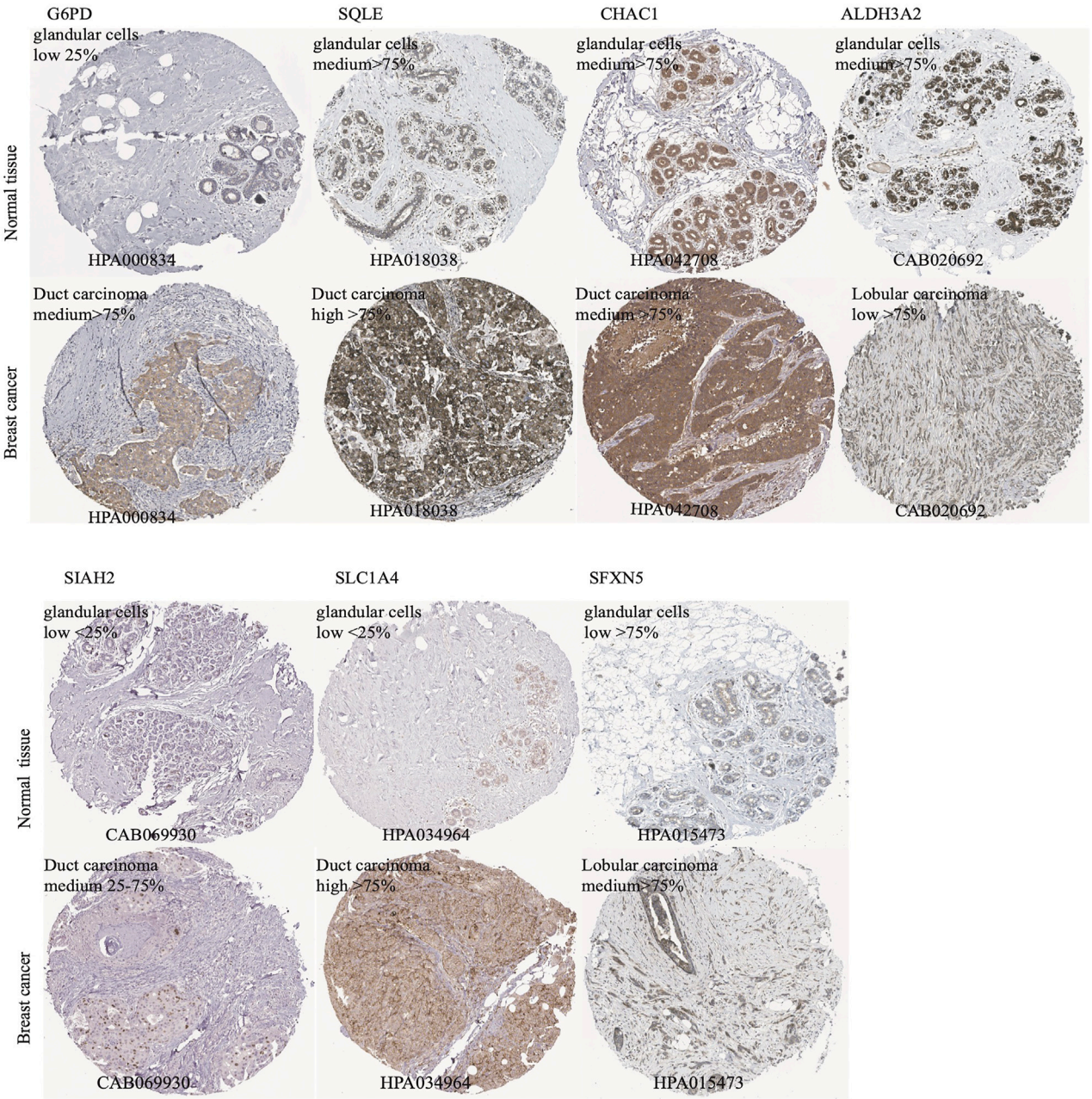

FIGURE 7 | The immunohistochemistry (IHC) of ferroptotic prognostic protein images from the HPA database. The G6PD, SQLE, CHAC1, ALDH3A2, SIAH2, SLC1A4, and SFXN5 proteins level in breast cancer and adjcent normal tissues were shown by the IHC staining.

CONCLUSION

We constructed a DSS prognostic prediction panel involving nine FRG genes in BRCA. This panel was based on FRG and DSS events. In the TCGA, METABRIC, and GSE3494 cohorts, our panel was independently correlated with DSS prognosis. We also found that the tumor immune microenvironment and ferroptosis may have a strong inherent connection with BRCA. This panel could be used to evaluate prognosis and to select patients for escalation/de-escalation treatment. Our research provides a preliminary theory for clinically individualized therapy by targeting ferroptosis genes.

DATA AVAILABILITY STATEMENT

Publicly available datasets were analyzed in this study. This data can be found here: https://portal.gdc.cancer.gov/repository http://www.cbioportal.org/study/summary?id=brca_metabric https://www.ncbi.nlm.nih.gov/gds/?term=GSE3494.

ETHICS STATEMENT

Ethical review and approval was not required for the study on human participants in accordance with the local legislation and institutional requirements. Written informed consent for participation was not required for this study in accordance with the national legislation and the institutional requirements. Written informed consent was not obtained from the individual(s) for the publication of any potentially identifiable images or data included in this article.

AUTHOR CONTRIBUTIONS

PL and BY planned and analyzed the study, and wrote the paper; YC, BX assisted in the study. JX and JW revise the manuscript. The final manuscript was read and accepted by all contributors.

FUNDING

The National Natural Science Foundation of China (82072920) and China's National Key R&D Program funded this research (2017YFC1311004).

ACKNOWLEDGMENTS

We would like to thank Hongda Pan for his guidance on computer software operation and code usage. We would like to thank Editage for English language editing.

SUPPLEMENTARY MATERIAL

The Supplementary Material for this article can be found online at: https://www.frontiersin.org/articles/10.3389/fcell.2021.709180/full#supplementary-material

REFERENCES

Cesca, M. G., Vian, L., Cristóvão-Ferreira, S., Pondé, N., and de Azambuja, E. (2020). HER2-positive Advanced Breast Cancer Treatment in 2020. *Cancer Treat. Rev.* 88, 102033. doi:10.1016/j.ctrv.2020.102033

Charoentong, P., Finotello, F., Angelova, M., Mayer, C., Efremova, M., Rieder, D., et al. (2017). Pan-cancer Immunogenomic Analyses Reveal Genotype-Immunophenotype Relationships and Predictors of Response to Checkpoint Blockade. *Cel Rep.* 18, 248–262. doi:10.1016/j.celrep.2016.12.019

Cheang, M. C. U., Martin, M., Nielsen, T. O., Prat, A., Voduc, D., Rodriguez-Lescure, A., et al. (2015). Defining Breast Cancer Intrinsic Subtypes by Quantitative Receptor Expression. *The Oncologist* 20, 474–482. doi:10.1634/theoncologist.2014-0372

Chen, M.-S., Wang, S.-F., Hsu, C.-Y., Yin, P.-H., Yeh, T.-S., Lee, H.-C., et al. (2017). CHAC1 Degradation of Glutathione Enhances Cystine-Starvation-Induced Necroptosis and Ferroptosis in Human Triple Negative Breast Cancer Cells via the GCN2-eIF2α-ATF4 Pathway. *Oncotarget* 8, 114588–114602. doi:10.18632/oncotarget.23055

Chen, X., Kang, R., Kroemer, G., and Tang, D. (2021). Broadening Horizons: the Role of Ferroptosis in Cancer. *Nat. Rev. Clin. Oncol.* 18, 280-296. doi:10.1038/s41571-020-00462-0

Chen, X., Xu, Z., Zhu, Z., Chen, A., Fu, G., Wang, Y., et al. (2018). Modulation of G6PD Affects Bladder Cancer via ROS Accumulation and the AKT Pathway *In Vitro*. *Int. J. Oncol.* 53, 1703–1712. doi:10.3892/ijo.2018.4501

Chillappagari, S., Belapurkar, R., Möller, A., Molenda, N., Kracht, M., Rohrbach, S., et al. (2020). SIAH2-mediated and Organ-specific Restriction of HO-1 Expression by a Dual Mechanism. *Sci. Rep.* 10, 2268. doi:10.1038/s41598-020-59005-3

Cortes, J., Cescon, D. W., Rugo, H. S., Nowecki, Z., Im, S. A., Yusof, M. M., et al. (2020). Pembrolizumab Plus Chemotherapy versus Placebo Plus Chemotherapy for Previously Untreated Locally Recurrent Inoperable or Metastatic Triple-Negative Breast Cancer (KEYNOTE-355): a Randomised, Placebo-Controlled, Double-Blind, Phase 3 Clinical Trial. *Lancet* 396, 1817–1828. doi:10.1016/S0140-6736(20)32531-9

Ding, Y., Chen, X., Liu, C., Ge, W., Wang, Q., Hao, X., et al. (2021). Identification of a Small Molecule as Inducer of Ferroptosis and Apoptosis through Ubiquitination of GPX4 in Triple Negative Breast Cancer Cells. *J. Hematol. Oncol.* 14, 19. doi:10.1186/s13045-020-01016-8

Dixon, S. J., Lemberg, K. M., Lamprecht, M. R., Skouta, R., Zaitsev, E. M., Gleason, C. E., et al. (2012). Ferroptosis: an Iron-dependent Form of Nonapoptotic Cell Death. *Cell* 149, 1060–1072. doi:10.1016/j.cell.2012.03.042

Foulkes, W. D., Smith, I. E., and Reis-Filho, J. S. (2010). Triple-negative Breast Cancer. *N. Engl. J. Med.* 363, 1938–1948. doi:10.1056/nejmra1001389

Friedmann Angeli, J. P., Krysko, D. V., and Conrad, M. (2019). Ferroptosis at the Crossroads of Cancer-Acquired Drug Resistance and Immune Evasion. *Nat. Rev. Cancer* 19, 405–414. doi:10.1038/s41568-019-0149-1

Garcia-Bermudez, J., Baudrier, L., Bayraktar, E. C., Shen, Y., La, K., Guarecuco, R., et al. (2019). Squalene Accumulation in Cholesterol Auxotrophic Lymphomas Prevents Oxidative Cell Death. *Nature* 567, 118–122. doi:10.1038/s41586-019-0945-5

Goebel, G., Berger, R., Strasak, A. M., Egle, D., Müller-Holzner, E., Schmidt, S., et al. (2012). Elevated mRNA Expression of CHAC1 Splicing Variants Is Associated with Poor Outcome for Breast and Ovarian Cancer Patients. *Br. J. Cancer* 106, 189–198. doi:10.1038/bjc.2011.510

Hangauer, M. J., Viswanathan, V. S., Ryan, M. J., Bole, D., Eaton, J. K., Matov, A., et al. (2017). Drug-tolerant Persister Cancer Cells Are Vulnerable to GPX4 Inhibition. *Nature* 551, 247–250. doi:10.1038/nature24297

Hao, S., Liang, B., Huang, Q., Dong, S., Wu, Z., He, W., et al. (2018). Metabolic Networks in Ferroptosis. *Oncol. Lett.* 15, 5405–5411. doi:10.3892/ol.2018.8066

Harbeck, N., Penault-Llorca, F., Cortes, J., Gnant, M., Houssami, N., Poortmans, P., et al. (2019). Breast Cancer. *Nat. Rev. Dis. Primers* 5, 66. doi:10.1038/s41572-019-0111-2

Hassannia, B., Vandenabeele, P., and Vanden Berghe, T. (2019). Targeting Ferroptosis to Iron Out Cancer. *Cancer Cell* 35, 830–849. doi:10.1016/j.ccell.2019.04.002

Jiang, Z., Lim, S-O., Yan, M., Hsu, J. L., Yao, J., Wei, Y., et al. (2021). TYRO3 Induces Anti-PD-1/pd-L1 Therapy Resistance by Limiting Innate Immunity and Tumoral Ferroptosis. *J. Clin. Invest.* 131, e139434. doi:10.1172/jci139434

Ju, H.-Q., Lu, Y.-X., Wu, Q.-N., Liu, J., Zeng, Z.-L., Mo, H.-Y., et al. (2017). Disrupting G6PD-Mediated Redox Homeostasis Enhances Chemosensitivity in Colorectal Cancer. *Oncogene* 36, 6282–6292. doi:10.1038/onc.2017.227

Kang, Y., Tiziani, S., Park, G., Kaul, M., and Paternostro, G. (2014). Cellular protection Using Flt3 and PI3Kα Inhibitors Demonstrates Multiple

Mechanisms of Oxidative Glutamate Toxicity. *Nat. Commun.* 5, 3672. doi:10.1038/ncomms4672

Li, D., Liu, S., Xu, J., Chen, L., Xu, C., Chen, F., et al. (2021). Ferroptosis-related Gene CHAC1 Is a Valid Indicator for the Poor Prognosis of Kidney Renal clear Cell Carcinoma. *J. Cel Mol Med* 27, 3610-3621. doi:10.1111/jcmm.16458

Li, J.-H., Liu, S., Zhou, H., Qu, L.-H., and Yang, J.-H. (2013). starBase v2.0: Decoding miRNA-ceRNA, miRNA-ncRNA and Protein-RNA Interaction Networks from Large-Scale CLIP-Seq Data. *Nucl. Acids Res.* 42, D92–D97. doi:10.1093/nar/gkt1248

Lin, Y., Lin, L., Fu, F., Wang, C., Hu, A., Xie, J., et al. (2021). Quantitative Proteomics Reveals Stage-specific Protein Regulation of Triple Negative Breast Cancer. *Breast Cancer Res. Treat.* 185, 39–52. doi:10.1007/s10549-020-05916-8

Ma, S., Henson, E. S., Chen, Y., and Gibson, S. B. (2016). Ferroptosis Is Induced Following Siramesine and Lapatinib Treatment of Breast Cancer Cells. *Cell Death Dis* 7–e2307. doi:10.1038/cddis.2016.208

Nagpal, A., Redvers, R. P., Ling, X., Ayton, S., Fuentes, M., Tavancheh, E., et al. (2019). Neoadjuvant Neratinib Promotes Ferroptosis and Inhibits Brain Metastasis in a Novel Syngeneic Model of Spontaneous HER2+ve Breast Cancer Metastasis. *Breast Cancer Res.* 21, 94. doi:10.1186/s13058-019-1177-1

Park, H. G., Kim, J. H., Dancer, A. N., Kothapalli, K. S., and Brenna, J. T. (2021). The Aromatase Inhibitor Letrozole Restores FADS2 Function in ER+ MCF7 Human Breast Cancer Cells. *Prostaglandins, Leukot. Essent. Fatty Acids* 171, 102312. doi:10.1016/j.plefa.2021.102312

Qin, Y., Hou, Y., Liu, S., Zhu, P., Wan, X., Zhao, M., et al. (2021). A Novel Long Non-Coding RNA Lnc030 Maintains Breast Cancer Stem Cell Stemness by Stabilizing SQLE mRNA and Increasing Cholesterol Synthesis. *Adv. Sci.* 8, 2002232. doi:10.1002/advs.202002232

Rooney, M. S., Shukla, S. A., Wu, C. J., Getz, G., and Hacohen, N. (2015). Molecular and Genetic Properties of Tumors Associated with Local Immune Cytolytic Activity. *Cell* 160, 48–61. doi:10.1016/j.cell.2014.12.033

Shen, C.-J., Kuo, Y.-L., Chen, C.-C., Chen, M.-J., and Cheng, Y.-M. (2017). MMP1 Expression Is Activated by Slug and Enhances Multi-Drug Resistance (MDR) in Breast Cancer. *PLoS One* 12, e0174487. doi:10.1371/journal.pone.0174487

Shuai, C., Yang, X., Pan, H., and Han, W. (2020). Estrogen Receptor Downregulates Expression of PD-1/pd-L1 and Infiltration of CD8+ T Cells by Inhibiting IL-17 Signaling Transduction in Breast Cancer. *Front. Oncol.* 10, 582863. doi:10.3389/fonc.2020.582863

Stockwell, B. R., Friedmann Angeli, J. P., Bayir, H., Bush, A. I., Conrad, M., Dixon, S. J., et al. (2017). Ferroptosis: A Regulated Cell Death Nexus Linking Metabolism, Redox Biology, and Disease. *Cell* 171, 273–285. doi:10.1016/j.cell.2017.09.021

Tibshirani, R. (1997). The Lasso Method for Variable Selection in the Cox Model. *Statist. Med.* 16, 385–395. doi:10.1002/(sici)1097-0258(19970228)16:4<385:aid-sim380>3.0.co;2-3

Tifoun, N., De Las Heras, J. M., Guillaume, A., Bouleau, S., Mignotte, B., and Le Floch, N. (2021). Insights into the Roles of the Sideroflexins/SLC56 Family in Iron Homeostasis and Iron-Sulfur Biogenesis. *Biomedicines* 9, 103. doi:10.3390/biomedicines9020103

Waks, A. G., and Winer, E. P. (2019). Breast Cancer Treatment: A Review. *JAMA* 321, 288–300. doi:10.1001/jama.2018.19323

Wang, W., and Liu, W. (2020). Integration of Gene Interaction Information into a Reweighted Lasso-Cox Model for Accurate Survival Prediction. *Bioinformatics* 26. 5405-5414. doi:10.1093/bioinformatics/btaa1046

Wang, W., Green, M., Choi, J. E., Gijón, M., Kennedy, P. D., Johnson, J. K., et al. (2019). CD8+ T Cells Regulate Tumour Ferroptosis during Cancer Immunotherapy. *Nature* 569, 270–274. doi:10.1038/s41586-019-1170-y

Wu, Z.-H., Tang, Y., Yu, H., and Li, H.-D. (2021). The Role of Ferroptosis in Breast Cancer Patients: a Comprehensive Analysis. *Cell Death Discov.* 7, 93. doi:10.1038/s41420-021-00473-5

Xu, H., Zhou, S., Tang, Q., Xia, H., and Bi, F. (2020). Cholesterol Metabolism: New Functions and Therapeutic Approaches in Cancer. *Biochim. Biophys. Acta (Bba) - Rev. Cancer* 1874, 188394. doi:10.1016/j.bbcan.2020.188394

Yang, M., Chen, P., Liu, J., Zhu, S., Kroemer, G., Klionsky, D. J., et al. (2019). Clockophagy Is a Novel Selective Autophagy Process Favoring Ferroptosis. *Sci. Adv.* 5, eaaw2238. doi:10.1126/sciadv.aaw2238

Yusuf, R. Z., Saez, B., Sharda, A., van Gastel, N., Yu, V. W. C., Baryawno, N., et al. (2020). Aldehyde Dehydrogenase 3a2 Protects AML Cells from Oxidative Death and the Synthetic Lethality of Ferroptosis Inducers. *Blood* 136, 1303–1316. doi:10.1182/blood.2019001808

Zaccara, S., Ries, R. J., and Jaffrey, S. R. (2019). Reading, Writing and Erasing mRNA Methylation. *Nat. Rev. Mol. Cel Biol* 20, 608–624. doi:10.1038/s41580-019-0168-5

Zhang, H. S., Zhang, Z. G., Du, G. Y., Sun, H. L., Liu, H. Y., Zhou, Z., et al. (2019). Nrf2 Promotes Breast Cancer Cell Migration via Up-regulation of G6PD/HIF-1α/Notch1 axis. *J. Cel Mol Med* 23, 3451–3463. doi:10.1111/jcmm.14241

Zhang, Z., Lu, M., Chen, C., Tong, X., Li, Y., Yang, K., et al. (2021). Holo-lactoferrin: the Link between Ferroptosis and Radiotherapy in Triple-Negative Breast Cancer. *Theranostics* 11, 3167–3182. doi:10.7150/thno.52028

Zhou, N., and FerrDb, Bao. J. (2020). A Manually Curated Resource for Regulators and Markers of Ferroptosis and Ferroptosis-Disease Associations. *Database* 2020, baaa021. doi:10.1093/database/baaa021

Zhu, J., Dai, P., Liu, F., Li, Y., Qin, Y., Yang, Q., et al. (2020). Upconverting Nanocarriers Enable Triggered Microtubule Inhibition and Concurrent Ferroptosis Induction for Selective Treatment of Triple-Negative Breast Cancer. *Nano Lett.* 20, 6235–6245. doi:10.1021/acs.nanolett.0c00502

Zhu, L., Tian, Q., Jiang, S., Gao, H., Yu, S., Zhou, Y., et al. (2021). A Novel Ferroptosis-Related Gene Signature for Overall Survival Prediction in Patients with Breast Cancer. *Front. Cel Dev. Biol.* 9, 670184. doi:10.3389/fcell.2021.670184

Zhu, L., Yang, F., Wang, L., Dong, L., Huang, Z., Wang, G., et al. (2021). Identification the Ferroptosis-Related Gene Signature in Patients with Esophageal Adenocarcinoma. *Cancer Cel Int* 21, 124. doi:10.1186/s12935-021-01821-2

Conflict of Interest: The authors declare that the research was conducted in the absence of any commercial or financial relationships that could be construed as a potential conflict of interest.

Publisher's Note: All claims expressed in this article are solely those of the authors and do not necessarily represent those of their affiliated organizations, or those of the publisher, the editors and the reviewers. Any product that may be evaluated in this article, or claim that may be made by its manufacturer, is not guaranteed or endorsed by the publisher.

frontiers in Cell and Developmental Biology

ORIGINAL RESEARCH
published: 25 November 2021
doi: 10.3389/fcell.2021.770115

Establishment and Validation of Prognostic Nomograms Based on Serum Copper Level for Patients With Early-Stage Triple-Negative Breast Cancer

*Fangfang Duan[1†], Jianpei Li[2†], Jiajia Huang[1†], Xin Hua[1†], Chenge Song[1], Li Wang[1], Xiwen Bi[1], Wen Xia[1] and Zhongyu Yuan[1]**

[1]*Departments of Medical Oncology, The State Key Laboratory of Oncology in South China, Collaborative Innovation Center for Cancer Medicine, Sun Yat-sen University Cancer Center, Guangzhou, China,* [2]*Departments of Clinical Laboratory Medicine, The State Key Laboratory of Oncology in South China, Collaborative Innovation Center for Cancer Medicine, Sun Yat-sen University Cancer Center, Guangzhou, China*

OPEN ACCESS

Edited by:
Ahmed Hamaï,
Institut National de la Santé et de la Recherche Médicale (INSERM), France

Reviewed by:
Xinhua Xie,
Sun Yat-sen University Cancer Center (SYSUCC), China
Ke-Da Yu,
Fudan University, China

***Correspondence:**
Zhongyu Yuan
yuanzhy@sysucc.org.cn

†These authors share first authorship

Specialty section:
This article was submitted to Molecular and Cellular Oncology, a section of the journal Frontiers in Cell and Developmental Biology

Received: *03 September 2021*
Accepted: *25 October 2021*
Published: *25 November 2021*

Citation:
Duan F, Li J, Huang J, Hua X, Song C, Wang L, Bi X, Xia W and Yuan Z (2021) Establishment and Validation of Prognostic Nomograms Based on Serum Copper Level for Patients With Early-Stage Triple-Negative Breast Cancer. Front. Cell Dev. Biol. 9:770115. doi: 10.3389/fcell.2021.770115

Background: Altered copper levels have been observed in several cancers, but studies on the relationship between serum copper and early-stage triple-negative breast cancer (TNBC) remain scare. We sought to establish a predictive model incorporating serum copper levels for individualized survival predictions.

Methods: We retrospectively analyzed clinicopathological information and baseline peripheric blood samples of patients diagnosed with early-stage TNBC between September 2005 and October 2016 at Sun Yat-sen University Cancer Center. The optimal cut-off point of serum copper level was determined using maximally selected log-rank statistics. Kaplan-Meier curves were used to estimate survival probabilities. Independent prognostic indicators associated with survival were identified using multivariate Cox regression analysis, and subsequently, prognostic nomograms were established to predict individualized disease-free survival (DFS) and overall survival (OS). The nomograms were validated in a separate cohort of 86 patients from the original randomized clinical trial SYSUCC-001 (SYSUCC-001 cohort).

Results: 350 patients were eligible in this study, including 264 in the training cohort and 86 in the SYSUCC-001 cohort. An optimal cut-off value of 21.3 μmol/L of serum copper was determined to maximally divide patients into low- and high-copper groups. After a median follow-up of 87.1 months, patients with high copper levels had significantly worse DFS (p = 0.002) and OS (p < 0.001) than those with low copper levels in the training cohort. Multivariate Cox regression analysis revealed that serum copper level was an independent factor for DFS and OS. Further, prognostic models based on serum copper were established for individualized predictions. These models showed excellent discrimination [C-index for DFS: 0.689, 95% confidence interval (CI): 0.621–0.757; C-index for OS: 0.728, 95% CI: 0.654–0.802] and predictive calibration, and were validated in the SYSUCC-001 cohort.

Conclusion: Serum copper level is a potential predictive biomarker for patients with early-stage TNBC. Predictive nomograms based on serum copper might be served as a practical tool for individualized prognostication.

Keywords: serum copper level, early-stage triple-negative breast cancer, prognostic nomograms, maximally selected log-rank statistics, survival

INTRODUCTION

Triple-negative breast cancer (TNBC), characterized by the absence of estrogen receptor (ER), progesterone receptor (PR), and human epidermal growth factor receptor 2 (HER-2), is a heterogenic and aggressive subtype of breast cancer. TNBC is associated with a high risk of early relapse, a high degree of invasiveness, and poor prognosis (Kim et al., 2018; Wang et al., 2021). Early-stage TNBC, defined as staged at I-III according to the American Joint Committee on Cancer (AJCC) 2016 (eighth edition) staging criteria (Amin et al., 2017), accounts for 15–20% of all newly diagnosed cases of early breast cancer (Dawson et al., 2009), and its treatment mainly depends on chemotherapy. Despite recent therapeutic advances, nearly 30% of patients with early-stage TNBC remain to develop disease progression within 3–5 years after the diagnosis despite receiving standard chemotherapy (Haffty et al., 2006; Dent et al., 2007; Chaudhary, 2020). Therefore, the identification of effective prognostic markers and development of individualized therapeutic strategies for TNBC patients are critical and necessary.

Copper is an essential element involving in many biological functions, including protein formation, enzyme activation, oxidation-reduction reactions, immunity development, and signaling pathways (Denoyer et al., 2015; Setty et al., 2008; Bhattacharjee et al., 2017). Copper deficiency has been associated with multiple diseases, such as Menkes disease, mild occipital horn syndrome, and bone marrow suppression (Brewer et al., 2000; Tang et al., 2006; Kaler, 2011; Chan et al., 2017). In addition, excessive copper is also harmful and related to diseases like Wilson disease, lymphoma, breast, colon, and lung cancers (Terada et al., 1999; Gupte and Mumper, 2009; Juloski et al., 2020). Copper chelators have been explored to decrease cell proliferation, angiogenesis, tumor growth, and reverse epithelial-mesenchymal transition (Ishida et al., 2013; Brady et al., 2014; MacDonald et al., 2014; Chan et al., 2017). Furthermore, increased serum copper levels have been associated with disease progression or drug resistance in several malignancies, including advanced breast cancer (Mookerjee et al., 2006; Gupte and Mumper, 2009; Majumder et al., 2009; Kaiafa et al., 2012). These findings suggest that the serum copper level might be served as a biomarker for monitoring tumor progression and treatment efficacy. However, the clinical value of serum copper in patients with early-stage TNBC is poorly investigated.

To address this need, we aimed to explore the relationship between baseline serum copper levels and the survival prognosis of patients with early-stage TNBC in this study, furtherly, we hoped to develop prognostic models combining serum copper levels and clinicopathological factor for individualized survival predictions and personalized decision-making.

METHODS AND PATIENTS

Study Design and Patient Eligibility

This study retrospectively analyzed the relationship between serum copper levels and the prognosis of patients with newly diagnosed TNBC at Sun Yat-sen University Cancer Center (SYSUCC) between September 2005 and October 2016. The study was approved by the ethics committee of SYSUCC (Registration number: B2021-218-01), written informed consent from patients was waived because of the retrospective nature of current study and the anonymous processing of patient information. We covered all personal data confidentially and conducted this study in accordance with the Declaration of Helsinki.

Patients were eligible for inclusion in this study if they met the following criteria: 1) women with pathologically diagnosed breast cancer without distant metastasis (e.g. brain, bone, live, lung) at the time of diagnosis, 2) age ≥18 years old, 3) ER/PR-negative, which was considered as <1% positive cells by immunohistochemistry (IHC) staining; HER2-negative tumor, which was defined as a score of 0 or 1 + on IHC or a score of 2 + on IHC without ERBB2 gene amplification on fluorescence *in situ* hybridization, 4) early-stage tumor, i.e., T1-4N0-3M0 according to the AJCC 2016 criteria (eighth edition) (Amin et al., 2017), and 5) availability of complete clinicopathological data and peripheric blood samples obtained within 1 week of the diagnosis for serum copper detection. Key exclusion criteria included: 1) pregnancy or lactation, 2) a history of breast cancer and other primary tumors, 3) severe or uncontrolled infection, and 4) severe metabolic disorder.

Sample Collection and Serum Copper Measurement

Patients' clinicopathological data were hand-retrieved from the electronic medical records system of SYSUCC. The peripheric blood samples collected at the time of diagnosis and before the initiation of any anti-cancer treatment were obtained from the tumor resource library of SYSUCC. The serum copper level of the participants was measured using the Copper Assay Kit (PAESA chromogenic method) of the Roche cobas 8,000 system (BSBE, Beijing, China).

Follow-Up and Endpoints

Patients were monitored every 3 months during the first 2 years, every 6 months during the subsequent 5 years, and once a year thereafter. The monitoring assessments included routine hematological and laboratory tests, menopausal status, breast and abdominal ultrasonography or computed tomography. X-ray and bone scans were performed annually.

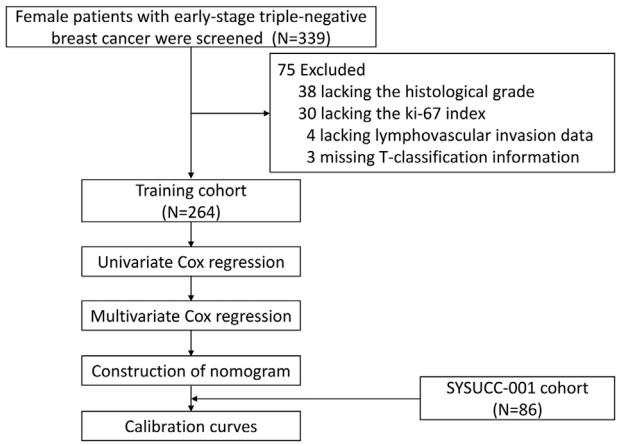

FIGURE 1 | Flow chart of patient selection in this study.

The primary endpoint was disease-free survival (DFS), which was defined as the time from the date of diagnosis to the date of first sign of disease progression or death due to any cause. The secondary endpoint was overall survival (OS), which was defined as the time from the date of diagnosis to the date of death due to any cause.

Statistical Analysis

Age was listed as mean with range, and categorical variables were represented as frequencies with percentages. The optimal cut-off value of serum copper level was determined by the maximally selected log-rank statistics using the "*maxstat*" package of R software (Hothorn and Zeileis, 2008). X-tile analysis of the 10-years OS was also conducted using the survival data of patients in the training cohort to decide the best cut-off point for serum copper level (Camp et al., 2004). Survival curves were estimated using the Kaplan-Meier method and compared with the log-rank test between the copper-high group and copper-low group. Variables achieving a p value <0.05 in the univariate Cox regression analysis could enter the backward stepwise multivariate Cox proportional hazards model, which has been tested on basis of the Schoenfeld residuals (Wileyto et al., 2013), and their hazard ratios (HRs) with 95% confidence intervals (CIs) were estimated. A predictive model incorporating serum copper and other independent clinicopathological factors identified from the multivariate Cox regression analysis was established and graphically presented as a nomogram, its discriminative performance and predictive accuracy were evaluated using the concordance index (C-index), which ranges from 0.5 (random chance) to 1.0 (perfect prediction), and calibration curves, whose Y-axis represents the actual observation of the survival rate, X-axis represents the survival rate predicted by the established nomogram, in both the training cohort and theSYSUCC-001 cohort. A two-sided p *value* < 0.05 was considered statistically significant. All statistical analyses were performed using R software ("rms" package, version 4.0.1; Vanderbilt University, Nashville, TN).

RESULTS

Clinicopathological Characteristics of Patients in the Training Cohort

After removing 75 patients with incomplete information, including 30 patients without Ki-67 index data, 38 patients without histological tumor grades, 4 patients without lymphovascular invasion data, and 3 patients without T-stage information (**Figure 1**), a total of 350 women with early-stage TNBC were eligible in the final analysis, including 264 patients in the training cohort, 86 patients in the SYSUCC-001 cohort. Specific patient clinicopathological characteristics in the training and SYSUCC-001 validation cohorts are shown in **Table 1**. In the training cohort, the mean age was 48 years [interquartile range (IQR), 41–57 years]. 169 (64.0%) women were premenopausal. Majority patients (98.9%) were pathologically diagnosed with invasive ductal carcinoma, and over half patients (56.1%) had tumors with a histological grade of 3. T1, T2, T3, and T4 tumors were presented in 90 (34.1%), 145 (54.9%), 23 (8.7%), and 6 (2.3%) patients, respectively. More than half the women (58.0%) were staged at N0, while the N1, N2, and N3 stages were present in 60 (22.7%), 27 (10.2%), and 24 (9.1%) women, respectively. In the SYSUCC-001 cohort, the mean age was 43.5 years (IQR, 37–51 years). Premenopausal women accounted for 79.1% (68). All patients were pathologically diagnosed with invasive ductal carcinoma, and 69 (80.2%) patients were histologically graded at 3. T1, T2, T3, and T4 tumors were showed in 29 (33.7%), 53 (61.6%), 2 (2.3%), and 2 (2.3%) patients, respectively. 52 (60.5%) women were staged at N0, and the N1, N2, and N3 stages were present in 19 (22.1%), 6 (7.0%), and 9 (10.5%) women, respectively.

Optimal Cut-Off Value of Serum Copper Level in the Training Cohort

Using maximally selected log-rank statistics, we determined that a cut-off point of 21.3 μmol/L for the baseline serum copper level would maximally divide patients into two copper-stratified groups (**Figure 2**), i.e., the copper-high group and the copper-low group. Consistently, the X-tile analysis based on the 10-years OS (**Supplementary Figure S1**) also resulted in a same cut-off serum copper level of 21.3 μmol/L (χ^2 log-rank value, 11.5172). In the training cohort, the serum copper level was ≤21.3 μmol/L among 237 (89.8%) women and >21.3 μmol/L among 27 (10.2%) women. In the SYSUCC-001 cohort, 84 (97.7%) TNBC patients had a value ≤21.3 of the serum copper and 2 (2.3%) patients had the serum copper level >21.3 μmol/L.

Survival Outcomes

After a median follow-up of 87.1 months (interquartile range, 67.6–113.4 months), we observed 64 DFS events and 51 deaths in training cohort, whose estimated 5-years DFS rates and 5-years OS rates were 79.6% (95% CI 74.8–84.6) and 83.7% (95% CI 79.3–88.4), respectively (**Supplementary Figure S2**).

In the training cohort, patients with high copper levels had significantly worse DFS (p = 0.002) and OS (p < 0.001) than

TABLE 1 | Characteristics of patients eligible in this study.

Characteristic	Number of cases (%)	
	Training cohort (*N* = 264)	**SYSUCC-001 cohort (*N* = 86)**
Age (years) at diagnosis	—	—
≤50	151 (57.2)	64 (74.4)
>50	113 (42.8)	22 (25.6)
Median	48	43.5
Interquartile range	41–57	37–51
Menopausal status	—	—
Premenopausal	169 (64.0)	68 (79.1)
Postmenopausal	95 (36.0)	18 (20.9)
Histological type	—	—
Invasive ductal carcinoma	261 (98.9)	86 (100.0)
Others	3 (1.1)	0
Histological grade[a]	—	—
1	6 (2.3)	1 (1.2)
2	110 (41.7)	16 (18.6)
3	148 (56.1)	69 (80.2)
Lymphovascular invasion	—	—
No	209 (79.2)	71 (82.6)
Yes	55 (20.8)	15 (17.4)
Ki-67 index at diagnosis <30%[b]	—	—
No	201 (76.1)	74 (86.0)
Yes	63 (23.9)	12 (14.0)
T stage[c]	—	—
1	90 (34.1)	29 (33.7)
2	145 (54.9)	53 (61.6)
3	23 (8.7)	2 (2.3)
4	6 (2.3)	2 (2.3)
N stage[c]	—	—
0	153 (58.0)	52 (60.5)
1	60 (22.7)	19 (22.1)
2	27 (10.2)	6 (7.0)
3	24 (9.1)	9 (10.5)
Serum copper (μmol/L)[d]	—	—
≤21.3	237 (89.8)	84 (97.7)
>21.3	27 (10.2)	2 (2.3)

[a]*Histological grade at diagnosis was based on the degree of histological tumor differentiation.*
[b]*The Ki-67 index at diagnosis indicates DNA, synthetic activity as measured using immunocytochemistry.*
[c]*Diagnosed based on the AJCC, 2016 criteria (eighth edition).*
[d]*Cut-off values were determined using maximally selected log-rank statistics.*

patients with low copper levels (**Figure 3**). The estimated 5-years DFS rates in the copper-high and copper-low groups were 61.3% (95% CI: 45.0–83.4) and 81.6% (95% CI: 76.8–86.1), respectively (**Figure 3A**). The estimated 5-years OS rates in the copper-high versus copper-low groups were 69.4% (95% CI: 53.8–89.6) versus 85.3% (95% CI: 80.9–90.0) (**Figure 3B**).

Establishment of the Prognostic Model

The results of the univariate Cox regression analyses of DFS and OS in the training cohort are shown in **Table 2**, which identified following indicators associated with DFS among women with early-stage TNBC: age, lymphovascular invasion, T stage, N stage and serum copper level. Further multivariate Cox regression analysis demonstrated that N stage and serum copper level remained independent factors for DFS (**Figure 4A**). Based on the above two independent prognostic indicators, a prognostic model for individualized prediction of DFS was constructed and represented as a graphical diagram (**Figure 5A**).

Variates achieving the predetermined significance level ($p < 0.05$) in the univariate Cox regression analysis of OS in the training cohort (**Table 2**), including age, menopausal status, lymphovascular invasion, T stage, N stage and serum copper level, were furtherly analyzed in the multivariate Cox regression analysis (**Figure 4B**), which revealed that age, N stage and serum copper level were still significantly associated with OS. Using these three independent prognostic indicators, we developed a prognostic model for the individualized prediction of OS (**Figure 6A**). Through our nomogram models, clinicians and patients could individually predict patients' prognosis, for example, patients with high serum copper levels assign a high score both on its point scale and on the total point scale, which determinates a poor prognosis, additional care and frequently monitoring are essential for them.

Evaluation of the Performance of the Prognostic Model

The prognostic nomogram of DFS showed excellent discriminative ability and predictive accuracy. The C-index after bootstrap correction was 0.689 (95% CI 0.621–0.757) in

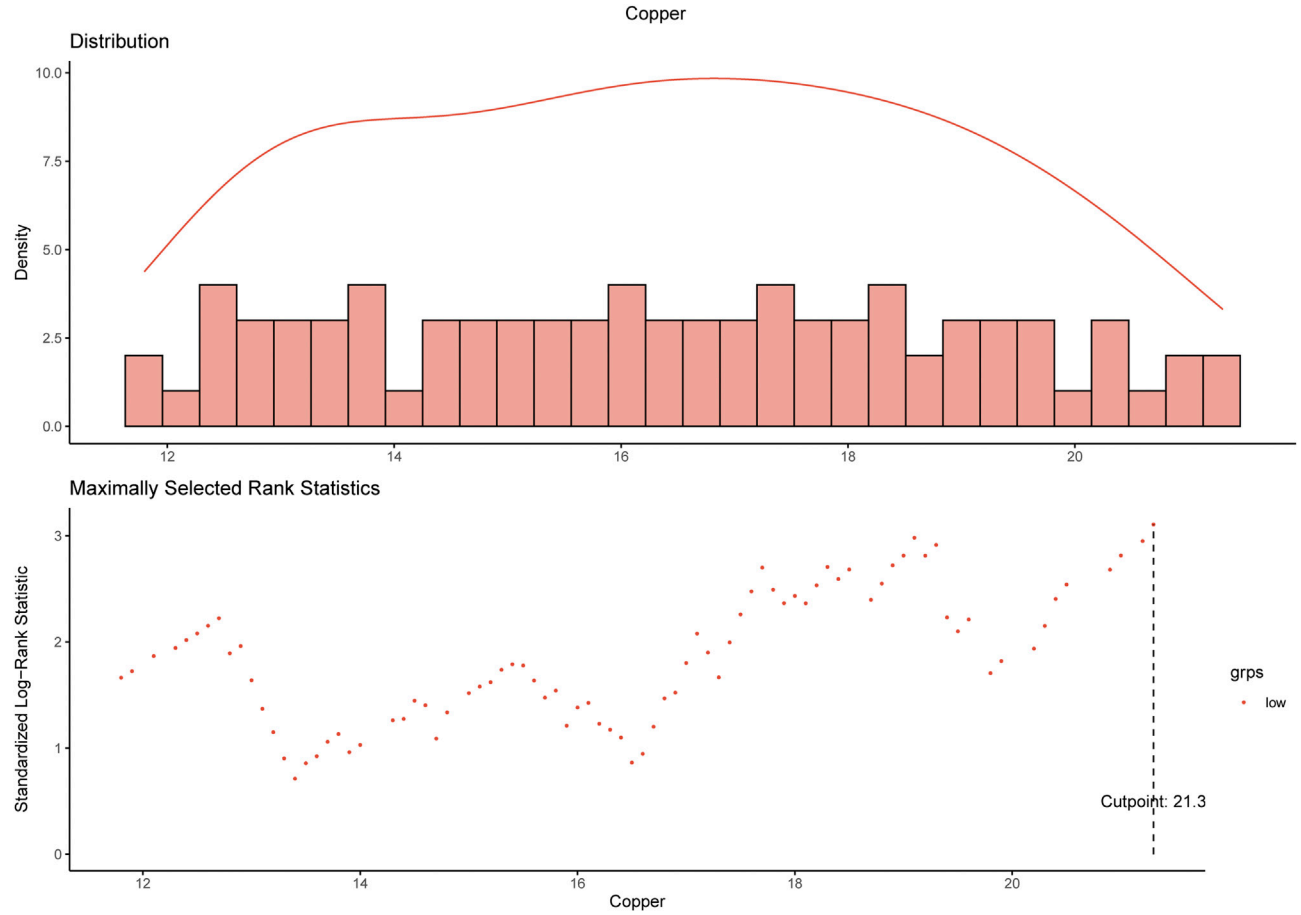

FIGURE 2 | Determination of the cut-off value of 21.3 μmol/L for serum copper level by using maximally selected log-rank statistics.

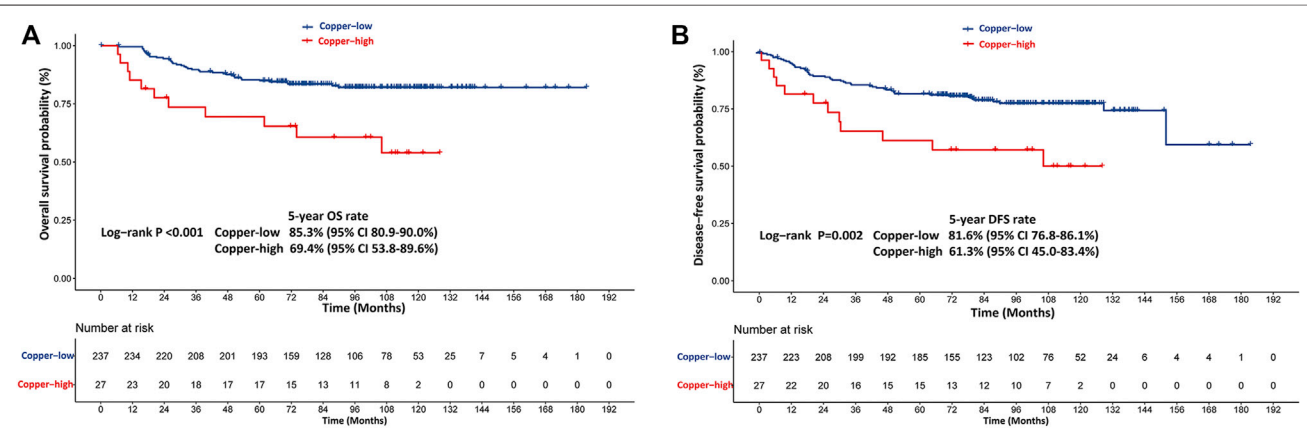

FIGURE 3 | Kaplan-Meier survival curves stratified based on the baseline serum copper level in the training cohort. **(A)** Kaplan-Meier estimates of disease-free survival (DFS) probability. **(B)** Kaplan-Meier estimates of overall survival (OS) probability. Copper-low level: ≤21.3 μmol/L, Copper-high level: >21.3 μmol/L.

the training cohort and 0.704 (95% CI 0.577–0.831) in the SYSUCC-001 cohort. Calibration curves for the DFS probability at 1-, 3-, and 5-years in the training and SYSUCC-001 cohorts both demonstrated satisfactory consistency between the nomogram-predicted and actual survival (**Figures 5B,C**).

TABLE 2 | Univariate Cox regression analysis of disease-free survival and overall survival in women with breast cancer in the training cohort.

Characteristics	Disease-free survival		Overall survival	
	Hazard ratio (95%CI)	*p* value	Hazard ratio (95%CI)	*p* value
Age (year)				
≤50	Reference	—	Reference	—
>50	1.643 (1.004–2.687)	0.048*	2.063 (1.181–3.604)	0.011*
Menopausal status				
Premenopausal	Reference	—	Reference	—
Postmenopausal	1.563 (0.955–2.559)	0.076	1.815 (1.048–3.144)	0.033*
Histological grade[a]	—	—	—	—
1/2	Reference	—	Reference	—
3	1.140 (0.694–1.873)	0.605	1.305 (0.743–2.289)	0.354
Lymphovascular invasion				
No	Reference	—	Reference	—
Yes	2.495 (1.481–4.205)	0.001*	2.728 (1.542–4.827)	0.001*
Ki-67 index at diagnosis <30%[b]				
No	Reference	—	Reference	—
Yes	0.999 (0.565–1.761)	0.996	0.836 (0.429–1.630)	0.600
T stage[c]				
1	Reference	—	Reference	—
2	0.870 (0.505–1.499)	0.616	0.863 (0.464–1.607)	0.642
3	1.079 (0.437–2.663)	0.868	1.384 (0.546–3.511)	0.494
4	3.529 (1.213–10.265)	0.021*	4.905 (1.647–14.605)	0.004*
N stage[c]				
0	Reference	—	Reference	—
1	2.537 (1.348–4.774)	0.004*	1.976 (0.943–4.138)	0.071
2	3.633 (1.786–7.392)	<0.001*	3.665 (1.677–8.009)	0.001*
3	6.328 (3.150–12.711)	<0.001*	7.099 (3.375–14.932)	<0.001*
Serum Copper (umol/L)[d]				
≤21.3	Reference	—	Reference	—
>21.3	2.560 (1.363–4.811)	0.003 *	3.006 (1.542–5.861)	0.001*

*p < *0.05.*

[a]*Histological grade at diagnosis was based on the degree of histological tumor differentiation.*

[b]*The Ki-67, index at diagnosis indicates DNA, synthetic activity as measured using immunocytochemistry.*

[c]*Diagnosed based on the AJCC 2016 criteria (eighth edition).*

[d]*Cut-off values were determined using maximally selected log-rank statistics.*

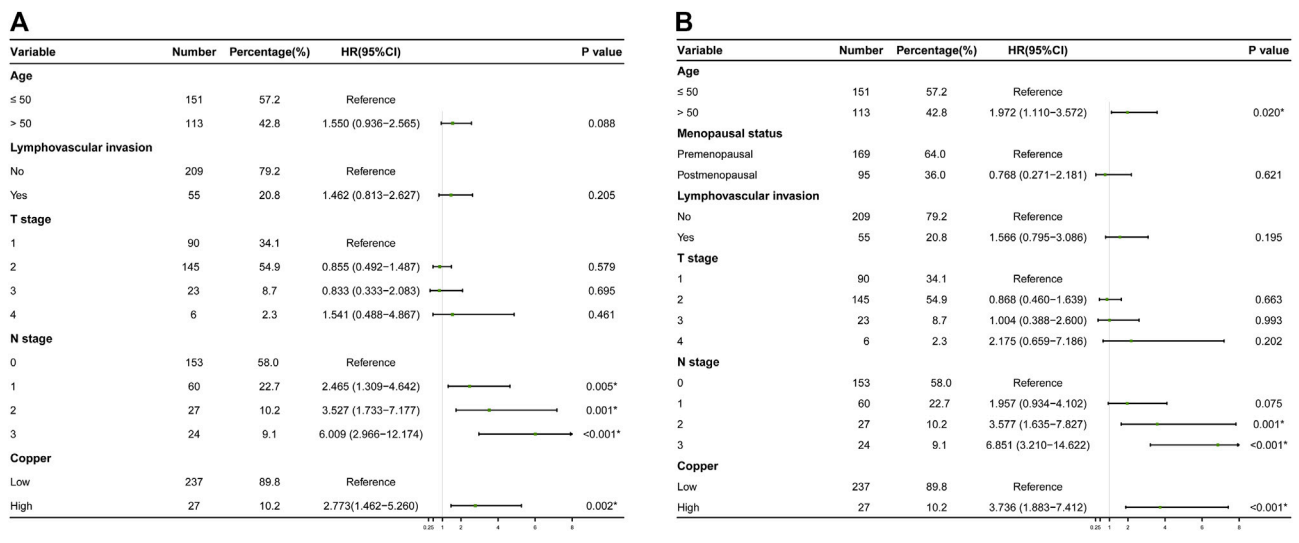

FIGURE 4 | Results of final multivariate Cox regression analyses in the training cohort are represented as forest plots. **(A)** Forest plot of disease-free survival (DFS) probability. **(B)** Forest plot of overall survival (OS).

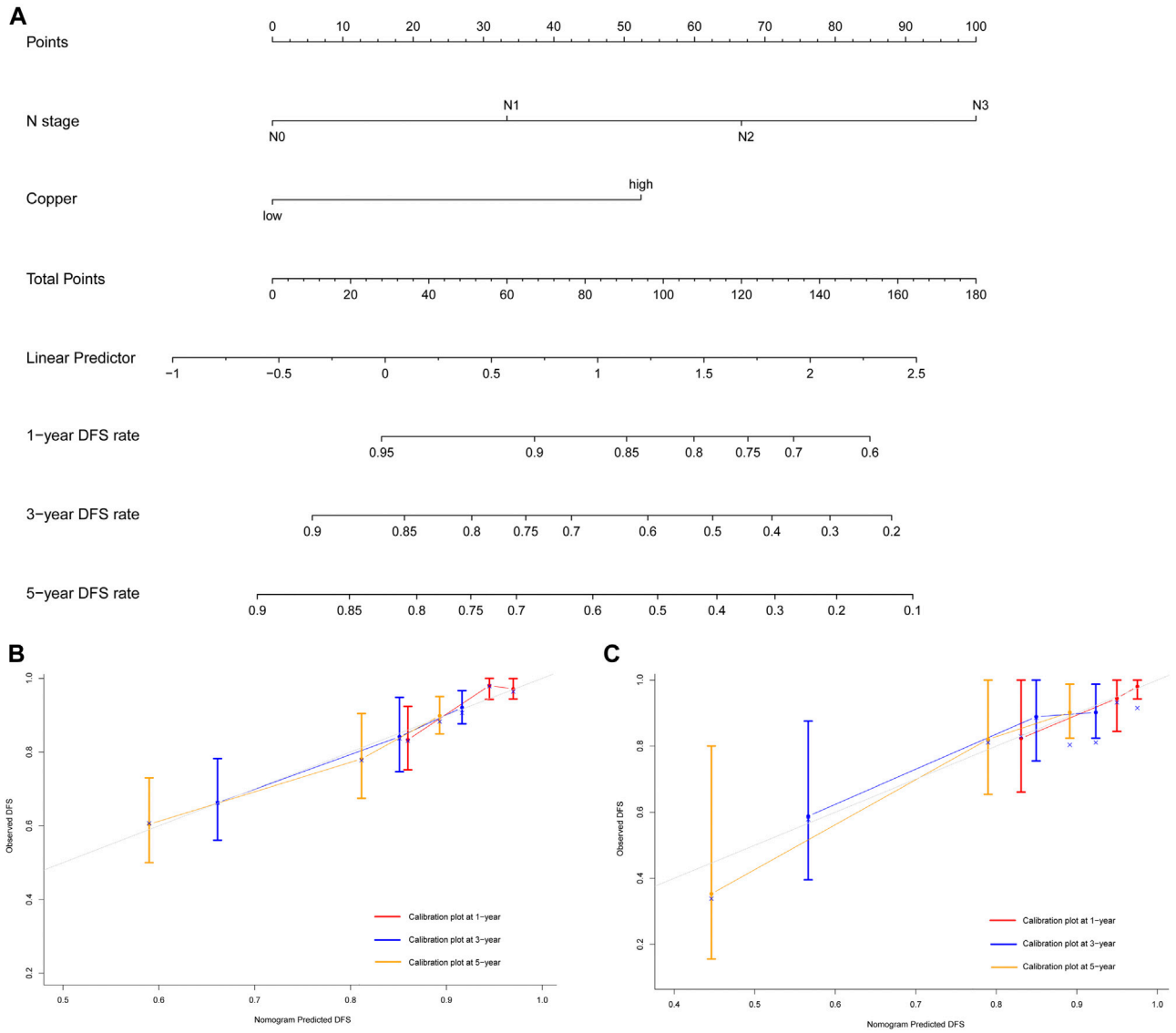

FIGURE 5 | Development and validation of prognostic model for individualized prediction of disease-free survival (DFS). **(A)** Nomogram of current prognostic model for patients with early-stage triple-negative breast cancer. **(B)** Calibration curves for predicting DFS at 1-, 3-, and 5-years in the training cohort. **(C)** Calibration curves for predicting DFS at 1-, 3-, and 5-years in the SYSUCC-001 cohort.

The prognostic nomogram of OS also showed satisfactory discrimination, with an excellent C-index of 0.728 (95% CI 0.654–0.802) in the training cohort and 0.653 (95% CI 0.487–0.819) in the SYSUCC-001 cohort. The calibration curves for the probability of OS at 1-, 3-, and 5-years (**Figures 6B,C**) also suggested good agreement between the observed and nomogram-predicted survival.

DISCUSSION

In current study, we found that patients with early-stage TNBC were a heterogeneous population with different serum copper levels. According to maximally selected log-rank statistics, we determined that 21.3 μmol/L was the best cut-off value of serum copper to stratify patients into two different groups. Moreover, multivariate Cox analysis identified high serum copper level as an independent factor influencing survival. Prognostic nomograms incorporating serum copper level and other clinicopathological factors were developed, which showed excellent discrimination and good consistency between the nomogram-predicted survival and actual observations in both the training and SYSUCC-001 cohorts.

As a catalytic cofactor and a structural component of various proteins and enzymes, copper is indispensable for organisms, and its homeostasis is crucial for many physiological functions (Denoyer et al., 2015; Setty et al., 2008; Bhattacharjee et al., 2017; Juloski et al., 2020; Shanbhag et al., 2019; Chan et al., 2020). Copper dysregulation and variations in copper metabolism-related

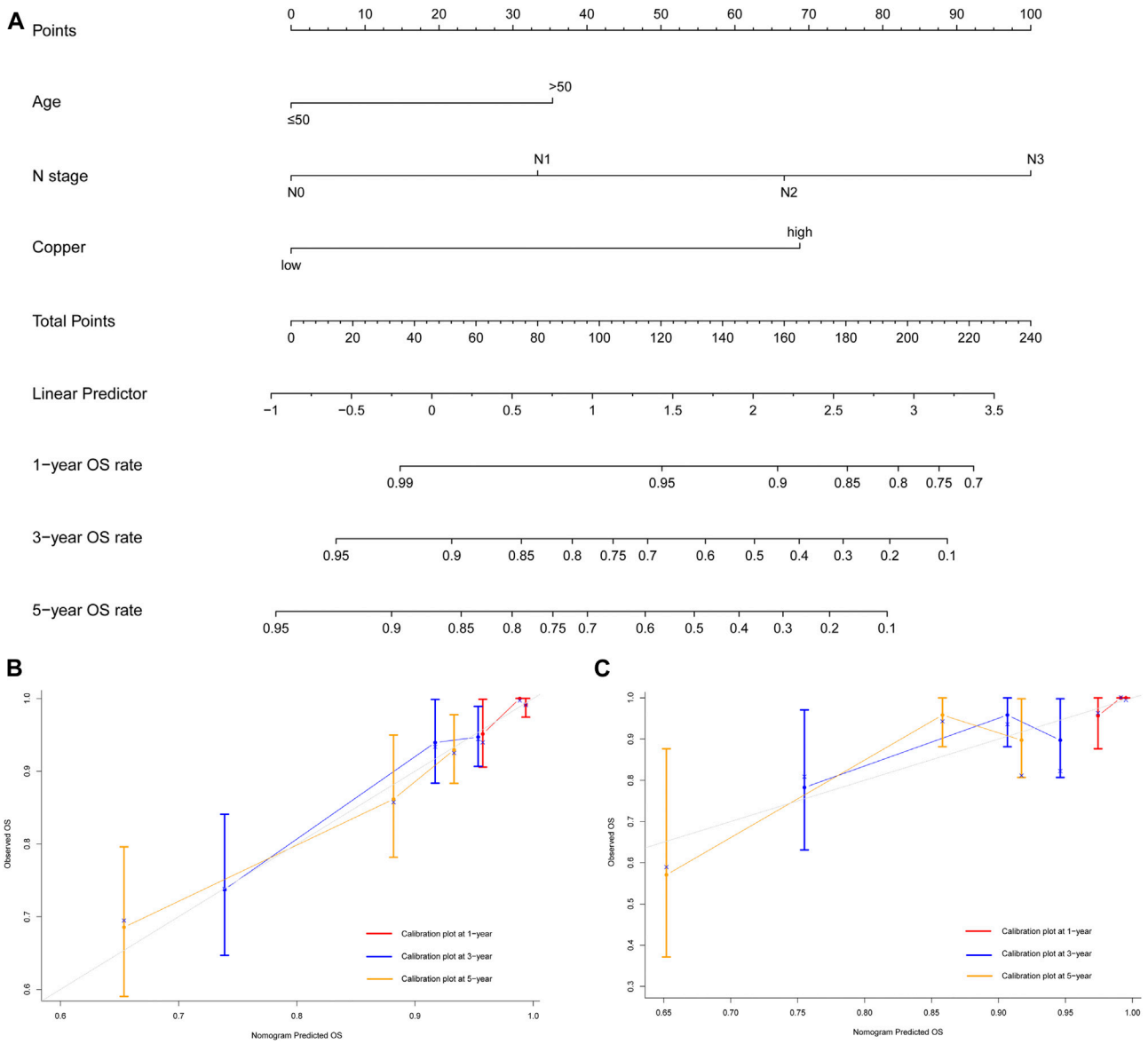

FIGURE 6 | Development and validation of prognostic model for individualized prediction of overall survival (OS). **(A)** Nomogram of current prognostic model for patients with early-stage triple-negative breast cancer. **(B)** Calibration curves for predicting OS at 1-, 3-, and 5-years in the training cohort. **(C)** Calibration curves for predicting OS at 1-, 3-, and 5-years in the SYSUCC-001 cohort.

proteins have been found in many tumors, including breast cancer (Terada et al., 1999; Gupte and Mumper, 2009; Hlynialuk et al., 2015; Juloski et al., 2020). The multifaceted effect of copper on carcinogenesis has been confirmed, it not only interrupts the initiation and progression of tumors but also promotes cell proliferation, angiogenesis, cell growth, and cell migration (Brady et al., 2014; Angelé-Martínez et al., 2017; Lelièvre et al., 2020). Thus, copper chelators or ionophores that deplete or increase the copper level in tumors have been explored in preclinical studies, and been reported to have promising clinical value (Chan et al., 2017; Xu et al., 2018; Chan et al., 2020; Cui et al., 2021).

In 1975, Schwartz firstly reported the potential value of copper in the diagnosis and prognostication of tumors (Schwartz 1975). Gupte and Mumper recently found increased serum copper levels and oxidative stress in multiple malignancies, these factors are the hallmarks of a range of cancers, and may thus provide a basis for the development of potential novel anti-cancer treatments, such as copper chelators (Gupte and Mumper, 2009). A study of patients with hematological malignancies demonstrated that serum copper levels declined and even normalized during tumor remission, but rebounded to the pre-treatment levels when relapses occurred (Kaiafa et al., 2012). High serum copper levels have also been confirmed to be associated with

tumor progression, staging, and chemotherapy resistance among patients with metastatic colon, advanced breast, and lung cancers, serum copper levels among non-responders were approximately 130–160% of that in responders (Denoyer et al., 2015; Majumder et al., 2009; Lelièvre et al., 2020). Given the short half-life of copper (Lelièvre et al., 2020), and its central role in cancer development from tumorigenesis to metastasis, we think that serum copper level may be a promising biomarker for prognostication and the monitoring of treatment efficacy.

However, some studies on breast and colon cancers have reported that the serum copper level was lower in tumor tissues than in normal tissues (Lelièvre et al., 2020; Kucharzewski et al., 2003). Leila et al. also did not support the association between copper level and breast cancer in their meta-analysis, but the heterogeneity among the original studies enrolled in this meta-analysis should be noted (Jouybari et al., 2020), which is similar to other meta-analyses on Hodgkin lymphoma and lung cancer (Mahabir et al., 2010; Thompson et al., 2010). At present, there is no consensus on the relationship between serum copper level and cancers, and studies investigating this associations especially in early-stage TNBC remain rare. Thus, it is necessary to explore the relationship between serum copper and TNBC.

Based on the stratification of serum copper levels, we established prognostic models that incorporated the serum copper level and other clinicopathological factors, including age and N stage, which is an indicator of metastasis (Amin et al., 2017). Compared with the previous 21-gene, MammaPrint, and PAM50 predictive models, our nomograms are more economical and easily applicable in clinical practice. The 21-gene test is limited to lymph node-negative patients with early-stage ER+/PR+, HER2-breast cancer, its prognostic performance in other breast cancer subtypes and in lymph node-positive breast cancers is poorly understood (Poorvu et al., 2020). PAM50 was developed based on the mRNA levels of 50 genes in order to discriminate intrinsic breast cancer subtypes and stratify relapse risks, the C-index of its prognostic value is 0.63–0.67 (Gnant et al., 2015; Wallden et al., 2020). MammaPrint is a diagnostic assay based on 70 genes and evaluates the distant recurrence risk in early-stage breast cancer. This test has been validated in a real-world study, wherein it achieved a C-index of 0.614 (Ibraheem et al., 2020). These findings suggest that our prognostic models have a better predictive accuracy. Additionally, despite the TNM staging system, several predictive models were explored according to inflammatory status, tumor marker, stromal tumor-infiltrating lymphocytes, gene signature and so on with C-index from 0.69 to 0.77 (Shi et al., 2019; Yang et al., 2019; Zheng et al., 2020), compared with these models, our predictive nomogram achieved a comparative prognostic accuracy, and is more economic and convenient. Moreover, our study innovatively proposes a prognostic model in view of the impact of trace element copper with clinicopathological factors.

There are some limitations to our study. Firstly, as a retrospective study, selection bias and incomplete data were inevitable, an external validation rather than a same-institute validation might enhance the power of our predictive models. We minimized the risk of selection bias by enrolling all eligible patients to date and validating our results in a relatively separate cohort. Secondly, the serum cooper might be influenced by food, but we failed to obtain and explore information of patients' dietary, so a prospective study to control these potential confounding factors and validate the prognostic value of our nomograms is warranted in future. Thirdly, we only explored the relationship between the baseline serum copper level at the time of diagnosis and early-stage TNBC. We did not measure the serum copper levels in healthy control subjects without TNBC, and monitor the dynamic changes in serum copper levels during the treatment of TNBC. Fourthly, this study was limited to patients from China, so the extension of our results to patients from other geographic regions or with other racial backgrounds should be done with caution. Finally, fundamental cytological studies and investigations of the underlying mechanisms are necessary to further explore the usefulness of serum copper levels in early-stage TNBC.

In conclusion, we proposed an optimal cut-off value of baseline serum copper levels to maximally distinguish women with early-stage TNBC into different risk groups in current study. Based on this serum copper level cut-off, we developed and validated prognostic models for personalized survival predictions, resulting in satisfactory discrimination and good agreement between the nomogram-predicted and actual survival for survival in training and validations cohorts.

DATA AVAILABILITY STATEMENT

The datasets presented in this study can be found in online repositories. The names of the repository/repositories and accession number(s) can be found below: Research Data Deposit public platform (www.researchdata.org.cn), with the approval RDD number, RDDA2021002097.

ETHICS STATEMENT

The studies involving human participants were reviewed and approved by his study was approved by the ethics committee of Sun Yat-sen University Cancer Center (registration number: B2021-218-01) with a waiver of requirement of patient informed consent because we just retrospectively reviewed their medical data without impairing their health. We covered patient data confidentially and conducted this study in accordance with the Declaration of Helsinki. The ethics committee waived the requirement of written informed consent for participation.

AUTHOR CONTRIBUTIONS

ZY contributed to the design and conception of this study. FD, JL, JH, and XH contributed to the collection, primary analysis, and interpretation of data. FD, JH, XH, CS, and LW participating in the drafting of the manuscript. FD, JL, JH, WX, XB, and ZY contributed in administrative, technical, or material support. All authors contributed to revision of this manuscript and approved the final summitted version.

FUNDING

This study was funded by the Natural Science Foundation of Guangdong Province (No. 2019A151011781), the Sci-Tech Project Foundation of Guangzhou City (No. 202002020033), and the cultivation foundation for the junior teachers in Sun Yat-sen University (No. 20ykpy164).

ACKNOWLEDGMENTS

We gratefully acknowledge patients and their family for all their help in enabling completion of this study.

SUPPLEMENTARY MATERIAL

The Supplementary Material for this article can be found online at: https://www.frontiersin.org/articles/10.3389/fcell.2021.770115/full#supplementary-material

Supplementary Figure S1 | Determination of the cut-off value of serum copper level and survival analyses. X-tile analysis of 10-year OS was performed using the patients' data to identify the best cut off value for serum copper level. The optimal cut-off points highlighted by the black circles in the left panels are shown as histograms of the entire cohort (middle panels), and Kaplan-Meier plots are displayed in the right panels. The optimal cut-off value for serum copper level was 21.3 μmol/L ($\chi 2$ = 11.5172, P = 0.0189).

Supplementary Figure S2 | Kaplan-Meier survival curves with log-rank test in the training cohort. A: Kaplan-Meier estimates of disease-free survival (DFS) probability. B: Kaplan-Meier estimates of overall survival (OS) probability.

REFERENCES

Amin, M. B., Greene, F. L., Edge, S. B., Compton, C. C., Gershenwald, J. E., Brookland, R. K., et al. (2017). The Eighth Edition AJCC Cancer Staging Manual: Continuing to Build a Bridge from a Population-Based to a More "personalized" Approach to Cancer Staging. *CA: A Cancer J. Clinicians* 67 (2), 93–99. doi:10.3322/caac.21388

Angelé-Martínez, C., Nguyen, K. V. T., Ameer, F. S., Anker, J. N., and Brumaghim, J. L. (2017). Reactive Oxygen Species Generation by Copper(II) Oxide Nanoparticles Determined by DNA Damage Assays and EPR Spectroscopy. *Nanotoxicology* 11 (2), 278–288. doi:10.1080/17435390.2017.1293750

Bhattacharjee, A., Chakraborty, K., and Shukla, A. (2017). Cellular Copper Homeostasis: Current Concepts on its Interplay with Glutathione Homeostasis and its Implication in Physiology and Human Diseases. *Metallomics* 9 (10), 1376–1388. doi:10.1039/c7mt00066a

Brady, D. C., Crowe, M. S., Turski, M. L., Hobbs, G. A., Yao, X., Chaikuad, A., et al. (2014). Copper Is Required for Oncogenic BRAF Signalling and Tumorigenesis. *Nature* 509 (7501), 492–496. doi:10.1038/nature13180

Brewer, G. J., Dick, R., Grover, D., LeClaire, V., Tseng, M., Wicha, M., et al. (2000). Treatment of Metastatic Cancer with Tetrathiomolybdate, an Anticopper, Antiangiogenic Agent: Phase I Study. *Clin. Cancer Res. : Official J. Am. Assoc. Cancer Res.* 6 (1), 1–10. doi:10.1097/01.gim.0000245578.94312.1e

Camp, R. L., Dolled-Filhart, M., and Rimm, D. L. (2004). X-tile. *Clin. Cancer Res.* 10 (21), 7252–7259. doi:10.1158/1078-0432.CCR-04-0713

Chan, N., Willis, A., Kornhauser, N., Ward, M. M., Lee, S. B., Nackos, E., et al. (2020). Correction: Influencing the Tumor Microenvironment: A Phase II Study of Copper Depletion Using Tetrathiomolybdate in Patients with Breast Cancer at High Risk for Recurrence and in Preclinical Models of Lung Metastases. *Clin. Cancer Res.* 26 (18), 5051. doi:10.1158/1078-0432.CCR-20-3177

Chan, N., Willis, A., Kornhauser, N., Ward, M. M., Lee, S. B., Nackos, E., et al. (2017). Influencing the Tumor Microenvironment: A Phase II Study of Copper Depletion Using Tetrathiomolybdate in Patients with Breast Cancer at High Risk for Recurrence and in Preclinical Models of Lung Metastases. *Clin. Cancer Res.* 23 (3), 666–676. doi:10.1158/1078-0432.CCR-16-1326

Chaudhary, L. N. (2020). Early Stage Triple Negative Breast Cancer: Management and Future Directions. *Semin. Oncol.* 47 (4), 201–208. doi:10.1053/j.seminoncol.2020.05.006

Cui, L., Gouw, A. M., LaGory, E. L., Guo, S., Attarwala, N., Tang, Y., et al. (2021). Mitochondrial Copper Depletion Suppresses Triple-Negative Breast Cancer in Mice. *Nat. Biotechnol.* 39 (3), 357–367. doi:10.1038/s41587-020-0707-9

Dawson, S. J., Provenzano, E., and Caldas, C. (2009). Triple Negative Breast Cancers: Clinical and Prognostic Implications. *Eur. J. Cancer* 45, 27–40. Oxford, England : 1990. doi:10.1016/S0959-8049(09)70013-9

Denoyer, D., Masaldan, S., La Fontaine, S., and Cater, M. A. (2015). Targeting Copper in Cancer Therapy: 'Copper that Cancer'. *Metallomics* 7 (11), 1459–1476. doi:10.1039/c5mt00149h

Dent, R., Trudeau, M., Pritchard, K. I., Hanna, W. M., Kahn, H. K., Sawka, C. A., et al. (2007). Triple-negative Breast Cancer: Clinical Features and Patterns of Recurrence. *Clin. Cancer Res.* 13, 4429–4434. doi:10.1158/1078-0432.CCR-06-3045

Gnant, M., Sestak, I., Filipits, M., Dowsett, M., Balic, M., Lopez-Knowles, E., et al. (2015). Identifying Clinically Relevant Prognostic Subgroups of Postmenopausal Women with Node-Positive Hormone Receptor-Positive Early-Stage Breast Cancer Treated with Endocrine Therapy: a Combined Analysis of ABCSG-8 and ATAC Using the PAM50 Risk of Recurrence Score and Intrinsic Subtype. *Ann. Oncol.* 26 (8), 1685–1691. doi:10.1093/annonc/mdv215

Gradishar, W. J., Anderson, B. O., Abraham, J., Aft, R., Agnese, D., Allison, K. H., et al. (2020). Breast Cancer, Version 3.2020, NCCN Clinical Practice Guidelines in Oncology. *J. Natl. Compr. Cancer Netw. : JNCCN* 18 (4), 452–478. doi:10.6004/jnccn.2020.0016

Gupte, A., and Mumper, R. J. (2009). Elevated Copper and Oxidative Stress in Cancer Cells as a Target for Cancer Treatment. *Cancer Treat. Rev.* 35 (1), 32–46. doi:10.1016/j.ctrv.2008.07.004

Haffty, B. G., Yang, Q., Reiss, M., Kearney, T., Higgins, S. A., Weidhaas, J., et al. (2006). Locoregional Relapse and Distant Metastasis in Conservatively Managed Triple Negative Early-Stage Breast Cancer. *Jco* 24 (36), 5652–5657. doi:10.1200/jco.2006.06.5664

Hlynialuk, C. J., Ling, B., Baker, Z. N., Cobine, P. A., Yu, L. D., Boulet, A., et al. (2015). The Mitochondrial Metallochaperone SCO1 Is Required to Sustain Expression of the High-Affinity Copper Transporter CTR1 and Preserve Copper Homeostasis. *Cel. Rep.* 10 (6), 933–943. doi:10.1016/j.celrep.2015.01.019

Hothorn, T., and Zeileis, A. (2008). Generalized Maximally Selected Statistics. *Biometrics* 64 (4), 1263–1269. doi:10.1111/j.1541-0420.2008.00995.x

Ibraheem, A., Olopade, O. I., and Huo, D. (2020). Propensity Score Analysis of the Prognostic Value of Genomic Assays for Breast Cancer in Diverse Populations Using the National Cancer Data Base. *Cancer* 126 (17), 4013–4022. doi:10.1002/cncr.32956

Ishida, S., Andreux, P., Poitry-Yamate, C., Auwerx, J., and Hanahan, D. (2013). Bioavailable Copper Modulates Oxidative Phosphorylation and Growth of Tumors. *Proc. Natl. Acad. Sci.* 110 (48), 19507–19512. doi:10.1073/pnas.1318431110

Jouybari, L., Kiani, F., Islami, F., Sanagoo, A., Sayehmiri, F., Hosnedlova, B., et al. (2020). Copper Concentrations in Breast Cancer: A Systematic Review and Meta-Analysis. *Cmc* 27 (37), 6373–6383. doi:10.2174/0929867326666190918120209

Juloski, J. T., Rakic, A., Ćuk, V. V., Ćuk, V. M., Stefanović, S., Nikolić, D., et al. (2020). Colorectal Cancer and Trace Elements Alteration. *J. Trace Elem. Med. Biol.* 59, 126451. doi:10.1016/j.jtemb.2020.126451

Kaiafa, G. D., Saouli, Z., Diamantidis, M. D., Kontoninas, Z., Voulgaridou, V., Raptaki, M., et al. (2012). Copper Levels in Patients with Hematological Malignancies. *Eur. J. Intern. Med.* 23 (8), 738–741. doi:10.1016/j.ejim.2012.07.009

Kaler, S. G. (2011). ATP7A-related Copper Transport Diseases-Emerging Concepts and Future Trends. *Nat. Rev. Neurol.* 7 (1), 15–29. doi:10.1038/nrneurol.2010.180

Kim, C., Gao, R., Sei, E., Brandt, R., Hartman, J., Hatschek, T., et al. (2018). Chemoresistance Evolution in Triple-Negative Breast Cancer Delineated by

Single-Cell Sequencing. *Cell* 173 (4), 879–893. e13. doi:10.1016/j.cell.2018.03.041

Kucharzewski, M., Braziewicz, J., Majewska, U., and Gózdz, S. (2003). Selenium, Copper, and Zinc Concentrations in Intestinal Cancer Tissue and in colon and Rectum Polyps. *Bter* 92 (1), 1–10. doi:10.1385/BTER:92:1:1

Lelièvre, P., Sancey, L., Coll, J.-L., Deniaud, A., and Busser, B. (2020). The Multifaceted Roles of Copper in Cancer: A Trace Metal Element with Dysregulated Metabolism, but Also a Target or a Bullet for Therapy. *Cancers* 12 (12), 3594. doi:10.3390/cancers12123594

MacDonald, G., Nalvarte, I., Smirnova, T., Vecchi, M., Aceto, N., Doelemeyer, A., et al. (2014). Memo Is a Copper-dependent Redox Protein with an Essential Role in Migration and Metastasis. *Sci. Signal.* 7 (329), ra56. doi:10.1126/scisignal.2004870

Mahabir, S., Forman, M. R., Dong, Y. Q., Park, Y., Hollenbeck, A., and Schatzkin, A. (2010). Mineral Intake and Lung Cancer Risk in the NIH-American Association of Retired Persons Diet and Health Study. *Cancer Epidemiol. Biomarkers Prevcosponsored By Am. Soc. Prev. Oncol.* 19 (8), 1976–1983. doi:10.1158/1055-9965.EPI-10-0067

Majumder, S., Chatterjee, S., Pal, S., Biswas, J., Efferth, T., and Choudhuri, S. K. (2009). The Role of Copper in Drug-Resistant Murine and Human Tumors. *Biometals* 22 (2), 377–384. doi:10.1007/s10534-008-9174-3

Mookerjee, A., Mookerjee Basu, J., Dutta, P., Majumder, S., Bhattacharyya, S., Biswas, J., et al. (2006). Overcoming Drug-Resistant Cancer by a Newly Developed Copper Chelate through Host-Protective Cytokine-Mediated Apoptosis. *Clin. Cancer Res.* 12, 4339–4349. doi:10.1158/1078-0432.CCR-06-0001

Poorvu, P. D., Gelber, S. I., Rosenberg, S. M., Ruddy, K. J., Tamimi, R. M., Collins, L. C., et al. (2020). Prognostic Impact of the 21-Gene Recurrence Score Assay Among Young Women with Node-Negative and Node-Positive ER-Positive/HER2-Negative Breast Cancer. *Jco* 38 (7), 725–733. doi:10.1200/JCO.19.01959

Schwartz, M. K. (1975). Role of Trace Elements in Cancer. *Cancer Res.* 35, 3481–3487.

Setty, S. R. G., Tenza, D., Sviderskaya, E. V., Bennett, D. C., Raposo, G., and Marks, M. S. (2008). Cell-specific ATP7A Transport Sustains Copper-dependent Tyrosinase Activity in Melanosomes. *Nature* 454 (7208), 1142–1146. doi:10.1038/nature07163

Shanbhag, V., Jasmer-McDonald, K., Zhu, S., Martin, A. L., Gudekar, N., Khan, A., et al. (2019). ATP7A Delivers Copper to the Lysyl Oxidase Family of Enzymes and Promotes Tumorigenesis and Metastasis. *Proc. Natl. Acad. Sci. USA* 116 (14), 6836–6841. doi:10.1073/pnas.1817473116

Shi, H., Wang, X.-H., Gu, J.-W., and Guo, G.-L. (2019). Development and Validation of Nomograms for Predicting the Prognosis of Triple-Negative Breast Cancer Patients Based on 379 Chinese Patients. *Cmar* l1, 10827–10839. doi:10.2147/cmar.s234926

Tang, J., Robertson, S., Lem, K. E., Godwin, S. C., and Kaler, S. G. (2006). Functional Copper Transport Explains Neurologic Sparing in Occipital Horn Syndrome. *Genet. Med.* 8 (11), 711–718. doi:10.1097/01.gim.0000245578.94312.1eBrewer

Terada, K., Aiba, N., Yang, X.-L., Iida, M., Nakai, M., Miura, N., et al. (1999). Biliary Excretion of Copper in LEC Rat after Introduction of Copper Transporting P-type ATPase, ATP7B. *FEBS Lett.* 448 (1), 53–56. doi:10.1016/s0014-5793(99)00319-1

Thompson, C. A., Habermann, T. M., Wang, A. H., Vierkant, R. A., Folsom, A. R., Ross, J. A., et al. (2010). Antioxidant Intake from Fruits, Vegetables and Other Sources and Risk of Non-hodgkin's Lymphoma: the Iowa Women's Health Study. *Int. J. Cancer* 126 (4), 992–1003. doi:10.1002/ijc.24830

Wallden, B., Storhoff, J., Nielsen, T., Dowidar, N., Schaper, C., Ferree, S., et al. (2015). Development and Verification of the PAM50-Based Prosigna Breast Cancer Gene Signature Assay. *BMC Med. Genomics* 8, 54. doi:10.1186/s12920-015-0129-6

Wang, X., Wang, S.-S., Huang, H., Cai, L., Zhao, L., Peng, R.-J., et al. (2021). Effect of Capecitabine Maintenance Therapy Using Lower Dosage and Higher Frequency vs Observation on Disease-free Survival Among Patients with Early-Stage Triple-Negative Breast Cancer Who Had Received Standard Treatment. *JAMA* 325 (1), 50–58. doi:10.1001/jama.2020.23370

Wileyto, E. P., Li, Y., Chen, J., and Heitjan, D. F. (2013). Assessing the Fit of Parametric Cure Models. *Biostatistics* 14 (2), 340–350. doi:10.1093/biostatistics/kxs043

Xu, M., Casio, M., Range, D. E., Sosa, J. A., and Counter, C. M. (2018). Copper Chelation as Targeted Therapy in a Mouse Model of Oncogenic BRAF-Driven Papillary Thyroid Cancer. *Clin. Cancer Res.* 24 (17), 4271–4281. doi:10.1158/1078-0432.CCR-17-3705

Yang, Y., Wang, Y., Deng, H., Tan, C., Li, Q., He, Z., et al. (2019). Development and Validation of Nomograms Predicting Survival in Chinese Patients with Triple Negative Breast Cancer. *BMC Cancer* 19 (1), 541. doi:10.1186/s12885-019-5703-4

Zheng, S., Zou, Y., Liang, J. y., Xiao, W., Yang, A., Meng, T., et al. (2020). Identification and Validation of a Combined Hypoxia and Immune index for Triple-negative Breast Cancer. *Mol. Oncol.* 14 (11), 2814–2833. doi:10.1002/1878-0261.12747

Conflict of Interest: The authors declare that the research was conducted in the absence of any commercial or financial relationships that could be construed as a potential conflict of interest.

Publisher's Note: All claims expressed in this article are solely those of the authors and do not necessarily represent those of their affiliated organizations, or those of the publisher, the editors and the reviewers. Any product that may be evaluated in this article, or claim that may be made by its manufacturer, is not guaranteed or endorsed by the publisher.

frontiers in Cell and Developmental Biology

ORIGINAL RESEARCH
published: 07 December 2021
doi: 10.3389/fcell.2021.788451

A Novel lncRNA Panel Related to Ferroptosis, Tumor Progression, and Microenvironment is a Robust Prognostic Indicator for Glioma Patients

Yikang He[1], *Yangfan Ye*[2,3], *Wei Tian*[2,3]* *and Huaide Qiu*[4]*

[1]Department of Rehabilitation, Zhongda Hospital, School of Medicine, Southeast University, Nanjing, China, [2]Department of Neurosurgery, The First Affiliated Hospital of Nanjing Medical University, Nanjing, China, [3]The First Clinical Medical College, Nanjing Medical University, Nanjing, China, [4]Center of Rehabilitation Medicine, The First Affiliated Hospital of Nanjing Medical University, Nanjing, China

OPEN ACCESS

Edited by:
Maryam Mehrpour,
Université Paris Descartes, France

Reviewed by:
Ian Kerr,
University of Nottingham, United Kingdom
Ella L. Kim,
Johannes Gutenberg University Mainz, Germany

***Correspondence:**
Wei Tian
a983314518@126.com
Huaide Qiu
James55@njmu.edu.cn

Specialty section:
This article was submitted to Molecular and Cellular Oncology, a section of the journal Frontiers in Cell and Developmental Biology

Received: 02 October 2021
Accepted: 16 November 2021
Published: 07 December 2021

Citation:
He Y, Ye Y, Tian W and Qiu H (2021) A Novel lncRNA Panel Related to Ferroptosis, Tumor Progression, and Microenvironment is a Robust Prognostic Indicator for Glioma Patients. Front. Cell Dev. Biol. 9:788451. doi: 10.3389/fcell.2021.788451

Objective: To establish a lncRNA panel related to ferroptosis, tumor progression, and microenvironment for prognostic estimation in patients with glioma.

Methods: LncRNAs associated with tumor progression and microenvironment were screened via the weighted gene co-expression network analysis (WGCNA). Overlapped lncRNAs highlighted in WGCNA, related to ferroptosis, and incorporated in Chinese Glioma Genome Atlas (CGGA) were identified as hub lncRNAs. With expression profiles of the hub lncRNA, we conducted the least absolute shrinkage and selection operator (LASSO) regression and built a ferroptosis-related lncRNA signature to separate glioma patients with distinct survival outcomes. The lncRNA signature was validated in TCGA, the CGGA_693, and CGGA_325 cohorts using Kaplan-Meier survival analysis and ROC curves. The ferroptosis-related lncRNA panel was validated with 15 glioma samples using quantitative real-time PCR (qRT-PCR). Multivariate Cox regression was performed, and a nomogram was mapped and validated. Immune infiltration correlated to the signature was explored using TIMER and CIBERSORT algorithms.

Results: The present study identified 30 hub lncRNAs related to ferroptosis, tumor progression, and microenvironment. With the 30 hub lncRNAs, we developed a lncRNA signature with distinct stratification of survival chance in patients with glioma in two independent cohorts (HRs>1, $p < 0.05$). The lncRNA signature revealed a panel of 14 lncRNAs, i.e., APCDD1L-AS1, H19, LINC00205, LINC00346, LINC00475, LINC00484, LINC00601, LINC00664, LINC00886, LUCAT1, MIR155HG, NEAT1, PVT1, and SNHG18. These lncRNA expressions were validated in clinical specimens using qRT-PCR. Robust predictive accuracies of the signature were present across different datasets at multiple timepoints. With univariate and multivariate regressions, we demonstrated that the risk score based on the lncRNA signature is an independent prognostic indicator after clinical factors were adjusted. A nomogram was constructed with these prognostic factors, and it has demonstrated decent classification and accuracy. Additionally, the

signature-based classification was observed to be correlated with multiple clinical characteristics and molecular subtypes. Further, extensive immune cells were upregulated in the high-risk group, such as $CD8^+$ T cell, neutrophil, macrophage, and myeloid dendritic cell, indicating increased immune infiltrations.

Conclusion: We established a novel ferroptosis-related lncRNA signature that could effectively stratify the prognosis of glioma patients with adequate predictive performance.

Keywords: long non-coding RNAs, prognostic signature, glioma, the cancer genome atlas, chinese glioma genome atlas

INTRODUCTION

Glioma is the most common intracranial malignancy, accounting for 80% of brain malignancies and 30% of brain tumors (de Robles et al., 2015). Adult diffused gliomas were classified into lower-grade glioma (LGG) and glioblastoma multiforme (GBM), as indicated in the 2016 World Health Organization (WHO) classification (Louis et al., 2016; Wen and Huse, 2017). While GBM presents an inferior prognosis with a median survival of 14.6 months (Lara-Velazquez et al., 2017), most LGG progresses to GBM, leading to an unfavorable overall survival rate (Ostrom et al., 2014; Claus et al., 2015; Lim et al., 2018; Kirby and Finnerty, 2020). Interestingly, patients with LGG could decease within months post-surgery while those with GBM lived for years in some cases, which indicates that the current classification of gliomas does not reflect the distinct survival outcomes (Chen et al., 2017). To evaluate prognosis and develop therapeutic strategies, molecular biomarkers including O6-methylguanine-DNA methyltransferase (MGMT) methylation, codeletion of chromosome 1 and 19 (1p/19q), mutations in isocitrate dehydrogenase (IDH) are under active investigation in patients with glioma (Molinaro et al., 2019). Although these molecular biomarkers are implicated in the regulation of cancer cell proliferation and death (Ceccarelli et al., 2016), it remains a challenge to inform individual prognosis and treatment. Therefore, novel biomarkers are warranted for prognostic stratification and therapeutic strategies.

Ferroptosis, a novel form of programmed cell death, is characterized by the aberrant accumulation of lipid peroxide related to iron metabolism (Dixon et al., 2012). Various types of cancer cells were observed to be sensitive to ferroptosis (Eling et al., 2015; Belavgeni et al., 2019; Carbone and Melino, 2019), which may alter the process of cancer development and therapies (Gan, 2019; Liang et al., 2019; Stockwell and Jiang, 2019). Additionally, genes with regulatory effects on ferroptosis, such as P53 (Junttila and Evan, 2009), DPP4 (Enz et al., 2019), and HSPB1 (Arrigo and Gibert, 2012), are associated with the development and progression of cancers. Besides, ferroptosis-related genes have shown potentials to be prognostic biomarkers in glioma (Liu et al., 2020; Zhuo et al., 2020), indicating the significance of ferroptosis in glioma.

Long non-coding RNAs (lncRNAs) are a type of transcripts with more than 200 nucleotides which does not code for proteins (Clark et al., 2012). lncRNAs are the major component of human transcriptome with a proportion up to 80% (Hong et al., 2020). Owing to the ubiquitous regulatory effect of lncRNAs, it is involved in tumorigenesis in numerous cancers. Moreover, dysregulation of lncRNAs has been reported to be associated with the pathogenicity of gliomas (Bhan et al., 2017). Further, there has been emerging reports of lncRNA signatures in predicting survival of glioma patients (Wang et al., 2018; Luan et al., 2019; Xia et al., 2020). A ferroptosis-related lncRNAs signature was observed to be associated with prognosis, tumor microenvironment, and response to radiotherapy in glioma (Zheng et al., 2021). However, the previous study used median risk scores for each dataset, leading to half-by-half classifications and potential false-positive results. In machine learning models, a consistent cutoff value for different datasets enhances generalizability, and thereby increasing applicability in real world.

In the present study, we sought to establish a ferroptosis-related lncRNA signature with transcriptomic and clinical data from the Cancer Genome Atlas (TCGA) and two cohorts from the Chinese Glioma Genome Atlas (CGGA). We analyzed the expression profiles of ferroptosis-related lncRNAs and fitted key lncRNAs into a prediction model, which was rigorously validated in three datasets with the same cutoff value. Our data indicate that the ferroptosis-related lncRNA signature is ready to serve as a novel prognostic panel, and therapies targeting these lncRNAs might yield effective results.

MATERIALS AND METHODS

Data Collection

RNA sequencing (RNA-seq) data and corresponding clinical information of 698 glioma samples were taken from TCGA (https://portal.gdc.cancer.gov), while the test datasets with 693 glioma samples (CGGA_693) as well as with 325 samples (CGGA_325) was retrieved from the CGGA (http://www.cgga.org.cn). Then ferroptosis-related genes were retrieved from previous literature (Liu et al., 2020).

Coexpression Network Identified Clinically Relevant Long Non-Coding RNAs

The lncRNAs associated with tumor progression and microenvironment were screened using the weighted gene co-expression network analysis (WGCNA) package (Langfelder and Horvath, 2008). Samples and lncRNAs were filtered with

statistical tests, while outliers were detected with hierarchical clustering. Then we selected the soft threshold and engendered the hierarchical clustering tree. Module eigengene (ME) representing the overall expression level of the module was calculated, and the Pearson correlation coefficients between lncRNA modules and clinical traits were calculated to identify modules of interest. Modules with correlation coefficients >0.5 with regarding to tumor grade and ESTIMATE scores were identified, and lncRNAs in these modules were identified as clinically relevant lncRNAs.

Subsequently, we calculated the correlation coefficients between each gene expression in the specific module and clinical trait, and the value of coefficients were defined as gene significance (GS). Module memberships (MMs) were defined as the coefficients between gene expression and MEs. Correlations between GS and MMs were analyzed to verify the significance of lncRNAs in the specific module.

Identification of Hub Long Non-Coding RNAs and Development of a Prognostic Signature

Based on the list of clinically relevant lncRNAs, we identified specific ferroptosis-related lncRNAs whose expression was correlated to ferroptosis-related genes (Pearson Cor>0.5 and $p < 0.05$). Overlapped lncRNAs indexed in the ferroptosis-related lncRNA list, highlighted in WGCNA, and incorporated in CGGA were identified as hub lncRNAs. With expression profiles of the hub lncRNA, we conducted the least absolute shrinkage and selection operator (LASSO) regression analysis (Meier et al., 2008) and selected key lncRNAs in TCGA dataset. Subsequently, we calculated the individualized risk score with coefficients and expression levels of the key lncRNAs, which stands for a ferroptosis-related prognostic signature that separates the high-risk glioma patients from the low-risk ones. The formulae for risk score were as follows.

$$\text{risk score} = \Sigma\beta_i{}^{*}X_i$$

(X_i represents the identified hub lncRNA expression, and β_i represents the corresponding coefficient.)

TCGA-glioma patients were divided into high-risk and low-risk groups based on the median risk score as the cutoff. Then the clinical relevance was validated using Kaplan-Meier survival analysis between risk groups. The prognostic signature was presented as a risk plot that includes the distribution of risk score and classification of survival status for patients in different groups. The time-dependent receiver operating characteristic (ROC) analysis was performed (Heagerty et al., 2000), and the area under the curve (AUC) was calculated to evaluate the prognostic accuracy in the TCGA-glioma patients at 1-year, 3-years, and 5-years post-operation. AUC>0.7 was considered adequate accuracy. The prognostic signature with the same risk score formula and cutoff value was then validated in the CGGA-glioma patients. It was then validated in CGGA using Kaplan-Meier survival analysis, ROC curves, as well as a risk plot.

The Independently Prognostic Value of the Signature

The univariate and multivariate Cox regressions were conducted to determine whether the prognostic signature was independent of clinical characteristics as well as to identify other independent prognostic factors. To determine whether the signature was independent of additional treatment, we also conducted subgroup survival analysis with variables of chemotherapy and radiotherapy. A nomogram was constructed with these prognostic factors using the rms R package, and it was validated using calibration plot (Qiu et al., 2020). Additionally, the correlation between the prognostic signature and clinical characteristics were explored by chi-square test using TCGA.

Quantitative Real-Time PCR Analysis of Long Non-Coding RNAs in Glioma Tissues

A total of 15 glioma specimens (nine LGG vs six high-grade gliomas [HGG]) were obtained from the Department of Neurosurgery, First Affiliated Hospital of Nanjing Medical University. All specimens were stored in liquid nitrogen, and all patients provided informed consent. The collecting of specimens was approved by the Ethics Committee of First Affiliated Hospital of Nanjing Medical University (No: 2020-SRFA-167).

Total RNA extraction was performed by standard procedures. quantitative real-time PCR (qRT-PCR) was conducted using Oligo primers (Tsingke Biotechnology, for indicated lncRNAs with AceQ qPCR SYBR Master Mix (Vazyme, Q141-02). In all assays, GAPDH served as normalization control. Data were analyzed using the $-\Delta\Delta$Ct method with each test performed in triplicate.

Immune Infiltration Correlated to the Long Non-Coding RNAs Signature

To explore the immune infiltration in the glioma samples stratified by the signature, immune cell abundances were calculated using TIMER (Li et al., 2020) and CIBERSORT (Newman et al., 2015). Between-group comparisons were conducted using Wilcoxon test, and immune cell types with $p < 0.05$ were kept for visualization.

Statistical Analysis

Cox regression analysis and Kaplan-Meier method were performed for survival analysis, where Cox p-values and log-rank p-values were calculated. Pearson correlation was applied to determine significant correlations between continuous variables, while chi-square test was adopted to delineate correlations between categorical variables. PCR data were analyzed with independent T tests between groups. Multiple T tests were corrected using the Two-stage linear step-up procedure of Benjamini, Krieger and Yekutieli, with q = 1% being statistically significant (Benjamini et al., 2006). Data were analyzed using R software 4.1.1 and GraphPad Prism 8.3.0, where p-value<0.05 was regarded as statistically significant.

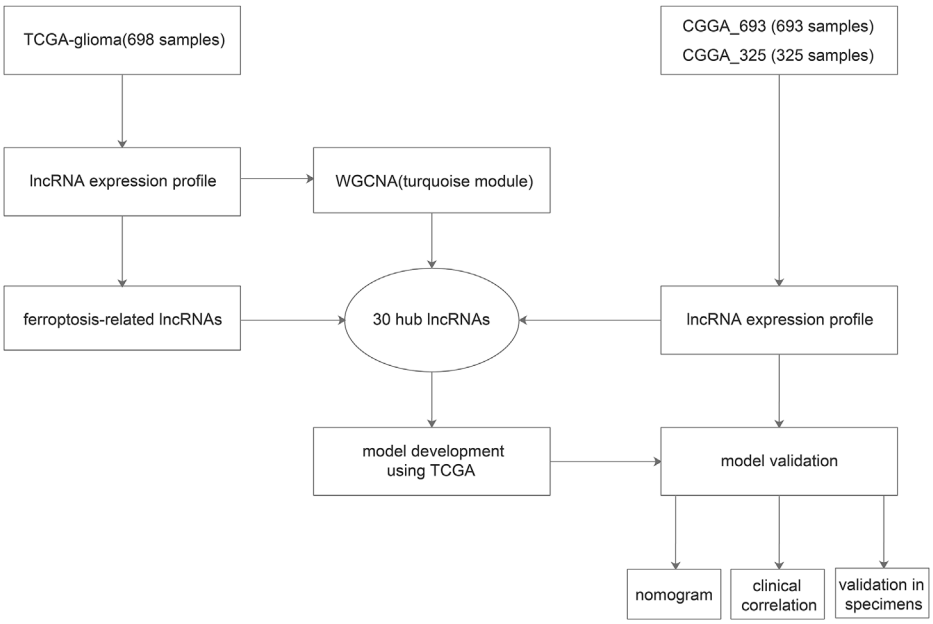

FIGURE 1 | Work flow of the present study.

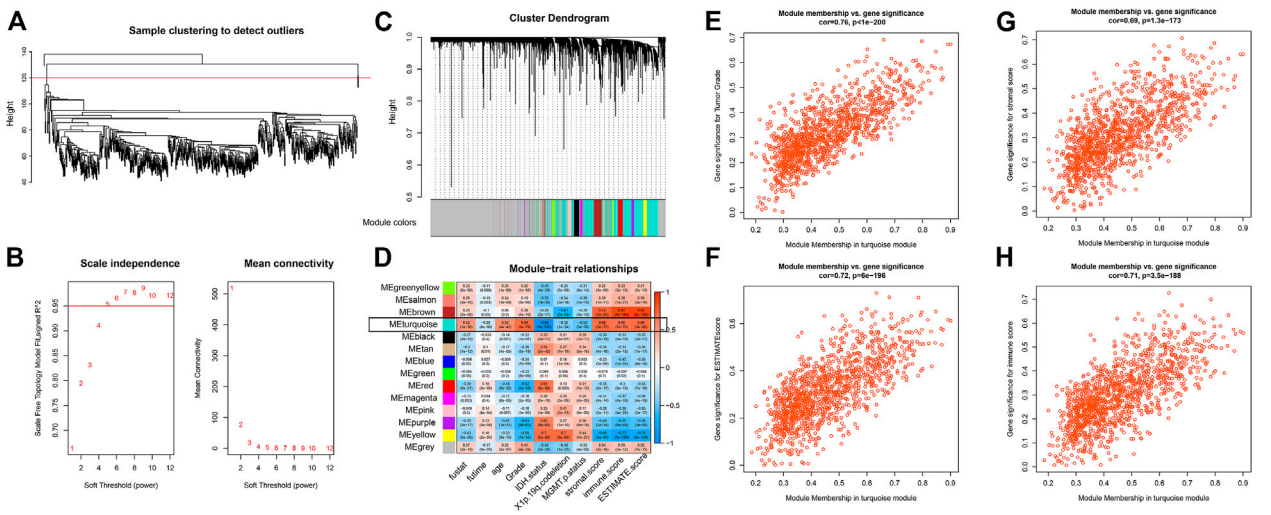

FIGURE 2 | WGCNA using lncRNA expressions **(A)** Sample clustering to detect outliers **(B)** Soft threshold selection **(C)** Cluster dendrogram to distinguish modules **(D)** Correlation matrix between modules and clinical traits **(E–H)** Scatter plot with GS and MM in the turquoise module with regard to tumor grade **(E)**, ESTIMATE combined score **(F)**, ESTIMATE stromal score **(G)**, and ESTIMATE immune score **(H)**.

RESULTS

Identification of Hub Long Non-Coding RNAs and Enrichment Analysis

The flow chart of the present study is presented in **Figure 1**. Using the WGCNA package, we performed the hierarchical clustering and detected one outlier (**Figure 2A**). With the cutoff value of 0.95 in Scale-free R^2, the soft-thresholding power was set to be five (**Figure 2B**). The clustering dendrograms identified 14 modules (**Figure 2C**), out of which the turquoise module was significantly correlated with tumor grade as well as tumor microenvironment (Cor>0.5, **Figure 2D**). To be specific, features including tumor grade, ESTIMATE combined score, stromal score, and immune score were highlighted. Scatterplots of GS for the aforementioned features versus MM in the turquoise module exhibit a marked correlation, suggesting the functional significance of these lncRNAs in the turquoise module (**Figures 2E–H**). Therefore, a total of 1223 clinically

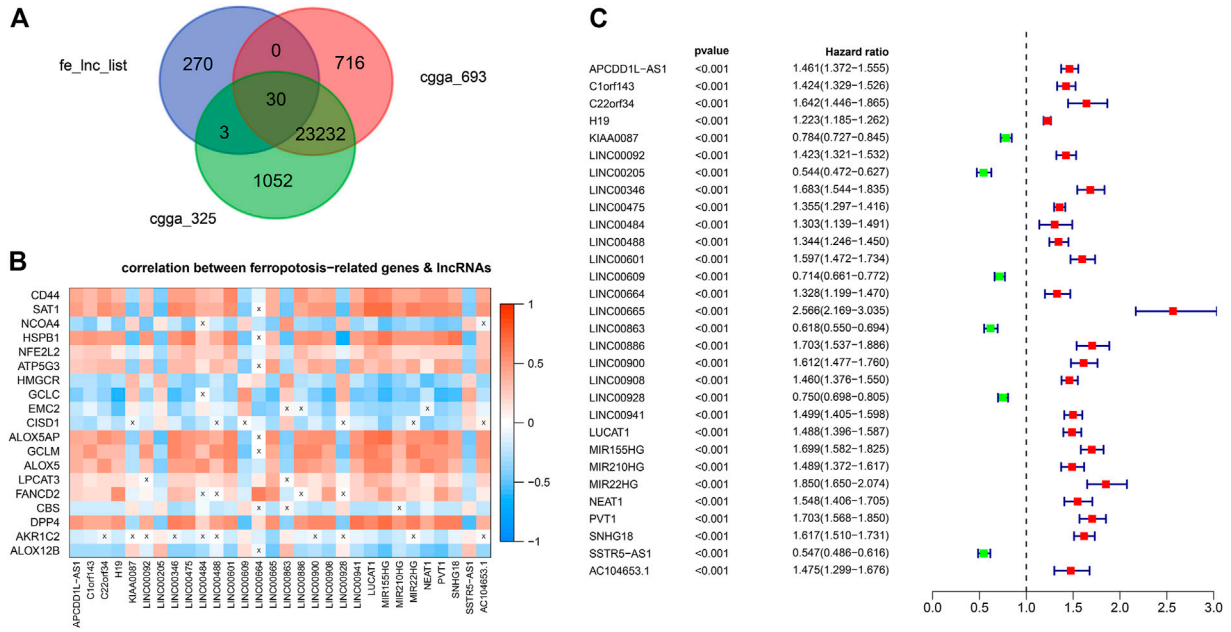

FIGURE 3 | Identification of hub lncRNAs **(A)** Venn Gram for identification of hub lncRNAs **(B)** Correlation matrix of hub lncRNAs and genes implicated in ferroptosis **(C)** Forest plot showing prognostic value of the 30 hub lncRNAs.

relevant lncRNAs embedded in the turquoise module were selected.

Development and Validation of the Prognostic Signature

Out of the 1223 lncRNAs in the turquoise module, 303 lncRNAs were related to ferroptosis. After intersecting the 303 ferroptosis-related lncRNAs with the gene list of CGGA, we retrieved 30 hub lncRNAs (**Figure 3A**). The correlation between the expressions of 30 hub lncRNAs (columns) and ferroptosis-related genes (rows) was presented in **Figure 3B**. The forest plot showing prognostic value of the 30 hub lncRNAs was presented in **Figure 3C**. With the 30 hub lncRNAs, we selected 14 key lncRNAs with Lasso regression using TCGA dataset (**Figures 4A,B**). As shown in **Figure 4C**, the 14 lncRNAs were as follows (with absolute value of model coefficients increasing): APCDD1L-AS1, H19, LINC00205, LINC00346, LINC00475, LINC00484, LINC00601, LINC00664, LINC00886, LUCAT1, MIR155HG, NEAT1, PVT1, and SNHG18. Except for LINC00205 exhibits a negative coefficient on risk score, which indicates its protective effects on prognosis, the other lncRNAs were observed to be risk factors with positive coefficients (**Figure 4C**). Subsequently, we calculated individualized risk scores with coefficient-weighted expression levels of 14 lncRNAs after extracting the coefficients. TCGA-glioma patients were divided into high-score and low-score groups based on the median risk score of 3.04 as the cutoff. Significant difference was shown between these two groups in survival analysis (**Figure 4D**, HR = 3.1, 95% CI = 2.7–3.6, $p < 0.001$). ROC curve analysis of the signature in TCGA-glioma patients achieved AUC of 0.853, 0.856, and 0.825 at 1-, 3- and 5-years (**Figure 4E**). The risk plot presented a clear separation of survival status between risk groups with red dots being ceased cases and blue ones alive (**Figure 4F**). Likewise, we calculated individualized risk scores in CCGA_693 and CGGA_325 glioma patients and divided them into high-risk and low-risk groups with the same cutoff value (3.04). The patients in high-risk group had worse prognosis compared to those in low-risk group (**Figures 4G,J**). And ROC curve analysis of the signature in CGGA_693 achieved AUCs of 0.719, 0.783, and 0.782 at 1-, 3- and 5-years respectively, indicating a moderately high sensitivity and specificity of the signature in predicting patients' survival (**Figure 4H**). Similar result was observed in ROC curve analysis of the signature based on the CGGA_325 (**Figure 4K**). Further, we revealed the distribution patterns of risk scores and survival status, and found that the survival time of patients with high-risk scores was markedly lower than that of patients with low-risk scores (**Figures 4I, 4L**).

Assessment of the Independence of the Prognostic Signature

We next sought to determine whether the risk score based on the lncRNA signature is an independent prognostic indicator of OS in glioma patients. The risk score and several clinicopathological variables such as gender, age, grade, IDH mutation status, 1p19q-codeletion status, MGMT promoter methylation status, radiotherapy and chemotherapy were included in univariate and multivariate Cox regression analyses. Univariate Cox regression analysis showed that risk score, age, grade,

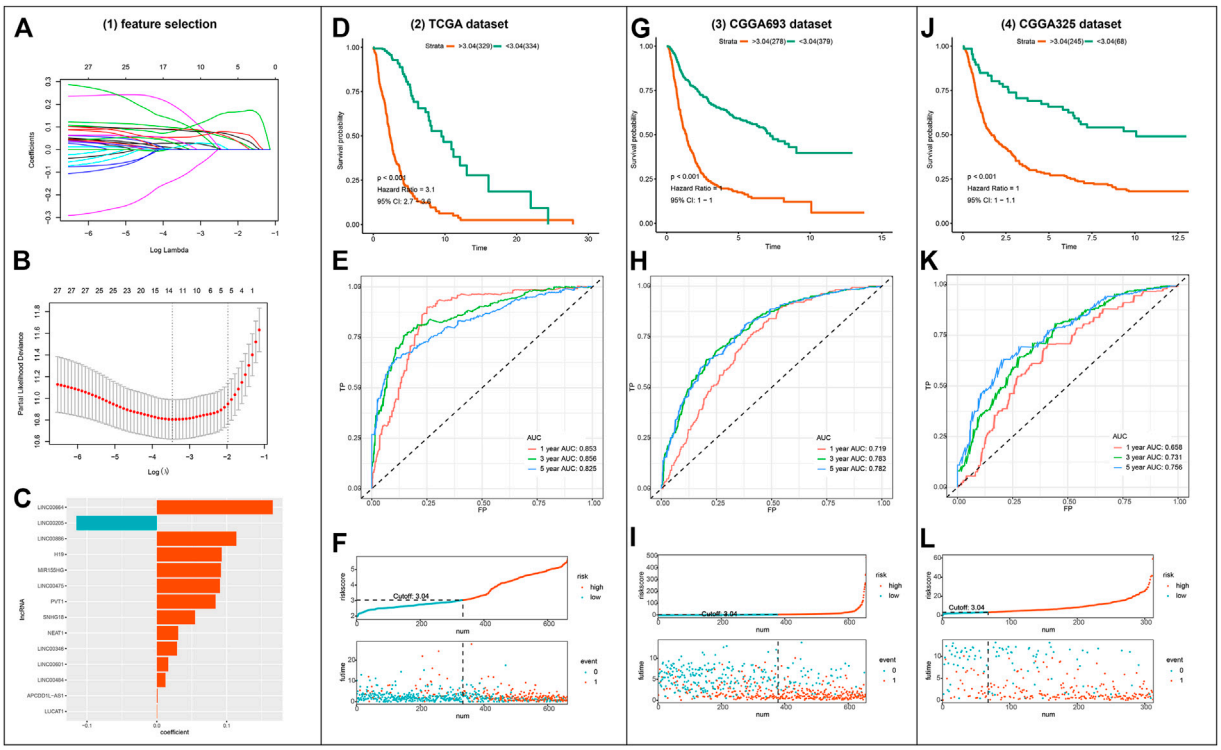

FIGURE 4 | Construction and validation of the ferroptosis-related lncRNA signature **(A–B)** Visualization of LASSO regression **(C)** Coefficients of the 14 lncRNAs fitted in the signature **(D)** Kaplan-Meier curve presenting survival of high-risk and low-risk groups in TCGA **(E)** Time-dependent ROC for the signature in TCGA **(F)** Discriminative plot of the signature using TCGA **(G, J)** Kaplan-Meier curve presenting survival of high-risk and low-risk groups in CGGA_693 or CGGA_325 respectively **(H, K)** Time-dependent ROC for the signature in CGGA_693 or CGGA_325 respectively **(I, L)** Discriminative plot of the signature using CGGA_693 or CGGA_325 separately.

radiotherapy, IDH mutation status, 1p19q-codeletion status and MGMT promoter methylation status were significantly correlated with the OS of glioma patients, whereas gender and chemotherapy did not show any correlation (**Figure 5A**, left panel). Four variables were further identified as independent prognostic factors of OS by multivariate analysis, including risk score (HR = 2.257, 95% CI = 1.437–3.544, $p < 0.001$), age (HR = 1.040, 95% CI = 1.022–1.059, $p < 0.001$), grade (HR = 2.130, 95% CI = 1.365–3.324, $p < 0.001$) and radiotherapy (HR = 0.507, 95% CI = 0.279–0.920, $p = 0.026$) (**Figure 5A**, right panel). Further, subgroup survival analysis showed the signature predicts overall survival in groups with chemotherapy (**Figure 5B**), without chemotherapy (**Figure 5C**), with radiotherapy (**Figure 5D**), and without radiotherapy (**Figure 5E**).

With the aforementioned independent prognostic factors, we established a nomogram for predicting individual OS. As presented in **Figure 5F**, the clinicians can predict survival outcome for individuals with known age, tumor grade, and risk score in an intuitive manner. The classification accuracy was 0.941, 0.964, and 0.897 for 1-, 3-, and 5-years survival prediction (**Figure 5G**). Further, the prediction accuracy was also evaluated with calibration plots, which showed that the nomogram-based prediction was highly consistent with the actual survival at 1-, 3-, and 5-years post-operation (**Figure 5H**).

Clinical Correlations of the Prognostic Classifier

As shown in **Figure 6A**, the prognostic classifier was significantly correlated with multiple clinical features, including age, grade, chemotherapy, radiotherapy and MGMT promoter methylation status, 1p19q-codeletion status, and IDH mutation status ($p < 0.001$). Notably, the correlation between the lncRNA signature and grade was prominent. Further, we analyzed the expressions of 14 lncRNA signatures between high-grade and lower-grade samples, and the between-group results were distinct ($p < 0.001$) (**Figure 6B**).

Validations for Long Non-Coding RNAs Expressions With Quantitative Real-Time PCR

Out of the 14 lncRNAs, high expressions of PVT1 and SNHG18 in glioblastoma samples as opposed to LGG was validated in the previous study (Zheng et al., 2021). Likewise, lncRNA MIR155HG was reported in high-grade glioma as compared to LGG (He et al., 2021). As such, we hereby validated the other 11 lncRNAs in clinical specimens. As shown in **Figure 6C**, we successfully validated 11 lncRNAs, i.e., APCDD1L-AS1, H19, LINC00205, LINC00346, LINC00475, LINC00484, LINC00601,

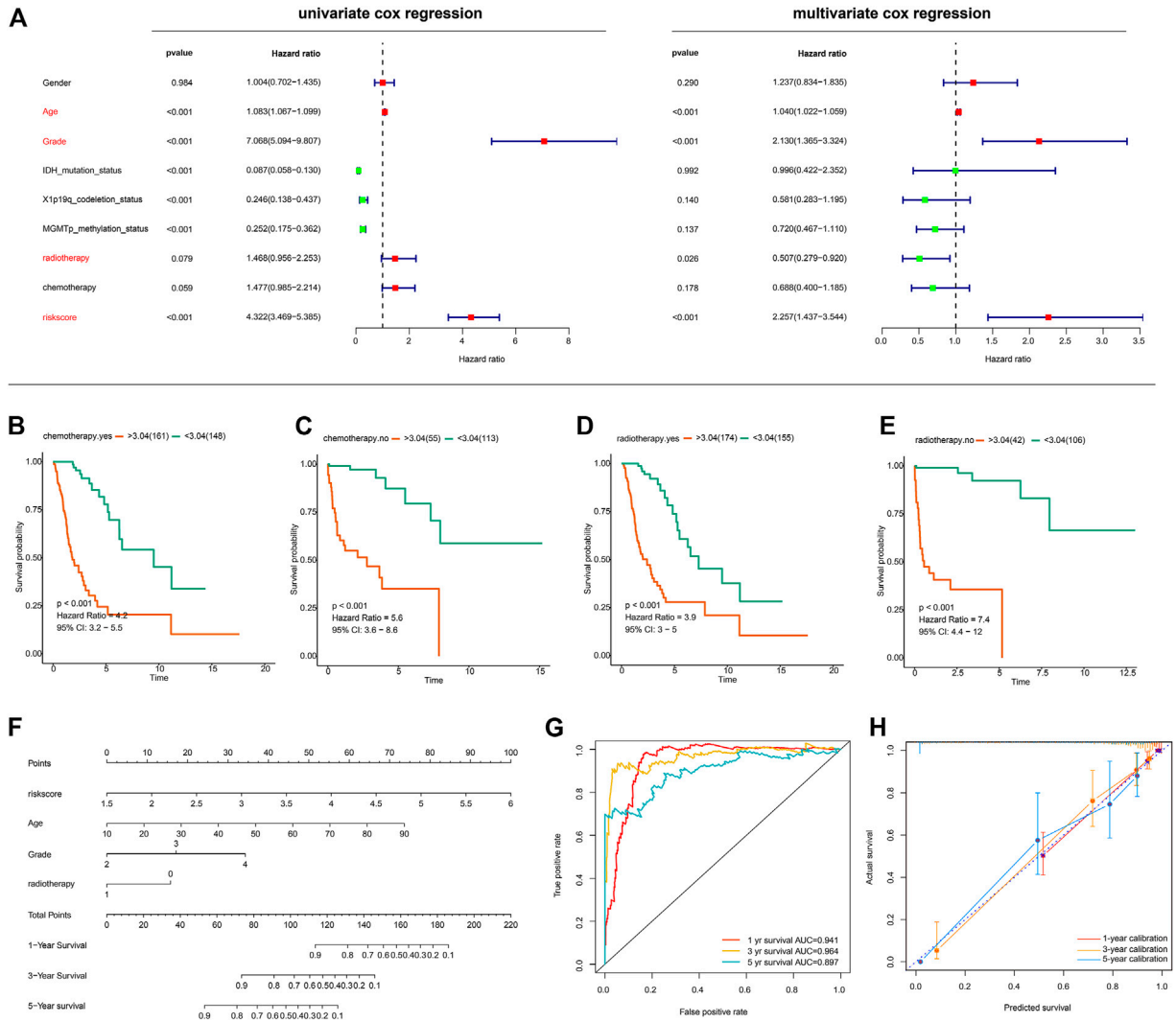

FIGURE 5 | Evaluation of the prognostic signature and establishment of a nomogram **(A)** Univariate and Multivariate Cox regression analysis of the ferroptosis-related lncRNA signature and other clinicopathological features in gliomas **(B–E)** Subgroup survival analysis using groups with chemotherapy **(B)**, without chemotherapy **(C)**, with radiotherapy **(D)**, without radiotherapy **(E)** **(F)** The nomogram incorporating independent prognostic factors **(G)** ROC curves for the nomogram-based classification at multiple timepoints **(H)** Calibration plots for 1-, 3-, and 5-years survival predictions.

LINC00664, LINC00886, LUCAT1, NEAT1 ($q < 0.0001$). Apart from LINC00205, all the other lncRNAs were upregulated in HGG (**Figures 6C,D**).

Immune Infiltration in the High-Risk Group

Using the TIMER algorithm, we identified four types of immune cells upregulated in the high-risk group, i.e., $CD8^+$ T cell, neutrophil, macrophage, and myeloid dendritic cell (**Figure 7**). With CIBERSORT algorithm, more extensive immune cell components were identified, such as B cell memory, T cell $CD4^+$ memory (resting and activated), macrophage (M0, M1, and M2), and mast cell activated. These results indicate there was increased immune infiltration in the high-risk group defined by the ferroptosis-related lncRNA signature (**Figure 7**).

DISCUSSION

Due to the inherent heterogeneity of glioma, the current WHO classification of gliomas does not sufficiently characterize the distinct survival outcomes. Even with well-established molecular markers, the prognosis stratification and treatment of glioma patients remain challenges. Ferroptosis is involved in the development and progression of cancers and its pivotal role in glioma has been recently unveiled (Liu et al., 2020). In this context, the present study aimed to establish a novel ferroptosis-related lncRNA signature for glioma.

Our study identified 30 ferroptosis-related lncRNAs in association with tumor grade and microenvironment via WGCNA. With the 30 hub lncRNAs, we developed a lncRNA signature for prognosis prediction. The ferroptosis-related lncRNA

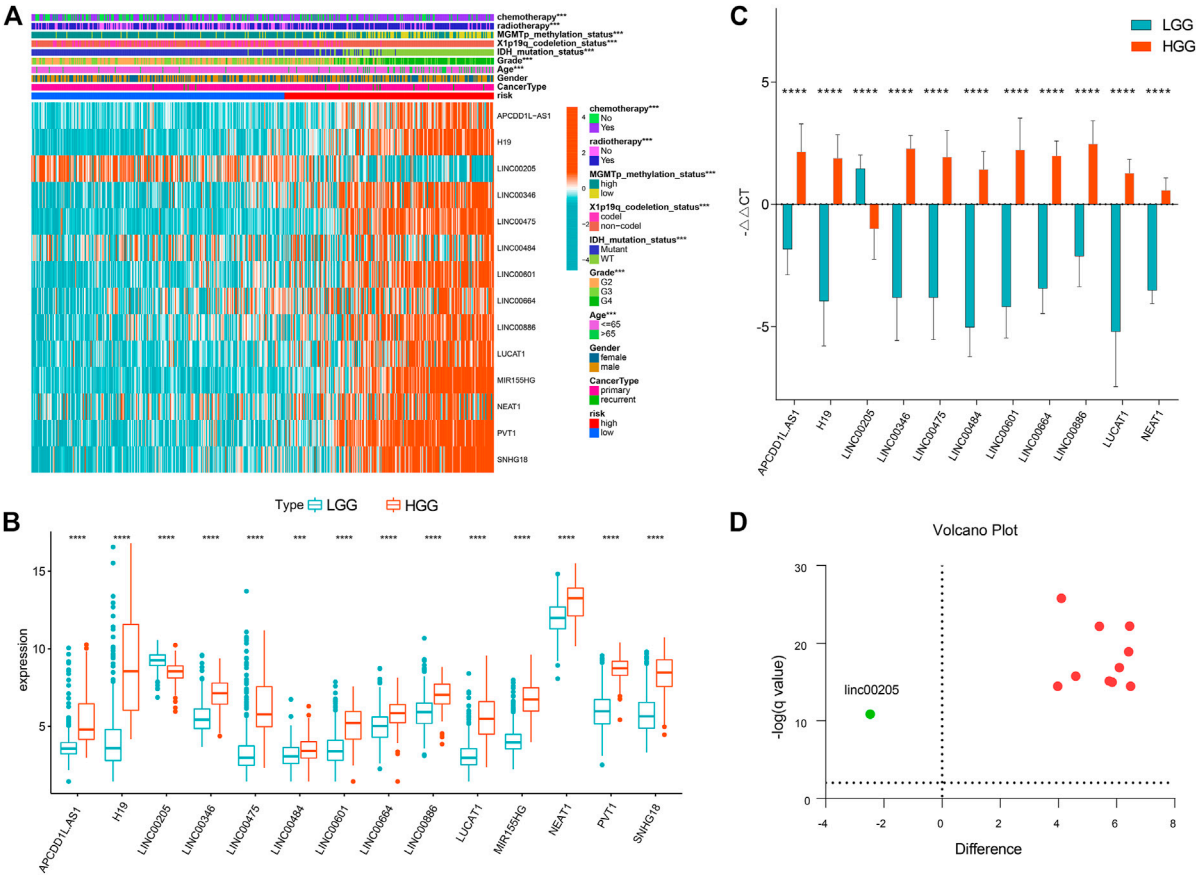

FIGURE 6 | Clinical correlation of the prognostic signature **(A)** Heatmap presenting correlations between the signature and clinical features **(B)** Boxplot showing lncRNA expressions between high-grade and lower-grade samples. ***$p < 0.001$, ****$p < 0.0001$ **(C)** Validation for the lncRNA signature in glioma samples using qRT-PCR. ****q < 0.0001. **(D)** Valcano plot showing expressions of the 14 lncRNAs across LGG and HGG. Red dots represent upregulated lncRNAs in HGG and the green dot represents downregulated lncRNA.

signature was clinically relevant with distinct stratification of survival chance in patients with glioma in two independent cohorts. Robust predictive accuracies of the signature were present across different datasets at multiple timepoints. With univariate and multivariate regressions, we demonstrated that the risk score based on the lncRNA signature is an independent prognostic indicator after clinical factors were adjusted. The nomogram incorporating age, tumor grade, radiotherapy and risk score was observed to be accurate in both classification and prediction performance. What's more, the signature-based stratification was observed to be correlated with extensive clinical characteristics, including tumor grade, MGMT promoter methylation status, 1p19q-codeletion status, and IDH mutation status. Further, increased immune infiltration was observed in the high-risk group as defined by the signature, which contributed to detrimental survival outcomes.

The ferroptosis-related lncRNA signature highlighted a total of 14 lncRNAs, i.e., APCDD1L-AS1, H19, LINC00205, LINC00346, LINC00475, LINC00484, LINC00601, LINC00664, LINC00886, LUCAT1, MIR155HG, NEAT1, PVT1, and SNHG18. Out of the 14 lncRNAs, eight of them were previously reported. H19 was reported to be upregulated in high-grade glioma and facilitated the proliferation of diffuse intrinsic pontine glioma (Roig-Carles et al., 2021). LINC00346 promotes cell migration, proliferation, and apoptosis by targeting ROCK1(Chen et al., 2020) and miR-128-3p/SZRD1 axis (Geng et al., 2020) in glioma. Overexpression of LINC00475 was observed in hypoxic gliomas and silencing LINC00475 results in suppression of tumor proliferation, migration, as well as invasion (Yu et al., 2020a). By regulating the miR-141-3p/YAP1 axis, LINC00475 facilitates tumor progression of glioma (Yu et al., 2020b). LUCAT1 is an oncogenic molecule in glioma, and its knockdown induced inhibition of cell viability and invasion by regulating miR-375 in glioma (Gao et al., 2018). LncRNA miR155HG contributes to tumor growth and progression in glioblastoma (Wu et al., 2019), and its prognostic value was also identified in previous bioinformatic analysis (Zheng et al., 2021). NEAT1 demonstrated to be a contributor to glioma cell migration, invasion, and tumor progression (Chen et al., 2018; Zhou et al., 2018). PVT1 promotes tumorigenesis and cancer progression of glioma via regulation of miR-128-3p/GREM1 Axis and BMP signaling pathway (Fu et al., 2018). Upregulation of SNHG18 promotes resistance to radiotherapy in glioma by repressing Semaphorin 5A (Zheng et al., 2016). High expressions of PVT1 and SNHG18 in glioblastoma samples as opposed to LGG was validated in the previous study (Zheng et al., 2021). Notably, the role of lncRNAs APCDD1L-AS1,

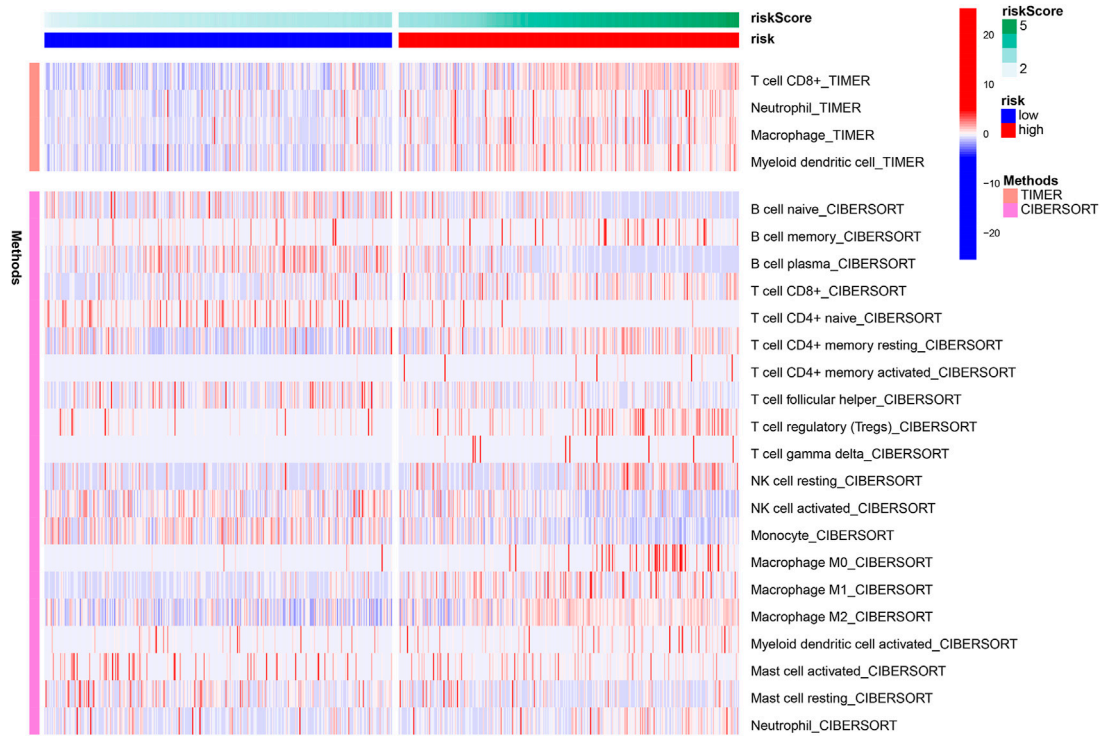

FIGURE 7 | Heatmap presenting immune infiltration correlated to the lncRNA signature.

LINC00205, LINC00484, LINC00601, LINC00664, and LINC00886 was first reported and validated in the present study.

Zheng et al. (Zheng et al., 2021) established a prognostic ferroptosis-Related lncRNAs signature correlated with immune landscape and radiotherapy response in Glioma. However, they applied median risk scores for three cohorts with a half-by-half classification in each cohort, thereby leading to potential false-positive results. Notably, there was no other report of ferroptosis-related lncRNA signature in gliomas. By contrast, the present study reports a ferroptosis-related lncRNA signature, which exhibits a distinct separation of survival rates in glioma patients with the same cutoff value across different cohorts. Further, expression levels of the ferroptosis-related lncRNAs signature were also validated between high-grade and lower-grade samples using qPCR. It could be translated to clinical settings as a test panel for informing individualized prognosis. Therapies targeting these lncRNAs could hold promise for enhanced efficacy. However, a lack of functional validation is considered as a major limitation in the present study. The functional implications of the lncRNAs require further validation with empirical data.

CONCLUSION

The present study established a ferroptosis-related lncRNA signature that could effectively stratify the prognosis of glioma patients, with superior predictive performance to all clinical index. These findings may pave the way for developing novel biomarkers for prognosis and treatments in gliomas.

DATA AVAILABILITY STATEMENT

The datasets presented in this study can be found in online repositories. The names of the repository/repositories and accession number(s) can be found in the article.

ETHICS STATEMENT

All specimens were stored in liquid nitrogen, and all patients provided informed consent. The collecting of specimens was approved by the Ethics Committee of First Affiliated Hospital of Nanjing Medical University (No: 2020-SRFA-167).

AUTHOR CONTRIBUTIONS

HQ conceived the project and designed the study. YH and HQ analyzed and interpreted the data. WT and YY collected clinical samples and conducted lab investigation. HQ and WT contributed to the revision of this manuscript. All authors have read and approved the final manuscript.

FUNDING

This study was funded by the Postgraduate Research; Practice Innovation Program of Jiangsu Province (SJCX20_0478 & SJCX20_0485).

REFERENCES

Arrigo, A.-P., and Gibert, B. (2012). HspB1 Dynamic Phospho-Oligomeric Structure Dependent Interactome as Cancer Therapeutic Target. *Curr. Mol. Med.* 12 (9), 1151–1163. doi:10.2174/156652412803306693

Belavgeni, A., Bornstein, S. R., von Mässenhausen, A., Tonnus, W., Stumpf, J., Meyer, C., et al. (2019). Exquisite Sensitivity of Adrenocortical Carcinomas to Induction of Ferroptosis. *Proc. Natl. Acad. Sci. USA* 116 (44), 22269–22274. doi:10.1073/pnas.1912700116

Benjamini, Y., Krieger, A. M., and Yekutieli, D. (2006). Adaptive Linear Step-Up Procedures that Control the False Discovery Rate. *Biometrika* 93 (3), 491–507. doi:10.1093/biomet/93.3.491

Bhan, A., Soleimani, M., and Mandal, S. S. (2017). Long Noncoding RNA and Cancer: a New Paradigm. *Cancer Res.* 77 (15), 3965–3981. doi:10.1158/0008-5472.can-16-2634

Carbone, M., and Melino, G. (2019). Stearoyl CoA Desaturase Regulates Ferroptosis in Ovarian Cancer Offering New Therapeutic Perspectives. *Cancer Res.* 79 (20), 5149–5150. doi:10.1158/0008-5472.can-19-2453

Ceccarelli, M., Barthel, F. P., Malta, T. M., Sabedot, T. S., Salama, S. R., Murray, B. A., et al. (2016). Molecular Profiling Reveals Biologically Discrete Subsets and Pathways of Progression in Diffuse Glioma. *Cell* 164 (3), 550–563. doi:10.1016/j.cell.2015.12.028

Chen, Q., Cai, J., Wang, Q., Wang, Y., Liu, M., Yang, J., et al. (2018). Long Noncoding RNA NEAT1, Regulated by the EGFR Pathway, Contributes to Glioblastoma Progression through the WNT/β-Catenin Pathway by Scaffolding EZH2. *Clin. Cancer Res.* 24 (3), 684–695. doi:10.1158/1078-0432.ccr-17-0605

Chen, R., Smith-Cohn, M., Cohen, A. L., and Colman, H. (2017). Glioma Subclassifications and Their Clinical Significance. *Neurotherapeutics* 14 (2), 284–297. doi:10.1007/s13311-017-0519-x

Chen, X., Li, D., Chen, L., Hao, B., Gao, Y., Li, L., et al. (2020). Long Noncoding RNA LINC00346 Promotes Glioma Cell Migration, Invasion and Proliferation by Up-regulating ROCK1. *J. Cel. Mol. Med.* 24 (22), 13010–13019. doi:10.1111/jcmm.15899

Clark, M. B., Johnston, R. L., Inostroza-Ponta, M., Fox, A. H., Fortini, E., Moscato, P., et al. (2012). Genome-wide Analysis of Long Noncoding RNA Stability. *Genome Res.* 22 (5), 885–898. doi:10.1101/gr.131037.111

Claus, E. B., Walsh, K. M., Wiencke, J. K., Molinaro, A. M., Wiemels, J. L., Schildkraut, J. M., et al. (2015). Survival and Low-Grade Glioma: the Emergence of Genetic Information. *Neurosurg Focus* 38 (1), E6. doi:10.3171/2014.10.focus12367

de Robles, P., Fiest, K. M., Frolkis, A. D., Pringsheim, T., Atta, C., St. Germaine-Smith, C., et al. (2015). The Worldwide Incidence and Prevalence of Primary Brain Tumors: a Systematic Review and Meta-Analysis. *Neuro Oncol.* 17 (6), 776–783. doi:10.1093/neuonc/nou283

Dixon, S. J., Lemberg, K. M., Lamprecht, M. R., Skouta, R., Zaitsev, E. M., Gleason, C. E., et al. (2012). Ferroptosis: an Iron-dependent Form of Nonapoptotic Cell Death. *Cell* 149 (5), 1060–1072. doi:10.1016/j.cell.2012.03.042

Eling, N., Reuter, L., Hazin, J., Hamacher-Brady, A., and Brady, N. R. (2015). Identification of Artesunate as a Specific Activator of Ferroptosis in Pancreatic Cancer Cells. *Oncoscience* 2 (5), 517–532. doi:10.18632/oncoscience.160

Enz, N., Vliegen, G., De Meester, I., and Jungraithmayr, W. (2019). CD26/DPP4 - a Potential Biomarker and Target for Cancer Therapy. *Pharmacol. Ther.* 198, 135–159. doi:10.1016/j.pharmthera.2019.02.015

Fu, C., Li, D., Zhang, X., Liu, N., Chi, G., and Jin, X. (2018). LncRNA PVT1 Facilitates Tumorigenesis and Progression of Glioma via Regulation of MiR-128-3p/GREM1 Axis and BMP Signaling Pathway. *Neurotherapeutics* 15 (4), 1139–1157. doi:10.1007/s13311-018-0649-9

Gan, B. (2019). DUBbing Ferroptosis in Cancer Cells. *Cancer Res.* 79 (8), 1749–1750. doi:10.1158/0008-5472.can-19-0487

Gao, Y.-S., Liu, X.-Z., Zhang, Y.-G., Liu, X.-J., and Li, L.-Z. (2018). Knockdown of Long Noncoding RNA LUCAT1 Inhibits Cell Viability and Invasion by Regulating miR-375 in Glioma. *Oncol. Res.* 26 (2), 307–313. doi:10.3727/096504017x15088061795756

Geng, Y. B., Pan, C. C., Xu, C., Zuo, P. C., Wang, Y., Li, X. O., et al. (2020). Long Non-coding RNA LINC00346 Regulates Proliferation and Apoptosis by Targeting miR-128-3p/SZRD1 axis in Glioma. *Eur. Rev. Med. Pharmacol. Sci.* 24 (18), 9581–9590. doi:10.26355/eurrev_202009_23046

He, X., Sheng, J., Yu, W., Wang, K., Zhu, S., and Liu, Q. (2021). LncRNA MIR155HG Promotes Temozolomide Resistance by Activating the Wnt/β-Catenin Pathway via Binding to PTBP1 in Glioma. *Cell Mol Neurobiol* 41 (6), 1271–1284. doi:10.1007/s10571-020-00898-z

Heagerty, P. J., Lumley, T., and Pepe, M. S. (2000). Time-Dependent ROC Curves for Censored Survival Data and a Diagnostic Marker. *Biometrics* 56 (2), 337–344. doi:10.1111/j.0006-341x.2000.00337.x

Hong, W., Liang, L., Gu, Y., Qi, Z., Qiu, H., Yang, X., et al. (2020). Immune-related lncRNA to Construct Novel Signature and Predict the Immune Landscape of Human Hepatocellular Carcinoma. *Mol. Ther. - Nucleic Acids* 22, 937–947. doi:10.1016/j.omtn.2020.10.002

Junttila, M. R., and Evan, G. I. (2009). p53 - a Jack of All Trades but Master of None. *Nat. Rev. Cancer* 9 (11), 821–829. doi:10.1038/nrc2728

Kirby, A. J., and Finnerty, G. T. (2020). New Strategies for Managing Adult Gliomas. *J. Neurol.* 268, 3666–3674. doi:10.1007/s00415-020-09884-3

Langfelder, P., and Horvath, S. (2008). WGCNA: an R Package for Weighted Correlation Network Analysis. *BMC Bioinformatics* 9, 559. doi:10.1186/1471-2105-9-559

Lara-Velazquez, M., Al-Kharboosh, R., Jeanneret, S., Vazquez-Ramos, C., Mahato, D., Tavanaiepour, D., et al. (2017). Advances in Brain Tumor Surgery for Glioblastoma in Adults. *Brain Sci.* 7 (12), 166. doi:10.3390/brainsci7120166

Li, T., Fu, J., Zeng, Z., Cohen, D., Li, J., Chen, Q., et al. (2020). TIMER2.0 for Analysis of Tumor-Infiltrating Immune Cells. *Nucleic Acids Res.* 48 (W1), W509–w514. doi:10.1093/nar/gkaa407

Liang, C., Zhang, X., Yang, M., and Dong, X. (2019). Recent Progress in Ferroptosis Inducers for Cancer Therapy. *Adv. Mater.* 31 (51), 1904197. doi:10.1002/adma.201904197

Lim, M., Xia, Y., Bettegowda, C., and Weller, M. (2018). Current State of Immunotherapy for Glioblastoma. *Nat. Rev. Clin. Oncol.* 15 (7), 422–442. doi:10.1038/s41571-018-0003-5

Liu, H.-j., Hu, H.-m., Li, G.-z., Zhang, Y., Wu, F., Liu, X., et al. (2020). Ferroptosis-Related Gene Signature Predicts Glioma Cell Death and Glioma Patient Progression. *Front. Cel Dev. Biol.* 8, 538. doi:10.3389/fcell.2020.00538

Louis, D. N., Perry, A., Reifenberger, G., von Deimling, A., Figarella-Branger, D., Cavenee, W. K., et al. (2016). The 2016 World Health Organization Classification of Tumors of the Central Nervous System: a Summary. *Acta Neuropathol.* 131 (6), 803–820. doi:10.1007/s00401-016-1545-1

Luan, F., Chen, W., Chen, M., Yan, J., Chen, H., Yu, H., et al. (2019). An Autophagy-related Long Non-coding RNA Signature for Glioma. *FEBS open bio* 9 (4), 653–667. doi:10.1002/2211-5463.12601

Meier, L., Van De Geer, S., and Bühlmann, P. (2008). The Group Lasso for Logistic Regression. *J. R. Stat. Soc. Ser. B (Stat Methodol)* 70 (1), 53–71. doi:10.1111/j.1467-9868.2007.00627.x

Molinaro, A. M., Taylor, J. W., Wiencke, J. K., and Wrensch, M. R. (2019). Genetic and Molecular Epidemiology of Adult Diffuse Glioma. *Nat. Rev. Neurol.* 15 (7), 405–417. doi:10.1038/s41582-019-0220-2

Newman, A. M., Liu, C. L., Green, M. R., Gentles, A. J., Feng, W., Xu, Y., et al. (2015). Robust Enumeration of Cell Subsets from Tissue Expression Profiles. *Nat. Methods* 12 (5), 453–457. doi:10.1038/nmeth.3337

Ostrom, Q. T., Bauchet, L., Davis, F. G., Deltour, I., Fisher, J. L., Langer, C. E., et al. (2014). The Epidemiology of Glioma in Adults: a "state of the Science" Review. *Neuro-Oncology* 16 (7), 896–913. doi:10.1093/neuonc/nou087

Qiu, H., Hu, X., He, C., Yu, B., Li, Y., and Li, J. (2020). Identification and Validation of an Individualized Prognostic Signature of Bladder Cancer Based on Seven Immune Related Genes. *Front. Genet.* 11, 12. doi:10.3389/fgene.2020.00012

Roig-Carles, D., Jackson, H., Loveson, K. F., Mackay, A., Mather, R. L., Waters, E., et al. (2021). The Long Non-coding RNA H19 Drives the Proliferation of Diffuse Intrinsic Pontine Glioma with H3K27 Mutation. *Int. J. Mol. Sci.* 22 (17). doi:10.3390/ijms22179165

Stockwell, B. R., and Jiang, X. (2019). A Physiological Function for Ferroptosis in Tumor Suppression by the Immune System. *Cel Metab.* 30 (1), 14–15. doi:10.1016/j.cmet.2019.06.012

Wang, W., Zhao, Z., Yang, F., Wang, H., Wu, F., Liang, T., et al. (2018). An Immune-Related lncRNA Signature for Patients with Anaplastic Gliomas. *J. Neurooncol.* 136 (2), 263–271. doi:10.1007/s11060-017-2667-6

Wen, P. Y., and Huse, J. T. (2017). 2016 World Health Organization Classification of Central Nervous System Tumors. *Continuum (Minneap Minn)* 23 (6), 1531–1547. doi:10.1212/CON.0000000000000536

Wu, W., Yu, T., Wu, Y., Tian, W., Zhang, J., and Wang, Y. (2019). The miR155HG/miR-185/ANXA2 Loop Contributes to Glioblastoma Growth and Progression. *J. Exp. Clin. Cancer Res.* 38 (1), 133. doi:10.1186/s13046-019-1132-0

Xia, P., Li, Q., Wu, G., and Huang, Y. (2020). An Immune-Related lncRNA Signature to Predict Survival in Glioma Patients. *Cell Mol. Neurobiol.* 41 (2), 365–375. doi:10.1007/s10571-020-00857-8

Yu, L., Gui, S., Liu, Y., Qiu, X., Qiu, B., Zhang, X., et al. (2020). Long Intergenic Non-protein Coding RNA 00475 Silencing Acts as a Tumor Suppressor in Glioma under Hypoxic Condition by Impairing microRNA-449b-5p-dependent AGAP2 Up-Regulation. *Ther. Adv. Med. Oncol.* 12, 1758835920940936. doi:10.1177/1758835920940936

Yu, M., Yi, B., Zhou, W., Gong, W., Li, G., and Yu, S. (2020). Linc00475 Promotes the Progression of Glioma by Regulating the miR-141-3p/YAP1 axis. *J. Cel Mol Med.* 25 (1), 463–472. doi:10.1111/jcmm.16100

Zheng, J., Zhou, Z., Qiu, Y., Wang, M., Yu, H., Wu, Z., et al. (2021). A Prognostic Ferroptosis-Related lncRNAs Signature Associated with Immune Landscape and Radiotherapy Response in Glioma. *Front. Cel Dev. Biol.* 9, 675555. doi:10.3389/fcell.2021.675555

Zheng, R., Yao, Q., Ren, C., Liu, Y., Yang, H., Xie, G., et al. (2016). Upregulation of Long Noncoding RNA Small Nucleolar RNA Host Gene 18 Promotes Radioresistance of Glioma by Repressing Semaphorin 5A. *Int. J. Radiat. Oncology*Biology*Physics* 96 (4), 877–887. doi:10.1016/j.ijrobp.2016.07.036

Zhou, K., Zhang, C., Yao, H., Zhang, X., Zhou, Y., Che, Y., et al. (2018). Knockdown of Long Non-coding RNA NEAT1 Inhibits Glioma Cell Migration and Invasion via Modulation of SOX2 Targeted by miR-132. *Mol. Cancer* 17 (1), 105. doi:10.1186/s12943-018-0849-2

Zhuo, S., Chen, Z., Yang, Y., Zhang, J., Tang, J., and Yang, K. (2020). Clinical and Biological Significances of a Ferroptosis-Related Gene Signature in Glioma. *Front. Oncol.* 10, 590861. doi:10.3389/fonc.2020.590861

Conflict of Interest: The authors declare that the research was conducted in the absence of any commercial or financial relationships that could be construed as a potential conflict of interest.

Publisher's Note: All claims expressed in this article are solely those of the authors and do not necessarily represent those of their affiliated organizations, or those of the publisher, the editors and the reviewers. Any product that may be evaluated in this article, or claim that may be made by its manufacturer, is not guaranteed or endorsed by the publisher.

frontiers in Cell and Developmental Biology

ORIGINAL RESEARCH
published: 18 January 2022
doi: 10.3389/fcell.2021.786684

An Iron Metabolism-Related Gene Signature for the Prognosis of Colon Cancer

*Jing Yuan, Tao Liu and Yuhong Zhang**

State Key Laboratory of Oncology in South China, Collaborative Innovation Center for Cancer Medicine, Sun Yat-sen University Cancer Center, Guangzhou, China

As an essential microelement, the iron ion is involved in cell proliferation, metabolism, and differentiation. Iron metabolism plays a crucial role in the occurrence and development of colon adenocarcinoma (COAD). In this study, univariate and multivariate Cox regression, and least absolute shrinkage and selection operator analyses were conducted to construct the gene signature, based on a dataset from The Cancer Genome Atlas. We identified the prognostic value of two iron metabolism-related genes [SLC39A8 (encoding solute carrier family 39 member 8) and SLC48A1 (encoding solute carrier family 48 member 1)] in COAD. A nomogram model was established to predict the overall survival of patients with COAD. Functional analysis showed that the tumor microenvironment and immune cell infiltrate were different between the low risk and high risk subgroups. This study verified that the iron metabolism-related gene signature (SLC39A8 and SLC48A1) could be used as a prognostic biomarker for patients with COAD.

Keywords: colon cancer, prognosis, iron metabolism, nomogram model, overall survival

OPEN ACCESS

Edited by:
Chang Gong,
Sun Yat-Sen University, China

Reviewed by:
Balamurugan Kuppusamy,
National Cancer Institute at Frederick, United States
Qisheng Su,
Guangxi Medical University, China

****Correspondence:***
Yuhong Zhang
zhangyh2@sysucc.org.cn

Specialty section:
This article was submitted to Molecular and Cellular Oncology, a section of the journal Frontiers in Cell and Developmental Biology

Received: *30 September 2021*
Accepted: *17 December 2021*
Published: *18 January 2022*

Citation:
Yuan J, Liu T and Zhang Y (2022) An Iron Metabolism-Related Gene Signature for the Prognosis of Colon Cancer. Front. Cell Dev. Biol. 9:786684. doi: 10.3389/fcell.2021.786684

INTRODUCTION

Colon adenocarcinoma (COAD) is one of the three most commonly diagnosed cancers, and is the second leading cause of cancer death worldwide. Although research enhanced the overall survival and led to good prognosis for patients with COAD, the mortality and disability caused by COAD are still very high (Xi and Xu, 2021).

At present, the biggest challenge to improving the survival of patients with COAD is metastasis or postoperative recurrence (Carethers and Jung, 2015). Therefore, a more accurate prognostic assessment model is required to allow individualized treatment and improve the prognosis of patients with COAD. There is increasing evidence that iron overload is closely associated with tumorigenesis in multiple types of human cancer. Cancers usually have a demand for iron, which is an essential element in biological processes, including DNA synthesis, energy metabolism, and immune function (Behr et al., 2018; Hassannia et al., 2019). Ferroptosis, an iron-dependent form of nonapoptotic cell death, has emerged recently as a novel method to treat cancer (Dixon et al., 2012). Pathways of iron metabolism, including iron acquisition, efflux, storage, and regulation, are unbalanced in cancer, indicating that iron metabolism plays a crucial rules in tumor cell survival (Torti and Torti, 2013). However, the prognostic value of genetic markers associated with iron metabolism in COAD has not been fully explored.

In this study, we constructed iron metabolism-related gene signature [*SLC39A8* (encoding solute carrier family 39 member 8) and *SLC48A1* (encoding solute carrier family 48 member 1)] using a dataset from The Cancer Genome Atlas (TCGA) and validated the stability and reliability of the

model in a Gene Expression Omnibus (GEO) dataset. Then, functional enrichment analysis was carried out to determine the potential mechanism of action of the proteins encoded by the two genes. Finally, experiments demonstrated the expression level and function of the two iron metabolism-related genes *in vitro* and *in vivo*.

METHODS

Data Collection

COAD gene expression profiles and corresponding clinical information were downloaded from the TCGA database (n = 512) and GEO database (GSE39582, n = 576). Seventy iron metabolism-related genes are listed in **Supplementary Table S1**, which were derived from a previous study (Wei et al., 2020). The GSE39582 dataset was used to validate the established signature.

Construction and Validation of an Iron Metabolism-Related Genes Risk Score

The TCGA dataset was used as the training dataset to build the iron metabolism-related genes risk score. Univariable Cox regression and Least absolute shrinkage and selection operator (LASSO) Cox analysis were performed to select iron metabolism-related genes associated with prognosis ($p < 0.05$). Then, multivariate Cox regression was used to further determine candidate iron metabolism-related genes associated with prognosis in COAD. Following this, the risk score for each patient was calculated as follows:

$$\text{Risk Score} = \text{coefficient } 1^{*}\text{Exp1} + \text{coefficient } 2^{*}\text{Exp2} + \ldots\ldots + \text{coefficient n}^{*}\text{Exp n}$$

where Exp represented the expression level of the candidate iron metabolism-related gene. Using the median of the above risk score as the cutoff point, patients with COAD in the training cohort and validation cohort were divided into low-risk and high-risk subgroups.

Validation of the Prognostic Model

Kaplan–Meier analysis was carried out to compare the prognostic difference between the two subgroups. Univariable and multivariate Cox regression were conducted to further evaluate the iron metabolism-related gene signature's prognostic value in the training cohort. Then, the prognostic gene signature was validated externally in the validation dataset, followed by further Kaplan–Meier analysis.

Constructing a Predictive Nomogram

Univariate and multivariate Cox regression analysis were carried out to determine the prognostic factors including the risk score established above, and age, sex, tumor stage, and tumor-node-metastasis (TNM) stage in COAD. The factors with a significant difference ($p < 0.05$) were selected to construct a nomogram model. A calibration curve was plotted to verify the accuracy of the nomogram.

Gene Set Enrichment Analysis

Enriched pathways in different iron metabolism risk score datasets were assessed using Gene Set Enrichment Analysis (GSEA) software (GSEAv4.0.1, https://www.gsea-msigdb.org/). The Hallmark (v7.1) gene set collections were used as references. $p < 0.05$ and a false discovery rate of q < 0.25 were considered significant.

Correlation of the Risk Score With the Proportion of Tumor-Infiltrating Immune Cells

The abundance of 22 TICs in each tumor sample in the COAD cohort were estimated using the CIBERSORT module in the R package. CIBERSORT (Chen et al., 2018) was performed to determine the relative mRNA expression levels in the high- and low-risk subgroups to characterize the cell composition of tumor tissues.

RNA Isolation and qRT-PCR Analysis

Total RNA from colon cancer cells were extracted using the TRIzol reagent (Takara Biotechnology, Dalian, China). Next, cDNA was prepared using a Revert Aid First Strand cDNA Synthesis kit (Thermo Fisher Scientific, Waltham, MA, United States). The cDNA was then used as a template in a quantitative real-time polymerase chain reaction (qPCR) to determine the expression levels of the iron metabolism-related genes using Japan). The qPCR amplification reactions conditions were as follows: 95°C for 15 min; followed by 40 cycles of 95°C for 30 s, 55°C for 1 min, and 72°C for 30 s. The expression levels were normalized to those of *ACTB* (encoding β-actin). All primers were synthesized by Sangon Biotech (Shanghai, China) and are listed in **Supplementary Table S2**. All PCR reactions were performed in triplicate, and the relative expression levels of mRNA were quantified using the 2-ΔΔCt method.

Immunohistochemistry Examination

This protocol was approved by the Ethics Committee of Sun Yat-Sen University Cancer Center (Guangzhou, China). Written informed consent was obtained from patients at their first visit. The surgically resected colon cancer tissues of eight patients at Sun Yat-sen University Cancer Center were included in this study. Tumors and corresponding nontumorous tissue were fixed in 4% paraformaldehyde, embedded in paraffin blocks, and processed into 4 μm-thick continuous sections. Immunohistochemical staining was performed to determine the distribution of SLC39A8 and SLC48A1. The antibodies used were: anti-SLC39A8 (1:200; 20459-1-AP; Proteintech) and anti-SLC48A1 (1:200; NBP1-91563; Novus Biologicals).

Cell Culture and Transfection

Colon cancer cells (DLD-1) were cultured in Dulbecco's modified Eagle Medium (Gibco, Grand Island, NY, United States) supplemented with 10% fetal bovine serum (Invitrogen, Carlsbad, CA, United States) at 37°C with 5% CO_2. Small

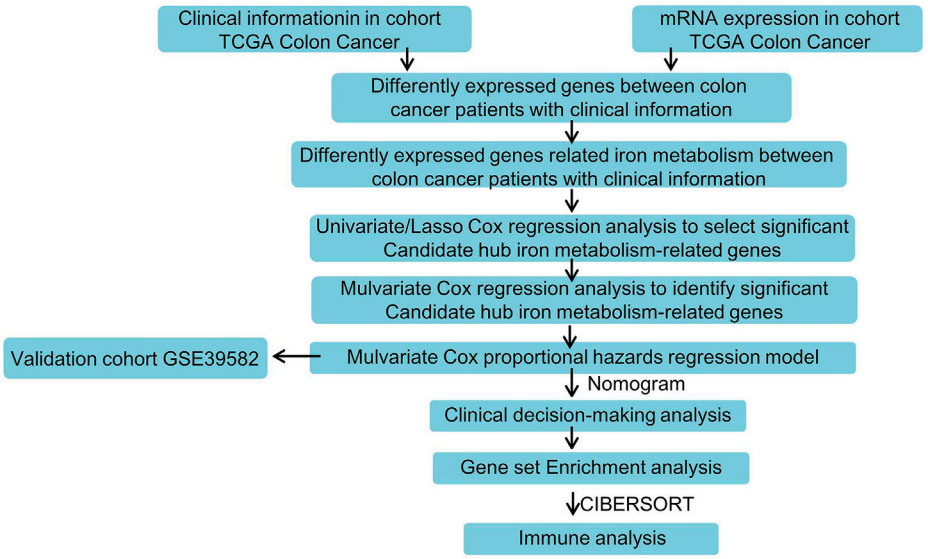

FIGURE 1 | Flowchart for analyzing iron metabolism-related gene signature associated with colon cancer.

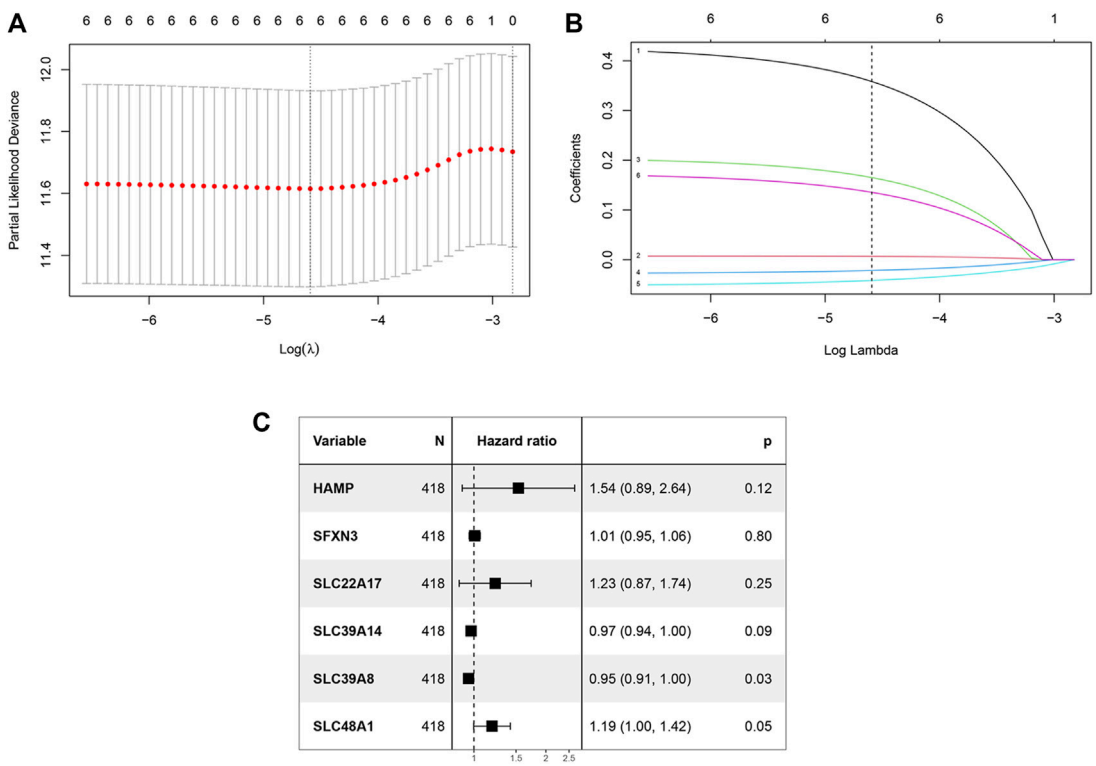

FIGURE 2 | Construction of the iron metabolism model. **(A)** 1000 bootstrap replicates by lasso Cox regression analysis for variable selection. **(B)** LASSO coefficients of iron metabolism genes. Each curve represents a metabolic gene. **(C)** Multivariate Cox regression analysis.

interfering RNAs (siRNAs) targeting *SLC39A8* and *SLC48A1* were synthesized by Sangon Biotech. The sequences of the siRNAs are listed in **Supplementary Table S4**. Transient transfection was performed using the Lipofectamine 2000 reagent (Invitrogen, Shanghai, China) according to the producer's protocol.

TABLE 1 | Multivariate Cox coefficients of iron metabolism related genes.

Gene	coef	exp (coef)	se (coef)	z	p
HAMP	0.4286	1.535065	0.276562	1.550	0.1212
SFXN3	0.0070	1.007071	0.027600	0.255	0.7985
SLC22A17	0.2046	1.227040	0.176986	1.156	0.2477
SLC39A14	−0.0277	0.972637	0.016133	−1.720	0.0855
SLC39A8	−0.0521	0.949228	0.024044	2.167	0.0302
SLC48A1	0.1739	1.189989	0.089898	1.935	0.0530

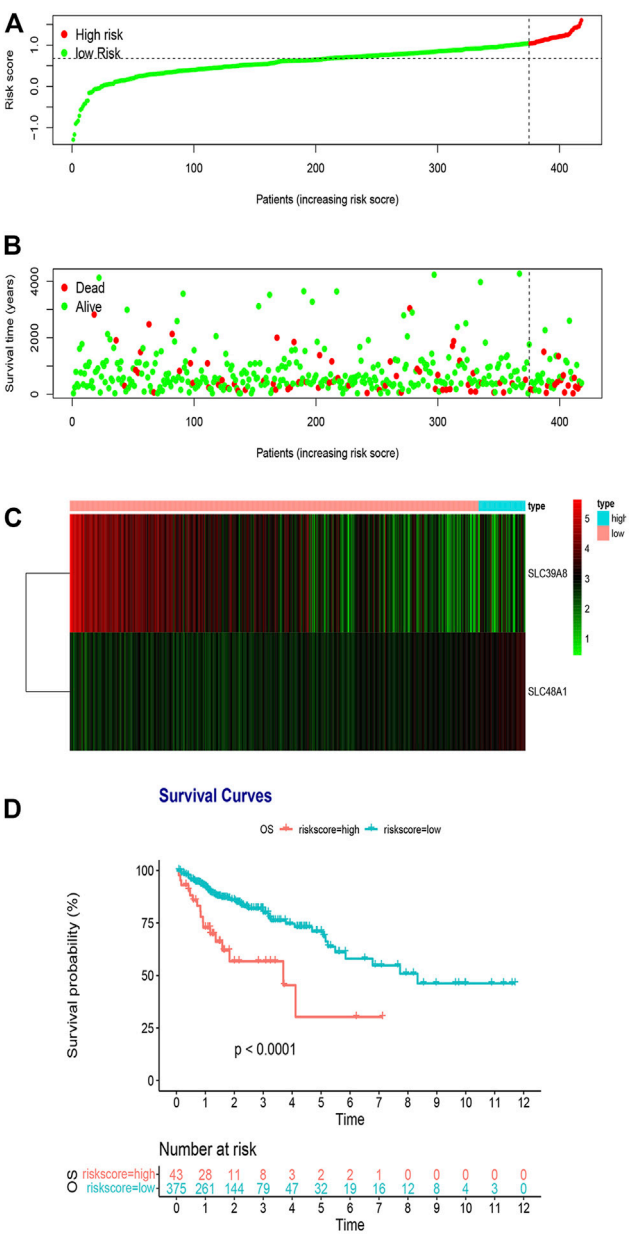

FIGURE 3 | Risk score analysis of the two-gene prognostic model in the TCGA training cohort. **(A)** Survival differences between high- and low-risk groups. **(B)** Dot plots comparing outcomes of subjects in the high- and low-risk groups. **(C)** Heat map for gene expressions in the high- and low-risk groups. **(D)** Kaplan Meier survival analysis of all patients with COAD in the high- and low-risk groups.

Cell Viability Assay

DLD-1 Cells were seeded to a 96-well plate and transfected with negative control (NC)-siRNA, *SLC39A8*-siRNA, or *SLC48A1*-siRNA for 24, 48, or 72 h, after which the cells were further incubated with 20 μL of MTS reagent for another 2 h. Cell viability was detected as the optical density (OD) value at 490 nm.

Colony Formation Assay

To study the effects of SLC39A8 and SLC48A1 on cell proliferation, DLD-1 Cells transfected with NC-siRNA, *SLC39A8*-siRNA, or *SLC48A1*-siRNA were seeded into 6-well plates and incubated for 14 days. Cells were then stained using Crystal Violet Staining Solution, and the number of colonies was detected using light microscopy.

Statistical Analysis

All statistical analyses were conducted using the R software. Kaplan–Meier analysis was used to compare the overall survival differences between the low- and high-risk subgroups. Given the possibility of multicollinearity, we used LASSO Cox regression analysis to identify the most valuable prognostic genes among all iron metabolism-related genes. An L1 penalty was set in the LASSO Cox model to shrink some regression coefficients to exactly zero and a 10-fold cross-validation with minimum criteria was performed to find the optimal λ value. Univariate and multivariate Cox proportional hazard regression analyses were carried out to evaluate the relationship between the risk score and overall survival. In all instances, a value of $p < 0.05$ was regarded as statistically significant.

RESULTS

Identification of Differentially Expressed Iron Metabolism-Related Genes

As shown in **Figure 1**, a systematic study was carried out for the pivotal roles and the latent prognostic values of iron metabolism-related genes in COAD. The mRNA expression profiles in tissues from patients with COAD ($n = 512$) were downloaded from the TCGA database as the training dataset. The GSE39582 dataset ($n = 576$) was used as validation cohort. Of the 56,753 genes in the TCGA expression data, 70 iron metabolism-related genes were selected.

Construction of the Iron Metabolism-Related Gene Signature in the TCGA Cohort

In the TCGA training dataset, single-factor Cox analysis was performed to analyze comprehensively the prognostic value of iron metabolism-related genes in COAD. We found that six genes [*HAMP* (encoding hepcidin antimicrobial peptide), *SFXN3* (encoding sideroflexin 3), *SLC22A17* (encoding solute carrier family 22 member 17), *SLC39A14* (encoding solute carrier family 39 member 14), *SLC39A8*, and *SLC48A1*] were significantly related to the prognosis of patients with COAD (**Supplementary Figure S1**). These iron metabolism-related

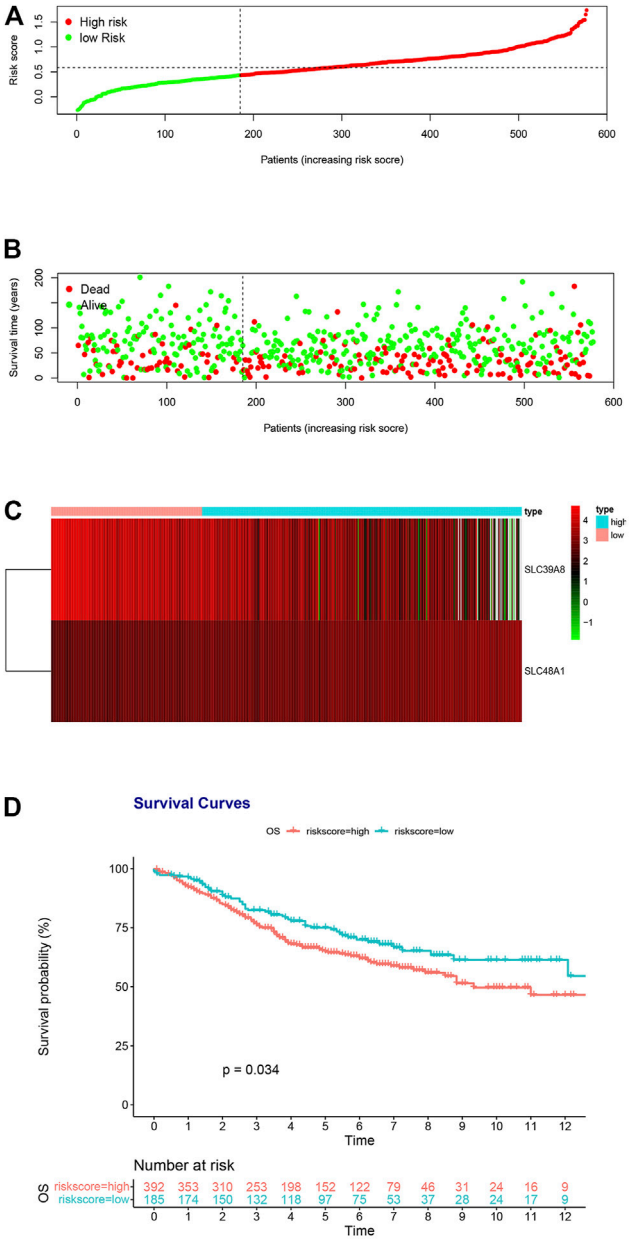

FIGURE 4 | Risk score analysis of the two-gene prognostic model in the GSE39582 validation cohort. **(A)** Survival differences between high- and low-risk groups. **(B)** Dot plots comparing outcomes of subjects in the high- and low-risk groups. **(C)** Heat map for gene expressions in the high- and low-risk groups. **(D)** Kaplan Meier survival analysis of all patients with COAD in the high- and low-risk groups.

genes were subsequently subjected to LASSO Cox regression analysis to avoid colinear influences, and regression coefficients were calculated (**Figure 2A**). When the six genes were incorporated, the model achieved the best performance (**Figure 2B**). These genes and their related coefficients are shown in **Supplementary Table S3**. The six iron metabolism-related genes were further analyzed by multivariate Cox regression. As shown in **Figure 2C**; **Table 1**, *SLC39A8* and *SLC48A1* were identified as independent predictors of prognosis for patients with COAD.

Model Construction and Analysis of the Prognosis-Related Genetic Risk Score

The two hub iron metabolism-related genes identified in *Construction of the Iron Metabolism-Related Gene Signature in the TCGA Cohort* were used to construct a prognosis-related genetic risk score. The risk score of each patient with COAD was calculated as follows:

$$\text{Risk Score} = -0.052106 \times \text{ExpSLC39A8} + 0.173944 \times \text{ExpSLC48A1}$$

We classified risk scores using the optimal cutoff points decided by the maximally selected log-rank statistics, in which patients with risk scores above the cutoff value were recognized as the high-risk group, and patients with risk scores below the cutoff value were recognized as the low-risk group. A survival analysis was performed to evaluate the predictive effect of this model. **Figure 3A** shows the distribution of the TCGA training cohort. Furthermore, dot plots were made to compare survival of patients in the high-risk and low risk-groups, which showed that survival in the high-risk group was worse than that in the low-risk group (**Figure 3B**). The heat maps in **Figure 3C** show the comparison of the expression levels of the two iron metabolism-related genes between the groups. The expression of *SLC39A8* was higher in the low-risk patients, while *SLC48A1* expression was higher in high-risk patients. Kaplan–Meier survival analyses found that patients with COAD in the high-risk group had worse prognosis compared with those in the low-risk group (**Figure 3D**; $p < 0.0001$).

Validation of Iron Metabolism-Related Genes Based on the GSE39582, GSE17536, and GSE38832 Dataset

To determine the accuracy of the two-gene prognostic model, we used the GSE39582 dataset as an external validation cohort. The distribution of the validation cohort is displayed in **Figure 4A**, **Supplementary Figures S2A, S3A**. The dot plot and heat map results were similar to those of the TCGA cohort (**Figures 4B,C**, **Supplementary Figures S2B,C, S3B,C**). Survival analysis indicated that the overall survival of the low-risk group was markedly longer than that of the high-risk group (**Figure 4D**; $p = 0.034$, **Supplementary Figure S2D**; $p = 0.053$ and **Supplementary Figure S3D**; $p = 0.021$).

Development of a Prognostic Model Based on Iron Metabolism-Related Genes and Clinical Factors

We next analyzed other co-variates using univariate and multivariate Cox regression to determine the prognostic factors in COAD. The results showed that risk score, N stage,

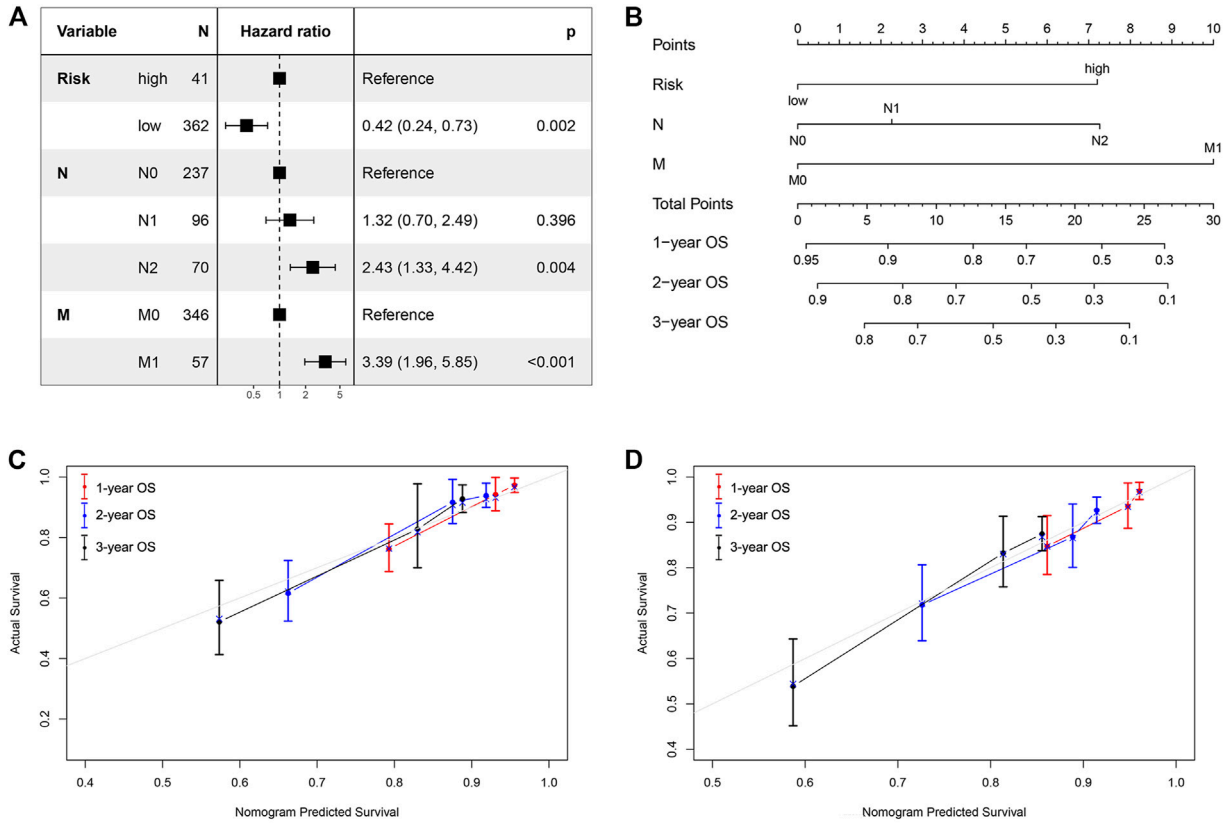

FIGURE 5 | Nomogram and calibration curve for predicting the probability of 1-, 2- and 3-years OS for patients with COAD. **(A)** The hazard ratios of the risk score and clinical factors based on multivariate COX analysis. **(B)** A nomogram integrates iron metabolism gene signature and other prognostic factors in patients with COAD; **(C, D)** The calibration curve of the nomogram in TCGA cohort and GSE39582 validation dataset.

and M stage correlated with survival in the multivariate analysis. The hazard ratios of the risk score and above clinical factors are listed in **Figure 5A**. We then constructed a nomogram using the risk score, N stage, and M stage as variables (**Figure 5B**). A lower point was related to a better prognostic result on the nomogram. The C-index was 0.8092 [95% confidence interval (CI): 0.7543–0.8642] for the nomogram, indicating that it had a good discriminating ability. Outcome was reported as 1-, 2- and 3-years overall survival. The associated calibration curves from the nomograms at 1, 2 and 3 years are displayed in **Figures 5C,D**, which showed a good performance of our nomogram in predicting 1-, 2- and 3- year survival. Therefore, this nomogram could be a useful model to predict the survival of patients with COAD.

Gene Set Enrichment Analysis With the Two Iron Metabolism-Related Genes

To explore the molecular functions of the identified iron metabolism-related genes in this study, we conducted GSEA analysis to determine the gene expression profile. The results are shown in **Figure 6**. Multiple functional gene sets were enriched significantly in the low-risk group containing HALLMARK_ANDROGEN_RESPONSE, HALLMARK_KRAS_SIGNALING_UP, HALLMARK_PI3K_AKT_MTOR_SIGNALING, HALLMARK_PROTEIN_SECRETION, and HALLMARK_UV_RESPONSE _DN. These findings suggested that the two iron metabolism-related genes were potentially closely correlated with the status of the COAD microenvironment.

Association of the Two Iron Metabolism-Related Genes With the Proportion of TICs

To further determine the relationship of the two iron metabolism-related genes with the immune microenvironment, we analyze the proportion of TIC subpopulations and constructed immune cell profiles in COAD using CIBERSORT. As shown in **Figures 7A,B**, a stacked bar plot and heat map were provided to describe the immune microenvironment in the high-risk and low-risk groups. Furthermore, the proportions of 22 immune cell proportions of COAD are shown in **Figure 7C**. The results showed that two TICs, regulatory T cells and eosinophils, were related to the two-gene signature risk score. The low- and high-risk score groups showed specific immune cell distributions.

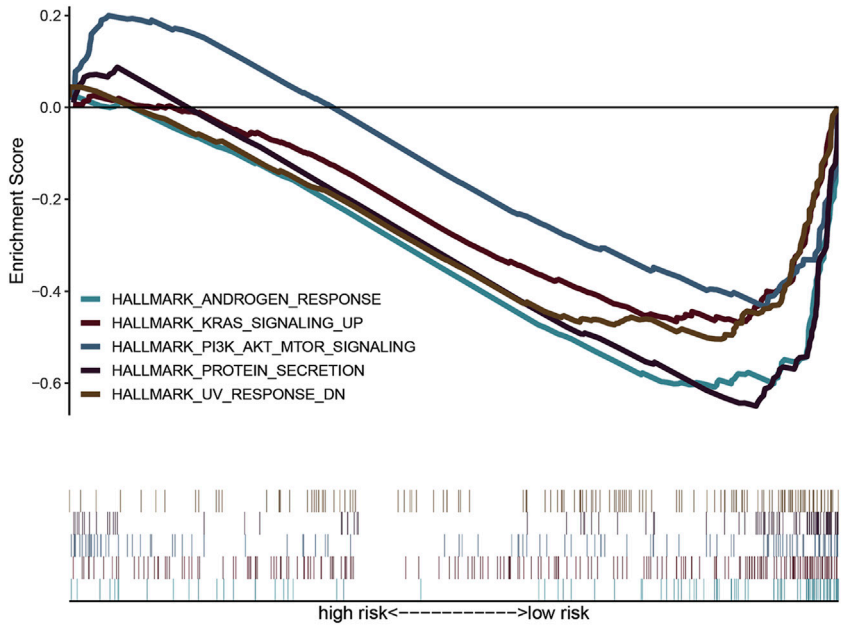

FIGURE 6 | Gene set variation analysis and gene set enrichment analysis of pathways. GSEA showed five pathways enriched in the low-risk group.

Expression Level Determination and Functional Analysis of the Iron Metabolism-Related Genes in COAD

To ascertain the expression levels of SLC39A8 and SLC48A1 in COAD tissues, eight colon cancer tissues and corresponding normal tissues were tested. Immunohistochemistry (**Figure 8A**) showed that the SLC39A8 level was downregulated in colon cancer tissues, and the SLC48A1 level was upregulated significantly in colon cancer tissues. Furthermore, the mRNA levels of *SLC39A8* and *SLC48A1* were successfully knocked down using siRNA in colon cancer cells *in vitro* (**Figure 8B**, **Supplementary Figure S4**). Next, we analyzed the potential function of SLC39A8 and SLC48A1 in colon cancer. Knocking down *SLC39A8* promoted the proliferation of different colon cancer cell lines (DLD1, HCT116, and HT29), and silencing *SLC48A1* suppressed the proliferation of colon cancer cells *in vitro* (**Figures 8C,D**, **Supplementary Figure S4**). These results indicated that *SLC39A8* might function as a tumor suppressor gene and *SLC48A1* might function as an oncogene in COAD.

DISCUSSION

The reasons for the occurrence and development of colon cancer are complex and may include interactions between environmental exposure, diet, and genetic factors (Brenner et al., 2014). In the pathogenesis of colon cancer, there are also many genetic and epigenetic changes in proliferation signaling pathways and tumor suppressor genes, such as the WNT pathway, the transforming growth factor beta (TGF-β) pathway, the phosphatidylinositol-4,5-bisphosphate 3-kinase (PI3K)-protein kinase (AKT) pathway, the mitogen activated protein kinase (MAPK) pathway, and the tumor protein p53 (TP53) pathway. Traditional TNM staging has some limitations for accurate prognostic prediction (Sjoblom et al., 2006). Although many molecular markers related to the prognosis of colon cancer have been reported, a single prognostic factor is often one-sided in the precision treatment system, whether it is a traditional pathological indicator or a new molecular marker. Studies have confirmed that the combination of molecular markers and traditional pathological prognostic indicators can predict the prognosis of patients with tumors more accurately. Therefore, in the construction of a prognosis prediction system for colon cancer, researchers have focused on integrating different types of prognostic factors to achieve the goal of predicting patient prognosis accurately.

Iron is an essential metal micronutrient for humans. At the cellular level, iron is involved in basic energy metabolism, mitochondrial function, and DNA synthesis (Imam et al., 2017). At the systemic level, iron metabolism is mainly regulated by the liver-derived endocrine hormone, ferrimodulin. Epidemiological data suggest that iron levels are associated with the risk of colorectal cancer. People with a high intake of red meat containing high amounts of heme iron and patients with iron overload disease had an increased risk of colorectal cancer (Martin et al., 2018). Colorectal cancer cells are enriched in iron relative to adjacent normal intestinal epithelial cells. Iron plays an important role in colorectal cancer. The tumor hypoxic environment induces heterotopic high expression of iron modulin in colorectal cancer epithelial cells through hypoxia-inducible factor 2 alpha (HIF2α) (Schwartz et al., 2021).

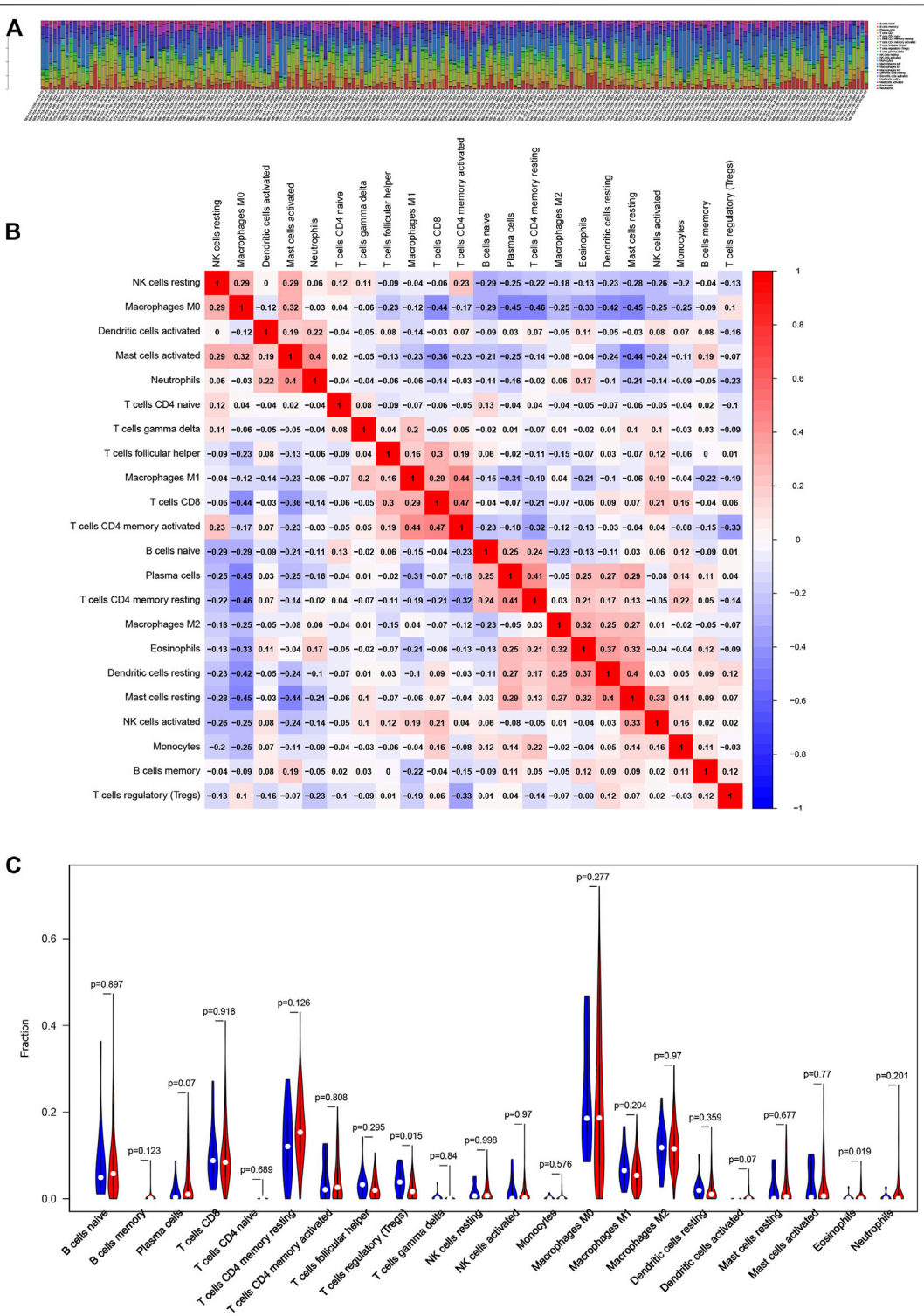

FIGURE 7 | Association of iron metabolism-related gene signature with the proportion of TICs **(A, B)** Bar plot and heat map for the immune microenvironment in the high-risk and low-risk groups **(C)** Distribution level of 22 types of immune cells in the high- and low-risk groups.

In this study, we downloaded data from the TCGA and GEO from public databases and extracted information about 70 genes related to iron metabolism. Univariate regression analysis, multivariate Cox regression analysis, and LASSO Cox analysis were used to identify the genes associated with iron metabolism prognosis in the TCGA cohort, and LASSO Cox regression

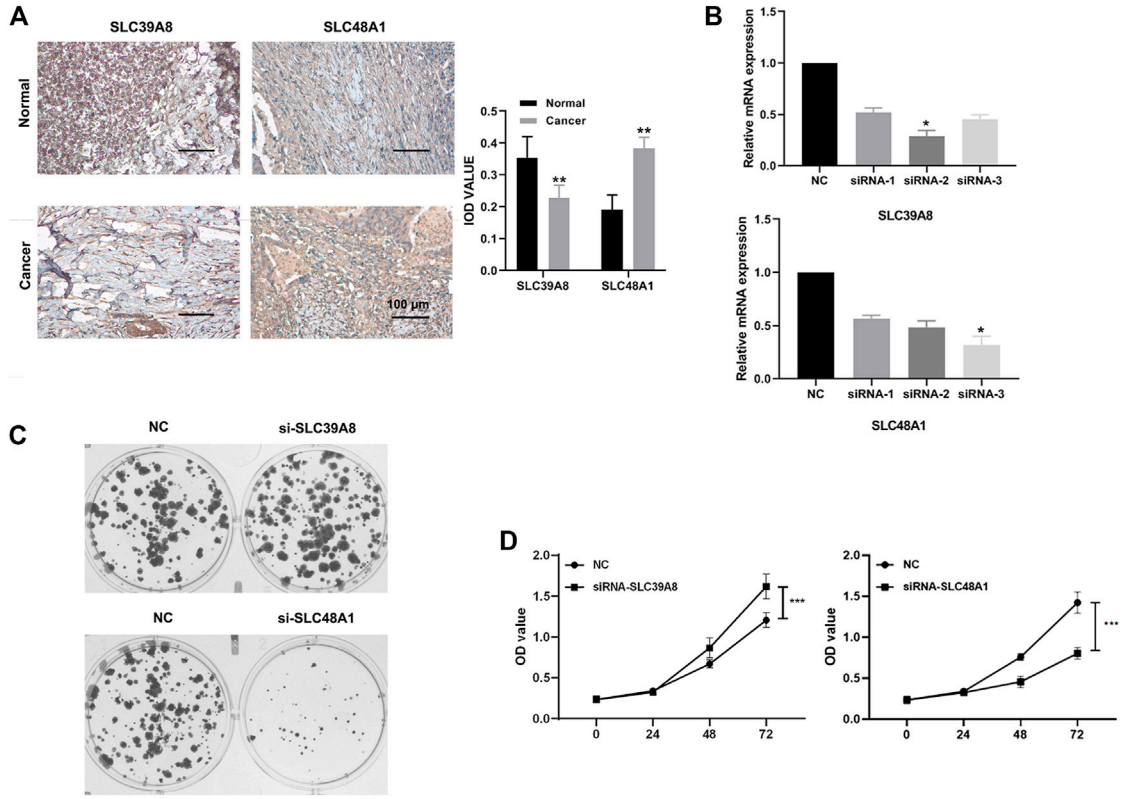

FIGURE 8 | Expression verification and functional analysis of genes related to iron metabolism. **(A)** Immunohistochemical results showed that SLC48A1 was highly expressed in human colon cancer tissues, while SLC39A8 was low expressed in human colon cancer tissues. **(B)** mRNA levels of SLC39A8 and SLC48A1 were knocked down using siRNAs in colon cancer cells. The results of cell clonal formation assay **(C)** and MTS **(D)** showed that knockdown SLC48A1 inhibited the proliferation of DLD1 cells, while knockdown SLC39A8 promoted the proliferation of DLD1 cells. Data are shown as mean ± SD; $^{*}p < 0.05$, $^{***}p < 0.001$ (versus NC group).

analysis was used to establish the prognostic model incorporating these genes. We identified two iron metabolism genes, *SLC48A1* and *SLC39A8*, which were associated with clinical survival. In the TCGA and GSE39582 datasets, genes related to iron metabolism can be used to predict the prognosis of patients with COAD. In different datasets of patients with colon cancer, *SLC48A1* and *SLC39A8* gene markers showed good prognostic performance.

The stability of the prediction model was verified in the GEO cohort, and a Nomogram model was constructed to predict the prognosis of patients with COAD. At the same time, the correlation of the *SLC48A1* and *SLC39A8* genes with tumor-infiltrating immune cells was analyzed. SLC48A1 regulates V-ATPase activity, which is a prerequisite for endosomal acidification, and enhances glucose transporter-1 (GLUT-1) transport, while increasing glucose uptake and lactate production. SLC48A1 also promotes the transport of the insulin-like growth factor I receptor (IGF-1R) (Fogarty et al., 2014). SLC39A8 is widely expressed and encodes the zrt- and irt-like protein 8 (ZIP8) protein. ZIP8 (also known as solute carrier family 39 member 8) is a membrane transporter that helps to absorb many substrates, including basic and toxic divalent metals (e.g., zinc, manganese, iron, and cadmium) and inorganic selenium (Liu et al., 2018). We found that high expression of *SLC39A8* and *SLC48A1* in patients with COAD was closely associated with reduced overall survival. Additionally, high expression of SLC48A1 drives glycolysis flux and promotes cancer cell growth, migration, and invasion, which is associated with poor prognosis (Sohoni et al., 2019). The loss of ZIP8 inhibits the migration potential of neuroblastoma cancer cells by reducing the expression level of matrix metalloproteinases (Mei et al., 2018). In this study, we revealed the prognostic value of iron metabolism-related genes *SLC48A1* and *SLC39A8* in colon cancer; however, their associated signaling pathways need to be further explored.

Univariate and multivariate Cox analyses in our training set (TCGA) and validation set (GSE39582) showed that iron metabolism-related genes were independent prognostic factors in patients with COAD. Colon cancer, including COAD, is insensitive to immunotherapy, which might be mediated by a series of immune escape mechanisms. To better understand the relationship between the risk score and immune components, we investigated the association of genes related to iron metabolism with various immune-infiltrating cells. The results showed that the a high risk score was closely related to regulatory T cells and eosinophils. This suggested that the poor prognosis in the high-risk group might be caused by immunosuppression induced by

regulatory T cells and eosinophils. Thus, the clinical prognosis of patients with colon cancer may be related to differences in immune cell compositions and genes related to iron metabolism might be involved in immunosuppression in colon cancer. This will provide new insights and targets for immunotherapy of colon cancer.

We used GSEA enrichment analysis to better understand the pathway of iron metabolism-related genes in colon cancer. The results showed that low-risk scores were enriched in KRAS and PI3K-AKT-mechanistic target of rapamycin (mTOR) signaling pathways. The KRAS subtype is mutated in 84% of RAS mutated cancers. In colon cancer, *KRAS* mutations are present in 30–50% of patients (Goel et al., 2015). The presence of *KRAS* mutations not only affects prognostic survival, but also predicts the responsiveness of patients with colon cancer to epidermal growth factor receptor (EGFR) signaling inhibitors (Stec et al., 2012). Overexpression of PI3K/AKT/mTOR signaling components has been reported in various types of cancer, and is especially closely related to the occurrence, development, and prognosis of colon cancer. In recent years, inhibitors targeting PI3K/AKT signaling have been shown to reduce the tumor burden in different experimental models and have been considered as potential therapeutic agents (Johnson et al., 2010; Narayanankutty, 2019). The possibility that iron metabolism might function through KRAS and PI3K-AKT-mTOR signaling pathways in colon cancer provides ideas for future research.

IHC was used to further verify the clinical samples, which showed high SLC39A8 levels in tumor tissues. Iron is known to be essential for the catalytic function of ribonucleotide reductase, the enzyme that converts ribonucleotides into deoxyribonucleotides, a rate-limiting step in DNA synthesis and an obligate step in cell replication (Torti and Torti, 2020). Moreover, iron was also proved to promote the proliferation and Warburg Effect of colon cancer cells through colony formation and MTS experiment *in vitro* (Yuan et al., 2021). HIF-2α promoted cell proliferation and survival by inducing iron accumulation in HCT116 cells, and low-iron diet reduced HIF-2α-mediated intestinal tumorigenesis and cellular proliferation (Xue et al., 2012). As we all know, cell colony formation assay and MTS assay are important techniques for detecting cell proliferation, invasiveness and sensitivity to killing factors. Therefore, we conducted colony formation and MTS experiment to determine the effect of knocking down iron metabolism-related genes on cell proliferation ability in different colorectal cancer cell lines, and the result showed that inhibition of SLC48A1 promoted the proliferation of colon cancer cells, and silencing of SLC39A8 expression suppressed the proliferation of colon cancer cells *in vitro*. These studies also suggest that SLC48A1 and SLC39A8 might be potential predictors of clinical prognosis and therapeutic targets for colon cancer.

Compared with markers based on single gene expression, multi-gene markers obtained by univariate and multivariate Cox and LASSO regression analysis of gene sets can compensate for individual differences, improve prediction and accuracy in tumors, and show better predictive performance. The mechanisms of action of the proteins encoded by iron metabolism-related genes in colon cancer require further study. Meanwhile, although we have noted correlations with immune cells, the function of iron metabolism in the tumor microenvironment and immunotherapy still needs to be clarified.

CONCLUSION

A novel iron metabolism-related gene signature based model was constructed that could be used for prognostic prediction in colon cancer. SLC39A8 and SLC48A1 play a role in the development of colon cancer and might be potential therapeutic targets.

DATA AVAILABILITY STATEMENT

The datasets presented in this study can be found in online repositories. The names of the repository/repositories and accession number(s) can be found in the article/ **Supplementary Material**.

ETHICS STATEMENT

The studies involving human participants were reviewed and approved by the Ethics Committee of Sun Yat-Sen University Cancer Center. The patients/participants provided their written informed consent to participate in this study.

AUTHOR CONTRIBUTIONS

JY and YZ did the literature search and designed the study. JY and YZ collected data. TL participated in the analysis and interpretation of data. All authors participated in revising the manuscript and approved the final version before submission.

ACKNOWLEDGMENTS

We thank Xin Hua, PhD, for help in the instruction in designing this study.

SUPPLEMENTARY MATERIAL

The Supplementary Material for this article can be found online at: https://www.frontiersin.org/articles/10.3389/fcell.2021.786684/full#supplementary-material

REFERENCES

Behr, S. C., Villanueva-Meyer, J. E., Li, Y., Wang, Y. H., Wei, J., Moroz, A., et al. (2018). Targeting Iron Metabolism in High-Grade Glioma with 68Ga-citrate PET/MR. *JCI Insight* 3 (21), e93999. doi:10.1172/jci.insight.93999

Brenner, H., Kloor, M., and Pox, C. P. (2014). Colorectal Cancer. *The Lancet* 383 (9927), 1490–1502. doi:10.1016/S0140-6736(13)61649-9

Carethers, J. M., and Jung, B. H. (2015). Genetics and Genetic Biomarkers in Sporadic Colorectal Cancer. *Gastroenterology* 149 (5), 1177–1190. doi:10.1053/j.gastro.2015.06.047

Chen, B., Khodadoust, M. S., Liu, C. L., Newman, A. M., and Alizadeh, A. A. (2018). Profiling Tumor Infiltrating Immune Cells with CIBERSORT. *Methods Mol. Biol.* 1711, 243–259. doi:10.1007/978-1-4939-7493-1_12

Dixon, S. J., Lemberg, K. M., Lamprecht, M. R., Skouta, R., Zaitsev, E. M., Gleason, C. E., et al. (2012). Ferroptosis: an Iron-dependent Form of Nonapoptotic Cell Death. *Cell* 149 (5), 1060–1072. doi:10.1016/j.cell.2012.03.042

Fogarty, F. M., O'Keeffe, J., Zhadanov, A., Papkovsky, D., Ayllon, V., and O'Connor, R. (2014). HRG-1 Enhances Cancer Cell Invasive Potential and Couples Glucose Metabolism to Cytosolic/extracellular pH Gradient Regulation by the Vacuolar-H+ ATPase. *Oncogene* 33 (38), 4653–4663. doi:10.1038/onc.2013.403

Goel, S., Huang, J., and Klampfer, L. (2015). K-ras, Intestinal Homeostasis and Colon Cancer. *Ccp* 10 (1), 73–81. doi:10.2174/1574884708666131111204440

Hassannia, B., Vandenabeele, P., and Vanden Berghe, T. (2019). Targeting Ferroptosis to Iron Out Cancer. *Cancer Cell* 35 (6), 830–849. doi:10.1016/j.ccell.2019.04.002

Imam, M., Zhang, S., Ma, J., Wang, H., and Wang, F. (2017). Antioxidants Mediate Both Iron Homeostasis and Oxidative Stress. *Nutrients* 9 (7), 671. doi:10.3390/nu9070671

Johnson, S. M., Gulhati, P., Rampy, B. A., Han, Y., Rychahou, P. G., Doan, H. Q., et al. (2010). Novel Expression Patterns of PI3K/Akt/mTOR Signaling Pathway Components in Colorectal Cancer. *J. Am. Coll. Surgeons* 210 (5), 767–776. doi:10.1016/j.jamcollsurg.2009.12.008

Liu, L., Geng, X., Cai, Y., Copple, B., Yoshinaga, M., Shen, J., et al. (2018). Hepatic ZIP8 Deficiency Is Associated with Disrupted Selenium Homeostasis, Liver Pathology, and Tumor Formation. *Am. J. Physiology-Gastrointestinal Liver Physiol.* 315 (4), G569–G579. doi:10.1152/ajpgi.00165.2018

Martin, O. C. B., Naud, N., Taché, S., Debrauwer, L., Chevolleau, S., Dupuy, J., et al. (2018). Targeting Colon Luminal Lipid Peroxidation Limits Colon Carcinogenesis Associated with Red Meat Consumption. *Cancer Prev. Res.* 11 (9), 569–580. doi:10.1158/1940-6207.CAPR-17-0361

Mei, Z., Yan, P., Wang, Y., Liu, S., and He, F. (2018). Knockdown of Zinc Transporter ZIP8 Expression Inhibits Neuroblastoma Progression and Metastasis Inï¿½vitro. *Mol. Med. Rep.* 18 (1), 477–485. doi:10.3892/mmr.2018.8944

Narayanankutty, A. (2019). PI3K/ Akt/ mTOR Pathway as a Therapeutic Target for Colorectal Cancer: A Review of Preclinical and Clinical Evidence. *Cdt* 20 (12), 1217–1226. doi:10.2174/1389450120666190618123846

Schwartz, A. J., Goyert, J. W., Solanki, S., Kerk, S. A., Chen, B., Castillo, C., et al. (2021). Hepcidin Sequesters Iron to Sustain Nucleotide Metabolism and Mitochondrial Function in Colorectal Cancer Epithelial Cells. *Nat. Metab.* 3 (7), 969–982. doi:10.1038/s42255-021-00406-7

Sjöblom, T., Jones, S., Wood, L. D., Parsons, D. W., Lin, J., Barber, T. D., et al. (2006). The Consensus Coding Sequences of Human Breast and Colorectal Cancers. *Science* 314 (5797), 268–274. doi:10.1126/science.1133427

Sohoni, S., Ghosh, P., Wang, T., Kalainayakan, S. P., Vidal, C., Dey, S., et al. (2019). Elevated Heme Synthesis and Uptake Underpin Intensified Oxidative Metabolism and Tumorigenic Functions in Non-small Cell Lung Cancer Cells. *Cancer Res.* 79 (10), 2511–2525. doi:10.1158/0008-5472.CAN-18-2156

Stec, R., Bodnar, L., Charkiewicz, R., Korniluk, J., Rokita, M., Smoter, M., et al. (2012). K-ras Gene Mutation Status as a Prognostic and Predictive Factor in Patients with Colorectal Cancer Undergoing Irinotecan- or Oxaliplatin-Based Chemotherapy. *Cancer Biol. Ther.* 13 (13), 1235–1243. doi:10.4161/cbt.21813

Torti, S. V., and Torti, F. M. (2013). Iron and Cancer: More Ore to Be Mined. *Nat. Rev. Cancer* 13 (5), 342–355. doi:10.1038/nrc3495

Torti, S. V., and Torti, F. M. (2020). Iron and Cancer: 2020 Vision. *Cancer Res.* 80 (24), 5435–5448. doi:10.1158/0008-5472.CAN-20-2017

Wei, J., Gao, X., Qin, Y., Liu, T., and Kang, Y. (2020). An Iron Metabolism-Related SLC22A17 for the Prognostic Value of Gastric Cancer. *Ott* Vol. 13, 12763–12775. doi:10.2147/ott.s287811

Xi, Y., and Xu, P. (2021). Global Colorectal Cancer burden in 2020 and Projections to 2040. *Translational Oncol.* 14 (10), 101174. doi:10.1016/j.tranon.2021.101174

Xue, X., Taylor, M., Anderson, E., Hao, C., Qu, A., Greenson, J. K., et al. (2012). Hypoxia-Inducible Factor-2α Activation Promotes Colorectal Cancer Progression by Dysregulating Iron Homeostasis. *Cancer Res.* 72 (9), 2285–2293. doi:10.1158/0008-5472.can-11-3836

Yuan, Y., Ni, S., Zhuge, A., Li, B., and Li, L. (2021). Iron Regulates the Warburg Effect and Ferroptosis in Colorectal Cancer. *Front. Oncol.* 11, 614778. doi:10.3389/fonc.2021.614778

Conflict of Interest: The authors declare that the research was conducted in the absence of any commercial or financial relationships that could be construed as a potential conflict of interest.

Publisher's Note: All claims expressed in this article are solely those of the authors and do not necessarily represent those of their affiliated organizations, or those of the publisher, the editors and the reviewers. Any product that may be evaluated in this article, or claim that may be made by its manufacturer, is not guaranteed or endorsed by the publisher.

frontiers in Cell and Developmental Biology

ORIGINAL RESEARCH
published: 23 February 2022
doi: 10.3389/fcell.2022.784179

The Iron-Inflammation Axis in Early-Stage Triple-Negative Breast Cancer

Fangfang Duan[1†], Muyi Zhong[2†], Jinhui Ye[3†], Li Wang[1], Chang Jiang[1], Zhongyu Yuan[1], Xiwen Bi[1‡] and Jiajia Huang[1*‡]*

[1]Department of Medical Oncology, The State Key Laboratory of Oncology in South China, Collaborative Innovation Center for Cancer Medicine, Sun Yat-sen University Cancer Center, Guangzhou, China, [2]Department of Breast Oncology, Dongguan People's Hospital, Dongguan, China, [3]Department of Breast Oncology, The First People's Hospital of Zhaoqing, Zhaoqing, China

OPEN ACCESS

Edited by:
Chang Gong,
Sun Yat-sen University, China

Reviewed by:
Margarida Barroso,
Albany Medical College, United States
Tira Tan,
National Cancer Centre Singapore, Singapore

***Correspondence:**
Xiwen Bi
bixw@sysucc.org.cn
Jiajia Huang
huangjiaj@sysucc.org.cn

†These authors have contributed equally to this work and share first authorship

‡These authors have contributed equally to this work

Specialty section:
This article was submitted to Molecular and Cellular Oncology, a section of the journal Frontiers in Cell and Developmental Biology

Received: 27 September 2021
Accepted: 09 February 2022
Published: 23 February 2022

Citation:
Duan F, Zhong M, Ye J, Wang L, Jiang C, Yuan Z, Bi X and Huang J (2022) The Iron-Inflammation Axis in Early-Stage Triple-Negative Breast Cancer. Front. Cell Dev. Biol. 10:784179. doi: 10.3389/fcell.2022.784179

The iron-related homeostasis and inflammatory biomarker have been identified as prognostic factors for cancers. We aimed to explore the prognostic value of a novel comprehensive biomarker, the iron-monocyte-to-lymphocyte ratio (IronMLR) score, in patients with early-stage triple-negative breast cancer (TNBC) in this study. We retrospectively analysed a total of 257 early-stage TNBC patients treated at Sun Yat-sen University Cancer Center (SYSUCC) between March 2006 and October 2016. Their clinicopathological information and haematological data tested within 1 week of the diagnosis were collected. According to the IronMLR score cutoff value of 6.07 μmol/L determined by maximally selected rank statistics, patients were stratified into the low- and high-IronMLR groups, after a median follow-up of 92.3 months (95% confidence interval [CI] 76.0–119.3 months), significant differences in 5-years disease-free survival (DFS) rate (81.2%, 95% CI 76.2%–86.5% *vs.* 65.5%, 95% CI 50.3%–85.3%, $p = 0.012$) and 5-years overall survival (OS) rate (86.0%, 95% CI 81.6%–90.7% *vs.* 65.5%, 95% CI 50.3%–85.3%, $p = 0.011$) were seen between two groups. Further multivariate Cox regression analysis revealed the IronMLR score as an independent predictor for DFS and OS, respectively, we then established a prognostic nomogram integrating the IronMLR score, T stage and N stage for individualized survival predictions. The prognostic model showed good predictive performance with a C-index of DFS 0.725 (95% CI 0.662–0.788) and OS 0.758 (95% CI 0.689–0.826), respectively. Besides, calibration curves for 1-, 3-, 5-DFS, and OS represented satisfactory consistency between actual and nomogram predicted survival. In conclusion, the Iron-inflammation axis might be a potential prognostic biomarker of survival outcomes for patients with early-stage TNBC, prognostic nomograms based on it with good predictive performance might improve individualized survival predictions.

Keywords: early-stage triple-negative breast cancer, serum iron level, monocyte-tolymphocyte ratio, predictive nomogram, survival

INTRODUCTION

Triple-negative breast cancer (TNBC), characterized by the absence of estrogen receptor (ER), progesterone receptor (PR), and human epidermal growth factor receptor 2 (HER-2) expression, accounts for approximately 15% of all breast cancers (Ferlay et al., 2021; Wang et al., 2021). Compared to other subtypes of breast cancers, patients with TNBC usually experience worse survival outcomes due to its increased aggressiveness, heterogeneity, and risks of recurrence and metastasis (Li et al., 2017). Over the past few decades, despite great therapeutic advances in TNBC, TNBC remains a considerable challenge for women worldwide due to its relatively high mortality (Dent et al., 2007; Bianchini et al., 2016; Garrido-Castro et al., 2019). Therefore, the discovery of novel, precise biomarkers, or individualized therapeutic targets for patients with TNBC is urgently needed.

As an essential trace element, iron is involved in activating many proteins, enzymes, and biological processes, such as cell respiration and various signalling pathways (Torti et al., 2018). Increasing studies have demonstrated that the dysregulation of systemic iron homeostasis is related to tumor initiation, growth, development, and progression (Chen et al., 2015; Radulescu et al., 2016). The depletion of iron using iron chelators or targeting increased serum iron has been explored as a novel therapeutic strategy for some cancers (Nutting et al., 2009; Yamasaki et al., 2011; List et al., 2012; Neufeld et al., 2012; Kalinowski et al., 2016; Stockwell et al., 2017; von Hagens et al., 2017). Moreover, ferroptosis, an iron-dependent programmed cell death, has been classified as a type of regulated necrosis and is also recognized as a new therapeutic target for tumours (Dixon et al., 2012). Given its immunogenicity, ferroptosis can induce cells to release damage-associated molecular patterns (DAMPs) and alarmins, which might enhance cell death and facilitate a series of inflammation-related responses (Martin-Sanchez et al., 2017; Proneth and Conrad, 2019; Sun et al., 2020). However, the role of ferroptosis in inflammation is multifaceted, it not only induces inflammatory activity but also suppresses inflammatory cell infiltration (Umemura et al., 2017; Tsurusaki et al., 2019; Sun et al., 2020; Zhou et al., 2020).

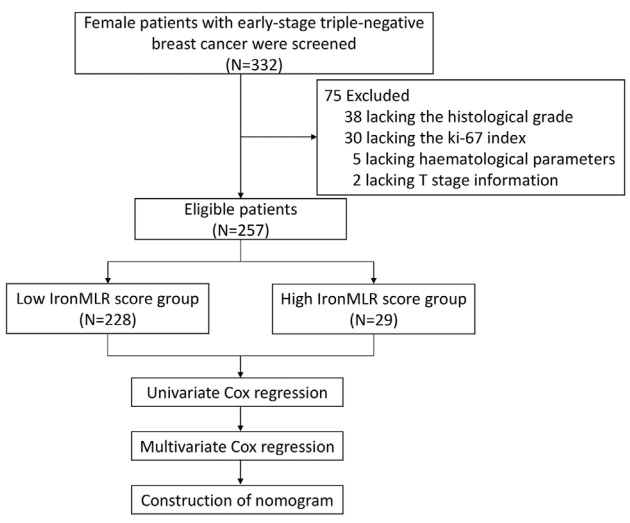

FIGURE 1 | Flow chart of patients selection in this study.

Monocytes have been explored for the suppression of lymphocyte activation, which is associated with aggressive tumors and metastasis (Tiainen et al., 2021). Peripheral lymphocytes or lymphocytes infiltrating in the tumour microenvironment (TME) play an important role in antitumour immunity by T cell-mediated cellular cytotoxicity (Andre et al., 2013). Therefore, the serum monocyte-to-lymphocyte ratio (MLR) might serve as a predictor of systemic inflammatory status, and an increased MLR might reflect poor antitumour immunity (Miklikova et al., 2020). The prognostic value of the MLR has been previously explored in breast cancer (De Giorgi et al., 2019). Thus, we hypothesized that a comprehensive biomarker based on iron homeostasis and systemic inflammation status might also show potential prognostic value. However, to date, no study has examined this aspect.

We aimed to explore the prognostic value of the novel comprehensive biomarker, the IronMLR score, calculated based on the serum iron level and MLR, for female patients with early-stage TNBC. Subsequently, we attempted to establish a prognostic model based on this Iron-inflammation axis for individualized survival predictions.

METHODS

Eligible Patients

We explored the predictive value of a novel biomarker, the IronMLR score, in female patients newly diagnosed with early-stage TNBC at Sun Yat-sen University Cancer Center (SYSUCC) between March 2006 and October 2016. Our study protocol was approved by the Ethics Committee of SYSUCC (registration number: B2021-282-01). Given the retrospective nature of the current study, the requirement of written informed consent from patients was waived. In addition, we anonymously analysed all personal data in line with the Declaration of Helsinki.

Patients were included if they met the following key inclusion criteria: 1) 18 ≤ age <75 years old; 2) pathological diagnosis of breast cancer; 3) absence of ER, PR, and HER2 expression (scored as 0, 1+, or 2+ by immunohistochemistry [IHC] without amplification of the ERBB2 gene on fluorescence *in situ* hybridization); 4) no local relapse or distant metastasis at the diagnosis; and 5) complete clinicopathological data and available haematological parameters assessed within 1 week of the date of diagnosis. All patients in this study were restaged according to the American Joint Committee on Cancer (AJCC 2010, seventh version).

Key exclusion criteria included 1) pregnancy or lactation; 2) a history of malignancy, including breast cancer; 3) medication

TABLE 1 | Characteristics of patients eligible in this study.

Characteristics	All (N = 257)	IronMLRscore		*p* value
		Low (N = 228)	High (N = 29)	
Age (years), median (IQR)	48.0 (41.0–57.0)	48.7 (47.3–50.2)	50.7 (46.2–55.1)	0.406
Age at diagnosis				0.332
≤50	150 (58.4%)	136 (59.6%)	14 (48.3%)	
>50	107 (41.6%)	92 (40.4%)	15 (51.7%)	
BMI, median (IQR)	23.4 (23.0–23.8)	23.5 (23.1–23.9)	22.3 (21.2–23.6)	0.064
BMI				0.029
≤23	132 (51.6%)	111 (48.9%)	21 (72.4%)	
>23	124 (48.4%)	116 (51.5%)	8 (27.6%)	
T stage[a]				0.232
T1	89 (34.6%)	78 (34.2%)	11 (37.9%)	
T2	141 (54.9%)	125 (54.8%)	16 (55.2%)	
T3	23 (8.9%)	21 (9.2%)	2 (6.9%)	
T4	4 (1.6%)	4 (1.8%)	0 (0.0%)	
N stage[a]				0.403
N0	152 (59.2%)	132 (57.9%)	20 (69.1%)	
N1	57 (22.2%)	54 (23.7%)	3 (10.3%)	
N2	24 (9.3%)	21 (9.2%)	3 (10.3%)	
N3	24 (9.3%)	21 (9.2%)	3 (10.3%)	
Stage[a]				0.986
I	59 (23.0%)	52 (22.8%)	7 (24.1%)	
II	143 (55.6%)	127 (55.7%)	16 (55.2%)	
III	55 (21.4%)	49 (21.5%)	6 (20.7%)	
Menstrual status				0.546
Premenopausal	168 (65.4%)	151 (66.2%)	17 (58.6%)	
Postmenopausal	89 (34.6%)	77 (33.8%)	12 (41.4%)	
Pathological grade[b]				0.999
1/2	112 (43.6%)	99 (43.4%)	13 (44.8%)	
3	145 (56.4%)	129 (56.6%)	16 (55.2%)	
KI-67 index[c]				0.028
<30%	60 (23.3%)	48 (21.1%)	12 (41.4%)	
≥30%	197 (76.7%)	180 (78.9%)	17 (58.6%)	
Lymphovascular invasion				0.502
No	205 (79.8%)	180 (78.9%)	25 (86.2%)	
Yes	52 (20.2%)	48 (21.1%)	4 (13.8%)	

[a]*Diagnosed based on the AJCC 2010 criteria (seventh edition).*
[b]*Histological grade at diagnosis was based on the degree of histological tumor differentiation.*
[c]*The Ki-67 index at diagnosis indicates DNA synthetic activity as measured using immunocytochemistry.*
[d]*The cut-off value was determined by means of maximally selected log-rank statistics.*
Abbreviation: IQR, interquartile ranges.

affecting the patient's inflammatory status before diagnosis; and 4) the presence of any severe or uncontrolled complications.

Information Collection and Measurement of Serum Iron Levels

Clinicopathological data were hand-retrieved from the electronic medical records system of our hospital and included age, menstrual status, histological type, T stage, N stage, histological grade, lymphovascular invasion, and Ki-67 index. Haematological parameters were assessed within 1 week of initiating any anti-tumor therapy, and the MLR was calculated as: MLR = monocyte count (10^9/L)/lymphocyte count (10^9/L). We acquired patient blood samples obtained within 1 week of diagnosis from the Tumor Resource Library of SYSUCC. The serum iron levels of patients were analysed using the Iron (Fe) Assay Kit (PAESA Chromogenic Method) with a Cobas 8,000 system (Roche Diagnostics, Basel, Switzerland). The IronMLR score was calculated as following: IronMLR score = serum iron level * MLR.

Follow-up and Endpoints

We retrieved patient follow-up information from the outpatient electronic records of our center or telephone interviews. Patients were monitored every 3 months during 2 years of the diagnosis, subsequently every 6 months to 5 years, and then once every year thereafter. The main follow-up items included routine laboratory tests, menstrual status, ultrasound (breast and abdomen), or computed tomography (CT). Patients underwent bone scintigraphy annually.

The primary endpoint of the current study was disease-free survival (DFS), which was defined as the time from the date of diagnosis to the date of disease progression or death due to any cause. The second endpoint was overall survival (OS), which was defined as the time from the date of diagnosis to the date of death due to any cause.

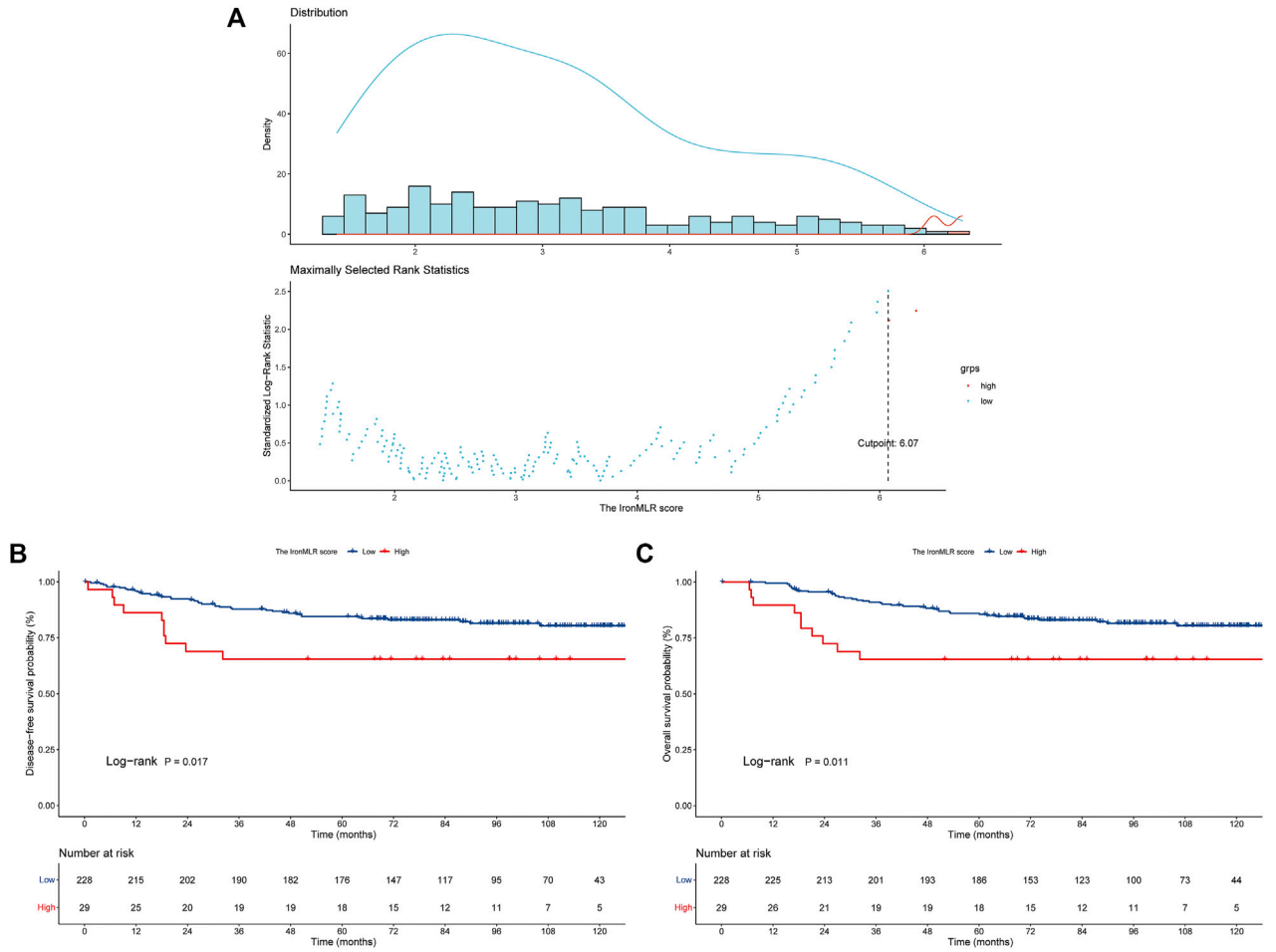

FIGURE 2 | Determination of the cutoff value of the IronMLR score and Survival risk stratification of patients. **(A)** A cutoff value of 6.07 μmol/L defined by maximally selected rank statistics. **(B)** Survival curves for disease-free survival (DFS) between different IronMLR score groups. **(C)** Survival curves for overall survival (OS) between different IronMLR score groups.

Statistical Analysis

Categorical variables are presented as frequencies with percentages, and continuous variables are listed as medians with interquartile ranges (IQRs). Chi-square tests and Mann-Whitney U tests were performed to compare the association between patient clinicopathological characteristics and the baseline IronMLR score. Patients with early-stage TNBC were stratified into high and low IronMLR groups according to the cut-off value of the IronMLR score determined by maximally selected rank statistics. The Kaplan-Meier method was performed to estimate survival curves of two different IronMLR score groups, and the log-rank test was used to compare their survival differences. Only variables with p values less than 0.05 in the univariate Cox analysis were included in the multivariate Cox regression model. Factors were tested according to the Schoenfeld residuals (Wileyto et al., 2013), and their corresponding hazard ratios (HRs) with 95% confidence intervals (CIs) were estimated. Then, we developed a prognostic model integrating the IronMLR score with other independent clinicopathological indicators from the multivariate Cox analysis, and we evaluated the prognostic accuracy and discriminative ability of the predictive model by means of the concordance index (C-index), calibration curves, and time-dependent receiver operating characteristic (ROC) curves. A two-sided $p < 0.05$ was regarded as significant, and all statistical analyses were performed using R 4.0.1.

RESULTS

Patient Clinicopathologic Characteristics According to the IronMLR Score

As presented in the flow chart in **Figure 1**, between March 2006 and October 2016, a total of 257 female patients with early-stage TNBC were eligible for inclusion in this study. A total of 75 patients were excluded due to a lack of complete information, i.e., 38 patients did not have complete histological grade data, 30 patients did not have Ki-67 index data, 5 patients lacked data on haematological parameters, and 2 patients had missing T stage information.

Table 2 | Univariate and multivariate cox regression analysis of disease-free survival.

Characteristics	Univariate cox analysis		Multivariate cox analysis	
	Hazard ratio (95%CI)	*p* value	Hazard ratio (95%CI)	*p* value
Age (year)				
≤50	Reference		Reference	
>50	1.723 (1.056–2.810)	0.029*	1.370 (0.810–2.310)	0.243
BMI				
≤23	Reference			
>23	0.946 (0.581-1.540)	0.823		
Menstrual status				
Premenopausal	Reference			
Postmenopausal	1.601 (0.974–2.632)	0.064		
Histological grade[a]				
1/2	Reference			
3	0.988 (0.605–1.613)	0.961		
Lymphovascular invasion				
No	Reference		Reference	
Yes	2.324 (1.358–3.979)	0.002*	1.560 (0.840–2.880)	0.157
Ki-67 index at diagnosis < 30%[b]				
No	Reference			
Yes	1.135 (0.655–1.964)	0.652		
T stage[c]				
1	Reference		Reference	
2	0.863 (0.506–1.474)	0.590	0.840 (0.490–1.460)	0.543
3	1.021 (0.415–2.508)	0.964	0.890 (0.350–2.250)	0.802
4	3.886 (1.165–12.970)	0.027*	2.660 (0.770–9.270)	0.123
N stage[c]				
0	Reference		Reference	
1	2.452 (1.325–4.538)	0.004*	2.360 (1.250–4.430)	0.008*
2	2.898 (1.381–6.083)	0.005*	2.560 (1.190–5.500)	0.016*
3	5.788 (2.925–11.453)	<0.001*	4.130 (1.910–8.920)	<0.001*
IronMLR score				
Low	Reference		Reference	
High	2.157 (1.171–3.974)	0.014*	2.310 (1.200–4.430)	0.012*

*p < *0.05*.

[a]*Histological grade at diagnosis was based on the degree of histological tumor differentiation.*

[b]*The Ki-67, index at diagnosis indicates DNA, synthetic activity as measured using immunocytochemistry.*

[c]*Diagnosed based on the AJCC, 2010 criteria (seventh edition).*

The baseline clinicopathological features are shown in **Table 1**. The median age at the diagnosis of all eligible patients was 48.0 (IQR: 41.0–57.0) years old, and 150 (58.4%) patients were ≤50 years old. The median BMI was 23.4 (IQR: 23.0–23.8) kg/m^2, and 132 (51.6%) patients had a value of BMI ≤23.0 kg/m^2. There were 168 (65.4%) patients in the premenopausal period and 197 (76.7%) with a Ki-67 index value ≥30%. According to the seventh AJCC staging criteria, stages I, II, and III accounted for 23.0, 55.6, and 21.4%, respectively.

The optimal cut-off value of the IronMLR score defined by the maximally selected rank statistics for OS was 6.07 umol/L (**Figure 2A**). Overall, 228 (88.7%) patients had a low IronMLR score, and 29 (11.3%) patients had a high IronMLR score. The baseline clinicopathological characteristics between these two IronMLR groups were much more balanced (**Table 1**). Compared to TNBC patients in the low IronMLR score group, a higher proportion of patients in the high IronMLR score group had a BMI ≤23 kg/m^2 (p = 0.029) and Ki-67 index <30% (p = 0.028).

Survival Outcomes

The median follow-up time was 92.3 months (95% CI 76.0–119.3 months). Compared to patients in the low IronMLR score group, early-stage TNBC patients in the high IronMLR score group had a significantly worse 5-years DFS rate (81.2%, 95% CI 76.2%–86.5% *vs.* 65.5%, 95% CI 50.3%–85.3%, p = 0.012) (**Figure 2B**) and 5-years OS rate (86.0%, 95% CI 81.6%–90.7% *vs.* 65.5%, 95% CI 50.3%–85.3%, p = 0.011) (**Figure 2C**).

Independent Indicators for Survival

As shown in **Table 2**, five factors were considered independent indicators for DFS according to the univariate Cox regression model, including age, lymphovascular invasion, T stage, N stage, and the IronMLR score. Further multivariate Cox analysis demonstrated that N stage and the IronMLR score remained independent predictors of DFS for patients with early-stage TNBC.

Table 3 presents that age, menstrual status, lymphovascular invasion, T stage, N stage, and the IronMLR score of patients achieved the predominate threshold of OS (p < 0.05) for early-stage TNBC female patients in the univariate Cox analysis. Then, these variables were further analysed in the multivariate Cox regression model, which revealed that T stage, N stage, and the IronMLR score continued to be significantly associated with OS.

TABLE 3 | Univariate and multivariate cox regression analysis of overall survival.

Characteristics	Univariate cox analysis		Multivariate cox analysis	
	Hazard ratio (95%CI)	*p* value	Hazard ratio (95%CI)	*p* value
Age (year)				
≤50	Reference		Reference	
>50	2.103 (1.199–3.689)	0.010*	1.770 (0.640–4.900)	0.272
BMI				
≤23	Reference			
>23	0.810 (0.463–1.416)	0.460		
Menstrual status				
Premenopausal	Reference		Reference	
Postmenopausal	1.859 (1.067–3.238)	0.029*	0.910 (0.320–2.570)	0.852
Histological grade[a]				
1/2	Reference			
3	1.235 (0.701–2.176)	0.464		
Lymphovascular invasion				
No	Reference		Reference	
Yes	2.689 (1.504–4.809)	0.001*	1.820 (0.920–3.600)	0.086
Ki-67 index at diagnosis < 30%[b]				
No	Reference			
Yes	0.891 (0.456–1.740)	0.735		
T stage[c]				
1	Reference		Reference	
2	0.880 (0.473–1.638)	0.686	0.820 (0.430–1.540)	0.535
3	1.363 (0.537–3.458)	0.514	1.020 (0.370–2.870)	0.963
4	5.251 (1.536–17.958)	0.008*	3.880 (1.070–13.990)	0.039*
N stage[c]				
0	Reference		Reference	
1	2.099 (1.002–4.397)	0.049*	1.990 (0.930–4.280)	0.077
2	3.640 (1.621–8.174)	0.002*	2.990 (1.260–7.060)	0.013*
3	7.134 (3.392–15.006)	<0.001*	4.510 (1.940–10.500)	<0.001*
IronMLR score				
Low	Reference		Reference	
High	2.404 (1.201–4.808)	0.013*	2.730 (1.310–5.710)	0.008*

*p < *0.05*.

[a]*Histological grade at diagnosis was based on the degree of histological tumor differentiation.*

[b]*The Ki-67 index at diagnosis indicates DNA synthetic activity as measured using immunocytochemistry.*

[c]*Diagnosed based on the AJCC 2010 criteria (seventh edition).*

Establishment and Evaluation of the Prognostic Model

Based on independent indicators for DFS identified in the above multivariate Cox analysis, i.e., N stage and the IronMLR score, we established a prognostic model for individualized DFS prediction for patients with early-stage TNBC. Given that T stage is commonly used in clinical practice, we also integrated it into the prognostic model (**Figure 3A**). The model showed perfect predictive performance with a good C-index of 0.725 (95% CI 0.662–0.788). Satisfactory consistency between observational 1-, 3-, and 5-years DFS rates and nomogram-predicted DFS rates was found in calibration curves (**Figure 3B**). Time-dependent ROC curves showed that the area under the curve (AUC) of our nomogram for DFS was higher than the AUCs for T stage, N stage, and the traditional tumor-node-metastasis (TNM) staging system (**Figure 3C**).

Similarly, we developed a prognostic model with independent indicators according to the multivariate Cox regression model, i.e., T stage, N stage, and IronMLR score, for individualized OS prediction (**Figure 4A**). The predictive accuracy of our nomogram for OS was very good, with a satisfactory C-index of 0.758 (95% CI 0.689–0.826). The calibration plots for 1-, 3-, and 5-years OS rates demonstrated good consistency between actual and nomogram-predicted OS rates (**Figure 4B**). Compared to traditional T stage, N stage, and TNM stage, our prognostic nomogram for OS achieved a higher AUC according to time-dependent ROC curves (**Figure 4C**).

DISCUSSION

In this study, we constructed a novel comprehensive biomarker based on the serum iron level and systemic inflammation status, the IronMLR score. According to a cut-off value of 6.07 determined by maximally selected rank statistics, heterogeneous patients with early-stage TNBC were divided into groups based on a low or high IronMLR score. Significant differences in DFS and OS were found between these two groups. Further univariate and multivariate Cox regression analyses demonstrated that a high IronMLR score was a negatively independent predictor of poor survival for early-stage TNBC patients. Subsequently, prognostic models integrating the IronMLR score and two clinicopathological features (T stage and N stage) for DFS and

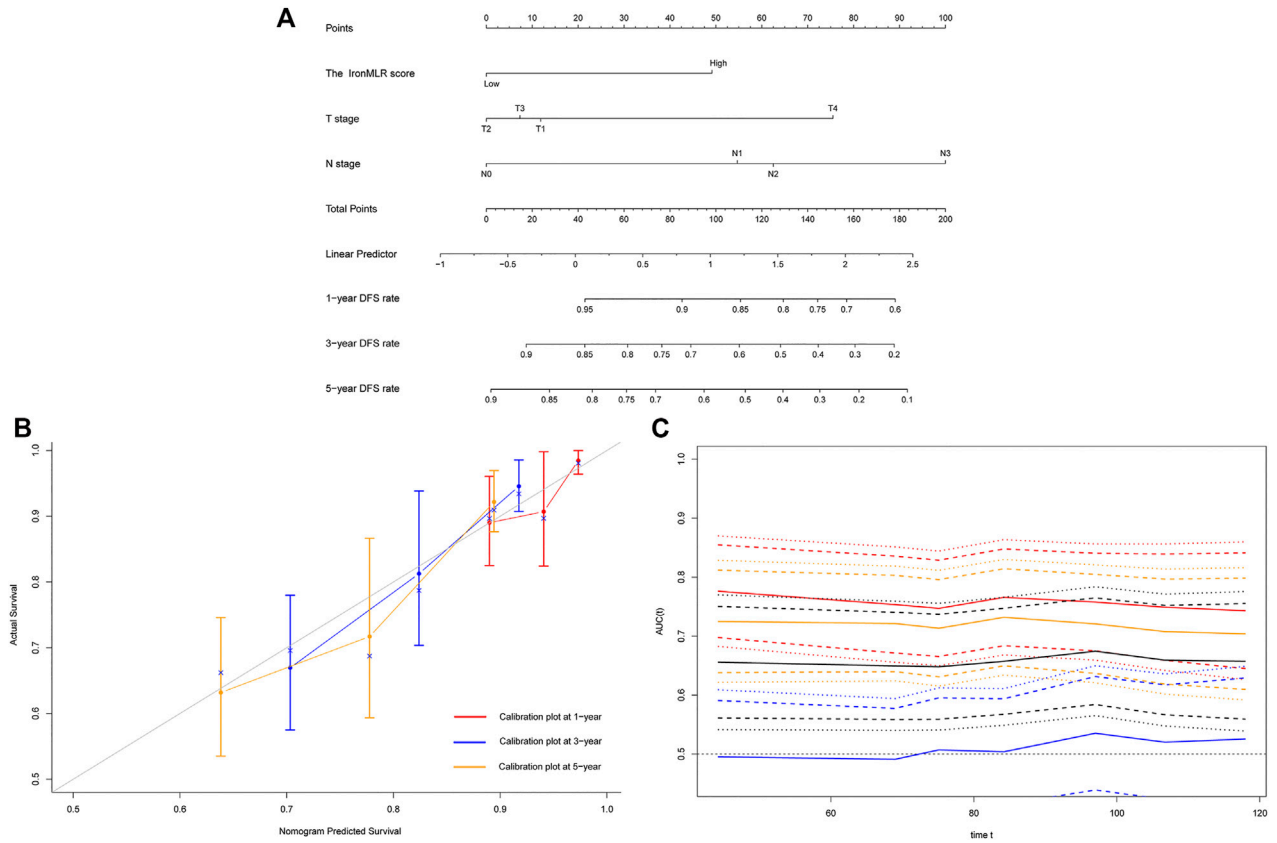

FIGURE 3 | Development and evaluation of a model for individualized prediction of disease-free survival (DFS). **(A)** Nomogram of prognostic model for patients with early-stage triple-negative breast cancer. **(B)** Calibration plots of 1-, 3-, and 5-years DFS predictions. **(C)** Time-dependent receiver operating characteristic (ROC) curves (Nomogram [red], T stage [blue], N stage [orange], TNM stage [black]).

OS were established and graphically depicted as nomograms. These prognostic nomograms presented good discriminative ability and satisfactory predictive agreement between observed clinical outcomes and the nomogram-predicted survival probability.

Although iron is indispensable for many proteins and enzymes, playing an important role in various biological processes (Hider and Maret, 2015; Torti et al., 2018), it also attributes to oxidative stress and DNA damage. Excess iron has been found to be significantly associated with tumor initiation, progression, aggressiveness, and metastasis (Chen et al., 2015; Guo et al., 2015; Radulescu et al., 2016). Increasing studies have found iron metabolic dysregulation, iron homeostatic disorder, and distribution changes in peripheral iron in patients with various malignancies, including breast cancer (Torti et al., 2018; Galaris et al., 2019). Meanwhile, iron accumulation could induce lipid peroxidation and facilitate lethal injury to tumor cells, which subsequently could contribute to inhibiting tumor initiation and progression (Chang et al., 2019; Forciniti et al., 2020; Yang et al., 2021). Iron accumulation is involved in some programmed cell death pathways, such as apoptosis, necroptosis, ferroptosis, and so on (Dixon et al., 2012; Torti et al., 2018). Thus, iron-related metabolism or iron chelators might be potential novel therapeutic targets and strategies for antitumor treatment (Nutting et al., 2009; Yamasaki et al., 2011; List et al., 2012; Neufeld et al., 2012; Kalinowski et al., 2016). Hence, the measurement of iron levels is necessary. Many previous studies have used iron-bound proteins such as transferrin and ferritin to reflect body iron levels (Fonseca-Nunes et al., 2014; Torti et al., 2018; Morales and Xue, 2021), but this indirect test might produce errors in reflecting actual iron levels, direct detection of serum iron would be better (Torti et al., 2018; El Hout et al., 2018). Thus, we adopted the peripheral iron level to construct the IronMLR score in this study.

Inflammation, a hallmark feature of tumors, has shown a significant association with tumorigenesis, progression, development, and metastasis (Diakos, et al., 2014). Cancer-associated inflammation refers to complicated connections between tumors and inflammatory responses, and it might show a significant relation to poor prognosis and therapeutic failure (Zitvogel et al., 2017; Li et al., 2021). As vital inflammatory mediators, peripheral inflammatory cells or inflammatory cells infiltrating in the TME are potential prognostic biomarkers for breast cancer (Diakos et al., 2014; van der Willik et al., 2018). Among inflammatory cells, monocytes have been identified as inhibitors of lymphocyte activation and play an important role in tumor aggressiveness and metastasis (Tiainen et al., 2021). Circulating lymphocytes or lymphocytes infiltrating in the

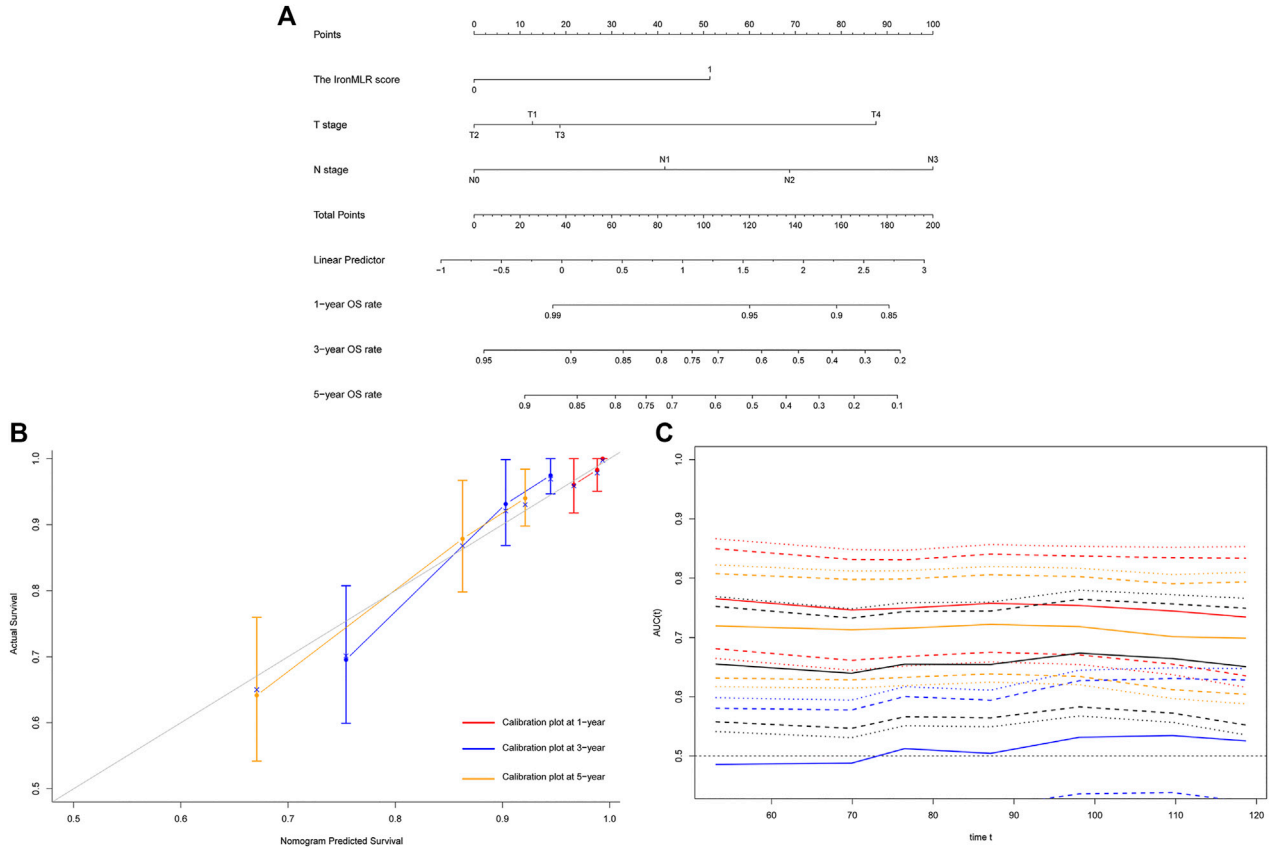

FIGURE 4 | Development and evaluation of a model for individualized prediction of overall survival (OS). **(A)** Nomogram of prognostic model for patients with early-stage triple-negative breast cancer. **(B)** Calibration plots for predicting OS at 1-, 3-, and 5-years. **(C)** Time-dependent receiver operating characteristic (ROC) curves (Nomogram [red], T stage [blue], N stage [orange], TNM stage [black]).

TME are both involved in antitumor immune responses (Andre et al., 2013). Therefore, the circulating marker MLR might reflect systemic inflammatory status, an elevated MLR indicates an increased monocyte count or a reduced lymphocyte count, which suggests poor antitumor immunity (Miklikova et al., 2020). The negative association between the MLR and survival outcomes of breast cancer patients has also been explored (De Giorgi et al., 2019).

Nowadays, the underlying association between iron and inflammation is still poorly understood. As previously mentioned, ferroptosis plays multifaceted functions in cancer-related inflammation, activation, and infiltration of inflammatory cells (Umemura et al., 2017; Tsurusaki et al., 2019; Sun et al., 2020; Zhou et al., 2020). In addition, IL-6, an inflammatory cytokine, is secreted locally in the TME of breast cancer such as monocytes (Masjedi et al., 2018), and it has been demonstrated to directly regulate systemic iron homeostasis through IL6/IL6R/Janus kinase 2 (JAK2)/signal transducer and activator of transcription 3 (STAT3) signaling pathway (Hentze et al., 2010; Ganz and Nemeth, 2011; Guo et al., 2015). Moreover, IL-6 also likely contributes to the dysregulated hepcidin/ferroportin signaling in breast cancer and mediates further iron homeostasis (Masjedi et al., 2018). So, the blockade of IL-6 inflammatory signaling cascade has been investigated as a potential therapeutic strategy to suppress hepcidin in breast cancer and for anaemic cancer patients (Jiang et al., 2011; Guo et al., 2015). In recent years, researchers have taken great interest in developing prognostic models for risk stratification and clinical outcomes predictions. Predictive models incorporating multiple biomarkers rather than a single marker have higher prognostic accuracy (Li et al., 2021). Thus, we comprehensively developed a new biomarker integrating serum iron with systemic inflammatory markers. Our analyses showed that the novel IronMLR score is an independent indicator of the survival of patients with early-stage TNBC, and patients stratified according to its cut-off value experience significantly different survival outcomes.

Based on the classification of the IronMLR score, prognostic nomogram incorporating it and the commonly used T stage and N stage were established. In clinical practice, 21-gene tests, 70-gene assays, and PAM50 predictive models are widely applied for risk stratification or therapeutic recommendations, but these genetic models are restricted to patients with specific subtypes, lymph node-negative patients or women at high clinical risk of recurrence from breast cancer, with limited prognostic accuracy (Dixon et al., 2012; Gnant et al., 2015; Ibraheem et al., 2020;

Poorvu et al., 2020). Comparatively speaking, the predictive nomogram developed in our study were more accurate with a high C-index, economic, convenient, and easier to be applied in primary hospitals. Clinicians and patients usually use the TNM staging system to stratify recurrence or death risks and to guide therapeutic strategies, however, the TNM criteria just incorporate a limited number of clinical features, so its predictive accuracy is limited due to the heterogeneity observed among patients (Bareche et al., 2018; Grosselin et al., 2019). Our time-dependent ROC curves showed that compared to the common TNM staging system, higher AUCs for DFS and OS were achieved with our prognostic nomograms, which suggested that our predictive models have greater predictive accuracy and might be a strong supplement to traditional TNM criteria. For example, TNBC patients with high IronMLR scores tended to have poorer prognosis, for them, more intensive care, closer follow-up, and more precise routine imaging monitor such as CT or magnetic resonance imaging (MRI) instead of breast/abdominal ultrasound would be much meaningful to monitor their tumor condition and improve their survival outcomes as much as possible.

Our study had several limitations, which should be acknowledged. First, because we retrospectively explored the prognostic value of the IronMLR score, selection bias is inevitable. Second, we only evaluated the baseline serum iron level and MLR before the initiation of any anti-tumor therapy, but we failed to explore the dynamic changes of the serum iron level and inflammatory status of patients during subsequent treatment. Monitoring changes in these parameters might help clinicians both to adjust the therapeutic strategy in time and to guide personalized treatment. Third, this study was a preliminary research, underlying mechanisms of the IronMLR on TNBC, and the relationship between MLR and iron require more investigations. Finally, patients with early-stage TNBC included in this study were from only a single centre in China. Further large or multicentre cohort studies are warrant to enhance the power of our results. Although we actively sought help and cooperation from other hospitals to validate our prognostic models, unfortunately, we failed to obtain complete haematological parameters and follow-up information. Thus, the prognostic accuracy of our nomograms for early-stage TNBC patients from other geographic backgrounds requires further evaluation in future studies.

CONCLUSION

In conclusion, we propose the Iron-inflammation axis, the IronMLR score, as a novel prognostic biomarker for trace element and systemic inflammatory status in female patients with early-stage TNBC. Prognostic models based on the IronMLR score for individualized survival predictions showed good predictive performance and discriminative accuracy, but validation of the predictive role of the IronMLR score is needed in a large or multicentre cohort. Additional studies, especially those exploring the IronMLR score as a potential dynamic biomarker related to survival outcomes during treatment, are warranted in future.

DATA AVAILABILITY STATEMENT

The raw data supporting the conclusion of this article will be made available by the authors, without undue reservation.

ETHICS STATEMENT

The studies involving human participants were reviewed and approved by the Ethics Committee of Sun Yat-sen University Cancer Center. The ethics committee waived the requirement of written informed consent for participation.

AUTHOR CONTRIBUTIONS

JH and XB designed this study. FD, MZ, and JY collected, primarily analysed, and interpreted data. FD, MZ, JY, LW, and CJ participated in the drafting of the manuscript. FD, MZ, JY, ZY, XB, and JH contributed to administrative, technical, or material support. All authors revised this manuscript and approved the final summitted version.

FUNDING

This study was funded by the Natural Science Foundation of Guangdong Province (No. 2019A151011781), the Sci-Tech Project Foundation of Guangzhou City (No. 202002020033), and the cultivation foundation for the junior teachers in Sun Yat-sen University (No. 20ykpy164).

ACKNOWLEDGMENTS

We gratefully acknowledge patients and their family for all their help in enabling completion of this study.

REFERENCES

Andre, F., Dieci, M. V., Dubsky, P., Sotiriou, C., Curigliano, G., Denkert, C., et al. (2013). Molecular Pathways: Involvement of Immune Pathways in the Therapeutic Response and Outcome in Breast Cancer. *Clin. Cancer Res.* 19 (1), 28–33. doi:10.1158/1078-0432.CCR-11-2701

Bareche, Y., Venet, D., Ignatiadis, M., Aftimos, P., Piccart, M., Rothe, F., et al. (2018). Unravelling Triple-Negative Breast Cancer Molecular Heterogeneity Using an Integrative Multiomic Analysis. *Ann. Oncol.* 29 (4), 895–902. doi:10.1093/annonc/mdy024

Bianchini, G., Balko, J. M., Mayer, I. A., Sanders, M. E., and Gianni, L. (2016). Triple-negative Breast Cancer: Challenges and Opportunities of a Heterogeneous Disease. *Nat. Rev. Clin. Oncol.* 13 (11), 674–690. doi:10.1038/nrclinonc.2016.66

Chang, V. C., Cotterchio, M., and Khoo, E. (2019). Iron Intake, Body Iron Status, and Risk of Breast Cancer: a Systematic Review and Meta-Analysis. *BMC Cancer* 19 (1), 543. doi:10.1186/s12885-019-5642-0

Chen, Y., Zhang, S., Wang, X., Guo, W., Wang, L., Zhang, D., et al. (2015). Disordered Signaling Governing Ferroportin Transcription Favors Breast Cancer Growth. *Cell Signal.* 27 (1), 168–176. doi:10.1016/j.cellsig.2014.11.002

De Giorgi, U., Mego, M., Scarpi, E., Giordano, A., Giuliano, M., Valero, V., et al. (2019). Association between Circulating Tumor Cells and Peripheral Blood Monocytes in Metastatic Breast Cancer. *Ther. Adv. Med. Oncol.* 11, 175883591986606. doi:10.1177/1758835919866065

Dent, R., Trudeau, M., Pritchard, K. I., Hanna, W. M., Kahn, H. K., Sawka, C. A., et al. (2007). Triple-negative Breast Cancer: Clinical Features and Patterns of Recurrence. *Clin. Cancer Res.* 13 (15 Pt 1), 4429–4434. doi:10.1158/1078-0432.CCR-06-3045

Diakos, C. I., Charles, K. A., McMillan, D. C., and Clarke, S. J. (2014). Cancer-related Inflammation and Treatment Effectiveness. *Lancet Oncol.* 15 (11), e493–e503. doi:10.1016/S1470-2045(14)70263-3

Dixon, S. J., Lemberg, K. M., Lamprecht, M. R., Skouta, R., Zaitsev, E. M., Gleason, C. E., et al. (2012). Ferroptosis: an Iron-dependent Form of Nonapoptotic Cell Death. *Cell* 149 (5), 1060–1072. doi:10.1016/j.cell.2012.03.042

El Hout, M., Dos Santos, L., Hamaï, A., and Mehrpour, M. (2018). A Promising New Approach to Cancer Therapy: Targeting Iron Metabolism in Cancer Stem Cells. *Semin. Cancer Biol.* 53, 125–138. doi:10.1016/j.semcancer.2018.07.009

Ferlay, J., Colombet, M., Soerjomataram, I., Parkin, D. M., Piñeros, M., Znaor, A., et al. (2021). Cancer Statistics for the Year 2020: An Overview. *Int. J. Cancer* 149, 778–789. doi:10.1002/ijc.33588

Fonseca-Nunes, A., Jakszyn, P., and Agudo, A. (2014). Iron and Cancer Risk-A Systematic Review and Meta-Analysis of the Epidemiological Evidence. *Cancer Epidemiol. Biomarkers Prev.* 23 (1), 12–31. doi:10.1158/1055-9965.EPI-13-0733

Forciniti, S., Greco, L., Grizzi, F., Malesci, A., and Laghi, L. (2020). Iron Metabolism in Cancer Progression. *Ijms* 21 (6), 2257. doi:10.3390/ijms21062257

Galaris, D., Barbouti, A., and Pantopoulos, K. (2019). Iron Homeostasis and Oxidative Stress: An Intimate Relationship. *Biochim. Biophys. Acta (Bba) - Mol. Cel Res.* 1866 (12), 118535. doi:10.1016/j.bbamcr.2019.118535

Ganz, T., and Nemeth, E. (2011). The Hepcidin-Ferroportin System as a Therapeutic Target in Anemias and Iron Overload Disorders. *Hematol. Am Soc Hematol Educ Program* 2011, 538–542. doi:10.1182/asheducation-2011.1.538

Garrido-Castro, A. C., Lin, N. U., and Polyak, K. (2019). Insights into Molecular Classifications of Triple-Negative Breast Cancer: Improving Patient Selection for Treatment. *Cancer Discov.* 9 (2), 176–198. doi:10.1158/2159-8290.CD-18-1177

Gnant, M., Sestak, I., Filipits, M., Dowsett, M., Balic, M., Lopez-Knowles, E., et al. (2015). Identifying Clinically Relevant Prognostic Subgroups of Postmenopausal Women with Node-Positive Hormone Receptor-Positive Early-Stage Breast Cancer Treated with Endocrine Therapy: a Combined Analysis of ABCSG-8 and ATAC Using the PAM50 Risk of Recurrence Score and Intrinsic Subtype. *Ann. Oncol.* 26 (8), 1685–1691. doi:10.1093/annonc/mdv215

Grosselin, K., Durand, A., Marsolier, J., Poitou, A., Marangoni, E., Nemati, F., et al. (2019). High-throughput Single-Cell ChIP-Seq Identifies Heterogeneity of Chromatin States in Breast Cancer. *Nat. Genet.* 51 (6), 1060–1066. doi:10.1038/s41588-019-0424-9

Guo, W., Zhang, S., Chen, Y., Zhang, D., Yuan, L., Cong, H., et al. (2015). An Important Role of the Hepcidin-Ferroportin Signaling in Affecting Tumor Growth and Metastasis. *Acta Biochim. Biophys. Sin* 47 (9), 703–715. doi:10.1093/abbs/gmv063

Hentze, M. W., Muckenthaler, M. U., Galy, B., and Camaschella, C. (2010). Two to Tango: Regulation of Mammalian Iron Metabolism. *Cell* 142 (1), 24–38. doi:10.1016/j.cell.2010.06.028

Hider, R. C., and Maret, W. (2015). Iron and Zinc Sensing in Cells and the Body. *Metallomics* 7 (2), 200–201. doi:10.1039/c4mt90051k

Ibraheem, A., Olopade, O. I., and Huo, D. (2020). Propensity Score Analysis of the Prognostic Value of Genomic Assays for Breast Cancer in Diverse Populations Using the National Cancer Data Base. *Cancer* 126 (17), 4013–4022. doi:10.1002/cncr.32956

Jiang, X. P., Yang, D. C., Elliott, R. L., and Head, J. F. (2011). Down-regulation of Expression of Interleukin-6 and its Receptor Results in Growth Inhibition of MCF-7 Breast Cancer Cells. *Anticancer Res.* 31 (9), 2899–2906.

Kalinowski, D. S., Stefani, C., Toyokuni, S., Ganz, T., Anderson, G. J., Subramaniam, N. V., et al. (2016). Redox Cycling Metals: Pedaling Their Roles in Metabolism and Their Use in the Development of Novel Therapeutics. *Biochim. Biophys. Acta (Bba) - Mol. Cel Res.* 1863 (4), 727–748. doi:10.1016/j.bbamcr.2016.01.026

Li, W.-Z., Hua, X., Lv, S.-H., Liang, H., Liu, G.-Y., Lu, N., et al. (2021). A Scoring System Based on Nutritional and Inflammatory Parameters to Predict the Efficacy of First-Line Chemotherapy and Survival Outcomes for De Novo Metastatic Nasopharyngeal Carcinoma. *Jir* 14, 817–828. doi:10.2147/JIR.S296710

Li, X., Yang, J., Peng, L., Sahin, A. A., Huo, L., Ward, K. C., et al. (2017). Triple-negative Breast Cancer Has Worse Overall Survival and Cause-specific Survival Than Non-triple-negative Breast Cancer. *Breast Cancer Res. Treat.* 161 (2), 279–287. doi:10.1007/s10549-016-4059-6

List, A. F., Baer, M. R., Steensma, D. P., Raza, A., Esposito, J., Martinez-Lopez, N., et al. (2012). Deferasirox Reduces Serum Ferritin and Labile Plasma Iron in RBC Transfusion-dependent Patients with Myelodysplastic Syndrome. *Jco* 30 (17), 2134–2139. doi:10.1200/JCO.2010.34.1222

Martin-Sanchez, D., Ruiz-Andres, O., Poveda, J., Carrasco, S., Cannata-Ortiz, P., Sanchez-Niño, M. D., et al. (2017). Ferroptosis, but Not Necroptosis, Is Important in Nephrotoxic Folic Acid-Induced AKI. *Jasn* 28 (1), 218–229. doi:10.1681/asn.2015121376

Masjedi, A., Hashemi, V., Hojjat-Farsangi, M., Ghalamfarsa, G., Azizi, G., Yousefi, M., et al. (2018). The Significant Role of Interleukin-6 and its Signaling Pathway in the Immunopathogenesis and Treatment of Breast Cancer. *Biomed. Pharmacother.* 108, 1415–1424. doi:10.1016/j.biopha.2018.09.177

Miklikova, S., Minarik, G., Sedlackova, T., Plava, J., Cihova, M., Jurisova, S., et al. (2020). Inflammation-Based Scores Increase the Prognostic Value of Circulating Tumor Cells in Primary Breast Cancer. *Cancers (Basel)* 12 (5), 1134. doi:10.3390/cancers12051134

Morales, M., and Xue, X. (2021). Targeting Iron Metabolism in Cancer Therapy. *Theranostics* 11 (17), 8412–8429. doi:10.7150/thno.59092

Neufeld, E. J., Galanello, R., Viprakasit, V., Aydinok, Y., Piga, A., Harmatz, P., et al. (2012). A Phase 2 Study of the Safety, Tolerability, and Pharmacodynamics of FBS0701, a Novel Oral Iron Chelator, in Transfusional Iron Overload. *Blood* 119 (14), 3263–3268. doi:10.1182/blood-2011-10-386268

Nutting, C. M., van Herpen, C. M. L., Miah, A. B., Bhide, S. A., Machiels, J.-P., Buter, J., et al. (2009). Phase II Study of 3-AP Triapine in Patients with Recurrent or Metastatic Head and Neck Squamous Cell Carcinoma. *Ann. Oncol.* 20 (7), 1275–1279. doi:10.1093/annonc/mdn775

Poorvu, P. D., Gelber, S. I., Rosenberg, S. M., Ruddy, K. J., Tamimi, R. M., Collins, L. C., et al. (2020). Prognostic Impact of the 21-Gene Recurrence Score Assay Among Young Women with Node-Negative and Node-Positive ER-Positive/HER2-Negative Breast Cancer. *Jco* 38 (7), 725–733. doi:10.1200/JCO.19.01959

Proneth, B., and Conrad, M. (2019). Ferroptosis and Necroinflammation, a yet Poorly Explored Link. *Cell Death Differ* 26 (1), 14–24. doi:10.1038/s41418-018-0173-9

Radulescu, S., Brookes, M. J., Salgueiro, P., Ridgway, R. A., McGhee, E., Anderson, K., et al. (2016). Luminal Iron Levels Govern Intestinal Tumorigenesis after Apc Loss *In Vivo*. *Cel Rep.* 17 (10), 2805–2807. doi:10.1016/j.celrep.2016.10.028

Stockwell, B. R., Friedmann Angeli, J. P., Bayir, H., Bush, A. I., Conrad, M., Dixon, S. J., et al. (2017). Ferroptosis: A Regulated Cell Death Nexus Linking Metabolism, Redox Biology, and Disease. *Cell* 171 (2), 273–285. doi:10.1016/j.cell.2017.09.021

Sun, Y., Chen, P., Zhai, B., Zhang, M., Xiang, Y., Fang, J., et al. (2020). The Emerging Role of Ferroptosis in Inflammation. *Biomed. Pharmacother.* 127, 110108. doi:10.1016/j.biopha.2020.110108

Tiainen, S., Rilla, K., Hämäläinen, K., Oikari, S., and Auvinen, P. (2021). The Prognostic and Predictive Role of the Neutrophil-To-Lymphocyte Ratio and the Monocyte-To-Lymphocyte Ratio in Early Breast Cancer, Especially in the HER2+ Subtype. *Breast Cancer Res. Treat.* 185 (1), 63–72. doi:10.1007/s10549-020-05925-7

Torti, S. V., Manz, D. H., Paul, B. T., Blanchette-Farra, N., and Torti, F. M. (2018). Iron and Cancer. *Annu. Rev. Nutr.* 38, 97–125. doi:10.1146/annurev-nutr-082117-051732

Tsurusaki, S., Tsuchiya, Y., Koumura, T., Nakasone, M., Sakamoto, T., Matsuoka, M., et al. (2019). Hepatic Ferroptosis Plays an Important Role as the Trigger for Initiating Inflammation in Nonalcoholic Steatohepatitis. *Cell Death Dis* 10 (6), 449. doi:10.1038/s41419-019-1678-y

Umemura, M., Kim, J.-H., Aoyama, H., Hoshino, Y., Fukumura, H., Nakakaji, R., et al. (2017). The Iron Chelating Agent, Deferoxamine Detoxifies Fe(Salen)-Induced Cytotoxicity. *J. Pharmacol. Sci.* 134 (4), 203–210. doi:10.1016/j.jphs.2017.07.002

van der Willik, K. D., Koppelmans, V., Hauptmann, M., Compter, A., Ikram, M. A., and Schagen, S. B. (2018). Inflammation Markers and Cognitive Performance in Breast Cancer Survivors 20 Years after Completion of Chemotherapy: a Cohort Study. *Breast Cancer Res.* 20 (1), 135. doi:10.1186/s13058-018-1062-3

von Hagens, C., Walter-Sack, I., Goeckenjan, M., Osburg, J., Storch-Hagenlocher, B., Sertel, S., et al. (2017). Prospective Open Uncontrolled Phase I Study to Define a Well-Tolerated Dose of Oral Artesunate as Add-On Therapy in Patients with Metastatic Breast Cancer (ARTIC M33/2). *Breast Cancer Res. Treat.* 164 (2), 359–369. doi:10.1007/s10549-017-4261-1

Wang, X., Wang, S.-S., Huang, H., Cai, L., Zhao, L., Peng, R.-J., et al. (2021). Effect of Capecitabine Maintenance Therapy Using Lower Dosage and Higher Frequency vs Observation on Disease-free Survival Among Patients with Early-Stage Triple-Negative Breast Cancer Who Had Received Standard Treatment. *Jama* 325 (1), 50–58. doi:10.1001/jama.2020.23370

Wileyto, E. P., Li, Y., Chen, J., and Heitjan, D. F. (2013). Assessing the Fit of Parametric Cure Models. *Biostatistics* 14 (2), 340–350. doi:10.1093/biostatistics/kxs043

Yamasaki, T., Terai, S., and Sakaida, I. (2011). Deferoxamine for Advanced Hepatocellular Carcinoma. *N. Engl. J. Med.* 365 (6), 576–578. doi:10.1056/nejmc1105726

Yang, Y.-w., Dai, C.-m., Chen, X.-h., and Feng, J.-f. (2021). The Relationship between Serum Trace Elements and Oxidative Stress of Patients with Different Types of Cancer. *Oxidative Med. Cell Longevity* 2021, 1–13. doi:10.1155/2021/4846951

Zhou, Z., Ye, T. J., DeCaro, E., Buehler, B., Stahl, Z., Bonavita, G., et al. (2020). Intestinal SIRT1 Deficiency Protects Mice from Ethanol-Induced Liver Injury by Mitigating Ferroptosis. *Am. J. Pathol.* 190 (1), 82–92. doi:10.1016/j.ajpath.2019.09.012

Zitvogel, L., Pietrocola, F., and Kroemer, G. (2017). Nutrition, Inflammation and Cancer. *Nat. Immunol.* 18 (8), 843–850. doi:10.1038/ni.3754

Conflict of Interest: The authors declare that the research was conducted in the absence of any commercial or financial relationships that could be construed as a potential conflict of interest.

Publisher's Note: All claims expressed in this article are solely those of the authors and do not necessarily represent those of their affiliated organizations, or those of the publisher, the editors and the reviewers. Any product that may be evaluated in this article, or claim that may be made by its manufacturer, is not guaranteed or endorsed by the publisher.

Advantages of publishing in Frontiers

OPEN ACCESS
Articles are free to read for greatest visibility and readership

FAST PUBLICATION
Around 90 days from submission to decision

HIGH QUALITY PEER-REVIEW
Rigorous, collaborative, and constructive peer-review

TRANSPARENT PEER-REVIEW
Editors and reviewers acknowledged by name on published articles

Frontiers
Avenue du Tribunal-Fédéral 34
1005 Lausanne | Switzerland

Visit us: www.frontiersin.org
Contact us: frontiersin.org/about/contact

REPRODUCIBILITY OF RESEARCH
Support open data and methods to enhance research reproducibility

DIGITAL PUBLISHING
Articles designed for optimal readership across devices

FOLLOW US
@frontiersin

IMPACT METRICS
Advanced article metrics track visibility across digital media

EXTENSIVE PROMOTION
Marketing and promotion of impactful research

LOOP RESEARCH NETWORK
Our network increases your article's readership